frontiers | Research Topics

Heat stress: Response, mitigation, and tolerance in plants

Edited by
Ranjeet Ranjan Kumar, Biao Jin and Nianjun Teng

Published in
Frontiers in Plant Science

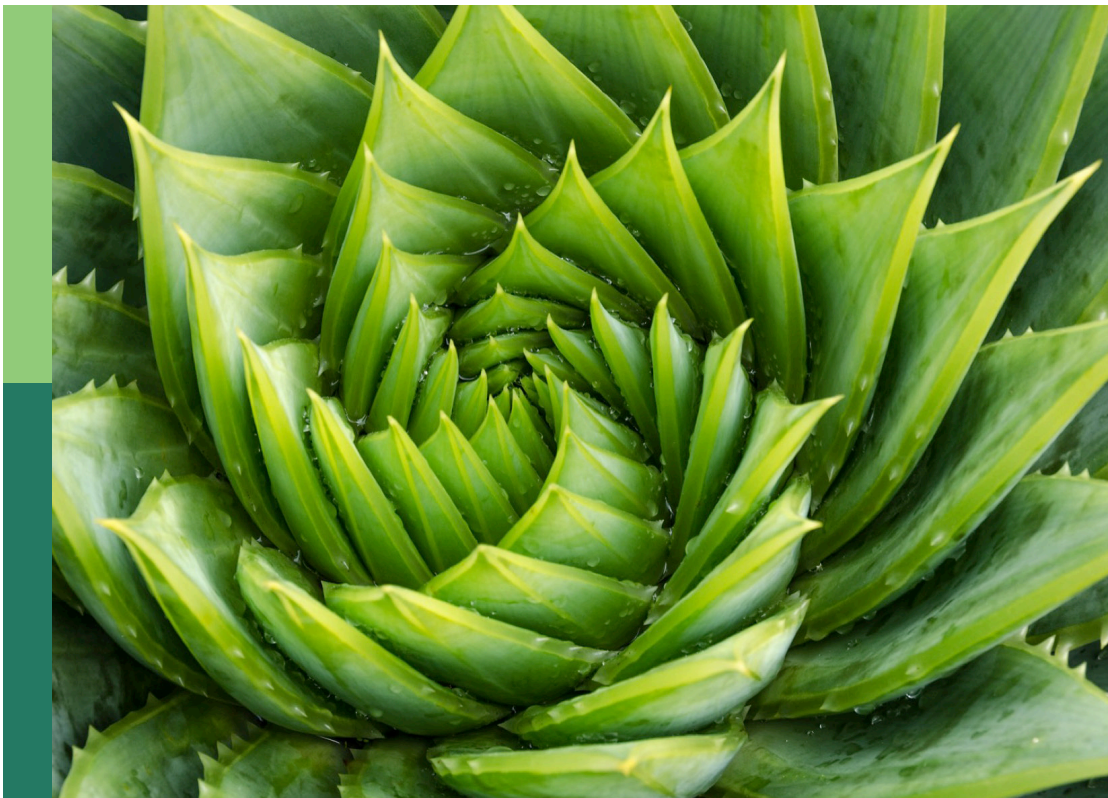

ISSN 1664-8714
ISBN 978-2-8325-3335-2
DOI 10.3389/978-2-8325-3335-2

About Frontiers

Frontiers is more than just an open access publisher of scholarly articles: it is a pioneering approach to the world of academia, radically improving the way scholarly research is managed. The grand vision of Frontiers is a world where all people have an equal opportunity to seek, share and generate knowledge. Frontiers provides immediate and permanent online open access to all its publications, but this alone is not enough to realize our grand goals.

Frontiers journal series

The Frontiers journal series is a multi-tier and interdisciplinary set of open-access, online journals, promising a paradigm shift from the current review, selection and dissemination processes in academic publishing. All Frontiers journals are driven by researchers for researchers; therefore, they constitute a service to the scholarly community. At the same time, the *Frontiers journal series* operates on a revolutionary invention, the tiered publishing system, initially addressing specific communities of scholars, and gradually climbing up to broader public understanding, thus serving the interests of the lay society, too.

Dedication to quality

Each Frontiers article is a landmark of the highest quality, thanks to genuinely collaborative interactions between authors and review editors, who include some of the world's best academicians. Research must be certified by peers before entering a stream of knowledge that may eventually reach the public - and shape society; therefore, Frontiers only applies the most rigorous and unbiased reviews. Frontiers revolutionizes research publishing by freely delivering the most outstanding research, evaluated with no bias from both the academic and social point of view. By applying the most advanced information technologies, Frontiers is catapulting scholarly publishing into a new generation.

What are Frontiers Research Topics?

Frontiers Research Topics are very popular trademarks of the *Frontiers journals series*: they are collections of at least ten articles, all centered on a particular subject. With their unique mix of varied contributions from Original Research to Review Articles, Frontiers Research Topics unify the most influential researchers, the latest key findings and historical advances in a hot research area.

Find out more on how to host your own Frontiers Research Topic or contribute to one as an author by contacting the Frontiers editorial office: frontiersin.org/about/contact

Heat stress: Response, mitigation, and tolerance in plants

Topic editors

Ranjeet Ranjan Kumar — Indian Agricultural Research Institute (ICAR), India

Biao Jin — Yangzhou University, China

Nianjun Teng — Nanjing Agricultural University, China

Citation

Kumar, R. R., Jin, B., Teng, N., eds. (2023). *Heat stress: Response, mitigation, and tolerance in plants*. Lausanne: Frontiers Media SA.

doi: 10.3389/978-2-8325-3335-2

Table of contents

frontiers | Frontiers in Plant Science

TYPE Editorial
PUBLISHED 14 August 2023
DOI 10.3389/fpls.2023.1266765

OPEN ACCESS

EDITED AND REVIEWED BY
Junya Mizoi,
The University of Tokyo, Japan

*CORRESPONDENCE
Ranjeet R. Kumar
ranjeetranjaniari@gmail.com
Biao Jin
bjin@yzu.edu.cn
Nianjun Teng
njteng@njau.edu.cn

†These authors have contributed equally to this work

RECEIVED 25 July 2023
ACCEPTED 07 August 2023
PUBLISHED 14 August 2023

CITATION
Kumar RR, Jin B and Teng N (2023) Editorial: Heat stress: response, mitigation, and tolerance in plants.
Front. Plant Sci. 14:1266765.
doi: 10.3389/fpls.2023.1266765

Editorial: Heat stress: response, mitigation, and tolerance in plants

Ranjeet R. Kumar[1*†], Biao Jin[2*†] and Nianjun Teng[3*†]

[1]Division of Biochemistry, Indian Council of Agricultural Research (ICAR)-Indian Agricultural Research Institute, New Delhi, India, [2]College of Horticulture and Landscape, Yangzhou University, Yangzhou, China, [3]College of Horticulture, Nanjing Agricultural University, Nanjing, China

KEYWORDS

heat stress, signalling molecule, stress-associated genes, transcription factor, thermotolerance, phytohormones, secondary metabolites, heat shock proteins

Editorial on the Research Topic
Heat stress: response, mitigation, and tolerance in plants

Heat stress is one of the major problems affecting the growth and yield of most of the agriculturally important crops. It causes oxidative bursts inside the cells, damaging the cell organelles, membranes, and leads to the denaturation/aggregation of enzymes (Kumar et al., 2023). In order to cope with the fluctuation in temperature, plants have developed various mechanisms like the expression of signalling molecules (like MAPK, CDPK, etc.), antioxidant enzymes (SOD, CAT, GPx, etc.), Heat shock transcription factors (TaHSFA6e, HSF3, etc.), heat shock proteins (sHSPs like HSP17, HSP26, etc.) and many other stress-associated genes like pyrrolyl disulphide isomerase, ABC-Transporter, universal stress proteins, etc. (Azameti et al., 2022).

This Research Topic has been meticulously organized, featuring thirteen original research articles that have been divided into two broad areas to emphasize the findings in the best possible manner: (1) Response of plants to stress/secondary metabolites or hormones, and (2) Omics approaches for the identification of stress-associated genes and proteins.

Response of plants to stress/secondary metabolites or hormones

The intensity and duration of heat stress have severe implications for plant growth and development. Various priming agents and hormones have been reported to modulate the HS-tolerance level of the plant. Otálora et al. reported that MeJA does not affect the gas exchange, chlorophyll A concentration, and the efficiency of the photosystem under HS. The ameliorative impact of MeJA on plants can be utilized to develop thermotolerant crop with improved grain-quality.

Secondary metabolites have been reported as one of the very important metabolites that are mainly utilized by plants as protectants against biotic stresses. Xu et al. reported that monoterpenes (eucalyptol, camphor, linalool, and borneol) modulates the

antioxidant enzymes activities of *Cinnamomum camphora* under HS due to the alterations in expression of the genes related to non-enzymatic and enzymatic antioxidant formation. Various exogenous treatments using phytohormones, polyamines or organic chemicals have been reported to enhance the thermotolerance level of plants. Zhang et al. reported that brassinolide and salicylic acid reduces the damage caused by the accumulation of reactive oxygen species in rice and helps in enhancing the HS-tolerance level. Volatile organic compounds have been reported to block signalling molecules and compromise the response of plants under biotic and abiotic stresses. Pavlovič et al. reported an increase in the cytoplasmic calcium level [Ca^{2+}]cyt in response to diethyl ether application in *Arabidopsis thaliana*, which in turn enhances the tolerance of photosystem II by enhancing the expression of HSPs. Exogenous application of volatile organic compounds can be used as potential method to modulate the tolerance level of the plants under different stresses.

The combined effect of heat and drought has been observed to disturb many ecosystems in terms of their water and carbon budgets. Li et al. reported that dew benefits are cancelled by the heatwave due to the minor contribution of dew in leaf water. Heat-induced reductions in net ecosystem production (NEP) were intensified by the combined effect of drought stress.

Agricultural and horticultural crops are highly prone to HS, since it has very drastic effects on different biological functions like fertilization, cell growth, fruit setting, etc. Tomato, being sensitive to HS, showed a severe decrease in yield and quality under HS. Nutrient management has been used in the past to enhance the tolerance level of the plant against abiotic stresses and has been observed to be quite effective in the case of horticultural crops. Luo et al. reported that short-term sub-high temperature (SHT) stress in tomato grown under nitrogen supplement improved the photosynthetic efficiency, nitrogen metabolism, and fruit quality. Moderate nitrogen application stabilizes the photosynthesis and nitrogen efficiency in tomato under HS and can be recommended as one of the approaches to enhance the tolerance and fruit quality of the tomato plant. Similarly, Mubarok et al. developed parthenocarpic tomato mutants and reported enhanced plant adaptability and fruiting ability under HS. Development of parthenocarpic fruit can be used as one of the approaches to enhance the tolerance and fruiting ability of the horticultural crops.

Omics approaches for the identification of stress-associated genes/proteins

With the advent of technologies, different omics approaches are used to identify novel or putative genes, stress-associated proteins, and metabolites linked with HS-tolerance, in order to understand the mechanism of HS-tolerance. Ikram et al. used the RNA-seq method to identify stress-associated genes in flowering Chinese cabbage (*Brassica campestris* L. ssp. chinensis) and identified 20,680 differentially expressed genes (DEGs) consisting of signalling molecules, transcription factors, and regulatory proteins. Phospholipase C (PLC) has been characterized as playing a very important role in signalling the plant against HS. Annum et al. reported that over-expression of PLC5 (PLC5 OE) in *Arabidopsis thaliana* protects the disintegration of chlorophyll in leaves and has well-developed root architecture under HS. This mechanism can be used in other crop plants to modulate their tolerance level under HS. Similarly, Xue et al. reported that with an increase in temperature, an upregulation of stress-associated genes like CfAPX1, CfAPX2, CfHSP11, CfHSP21, CfHSP70, CfHSFA1a, CfHSFB2a, and CfHSFB4 were observed in *Cryptomeria fortunei* under HS.

Heat stress during pollination has a severe effect on spikelet fertility and yield in rice. Mo et al. reported that sequence variations in OsGRF4 (*Oryza sativa* growth-regulating factor 4; $OsGRF4^{AA}$) helps in escaping the microRNA miR396-mediated degradation of this gene at the mRNA level and affects proper transcriptional and splicing regulation of genes under HS, regulates carbohydrate and nitrogen metabolism, and results in compromised tolerance behaviour in rice pollen. Huang et al. identified differentially expressed genes involved in HS-adaptation of *Gracilaria bailinae* (macroalgae) using RNA-seq and observed downregulation of most of the identified DEGs. These DEGs involved in spikelet fertility can be manipulated to enhance the tolerance under HS.

Various gene regulatory networks operate inside the plant system and play important roles in multiple adaptive processes. Xu et al. reported that drought- and cold-responsive gene regulatory networks (GRNs) in *Myrica rubra* have been built according to the timing of transcription under both abiotic stresses, and have a conserved trans-regulator and a common regulatory network. Functional validation showed MrbHLH10 to mitigate abiotic stresses through the modulation of ROS scavenging.

Overall, this Research Topic provides very significant information on role of different elicitors/metabolites in modulating the HS-tolerance, putative stress-responsive genes and their regulatory networks, and nutrient management approach to enhance the tolerance of horticultural crops. There is further need to elucidate the mechanism of heat stress tolerance in plants and identification of potential markers for evaluating the diverse germplasm of crops. This will pave the way for the development of 'climate-smart' crops.

Author contributions

RK: Writing – original draft. BJ: Writing – review & editing. NT: Writing – review & editing.

Acknowledgments

We express our sincere gratitude to all the authors who contributed their original research articles or reviews to this Research Topic. RK acknowledges the support from the Indian Council of Agricultural Research (ICAR) under National Innovations on Climate Resilient Agriculture (NICRA) project

(Sanction no. TG-3079) and CABin project (sanction no. 21-56, TG3064).

Conflict of interest

The authors declare that the research was conducted in the absence of any commercial or financial relationships that could be construed as a potential conflict of interest.

Publisher's note

References

Azameti, M. K., Ranjan, A., Singh, P. K., Gaikwad, K., Singh, A. K., Dalal, M., et al. (2022). Transcriptome profiling reveals the genes and pathways involved in thermotolerance in wheat (Triticum aestivum L.) genotype Raj 3765. *Sci. Rep.* 12 (1), 14831. doi: 10.1038/s41598-022-18625-7

Kumar, R. R., Rai, G. K., Kota, S., Watts, A., Sakhare, A., Kumar, S., et al. (2023). Fascinating dynamics of silicon in alleviation of heat stress induced oxidative damage in plants. *Plant Growth Regul.* 100 (2), 321–335. doi: 10.1007/s10725-022-00879-w

frontiers | Frontiers in Plant Science

TYPE Original Research
PUBLISHED 12 September 2022
DOI 10.3389/fpls.2022.995001

OPEN ACCESS

EDITED BY
Nianjun Teng,
Nanjing Agricultural University,
China

REVIEWED BY
Daqiu Zhao,
Yangzhou University,
China
Shu Yuan,
Sichuan Agricultural University,
China

*CORRESPONDENCE
Andrej Pavlovič
andrej.pavlovic@upol.cz

SPECIALTY SECTION
This article was submitted to Plant Abiotic Stress, a section of the journal Frontiers in Plant Science

RECEIVED 15 July 2022
ACCEPTED 18 August 2022
PUBLISHED 12 September 2022

CITATION
Pavlovič A, Jakšová J, Kučerová Z, Špundová M, Rác M, Roudnický P and Mithöfer A (2022) Diethyl ether anesthesia induces transient cytosolic [Ca^{2+}] increase, heat shock proteins, and heat stress tolerance of photosystem II in *Arabidopsis*. *Front. Plant Sci.* 13:995001. doi: 10.3389/fpls.2022.995001

Diethyl ether anesthesia induces transient cytosolic [Ca^{2+}] increase, heat shock proteins, and heat stress tolerance of photosystem II in *Arabidopsis*

Andrej Pavlovič[1]*, Jana Jakšová[1], Zuzana Kučerová[1], Martina Špundová[1], Marek Rác[1], Pavel Roudnický[2] and Axel Mithöfer[3]

[1]Department of Biophysics, Faculty of Science, Palacký University, Olomouc, Czechia, [2]Central European Institute of Technology, Masaryk University, Brno, Czechia, [3]Research Group Plant Defense Physiology, Max Planck Institute for Chemical Ecology, Jena, Germany

General volatile anesthetic diethyl ether blocks sensation and responsive behavior not only in animals but also in plants. Here, using a combination of RNA-seq and proteomic LC–MS/MS analyses, we investigated the effect of anesthetic diethyl ether on gene expression and downstream consequences in plant *Arabidopsis thaliana*. Differential expression analyses revealed reprogramming of gene expression under anesthesia: 6,168 genes were upregulated, 6,310 genes were downregulated, while 9,914 genes were not affected in comparison with control plants. On the protein level, out of 5,150 proteins identified, 393 were significantly upregulated and 227 were significantly downregulated. Among the highest significantly downregulated processes in etherized plants were chlorophyll/tetrapyrrole biosynthesis and photosynthesis. However, measurements of chlorophyll *a* fluorescence did not show inhibition of electron transport through photosystem II. The most significantly upregulated process was the response to heat stress (mainly heat shock proteins, HSPs). Using transgenic *A. thaliana* expressing *APOAEQUORIN*, we showed transient increase of cytoplasmic calcium level $[Ca^{2+}]_{cyt}$ in response to diethyl ether application. In addition, cell membrane permeability for ions also increased under anesthesia. The plants pre-treated with diethyl ether, and thus with induced HSPs, had increased tolerance of photosystem II to subsequent heat stress through the process known as cross-tolerance or priming. All these data indicate that diethyl ether anesthesia may partially mimic heat stress in plants through the effect on plasma membrane.

KEYWORDS

anesthesia, *Arabidopsis*, chlorophyll, diethyl ether, heat shock proteins, heat stress, photosystem II

Introduction

General volatile anesthetics (GVAs) are usually defined as compounds, which induce reversible loss of consciousness in humans (Franks, 2006). The clinical definition of anesthesiology states that it is the practice of medicine providing insensibility to pain during surgical, obstetric, therapeutic, and diagnostic procedures. Diethyl ether and chloroform were used as sole agents in a general anesthetic procedure for almost a century, and the term anesthesia was introduced soon after the discovery of etherization. In fact, the term anesthesia was coined to describe what happens during the process of etherization. GVAs produce unconsciousness, analgesia, amnesia, immobility, and lack of stress and hemodynamic responses in response to noxious stimulation (Urban and Bleckwenn, 2002). However, such narrow definitions are applicable only for subset of organisms with cortical networks that are susceptible to being anesthetized. Because the anesthetic drugs are also effective in organisms from protists, through plants, to primate, Kelz and Mashour (2019) proposed new definition for anesthetics applicable across whole tree of life as compounds which cause disconnection from environment, both in receptive (e.g., sensation) and expressive (e.g., motoric responses) arms of interaction.

If plants are exposed to GVAs, they indeed lost ability to sense their environment. In previous studies, it was shown that plants exposed to diethyl ether anesthesia were neither able to sense mechanical stimuli, wounding, or light and lack also expressive motoric responses. For example, touch-induced leaf movement in sensitive plant *Mimosa pudica*, trap closing reactions in carnivorous plant *Dionaea muscipula*, trap bending movement in carnivorous sundew *Drosera capensis* and autonomous circumnutations movements of tendrils of pea (*Pisum sativum*) were completely stopped (Milne and Beamish, 1999; De Luccia, 2012; Yokawa et al., 2018; Pavlovič et al., 2020; Böhm and Scherzer, 2021; Scherzer et al., 2022). We found that disappearance of some of these plant reactions were caused by inhibition of electrical signal generation and propagation, a target of anesthetics is remarkably similar to animal organisms. Also in the case of *Arabidopsis thaliana* plants, in which motoric responses are not easily observable, etherized individuals lost ability of systemic electrical and Ca^{2+} signals propagation from damaged to neighboring leaves after heat wounding (Jakšová et al., 2021). Since electrical and Ca^{2+} signal propagation is dependent on ligand-gated glutamate receptor like channels (GLRs, Mousavi et al., 2013; Toyota et al., 2018), and diethyl ether attenuated also glutamate-induced Ca^{2+} signal (Jakšová et al., 2021; Scherzer et al., 2022), GLR channels have been suspected as the possible targets of anesthesia in plants, like in animals. In the absence of electrical signals in etherized plants, the downstream sequence of events in systemic leaves were blocked, including accumulation of phytohormones of the jasmonates (JA) group and expression of JA-responsive genes, indicating the inhibition of sensing as well as responsive behavior in plants (Pavlovič et al., 2020; Jakšová et al., 2021).

The exact mode of GVA action in animals and plants is still a mystery. In the membrane theory, Meyer (1899) and Overton (1901) assumed that solubilization of lipophilic GVA in lipid bilayer of the neurons causes their fluidizing and malfunction, and anesthetic effect. In the modern lipid hypothesis, anesthetics do not act directly through the membrane, but rather perturb specialized lipid matrices at the protein-lipid interface (Lerner, 1997; Pavel et al., 2020). The protein theory of GVA action was put forward, when Franks and Lieb (1984) demonstrated that the anesthetic effect can be reproduced on a soluble luciferase protein in the absence of lipids. It was believed that GVAs bind to their target ion channel by a key-lock mechanism and change their structure dramatically from open to closed conformation. The modern protein theory suggests that GVAs do not change structure of membrane channel but change its dynamics, especially dynamics in the flexible loops that connect α-helices in a bundle and are exposed to the membrane-water interface (Tang and Xu, 2002). Recent findings indicate that GVAs disrupt lipid rafts, regions of ordered lipids which allow nanoscale compartmentalization of proteins and lipids (Pavel et al., 2020).

In this study, we focused on molecular responses to diethyl ether anesthesia in *A. thaliana* using transcriptomic (RNA-seq) and proteomic (LC–MS/MS) analyses. Although recent studies have shown that diethyl ether anesthesia blocks sensation and responsive behavior in plants, here we show for the first time that it also induced huge reprogramming of gene expression. Our data strongly suggest that GVA diethyl ether mimics a heat stress probably through the effect on plasma membrane.

Materials and methods

Plant material, culture conditions, and experimental setup

Plants of *Arabidopsis thaliana* (L.) Heynh. (Col-0) and transgenic *A. thaliana* (L.) Heynh. (Col-0), expressing the *APOAEQUORIN* gene under control of the CaMV 35S promoter, were grown on a soil substrate (Potgrond H, Klasmann-Deilmann, Germany) in a growth chamber (AR75L; Percival-Scientific, United States) for 6–7 weeks under 8 h light (100 µmol photons m^{-2} s^{-1} PAR)/16 h dark cycle (21/21°C) and 60% relative air humidity. The 6–7 weeks old plants were enclosed into polypropylene bags or transparent boxes and diethyl ether was applied. By adding a corresponding volume of liquid phase of diethyl ether to a certain volume of air, 15% vapor of diethyl ether was obtained (see Yokawa et al., 2018). Then, after 2.5 and 5.5 h, the leaf samples were collected and immediately frozen in liquid nitrogen and stored at −80°C. At the same time the leaf samples from controlled bagged plants without diethyl ether were also sampled by the same way.

RNA-seq analyses

A single eighth leaf (for leaf numbering see Jakšová et al., 2021) of 2.5 h etherized and control plants of *A. thaliana* were cut,

immediately frozen in liquid nitrogen and weighted. 50–60 mg of leaf material was homogenized in a Geno/Grinder® 2010 (Spex Sample Prep, Stanmore, United Kingdom) equipped with aluminum racks. The racks were cooled in liquid nitrogen prior to usage to prevent a thawing of leaf material during the whole homogenization process. RNA was extracted and purified using Trizol reagent (Invitrogen, Carlsbad, CA, United States) followed by the RNA Clean & Concentrator TM-5 kit (Zymo Research, Irvine, CA, United States), including DNase digestion to remove genomic DNA contamination. A total amount of 1 μg RNA per sample was used as input material for the RNA sample preparations. Sequencing libraries were generated using NEBNext® UltraTM RNA Library Prep Kit for Illumina® (NEB, United States) following manufacturer's recommendations and index codes were added to attribute sequences to each sample. Briefly, mRNA was purified from total RNA using poly-T oligo-attached magnetic beads. Fragmentation was carried out using divalent cations under elevated temperature in NEBNext First Strand Synthesis Reaction Buffer (5X). First strand cDNA was synthesized using random hexamer primer and M-MuLV Reverse Transcriptase (RNase H-). Second strand cDNA synthesis was subsequently performed using DNA Polymerase I and RNase H. Remaining overhangs were converted into blunt ends *via* exonuclease/polymerase activities. After adenylation of 3′ ends of DNA fragments, NEBNext Adaptor with hairpin loop structure were ligated to prepare for hybridization. In order to select cDNA fragments of preferentially 150–200 bp in length, the library fragments were purified with AMPure XP system (Beckman Coulter, Beverly, United States). Then 3 μl USER Enzyme (NEB, United States) was used with size-selected, adaptor ligated cDNA at 37°C for 15 min followed by 5 min at 95°C before PCR. Then PCR was performed with Phusion High-Fidelity DNA polymerase, Universal PCR primers and Index (X) Primer. At last, PCR products were purified (AMPure XP system) and library quality was assessed on the Agilent Bioanalyzer 2100 system. The clustering of the index-coded samples was performed on a cBot Cluster Generation System using PE Cluster Kit cBot-HS (Illumina) according to the manufacturer's instructions. After cluster generation, the library preparations were sequenced on an Illumina platform and paired-end reads were generated. Raw data (raw reads) of FASTQ format were firstly processed through FASTP. In this step, clean data (clean reads) were obtained by removing reads containing adapter and poly-N sequences and reads with low quality from raw data. At the same time, Q20, Q30, and GC content of the clean data were calculated. All the downstream analyses were based on the clean data with high quality. Differential expression analysis between two conditions/groups four biological replicates per condition was performed using DESeq2R package. DESeq2 provides statistical routines for determining differential expression in digital gene expression data using a model based on the negative binomial distribution. The resulting p values were adjusted using the Benjamini and Hochberg's approach for controlling the False Discovery Rate (FDR). Genes with an adjusted p value <0.05 found by DESeq2 were assigned as differentially expressed. Gene Ontology (GO) enrichment analysis of differentially expressed genes was implemented by the clusterProfiler R package, in which gene length bias was corrected. GO terms with corrected p value less than 0.05 were considered significantly enriched by differential expressed genes. The RNA-seq experiment was commercially done by NovoGene.

LC–MS/MS analyses

A single eight leaf from etherized *A. thaliana* plants for 5.5 h and non-etherized leaf from control plants were homogenized by mortar and pestle in liquid nitrogen after diethyl ether treatment. Homogenates were then lysed in SDT buffer (4% SDS, 0.1 M DTT, 0.1 M Tris/HCl, and pH 7.6) in a thermomixer (Eppendorf ThermoMixer® C, 60 min, 95°C, 750 rpm). After that, samples were centrifuged (15 min, 20,000 × g) and the supernatants (ca 100 μg of total protein) used for filter-aided sample preparation (FASP) as described elsewhere (Wiśniewski et al., 2009) using 0.75 μg of trypsin (sequencing grade; Promega). Resulting peptides were analyzed by LC–MS/MS.

LC–MS/MS analyses of all peptides were done using nanoElute system (Bruker) connected to timsTOF Pro spectrometer (Bruker). Two column (trapping column: Acclaim™ PepMap™ 100 C18, dimensions 300 μm ID, 5 mm long, 5 μm particles, Thermo Fisher Scientific; separation column: Aurora C18, 75 μm ID, 250 mm long, 1.6 μm particles, IonOpticks) mode was used on nanoElute system with default equilibration conditions (trap column: 10 volumes at 217.5 bars; separation column: 4 column volumes at 800 bars). Sample loading was done using three pickup volumes +2 μl at 100 bars. Trapped peptides were eluted by 120 min linear gradient program (flow rate 400 nl min^{-1}, 3–80% of mobile phase B; mobile phase A: 0.1% FA in water; and mobile phase B: 0.1% FA in ACN). The analytical column was placed inside the Column Toaster (40°C; Bruker) and its emitter side was installed into CaptiveSpray ion source (Bruker). MSn data were acquired in m/z range of 100–1,700 and 1/k0 range of 0.6–1.6 $V \times s \times cm^{-2}$ using DDA-PASEF method acquiring 10 PASEF scans with scheduled target intensity of 20,000 and intensity threshold of 2,500. Active exclusion was set for 0.4 min with precursor reconsideration for 4× more intense precursors.

For data evaluation, we used MaxQuant software (v1.6.17; Cox and Mann, 2008) with in built Andromeda search engine (Cox et al., 2011). Search was done against protein databases of *A. thaliana* (27,468 protein sequences, version from 2020-12-02, downloaded from ftp://ftp.uniprot.org/pub/databases/uniprot/current_release/knowledgebase/reference_proteomes/Eukaryota/UP000006548/UP000006548_3702.fasta.gz) and cRAP contaminants (112 sequences, version from 2018-11-22, downloaded from http://www.thegpm.org/crap). Modifications were set as follows for database search: oxidation (M), deamidation (N, Q), and acetylation (Protein N-term) as variable modifications, with carbamidomethylation (C)

as a fixed modification. Enzyme specificity was tryptic with two permissible miscleavages. Only peptides and proteins with false discovery rate threshold under 0.01 were considered. Relative protein abundance was assessed using protein intensities calculated by MaxQuant. Intensities of reported proteins were further evaluated using software container environment (https://github.com/OmicsWorkflows/KNIME_docker_vnc; version 4.1.3a). Processing workflow is available upon request and it covers, in short, reverse hits and contaminant protein groups (cRAP) removal, protein group intensities log2 transformation and normalization (loessF), and LIMMA statistical tests. Significantly up/downregulated protein groups were further subjected to functional enrichment analysis using g:Profiler web tool (significance threshold g:SCS; user threshold 0.05; Raudvere et al., 2019).

Western blotting

Total protein from the eighth leaf of 5.5 h etherized and control plants of *A. thaliana* was isolated using extraction buffer containing 28 mM DTT, 28 mM Na_2CO_3, 175 mM sucrose, 5% SDS, 10 mM EDTA, and protease inhibitors (Set VI, Calbiochem, Darmstadt, Germany). The samples were heated for 30 min at 70°C. The concentration of total soluble proteins in the samples was determined using the Bicinchoninic Acid Kit for Protein Determination (Sigma-Aldrich, St. Louis, MO, United States), and absorbance was measured at 562 nm (Thermo Spectronic UV500, UV–Vis Spectro, MA, United States). The same amount of protein was separated in a 10% (v/v) SDS–polyacrylamide gel (Schägger, 2006) followed by transfer to a nitrocellulose membrane (Bio-Rad, Germany) by Trans-Blot SD Semi-Dry Electrophoretic Transfer Cell (Bio-Rad, Hercules, CA, United States). To check the correct protein transfer, the membranes were stained by Ponceau-S. After blocking in TBS-T containing 5% BSA overnight at 4°C, the membranes were incubated with the primary antibody at room temperature with soft agitation. Antibodies against proteins HSP70 (AS08371), HSP90-1 (AS08346), GluTR (AS10689), LPOR (AS05067), RbcL (AS03037), and actin (AS13 2640) were purchased from Agrisera (Vännäs, Sweden). After washing, the membrane was incubated 1 h with the secondary antibody [goat anti-rabbit IgG (H + L)-horseradish peroxidase conjugate] with dilution 1:10,000 (Bio-Rad, Hercules, CA, United States). Signals were visualized and quantified using Immobilon Western chemiluminescent HRP substrate (Millipore, Billerica, MA, United States) on an Amersham Imager 600 (GE HealthCare Life Sciences, Japan). The data were checked for homogeneity of variance and significant differences were evaluated by Student's *t*-test. If non-homogeneity was present, Welch's *t*-test was used instead (Microsoft Excel).

Aequorin luminescence imaging

Transgenic *A. thaliana* (L.) Heynh Col-0 wild-type expressing the *APOAEQUORIN* gene under control of the CaMV 35S promoter was used for $[Ca^{2+}]_{cyt}$ analyses (Kiep et al., 2015). Aequorin was reconstituted by spraying plants with 10 µM coelenterazine (Invitrogen, Eugene, OR, United States) in 0.01% Tween 20 (Sigma-Aldrich, United Kingdom) and subsequent incubation for 5 h in the dark. Aequorin luminescence imaging was performed using a highly sensitive CCD camera iKon-XL (Oxford Instruments plc, Tubney Woods, Abingdon, United Kingdom). To reduce the dark current, CCD camera was cooled down to −100°C. The CCD camera was equipped with a 50-mm focal distance lens with an f-number of 1.2 (Nikon, Tokyo, Japan) to enhance the light collecting efficiency. Spectral sensitivity of CCD camera was within the range of λ = 200–1,000 nm with almost 90% quantum efficiency in the visible range of the spectrum. The spectral sensitivity was limited to λ = 350–1,000 nm by the lenses. CCD camera parameters were as follows: scan rate, 100 kHz; gain, 2. Photons were captured in photon-counting mode with a 5 min acquisition time. Signal acquisition and processing were performed with Andor Solis (Oxford Instruments plc, Tubney Wood, Abingdon, United Kingdom) and ImageJ 1.49 (NIH, United States), respectively. The CCD camera was situated in the experimental dark room (3 m × 1.5 m × 2.5 m) painted in black. The door in the experimental dark room was protected completely with a black curtain to restrict any external light. The plants were imaged 10 min before, during and 2.5 h after diethyl ether application. All experiments were repeated several times to ensure reproducibility.

Chlorophyll *a* fluorescence quenching analysis

Chlorophyll *a* fluorescence quenching analysis was measured using a FluorCam imaging system (800–0, PSI, Czech Republic) on the plants enclosed in the transparent boxes. The plants were treated by diethyl ether for 5.5 h and measured immediately still under the effect of diethyl ether. Control plants were also enclosed in the box before and during the measurement in order to maintain the same optical conditions of the measurement. Before measurements, the plants were dark-adapted for 20 min. A kinetics of three parameters—an effective quantum yield of photosystem II (PSII; Φ_{PSII}), excitation pressure on PSII ($1-q_P$), and non-photochemical quenching of chlorophyll fluorescence (NPQ) were evaluated after switching on actinic light (red light, 100 µmol photons m^{-2} s^{-1} PAR) and during subsequent dark relaxation. Φ_{PSII} was calculated as $\Phi_{PSII} = (F_M' - F_t)/F_M'$, the excitation pressure $1-q_P = 1 - (F_M' - F_t)/(F_M' - F_0')$, and $NPQ = (F_M - F_M')/F_M'$ (Maxwell and Johnson, 2000). Maximum fluorescence in dark (F_M) and light-adapted state (F_M') was determined by applying the 1.6 s saturating pulse (blue light, 3,000 µmol photons m^{-2} s^{-1} PAR). The actual fluorescence signal at the time *t* of actinic illumination (F_t) was measured immediately prior to the application of saturating pulse. Minimum fluorescence in light-adapted state (F_0') was estimated by the formula $F_0' \approx F_0/[(F_M - F_0)/F_M + F_0/F_M']$. F_0 (minimum fluorescence in

dark-adapted state) was determined by applying several μ-seconds-long measuring flashes (red light, 0.1 μmol photons m^{-2} s^{-1} PAR) at the beginning of the procedure. The data were checked for homogeneity of variance and significant differences were evaluated by Student's *t*-test, if non-homogeneity was present, Welch's *t*-test was used instead (Microsoft Excel).

Measurements of fast chlorophyll *a* fluorescence transient

To investigate the effect of diethyl ether mediated cross-tolerance or priming on subsequent heat–stress response, we measured fast chlorophyll *a* fluorescence transient. The measurements were done in control plants and plants incubated 5.5 h in diethyl ether. Then the plants were removed from the boxes and after 30 min of their recovery (15 min under dim light and then 15 min in darkness), leaves were detached from the plants and incubated for 5 min in a water bath at room temperature (RT) or at 40, 42, 43, 45, and 46°C (in darkness). Immediately after the heat treatment, chlorophyll *a* fluorescence induction transient (OJIP curve) was measured by a Plant Efficiency Analyzer (Hansatech Instruments, United Kingdom) at RT from the adaxial side of the leaves. Excitation light intensity of 2,500 μmol photons m^{-2} s^{-1} PAR (red light) and 2 s detection time were used for the measurement. A maximal quantum yield of PSII photochemistry was estimated as $F_V/F_M = (F_M - F_0)/F_M$, where F_M is maximal fluorescence (corresponding to the fluorescence intensity in P-level in the OJIP curve) and F_0 minimal fluorescence in dark-adapted leaves (Maxwell and Johnson, 2000). The measured O(K)JIP curves were normalized to variable fluorescence ($F_V = F_M - F_0$) and to variable fluorescence at 2 ms [$F_{V(2ms)} = F_{(2ms)} - F_0$] in order to better visualize a K-band indicating high temperature-induced inhibition of oxygen evolving complex (Guissé et al., 1995; Srivastava et al., 1997). The data were checked for homogeneity of variance and significant differences were evaluated by Student's *t*-test, if non-homogeneity was present, Welch's *t*-test was used instead (Microsoft Excel).

Measurements of cell membrane permeability for ions

For the determination of the extent of ion leakage from leaf tissue, as a measure of cell membrane permeability for ions associated with membrane damage and/or increased fluidity, leaf disks (diameter of 12 mm) were cut out from leaves of the control plants and plants, which had been incubated in diethyl ether for 5.5 h before. Three leaf disks (representing one sample) were immediately put into test tube containing 5 ml of deionized water and incubated in water bath at RT or temperature of 42 or 45°C. The electrical conductivity (EC) of the solutions was measured in 10 min intervals (at RT) or after 60 min of incubation of the samples at a given temperature with a digital conductivity meter (GMH 3430, Greisinger, Germany). The total electrical conductivity (EC_T) was measured after autoclaving the samples for 15 min at 121°C. The relative conductivity (%) was calculated as EC/EC_T 100. The data were checked for homogeneity of variance and significant differences were evaluated by Student's *t*-test, if non-homogeneity was present, Welch's *t*-test was used instead (Microsoft Excel).

Results

Transcriptomic analyses

We performed transcriptomic studies with *A. thaliana* plants that were exposed to diethyl ether anesthesia for 2.5 h. Differential expression analyses revealed that under anesthesia 9,914 genes were not affected, 6,168 genes were upregulated and 6,310 genes were downregulated at $p < 0.05$ in comparison to control plants (Figure 1). The complex lists of upregulated and downregulated genes are available in Supplementary Table S1. For annotation and categorization a gene product's molecular function (MF), cell compartment (CC) and associated biological process (BP) gene ontology enrichment analyses (GO) were performed (Figure 2). Among the top 20 downregulated processes in etherized plants were biological processes (GO-BP) involved in photosynthesis, chlorophyll/tetrapyrrole biosynthesis, amino acids metabolism, and cofactor/coenzyme biosynthesis (Figure 2A). Not surprisingly, the locations relative to cellular structures in which the downregulated gene products perform a function (GO-CC) were chloroplasts and thylakoid membranes (Figure 2C). Molecular function activities (GO-MF) involved ligase, isomerase, transferase, oxidoreductase, and galactosidase activities (Figure 2E). Among the top 20 upregulated processes in etherized plants were biological processes (GO-BP) involved in heat response, response to chitin and bacterium, vesicle-mediated transport, immune system responses, response to (organo) nitrogen compounds etc. (Figure 2B). The locations where the upregulated genes perform their function (GO-CC) were mainly in endomembrane system (Figure 2D). The upregulated molecular functions (GO-MF) were represented by protein degradation (ubiquitin system), modification (phosphatases), folding (heat shock protein binding), vesicular transport (clathrin and SNARE binding), and calcium ion and calmodulin binding (Figure 2F). The complex lists of significantly enriched GO terms are available in Supplementary Table S2.

Proteomic analysis

To validate the RNA-seq data and to confirm if increased/decreased level of mRNA is mirrored also on protein level, we performed proteomic analysis of plants etherized for 5.5 h. This longer treatment was chosen based on the fact that proteins have slower turnover rate than mRNA. Out of 5,150 proteins

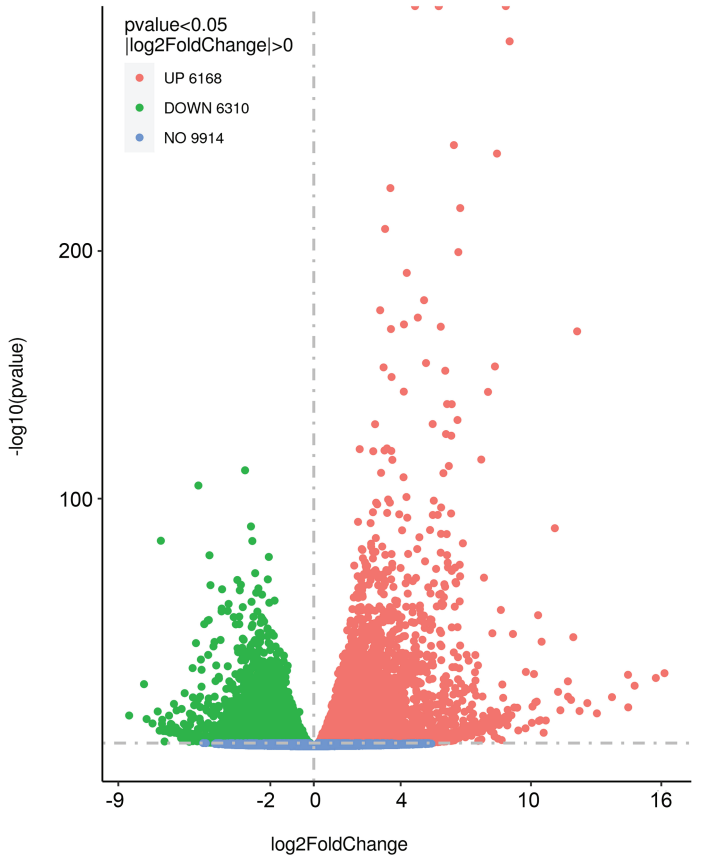

DOWN
Expansin-A8 EXPA8
Dirigent protein 6 DIR6
Fatty acid desaturase 4-like 2, chloroplastic FAD4L2
3-ketoacyl-CoA synthase 19 KSC19
Amine oxidase
Hevein-like preproprotein HEL
Peroxidase 32 PER32
Glutathione S-transferase F3 GSTF3
PDF1.2b
SAUR-like auxin-responsive protein family
Nudix hydrolase 18, mitochondrial NUDT18
RING/U-box superfamily protein
Organic cation/carnitine transporter 3 OCT3
Serine/threonine-protein phosphatase 6 regulatory ankyrin repeat subunit
MATH domain and coiled-coil domain-containing protein At3g58200
Chalcone--flavonone isomerase 1 CHI1
Putative cysteine-rich receptor-like protein kinase 30
Protamine P1 family protein
Peroxidase (DUF 3339)
Transcription factor bHLH61

UP
Subtilisin-like protease SBT3.3
Glycosyltransferase (Fragment) UGT74E2
UDP-glycosyltransferase UGT73C1
Serine/threonine-protein kinase OXI1
Ethylene-responsive transcription factor ERF071
BPS1-like protein
Putative F-box protein
Regulator of chromosome condensation (RCC1) family protein
Ethylene-responsive transcription factor ERF020
Formin-like protein 12 FH12
ACD11 homolog protein
ARM repeat superfamily protein
ATPase 9, plasma membrane-type AHA9
Putative glutamine amidotransferase GAT1_2.1
Glutathione S-transferase GSTU25
23.5 kDa heat shock protein, mitochondrial HSP23.5
Putative disease resistance protein
17.6 kDa class II heat shock protein HSP17.6
Zinc finger AN1 domain-containing stress-associated protein 12 SAP12
Protein DETOXIFICATION 3 DTX3

FIGURE 1
Summary of the RNA-seq results and differentially expressed genes (DEG) in response to diethyl ether anesthesia in *Arabidopsis thaliana*. Volcano plot representation of differential expression analysis of genes in the control *vs*. diethyl ether treated plants. Green and red points mark the genes with significantly decreased or increased expression, respectively in diethyl ether treated plants compared to controls ($p < 0.05$). Blue points mark the genes that are not significantly differentially expressed. The *x*-axis shows $\log_2$ fold changes in expression and the *y*-axis the $\log_{10}$ *p* values of a gene being differentially expressed. On the right, top 20 upregulated and top 20 downregulated genes based on $\log_2$ fold change are listed. The complete list of DEG is available as Supplementary Table S1.

detected and identified, 393 proteins were significantly upregulated, and 227 proteins were significantly downregulated at $p < 0.05$ in etherized plants in comparison to control plants. The list of upregulated and downregulated proteins is available as Supplementary Table S3. As in the case of RNA-seq experiment, GO analysis was performed (Figure 3). Among the significantly downregulated processes in etherized plants were biological processes involved in chlorophyll/tetrapyrrole biosynthesis, uronic acid and galacturonate metabolic processes and thiamine metabolism (GO-BP, Figure 3A), which were located in different parts of plastid/chloroplast and Golgi network (GO-CC, Figure 3C). UDP-glucuronate 4-epimerase activity and Rho GDP-dissociation inhibitor activity were the only two significantly downregulated molecular functions (GO-MF, Figure 3E). Among the significantly upregulated processes in etherized plants were biological processes involved in response to cadmium/metal ions, responses to different biotic/abiotic stimuli, response to heat etc. (GO-BP, Figure 3B) in different cell parts (Figure 3D). The upregulated molecular functions (GO-MF) involved glucosyltransferase activity, xyloglucan/xyloglucosyl transferase activity and *cis*/*trans* zeatin O-beta-D-glucosyltransferase activity, protein folding (heat-shock protein binding, misfolded protein binding, and protein folding chaperone) etc. (GO-MF, Figure 3F).

Anesthesia with diethyl ether downregulated chlorophyll metabolism and upregulated heat shock proteins

When comparing RNA-seq experiments and proteomic analyses one might notice that anesthesia with diethyl ether upregulated genes and proteins involved in reparation of misfolded proteins (mainly HSPs) and downregulated photosynthesis/chlorophyll metabolism. Among other processes were upregulation of endomembrane/vesicular transport associated genes and downregulated vitamin/thiamine metabolic processes. Indeed heat maps indicate that

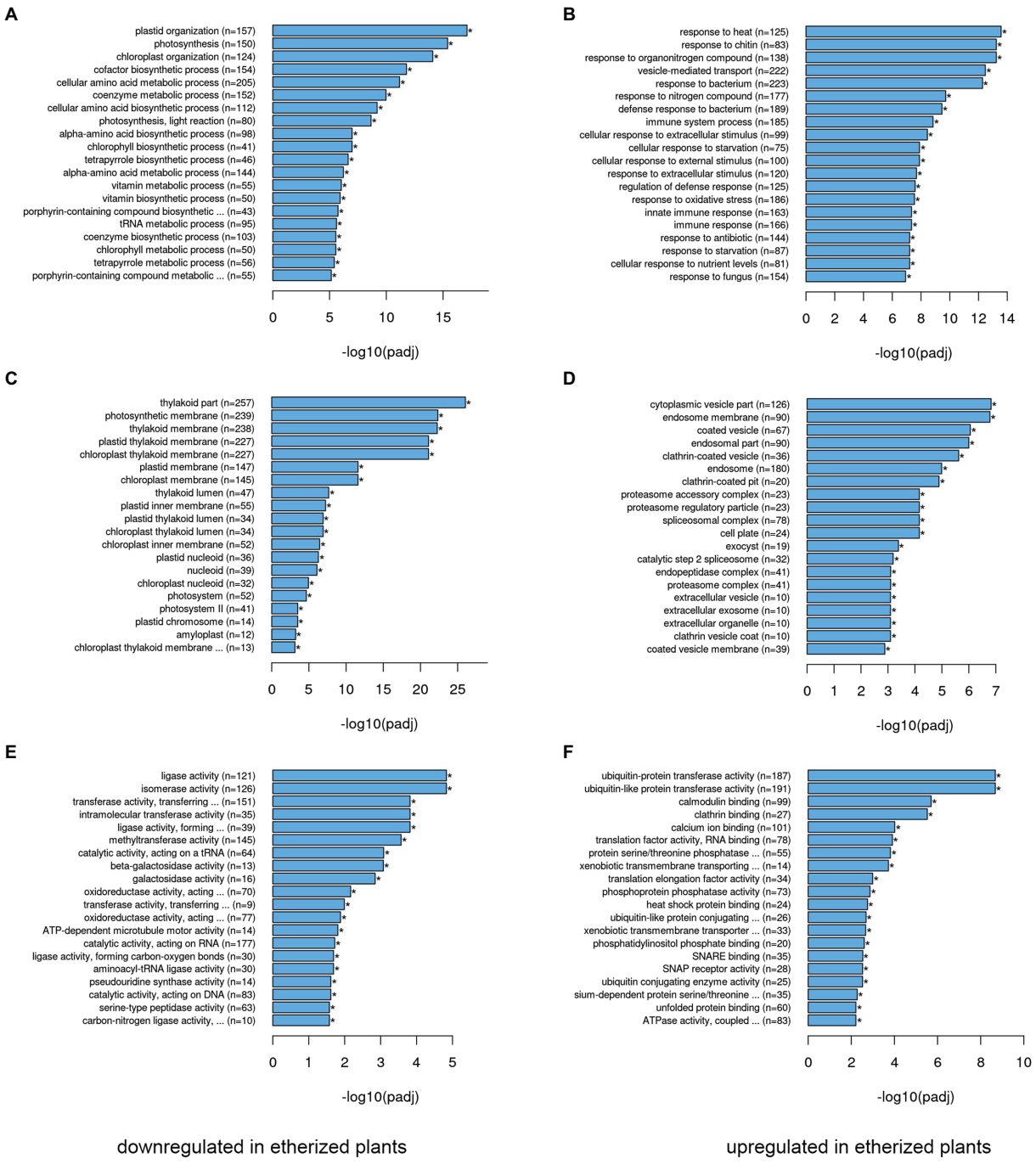

FIGURE 2
Gene ontology (GO) functional analysis of differentially expressed genes (DEGs) in *Arabidopsis thaliana*. The 20 most significantly ($p < 0.05$) enriched downregulated GO terms in biological process **(A)**, cellular component **(C)**, and molecular function **(E)** branches in etherized plants compared to control are presented. The 20 most significantly ($p<0.05$) enriched upregulated GO terms in biological process **(B)**, cellular component **(D)**, and molecular function **(F)** branches in etherized plants compared to control are presented. All the adjusted statistically significant values of the terms were negative 10-base log transformed. Asterisks (*) denote significantly different GO terms at $p < 0.05$. A complete list of GO terms is available as Supplementary Table S2.

majority of HSPs mRNA/proteins were significantly upregulated and mRNA/proteins involved in chlorophyll metabolism were significantly downregulated (Figure 4). The proteins involved in photosynthesis were significantly downregulated only in three cases (PsaO, Lhca5, and Lhca6) despite significant transcriptional downregulation of many genes involved in photosynthesis (Figure 4). This was probably caused by the high abundance of majority of photosynthesis-related proteins which

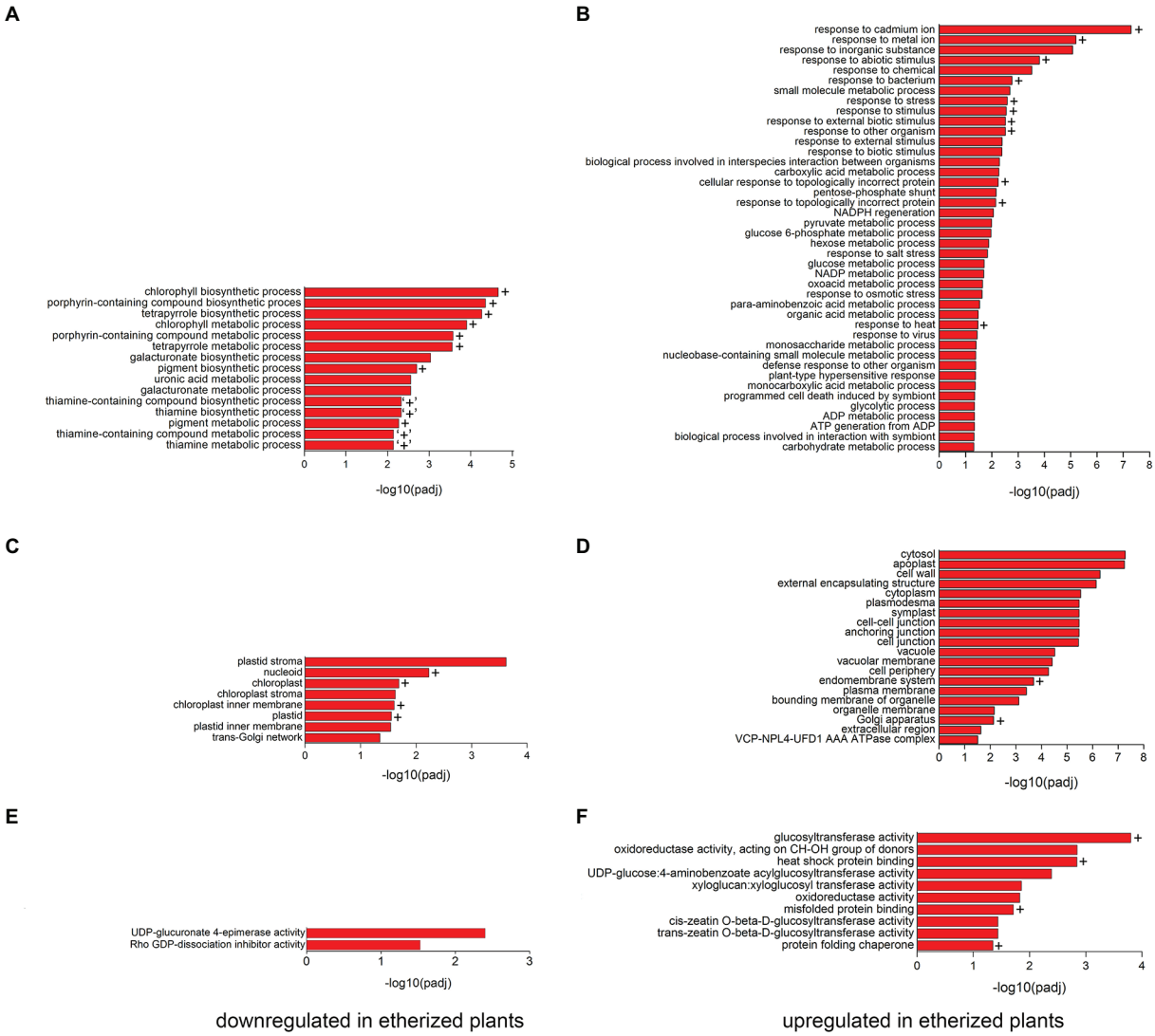

FIGURE 3
Gene ontology (GO) functional analysis of differentially expressed proteins (DEPs) in *Arabidopsis thaliana*. All the significantly ($p < 0.05$) enriched downregulated GO terms in biological process **(A)**, cellular component **(C)**, and molecular function **(E)** branches in etherized plants compared to control are presented. All the significantly ($p < 0.05$) enriched upregulated GO terms in biological process **(B)**, cellular component **(D)**, and molecular function **(F)** branches in etherized plants compared to control are presented. All the adjusted statistically significant values of the terms were negative 10-base log transformed. Crosses (+) denote the same or very similar GO terms, which were enriched also in RNA-seq experiments. "+" denote similar GO term from RNA-seq experiments (vitamin metabolic and vitamin biosynthetic processes) which contain downregulated genes for thiamine biosynthesis. A complete list of DEP is available as Supplementary Table S3.

accumulated 6–7 weeks before short diethyl ether treatment (5.5 h) what was a too short time to reverse the accumulation. This is in line with chlorophyll concentration which did not differ significantly between control and etherized plants (data not shown).

Western blotting using commercial antibodies reacting with different isoforms of heat shock proteins HSP70 and HSP90 showed only negligible increase of HSP70 isoforms (reacting with HSP70-1, HSP70-2, and HSP70-3) in response to diethyl ether treatment, however antibodies against HSP90 reacting with HSP90-1 and HSP90-2 showed significant increase in etherized plants. The key regulatory enzymes in chlorophyll biosynthesis glutamyl-tRNA reductase (GluTR or HEMA) and light-dependent protochlorophyllide oxidoreductase (POR) were also immunoblotted. The antibody against GluTR reacting with two isoforms (HEMA1 and HEMA2) in *Arabidopsis* showed slightly higher enzyme abundance in etherized plants but not significant. On the contrary, POR was significantly less abundant in etherized plants (Figure 5). The antibody against large subunit of Rubisco (RbcL) and actin were used as loading controls and their content was not affected by diethyl ether treatment as data from proteomic analyses indicates. Western blotting analyses confirmed RNA-seq and proteomic data.

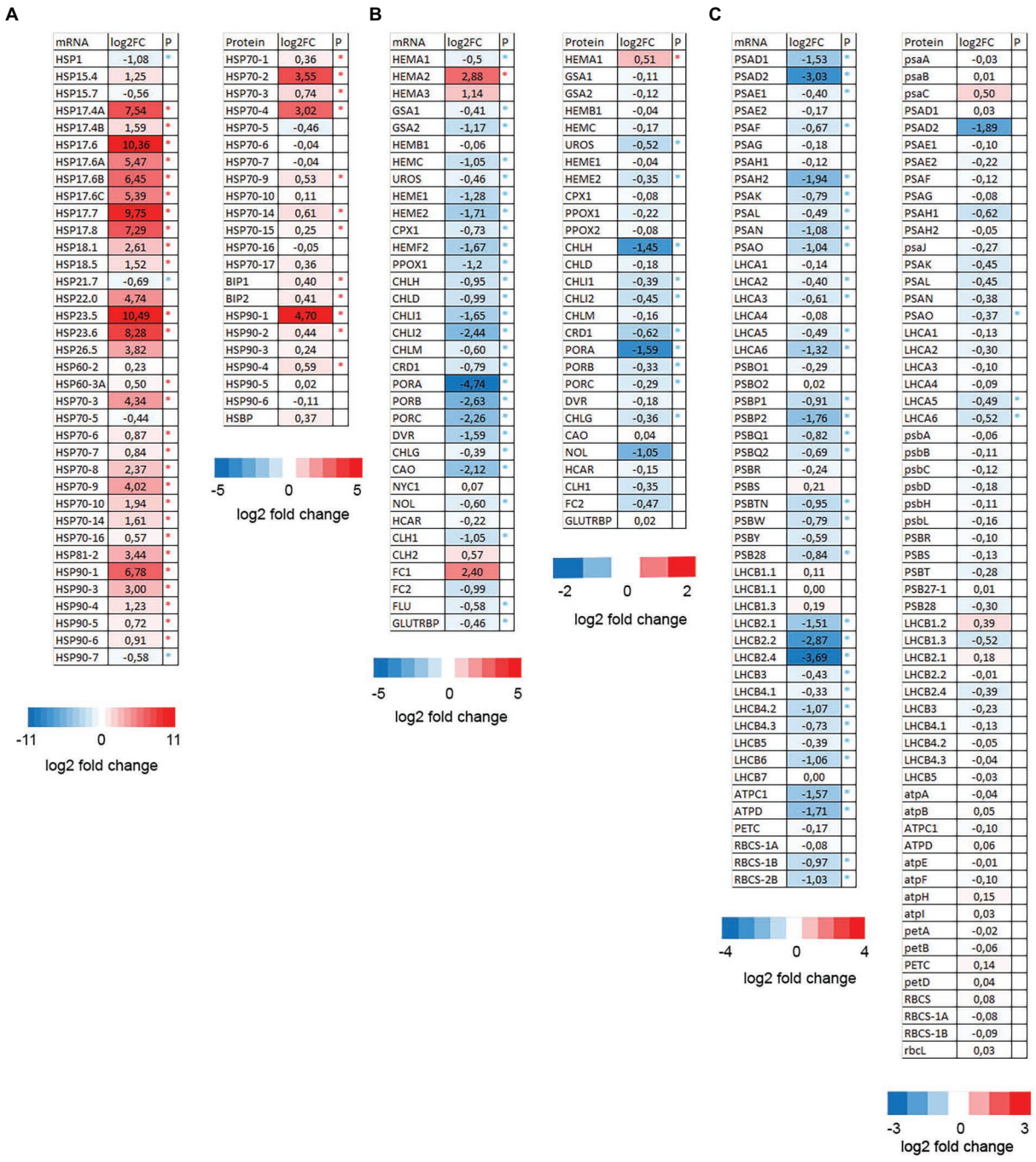

FIGURE 4
Heat maps showing the expression pattern of HSPs **(A)**, chlorophyll metabolism **(B)**, and photosynthesis-related genes **(C)** in *Arabidopsis thaliana*. Log_2 fold changes in the mRNA (from RNA-seq experiment) and proteins (LC–MS/MS analysis) in diethyl ether treated plants compared to controls (asterisk denote significant differences at $p < 0.05$, $n = 4$).

Diethyl ether induced calcium entry into the cells

Because heat shock response and accumulation of HSPs were attributed to the entry of Ca^{2+} into the cytosol (Saidi et al., 2009), we measured $[Ca^{2+}]_{cyt}$ in transgenic *A. thaliana* plants expressing *APOAEQUORIN* treated with coelenterazine for AEQUORIN reconstitution, in response to diethyl ether application. Within few minutes after diethyl ether application, the rapid rise of $[Ca^{2+}]_{cyt}$ signal was detected and the signal slowly decayed later (Figure 6; Supplementary Video S1). To prove that the signal is not an ultra-weak photon emission, the experiments were repeated also with transgenic plants without coelenterazine treatment. No clear signal in response to diethyl ether application was detected (Figure 6; Supplementary Video S2) confirming

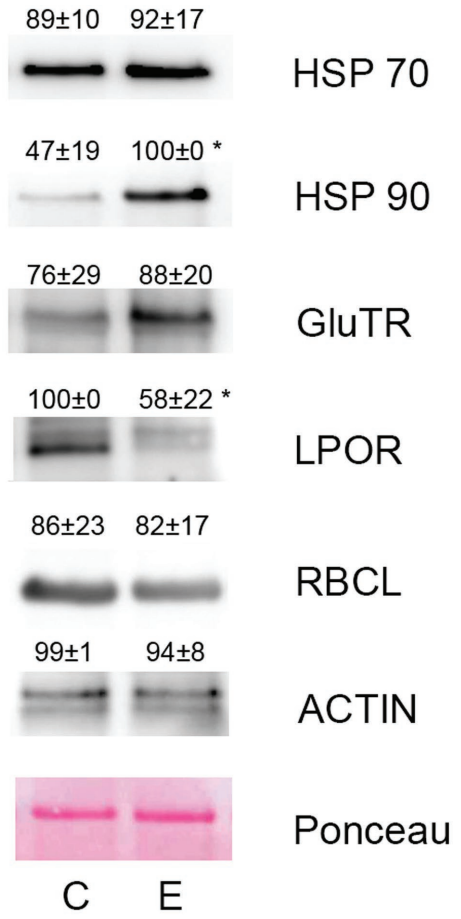

FIGURE 5
Western blotting of selected proteins involved in heat stress response and chlorophyll metabolism in *Arabidopsis thaliana*. The same protein amount was separated in 10% (v/v) SDS-PAGE and subjected to Western blot analysis. Antibodies against HSP70, HSP90, GluTR, LPOR, RbcL, and actin were used. The representative blots from three independent isolations are shown. The quantification of chemiluminescence signal is shown above the corresponding band. Means±SD. C, control plants; E, etherized plants. Asterisks (*) denote significant differences at $p < 0.05$ (Student's or Welch's *t*-test), $n = 3$.

that the signal in AEQUORIN plants came from increased $[Ca^{2+}]_{cyt}$.

Diethyl ether affected photosynthetic parameters in etherized plants

Due to the significant effect of diethyl ether on chlorophyll biosynthesis and photosynthesis, we investigated changes in chlorophyll *a* fluorescence parameters reflecting transition of photosynthetic apparatus from dark- to light-adapted state by measurements of chlorophyll *a* fluorescence quenching analysis. We found that etherized plants exhibited lower Φ_{PSII}, higher 1-qP, and lower NPQ during the first 30 s of actinic illumination. Later, after steady-state conditions were achieved, higher Φ_{PSII}, lower 1-qP, and higher NPQ were found in etherized plants (Figure 7).

Diethyl ether anesthesia protected OEC and PSII against subsequent heat stress

Because anesthesia induced HSPs, we decided to investigate a possible protective role of diethyl ether anesthesia against subsequent heat stress. Among the primary target of thermal damage in plants is the oxygen evolving complex (OEC) in PSII, which can be easily monitored by measurements of fast induction kinetics of chlorophyll *a* fluorescence. We monitored the appearance of K-step which is a sensitive indicator of OEC and PSII damage (Lazár et al., 1997; Srivastava et al., 1997) in response to increasing temperature. At room temperature, no clear K-step was detectable, but increasing the temperature above 40°C for 5 min resulted in appearance of K-step at about 0.5 ms (Figure 8) and decrease of maximum quantum yield of PSII (F_v/F_m, Figure 9). Both the less pronounced K-step and the significantly reduced decrease of F_v/F_m upon increasing temperature in diethyl ether exposed plants indicate protective effects of diethyl ether anesthesia against high temperatures caused damage of OEC and PSII.

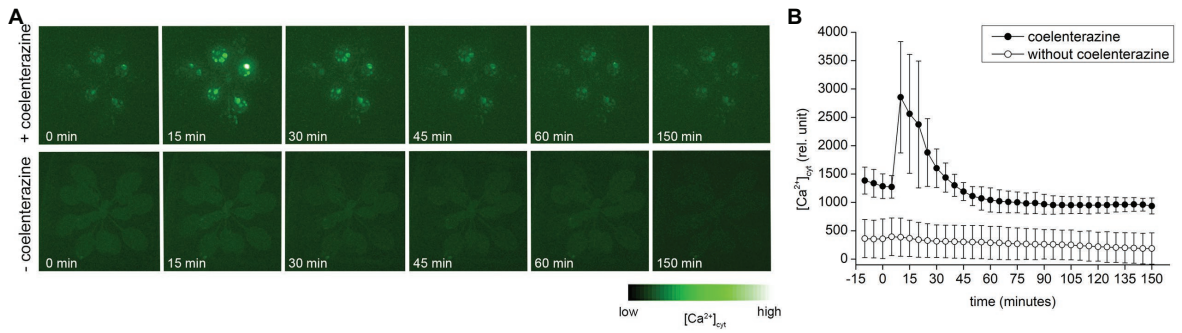

FIGURE 6
The cytoplasmic Ca^{2+} $[Ca^{2+}]_{cyt}$ signals in whole *Arabidopsis thaliana* rosette expressing *APOAEQUORIN* in response to diethyl ether application. **(A)** Representative images of selected time points of plants treated (upper row) and non-treated (lower row) with coelenterazine. **(B)** Time course (0–250 min) of average $[Ca^{2+}]_{cyt}$ accumulation in whole rosette in response to diethyl ether application. Plants treated with coelenterazine (closed circles) or without it (open circles). The diethyl ether was applied at time point 1 min. Means±SD, $n = 4$. The time lapse video of $[Ca^{2+}]_{cyt}$ is available as Supplementary Videos S1, S2.

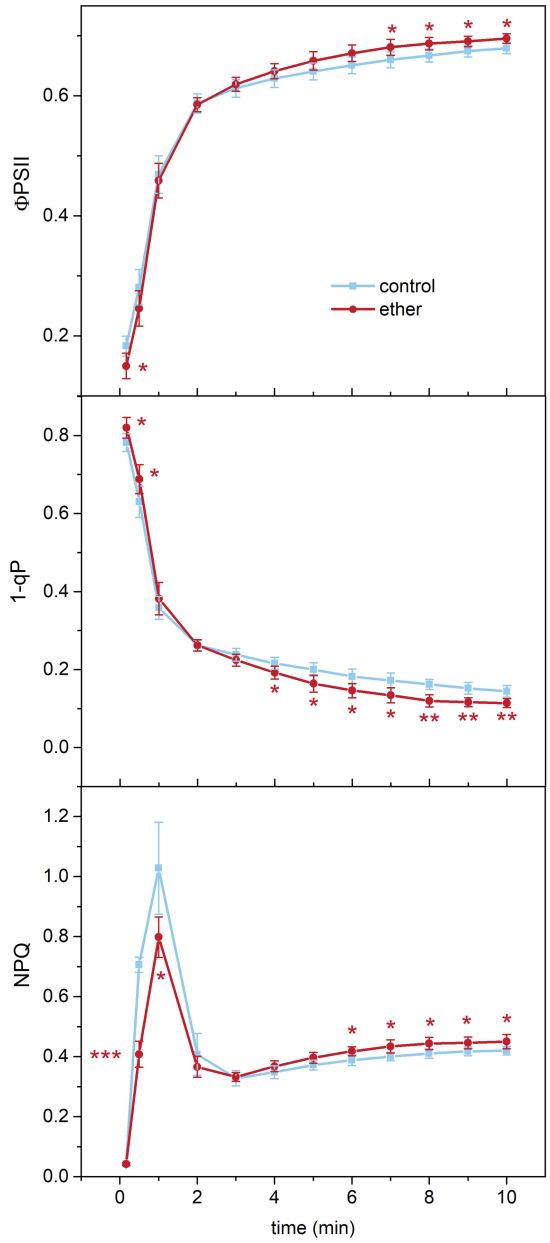

FIGURE 7
Chlorophyll *a* fluorescence parameters in *Arabidopsis thaliana*. A kinetics of effective photochemical quantum yield of PSII (Φ_{PSII}), excitation pressure on PSII (1−qP), and non-photochemical quenching (NPQ) of chlorophyll *a* fluorescence after switching on actinic light (time point 0min) in control and etherized plants. Asterisks denote significant difference at $p < 0.01$ (**) and $p < 0.05$ (*), (Student *t*-test). Means±SD, $n = 5$ (Student's *t*-test).

Diethyl ether increased membrane permeability for ions in etherized plants at room temperature

Because cell membranes including their permeability for ions are strongly affected by higher temperatures (Saidi et al., 2009), we next investigated the effect of diethyl ether on ion leakage from leaf samples. At room temperature, the relative electrical conductivity was slightly but significantly higher in etherized plants for the first 20 min of measurements indicating higher ion leakage (Figure 10A). Later, the difference between etherized and control plants were not significant probably due to longer measuring period and recovery from diethyl ether treatment. In an additional experiment, we compared the relative conductivity of leaves exposed for 60 min to RT, 42 and 45°C. Typically, the relative conductivity increased with increasing temperature reflecting an increase in membrane permeability for ions due to membrane changes not related to damage (leading probably to the efflux of K^+ ions together with their counter ions, Demidchik et al., 2014; Ilík et al., 2018). Diethyl ether had no additional effect on the ion leakage at higher temperature (Figure 10B).

Discussion

Recent studies showed that the anesthetic diethyl ether strongly suppresses the sensing of different stimuli in plants (e.g., light, touch, or wounding, Milne and Beamish, 1999; De Luccia, 2012; Yokawa et al., 2018; Pavlovič et al., 2020; Böhm and Scherzer, 2021; Jakšová et al., 2021; Scherzer et al., 2022). Here we show it concomitantly triggers also a strong cellular response. This omics-based study demonstrates that exposure of plants to GVA diethyl ether strongly reprogrammed gene expression in *A. thaliana*. Among the most obvious upregulated genes/proteins were HSPs (Figure 4), but also other heat responsive genes (e.g., WRKY transcription factors, Cheng et al., 2021). Studies on animals also found that GVA profoundly changed gene expression pattern (Sergeev et al., 2004) and increased expression of HSPs (HSP-10, HSP-27, and HSP70-1; Sergeev et al., 2004; Coghlan et al., 2018; Upton et al., 2020). HSPs are essential components contributing to cellular homeostasis under both optimal and detrimental conditions and are responsible for protein folding, assembly, translocation, and degradation during growth and development (Park and Seo, 2015). They originally were described in relation to heat shock (Ritossa, 1962) but are induced also by various stresses, such as cold, osmotic stress, anoxia, salinity, water stress, UV-B light etc. (Park and Seo, 2015). Several proposed models tried to explain the increased expression of HSPs in response to heat stress. The protein unfolding model suggests that heat-damaged proteins in the cytoplasm presumably recruit the cytoplasmic chaperones, thereby allowing inactive heat shock transcription factors (HSFs) to undergo phosphorylation, oligomerization, and translocation to the nucleus to transcribe HSP genes (Morimoto, 1998). The plasma membrane model suggests that heat-induced increase of membrane fluidity and changes in microdomain organization (i.e., lipid rafts) can generate a significant HSP expression (Horváth et al., 1998; Vigh et al., 2007; Saidi et al., 2009). Saidi et al. (2009) showed that increased expression of HSPs is strongly dependent on a preceding Ca^{2+} transient through Ca^{2+} permeable channel, which is also activated by membrane fluidizers. Changes in membrane

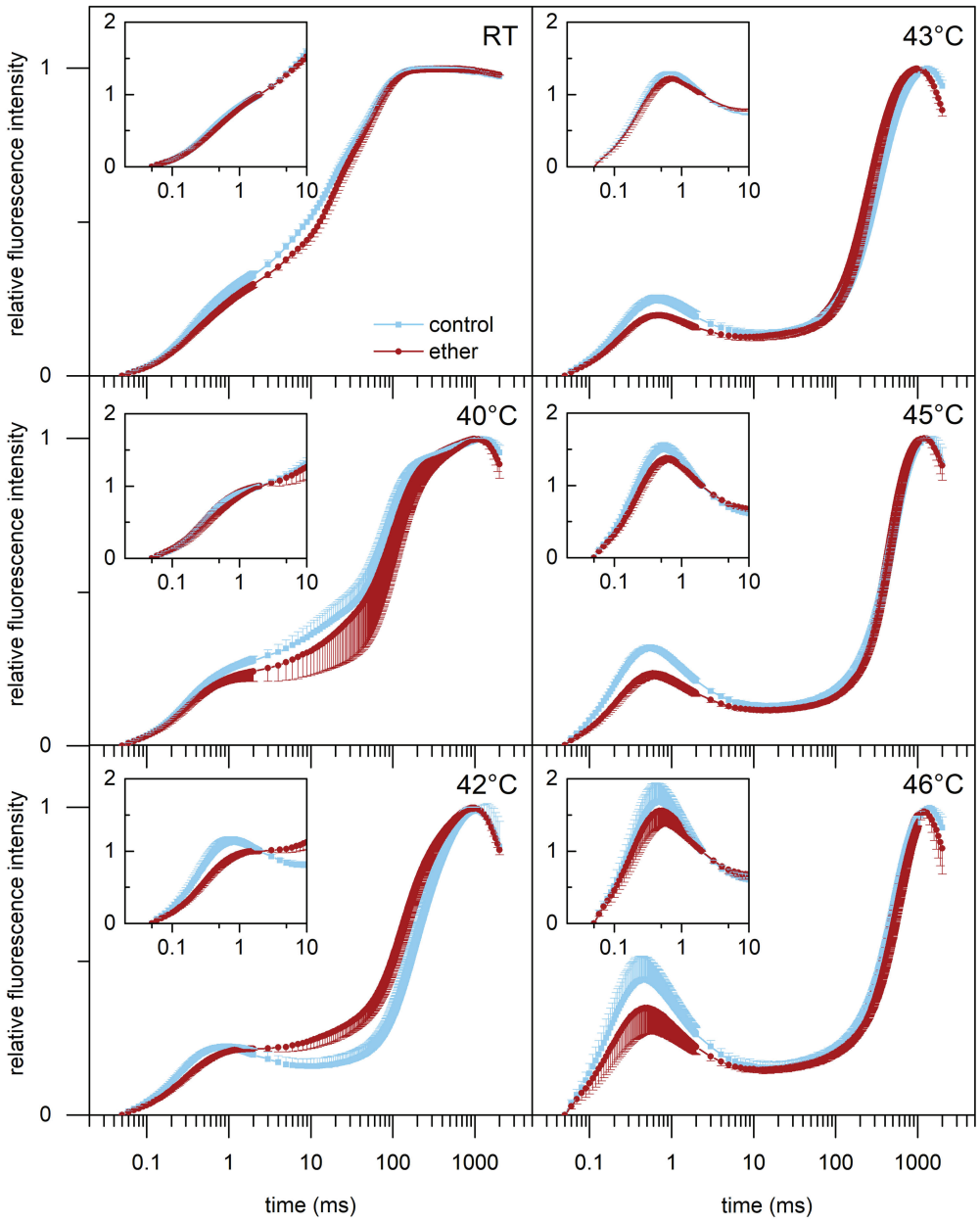

FIGURE 8
Effect of high-temperature treatment on chlorophyll *a* fluorescence induction transient in leaves of control and diethyl ether pre-treated *Arabidopsis thaliana* plants. Detached leaves were incubated for 5 min in a water bath of given temperature in darkness. RT, room temperature. The transients are normalized to variable fluorescence ($F_V=F_M - F_0$) or to variable fluorescence at 2ms [$F_{V(2ms)}=F_{(2ms)} - F_0$; inlets]. Means±SD, n = 5.

fluidity have been previously found to impact ion channel activity (Collins et al., 1993). This may explain the increased HSP expression after diethyl ether treatment in our study, because diethyl ether also increased $[Ca^{2+}]_{cyt}$ (Figure 6) and ion leakage at room temperature (Figure 10), membrane fluidity, and disrupted lipid rafts (Lerner, 1997; Pavel et al., 2020). Significantly upregulated GO-MF categories of "calcium ion binding" and "calmodulin binding" are in accordance with the role of Ca^{2+} in signaling during anesthesia (Figure 2F). This finding is partially interesting in the view of recent studies showing that diethyl ether blocked wound-induced glutamate-dependent Ca^{2+} transient and systemic response mediated by GLR channels in *A. thaliana* (Jakšová et al., 2021) and *D. muscipula* (Scherzer et al., 2022). Different kinetics of these $[Ca^{2+}]_{cyt}$ responses suggest participation of two different Ca^{2+} channels. This different effect of diethyl ether on Ca^{2+} transient in response to wounding in etherized plants and ether itself is another piece of evidence of complicated network of so called calcium signature (McAinsh and Pittman, 2009). A third model for HSPs induction suggests the role of reactive oxygen species (ROS). In addition to their detrimental character, ROS are also considered as important signaling molecules, which can induce expression of HSPs (Volkov et al., 2006; Scarpeci et al., 2008; Driedonks et al.,

2015). ROS formation after plant exposure to diethyl ether anesthesia was recently documented in *A. thaliana* roots (Yokawa et al., 2018, 2019).

The role of HSPs in multiple stress responses might explain the phenomenon of cross-tolerance or priming, where exposure to a certain stress factors improves tolerance to a subsequent different stress factors in plants (Bowler and Fluhr, 2000; Driedonks et al., 2015; Nair et al., 2022). In animals, such anesthetic preconditioning has been also suggested (Sergeev et al., 2004; Kitahata et al., 2008; Pagel, 2008). Therefore, we investigated whether GVA application and HSP induction can protect plant against subsequent heat stress by measuring a fast chlorophyll *a* fluorescence induction. One of the target site for elevated temperature-induced damage is PSII. Heat stress induces detachment of OEC proteins, loss of cofactors (Mn) from PSII and cleavage of D1 protein (Yoshioka et al., 2006). Our results showed increased thermal stability of PSII in plants exposed to diethyl ether for 5.5 h prior to subsequent heat–stress (Figure 8), indicating that diethyl ether provided protective role against heat–stress probably through induced HSPs. Indeed, the experiments of other authors demonstrated that HSPs can associate with thylakoids and protects O_2 evolution and OEC proteins of PSII against heat stress. It has been considered that HSPs in chloroplasts do not participate in the repair of stress-related damage but rather function as molecular chaperons to prevent protein denaturation and aggregation (Downs et al., 1999; Allakhverdiev et al., 2008). Saidi et al. (2009) also documented increased thermotolerance of PSII after priming with membrane fluidizer benzylalcohol in *Physcomitrella patens,* what is in accordance with our study.

Other class of genes/proteins upregulated by diethyl ether is involved in vesicle-mediated transport (Figure 2D). This finding is interesting and in accordance with a previous study, where it has been shown that the 15% diethyl ether and 1% lidocaine treatments slowed the rate of endocytic vesicle recycling in *Arabidopsis* root epidermal cells (Yokawa et al., 2018). Although

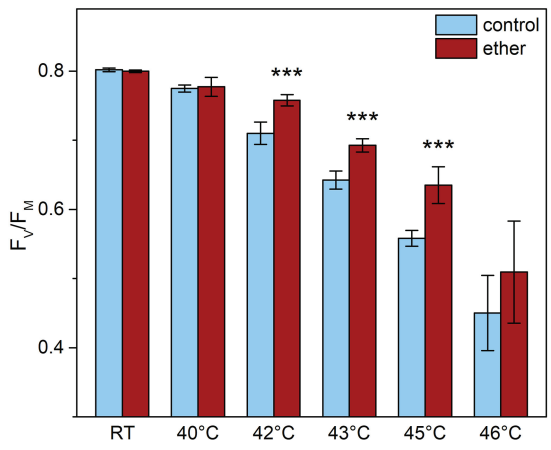

FIGURE 9
Maximal quantum yield of PSII photochemistry (F_V/F_M) in leaves of control and diethyl ether pre-treated *Arabidopsis thaliana* plants. Detached leaves were incubated for 5 min in a water bath of given temperature in darkness. RT, room temperature. Means±SD, n = 5. Asterisks (***) indicate statistically significant difference from untreated samples ($p < 0.001$; Student's or Welch's t-test).

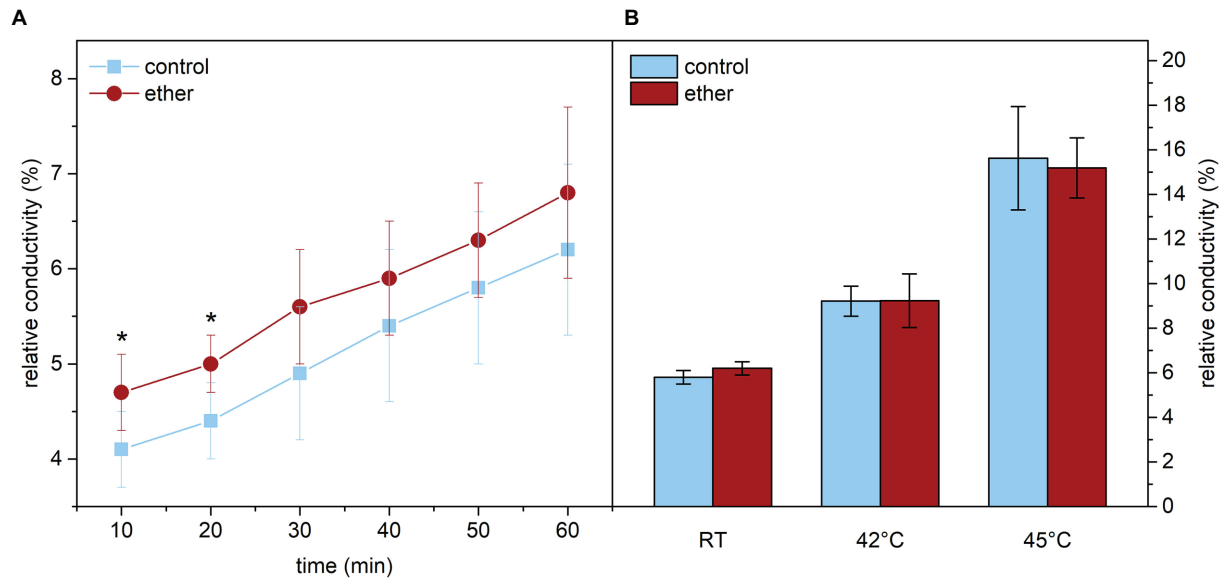

FIGURE 10
Relative conductivity reflecting ion leakage from leaf samples of *Arabidopsis thaliana*. **(A)** Relative conductivity at room temperature (RT) measured in 10min intervals immediately after diethyl ether treatment and in control samples. **(B)** Relative conductivity after 60min incubation of leaf samples at given temperature. Expressed in % of maximum conductivity measured in leaf samples with fully disintegrated membranes. Means±SD, n=5. Asterisks (*) indicate statistically significant difference from untreated samples ($p < 0.05$; Student's or Welch's t-test).

the mechanism involved remains unclear, these results indicate that anesthetics alter normal membrane properties and interact with vesicle trafficking in plants (Yokawa et al., 2019). The important implication of this finding in plants is applicable for presynaptic release of neurotransmitter in animal neurons. Worms with altered sensitivity to GVA were found to have mutation in syntaxin forming the SNARE complex that regulates presynaptic neurotransmitter release (van Swinderen et al., 1999). Interestingly, genes encoding "SNARE binding" were among enriched GO-MF categories also in *Arabidopsis* (Figure 2F).

Our recent study has found inhibition of chlorophyll accumulation during de-etiolization under diethyl ether anesthesia in garden cress (Yokawa et al., 2018). In our experiments with circadian grown plants, the chlorophyll $a+b$ concentration was not significantly different (data not shown) due to the high amount of chlorophylls which were pre-synthetized 6–7 weeks before 5.5 h diethyl ether treatment. However, our analysis found that chlorophyll biosynthesis is transcriptionally downregulated also in mature circadian-grown plants, because 26 out of 34 genes encoding proteins involved in tetrapyrrole biosynthesis were significantly downregulated (Figure 4). This was mirrored also on protein level (Figure 4). Concomitantly, the transcription of many photosynthesis-related genes was also downregulated (Figure 4). If this was a result of plastid to nucleus retrograde redox signaling (e.g., through changes of redox state of plastoquinone pool indicating by differences in 1-qP, Figure 7) or direct effect of diethyl ether remains unknown. Recently, it was found that increased $[Ca^{2+}]_{cyt}$, which was also documented in this study (Figure 6), is responsible for repression of *LHCB* genes mediated by MAP kinases phosphorylation of ABI4 (Guo et al., 2016). Chlorophyll metabolism is tightly regulated by different factors like heat, light, cold, phytohormones and is also non-specific indicator of any plant stress (Kruse et al., 1997; Tewari and Tripathy, 1998; Matsumoto et al., 2004; Mohanty et al., 2006; Yaronskaya et al., 2006; Kobayashi and Masuda, 2016). It is known for decades that GVA and lidocaine inhibited photosynthetic reactions in isolated chloroplasts (Wu and Berkowitz, 1991; Nakao et al., 1998). In our study, we measured photosynthetic reactions by *in vivo* chlorophyll *a* fluorescence in intact plants and we did not find anesthesia-induced inhibition of photosynthesis. On the contrary, after reaching steady-state conditions, the rate of photosynthetic electron transport (expressed as Φ_{PSII}) was even slightly higher in etherized plants (Figure 7).

Our study showed that plants under anesthesia with diethyl ether had not only decreased ability to sense their environment (Yokawa et al., 2018; Pavlovič et al., 2020; Jakšová et al., 2021; Scherzer et al., 2022) but surprisingly also strongly reprogrammed gene expression. The possible underlying mechanism involved Ca^{2+} entry into the cells through the effect on plasma membranes and thus resembles the effect of heat stress (Figure 11). While the effect on primary photosynthetic reactions is rather marginal in etherized plants, exposure of plants to anesthetic may protect the PSII against subsequent heat stress through the effect of cross-tolerance or priming. This study has shown that the effects of anesthesia and term anesthesia go far beyond consciousness and

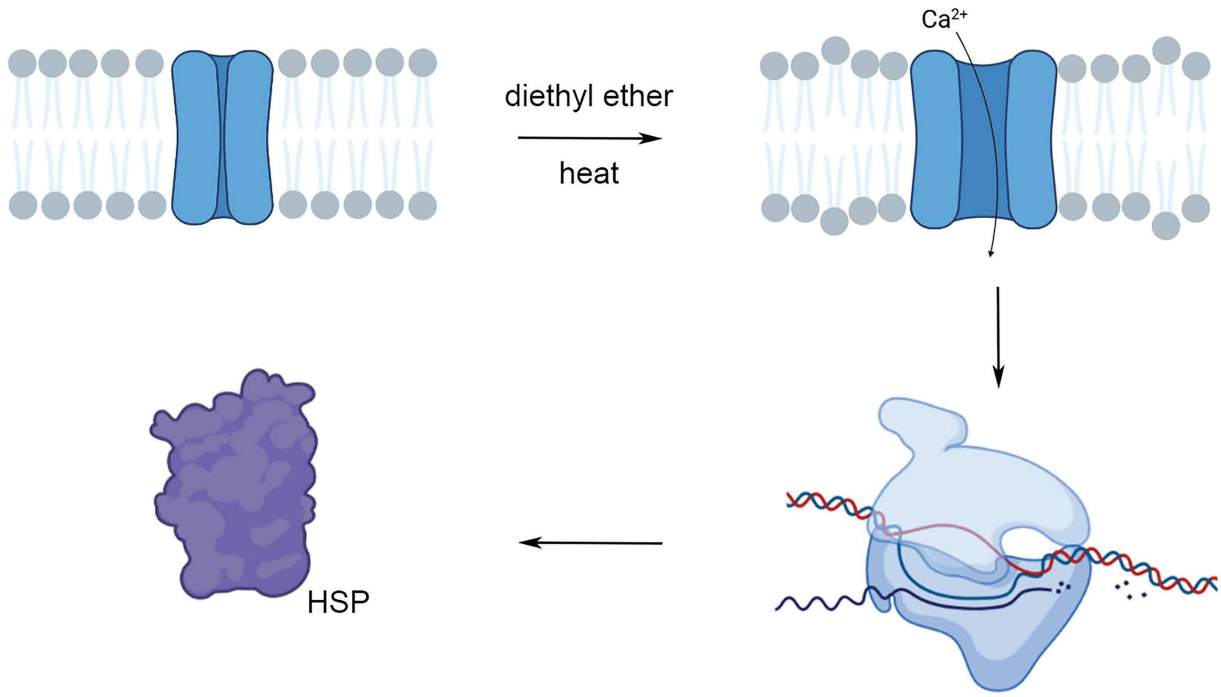

FIGURE 11
The hypothesis about similar action of diethyl ether anesthesia and heat stress on HSP expression. Both, anesthesia and heat stress fluidizes a membrane and affect Ca^{2+} channel function. The consequent Ca^{2+} entry into the cytoplasm triggers signaling cascade leading to the changes of gene expression (e.g., induction of HSPs). Created in BioRender.com.

modern medicine having wider implications for a variety of organisms and deserve our further attention.

Data availability statement

The datasets presented in this study can be found in online repositories. The names of the repository/repositories and accession number(s) can be found at: https://datadryad.org/stash, doi: 10.5061/dryad.wm37pvmqq.

Author contributions

AP designed the research, analyzed the data, and wrote the manuscript. AP and AM provided material and financial support. JJ did Western blots and isolated RNA for RNA-seq experiments. PR performed proteomic analysis. MŠ and ZK measured chlorophyll *a* fluorescence and relative conductivity. MR and AP measured $[Ca^{2+}]_{cyt}$ signals. All authors contributed to the article and approved the submitted version.

Funding

The study was supported by the Czech Science Foundation Agency GAČR (21-03593S). CIISB, Instruct-CZ Center of Instruct-ERIC EU consortium, funded by MEYS CR infrastructure project LM2018127, is also gratefully acknowledged for the financial support of the measurements at the CF Prot.

Conflict of interest

The authors declare that the research was conducted in the absence of any commercial or financial relationships that could be construed as a potential conflict of interest.

Publisher's note

Supplementary material

The Supplementary material for this article can be found online at: https://www.frontiersin.org/articles/10.3389/fpls.2022.995001/full#supplementary-material

SUPPLEMENTARY TABLE S1
The complete list of significantly upregulated and downregulated differentially expressed genes (DEGs) in *A. thaliana* arranged from the highest to lowest $\log_2$ fold change ($p < 0.05$).

SUPPLEMENTARY TABLE S2
The complete list of significantly enriched GO terms at $p < 0.05$ arranged from the lowest to highest adjusted p values (p_{adj}) in *A. thaliana*.

SUPPLEMENTARY TABLE S3
The complete list of significantly upregulated and downregulated differentially expressed proteins (DEPs) in *A. thaliana* arranged from the highest to lowest $\log_2$ fold change ($p < 0.05$).

SUPPLEMENTARY VIDEO S1
Luminescence in whole *A. thaliana* rosette expressing the APOAEQUORIN gene with coelenterazine in response to diethyl ether application at time point 1 min. The plants were sprayed with coelenterazine and the signal is indicator of $[Ca^{2+}]_{cyt}$. Photons were captured in photon-counting mode with a 5 min acquisition time.

SUPPLEMENTARY VIDEO S2
Luminescence in whole *A. thaliana* rosette expressing the APOAEQUORIN gene without coelenterazine in response to diethyl ether application at time point 1 min. The plants were not sprayed with coelenterazine before measurements and the possible signal is indicator of ROS production. Photons were captured in photon-counting mode with a 5 min acquisition time.

References

Allakhverdiev, S. I., Kreslavski, V. D., Klimov, V. V., Los, D. A., Carpentier, R., and Mohanty, P. (2008). Heat stress: an overview of molecular responses in photosynthesis. *Photosynth. Res.* 98, 541–550. doi: 10.1007/s11120-008-9331-0

Böhm, J., and Scherzer, S. (2021). Signaling and transport processes related to the carnivorous lifestyle of plants living on nutrient-poor soil. *Plant Physiol.* 187, 2017–2031. doi: 10.1093/plphys/kiab297

Bowler, C., and Fluhr, R. (2000). The role of calcium and activated oxygens as signals for controlling cross-tolerance. *Trends Plant Sci.* 5, 241–246. doi: 10.1016/s1360-1385(00)01628-9

Cheng, Z., Luan, Y., Meng, J., Sun, J., Tao, J., and Zhao, D. (2021). WRKY transcription factor response to high-temperature stress. *Plants* 10:2211. doi: 10.3390/plants10102211

Coghlan, M., Richards, E., Shaik, S., Rossi, P., Vanama, R. B., Ahmadi, S., et al. (2018). Inhalation anesthetics induce neuronal protein aggregation and use affect ER trafficking. *Sci. Rep.* 8:5275. doi: 10.1038/s41598-018-23335-0

Collins, A. C., Wehner, J. M., and Wilson, W. R. (1993). Animal models for alcoholism: genetic strategies and neurochemical mechanisms. *Biochem. Soc. Symp.* 59, 173–191. PMID: 8192685

Cox, J., and Mann, M. (2008). MaxQuant enables high peptide identification rates, individualized p.p.b.-range mass accuracies and proteome-wide protein quantification. *Nat. Biotechnol.* 26, 1367–1372. doi: 10.1038/nbt.1511

Cox, J., Neuhauser, N., Michalski, A., Scheltema, R. A., Olsen, J. V., and Mann, M. (2011). Andromeda: a peptide search engine integrated into the MaxQuant environment. *J. Proteome Res.* 10, 1794–1805. doi: 10.1021/pr101065j

De Luccia, T. P. B. (2012). *Mimosa pudica*, *Dionaea muscipula* and anesthetics. *Plant Signal. Behav.* 7, 1163–1167. doi: 10.4161/psb.21000

Demidchik, V., Straltsova, D., Medvedev, S. S., Pozhvanov, G. A., Sokolik, A., and Yurin, V. (2014). Stress-induced electrolyte leakage: the role of K+-permeable channels and involvement in programmed cell death and metabolic adjustment. *J. Exp. Bot.* 65, 1259–1270. doi: 10.1093/jxb/eru004

Downs, C. A., Coleman, J. S., and Heckathorn, S. A. (1999). The chloroplast 22-ku heat-shock protein: a lumenal protein that associates with the oxygen evolving complex and protects photosystem II during heat stress. *J. Plant Physiol.* 155, 477–487. doi: 10.1016/S0176-1617(99)80042-X

Driedonks, N., Xu, J., Peters, J. L., Park, S., and Rieu, I. (2015). Multi-level interactions between heat shock factors, heat shock proteins, and the redox system regulate acclimation to heat. *Front. Plant Sci.* 6:999. doi: 10.3389/fpls.2015.00999

Franks, N. P. (2006). Molecular targets underlying general anesthesia. *Br. J. Pharmacol.* 147, S72–S81. doi: 10.1038/sj.bjp.0706441

Franks, N. P., and Lieb, W. R. (1984). Do general anesthetics act by competitive binding to specific receptors? *Nature* 310, 599–601. doi: 10.1038/310599a0

Guissé, B., Srivastava, A., and Strasser, R. J. (1995). The polyphasic rise of the chlorophyll a fluorescence (O-K-J-I-P) in heat stressed leaves. *Arch. Sci. Genev.* 48, 147–160.

Guo, H., Feng, P., Chi, W., Sun, X., Xu, X., Li, Y., et al. (2016). Plastid-nucleus communication involves calcium-modulated MAPK signalling. *Nature Comm.* 7:12173. doi: 10.1038/ncomms12173

Horváth, I., Glatz, A., Varvasovszki, V., Török, Z., Páli, T., Balogh, G., et al. (1998). Membrane physical state controls the signaling mechanism of the heat shock response in *Synechocystis* PCC 6803: identification of *hsp17* as a "fluidity gene". *Proc. Natl. Acad. Sci. U. S. A.* 95, 3513–3518. doi: 10.1073/pnas.95.7.3513

Ilík, P., Špundová, M., Šicner, M., Melkovičová, H., Kučerová, Z., Krchňák, P., et al. (2018). Estimating heat tolerance of plants by ion leakage: a new method based on gradual heating. *New Phytol.* 218, 1278–1287. doi: 10.1111/nph.15097

Jakšová, J., Rác, M., Bokor, B., Petřík, I., Novák, O., Reichelt, M., et al. (2021). Anesthetic diethyl ether impairs systemic electrical and jasmonate signaling in *Arabidopsis thaliana*. *Plant Physiol. Biochem.* 169, 311–321. doi: 10.1016/j.plaphy.2021.11.019

Kelz, M. B., and Mashour, G. A. (2019). The biology of general anesthesia from paramecium to primate. *Curr. Biol.* 29, R1199–R1210. doi: 10.1016/j.cub.2019.09.071

Kiep, V., Vadassery, J., Lattke, J., Maaß, J.-P., Boland, W., Peiter, E., et al. (2015). Systemic cytosolic Ca^{2+} elevation is activated upon wounding and herbivory in Arabidopsis. *New Phytol.* 207, 996–1004. doi: 10.1111/nph.13493

Kitahata, H., Nozaki, J., Kawahito, S., Tomino, T., and Oshita, S. (2008). Low-dose sevoflurane inhalation enhances late cardioprotection from anti-ulcer drug geranygeranylacetone. *Anesth. Analg.* 107, 755–761. doi: 10.1213/ane.0b013e31817f0e61

Kobayashi, K., and Masuda, T. (2016). Transcriptional regulation of tetrapyrrole biosynthesis in *Arabidopsis thaliana*. *Front. Plant Sci.* 7:1811. doi: 10.3389/fpls.2016.01811

Kruse, E., Grimm, B., Beator, J., and Kloppstech, K. (1997). Developmental and circadian control of the capacity for δ-aminolevulinic acid synthesis in green barley. *Planta* 202, 235–241. doi: 10.1007/s004250050124

Lazár, D., Pospíšil, P., and Nauš, J. (1997). Decrease of fluorescence intensity after the K step in chlorophyll a fluorescence induction is suppressed by electron acceptors and donors to photosystem 2. *Photosynthetica* 37, 255–265. doi: 10.1023/A:1007112222952

Lerner, R. A. (1997). A hypothesis about the endogenous analogue of general anesthesia. *Proc. Natl. Acad. Sci. U. S. A.* 94, 13375–13377. doi: 10.1073/pnas.94.25.13375

Matsumoto, F., Obayashi, T., Sasaki-Sekimoto, Y., Ohta, H., Takamiya, K., and Masuda, T. (2004). Gene expression profiling of the tetrapyrrole metabolic pathway in Arabidopsis with a mini-array system. *Plant Physiol.* 135, 2379–2391. doi: 10.1104/pp.104.042408

Maxwell, K., and Johnson, G. N. (2000). Chlorophyll fluorescence—a practical guide. *J. Exp. Bot.* 51, 659–668. doi: 10.1093/jxb/51.345.659

McAinsh, M. R., and Pittman, J. K. (2009). Shaping the calcium signature. *New Phytol.* 181, 275–294. doi: 10.1111/j.1469-8137.2008.02682.x

Meyer, H. (1899). Zur Theorie der Alkoholnarkose. *Arch. Exp. Pathol. Pharmakol.* 42, 109–118. doi: 10.1007/BF01834479

Milne, A., and Beamish, T. (1999). Inhalational and local anesthetics reduce tactile and thermal responses in *Mimosa pudica*. *Can. J. Anaesth.* 46, 287–289. doi: 10.1007/BF03012612

Mohanty, S., Grimm, B., and Tripathy, B. C. (2006). Light and dark modulation of chlorophyll biosynthetic genes in response to temperature. *Planta* 224, 692–699. doi: 10.1007/s00425-006-0248-6

Morimoto, R. I. (1998). Regulation of the heat shock transcriptional response: cross talk between a family of heat shock factors, molecular chaperones, and negative regulators. *Genes Dev.* 12, 3788–3796. doi: 10.1101/gad.12.24.3788

Mousavi, S. A. R., Chauvin, A., Pascaud, F., Kellenberger, S., and Farmer, E. E. (2013). Glutamate receptor-like genes mediate leaf-to-leaf wound signals. *Nature* 500, 422–426. doi: 10.1038/nature12478

Nair, A., Bhukya, D. P. N., Sunkar, R., Chavali, S., and Allu, A. D. (2022). Molecular basis of priming-induced acquired tolerance to multiple abiotic stresses in plants. *J. Exp. Bot.* 73, 3355–3371. doi: 10.1093/jxb/erac089

Nakao, H., Ogli, K., Yokono, S., Ono, J., and Miyatake, A. (1998). The effect of volatile anesthetics on light-induced phosphorylation in spinach chloroplasts. *Toxicol. Lett.* 100-101, 135–138. doi: 10.1016/s0378-4274(98)00177-5

Overton, C. E. (1901). *Studien über die Narkose Zugleich ein Beitrag zur Allgemeinen Pharmakologie*. Jena, Germany: Fischer Verlag.

Pagel, P. S. (2008). Induction of heat shock protein 70 and preconditioning by sevoflurane: a potent protective interaction against myocardial ischemia-reperfusion injury. *Anesth. Analg.* 107, 742–745. doi: 10.1213/ane.0b013e31817f6d40

Park, C.-J., and Seo, Y.-S. (2015). Heat shock proteins: a review of the molecular chaperones for plant immunity. *Plant Pathol. J.* 31, 323–333. doi: 10.5423/PPJ.RW.08.2015.0150

Pavel, M. A., Petersen, N., Wang, H., Lerner, R. A., and Hansen, S. B. (2020). Studies on the mechanism of general anesthesia. *Proc. Natl. Acad. Sci. U. S. A.* 117, 13757–13766. doi: 10.1073/pnas.2004259117

Pavlovič, A., Libiaková, M., Bokor, B., Jakšová, J., Petřík, I., Novák, O., et al. (2020). Anaesthesia with diethyl ether impairs jasmonate signaling in the carnivorous plant Venus flytrap (*Dionaea muscipula*). *Ann. Bot.* 125, 173–183. doi: 10.1093/aob/mcz177

Raudvere, U., Kolberg, L., Kuzmin, I., Arak, T., Adler, P., Peterson, H., et al. (2019). G:profiler: a web server for functional enrichment analysis and conversions of gene lists (2019 update). *Nucleic Acids Res.* 47, W191–W198. doi: 10.1093/nar/gkz369

Ritossa, F. (1962). A new puffing pattern induced by temperature shock and DNP in drosophila. *Experientia* 18, 571–573. doi: 10.1007/BF02172188

Saidi, Y., Finka, A., Muriset, M., Bromberg, Z., Weiss, Y. G., Maathuis, F. J. M., et al. (2009). The heat shock response in moss plants is regulated by specific calcium-permeable channels in the plasma membrane. *Plant Cell* 21, 2829–2843. doi: 10.1105/tpc.108.065318

Scarpeci, T. E., Zanor, M. I., and Valle, E. M. (2008). Investigating the role of plant heat shock proteins during oxidative stress. *Plant Signal. Behav.* 3, 856–857. doi: 10.4161/psb.3.10.6021

Schägger, H. (2006). Tricine–SDS-PAGE. *Nat. Protoc.* 1, 16–22. doi: 10.1038/nprot.2006.4

Scherzer, S., Huang, S., Iosip, A., Kreuzer, I., Yokawa, K., Al-Rasheid, K. A. S., et al. (2022). Ether anesthetics prevents touch-induced trigger hair calcium-electrical signals excite the Venus flytrap. *Sci. Rep.* 12:2851. doi: 10.1038/s41598-022-06915-z

Sergeev, P., da Silva, R., Lucchinetti, E., Zaugg, K., Pasch, T., Schaub, M. C., et al. (2004). Trigger-dependent gene expression profiles in cardiac preconditioning. Evidence for distinct genetic programs in ischemic and anesthetic preconditioning. *Anesthesiology* 100, 474–488. doi: 10.1097/00000542-200403000-00005

Srivastava, A., Guissé, B., Greppin, H., and Strasser, R. J. (1997). Regulation of antenna structure and electron transport in photosystem II of Pisum sativum under elevated temperature probed by the fast polyphasic chlorophyll *a* fluorescence transient: OKJIP. *Biochim. Biophys. Acta-Bioenerget.* 1320, 95–106. doi: 10.1016/S0005-2728(97)00017-0

Tang, P., and Xu, Y. (2002). Large-scale molecular dynamics simulations of general anesthetic effects on the ion channel in the fully hydrated membrane: the implication of molecular mechanisms of general anesthesia. *Proc. Natl. Acad. Sci. U. S. A.* 99, 16035–16040. doi: 10.1073/pnas.252522299

Tewari, A. K., and Tripathy, B. C. (1998). Temperature-stress-induced impairment of chlorophyll biosynthetic reactions in cucumber and wheat. *Plant Physiol.* 117, 851–858. doi: 10.1104/pp.117.3.851

Toyota, M., Spencer, D., Sawai-Toyota, S., Jiaqi, W., Zhang, T., Koo, A. J., et al. (2018). Glutamate triggers long-distance, calcium-based plant defense signaling. *Science* 361, 1112–1115. doi: 10.1126/science.aat7744

Upton, D. H., Popovic, K., Fulton, R., and Kassiou, M. (2020). Anesthetic-dependent changes in gene expression following acute and chronic exposure in the rodent brain. *Sci. Rep.* 10:9366. doi: 10.1038/s41598-020-66122-6

Urban, B. W., and Bleckwenn, M. (2002). Concepts and correlations relevant to general anaesthesia. *Br. J. Anaesth.* 89, 3–16. doi: 10.1093/bja/aef164

van Swinderen, B., Saifee, O., Shebester, L., Roberson, R., Nonet, M. L., and Crowder, C. M. (1999). A neomorphic syntaxin mutation blocks volatile-anesthetic action in *Caenorhabditis elegans*. *Proc. Natl. Acad. Sci. U. S. A.* 96, 2479–2484. doi: 10.1073/pnas.96.5.2479

Vigh, L., Horváth, I., Maresca, B., and Harwood, J. L. (2007). Can the stress protein response be controlled by 'membrane-lipid therapy'? *Trends Biochem. Sci.* 32, 357–363. doi: 10.1016/j.tibs.2007.06.009

Volkov, R. A., Panchuk, I. I., Mullineaux, P. M., and Schöffl, F. (2006). Heat stress-induced $H_{(2)}O_{(2)}$ is required for effective expression of heat shock genes in Arabidopsis. *Plant Mol. Biol.* 61, 733–746. doi: 10.1007/s11103-006-0045-4

Wiśniewski, J. R., Zougman, A., Nagaraj, N., and Mann, M. (2009). Universal sample preparation method for proteome analysis. *Nat. Methods* 6, 359–362. doi: 10.1038/nmeth.1322

Wu, W., and Berkowitz, G. A. (1991). Lidocaine and ATPase inhibitor interaction with the chloroplast envelope. *Plant Physiol.* 97, 1551–1557. doi: 10.1104/pp.97.4.1551

Yaronskaya, E., Vershilovskaya, I., Poers, Y., Alawady, A. E., Averina, N., and Grimm, B. (2006). Cytokinin effects on tetrapyrrole biosynthesis and photosynthetic activity in barley seedlings. *Planta* 224, 700–709. doi: 10.1007/s00425-006-0249-5

Yokawa, K., Kagenishi, T., and Baluška, F. (2019). Anesthetics, anesthesia, and plants. *Trends Plant Sci.* 24, 12–14. doi: 10.1016/j.tplants.2018.10.006

Yokawa, K., Kagenishi, T., Pavlovič, A., Gall, S., Weiland, M., Mancuso, S., et al. (2018). Anesthetics stop diverse plant organ movements, affect endocytic vesicle recycling and ROS homeostasis, and block action potentials in Venus flytraps. *Ann. Bot.* 122, 747–756. doi: 10.1093/aob/mcx155

Yoshioka, M., Uchida, S., Mori, H., Komayama, K., Ohira, S., Morita, N., et al. (2006). Quality control of photosystem II. Cleavage of reaction center D1 protein in spinach thylakoids by Fts H protease under moderate heat stress. *J. Biol. Chem.* 281, 21660–21669. doi: 10.1074/jbc.M602896200

frontiers | Frontiers in Plant Science

TYPE Original Research
PUBLISHED 23 September 2022
DOI 10.3389/fpls.2022.1014230

OPEN ACCESS

EDITED BY
Biao Jin,
Yangzhou University, China

REVIEWED BY
Raj Kumar Joshi,
Rama Devi Women's University, India
Ze Wu,
Nanjing Agricultural University, China

*CORRESPONDENCE
Ginés Otálora
gines.oralora@carm.es
Francisco M. del Amor
franciscom.delamor@carm.es

SPECIALTY SECTION
This article was submitted to Plant Abiotic Stress, a section of the journal Frontiers in Plant Science

RECEIVED 08 August 2022
ACCEPTED 08 September 2022
PUBLISHED 23 September 2022

CITATION
Otálora G, Piñero MC, Collado-González J, Gálvez A, López-Marín J and del Amor FM (2022) Heat-shock and methyl-jasmonate: The cultivar-specific responses of pepper plants. *Front. Plant Sci.* 13:1014230. doi: 10.3389/fpls.2022.1014230

Heat-shock and methyl-jasmonate: The cultivar-specific responses of pepper plants

Ginés Otálora*, María Carmen Piñero, Jacinta Collado-González, Amparo Gálvez, Josefa López-Marín and Francisco M. del Amor*

Department of Crop Production and Agri-Technology, Murcia Institute of Agri-Food Research and Development (IMIDA), Murcia, Spain

Frequency, intensity and duration heat-related events have profound implications for future food supply through effects on plant growth and development. This concern needs effective and urgent mitigation tools. However, the effectiveness of potential solutions may decrease according to the specific cultivar response rather consider at specie level. The metyl-jasmonates are essential cellular regulators which are involved in pivotal plant development processes and related to confer protection to heat shock. Thus, our aim was to study the response of three pepper cultivars, Agio (Hungarian type), Basque (Chilli type), and Loreto (Lamuyo type), subjected to heat shock (40°C/72 h) and foliarly-sprayed with methyl-jasmonate (MeJA; 100 µmol), and the effects on several physiological traits. Our results show that despite the important differential impact of heat shock caused on each cultivar, MeJA application did not affect gas exchange, chlorophyll A concentration or efficiency of the photosystem in these cultivars. However, P concentration was reduced when MeJA was applied to Basque chilli, and a significant effect on leaf carbohydrates concentration was observed for Agio and Loreto. Moreover, Agio was the only cultivar in which the amino-acid profile was affected by MeJA under heat shock. Under that condition, putrescine increased for all cultivars, whist the effect of MeJA was only observed for spermine and histamine for Agio and Loreto. Thus, the results indicated that the ameliorative impact of MeJA on this stressor was clearly influenced by cultivar, revealing specific traits. Thus, these results could be used as valuable tools for the characterization of this intraspecific tolerance to heat shock during the vegetative growth stage of pepper.

KEYWORDS

***Capsicum annuun L.*, mineral concentration, polyamines, sugars, sustainable strategic management, thermotolerance**

Introduction

The current climate crisis demands challenging solutions from agronomists, who have to cope with the new requirements of food and nutrition security, sustainability, and economic welfare (Dhankher and Foyer, 2018). However, the increase in food production under the context of non-optimal climate conditions for crop production (as a result of the increase in frequency and intensity of heat waves), may exceed the physiological thresholds of tolerance of many crops (Russo et al., 2014; Christidis et al., 2015). In Europe's ecosystem, the gross primary production was reduced by 30% during the heatwave in the summer of 2003 (Ciais et al., 2005), while in the Russian heat wave in summer 2010, this impact was aggravated and estimated at 50% (Bastos et al., 2013). Consequently, new studies to increase product yield whilst maintaining quality are urgently required. Thus, this forces farmers to look for new and more efficient technologies in crop management along with more resilient crop varieties. In fact, changing cultivars could be a useful strategy for climate crisis (Waha et al., 2013), although ignoring cultivar effects, especially for heat stress intensity, could provide biased results and introduce errors in the climate impact assessment results (Rezaei et al., 2018). Presently, it is becoming more frequent to read reports about significant reductions in major crops worldwide (Tito et al., 2018), in which the sensitivity to high temperatures is not only dependent on stress intensity and duration but greatly varies among species (Weng and Lai, 2005) and cultivars (Camejo et al., 2005; Balla et al., 2019). Thus, this stressor can differentially affect plant development and yield and quality, comprising molecular, biochemical, physiological, and morphological alterations (Zandalinas et al., 2018), with their identification and quantification being of paramount importance to achieve the required higher tolerance.

Methyl jasmonate (MeJA) is a natural plant growth regulator that was found to be active in many physiological processes. For example, it can induce some specific proteins that are similar to those induced by heat shock (Weidhase et al., 1987). It was recently indicated that both MeJA biosynthesis and signaling are required for thermotolerance in Arabidopsis (Clarke et al., 2009; Kazan, 2015), thus underlining the importance of the exogenous application of MeJA to confer heat tolerance to horticultural crops. On the other hand, heat stress (HS), defined as short-term temperature increases above the optimum range (Wahid et al., 2007) threatens crop productivity in many areas of the world given the prediction of extreme conditions, and urgently highlights the lack of readiness of our current crop genotypes to cope with future climate extremes (Chavan et al., 2019). Heat shock stress has a complex effect on crops, and to further improve sweet pepper plant tolerance, it is necessary to evaluate and characterize the various mechanisms involved in this crop's tolerance. However, not enough research has been conducted to compare the main abiotic stress-tolerance traits of sweet pepper cultivars. This crop has been pointed out as sensitive to heat stress, which affects yield and fruit quality (Mateos et al., 2013). Thus, the assessment of heat tolerance in this crop is important in climate-response breeding programs.

Sweet pepper is an important crop species in the Mediterranean-climate areas worldwide, which are some of the climate regions most impacted by the climate crisis (Woetzel et al., 2020). Therefore, the importance of our research is twofold: to gain insights into the physiological processes of the response of pepper to heat stress in relation to the response to MeJA, and to elucidate the way in which these responses are modulated by cultivar. Consequently, we studied photosynthesis and chlorophyll fluorescence, mineral content, carbohydrates, polyamines, and the amino acid profile. The information gained about the role of these traits could establish new ways for managing plant resilience to severe heat waves for this crop.

Material and methods

Plant material, growth conditions, and treatments

Three pepper cultivars (*Capsicum annuum* L.) Basque chilli (Chilli pepper type; Ramiro Arnedo Spain S.A.U.), Loreto (Lamuyo type; Syngenta Spain S.A.U.) and Agio (Hungarian type, Nunhems Spain S.A.U.) were obtained from a commercial nursery. Homogeneous pepper seedlings were selected and transplanted into black 5 L containers filled with coconut coir fiber (Pelemix, Alhama de Murcia, Murcia, Spain). Irrigation was supplied by self-compensating drippers (2 L h^{-1}). Nutrient solution drainage was monitored to avoid salt accumulation and ionic interference in the rhizosphere, and fresh nutrient solution was provided with minimum drainage of 35%. The experiment was carried out in a climate chamber, as described in del Amor et al. (2010).The acclimation stage lasted 18 days, and the environmental conditions were 60% relative humidity, 16/8 h day/night photoperiod, 26/18°C, and photosynthetically active radiation (PAR) of 250 µmol m^{-2} s^{-1}. The nutrient solution (modified Hoagland solution) contained the following minerals: NO_3^- : 12.0; $H_2PO_4^-$: 1.0; SO_4^{2-} : 3.5; K^+:7.0; Ca^{2+}:4.5; Mg^{2+}:2.0. Plants were subjected to heat stress for 72 h in the climate-controlled chamber and the temperature was increased to 40/33/28°C for 12/4/6h and 18/8h day/night photoperiod. At the beginning of the stress period, half of the plants were homogenously sprayed a solution containing MeJA (100µM) and 0.01% Tween-20 as the surfactant. Phenotype picture (control plants) is provided in Supplementary Figure 1. Six plants were analyzed per each treatment (sprayed and non-sprayed and heat treatments for 72 h).

Gas exchange

The net CO_2 assimilation (ACO_2), internal [CO_2] (Ci), transpiration rate (E), and stomatal conductance (gs) were measured in the youngest fully-expanded leaf of each plant, using a CIRAS-2 (PP system, Amesbury, MA) with a PLC6 (U) Automatic Universal Leaf Cuvette, measuring both sides of the leaves. The cuvette provided light (LED) with a photon flux of 1,300 m-2 s-1, 360 or 800 µmol mol-1 CO2, a leaf temperature of 25°C, and 75% relative humidity. The intrinsic water use efficiency (WUE) of leaf gas exchange was calculated from the gas exchange data as ACO_2/E, where ACO_2 is the carbon assimilated through photosynthesis, and E is the amount of water lost *via* transpiration.

Chlorophyll content and fluorescence

Chlorophylls were extracted from samples of the youngest leaf with N,N dimethylformamide, for 72 h, in darkness at 4°C. Subsequently, the absorbance was measured in a spectrophotometer at 750, 664, and 647 nm, and the quantities of Chlorophylls a (Chl a), b (Chl b), and a+b (Chl a+b) were calculated according to the method by Porra et al. (1989). On the leaf used for gas exchange, the dark-adapted maximum fluorescence (Fm) and minimum fluorescence (Fo), and the light adapted, steady-state chlorophyll fluorescence (F) and maximum fluorescence (Fm′) were measured with a portable modulated fluorometer, model OS-30P (Opti-Science, USA). The ratio between the variable fluorescence from a dark-adapted leaf (Fv) and the maximal fluorescence from a dark-adapted, youngest fully-expanded leaf (Fm) – called the maximum potential quantum efficiency of photosystem II (Fv/Fm) - was calculated. A leaf clip holder was placed on each leaf to maintain dark conditions for at least 30 min before reading.

Mineral composition

The leaf anion concentrations were determined in dry matter, as previously described by Piñero et al. (2016). The anions were analyzed in an ion chromatograph (Metrohm 861 Advanced Compact IC; Metrohm 838 Advanced Sampler); the column used was a Metrohm Metrosep A Supp7 250/4.0 mm. The cation concentrations were analyzed on lyophilized leaves (0.1 g) according to Otálora et al. (2018), by acid digestion, using an ETHOS ONE microwave digestion system (Milestone Inc., Shelton, CT, USA).

Sugars content

Leaf sugars (glucose, fructose, and sucrose) were determined in leaves by ion chromatography, using an 817 Bioscan (Metrohm, Herisau, Switzerland) system equipped with a pulsed amperometric detector (PAD) and a gold electrode. The column used was a Metrohm Metrosep Carb 1-150 IC column (4.6 x 250 mm), which was heated to 32°C.

Polyamines

The polyamines content were determined according to Del Rodriguez et al. (2001), with modifications. Pepper leaf samples (5 g), previously stored at -80°C, were mixed with 5 mL of perchloric acid (5%), homogenized for 2 min, and kept for 1 h under refrigeration with periodic stirring, and centrifuged at 5000 x g for 8 min. The supernatant, containing free polyamines, was placed in plastic jars and kept in a freezer at -20°C until use. Free polyamines were benzoylated, 1 mL of sample was taken and mixed with 1 mL of 2 M NaOH and 20 µL of benzoyl chloride. The mixture was stirred in a vortex mixer for 15 s and allowed to rest for 20 min at room temperature. Subsequently, 4 mL of a saturated sodium chloride solution were added, and the system was stirred while 2 mL of diethyl ether were added. The system was left to rest for 30 min at -20°C. Then, 1 mL of the diethyl ether phase was taken and evaporated. The residue was re-suspended in 0.5 mL of acetonitrile/water (56/44 v/v). The polyamines present were analyzed with an ACQUITY UPLC system (Waters, Milford, MA, USA) equipped with a UV detector (230 nm) and a reversed-phase column (ACQUITY UPLC HSS T3 1.8 µm, 2.1 x 100 mm), at 40°C. A mixture of acetonitrile/water (42/58 v/v) was used as the elution solvent, with a flow rate of 0.55 mL/min.

Free amino acids

Free amino acids were extracted from leaves frozen at -80°C. The pepper leaves were analyzed with the AccQ·Tag-ultra performance liquid chromatography (UPLC) method [Waters, UPLC Amino Acid Analysis Solution. Waters Corporation, Milford, MA (2006)] equipped with a fluorescence detector, as described in Piñero et al. (2017). The amino acids measured were (Arg) arginine; (Ala) alanine; (Asp) aspartic acid; (Ser) serine; (His) histidine; (Ile) isoleucine; (Leu) leucine; (Phe) phenylalanine; (Met) methionine; (Pro) proline; (Gly) glycine; (Thr) threonine; (Lys) lysine; glutamic acid (Glu) and (Val) valine.

Statistical analysis

The data were tested first for homogeneity of variance and normality of distribution. Significance was determined by analysis of variance (ANOVA), and the significance ($p \leq 0.05$) of differences between means was tested with Duncan's Multiple

Range Test using Statgraphics Centurion® XVI software (StatPoint Technologies, Inc). Each treatment had six replicates.

Results

Leaf gas exchange and chlorophyll fluorescence parameters

The effect of the imposed heat stress was different depending of the cultivar studied. The induced heat shock wave produced a significant increase in the net photosynthetic rate for all cultivars, with this effect being cultivar-dependent (Figure 1A). Thus, the impact of the stress was significantly higher for the Basque chilly, as shown by the increased leaf photosynthesis of 27.7%, as compared with the less affected cultivars Hungarian type (Agio) or Lamuyo type (Loreto), with an increase of 22.3% and 18.3%, respectively. The application of MeJA before stress had a relatively minor effect on the three cultivars, but Loreto showed the highest photosynthetic values. The response for leaf stomatal conductance and transpiration, and consequently intrinsic water use efficiency, were less affected among cultivars, as compared to the data observed for leaf photosynthesis, with the effect of the cultivar being not significant. As expected, the transpiration rate (Figure 1B) was higher when heat stress was applied, although the effects of the cultivar and MeJA were not significant. Accordingly, intrinsic water use efficiency (Figure 1D) had the same effect. The response for leaf stomatal conductance (Figure 1C) with increasing temperature was not affected in the three cultivars. The impact of heat stress on chlorophyll A (Chll A) concentration (Figure 2A) was remarkable in Agio, but not for Basque chilli or Loreto. However, chlorophyll B (Chll B) (Figure 2B) was clearly affected in the three cultivars to a large extent. Thus, when cultivars were subjected to heat stress for 72 h, a significant leap was observed for Chll B in Basque chilli and Agio (47.9% and 115.1%) although this was lower for Loreto (12.4%). The application of MeJA caused no impact on Basque

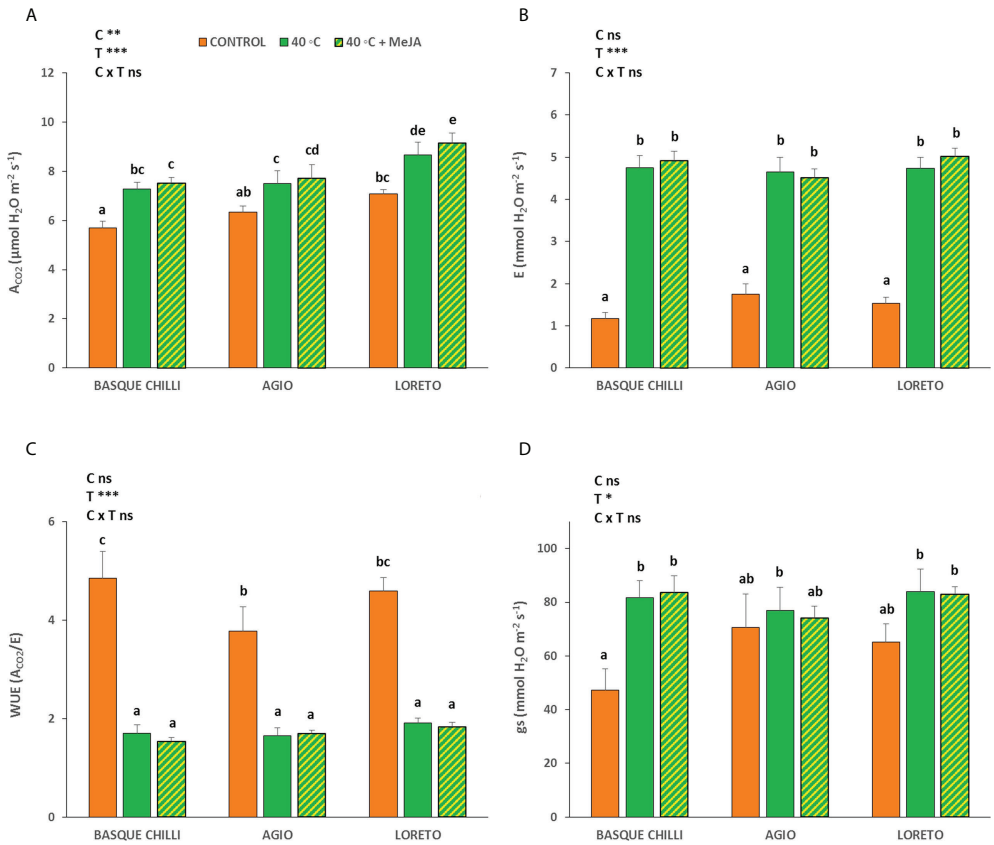

FIGURE 1
Effects of heat shock and MeJA on **(A)** the net CO_2 assimilation rate (A_{CO2}), **(B)** transpiration (E), **(C)** stomatal conductance (gs), and **(D)** intrinsic water use efficiency (WUE) in leaves of the three pepper cultivars. Values are means ± SE. Different letters indicate significant differences between treatments according to Duncan's test at the 95% confidence level. The * refers to significant differences at the level of $p \leq 0.05$; **$p \leq 0.005$; ***$p \leq 0.001$; n.s., not significant. C is cultivar; T is temperature.

10.3389/fpls.2022.1014230

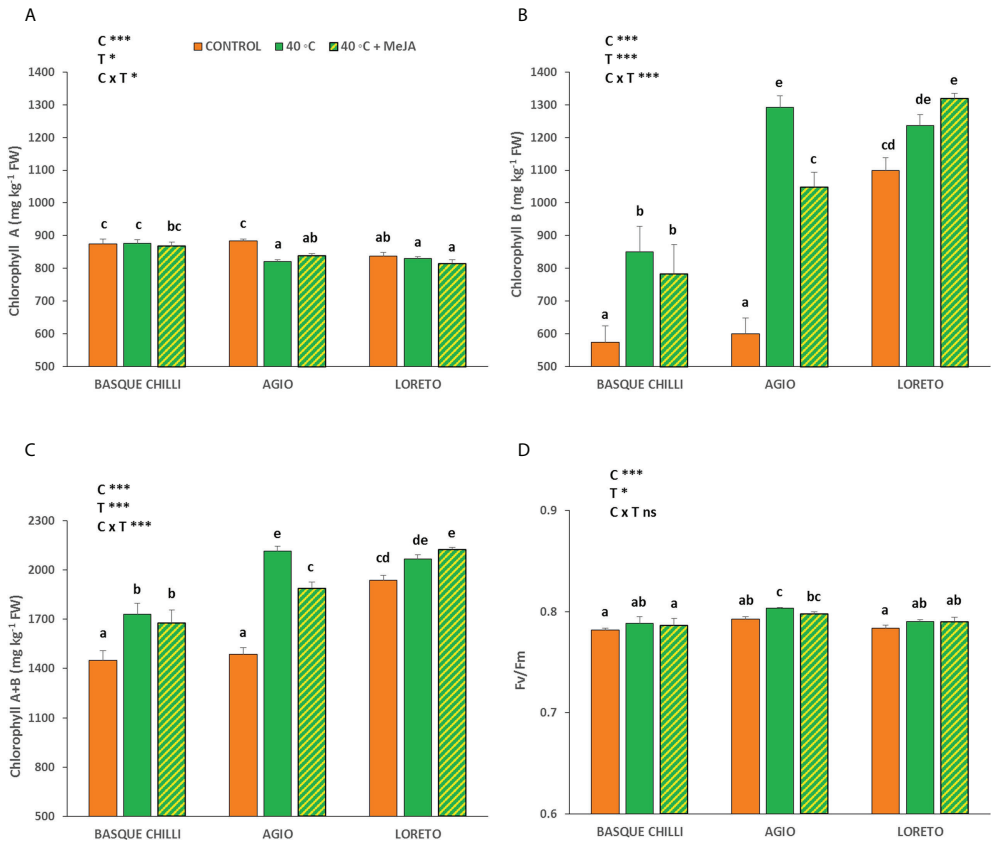

FIGURE 2
Effects of heat shock and MeJA on **(A)** Chlorophyll a, **(B)** Chlorophyll b, **(C)** total Chlorophylls (a+b), and **(D)** the maximum potential quantum efficiency of photosystem II (Fv/Fm) in leaves of the three pepper cultivars. Values are means ± SE. Different letters indicate significant differences between treatments according to Duncan's test at the 95% confidence level. The * refers to significant differences at the level of $p \leq 0.05$; ***$p \leq 0.001$; n.s., not significant. C is cultivar; T is temperature.

chilli or Loreto, although Agio showed the highest response (reducing the observed increase in Chll B due to heat stress to 74.5% with respect the non-stressed plants). In addition, a similar effect as Chll B was found for total chlorophylls (Figure 2C), as Chll B, was a major component of this parameter. Moreover, we found a weak effect of both treatments on chlorophyll fluorescence (Figure 2D) and only Agio showed a slight increase (1.3%) with heat shock, although the application MeJA did not have a significant effect.

Leaf mineral concentration

Leaf nitrate concentration significantly increased in the three studied cultivars after heat stress, with Basque chilli being the most responsive, with an increase of 26.7%, followed by Loreto (19.4%) and Agio (18.4%) with respect of non-stressed plants for the same cultivar (Table 1). The concentrations of phosphates, sulfates, and chlorides concentration were more affected according to cultivar. Loreto showed a clearly distinctive pattern with heat stress, with a significant reduction observed for phosphates and chlorides, whilst the increase in sulfates was more attenuated as compared with Basque chilli and Agio. Loreto was also the cultivar where the addition of MeJA resulted in a reduction of nitrate concentration as compared with stressed plants, without significant differences observed with respect to non-stressed plants. The concentration of cations varied among cultivars (Tables 2, 3). Control plants of Basque chilli showed the lowest Ca concentration, whilst Loreto had the highest P and Mg concentrations. When subjected to heat stress, the Basque chilli cultivar was less affected with respect to the cation concentrations, but interestingly, MeJA attenuated the accumulation of P after heat stress. Agio had a similar response for P, but this effect was not observed for Loreto, which prompted the highest Na concentration in the leaves. Micronutrients (Table 3) concentrations were markedly affected, where B concentration increased by 17.6% and 33.8%, respectively, in Basque chilli and Agio, by the heat stress. Loreto

10.3389/fpls.2022.1014230

TABLE 1 Effects of heat shock and MeJA on leaf anion concentration (g kg^{-1} DW) of the three pepper cultivars.

Cultivar	Treatment	Chlorides	Nitrates	Phosphates	Sulfates
BASQUE CHILLI	Control	1.06 ± 0.10 c	39.29 ± 1.12 abc	14.05 ± 0.40 bc	6.08 ± 0.19 a
	40°C	0.96 ± 0.06 bc	49.77 ± 1.88 de	17.72 ± 0.56 d	7.17 ± 0.36 abc
	40°C + MeJA	0.97 ± 0.03 bc	49.06 ± 2.09 de	13.66 ± 0.88 bc	6.86 ± 0.58 ab
AGIO	Control	1.01 ± 0.08 bc	43.90 ± 4.02 cd	13.95 ± 2.10 bc	6.82 ± 0.78 ab
	40°C	1.17 ± 0.12 c	51.98 ± 1.34 e	16.94 ± 0.91 cd	8.44 ± 0.24 c
	40°C + MeJA	0.99 ± 0.07 bc	53.65 ± 1.90 e	16.40 ± 0.70 cd	8.50 ± 0.30 c
LORETO	Control	0.76 ± 0.07 b	34.46 ± 1.43 a	16.54 ± 2.10 cd	7.12 ± 0.20 abc
	40°C	0.48 ± 0.05 a	41.15 ± 1.37 bc	11.18 ± 0.79 ab	7.60 ± 0.41 bc
	40°C + MeJA	0.44 ± 0.05 a	36.74 ± 1.82 ab	9.71 ± 1.02 a	6.67 ± 0.52 ab
ANOVA	Cultivar (C)	***	***	**	*
	Temperature (T)	ns	***	ns	*
	C x T	ns	ns	***	ns

Values are means ± SE. Different letters indicate significant differences between treatments according to Duncan's test at the 95% confidence level. The * refers to significant differences at the level of $p \leq 0.05$; **$p \leq 0.005$; ***$p \leq 0.001$; n.s., not significant.

showed differences for Cu and Zn (which increased 50.8% and 15.84%), while Mn concentration was affected in Agio and Loreto (42.3% and 82.7%), although Basque Chilli did not show a significant difference for this macronutrient after heat stress. MeJA did not affect the response of leaf micronutrients in the pepper plants subjected to heat stress.

Leaf sugars concentration

The heat stress differentially impacted the cultivars, and the leaf carbohydrates concentrations varied by cultivar (Figure 3). Glucose concentration was not altered by heat in Basque chilli, but Agio and Loreto increased its concentration in a similar way (52.7% and 52.5%) as compared with the non-stressed plant of the same cultivar. However, fructose was only increased in Agio (16.8%) when heat shock was applied. On the other hand, sucrose was noticeably impacted in Basque chilli, which was the only sugar affected in this cultivar after stress (61% increase). The behavior of sucrose for Agio was similar to Basque chilli, while Loreto experienced a significant increase for this carbohydrate when MeJA was applied.

Polyamines

MeJA had an important effect on the putrescine concentration and showed similar results for all cultivars (Figure 4). Thus, while heat stress significantly reduced putrescine by 55.1%, 71.5%, and 85.5% for Chilli, Agio and Loreto, with respect non-stressed plants, the application of MeJA to the stressed ones remarkably increased putrescine

TABLE 2 Effects of heat shock and MeJA on leaf cation concentration (g kg^{-1} DW) of the three pepper cultivars.

Cultivar	Treatment	Ca	K	Mg	Na	P
BASQUE CHILLI	Control	9.28 ± 0.22 a	57.48 ± 1.40 a	5.08 ± 0.14 a	0.15 ± 0.01 a	4.72 ± 0.13 a
	40°C	10.28 ± 0.27 a	61.02 ± 1.87 ab	5.71 ± 0.29 abc	0.16 ± 0.01 a	5.92 ± 0.08 cd
	40°C + MeJA	9.90 ± 0.28 a	59.73 ± 1.25 ab	5.54 ± 0.31 ab	0.18 ± 0.01 ab	5.05 ± 0.29 ab
AGIO	Control	14.36 ± 0.68 cd	58.86 ± 2.49 ab	5.04 ± 0.28 a	0.19 ± 0.02 abc	5.20 ± 0.40 ab
	40°C	15.33 ± 0.69 de	59.59 ± 1.58 ab	5.60 ± 0.25 abc	0.20 ± 0.01 abc	5.89 ± 0.17 cd
	40°C + MeJA	16.42 ± 0.78 e	62.88 ± 2.15 ab	5.67 ± 0.24 abc	0.23 ± 0.02 bcd	5.44 ± 0.12 bc
LORETO	Control	13.90 ± 0.71 bcd	62.41 ± 1.26 ab	6.05 ± 0.21 bc	0.24 ± 0.01 cde	5.92 ± 0.32 cd
	40°C	13.34 ± 0.58 bc	64.01 ± 0.96 b	6.41 ± 0.17 c	0.27 ± 0.01 de	6.88 ± 0.10 e
	40°C + MeJA	12.40 ± 0.34 b	63.73 ± 1.49 b	6.05 ± 0.17 bc	0.30 ± 0.02 e	6.49 ± 0.17 de
	Cultivar (C)	***	*	**	***	***
ANOVA	Temperature (T)	ns	ns	ns	*	***
	C x T	ns	ns	ns	ns	ns

Values are means ± SE. Different letters indicate significant differences between treatments according to Duncan's test at the 95% confidence level. The * refers to significant differences at the level of $p \leq 0.05$; **$p \leq 0.005$; ***$p \leq 0.001$; n.s., not significant.

10.3389/fpls.2022.1014230

TABLE 3 Effects of heat shock and MeJA on leaf cation concentration (mg kg^{-1} DW) of the three pepper cultivars.

Cultivar	Treatment	B	Cu	Fe	Mn	Zn
BASQUE CHILLI	Control	33.83 ± 1.26 a	7.67 ± 0.72 a	122.12 ± 6.51 ab	12.58 ± 1.13 a	48.83 ± 2.07 a
	40°C	39.77 ± 1.24 b	10.94 ± 0.97 bc	116.05 ± 3.30 a	15.88 ± 1.57 ab	62.75 ± 1.98 b
	40°C + MeJA	40.93 ± 0.58 b	9.95 ± 1.43 abc	114.22 ± 4.98 a	12.02 ± 1.54 a	56.75 ± 4.43 ab
AGIO	Control	31.06 ± 1.54 a	7.18 ± 0.51 a	118.36 ± 4.36 ab	12.54 ± 1.90 a	66.05 ± 6.17 bc
	40°C	41.55 ± 1.35 b	8.77 ± 0.77 ab	115.89 ± 3.39 a	17.85 ± 1.96 b	76.12 ± 3.52 c
	40°C + MeJA	42.13 ± 0.94 b	8.45 ± 0.67 ab	115.73 ± 2.25 a	18.48 ± 1.33 b	74.58 ± 2.02 c
LORETO	Control	30.43 ± 2.44 a	7.76 ± 0.86 a	125.57 ± 8.76 ab	11.31 ± 1.44 a	77.38 ± 3.98 c
	40°C	33.56 ± 0.64 a	11.70 ± 0.63 c	133.09 ± 4.09 b	20.66 ± 0.76 b	99.06 ± 3.58 d
	40°C + MeJA	32.50 ± 0.70 a	12.40 ± 0.76 c	128.41 ± 6.89 ab	19.05 ± 2.22 b	89.64 ± 3.92 d
	Cultivar (C)	***	*	*	*	***
ANOVA	Temperature (T)	***	***	ns	***	***
	C x T	*	ns	ns	ns	ns

Values are means ± SE. Different letters indicate significant differences between treatments according to Duncan's test at the 95% confidence level. The * refers to significant differences at the level of $p \leq 0.05$; ***$p \leq 0.001$; n.s., not significant.

concentration by 213.9%, 174.3% and 297.6%, respectively. The results for spermidine were more attenuated and only the Basque chilli showed a significant effect on the MeJA application. Spermine concentration also increased after MeJA application as compared with stressed plants without MeJA, but only for Basque chilli and Agio (37.9% and 46.7%), with no significant differences observed for Loreto. Cadaverine showed a pattern similar to spermidine. Histamine concentration was also reduced after 72 h of the imposed stress by 44.8%, 39.2%, and 38.5% for Basque chilli, Agio and Loreto, respectively, but the application of MeJA before stress restored them to non-stressed values.

Free amino acids

The leaf amino acid concentration in the studied cultivars had a broad and diverse response to heat stress. Thus, the Basque chilly response was the most attenuated to both heat stress and MeJA (Figure 5A), whilst the Agio (Figure 5B) and Loreto (Figure 5C) cultivars showed a more specific response. Agio showed a remarkable effect after the application of MeJA before heat stress and the amino acids histidine, serine, arginine, threonine, valine, and isoleucine were significantly affected and as compared with stressed plants, the concentrations in the leaf increased by 144.5%, 102.5%, 220.3%, 174.5%,104.6%, and 105.5%, respectively. These increases were also very significant although lower when these were compared with the MeJA amendment and with the non-stressed plants. In the case of Loreto, the application of MeJA had a very reduced effect, with the response mainly attributed to the heat stress alone. In this case, we observed differences for Arginine, Alanine, Proline, and Lysine, and the decreases (instead of increases reported for Agio) were (compared with the non-stressed ones) 20.9%, 40.1%, 46.4%,35.0%.The most abundant amino acids found in the three untreated pepper cultivars were Ser,Arg, Asp, Ala and

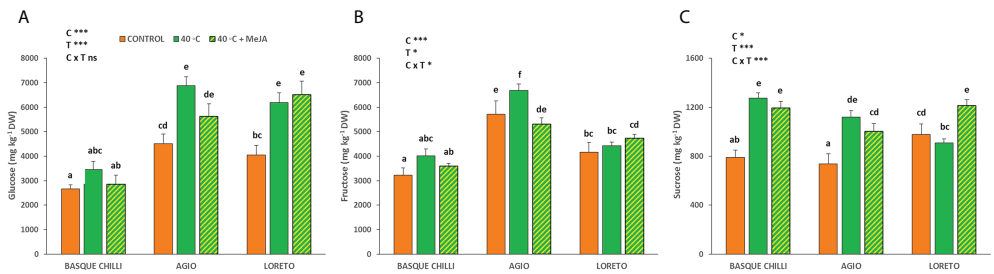

FIGURE 3
Effects of heat shock and MeJA on leaf carbohydrate concentration [**(A)** glucose, **(B)** fructose and **(C)** sucrose] of the three pepper cultivars. Values are means ± SE. Different letters indicate significant differences between treatments according to Duncan's test at the 95% confidence level. The * refers to significant differences at the level of $p \leq 0.05$; ***$p \leq 0.001$; n.s., not significant. C is cultivar; T is temperature.

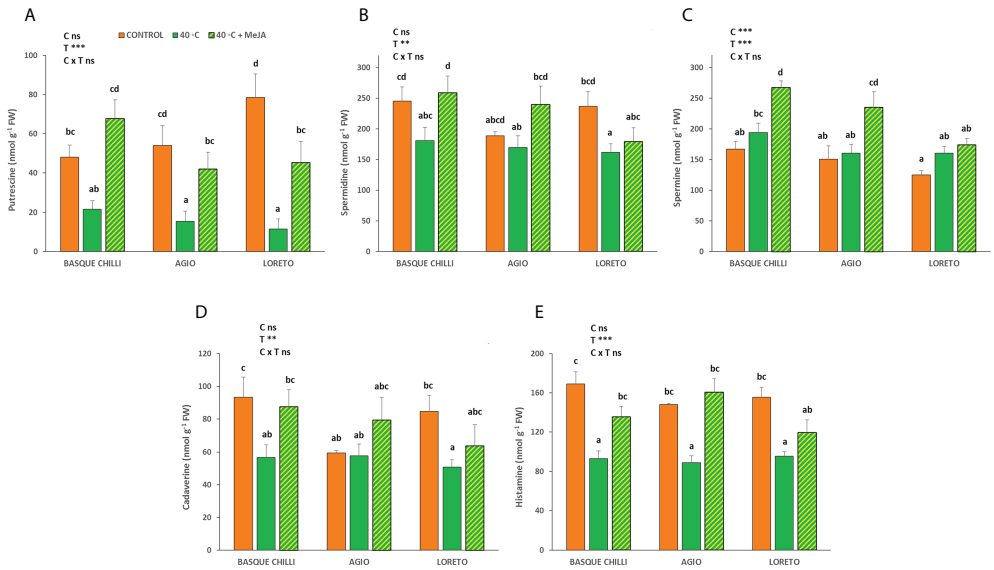

FIGURE 4
Effects of heat shock and MeJA on leaf polyamines (**(A)** putrescine, **(B)** spermidine, **(C)** spermine, **(D)** cadaverine and **(E)** histamine) of the three pepper cultivars. Values are means ± SE. Different letters indicate significant differences between treatments according to Duncan's test at the 95% confidence level. The ** refers to significant differences at the level of $p \leq 0.005$; ***$p \leq 0.001$; n.s., not significant. C is cultivar; T is temperature.

Glu, representing around 70%, 75%, and 73% of the total amino acids in Basque chilli, Agio, and Loreto, respectively. MeJA applied to Basque chilli and Loreto pepper plants had a lesser effect on the content of these compounds than in Agio pepper plants.

Table 4 shows the percentage of variance attributable to temperature, variety, and their interaction on pepper amino acid content. Temperature × variety was the most dominant factor for the concentrations of Ser, Arg, Gly, Asp, Thr, Met, Ile, and total amino acids.Temperature was the most dominant factor of variation for the concentrations of Ala and Glu. Variety was the most dominant factor of variation for the concentrations of His, Pro, Lys, Val, Leu, and Phe.

Discussion

Our data showed that the imposed heat stress had a positive effect on increasing leaf net CO2 assimilation rate for all the studied cultivars. Griffin et al. (2004) reported that Rubisco, the central enzyme of photosynthesis, is disrupted if the temperature increases from 35°C, stopping the photosynthetic process. That reduction in the photosynthetic process has been attributed to the inhibition of photosystem II in the thylakoid membrane, which impairs chlorophyll fluorescence (Chen et al., 2017) while decreasing stomatal conductance and transpiration (Fahad et al., 2016). However, these effects attributable to stomatal closure and/or inhibition of the inactivation of Rubisco, and the loss of chlorophyll contents (Ristic et al., 2008) were not detected in our experiment with pepper at a higher temperature, which increased or maintained Chlorophylls (a+b) content whilst increasing leaf transpiration, although WUE was reduced. The resilience of the photosynthetic machinery to high temperatures was also reported in our previous work with sweet pepper and elevated CO2 concentration during the vegetative growth stage (Pérez-Jiménez et al., 2019). At this point, we agreed with Rizhsky et al. (Rizhsky et al., 2002) who also indicated that high temperatures do not impair photosynthesis along with the intensification of the stomatal conductance. However, Pagamas and Nawata (2008) and Lee et al. (2018) pointed out the beneficial effect of high temperature on vegetative parameters. Interestingly we observed a differential response for Agio, where chlorophyll B clearly increased in concentration by heat (a similar response for all cultivars), but chlorophyll A was reduced. In squash, Ara et al. (2013) reported that Chl. B degraded more drastically under high temperature than Chll A, with the destruction of photosynthetic pigments under heat stress providing a clue for determining thermotolerance. However, Zhou et al. (2015), when screening heat tolerance for tomato genotypes, observed that heat stress led to a significant increase in the content of Chll A, Chl. B, and total chlorophyll contents in the heat-tolerant group, while in the heat-sensitive group, a significant decrease in the pigment contents was observed. In our experiment only Agio was

10.3389/fpls.2022.1014230

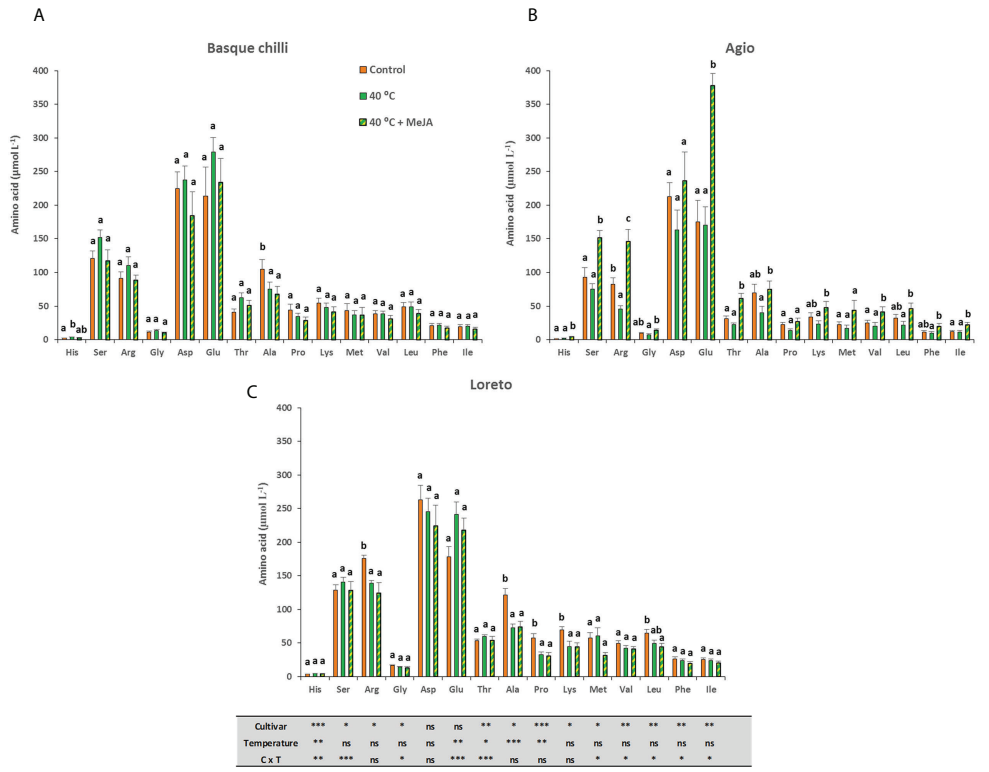

FIGURE 5
Effects of heat shock and MeJA on leaf amino acids concentration (µmol L^{-1}) of the three pepper cultivars [**(A)** Basque chilli, **(B)** Agio and **(C)** Loreto]. Values are means ± SE. Different letters indicate significant differences between treatments according to Duncan's test at the 95% confidence level. The * refers to significant differences at the level of $p \leq 0.05$; **$p \leq 0.005$; ***$p \leq 0.001$; n.s., not significant.

TABLE 4 Percentage of variance attributable to temperature, variety and their interaction for each amino acid of the three pepper cultivars.

	Temperature (%)	Variety (%)	Temperature x variety (%)	Residual (%)
His	17.26 **	26.54 ***	19.47 **	36.71
Ser	4.80 NS	12.13 *	36.14 ***	46.92
Arg	5.33 NS	35.80 ***	38.98 ***	19.87
Gly	0.87 NS	20.03 *	24.04 *	55.05
Asp	1.65 NS	7.08 NS	12.68 NS	78.57
Glu	19.83 **	3.25 NS	37.97 ***	38.93
Thr	10.12 *	18.83 **	30.73 ***	40.29
Ala	25.05 ***	16.56 *	12.07 NS	46.31
Pro	17.57 **	29.70 ***	13.01 NS	39.70
Lys	9.66 NS	17.55 *	16.87 NS	55.90
Met	0.67 NS	20.80 *	26.88 *	51.64
Val	2.32 NS	23.34 **	20.48 *	53.84
Leu	4.17 NS	23.68 **	20.22 *	51.92
Phe	0.33 NS	26.36 **	17.89 *	55.41
Ile	0.47 NS	22.13 **	23.07 *	54.32
Total aas	11.20 *	13.56 **	42.68 ***	32.55

Statistically significant at *$p \leq 0.05$, **$p \leq 0.01$ and ***$p \leq 0.001$, respectively. NS, not significant.

affected (reduced Chll A content), and despite Chll A being a primary electron donor in the electron transport chain and the primary pigment in photosynthesis, photosynthesis was not affected after heat stress in this cultivar. Moreover, an increase in Chll B was identified for all cultivars, probably attributed to an adaptation to high temperature for this species. The application of MeJA did not increase any gas exchange parameters beyond the temperature effects alone.The concentrations of leaf mineral nutrients were different under non-stressed conditions for the three cultivars. This is in agreement with the results from Ropokis et al. (2018), which uptake of nutrients was different under the same water regime, nutritional supply, and environmental conditions. Under heat stress, leaf NO3- concentration was significantly increased, although this increase was different depending on the cultivar, with Loreto being the least responsive. However, MeJA did not alter the response of the stressed cultivars. Huang et al. (Huang et al., 2017) indicated that exogenously applied jasmonate was related with inhibition of primary root growth. The effect of MeJA on root morphology could trigger alterations in nutrient uptake, especially under this stress condition, although a marginal effect was found for these pepper cultivars. This smaller effect can be attributable to the reduced time (72h) of the application to harvest, which reduced the effect on the accumulated growth. Sugar can act as signal molecules in the leaves, playing a pivotal role in regulating development, and triggering leaf senescence (Van Doorn, 2008; Reinbothe et al., 2009). Sugars can also impair photosynthesis when overcoming threshold concentrations (Zhang and Zhou, 2013). In tomato, the maintenance or higher levels of non-structural carbohydrates in mature leaves were associated with heat tolerance under short-term heat stress (Zhou et al., 2017). Sucrose, the final product of photosynthesis, can either act as a signaling molecule or become a reactive oxygen species scavenger, at low or high concentrations, respectively (Frank et al., 2009), with the latter protecting the plants from cellular damages and degradation of pigments such as chlorophylls. Our data showed that heat shock had an impact on the plants, especially for the Agio cultivar, in which glucose, fructose and sucrose were clearly reduced when MeJA was applied; however, an increase in sucrose concentration was observed in Loreto. Such alterations in carbohydrate concentration did not impair CO2-fixation. Gómez et al. (2010) pointed out in tomato that MeJA produced a rapid increase in leaf export of photosynthates, which did not occur in pepper.

Recent works have indicated that endogenous polyamines could participate in sustaining membrane integrity in cauliflower, as protectors against damage under stress conditions, through the stabilization of cell membranes (Collado-González et al., 2021a; Collado-González et al., 2021b), and therefore, they could have an effect in delaying leaf-related-senescence disorders. As previously indicated for other species, the collateral effect of MeJA associated with early senescence, can be effectively counteracted by the increase in the concentration of endogenous polyamines in specific pepper cultivars. Thus, in our stress conditions, this remarkable effect of MeJA can partly mitigate further leaf damage. A decrease in amino acid contents has also been observed for tomato (Gómez et al., 2010) and Brassica rapa leaves (Liang et al., 2006) after treatment with the foliar application of MeJA, with no stress conditions. Our data showed, after thermal stress, that MeJA application only affected the Agio cultivar, which clearly increased the concentration of their leaf amino acids. Consequently, a cultivar-dependent response was observed for pepper after the application of MeJA. (Garde-Cerdán et al., 2016) indicated that the amino acid profile of grapes was altered after the application of MeJA. In this study, we found a smaller decrease in the total amino acid content under heat stress in Agio and Loreto as compared to Basque chilli. Also, the effect of MeJA increased total amino acid content in the Agio variety alone. The differential accumulation of free amino acids could be associated with the genetic variations of heat tolerance in pepper plants. Thus, the effects of MeJA on pepper amino acid concentration were conditioned by variety. Gutiérrez-Gamboa et al. (2018) showed that grape variety had a higher effect on must amino acid composition than the elicitation through MeJA and yeast extract treatments and their interaction (variety x treatment).

Conclusions

Horticultural production is one of the most vulnerable agrosystems to the temperature impacts of climate change, and the effectiveness of mitigation strategies (such as the application of elicitors) against to this constraint needs to be widely contrasted. Our work shows the differential effects of pepper cultivars to heat stress with the application of MeJA, and also describes and examines the physiological traits involved in heat tolerance and the physiological mechanics affected. However, more studies are needed to screen a wider range of stress intensities and durations during the vegetative phase of growth and throughout the other developmental stages. To date, very few studies have addressed the specific differences of cultivars to high temperature and MeJA to show their specific responses. To this end, our study sought to investigate the physiological traits involved in that specific response to provide new knowledge for the development of new cultivars, selected to withstand the impact of heat waves without compromising yields.

Data availability statement

The raw data supporting the conclusions of this article will be made available by the authors, without undue reservation.

Author contributions

GO: conceptualisation, methodology, formal analysis, investigation, writing, editing. JG and MP: methodology, and formal analysis. JL-M: supervision. FA: conceptualization, funding acquisition, resources, project administration, supervision. All authors contributed to the article and approved the submitted version. All authors contributed to the article and approved the submitted version.

Funding

This work was financed by the European Regional Development Fund (ERDF) 80% – Region de Murcia (FEDER 1420-30).

Acknowledgments

We thank José Manuel Gambín, Miguel Marín, José Sáez Sironi, and Raquel Roca, for their technical assistance.

Conflict of interest

The authors declare that the research was conducted in the absence of any commercial or financial relationships that could be construed as a potential conflict of interest

Publisher's note

Supplementary material

The Supplementary Material for this article can be found online at: https://www.frontiersin.org/articles/10.3389/fpls.2022.1014230/full#supplementary-material

References

Ara, N., Yang, J., Hu, Z., and Zhang, M. (2013). Determination of heat tolerance of interspecific (Cucurbita maxima x cucurbita moschata) inbred line of squash "Maxchata" and its parents through photosynthetic response. *Tar. Bil. Der.* 19, 188–197. doi: 10.1501/tarimbil_0000001244

Balla, K., Karsai, I., Bónis, P., Kiss, T., Berki, Z., Horváth, Á., et al. (2019). Heat stress responses in a large set of winter wheat cultivars (*Triticum aestivum* l.) depend on the timing and duration of stress. *PloS One* 14 (9), e0222639. doi: 10.1371/journal.pone.0222639

Bastos, A., Gouveia, C. M., Trigo, R. M., and Running, S. W. (2013). Comparing the impacts of 2003 and 2010 heatwaves in NPP over Europe. *Biogeosciences Discuss.* 10, 15879–15911. doi: 10.5194/bgd-10-15879-2013

Camejo, D., Rodríguez, P., Morales, M. A., Dell'Amico, J. M., Torrecillas, A., and Alarcón, J. J. (2005). High temperature effects on photosynthetic activity of two tomato cultivars with different heat susceptibility. *J. Plant Physiol.* 3, 281–289. doi: 10.1016/j.jplph.2004.07.014

Chavan, S. G., Duursma, R. A., Tausz, M., and Ghannoum, O. (2019). Elevated CO_2 alleviates the negative impact of heat stress on wheat physiology but not on grain yield. *J. Exp. Bot.* 70, (21) 6447–6459. doi: 10.1093/jxb/erz386

Chen, Y. E., Zhang, C. M., Su, Y. Q., Ma, J., Zhang, Z. W., Yuan, M., et al. (2017). Responses of photosystem II and antioxidative systems to high light and high temperature co-stress in wheat. *Environ. Exper. Bot.* 165, 45–55. doi: 10.1016/j.envexpbot.2016.12.001

Christidis, N., Jones, G. S., and Stott, P. A. (2015). Dramatically increasing chance of extremely hot summers since the 2003 European heatwave. *Nat. Clim. Change.* 5, 46–50. doi: 10.1038/nclimate2468

Ciais, P., Reichstein, M., Viovy, N., Granier, A., Ogée, J., Allard, V., et al. (2005). Europe-Wide reduction in primary productivity caused by the heat and drought in 2003. *Nature* 437, 529–533. doi: 10.1038/nature03972

Clarke, S. M., Cristescu, S. M., Miersch, O., Harren, F. J. M., Wasternack, C., and Mur, L. A. J. (2009). Jasmonates act with salicylic acid to confer basal thermotolerance in *Arabidopsis thaliana*. *N. Phytologist.* 182, 175–187. doi: 10.1111/j.1469-8137.2008.02735.x

Collado-González, J., Piñero, M. C., Otálora, G., López-Marín, J., and del Amor, F. M. (2021a). The effect of foliar putrescine application, ammonium exposure, and heat stress on antioxidant compounds in cauliflower waste. *Antioxidants* 10 (5), 707. doi: 10.3390/antiox10050707

Collado-González, J., Piñero, M. C., Otálora, G., López-Marín, J., and del Amor, F. M. (2021b). Merging heat stress tolerance and health-promoting properties: The effects of exogenous arginine in cauliflower (*Brassica oleracea* var. botrytis l.). *Foods* 10 (1), 30. doi: 10.3390/foods10010030

del Amor, F. M., Cuadra-Crespo, P., Walker, D. J., Cámara, J. M., and Madrid, R. (2010). Effect of foliar application of antitranspirant on photosynthesis and water relations of pepper plants under different levels of CO2 and water stress. *J. Plant Physiol.* 167 (15), 1232–1238. doi: 10.1016/j.jplph.2010.04.010

Del Rodriguez, S. C., López, B., and Chaves, A. R. (2001). Effect of different treatments on the evolution of polyamines during refrigerated storage of eggplants. *J. Agric. Food Chem.* 49 (10), 4700–4705. doi: 10.1021/jf0001031

Dhankher, O. P., and Foyer, C. H. (2018). Climate resilient crops for improving global food security and safety. *Plant Cell Environ.* 41, 877–884. doi: 10.1111/pce.13207

Fahad, S., Hussain, S., Saud, S., Hassan, S., Ihsan, Z., Shah, A. N., et al. (2016). Exogenously applied plant growth regulators enhance the morpho-physiological growth and yield of rice under high temperature. *Front. Plant Sci.* 7. doi: 10.3389/fpls.2016.01250

Frank, G., Pressman, E., Ophir, R., Althan, L., Shaked, R., Freedman, M., et al. (2009). Transcriptional profiling of maturing tomato (*Solanum lycopersicum* l.) microspores reveals the involvement of heat shock proteins, ROS scavengers, hormones, and sugars in the heat stress response. *J. Exper. Bot.* 60, 3891–3908. doi: 10.1093/jxb/erp234

Garde-Cerdán, T., Portu, J., López, R., and Santamaría, P. (2016). Effect of methyl jasmonate application to grapevine leaves on grape amino acid content. *Food Chem.* 203, 536–539. doi: 10.1016/j.foodchem.2016.02.049

Gómez, S., Ferrieri, R. A., Schueller, M., and Orians, C. M. (2010). Methyl jasmonate elicits rapid changes in carbon and nitrogen dynamics in tomato. *N. Phytol.* 188, 835–844. doi: 10.1111/j.1469-8137.2010.03414.x

Griffin, J. J., Ranney, T. G., and Pharr, D. M. (2004). Heat and drought influence photosynthesis, water relations, and soluble carbohydrates of two ecotypes of redbud (*Cercis canadensis*). *J. Am. Soc Hortic. Sci.* 129, 497–502. doi: 10.21273/jashs.129.4.0497

Gutiérrez-Gamboa, G., Portu, J., López, R., Santamaría, P., and Garde-Cerdán, T. (2018). Elicitor and nitrogen applications to garnacha, graciano and tempranillo vines: effect on grape amino acid composition. *J. Sci. Food Agric.* 98, 2341–2349. doi: 10.1002/JSFA.8725

Huang, H., Liu, B., Liu, L., and Song, S. (2017). Jasmonate action in plant growth and development. *J. Exp. Bot.* 68, 1349–1359. doi: 10.1093/jxb/erw495

Kazan, K. (2015). Diverse roles of jasmonates and ethylene in abiotic stress tolerance. *Trends Plant Sci.* 20, 219–229. doi: 10.1016/j.tplants.2015.02.001

Lee, S. G., Kim, S. K., Lee, H. J., Lee, H. S., and Lee, J. H. (2018). Impact of moderate and extreme climate change scenarios on growth, morphological features, photosynthesis, and fruit production of hot pepper. *Ecol. Evolution.* 8, 197–206. doi: 10.1002/ece3.3647

Liang, Y. S., Choi, Y. H., Kim, H. K., and Verpoorte, R. (2006). Metabolomic analysis of methyl jasmonate treated brassica rapa leaves by 2-dimensional NMR spectroscopy. *Phytochemistry* 67, 2503–2511. doi: 10.1016/j.phytochem.2006.08.018

Mateos, R. M., Jiménez, A., Román, P., Romojaro, F., Bacarizo, S., Leterrier, M., et al. (2013). Antioxidant systems from pepper (*Capsicum annuum* l.): Involvement in the response to temperature changes in ripe fruits. *Int. J. Mol. Sci.* 14, 9556–9580. doi: 10.3390/ijms14059556

Otálora, G., Piñero, M. C., López-Marín, J., Varó, P., and del Amor, F. M. (2018). Effects of foliar nitrogen fertilization on the phenolic, mineral, and amino acid composition of escarole (*Cichorium endivia* l. var. latifolium). *Sci. Hortic.* 239, 87–92. doi: 10.1016/j.scienta.2018.05.031

Pagamas, P., and Nawata, E. (2008). Sensitive stages of fruit and seed development of chili pepper (*Capsicum annuum* l. var. shishito) exposed to high-temperature stress. *Sci. Hortic.* 117, 21–25. doi: 10.1016/j.scienta.2008.03.017

Pérez-Jiménez, M., Piñero, M. C., and del Amor, F. M. (2019). Heat shock, high CO_2 and nitrogen fertilization effects in pepper plants submitted to elevated temperatures. *Sci. Hortic.* 244, 322–329. doi: 10.1016/j.scienta.2018.09.072

Piñero, M. C., Otálora, G., Porras, M. E., Sánchez-Guerrero, M. C., Lorenzo, P., Medrano, E., et al. (2017). The form in which nitrogen is supplied affects the polyamines, amino acids, and mineral composition of sweet pepper fruit under an elevated CO2 concentration. *J. Agric. Food Chem.* 65, 711–717. doi: 10.1021/acs.jafc.6b04118

Piñero, M. C., Pérez-Jiménez, M., López-Marín, J., and Del Amor, F. M. (2016). Changes in the salinity tolerance of sweet pepper plants as affected by nitrogen form and high CO_2 concentration. *J. Plant Physiol.* 200, 18–27. doi: 10.1016/j.jplph.2016.05.020

Porra, R. J., Thompson, W. A., and Kriedemann, P. E. (1989). Determination of accurate extinction coefficients and simultaneous equations for assaying chlorophylls a and b extracted with four different solvents: Verification of the concentration of chlorophyll standards by atomic absorption spectroscopy. *BBA - Bioenergetics.* 975, 384–394. doi: 10.1016/S0005-2728(89)80347-0

Reinbothe, C., Springer, A., Samol, I., and Reinbothe, S. (2009). Plant oxylipins: Role of jasmonic acid during programmed cell death, defence and leaf senescence. *FEBS J.* 276, 4666–4681. doi: 10.1111/j.1742-4658.2009.07193.x

Rezaei, E. E., Siebert, S., Hüging, H., and Ewert, F. (2018). Climate change effect on wheat phenology depends on cultivar change. *Sci. Rep.* 8, 4891. doi: 10.1038/s41598-018-23101-2

Ristic, Z., Bukovnik, U., Momčilović, I., Fu, J., and Vara Prasad, P. V. (2008). Heat-induced accumulation of chloroplast protein synthesis elongation factor, EF-tu, in winter wheat. *J. Plant Physiol.* 165, 192–202. doi: 10.1016/j.jplph.2007.03.003

Rizhsky, L., Liang, H., and Mittler, R. (2002). The combined effect of drought stress and heat shock on gene expression in tobacco. *Plant Physiol.* 130, 1143–1151. doi: 10.1104/pp.006858

Ropokis, A., Ntatsi, G., Kittas, C., Katsoulas, N., and Savvas, D. (2018). Impact of cultivar and grafting on nutrient and water uptake by sweet pepper (*Capsicum annuum* l.) grown hydroponically under mediterranean climatic conditions. *Front. Plant Sci.* 9. doi: 10.3389/fpls.2018.01244

Russo, S., Dosio, A., Graversen, R. G., Sillmann, J., Carrao, H., Dunbar, M. B., et al. (2014). Magnitude of extreme heat waves in present climate and their projection in a warming world. *J. Geo-phys. Res. Atmos.* 119, 500–12,512. doi: 10.1002/2014JD022098

Tito, R., Vasconcelos, H. L., and Feeley, K. J. (2018). Global climate change increases risk of crop yield losses and food insecurity in the tropical Andes. *Glob Change Biol.* 24, e592–e602. doi: 10.1111/gcb.13959

Van Doorn, W. G. (2008). Is the onset of senescence in leaf cells of intact plants due to low or high sugar levels? *J. Exper. Bot.* 59, 1963–1972. doi: 10.1093/jxb/ern076

Waha, K., Müller, C., Bondeau, A., Dietrich, J. P., Kurukulasuriya, P., Heinke, J., et al. (2013). Adaptation to climate change through the choice of cropping system and sowing date in sub-Saharan Africa. *Global Environ. Change.* 23, 130–143. doi: 10.1016/j.gloenvcha.2012.11.001

Wahid, A., Gelani, S., Ashraf, M., and Foolad, M. R. (2007). Heat tolerance in plants: An overview. *Environ. Exper Bot.* 61, 199–223. doi: 10.1016/J.ENVEXPBOT.2007.05.011

Weidhase, R. A., Kramell, H. M., Lehmann, J., Liebisch, H. W., Lerbs, W., and Parthier, B. (1987). Methyljasmonate-induced changes in the polypeptide pattern of senescing barley leaf segments. *Plant Sci.* 51, 177–186. doi: 10.1016/0168-9452(87)90191-9

Weng, J. H., and Lai, M. F. (2005). Estimating heat tolerance among plant species by two chlorophyll fluorescence parameters. *Photosynthetica* 43, 439–444. doi: 10.1007/s11099-005-0070-6

Woetzel, J., Pinner, D., Samandari, H., Engel, H., Krishnan, M., Boland, B., et al. (2020). *Climate risk and response, physical hazards and socioeconomic impacts* (United States: McKinsey. Global Institute), 152. Available at: www.mckinsey.com/mgi.

Zandalinas, S. I., Mittler, R., Balfagón, D., Arbona, V., and Gómez-Cadenas, A. (2018). Plant adaptations to the combination of drought and high temperatures. *Physiol. Plantarum* 162, 2–12. doi: 10.1111/ppl.12540

Zhang, H., and Zhou, C. (2013). Signal transduction in leaf senescence. *Plant Mol. Biol.* 82, 539–545. doi: 10.1007/s11103-012-9980-4

Zhou, R., Yu, X., Kjær, K. H., Rosenqvist, E., Ottosen, C. O., and Wu, Z. (2015). Screening and validation of tomato genotypes under heat stress using Fv/Fm to reveal the physiological mechanism of heat tolerance. *Environ. Exper. Bot.* 118, 1–11. doi: 10.1016/j.envexpbot.2015.05.006

Zhou, R., Yu, X., Ottosen, C. O., Rosenqvist, E., Zhao, L., Wang, Y., et al. (2017). Drought stress had a predominant effect over heat stress on three tomato cultivars subjected to combined stress. *BMC Plant Biol.* 17, 24. doi: 10.1186/s12870-017-0974-x

frontiers | Frontiers in Plant Science

TYPE Original Research
PUBLISHED 02 December 2022
DOI 10.3389/fpls.2022.1077920

OPEN ACCESS

EDITED BY
Adnan Mustafa,
Brno University of Technology,
Czechia

REVIEWED BY
Muhammad Waheed Riaz,
Zhejiang Agriculture and Forestry University, China
Rafaqat Ali Gill,
Oil Crops Research Institute (CAAS), China
Fazal Rehman,
South China Botanical Garden (CAS), China

*CORRESPONDENCE
Peiguo Guo
guopg@gzhu.edu.cn
Yanshi Xia
xiayanshi922@163.com

†These authors have contributed equally to this work

SPECIALTY SECTION
This article was submitted to Plant Abiotic Stress, a section of the journal Frontiers in Plant Science

RECEIVED 23 October 2022
ACCEPTED 21 November 2022
PUBLISHED 02 December 2022

CITATION
Ikram M, Chen J, Xia Y, Li R, Siddique KHM and Guo P (2022) Comprehensive transcriptome analysis reveals heat-responsive genes in flowering Chinese cabbage (*Brassica campestris* L. ssp. *chinensis*) using RNA sequencing.
Front. Plant Sci. 13:1077920.
doi: 10.3389/fpls.2022.1077920

Comprehensive transcriptome analysis reveals heat-responsive genes in flowering Chinese cabbage (*Brassica campestris* L. ssp. *chinensis*) using RNA sequencing

Muhammad Ikram[1†], Jingfang Chen[1†], Yanshi Xia[1*], Ronghua Li[1], Kadambot H. M. Siddique[2] and Peiguo Guo[1*]

[1]Guangdong Provincial Key Laboratory of Plant Adaptation and Molecular Design, International Crop Research Center for Stress Resistance, School of Life Sciences, Guangzhou University, Guangzhou, China, [2]The UWA Institute of Agriculture, UWA School of Agriculture & Environment, The University of Western Australia, Perth, WA, Australia

Flowering Chinese cabbage (*Brassica campestris* L. ssp. *chinensis* var. *utilis* Tsen et Lee, 2n=20, AA) is a vegetable species in southern parts of China that faces high temperatures in the summer and winter seasons. While heat stress adversely impacts plant productivity and survival, the underlying molecular and biochemical causes are poorly understood. This study investigated the gene expression profiles of heat-sensitive (HS) '3T-6' and heat-tolerant (HT) 'Youlu-501' varieties of flowering Chinese cabbage in response to heat stress using RNA sequencing. Among the 37,958 genes expressed in leaves, 20,680 were differentially expressed genes (DEGs) at 1, 6, and 12 h, with 1,078 simultaneously expressed at all time points in both varieties. Hierarchical clustering analysis identified three clusters comprising 1,958, 556, and 591 down-regulated, up-regulated, and up- and/or down-regulated DEGs (3205 DEGs; 8.44%), which were significantly enriched in MAPK signaling, plant–pathogen interactions, plant hormone signal transduction, and brassinosteroid biosynthesis pathways and involved in stimulus, stress, growth, reproductive, and defense responses. Transcription factors, including MYB (12), NAC (13), WRKY (11), ERF (31), HSF (17), bHLH (16), and regulatory proteins such as PAL, CYP450, and photosystem II, played an essential role as effectors of homeostasis, kinases/phosphatases, and photosynthesis. Among 3205 DEGs, many previously reported genes underlying heat stress were also identified, e.g., *BraWRKY25, BraHSP70, BraHSPB27, BraCYP71A23, BraPYL9*, and *BraA05g032350.3C*. The genome-wide comparison of HS and HT provides a solid foundation for understanding the molecular mechanisms of heat tolerance in flowering Chinese cabbage.

KEYWORDS

heat stress, transcriptome, differentially expressed genes, cluster analysis, flowering chinese cabbage, RT-qPCR

Introduction

Heat stress is an environmental factor affecting crop vegetative growth, performance, and productivity worldwide, even causing plant death (Caers et al., 1985; Song et al., 2014a). According to a crop-based algorithm study, a 1°C rise in seasonal temperature causes 2.5–16% direct yield losses for key crops in tropical and subtropical regions (Lobell et al., 2008). Furthermore, greenhouse gas emissions have increased atmospheric temperatures by 0.3°C per decade (Jones et al., 1999), indicating that extreme temperature and climate change events will threaten food security by decreasing crop production (Battisti and Naylor, 2009; Rosenzweig et al., 2014). Flowering Chinese cabbage (*Brassica campestris* L. ssp. *chinensis* var. *utilis* Tsen et Lee) is a commercial vegetable crop mainly cultivated in southern parts of China (Chen et al., 2017). The demand for flowering Chinese cabbage is increasing due to its rich source of vitamin C, favourable taste, soluble fiber, phenolics, glucosinolates, and other nutritional value (Huang et al., 2017), but southern China's high summer and autumn temperatures seriously impair crop quality and production (Fan et al., 2017). Heat stress adversely affects plant growth, phenological stages, grain filling, pollen viability, even the structural changes in tissues and cell organelles, loss of leaf water, cell membrane damage, and photosynthetic membranes (Yoshinaga et al., 2005). At a molecular level, heat stress also affects the synthesis of primary and secondary metabolites, antioxidant enzymes, and lipid peroxidation *via* the production of reactive oxygen species (ROS). However, plants have evolved various molecular and physiological mechanisms during domestication to resist heat stress (Wahid et al., 2007; Hasanuzzaman et al., 2013), such as accumulating different metabolites (antioxidants, osmoprotectants, etc.) and activation of signaling and metabolic pathways. Therefore, understanding the mechanism of signaling cascades and specific genes expressed in response to HT will be beneficial for developing stress-tolerant varieties.

Transcription factors (TFs), signal transduction components, and proteins related to metabolism are responsive to heat stress (Grover et al., 2013). Recently, heat-responsive siRNAs and miRNAs in flowering Chinese cabbage have been reported (Yu et al., 2012; Song et al., 2021), with most up-regulated under high temperature, and their target genes with differential gene expression involved in responses to temperature stimulus, cell membrane, signal transduction, and mitogen-activated protein kinase (MAPK) signaling pathways (Song et al., 2021). In Chinese cabbage, Song et al. (2016) used RNA-seq datasets of heat treatments to identify 14,329 DEGs and 9,687 novel LncRNAs, of which LncRNAs controlled 192 DEGs under heat stress. Transcriptome sequencing analysis of Chinese cabbage (*B. rapa* ssp. *pekinensis*) inbred lines revealed that heat stress affects many genes, including those linked with membrane leakage, heat-shock proteins (HSPs), and enzymes that regulate ROS homeostasis (Dong et al., 2015). Heat-shock transcriptional factors (HSFs), which stimulate the expression of HSPs and other stress proteins, play a critical role in modulating stress responses (Swindell et al., 2007; Dong et al., 2015; Liu et al., 2018; Yao et al., 2020). The HSF gene family has been identified in various species, including *Arabidopsis* (Nover et al., 2001), tomato (Yang et al., 2016), soybean (Li et al., 2014), potato (Dossa et al., 2016), and Chinese cabbage (Song et al., 2014b). HSF and HSP family members are involved in several stress response pathways, including heat, cold, osmotic, and salt, in *Arabidopsis* (Swindell et al., 2007), with 21 HSFs cloned and analyzed (Nover et al., 2001). In global transcription profiles, many HSFs/HSPs were up-regulated in *Brassica napus* siliques, with many other heat-responsive marker genes, such as *ROF2, MBF1c, DREB2a*, and *Hsa32*, involved in heat resistance in many plants (Yu et al., 2014). Another study found that genes involved in protein protection, biotic stress responses, oxidative stress, programmed cell death, and metabolism were differentially expressed during heat stress (Kotak et al., 2007). Only limited transcriptome data are available for flowering Chinese cabbage under heat stress relative to Chinese cabbage, maize, rice, and Arabidopsis (Song et al., 2014a; Chen et al., 2017; Fan et al., 2017; Huang et al., 2017; Ali et al., 2022).

In recent years, next-generation sequencing technologies have been developed and significantly reduced the cost and increased the efficiency of genome sequencing. Therefore, the entire genome of *B. rapa* (Chiifu-401-42) was sequenced using Illumina GA II sequencing and annotated (Wang et al., 2011), which provides the foundation to identify the heat-responsive genes in flowering Chinese cabbage. Using RNA-seq, researchers can identify the expressed genes, particularly those with low abundance. To date, microarrays and RNA-Seq projects have been undertaken in many species, including rice, Chinese cabbage, maize, cotton, Arabidopsis, and vegetables, to detect genes responsive to heat and cold stress (Grover et al., 2013; Nakashima et al., 2014; Ikram et al., 2020; Song et al., 2021; Ali et al., 2022). For example, in *Arabidopsis*, nearly 30% of DEGs associated with abiotic stresses were identified, and 2,409 genes were involved in salt, cold, and drought stresses (Kreps et al., 2002). In wheat, 2% of genes were found to be associated with cold stress (Winfield et al., 2010). In *A. mongolicus*, 9,309 and 23,419 up- and down-regulated genes were detected under cold stress (Pang et al., 2013). In previous studies, various genes have been functionally characterized for heat tolerance in different crop plants, such as *ZmWRKY106* (Wang et al., 2018), *PpEXP1* (Xu et al., 2014), *hsp26* (Xue et al., 2010), *WsSGTL1* (Mishra et al., 2013), and *OsOr-R115H* (Jung et al., 2021).

Our previous research identified expressed sequence tag-simple sequence repeat (EST-SSR) markers in flowering Chinese cabbage (Chen et al., 2017) and also detected significant SNPs/genes for plant height (Ikram et al., 2022a; Ikram et al., 2022b; Li et al., 2022) and wilt resistance (Lai et al., 2021) in tobacco. The present study used RNA-seq based on the Illumina HiSeq2000

platform to undertake a genome-wide analysis of gene expression in leaves of HT (Youlu-501) and HS (3T-6) flowering Chinese cabbage varieties under heat stress (0, 1, 6, and 12 h) to (1) identify DEGs in HS and HT genotypes after 1, 6, and 12 h of heat stress: (2) annotate these genes based on gene ontology (GO) and Kyoto Encyclopedia of Genes and Genomes (KEGG) enrichment analysis; (3) identify the expression pattern of genes using Hierarchical clustering analysis; (4) identify TFs associated with the DEGs and their role in heat stress. The findings of this study will provide new insights into the heat tolerance of flowering Chinese cabbage.

Materials and methods

Plant materials and physiological parameters

Two natural flowering Chinese cabbage (*Brassica campestris L. ssp. chinensis* var. *utilis Tsen et Lee*) varieties [3T-6 (heat-sensitive) and Youlu-501 (heat-tolerant)] were obtained from the Guangdong Academy of Agricultural Sciences, China. The seeds of both accessions were sterilized and then germinated in a growth chamber of our lab at the International Crop Research Center for Stress Resistance (113.37_E, 23.05_N), Guangzhou University, under the following condition: 28/22°C for 14/10 h (day/night) with 80% relative humidity. Fifteen-day-old seedlings at five-leaf stage were transferred into another chamber at 38/29°C (14/10 h day/night) for heat stress. After the heat-stress treatment, samples were collected at three time points from fully expanded upper leaves of heat-sensitive (HS-1h, HS-6h, and HS-12h) and heat-tolerant (HT-1h, HT-6h, and HT-12h) plants. For the control (CK), leaf samples were collected from HS (HS-CK) and HT (HT-CK) plants under normal conditions at 25°C. The harvested leaf samples were immediately frozen in liquid nitrogen and preserved at –80°C until RNA extraction. The experiment had five replicates. Peroxidase (POD), superoxide dismutase (SOD), and catalase (CAT) were assessed as described in previous studies (Kono, 1978; Aebi, 1984). The fresh plants were taken at different times to calculate the fresh weight in both varieties.

RNA extraction, cDNA library construction, and sequencing

For transcriptome assembly, total RNA was extracted from five biological replicates at CK, HS/HT-1h, HS/HT-6h, and HS/HT-12h using TRIzol reagent (Takara Bio, Ostu, Japan), following the manufacturer's recommendations. The RNA was pooled into a single sample in equal amounts to find the broad gene library associated with heat resistance. DNase I (Takara Bio, Ostu, Japan) was used to digest genomic DNA, and RNA integrity and quantity were assessed using 1% agarose gel electrophoresis and a microplate spectrophotometer (BioTek Company, USA). cDNA libraries were prepared using RNA with high purity. In brief, mRNAs were purified using poly-T oligo-attached magnetic beads from total RNA. Following fragmentation, first-strand cDNA was synthesized using a random hexamer primer, followed by second-strand cDNA synthesized using DNA Polymerase I and RNase H. The paired-end Illumina sequencing required the purification and ligation of the double-stranded cDNAs to adaptors. After PCR amplification, library quality was verified on the Agilent 2100 Bioanalyzer system before sequencing the cDNA libraries using the Illumina HiSeq2000 system by the Beijing Genomics Institute (BGI) to generate 125 bp paired-end reads.

RNA-seq data analysis and annotation

Before library assembly, the raw reads were processed using SOAPnuke v1.5.2 (https://github.com/BGI-flexlab/SOAPnuke; Cock et al., 2009) to remove low-quality reads with >50% of bases with Q ≤ 20 or >10% unknown (N) bases and adapter sequences. The raw reads with quality check parameters were transformed to clean reads for further analysis. Finally, clean reads were mapped and aligned to *B. rapa* cv. Chiifu v3.0 reference genome (http://brassicadb.org/brad/; Wang et al., 2011) using HISAT2 v2.1.0 (Kim et al., 2015) and Bowtie2 v2.2.5 (Langmead and Salzberg, 2012). For functional annotation, all assembled gene sequences were aligned to databases, including reference genome (BRAD database), NT, NR, UniProt, Cluster of Orthologous Groups of proteins (COG), KEGG, and GO using Trinotate software (http://trinotate.github.io/) with E value ≤1e-5. The mapped reads were used to measure expression levels in fragments per kilobase of exon per million mapped fragments (FPKM) using RSEM software (Li and Dewey, 2011). Pearson's correlation coefficients for the eight samples were estimated using the 'cor' function in R4.1.0 (http://www.r-project.org/) software based on FPKM values, and a correlation graph was drawn using the 'ggplot2' R package (https://cran.r-project.org/web/packages/ggplot2/index.html). The 'prcomp' function in R4.1.0 (http://www.r-project.org/) was used to perform principal component analysis (PCA).

Differential expression and cluster analyses

For HS and HT varieties, DEGs between control and heat-stress conditions were calculated using the DESeq2 R package (Love et al., 2014), a reliable and efficient package for detecting DEGs between diverse samples. The significant DEGs between heat stress and control conditions were identified at $|\log_2(\text{fold-change})| > 2$ and false discovery rate (FDR) adjusted $P < 0.001$.

Further, significant DEGs in HS or HT were exposed to hierarchical or K-mean clustering based on the hclust function in R4.1.0 (distance: euclidean; method: ward.d), with $\log_2$FC subjected as the input. Finally, DEGs were analyzed for soft clustering based on fuzzy c-mean using the R4.1.0 package 'Mfuzz' (Kumar and Futschik, 2007).

Gene ontology and KEGG pathway enrichment analysis of differentially expressed genes

GO and KEGG enrichment analysis was undertaken to reveal the functional annotation and pathways associated with up- and down-regulated DEGs in each cluster or group. An online tool (http://www.geneontology.org/) was used to conduct GO enrichment analysis at FDR adjusted $P \leq 0.05$, classifying the DEG functions into three categories: cellular component, biological process, and molecular function. Similarly, KEGG pathway enrichment analysis was performed using the KEGG database (https://www.genome.jp/kegg/pathway.html) with significant criteria at an adjusted $P \leq 0.05$ (Kanehisa and Goto, 2000).

Validation of RNA-seq result by real-time quantitative PCR

Ten genes were chosen randomly to confirm the reliability of RNA-seq results using RT-qPCR. The RNA was the same as that used for transcriptomic sequencing, with the relative expression calculated using ABIPrism7000 RT-qPCR platform (Applied Biosystems, USA). The PCR reaction volume was 10 mL with 1 µg cDNA, 5 mL SYBR Premix Ex Taq II (Takara, China), and 200 nM primers. Three technical and biological replicates for each sample were measured with the following protocol: 95°C for 5 min, followed by 40 cycles of 95°C for 15 s, 60°C for 60 s, and until 65°C to 97°C with a ramp rate of 0.02°C s^{-1} for dissociation curve analysis. *BraActin* was used as housekeeping gene to normalize the data. The relative expression level of all selected genes at each time point was calculated using the $2^{-\Delta\Delta CT}$ method. The in-house R script was used to conduct a student t-test at $P \leq 0.05$ to find the significant differences between time points.

Results

Plant phenotypic and enzymatic activities under heat stress

Heat stress significantly altered plant growth and the reproduction system. At the initial stage of stress, plant leaves exhibited moderate to high wilting symptoms. Twelve hours of heat stress significantly decreased whole plant weight (g) in both species relative to the control (Figure 1A). The heat treatment significantly increased catalase (CAT), superoxide dismutase (SOD), and peroxidase (POD) activities in plant leaves at all time points, relative to the control, and more so in Youlu-501 than 3T-6 (Figure 1A).

Overview of transcriptomic sequencing data

Libraries were constructed and sequenced on the IlluminaHiseq2000 deep sequencing platform using the PE125 protocol (Table S1). Each library generated 21.94–24.90 million raw reads. After removing joint contamination, low-quality reads, and reads with unknown base (N) content, 21.86–24.81 million clean reads (99.42–99.963%) were collected (Table S1). The clean Q30 base rates of the eight samples ranged from 89.71–91.04%. Of the clean reads, 88.59–92.06% total and 73.06–76.72% unique reads were mapped to the *B. rapa* reference genome (Table S1), with 46,250 predicted *B. rapa* genes (Figure 1B). The PCA revealed an overall 86.80% (PC1 = 73.40% and PC2 = 13.40%) variation in gene expression datasets, with the heat-stress conditions (HS-1h/HR-1h, HS-6h/HR-6h, and HS-12/HR-12) clustered or grouped nearby but separated from their corresponding control HS-CK/HR-CK (Figure S1). Pearson's correlation coefficient analysis based on FPKM values of each sample revealed a significant positive correlation between different time points; for example, HS-6h and HT-6h highly correlated with other time points compared to HS-12h and HR-12h (Figure 1C). The HS and HT varieties significantly differed based on the $\log_{10}$ transformation of FPKM (Figure 1D), with the FPKM values of most genes >10 (Figure 1E). Sixteen genes had FPKM values >2,000 in both varieties at all time points.

Differential expression profiling of two varieties under heat stress

$DESeq_2$ software was used to investigate DEGs with FPKM values >1. During heat stress, 30,842, 32,260, 32,926, 31,540, 32,635, and 33,113 genes were regulated for HS-1h, HS-6h, HS-12h, HT-1h, HT-6h, and HT-12h, respectively (Figures 2A, B). The DEGs were selected using the following criteria of $\log_2$ fold-change $|\log_2(\text{foldchange})| \geq 2$ and FDR adjusted $P \leq 0.001$. Volcano plots identified the significant up- or down-regulated genes during heat stress at each time point (Figure 2A), with 10,153 (1,115 up- and 9,038 down-regulated), 7,879 (4,438 up- and 3,441 down-regulated), and 7,662 (5,349 up- and 2,313 down-regulated) DEGs in 3T-6 at HS-1h, HS-6h, and HS-12h compared to the control (Figures 2A–C) and 13,704 (882 up-

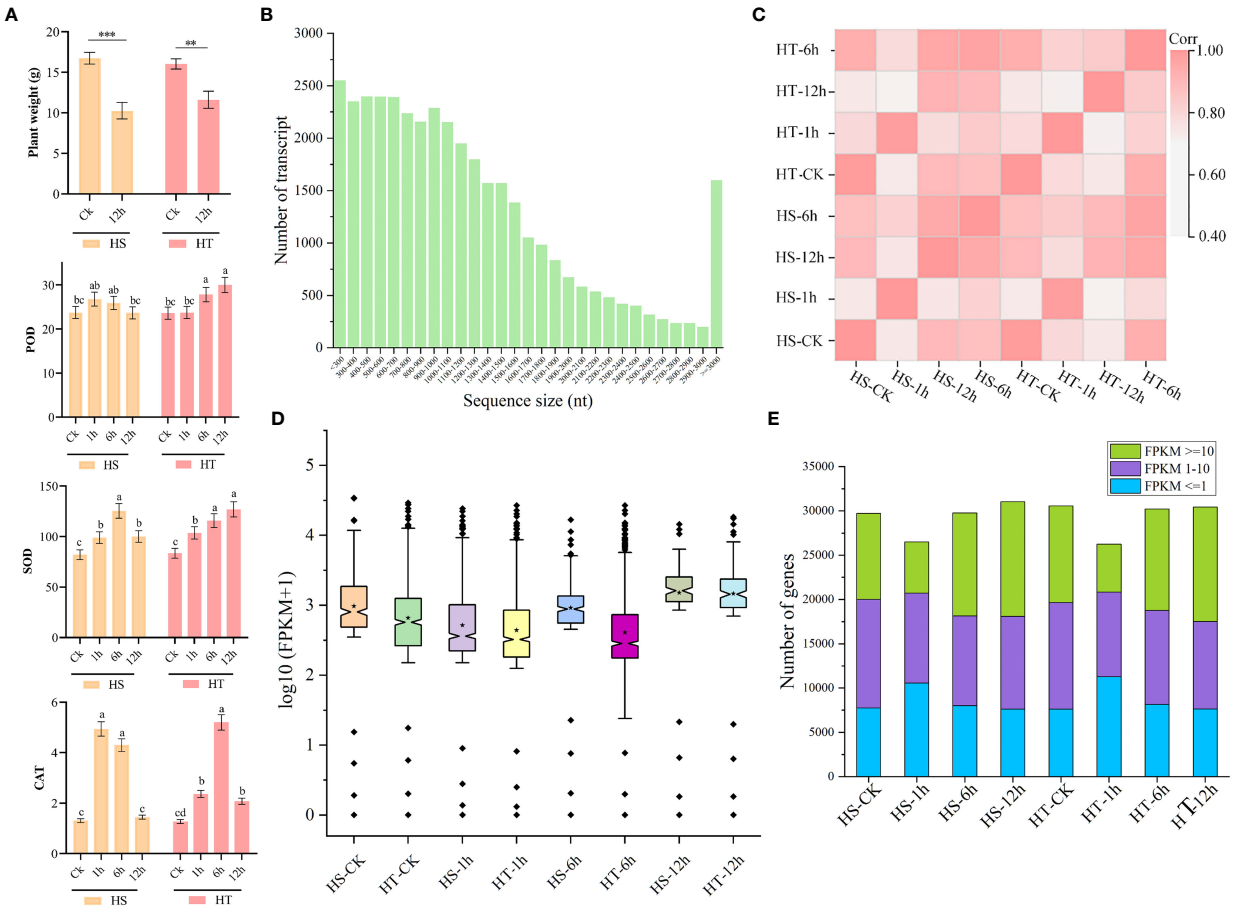

FIGURE 1
Phenotypic effect and overview of RNA sequencing data based on heat-sensitive and heat-tolerant flowering Chinese cabbage varieties. **(A)** Plant weight and enzymatic activities between control and stress conditions; **(B)** Number of transcripts and their sequence size; **(C)** Correlation analysis between heat-sensitive and heat-tolerant varieties at different time points; **(D)** $\log_{10}$ transformation of FPKM values at 0, 1, 6, and 12 h; **(E)** Distribution of genes based on FPKM values. The different small letters indicate the significant differences between the time points.

and 12,822 down-regulated), 5,161 (2,206 up- and 2,955 down-regulated), and 7,438 (3,989 up- and 3,449 down-regulated) DEGs in Youlu-501 at HT-1h, HT-6h, and HT-12h compared to the control (Figures 2A–C).

Subsequently, Sankey and Venn diagrams demonstrated the number of common and uniquely expressed genes at each time point or between two consecutive time points (Figures 2B, D–F), with 5,443 DEGs unique in all samples, and 7,025, 3,626, 2,382, 1,126, and 1,078 DEGs shared between two, three, four, five, and six samples (Figure 2B). Additionally, 2,073 and 2,210 DEGs were common at all time points of HS and HT genotypes, respectively (Figures 2D, E), indicating higher number of genes were regulated in heat-tolerant variety than sensitive. Of these, 1,078 DEGs were co-expressed differently in the HS and HT genotypes (Figure 2F), with 237 and 747 up- and down-regulated, respectively, and 94 differentially regulated. After 6 and 12 h of heat treatment, 328/325 and 330/323 more DEGs were up-regulated in HS/HT. Finally, 3,205 genes were differentially expressed at 1, 6, and 12 h in 3T-6 or Youlu-501 (Figures 2B, D–F).

Functional annotation of DEGs responsive to heat stress

GO enrichment analyses of up- and down-regulated genes in HS and HT at 1, 6, and 12 h categorized the heat stress-related genes associated with key biological processes. Figures 3, S2–S5 show the top 25 GO terms in three categories. In HS, for HS-CK vs. HS-1h, 462 up-regulated genes were mainly involved in 'response to stimulus (GO:0009628),' 'cellular process (GO:0009987),' 'primary metabolic process (GO:0044238),' 'response to abiotic stimulus (GO:0009628),' 'developmental process involved in reproduction (GO:0003006),' and 'response to heat

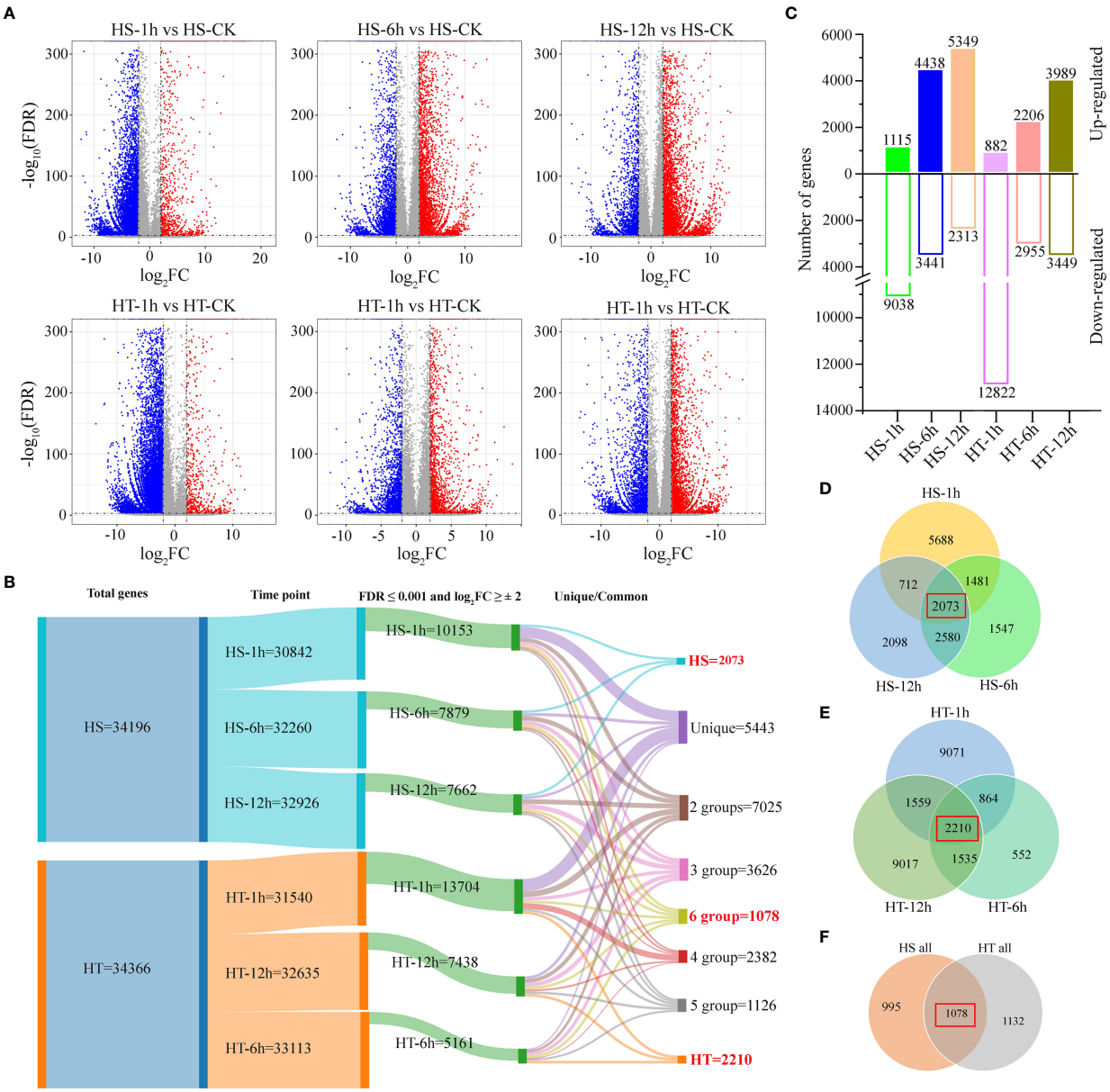

FIGURE 2
Analysis of differentially expressed genes in flowering Chinese cabbage varieties in response to heat stress. **(A)** Volcano plots of all expressed genes in heat-sensitive (HS) and heat-tolerant (HT) varieties at different time points relative to CK, with $\log_2$FC values drawn against $-\log_{10}$ (FDR) adjusted *P*-values. Red and blue dots represent up- and down-regulated DEGs based on $|\log_2(\text{foldchange})| \geq 2$ and FDR ≤ 0.001; gray dots represent non-significant DEGs; **(B)** The Sankey diagram represents the number of common and unique DEGs between each stress point; **(C)** Number of up and down-regulated DEGs identified under different heat-stress treatments relative to control HS and HT varieties; **(D)** Common and unique DEGs under different heat-stress treatments in HS variety; **(E)** Common and unique DEGs in HT under different heat-stress treatments; **(F)** Common DEGs in all heat-stress treatments in HS and HT.

(GO:0009408)' (Figure 3A). In comparison, most of the 4,055 down-regulated genes were involved in 'tissue development (GO:0009888),' 'auxin-activated signaling pathway (GO:0009734),' 'cell part (GO:0044464),' 'intracellular part (GO:0044424),' 'cellular response to abiotic stimulus (GO:0071214),' 'cell (GO:0005623),' 'intracellular (GO:0005622),' and 'cellular process (GO:0009987)' (Figure 3A). For HS-CK vs. HS-6h and HS-CK vs. HS-12h, 2,046 and 2,275 up-regulated genes were significantly enriched in 'anion binding (GO:0043168),' 'nucleotide binding (GO:0000166),' 'response to temperature stimulus (GO:0009266),' 'purine nucleotide binding (GO:0017076),' 'carbohydrate derivative binding (GO:0097367),'

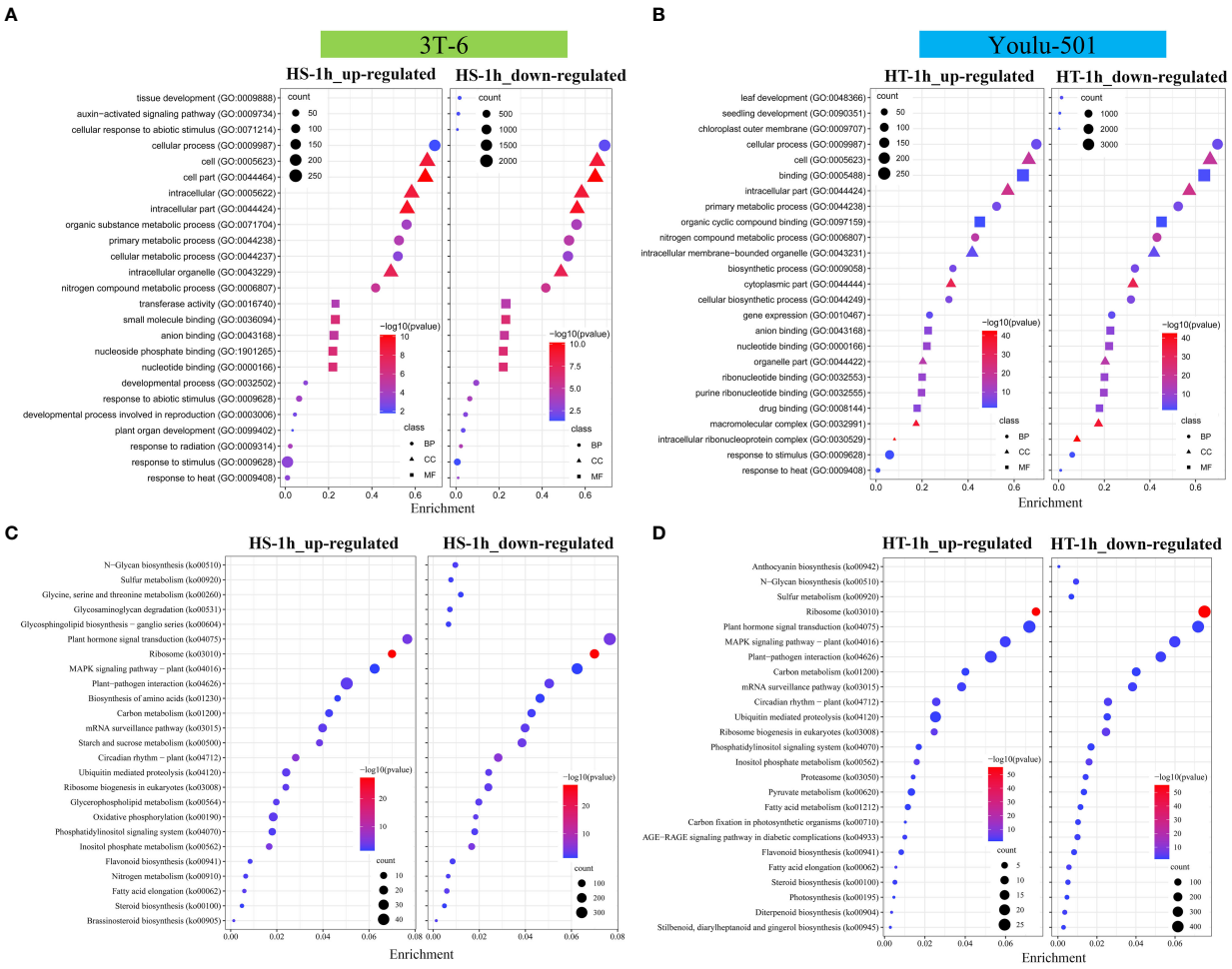

FIGURE 3
GO and KEGG enrichment analysis of up- and down-regulated genes in heat-sensitive (3T-6) and heat-tolerant (Youlu-501) flowering Chinese cabbage. **(A, B)** The top 25 GO terms in three categories are listed at HS-1h vs. HS-CK and HT-1h vs. HT-CK at $P \leq 0.05$; **(C, D)** The top 25 KEGG pathways and their corresponding number of genes HS-1h vs. HS-CK and HT-1h vs. HT-CK at $P \leq 0.05$. The x-axis represents the enrichment factor, the y-axis represents GO/KEGG terms with the number of genes, and the blue to red color indicates the significance and number of genes.

'response to abiotic stimulus (GO:0009628),' and 'photosynthesis (GO:0015979)' (Figure S2). In contrast, 1,568 and 902 down-regulated genes were mainly enriched in 'metabolic process (GO:0008152),' 'detoxification (GO:0071722),' 'intracellular organelle (GO:0043229),' 'chloroplast (GO:0009507),' and 'RNA binding (GO:0003723)' (Figure S2). In HT, for HT-CK vs. HT-1h, 418 up-regulated genes were involved in 'binding (GO:0005488)' 'cellular process (GO:0009987),' and 'primary metabolic process (GO:0044238)', and 6,626 down-regulated genes were enriched in 'leaf development (GO:0048366),' 'response to stimulus (GO:0009628),' 'chloroplast outer membrane (GO:0009707),' and 'biosynthetic process (GO:0009058)' (Figure 3B). Similarly, the highest number of DEGs for HT-6h and HT-12 were involved in 'response to stimulus (GO:0009628),' 'chloroplast (GO:0009507),' 'cell periphery (GO:0071944),' 'auxin homeostasis (GO:0010252),' 'membrane-bounded organelle (GO:0043227),' and 'photosynthesis (GO:0015979)' (Figure S3). The GO enrichment analysis indicated that HT had more enriched DEGs for each term than HS; for example, 1,410 HT and 415 HS genes were involved in 'response to stimulus' (Figures 3A, B, S2, S3).

The KEGG database was used to investigate the key genes involved in KEGG pathways, with 2,389 and 1,453 up-regulated and 3,390 and 4,286 down-regulated genes in HS and HT, respectively, enriched in 39 KEGG pathways (adjusted $P \leq 0.05$), including 'plant-pathogen interaction (ko04626),' 'oxidative phosphorylation (ko00190),' 'sulfur metabolism (ko00920),' 'steroid biosynthesis (ko00100),' 'nitrogen metabolism (ko00910),' 'plant hormone signal transduction (ko04075),' 'brassinosteroid biosynthesis (ko00905),' 'MAPK signaling pathway - plant (ko04016),' 'circadian rhythm - plant (ko04712),' 'carbon metabolism (ko01200),' and 'photosynthesis (ko00195)' (Figures 3C, D, S4, S5). The HT

genes were more involved in signal transduction and MAPK pathways than the HS genes (Figures 3C, D).

Cluster analysis of differentially expressed genes

We used gene expression changes (log_2FC value) to perform hierarchical clustering for 3205 DEGs (Figures 2D–F) in response to heat stress among flowering Chinese cabbage varieties. The clusters with similar patterns of expression change were identified using the hclust method. As a result, we found three clusters of genes response to heat stress at three time points relative to control and a black line representing the mean changes in expression (Figures 4A–C and Table S2). Cluster 1 contained 1,958 DEGs that were down-regulated in both varieties at 1, 6, and 12 h, and the expression variations of cluster 1 genes in Youlu-501 were comparatively more repressed than in 3T-6 (Figures 4A, B; Table S2). Interestingly, cluster 2 included 691 DEGs, the expression changes were down-regulated at 1h in both varieties compared to the control and up-regulated at 6 and 12 h, but expression patterns of HT were relatively higher than HS at 6 and 12 h stress condition (Figures 4A, B; Table S2). A total of 556 DEGs were found in Cluster 3, and most of them were up-regulated by heat stress in both varieties. The difference in Cluster 3 was that the genes had moderately greater induced expression levels in HS than in HT during heat stress except for 12h (Figures 4A, B; Table S2).

Further, we investigated the biological functions of these clusters using GO enrichment analysis (Figure 4C; Table S2). The cluster 1 DEGs were mainly involved in cellular component organization or biogenesis (91), biological regulation (143), cellular process (394), developmental process (46), metabolic process (379), and response to stimulus (165). The DEGs belonging to developmental process (24), growth (10), response to stimulus (54), localization (22), metabolic process (155), and multi-organism process (17) were also significantly enriched in cluster 2. In addition, DEGs in cluster 3, which were up-regulated in both varieties, were involved in biological regulation (41), carbon utilization (8), biogenesis (28), reproduction (7), and response to stimulus (59). The fold-change expression values were higher in HT Youlu-501 than in HS 3T-6 (Figure 4A; Table S2). In brief, the top 15 potential DEGs expressed in all stages were identified, and their homologous have been reported to play an essential role in heat stress (Table 1).

Gene families associated with heat stress

Gene families, including HSPs, cytochrome P450 (CYP), photosystem II (PSII), MAPK, and phenylalanine ammonia-lyase (PAL), play a significant role in plant abiotic and biotic stresses. HSP genes were clustered into two groups: (1) two genes up-regulated at high-stress conditions; (2) initially up-regulated and then down-regulated under high stress (Figures 5A–F; Table S3). Forty-two cytochrome P450 (CYP450) genes were differentially expressed under heat stress, with 16 were up-regulated in both varieties at 1, 6, and 12 h, including *BraCYP98A3*, *BraCYP82G1* *BraCYP83A1, BraCYP83A1, BraCYP72A13*, and *BraCYP94B3* (Figure 5A; Table S3). Of 16 DEGs, three genes (*BraCYPBC1*, *BraCYP97B3*, and *BraCYP77A4*) were up-regulated at 1, 6, and 12 h, while the others were up-regulated after 6 and 12 h stress (Figure 5A). Furthermore, *BraA01g002420.3C* (*BraCYP84A1-X1*) was down-regulated under heat stress (Figure 5A), with similar results obtained using RT-qPCR (Figure 5B). Photosynthesis is mainly sensitive to heat stress, and photosystem II (PSII) is the stress-sensitive site with its oxygen-evolving complex. Three PSII genes [*PSBQ3 (BraA02g017000.3C), PSBQ2 (BraA03g024820.3C)*, and *Psb27 (BraA08g035330.3C)*] were negatively expressed in HS (Figure 5D; Table S3). Another gene, *PSBQ2 (BraA05g013730.3C)*, encoding PSII oxygen-evolving enhancer protein 2, was up-regulated in HS and HT varieties. Moreover, 5 MAPK and 2 PAL gene expressions significantly differed in HS and HT after 1, 6, and 12 h. PAL1 and PAL3 have a redundant role in flavonoid biosynthesis (Table S3). *BraA09g032810.3C* (*MPK-10)* gene was down-regulated, while other genes were up- and down-regulated at different time points (Figure 5C).

Differential expression of transcription factors during heat stress

TF families of flowering Chinese cabbage were retrieved from the PlantTFDB database for enrichment analysis. We analyzed the DEGs related to heat-responsive TFs, such as MYBs, ARFs, HSFs, NACs, ERFs, and WRKYs families, which could be involved in regulating genes during heat stress (Figures 6A–I; Table S4), identifying 12 MYBs, 13 NACs, 11 WRKYs, 31 ERFs, 17 HSFs, six ARFs, and 16 bHLHs TFs (Table S4). Apart from partial bHLH TFs family members, heat stress significantly up-regulated most gene family members of MYBs, NACs, WRKYs, and ERFs. For example, *BraA03g051480.3C (WRKY53)* in HS at 1, 6, and 12 h, with similar results obtained using RT-qPCR (Figures 6H, I). *WRKY18* was down-regulated at the initial stress but up-regulated under high-stress conditions in HT (Figure 6I). HSFs encoding HSPs, as direct transcriptional activators of genes regulated by heat stress, showed higher up-regulated expression levels in HT than HS: *BraA02g043370.3C* encodes heat stress transcription factor B-2a-like (*HsfB-2a*) and had higher expression levels at 1, 6, and 12 h in HS and HT (Figures 6F, G; Table S4). Similarly, three bZIP TFs (*BZIPHY5*, *BZIPHY5-X1*, and *BZIP61*) were differentially expressed after heat stress. Of 12 MYBs, *BraA07g030110.3C (MYB1R1)* and *BraA03g044990.3C (MYB44)* were up-regulated at 1, 6, and 12 h, with the remaining ten down-regulated (Figure 6F; Table S4). Among 13 NACs, nine genes,

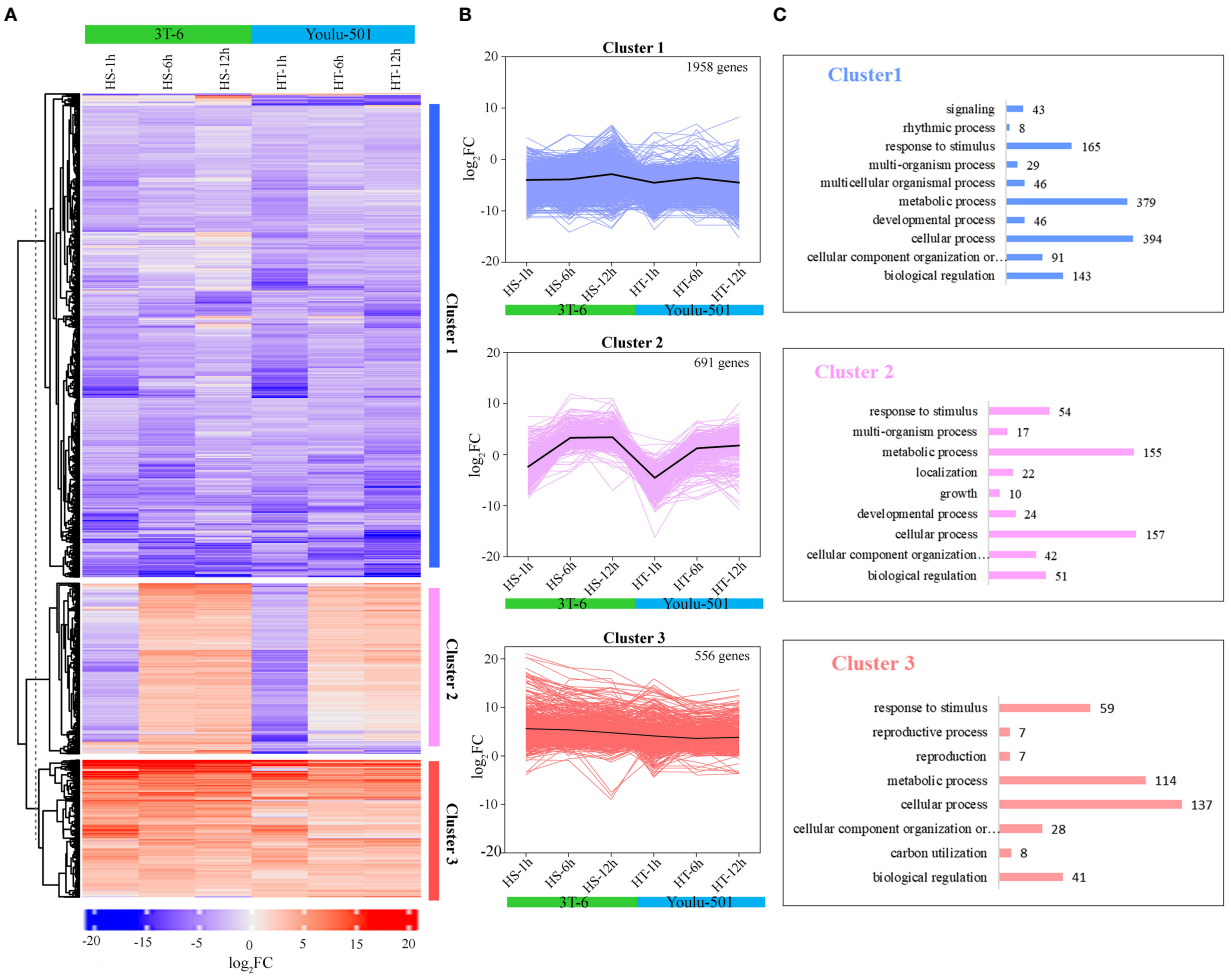

FIGURE 4
Expression patterns of differentially expressed genes (DEGs) and their functional annotation in heat-sensitive (3T-6) and heat-tolerant (Youlu-501) flowering Chinese cabbage in response to heat stress. **(A)** Hierarchical clustering analysis indicates DEG expression patterns in 3T-6 and Youlu-501 after 1, 6, and 12 h of heat stress relative to their controls; **(B)** Cluster analysis shows that the lines reflect expression patterns for each DEG at heat-stress time points. Black lines in each cluster indicate mean changes in DEG expression; **(C)** Gene ontology enrichment analysis of DEGs in each cluster.

including five NACs (*BraA02g002870.3C, BraA03g053670.3C, BraA07g004020.3C, BraA07g034350.3C*, and *BraA10g031880.3C*) were up-regulated in HS and HT at 1, 6, and 12 h, while *BraA06g027220.3C, BraA07g014500.3C*, and *BraA10g000880.3C* were up-regulated under high stress. In addition, most of the auxin (ARFs) and ethylene-responsive transcription factor (ERFs) up-regulated at 12h; for example, e.g., *BraA01g030800.3C, BraA06g041230.3C, BraA09g022610.3C, BraA09g022620.3C*, and *BraA02g031120.3C*, were down-regulated at initial stress (1h) and up-regulated at 6 and 12 h in HS and HT (Figures 6A, C–I; Table S4). These transcription factors possibly involve different thermotolerance in the two genotypes (Table S4) and might play essential roles in flowering Chinese cabbage heat resistance during the reproductive stage.

Validation of RNA-seq data by quantitative real-time PCR

To verify the results of RNA-seq, ten genes with diverse expression profiles, including up-regulated or down-regulated at all stages and/or regulated in HT or HS, were randomly selected for real-time qPCR to measure expression levels. Table S5 lists the primer sequences of selected genes. The relative expression level was calculated with $2^{-\Delta\Delta CT}$ using *BraActin* as a reference gene (Table S5). As a result, two TFs genes, *WRKY53* and *HsfB-2a*, had similar expression patterns as those in RNA-seq (Figure 6G, I). In brief, all ten genes exhibited the same expression profile, with high correlation coefficients observed between RNA-seq data and RT-qPCR at HS-1h (r = 0.83, P =

TABLE 1 List of top potential differentially expressed genes involved in heat tolerance in flowering Chinese cabbage.

Clusters	Gene id	Log_2 fold-change						Functional annotation	
		HS-1h	HS-6h	HS-12h	HT-1h	HT-6h	HT-12h	Annotation	GO/KEGG pathways enrichment
Cluster3	*BraA07g024750.3C*	9.07	4.65	3.32	7.49	2.69	3.43	Abscisic acid receptor PYL9-like	MAPK signaling pathway - plant (ko04016); Plant hormone signal transduction (ko04075)
Cluster1	*BraA09g028180.3C*	–3.92	–4.92	–6.18	–3.67	–6.00	–7.19	Sodium transporter HKT1-like	
Cluster1	*BraA09g022320.3C*	–4.50	–3.13	–2.66	–4.92	–2.55	3.01	abscisic acid receptor PYR1-like	MAPK signaling pathway - plant (ko04016); Plant hormone signal transduction (ko04075)
Cluster1	*BraA09g047180.3C*	-4.96	-6.50	-2.38	-4.78	-2.22	-3.83	stomatal closure-related actin-binding protein 3	microspherule protein 1 (K11674); cytoskeletal protein binding (GO:0008092)
Cluster3	*BraA10g001200.3C*	3.67	7.01	3.98	-2.12	2.20	2.67	gibberellin 2-beta-dioxygenase 6	Biosynthesis of secondary metabolites (ko01110); oxidoreductase activity (GO:0016491); metal ion binding (GO:0046872)
Cluster2	*BraA10g011520.3C*	-2.31	2.21	3.13	-3.24	2.12	3.06	abscisic acid receptor PYL8-like	MAPK signaling pathway - plant (ko04016); Plant hormone signal transduction (ko04075)
Cluster3	*BraA10g016090.3C*	3.12	5.68	5.87	2.90	3.98	4.63	temperature-induced lipocalin-1-like	apolipoprotein D and lipocalin family protein (K03098); transporter activity (GO:0005215)
Cluster3	*BraA10g028350.3C*	4.58	6.06	4.35	4.03	5.64	4.56	abscisic acid receptor PYL5	MAPK signaling pathway - plant (ko04016); Plant hormone signal transduction (ko04075)
Cluster3	*BraA02g041550.3C*	5.16	4.93	4.36	3.58	3.35	4.59	E3 ubiquitin-protein ligase MIEL1	Ubiquitin mediated proteolysis (ko04120); cation binding (GO:0043169); metal ion binding (GO:0046872)
Cluster1	*BraA05g008340.3C*	-3.79	-8.87	-8.87	-3.12	-8.79	-8.79	indole-3-acetic acid-induced protein ARG7-like	Plant hormone signal transduction (ko04075); response to stimulus (GO:0050896); response to hormone (GO:0009725); response to auxin (GO:0009733)
Cluster1	*BraA06g037940.3C*	-7.17	-10.75	-5.54	-4.92	-3.45	-7.65	pollen-specific protein-like At4g18596	
Cluster1	*BraA07g002070.3C*	-5.62	-5.62	-4.04	-5.09	-3.60	-4.24	putative RING-H2 finger protein ATL49	E3 ubiquitin-protein ligase RNF38/44 [EC:2.3.2.27] (K19041); intrinsic component of membrane (GO:0031224)
Cluster3	*BraA05g042010.3C*	8.06	5.70	8.80	5.97	3.29	4.39	protein DETOXIFICATION 24-like	multidrug resistance protein (K03327); antiporter activity (GO:0015297); transporter activity (GO:0005215)
Cluster1	*BraA08g000300.3C*	-3.10	-4.78	-3.14	-2.98	-4.63	-3.50	cellulose synthase-like protein E1	cellulose synthase A [EC:2.4.1.12] (K10999)
Cluster1	*BraA05g032350.3C*	-3.28	-2.36	-5.58	-2.30	-4.73	-3.55	bidirectional sugar transporter SWEET2-like	solute carrier family 50 (K15382); cell wall organization or biogenesis (GO:0071554); organic substance biosynthetic process (GO:1901576)

HS, heat-sensitive; HT, heat-tolerant.

0.0032), HS-12h (r = 0.86, P = 0.0013), HT-1h (r = 0.88, P = 0.0017), and HT-12 (r = 0.86, P = 0.0028), indicating the consistency of RNA sequencing data (Figure 7).

Discussion

Flowering Chinese cabbage, domesticated from Chinese cabbage with flowering stalk, is a major food due to its high nutrient value (Wang et al., 2016). However, heat stress significantly affects the yield of flowering Chinese cabbage. Thus, developing new varieties with high heat resistance is critical for solving this dilemma. In previous studies, stress-associated genes have been reported and functionally annotated in different vegetable crops under biotic and abiotic stress conditions, including high temperature, salt stress, heavy metal stress, drought, nutrient deficiency, bacterial wilt, fungal stress, and UV-B radiation (Gill et al., 2016; Gill et al., 2017; Cai et al., 2020; Yao et al., 2020; Ikram et al., 2022a; Li et al., 2022). In this study, the comparative transcriptome analysis between the heat treatment and control in HS and HT accessions significantly identified 20,680 DEGs ($|\log_2(\text{foldchange})| \geq 2$, FDR ≤ 0.001) (Figures 2, 3), and 3,205 putative candidate genes involved in response to heat stress in flowering Chinese cabbage (Figure 4; Table S2).

Heat stress affects flowering Chinese cabbage growth and productivity and produces ROS in plant cells, causing oxidative damage. In response to stress, a plant defense mechanism against

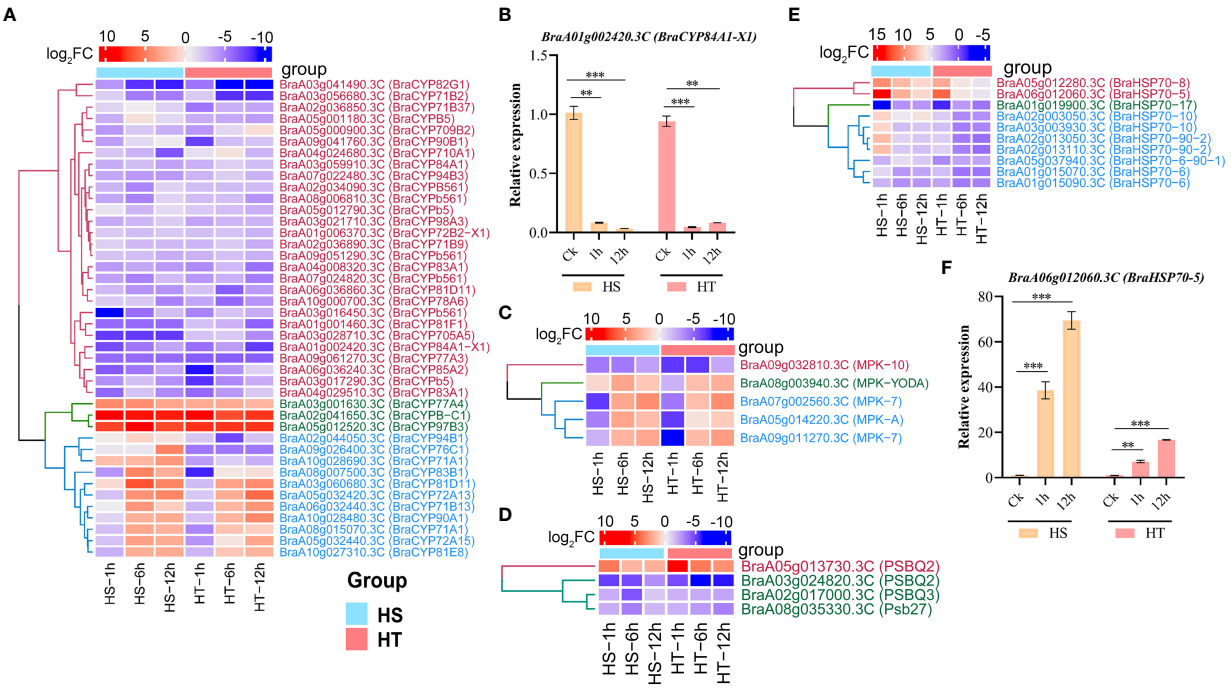

FIGURE 5
Heatmaps of up- and down-regulated genes in heat-sensitive (3T-6) and heat-tolerant (Youlu-501) Chinese flowering cabbage related to stress at different times and confirmation of two DEGs through RT-qPCR analysis. **(A)** Number of DEGs of cytochrome P450 gene family at four heat-stress time points; **(B)** *BraA01g002420.3C* (*BraCYP84A1-X1* cytochrome P450 84A1 isoform X1) showing similar expression pattern in RNA-seq data; Heatmaps of MAPK **(C)**, photosystem II **(D)**, and HSPs **(E)** related genes in HS and HT varieties under heat stress; **(F)** Confirmation of *BraHSP70-5* gene identified through RNA-seq using RT-qPCR analysis. Asterisks indicate significance between treatment and control using Student's t-test at **P < 0.01 and ***P < 0.001.

oxidative damage activated antioxidant enzymes, including SOD, POD, and CAT, that efficiently scavenge ROS (Wahid et al., 2007; Hasanuzzaman et al., 2013). In this study, SOD, POD, and CAT activities significantly increased under stress conditions compared to the control, more so in the HT genotype than the HS genotype (Figure 1A), as reported elsewhere (Wang et al., 2016; Song et al., 2019). Wahid et al. (2007) also measured increasing SOD, POD, and CAT activities in response to stress. Using RNA sequencing, we obtained 21.94–24.90 million raw reads from HS and HT accessions at 0, 1, 6, and 12 h, with 73.06–76.72% of the clean reads mapped to the *B. rapa* reference genome (Table S1) and higher from Chinese cabbage leaf RNA sequencing (Zhao et al., 2013) and flowering Chinese cabbage stalk RNA sequencing (Huang et al., 2017). We compared the expression data of leaves at 1, 6, and 12 h with the control, identifying 10,153, 7,879, 7,662, 13,704, 5,161, and 7,438 DEGs in HS-1h, HS-6h, HS-12h, HT-1h, HT-6h, and HT-12h, respectively (Figures 2A–C). Further, these genes were involved in cell division, cellular process, response to stimulus, primary metabolic process, response to heat, the developmental process involved in reproduction, photosynthesis, detoxification, RNA binding, and auxin homeostasis (Figures 3, S2, S3) in line with previous studies (Wang et al., 2016; Cai et al., 2020; Helal et al., 2021; Lai et al., 2021). In addition, most DEGs were enriched in the MAPK signaling pathway – plant, brassinosteroid biosynthesis, plant–pathogen interaction, plant hormone signal transduction, and circadian rhythm (Figures 3, S4, S5); these results are similar to previous reports (Song et al., 2014a; Song et al., 2021).

Hierarchical clustering analysis identified three clusters containing 1,958, 591, and 556 down-regulated, up- and down-regulated, and up-regulated, respectively (Figure 4; Table S2), involved in response to stimulus, biological regulation, oxidation, reproduction, cellular process, developmental process, and carbon utilization. These findings indicate that heat stress caused oxidative damage, leading to the up-regulation of genes to increase tolerance; for example, *BraA07g024750.3C* and *BraA10g001200.3C* encoded abscisic acid receptor *PYL9*-like and gibberellin 2-beta-dioxygenase 6, respectively (Table 1), and their homologous genes have been functionally characterized to mediate salt stress tolerance in *Arabidopsis* (Hichri et al., 2016) and cassava (Chang et al., 2020). *BraA05g032350.3C* encodes bidirectional sugar transporter SWEET2-like and plays a role in the organic substance biosynthetic process (Table 1). Moreover, cluster 3 DEGs were involved in sugar metabolism and proline/polyamine metabolism (Table S2), with the accumulation of sugar and proline detected as osmolytes, enhancing heat stress resistance

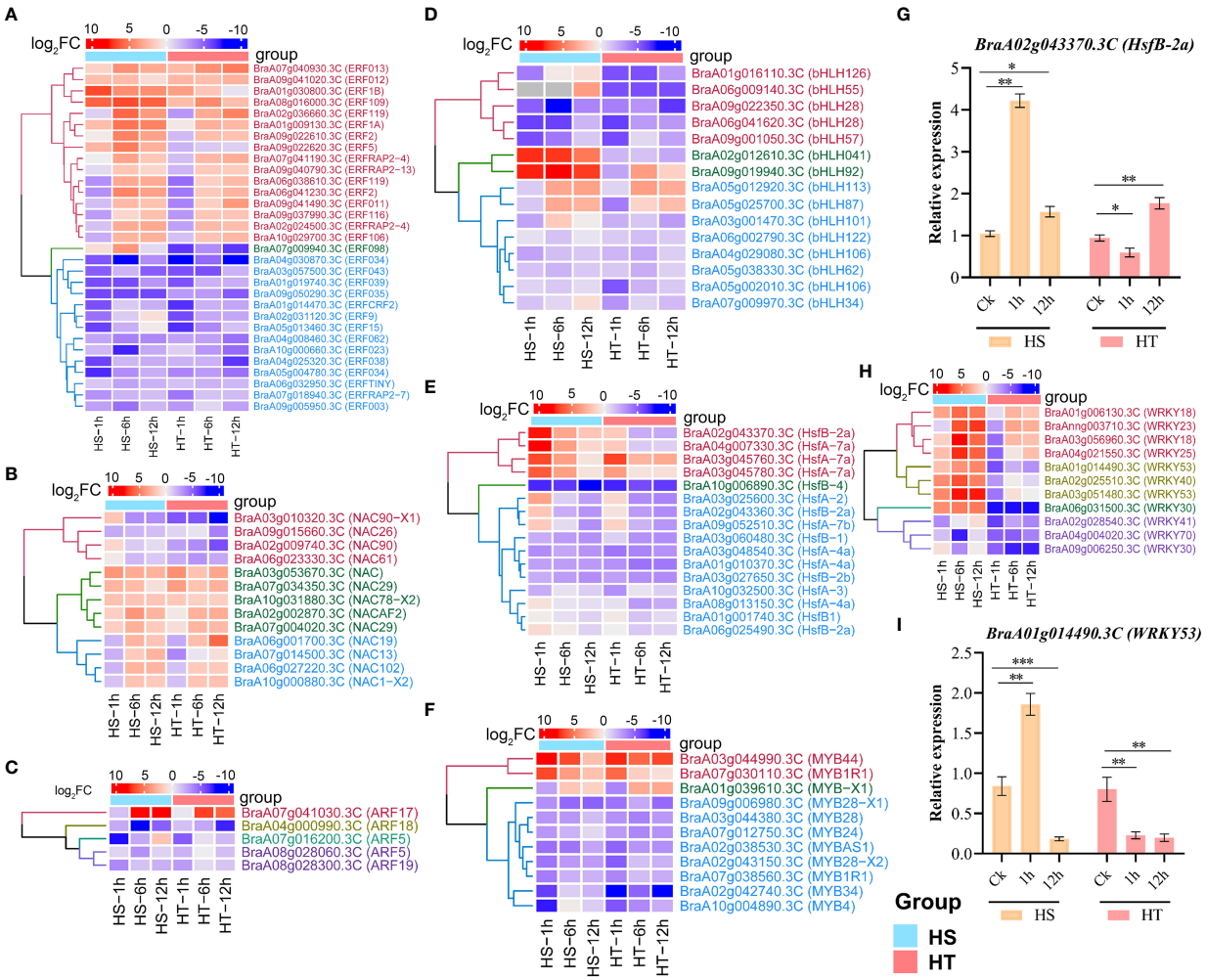

FIGURE 6
Heatmaps of transcription factor families involved in abiotic stress and validation of DEGs in heat-sensitive (3T-6) and heat-tolerant (Youlu-501) flowering Chinese cabbage using RT-qPCR analysis. The up- and down-regulated genes of TF families: **(A)** ERFs, **(B)** NAC, **(C)** ARFs, **(D)** bHLHs, **(E)** HSFs, **(F)** MYBs, and **(H)** WRKYs for different high-temperature treatments; **(G–I)** Confirmation of *HsfB-2a* and *WRKY53* using RT-qPCR. Asterisks indicate significance between treatment and control using Student's t-test at *P < 0.01, **P < 0.01, and ***P < 0.001.

(Wahid et al., 2007; Kumazaki and Suzuki, 2019; Song et al., 2019). The *Sid2-1* mutant was reported in *Arabidopsis*, significantly increasing soluble sugars to improve drought and heat stress (Kumazaki and Suzuki, 2019). Similarly, heat stress increased proline content in leaves of soybean (Amirjani, 2010), tomato (Rivero et al., 2004), chickpea (Chakraborty and Tongden, 2005), and *Arabidopsis* (Zhang and Huang, 2013; Gurrieri et al., 2020; Hoermiller et al., 2022). The cluster 2 DEGs (Figure 4; Table S2) are associated with late embryogenesis abundant protein (Magwanga et al., 2018) and ubiquitin (Qian et al., 2020a), which protect sub-cellular and cellular structures from dehydration and oxidative forces. Therefore, the transcriptomic results were similar to enzymatic activities, and the DEGs related to different proteins in flowering Chinese cabbage might be necessary for heat stress tolerance.

In this study, we identified 42 CYPs DEGs involved in primary and secondary metabolism, including *BraCYP83A1, BraCYP83B1, BraCYP71A1, BraCYP71B13, BraCYP71B2, BraCYP71B37*, and *BraCYP71B9* regulated in HS and HT (Figure 5; Table S3). *BraCYP83A1* was up-regulated at all time points (Figure 5), with a similar result reported in *Arabidopsis* that the *CYP83A1* was involved in flavonoid metabolism (Bilodeau et al., 1999). Similarly, *CYP71A1* genes were up-regulated in *Panicum virgatum* under heat stress and responsible for the synthesis of indole alkaloid (Li et al., 2013) and down-regulated in *Rhazya stricta* at high temperatures (Obaid et al., 2016). One gene (*CYP71A23)* in this study was previously identified using genome-wide association study, which caused pollen sterility in *Brassica napus* under heat stress (Rahaman et al., 2018). Similarly, five MAPK genes were identified in this study, which are critical

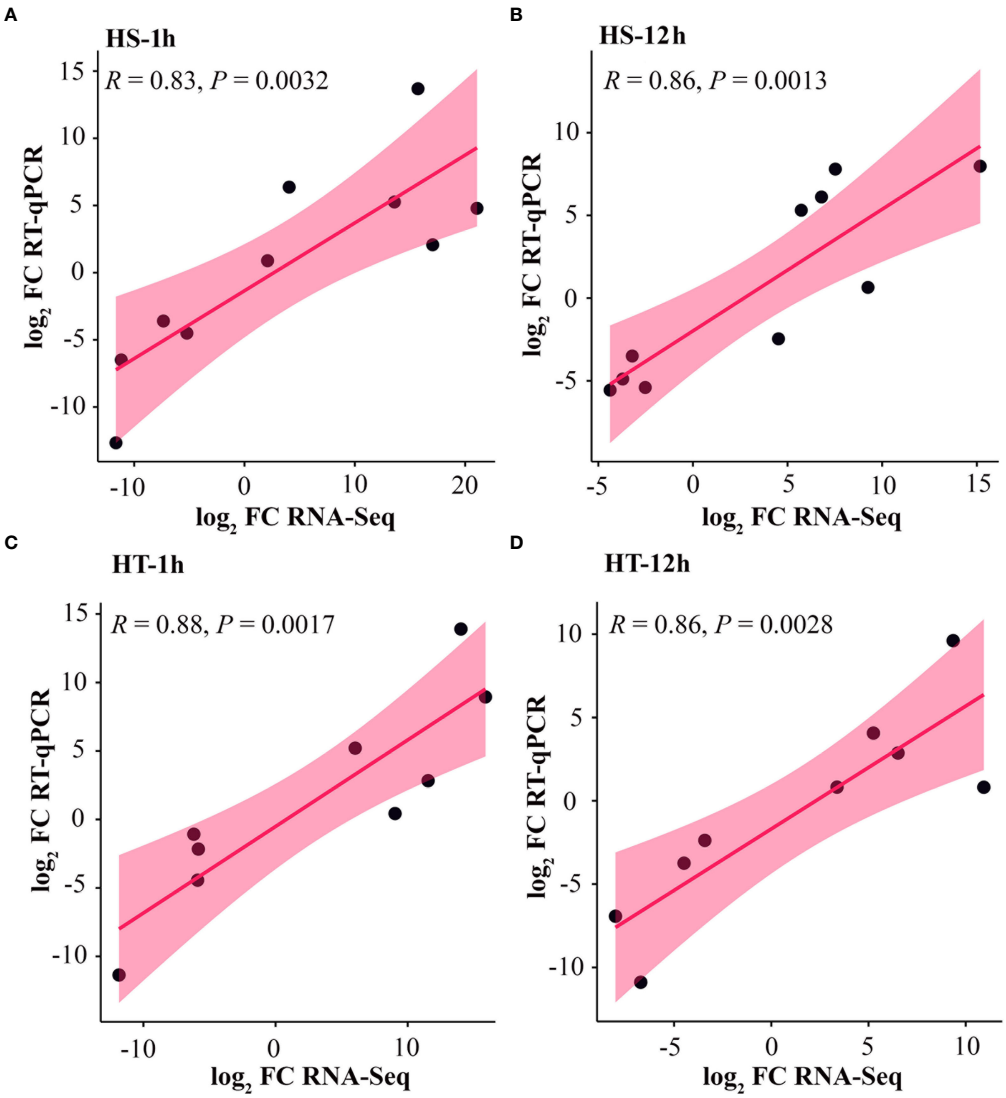

FIGURE 7
Validation of ten differentially expressed genes in heat-sensitive (3T-6) and heat-tolerant (Youlu-501) flowering Chinese cabbage based on RT-qPCR. The RNA-seq and RT-qPCR values in the form of $\log_2$ fold-change were plotted using linear regression analysis at **(A)** HS-1, **(B)** HS-12h, **(C)** HT-1h, and **(D)** HT-12h. *R* and *P* indicate the correlation coefficient and corresponding *P*-value.

regulators of plant growth in stress responses (Agrawal et al., 2002; Rohila and Yang, 2007). TFs are essential regulators of genes, involving many growth, developmental, and stress processes. The published studies have reported that heat stress increased the ethylene response, auxin response, zing finger proteins, MADS-box proteins, AP2 domain, WRKY, and leucine zipper factors (Chen et al., 2012; Zander et al., 2012; Kim et al., 2016; Wang et al., 2016; Gu et al., 2018; Rehman et al., 2021). RNA-seq analysis of HS and HT lines in rice and maize determined ethylene response factors that increased stress tolerance (Thirunavukkarasu et al., 2013; Minami et al., 2018). In this study, 31 ERFs were enriched, with >12 up-regulated at 6 and 12 h, possibly playing a significant role in heat tolerance (Figure 6A). Likewise, five WRKYs (*BraWRKY18, BraWRKY53, BraWRKY23, BraWRKY25*, and *BraWRKY40*) were up-regulated in HS and HT at 6 and 12 h (Figure 5; Table S4). Of these, *WRKY25* was also reported for heat tolerance in *Arabidopsis* (Chen et al., 2012), and *WRKY26* and *WRKY33* were also reported for stress resistance (Chen et al., 2012; Kim et al., 2016; Gu et al., 2018). Moreover, many other TFs, such as MYB, NAC, bHLH, and ARF, were detected (Figure 6; Table S4), indicating that TF families are directly related and enhance heat stress tolerance in flowering Chinese cabbage.

HSPs are expressed more during the initial stage of stress than long-term stress (Singh et al., 2019; Qian et al., 2020b). In this study, only ten DEGs were annotated as HSPs, including *BraHSP70-5, BraHSP70-10, BraHSP70-8*, and *BraHSP70-6* up-regulated at 1h

and *BraHSP70-6-90-1* and *BraHSP70-17* up-regulated at 12h (Figure 5; Table S3). Likewise, Wang et al. (2016) reported that *HSP70* and *HSPB27* were expressed in *B. rapa* after heat stress, with *HSP70* negatively controlling the heat stress response. *HSP70s* have been identified in many vegetables in response to heat stress, such as potato, tomato, cabbage, and pepper (Guo et al., 2016; Lee et al., 2017; Liu et al., 2018). Studies have demonstrated that HSFs are key regulators of HSPs under heat stress (Wang et al., 2016; Liu et al., 2018), with 35 HSF genes in A, B, and C groups reported in Chinese cabbage (Song et al., 2014b). However, 17 BraHSFs genes identified in this study, including *HsfB1, HsfB-2a, HsfA-7a, HsfB-1, HsfA-4a, HsfA-7b)*, and *HsfA-3*, were up-regulated at 1, 6, and 12 h in HS and HT (Figure 6; Table S4). Similarly, Scharf et al. (2012) identified *HSFA2* as a major heat stress factor that induces HSPs expression in stressed plants. Moreover, overexpression of *HSFA2* significantly increased salt, heat, light, and drought stress tolerance (Guo et al., 2016). A tomato *HSFA1-a* was identified as a master regulator for heat response in rice (Mishra et al., 2018). Thus, the present study increased our understanding of DEGs, their roles in stress, and *BraHSF* genes under heat stress.

Conclusion

We compared the transcriptomes of HS and HT varieties of flowering Chinese cabbage under heat stress. Approximately 3,205 genes were differentially expressed, with 1,078 DEGs identified at 1, 6, and 12 h after heat stress in both varieties. Cluster analysis divided these genes into three clusters containing 1,958, 591, and 556 genes, which participated in response to stimulus, cell division, cellular process, heat, programmed cell death, ribosome biogenesis, etc. Finally, 15 potential heat-tolerant genes were identified based on functional annotation and literature search. These results provide useful genetic resources for understanding the heat-tolerance mechanism in flowering Chinese cabbage, and these candidate genes require further functional validation and cloning to determine their actual role in heat tolerance.

Data availability statement

The original contributions presented in the study are publicly available. This data can be found here: NCBI, PRJNA885253.

Author contributions

PG and YX conceived and designed the experiments. JC, YX, MI, and RL performed the experiments and analyzed data. YX, MI, and RL contributed reagents/materials/analysis tools. MI, JC, YX, RL, KS, and PG wrote the paper. All authors contributed to the article and approved the submitted version.

Funding

This work was funded by the Natural Science Foundation of Guangdong Province, China (2019A1515011587).

Acknowledgments

We thank the Guangdong Academy of Agricultural Sciences, China, for providing flowering Chinese cabbage accessions.

Conflict of interest

The authors declare that the research was conducted in the absence of any commercial or financial relationships that could be construed as a potential conflict of interest.

Publisher's note

Supplementary material

The Supplementary Material for this article can be found online at: https://www.frontiersin.org/articles/10.3389/fpls.2022.1077920/full#supplementary-material

References

Aebi, H. (1984). Catalase *in vitro*. *Methods Enzymol.* 105, 121–126. doi: 10.1016/s0076-6879(84)05016-3

Agrawal, G. K., Rakwal, R., and Iwahashi, H. (2002). Isolation of novel rice (*Oryza sativa* l.) multiple stress responsive MAP kinase gene OsMSRMK2 whose mRNA accumulates rapidly in response to environmental cues. *Biochem. Biophys. Res. Commun.* 294, 1009–1016. doi: 10.1016/S0006-291X(02)00571-5

Ali, A., Wu, T., Xu, Z., Riaz, A., Alqudah, A. M., Iqbal, M. Z., et al. (2022). Phytohormones and transcriptome analyses revealed the dynamics involved in spikelet abortion and inflorescence development in rice. *Int. J. Mol. Sci.* 23, 7887. doi: 10.3390/ijms23147887

Amirjani, M. R. (2010). Effect of salinity stress on growth, mineral composition, proline content, antioxidant enzymes of soybean. *Am. J. Plant Physiol.* 5, 350–360. doi: 10.3923/ajpp.2010.350.360

Battisti, D. S., and Naylor, R. L. (2009). Historical warnings of future food insecurity with unprecedented seasonal heat. *Science* 323, 240–244. doi: 10.1126/science.1164363

Bilodeau, P., Udvardi, M. K., Peacock, W. J., and Dennis, E. S. (1999). A prolonged cold treatment-induced cytochrome P450 gene from *Arabidopsis thaliana*. *Plant Cell Environ.* 22, 791–800. doi: 10.1046/j.1365-3040.1999.00444.x

Caers, M., Rudelsheim, P., Van Onckelen, H., and Horemans, S. (1985). Effect of heat stress on photosynthetic activity and chloroplast ultrastructure in correlation with endogenous cytokinin concentration in maize seedlings. *Plant Cell Physiol.* 26, 47–52. doi: 10.1093/oxfordjournals.pcp.a076894

Cai, Z., He, F., Feng, X., Liang, T., Wang, H., Ding, S., et al. (2020). Transcriptomic analysis reveals important roles of lignin and flavonoid biosynthetic pathways in rice thermotolerance during reproductive stage. *Front. Genet.* 11. doi: 10.3389/fgene.2020.562937

Chakraborty, U., and Tongden, C. (2005). Evaluation of heat acclimation and salicylic acid treatments as potent inducers of thermotolerance in *Cicer arietinum* l. *Curr. Sci.* 89, 384–389.

Chang, Y., Bai, Y., Wei, Y., and Shi, H. (2020). CAMTA3 negatively regulates disease resistance through modulating immune response and extensive transcriptional reprogramming in cassava. *Tree Physiol.* 40, 1520–1533. doi: 10.1093/treephys/tpaa093

Chen, J., Li, R., Xia, Y., Bai, G., Guo, P., Wang, Z., et al. (2017). Development of EST-SSR markers in flowering Chinese cabbage (*Brassica campestris* l. ssp. chinensis var. utilis tsen et Lee) based on *de novo* transcriptomic assemblies. *PloS One* 12, e0184736. doi: 10.1371/journal.pone.0184736

Chen, L., Song, Y., Li, S., Zhang, L., Zou, C., and Yu, D. (2012). The role of WRKY transcription factors in plant abiotic stresses. *Biochim. Biophys. Acta - Gene Regul. Mech.* 1819, 120–128. doi: 10.1016/j.bbagrm.2011.09.002

Cock, P. J. A., Fields, C. J., Goto, N., Heuer, M. L., and Rice, P. M. (2009). The Sanger FASTQ file format for sequences with quality scores, and the Solexa/Illumina FASTQ variants. *Nucleic Acids Res.* 38, 1767–1771. doi: 10.1093/nar/gkp1137

Dong, X., Yi, H., Lee, J., Nou, I.-S., Han, C.-T., and Hur, Y. (2015). Global gene-expression analysis to identify differentially expressed genes critical for the heat stress response in *Brassica rapa*. *PloS One* 10, e0130451. doi: 10.1371/journal.pone.0130451

Dossa, K., Diouf, D., and Cissé, N. (2016). Genome-wide investigation of hsf genes in sesame reveals their segmental duplication expansion and their active role in drought stress response. *Front. Plant Sci.* 7. doi: 10.3389/fpls.2016.01522

Fan, Z.-Q., Tan, X.-L., Shan, W., Kuang, J.-F., Lu, W.-J., and Chen, J.-Y. (2017). BrWRKY65, a WRKY transcription factor, is involved in regulating three leaf senescence-associated genes in Chinese flowering cabbage. *Int. J. Mol. Sci.* 18, 1228. doi: 10.3390/ijms18061228

Gill, R. A., Ali, B., Cui, P., Shen, E., Farooq, M. A., Islam, F., et al. (2016). Comparative transcriptome profiling of two *Brassica napus* cultivars under chromium toxicity and its alleviation by reduced glutathione. *BMC Genomics* 17, 885. doi: 10.1186/s12864-016-3200-6

Gill, R. A., Ali, B., Yang, S., Tong, C., Islam, F., Gill, M. B., et al. (2017). Reduced glutathione mediates pheno-ultrastructure, kinome and transportome in chromium-induced *Brassica napus* l. *Front. Plant Sci.* 8. doi: 10.3389/fpls.2017.02037

Grover, A., Mittal, D., Negi, M., and Lavania, D. (2013). Generating high temperature tolerant transgenic plants: Achievements and challenges. *Plant Sci.* 205–206, 38–47. doi: 10.1016/j.plantsci.2013.01.005

Guo, M., Liu, J.-H., Ma, X., Zhai, Y.-F., Gong, Z.-H., and Lu, M.-H. (2016). Genome-wide analysis of the Hsp70 family genes in pepper (*Capsicum annuum* l.) and functional identification of CaHsp70-2 involvement in heat stress. *Plant Sci.* 252, 246–256. doi: 10.1016/j.plantsci.2016.07.001

Gurrieri, L., Merico, M., Trost, P., Forlani, G., and Sparla, F. (2020). Impact of drought on soluble sugars and free proline content in selected arabidopsis mutants. *Biol. (Basel).* 9, 1–14. doi: 10.3390/biology9110367

Gu, L., Wei, H., Wang, H., Su, J., and Yu, S. (2018). Characterization and functional analysis of GhWRKY42, a group IId WRKY gene, in upland cotton (*Gossypium hirsutum* l.). *BMC Genet.* 19, 48. doi: 10.1186/s12863-018-0653-4

Hasanuzzaman, M., Nahar, K., Alam, M. M., Roychowdhury, R., and Fujita, M. (2013). Physiological, biochemical, and molecular mechanisms of heat stress tolerance in plants. *Int. J. Mol. Sci.* 14, 9643–9684. doi: 10.3390/ijms14059643

Helal, M., Gill, R. A., Tang, M., Yang, L., Hu, M., Yang, L., et al. (2021). SNP- and haplotype-based GWAS of flowering-related traits in *Brassica napus*. *Plants* 10, 2475. doi: 10.3390/plants10112475

Hichri, I., Muhovski, Y., Clippe, A., Žižková, E., Dobrev, P. I., Motyka, V., et al. (2016). SlDREB2, a tomato dehydration-responsive element-binding 2 transcription factor, mediates salt stress tolerance in tomato and arabidopsis. *Plant Cell Environ.* 39, 62–79. doi: 10.1111/pce.12591

Hoermiller, I. I., Funck, D., Schönewolf, L., May, H., and Heyer, A. G. (2022). Cytosolic proline is required for basal freezing tolerance in arabidopsis. *Plant Cell Environ.* 45, 147–155. doi: 10.1111/pce.14196

Huang, X., Lei, Y., Guan, H., Hao, Y., Liu, H., Sun, G., et al. (2017). Transcriptomic analysis of the regulation of stalk development in flowering Chinese cabbage (*Brassica campestris*) by RNA sequencing. *Sci. Rep.* 7, 15517. doi: 10.1038/s41598-017-15699-6

Ikram, M., Han, X., Zuo, J. F., Song, J., Han, C. Y., Zhang, Y. W., et al. (2020). Identification of QTNs and their candidate genes for 100-seed weight in soybean (*Glycine max* l.) using multi-locus genome-wide association studies. *Genes (Basel).* 11, 1–22. doi: 10.3390/genes11070714

Ikram, M., Lai, R., Xia, Y., Li, R., Zhao, W., Siddique, K. H. M., et al. (2022a). Genetic dissection of tobacco (*Nicotiana tabacum* l.) plant height using single-locus and multi-locus genome-wide association studies. *Agronomy* 12, 1047. doi: 10.3390/agronomy12051047

Ikram, M., Xiao, J., Li, R., Xia, Y., Zhao, W., Yuan, Q., et al. (2022b). Identification of superior haplotypes and candidate genes for yield-related traits in tobacco (*Nicotiana tabacum* l.) using association mapping. *Ind. Crops Prod.* 189, 115886. doi: 10.1016/j.indcrop.2022.115886

Jones, P. D., New, M., Parker, D. E., Martin, S., and Rigor, I. G. (1999). Surface air temperature and its changes over the past 150 years. *Rev. Geophys.* 37, 173–199. doi: 10.1029/1999RG900002

Jung, Y. J., Go, J. Y., Lee, H. J., Park, J. S., Kim, J. Y., Lee, Y. J., et al. (2021). Overexpression of orange gene (OsOr-R115H) enhances heat tolerance and defense-related gene expression in rice (*Oryza sativa* l.). *Genes (Basel).* 12, 1891. doi: 10.3390/genes12121891

Kanehisa, M., and Goto, S. (2000). KEGG: Kyoto encyclopedia of genes and genomes. *Nucleic Acids Res.* 28, 27–30. doi: 10.1093/nar/28.1.27

Kim, D., Langmead, B., and Salzberg, S. L. (2015). HISAT: A fast spliced aligner with low memory requirements. *Nat. Methods* 12, 357–360. doi: 10.1038/nmeth.3317

Kim, C. Y., Vo, K. T. X., Nguyen, C. D., Jeong, D. H., Lee, S. K., Kumar, M., et al. (2016). Functional analysis of a cold-responsive rice WRKY gene, *OsWRKY71*. *Plant Biotechnol. Rep.* 10, 13–23. doi: 10.1007/s11816-015-0383-2

Kono, Y. (1978). Generation of superoxide radical during autoxidation of hydroxylamine and an assay for superoxide dismutase. *Arch. Biochem. Biophys.* 186, 189–195. doi: 10.1016/0003-9861(78)90479-4

Kotak, S., Larkindale, J., Lee, U., von Koskull-Döring, P., Vierling, E., and Scharf, K. D. (2007). Complexity of the heat stress response in plants. *Curr. Opin. Plant Biol.* 10, 310–316. doi: 10.1016/j.pbi.2007.04.011

Kreps, J. A., Wu, Y., Chang, H. S., Zhu, T., Wang, X., and Harper, J. F. (2002). Transcriptome changes for arabidopsis in response to salt, osmotic, and cold stress. *Plant Physiol.* 130, 2129–2141. doi: 10.1104/pp.008532

Kumar, L., and Futschik, M. E. (2007). Mfuzz: A software package for soft clustering of microarray data. *Bioinformation* 2, 5–7. doi: 10.6026/97320630002005

Kumazaki, A., and Suzuki, N. (2019). Enhanced tolerance to a combination of heat stress and drought in arabidopsis plants deficient in ICS1 is associated with modulation of photosynthetic reaction center proteins. *Physiol. Plant* 165, 232–246. doi: 10.1111/ppl.12809

Lai, R., Ikram, M., Li, R., Xia, Y., Yuan, Q., Zhao, W., et al. (2021). Identification of novel quantitative trait nucleotides and candidate genes for bacterial wilt resistance in tobacco (*Nicotiana tabacum* l.) using genotyping-by-sequencing and multi-locus genome-wide association studies. *Front. Plant Sci.* 12. doi: 10.3389/fpls.2021.744175

Langmead, B., and Salzberg, S. L. (2012). Fast gapped-read alignment with bowtie 2. *Nat. Methods* 9, 357–359. doi: 10.1038/nmeth.1923

Lee, S. S., Jung, W. Y., Park, H. J., Lee, A., Kwon, S.-Y., Kim, H.-S., et al. (2017). Genome-wide analysis of alternative splicing in an inbred cabbage (*Brassica oleracea* l.) line 'HO' in response to heat stress. *Curr. Genomics* 19, 12–20. doi: 10.2174/1389202918666170705151901

Li, B., and Dewey, C. N. (2011). RSEM: accurate transcript quantification from RNA-seq data with or without a reference genome. *BMC Bioinf.* 12, 323. doi: 10.1186/1471-2105-12-323

Li, H., Ikram, M., Xia, Y., Li, R., Yuan, Q., Zhao, W., et al. (2022). Genome-wide identification and development of InDel markers in tobacco (*Nicotiana tabacum* l.) using RAD-seq. *Physiol. Mol. Biol. Plants* 28, 1077–1089. doi: 10.1007/s12298-022-01187-3

Liu, J., Pang, X., Cheng, Y., Yin, Y., Zhang, Q., Su, W., et al. (2018). The Hsp70 gene family in *Solanum tuberosum*: Genome-wide identification, phylogeny, and expression patterns. *Sci. Rep.* 8, 16628. doi: 10.1038/s41598-018-34878-7

Li, Y.-F., Wang, Y., Tang, Y., Kakani, V. G., and Mahalingam, R. (2013). Transcriptome analysis of heat stress response in switchgrass (*Panicum virgatum* l.). *BMC Plant Biol.* 13, 153. doi: 10.1186/1471-2229-13-153

Li, P.-S., Yu, T.-F., He, G.-H., Chen, M., Zhou, Y.-B., Chai, S.-C., et al. (2014). Genome-wide analysis of the hsf family in soybean and functional identification of *GmHsf-34* involvement in drought and heat stresses. *BMC Genomics* 15, 1009. doi: 10.1186/1471-2164-15-1009

Lobell, D. B., Burke, M. B., Tebaldi, C., Mastrandrea, M. D., Falcon, W. P., and Naylor, R. L. (2008). Prioritizing climate change adaptation needs for food security in 2030. *Science* 319, 607–610. doi: 10.1126/science.1152339

Love, M. I., Huber, W., and Anders, S. (2014). Moderated estimation of fold change and dispersion for RNA-seq data with DESeq2. *Genome Biol.* 15, 550. doi: 10.1186/s13059-014-0550-8

Magwanga, R. O., Lu, P., Kirungu, J. N., Lu, H., Wang, X., Cai, X., et al. (2018). Characterization of the late embryogenesis abundant (LEA) proteins family and their role in drought stress tolerance in upland cotton. *BMC Genet.* 19, 6. doi: 10.1186/s12863-017-0596-1

Minami, A., Yano, K., Gamuyao, R., Nagai, K., Kuroha, T., Ayano, M., et al. (2018). Time-course transcriptomics analysis reveals key responses of submerged deepwater rice to flooding. *Plant Physiol.* 176, 3081–3102. doi: 10.1104/pp.17.00858

Mishra, M. K., Chaturvedi, P., Singh, R., Singh, G., Sharma, L. K., Pandey, V., et al. (2013). Overexpression of *WsSGTL1* gene of withania somnifera enhances salt tolerance, heat tolerance and cold acclimation ability in transgenic arabidopsis plants. *PloS One* 8, e63064. doi: 10.1371/journal.pone.0063064

Mishra, N., Srivastava, A. P., Esmaeili, N., Hu, W., and Shen, G. (2018). Overexpression of the rice gene *OsSIZ1* in arabidopsis improves drought-, heat-, and salt-tolerance simultaneously. *PloS One* 13, e0201716. doi: 10.1371/journal.pone.0201716

Nakashima, K., Yamaguchi-Shinozaki, K., and Shinozaki, K. (2014). The transcriptional regulatory network in the drought response and its crosstalk in abiotic stress responses including drought, cold, and heat. *Front. Plant Sci.* 5. doi: 10.3389/fpls.2014.00170

Nover, L., Bharti, K., Döring, P., Mishra, S. K., Ganguli, A., and Scharf, K. D. (2001). Arabidopsis and the heat stress transcription factor world: How many heat stress transcription factors do we need? *Cell Stress Chaperones* 6, 177–189. doi: 10.1379/1466-1268(2001)006<0177:aathst>2.0.co;2

Obaid, A. Y., Sabir, J. S. M., Atef, A., Liu, X., Edris, S., El-Domyati, F. M., et al. (2016). Analysis of transcriptional response to heat stress in *Rhazya stricta*. *BMC Plant Biol.* 16, 252. doi: 10.1186/s12870-016-0938-6

Pang, T., Ye, C.-Y., Xia, X., and Yin, W. (2013). *De novo* sequencing and transcriptome analysis of the desert shrub, *Ammopiptanthus mongolicus*, during cold acclimation using Illumina/Solexa. *BMC Genomics* 14, 488. doi: 10.1186/1471-2164-14-488

Qian, Y., Cao, L., Zhang, Q., Amee, M., Chen, K., and Chen, L. (2020b). SMRT and illumina RNA sequencing reveal novel insights into the heat stress response and crosstalk with leaf senescence in tall fescue. *BMC Plant Biol.* 20, 366. doi: 10.1186/s12870-020-02572-4

Qian, H., Zhang, Y., Wu, B., Wu, S., You, S., Zhang, N., et al. (2020a). Structure and function of HECT E3 ubiquitin ligases and their role in oxidative stress. *J. Transl. Intern. Med.* 8, 71–79. doi: 10.2478/jtim-2020-0012

Rahaman, M., Mamidi, S., and Rahman, M. (2018). Genome-wide association study of heat stress-tolerance traits in spring-type *Brassica napus* l. under controlled conditions. *Crop J.* 6, 115–125. doi: 10.1016/j.cj.2017.08.003

Rehman, A., Azhar, M. T., Hinze, L., Qayyum, A., Li, H., Peng, Z., et al. (2021). Insight into abscisic acid perception and signaling to increase plant tolerance to abiotic stress. *J. Plant Interact.* 16, 222–237. doi: 10.1080/17429145.2021.1925759

Rivero, R. M., Ruiz, J. M., and Romero, L. M. (2004). Importance of n source on heat stress tolerance due to the accumulation of proline and quaternary ammonium compounds in tomato plants. *Plant Biol.* 6, 702–707. doi: 10.1055/s-2004-821293

Rohila, J. S., and Yang, Y. (2007). Rice mitogen-activated protein kinase gene family and its role in biotic and abiotic stress response. *J. Integr. Plant Biol.* 49, 751–759. doi: 10.1111/j.1744-7909.2007.00501.x

Rosenzweig, C., Elliott, J., Deryng, D., Ruane, A. C., Müller, C., Arneth, A., et al. (2014). Assessing agricultural risks of climate change in the 21st century in a global gridded crop model intercomparison. *Proc. Natl. Acad. Sci. U. S. A.* 111, 3268–3273. doi: 10.1073/pnas.1222463110

Scharf, K. D., Berberich, T., Ebersberger, I., and Nover, L. (2012). The plant heat stress transcription factor (Hsf) family: Structure, function and evolution. *Biochim. Biophys. Acta - Gene Regul. Mech.* 1819, 104–119. doi: 10.1016/j.bbagrm.2011.10.002

Singh, D., Singh, C. K., Taunk, J., Jadon, V., Pal, M., and Gaikwad, K. (2019). Genome wide transcriptome analysis reveals vital role of heat responsive genes in regulatory mechanisms of lentil (*Lens culinaris medikus*). *Sci. Rep.* 9, 12976. doi: 10.1038/s41598-019-49496-0

Song, X., Hu, J., Wu, T., Yang, Q., Feng, X., Lin, H., et al. (2021). Comparative analysis of long noncoding RNAs in angiosperms and characterization of long noncoding RNAs in response to heat stress in Chinese cabbage. *Hortic. Res.* 8, 48. doi: 10.1038/s41438-021-00484-4

Song, X., Li, Y., Liu, T., Duan, W., Huang, Z., Wang, L., et al. (2014a). Genes associated with agronomic traits in non-heading Chinese cabbage identified by expression profiling. *BMC Plant Biol.* 14, 71. doi: 10.1186/1471-2229-14-71

Song, X., Liu, G., Duan, W., Liu, T., Huang, Z., Ren, J., et al. (2014b). Genome-wide identification, classification and expression analysis of the heat shock transcription factor family in Chinese cabbage. *Mol. Genet. Genomics* 289, 541–551. doi: 10.1007/s00438-014-0833-5

Song, X., Liu, G., Huang, Z., Duan, W., Tan, H., Li, Y., et al. (2016). Temperature expression patterns of genes and their coexpression with LncRNAs revealed by RNA-seq in non-heading Chinese cabbage. *BMC Genomics* 17, 297. doi: 10.1186/s12864-016-2625-2

Song, Q., Yang, F., Cui, B., Li, J., Zhang, Y., Li, H., et al. (2019). Physiological and molecular responses of two Chinese cabbage genotypes to heat stress. *Biol. Plant* 63, 548–555. doi: 10.32615/bp.2019.097

Swindell, W. R., Huebner, M., and Weber, A. P. (2007). Transcriptional profiling of arabidopsis heat shock proteins and transcription factors reveals extensive overlap between heat and non-heat stress response pathways. *BMC Genomics* 8, 125. doi: 10.1186/1471-2164-8-125

Thirunavukkarasu, N., Hossain, F., Mohan, S., Shiriga, K., Mittal, S., Sharma, R., et al. (2013). Genome-wide expression of transcriptomes and their co-expression pattern in subtropical maize (*Zea mays* l.) under waterlogging stress. *PloS One* 8, 125, e70433. doi: 10.1371/journal.pone.0070433

Wahid, A., Gelani, S., Ashraf, M., and Foolad, M. R. (2007). Heat tolerance in plants: An overview. *Environ. Exp. Bot.* 61, 199–223. doi: 10.1016/j.envexpbot.2007.05.011

Wang, A., Hu, J., Huang, X., Li, X., Zhou, G., and Yan, Z. (2016). Comparative transcriptome analysis reveals heat-responsive genes in Chinese cabbage (*Brassica rapa* ssp. chinensis). *Front. Plant Sci.* 7. doi: 10.3389/fpls.2016.00939

Wang, C.-T., Ru, J.-N., Liu, Y.-W., Li, M., Zhao, D., Yang, J.-F., et al. (2018). Maize WRKY transcription factor ZmWRKY106 confers drought and heat tolerance in transgenic plants. *Int. J. Mol. Sci.* 19, 3046. doi: 10.3390/ijms19103046

Wang, X., Wang, H., Wang, J., Sun, R., Wu, J., Liu, S., et al. (2011). The genome of the mesopolyploid crop species *Brassica rapa*. *Nat. Genet.* 43, 1035–1040. doi: 10.1038/ng.919

Winfield, M. O., Lu, C., Wilson, I. D., Coghill, J. A., and Edwards, K. J. (2010). Plant responses to cold: transcriptome analysis of wheat. *Plant Biotechnol. J.* 8, 749–771. doi: 10.1111/j.1467-7652.2010.00536.x

Xue, Y., Peng, R., Xiong, A., Li, X., Zha, D., and Yao, Q. (2010). Over-expression of heat shock protein gene *hsp26* in *Arabidopsis thaliana* enhances heat tolerance. *Biol. Plant* 54, 105–111. doi: 10.1007/s10535-010-0015-1

Xu, Q., Xu, X., Shi, Y., Xu, J., and Huang, B. (2014). Transgenic tobacco plants overexpressing a grass *PpEXP1* gene exhibit enhanced tolerance to heat stress. *PloS One* 9, e100792. doi: 10.1371/journal.pone.0100792

Yang, X., Zhu, W., Zhang, H., Liu, N., and Tian, S. (2016). Heat shock factors in tomatoes: genome-wide identification, phylogenetic analysis and expression profiling under development and heat stress. *PeerJ* 4, e1961. doi: 10.7717/peerj.1961

Yao, S., Liang, F., Gill, R. A., Huang, J., Cheng, X., Liu, Y., et al. (2020). A global survey of the transcriptome of allopolyploid brassica napus based on single-molecule long-read isoform sequencing and illumina-based RNA sequencing data. *Plant J.* 103, 843–857. doi: 10.1111/tpj.14754

Yoshinaga, K., Arimura, S. I., Niwa, Y., Tsutsumi, N., Uchimiya, H., and Kawai-Yamada, M. (2005). Mitochondrial behaviour in the early stages of ROS stress leading to cell death in *Arabidopsis thaliana*. *Ann. Bot.* 96, 337–342. doi: 10.1093/aob/mci181

Yu, E., Fan, C., Yang, Q., Li, X., Wan, B., Dong, Y., et al. (2014). Identification of heat responsive genes in *Brassica napus* siliques at the seed-filling stage through transcriptional profiling. *PloS One* 9, e101914. doi: 10.1371/journal.pone.0101914

Yu, X., Wang, H., Lu, Y., De Ruiter, M., Cariaso, M., Prins, M., et al. (2012). Identification of conserved and novel microRNAs that are responsive to heat stress in *Brassica rapa*. *J. Exp. Bot.* 63, 1025–1038. doi: 10.1093/jxb/err337

Zander, M., Chen, S., Imkampe, J., Thurow, C., and Gatz, C. (2012). Repression of the *arabidopsis thaliana* jasmonic acid/ethylene-induced defense pathway by tga-interacting glutaredoxins depends on their c-terminal alwl motif. *Mol. Plant* 5, 831–840. doi: 10.1093/mp/ssr113

Zhang, Z., and Huang, R. (2013). Analysis of malondialdehyde, chlorophyll proline, soluble sugar, and glutathione content in arabidopsis seedling. *BIO-PROTOCOL* 3, 817. doi: 10.21769/BioProtoc.817

Zhao, Q., Zou, J., Meng, J., Mei, S., and Wang, J. (2013). Tracing the transcriptomic changes in synthetic trigenomic allohexaploids of brassica using an rna-seq approach. *PloS One* 8, e68883. doi: 10.1371/journal.pone.0068883

frontiers | Frontiers in Plant Science

TYPE Original Research
PUBLISHED 15 December 2022
DOI 10.3389/fpls.2022.1072931

OPEN ACCESS

EDITED BY
Nianjun Teng,
Nanjing Agricultural University, China

REVIEWED BY
Zhaogeng Lu,
Yangzhou University, China
Jianmin Bian,
Jiangxi Agricultural University, China

*CORRESPONDENCE
Zhaojiang Zuo
zuozhaojiang@126.com

†These authors have contributed equally to this work

SPECIALTY SECTION
This article was submitted to Plant Abiotic Stress, a section of the journal Frontiers in Plant Science

RECEIVED 18 October 2022
ACCEPTED 28 November 2022
PUBLISHED 15 December 2022

CITATION
Xu C, Wang B, Luo Q, Ma Y, Zheng T, Wang Y, Cai Y and Zuo Z (2022) The uppermost monoterpenes improving *Cinnamomum camphora* thermotolerance by serving signaling functions. *Front. Plant Sci.* 13:1072931. doi: 10.3389/fpls.2022.1072931

The uppermost monoterpenes improving *Cinnamomum camphora* thermotolerance by serving signaling functions

Chenyi Xu[1,2†], Bin Wang[1,2†], Qingyun Luo[1,2†], Yuandan Ma[1,2], Tiefeng Zheng[1,2], Yingying Wang[1,2], Yuyan Cai[1,2] and Zhaojiang Zuo[1,2*]

[1]State Key Laboratory of Subtropical Silviculture, Zhejiang A&F University, Hangzhou, China, [2]Zhejiang Provincial Key Laboratory of Forest Aromatic Plants-based Healthcare Functions, Zhejiang A&F University, Hangzhou, China

Terpenes serve important functions in enhancing plant thermotolerance. *Cinnamomum camphora* mainly has eucalyptol (EuL), camphor (CmR), linalool (LnL) and borneol (BeL) chemotypes basing on the uppermost monoterpenes. To reveal the thermotolerance mechanisms of these uppermost monoterpenes (eucalyptol, camphor, linalool, and borneol) in *C. camphora*, we surveyed the ROS metabolism and photosynthesis in the 4 chemotypes fumigated with the corresponding uppermost monoterpene after fosmidomycin (Fos) inhibiting monoterpene synthesis under high temperature at 38°C (Fos+38°C+monoterpene), and investigated the related gene expression in EuL and CmR. Meanwhile, the thermotolerance differences among the 4 uppermost monoterpenes were analyzed. In contrast to normal temperature (28°C), ROS levels and antioxidant enzyme activities in the 4 chemotypes increased under 38°C, and further increased in the treatment with Fos inhibiting monoterpene synthesis at 38°C (Fos+38°C), which may be caused by the alterations in expression of the genes related with non-enzymatic and enzymatic antioxidant formation according to the analyses in EuL and CmR. Compared with Fos+38°C treatment, Fos+38°C+monoterpene treatments lowered ROS levels and antioxidant enzyme activities for the increased non-enzymatic antioxidant gene expression and decreased enzymatic antioxidant gene expression, respectively. High temperature at 38°C reduced the chlorophyll and carotenoid content as well as photosynthetic abilities, which may result from the declined expression of the genes associated with photosynthetic pigment biosynthesis, light reaction, and carbon fixation. Fos+38°C treatment aggravated the reduction. In contrast to Fos+38°C treatment, Fos+38°C+monoterpene treatments increased photosynthetic pigment content and improved photosynthetic abilities by up-regulating related gene expression. Among the 4 uppermost monoterpenes, camphor showed strong abilities in lowering ROS and maintaining photosynthesis, while eucalyptol showed weak abilities. This was consistent with the recovery effects

of the gene expression in the treatments with camphor and eucalyptol fumigation. Therefore, the uppermost monoterpenes can enhance *C. camphora* thermotolerance as signaling molecules, and may have differences in the signaling functions.

KEYWORDS

***Cinnamomum camphora*, gene expression, photosynthesis, reactive oxygen species, thermotolerance mechanism, uppermost monoterpene**

1 Introduction

Terpenes are one of the major group of volatile organic compounds (VOCs) released from plants (Holopainen and Blande, 2013), of which isoprene, monoterpenes and diterpenes are formed *via* methylerythritol-4-phosphate pathway (MEP) in plastids, and sesquiterpenes are formed *via* mevalonate pathway (MVA) in cytoplasm (Zuo, 2019). The formation and emission of terpenes are regulated by environmental conditions, such as temperature, CO_2, water, light, insect feeding (Zuo et al., 2019; Zheng et al., 2020; Tian et al., 2021). For the emitters, terpenes contribute to floral scents, fruit aromas and crop quality, and play important roles in attracting pollinators and seed dispersers (Mostafa et al., 2022). In ecosystems, terpenes not only serve important functions in ecological relationships between emitters and other plants or insects (Llusia et al., 2013; Vivaldo et al., 2017), but also play essential roles in protecting emitters against various stresses (Holopainen, 2011; Zuo, 2019).

Climate warming is one of global challenges not only for humans but also for plants, as high temperature seriously impacts plants by inducing reactive oxygen species (ROS) accumulation and damaging photosystems (Mathur et al., 2014; Wang et al., 2014). It is widely reported that high temperature can promote terpene emission from plants (Jardine et al., 2017; Guidolotti et al., 2019). Meanwhile, the terpene emission is beneficial to plant thermotolerance (Holopainen and Blande, 2013; Zuo et al., 2017; Tian et al., 2020). Isoprene-emitting *Arabidopsis thaliana* transformed with isoprene synthase gene (*ISPS*) enhanced the tolerance to high temperature at 40°C and even 60°C (Loivamäki et al., 2007; Sasaki et al., 2007; Zuo et al., 2019). After knocking down the *ISPS*, grey poplar (*Populus pruinosa* Schrenk) decreased photosystem II (PSII) efficiency and CO_2 assimilation rate in exposure to high temperature (Behnke et al., 2007). When isoprene emission from *Vismia guianensis* was inhibited by fosmidomycin (Fos) blocking MEP pathway, the plant reduced PSII efficiency under high temperature (Rodrigues et al., 2020). In fumigation with monoterpenes, *Quercus ilex* (Loreto et al., 1998; Peñuelas and Llusià, 2002) and *Q. suber* (Delfine et al., 2000) improved thermotolerance by declining leaf damage and maintaining photosynthetic abilities. In addition, monoterpenes and isoprene can also enhance plant tolerance to O_3, as blocking their synthesis by Fos resulted in ROS accumulation and photosynthesis reduction under O_3 stress (Loreto and Velikova, 2001; Loreto et al., 2004).

For the thermotolerance mechanisms of isoprene and monoterpenes, they has been mainly hypothesized that these small molecules can stabilize chloroplast membranes by intercalating into membranes against leakiness, and directly quench ROS as antioxidants (Sharkey et al., 2008; Velikova et al., 2011; Zuo et al., 2017). However, isoprene cannot dissolve into cellular membranes in great quantity, and is not involved in the formation of thylakoid membrane acyl lipids (Harvey et al., 2015). Meanwhile, there is a lack of an *in vivo* evidence about isoprene and monoterpenes with very low concentration quenching ROS in plant cells. Thus, the two hypotheses about the thermotolerance mechanisms are suspected by more and more people.

Recently, a new role about isoprene and monoterpenes regulating gene expression has been reported. In myrcene or ocimene fumigation, *A. thaliana* up-regulated the expression of the genes as transcription factors or involving in stress or defense responses (Godard et al., 2008). Riedlmeier et al. (2017) and Wenig et al. (2019) found that α-pinene and β-pinene fumigation can raise expression of the genes related with salicylic acid-mediated innate immune responses. In exposure to isoprene, *A. thaliana* changed expression of the genes that coded for proteins functionally associated with flavonoid and phenylpropanoid biosynthesis, cell wall synthesis, photosynthetic light reaction, stress responses, etc. (Harvey and Sharkey, 2016). When *A. thaliana* and tobacco (*Nicotiana tabacum*) were transferred into *ISPS* to become isoprene emitters, altered expression was found in the genes related with signaling networks and growth regulators, and up-regulated expression was found in the genes related with stress tolerance (Zuo et al., 2019). These findings demonstrate that monoterpenes and isoprene should play important signaling

roles in plant tolerating stresses (Lantz et al., 2019; Zuo et al., 2019; Tian et al., 2020).

Cinnamomum camphora (L.) J. Presl releases a wide spectrum of terpenes, and is used as Chinese herbal medicine, a flavor and fragrance agent, and excellent evergreen tree species for landscaping, etc. (Shi et al., 2016; Li et al., 2018; Yakefu et al., 2018). This species has 4 main chemotypes, including eucalyptol (EuL), camphor (CmR), linalool (LnL) and borneol (BeL) chemotypes (Luo et al., 2021). During one year, the 4 chemotypes of *C. camphora* improved monoterpene emission in hot months by raising expression of the genes associated with monoterpene synthesis (Tian et al., 2021). *C. camphora* is widely cultivated in southern China, an area frequently harmed by high temperature (Ma et al., 2019). In outdoor experiments, ROS accumulation and photosynthetic ability decline were found in the 4 chemotypes of adult *C. camphora* with inhibiting monoterpene synthesis under high temperature weather (Xu et al., 2022). Similar results were also found in indoor seedlings of EuL under high temperature, suggesting that monoterpene emission is beneficial to the plant tolerating high temperature (Zuo et al., 2017). When monoterpene synthesis in adult CmR was blocked by Fos, the fumigation with terpinene and β-pinene enhanced the plant thermotolerance by altering expression of 73 genes, demonstrating that the 2 monoterpenes may act as signals to enhance the plant thermotolerance (Tian et al., 2020).

Eucalyptol, camphor, linalool and borneol are the uppermost monoterpenes of *C. camphora*. Their emission amount more than 50% of total monoterpene emission amount in the corresponding chemotype, and seriously declined by more than 91% when Fos blocked the monoterpene synthesis (Tian et al., 2021). However, it is still unknown the roles of these uppermost monoterpenes in *C. camphora* tolerating high temperature. Therefore, in the present study, the ROS metabolism and photosynthetic abilities were investigated in the 4 main chemotypes of *C. camphora* that were fumigated with the corresponding uppermost monoterpenes under high temperature after Fos blocking monoterpene synthesis. The related gene expression was analyzed in EuL and CmR. Meanwhile, the thermotolerance differences among the uppermost monoterpenes were analyzed. The present findings not only uncover the thermotolerance mechanisms of the uppermost monoterpenes in *C. camphora*, but also provide a solid evidence for the new insight that monoterpenes and isoprene serve signaling functions in plants tolerating high temperature.

2 Materials and methods

2.1 Monoterpene fumigation

In each chemotype (EuL, CmR, LnL, and BeL), a random selection was carried out to obtain 4 adult *C. camphora* plants, whose growth conditions were detailedly described by Tian et al. (2021). For each selected plant, its southern branches with 15–18 leaves were randomly selected for the monoterpene fumigation. These branches were cut at 4: 00 PM, and immediately put into Hogland nutrient solution. In each chemotype, the branches from 4 plants were performed random grouping, and they were divided into 5 groups, with each branch from each plant as a replicate.

These branches were placed into a growth chamber with light intensity at 300 $\mu mol \cdot m^{-2} \cdot s^{-1}$ and temperature at 28°C for adaption. After 2 h, the branches in groups 3-5 were sprayed with 30 μM Fos to block monoterpene synthesis (Tian et al., 2020), while the branches in groups 1 and 2 were sprayed with distilled water. After that, these branches were still kept in the growth chamber for 4-h light and 8-h dark, and put into airtight transparent glass boxes (L×W×H, 35×24×19 cm), with each group in a box. For the groups 4 and 5, a piece of watch glass (diameter of 10 cm) was put into each box, and a certain volume of the uppermost monoterpene solution (consistent with the chemotype) was sprayed onto it. After full volatilization (about 1 h for the highest concentration), the monoterpene concentration in the box was 1 μM and 5 μM, respectively. Then, the group 1 (28°C) was till kept in the growth chamber at 28°C, while the group 2 (38°C), group 3 (Fos+38°C), group 4 (Fos+38°C +monoterpene 1) and group 5 (Fos+38°C+monoterpene 5) were placed into another growth chamber for the treatment with high temperature at 38°C. At the 5^{th} h during treatment, these groups were immediately changed to new preheating boxes (28°C for group 1, and 38°C for other groups) for ventilation, and then added into the uppermost monoterpene solution to perform the same treatment (about 25 min for the full volatilization of 5 μM monoterpene at 38°C) (Detailed procedure in Supplementary Table 1). After 10-h fumigation, the 3^{rd} and 4^{th} leaves in each branch from the top were used to measure the ROS levels, thiobarbituric acid reactive substance (TBARS) content, antioxidant enzyme activities, photosynthetic pigment levels and photosynthetic abilities in the 4 chemotypes, as well as the related gene expression in EuL and CmR.

2.2 Determination of ROS content

C. camphora leaves (0.2 g) were ground to homogenate with phosphate buffer solution (PBS) of 50 mM at pH 7.2 by using liquid nitrogen. After centrifugation at 12000 g at 4°C, the supernatant was collected to estimate $O_2^{-\cdot}$ content through hydroxylamine oxidation in description of Zuo et al. (2017).

H_2O_2 content was estimated following the method described by Tian et al. (2020). The leaf samples (0.5 g) were homogenized with cold acetone, and centrifuged at 12000 g at

4°C. After centrifugation, the extracted solution was mixed with 2 mL ddH_2O, and extracted with the solution that contained 1 volume of $CHCl_3$ and 3 volume of CCl_4. Then, the upper solution was used to estimate H_2O_2 levels by oxidizing xylenol orange.

2.3 Assessment of SOD and POD activities

The extraction of superoxide dismutase (SOD) and peroxidase (POD) followed the method of O_2–· extraction. For their activities, the inhibition of p-nitro blue tetrazolium chloride reduction was used to estimate the SOD activity, with the maximum absorption at 560 nm, while the oxidation of guaiacol was used to estimate the POD activity, with the maximum absorption at 470 nm (Zuo et al., 2017).

2.4 Determination of TBARS content

TBARS was extracted according to the O_2–· extraction method. The extracts of 1 ml were added into 2 ml 20% trichloroacetic acid which contained 0.5% thiobarbituric acid. The absorbance of the mixture was recorded at 450, 532 and 600 nm, and used to calculate TBARS content by using the formula described by Ma et al. (2019).

2.5 Determination of photosynthetic pigment levels

With aiding of a puncher (Φ 6.78 mm), 2 leaf discs were obtained from the 3rd and 4th leaves of the treated branches from the top, and were homogenized with 3 ml 80% acetone. After centrifugation at 8000 g, the supernatant was collected to measure the levels of chlorophyll (Chl) a, Chl b and carotenoids (Car) (Lichtenthaler and Welburn, 1983).

2.6 Assessment of Chl fluorescence transients

Following the previous procedure (Zuo et al., 2017), *C. camphora* leaves were dark-adapted for 30 min, and measured with YZQ500 Chl-fluorescence analyzer (YZQ Technology Co., China) for the Chl fluorescence transients (OJIP). To analyze the OJIP curve, the PSII maximum quantum yield of primary photochemistry (φPo) and non-photochemical deexcitation (φD_O) were calculated following the presentation of Strasser et al. (2004).

2.7 Transcriptome analysis

In EuL and CmR, 3 branches were randomly selected in each treatment. Total RNA were extracted from the 3rd and 4th leaves from the branch with an extraction kit. They were reverse transcribed into cDNA with reverse transcriptase (RNaseH) and random hexamer primer, according to the method described by Tian et al. (2020). After amplification through polymerase chain reaction (PCR), the cDNA from each sample (branch) was constructed a library for the sequence analysis in Novogene Bioinformatics Technology Co. (Beijing, China). (Zuo et al., 2018)

C. camphora transcriptome was assembled using the clean reads with Trinity software (Grabherr et al., 2011). The expression levels of the genes were determined according to the RNA-Seq method (Li and Dewey, 2011). DESeq R package and KOBAS were used to perform the analysis of differential expression genes with $P< 0.05$ and fold change >1 and annotation, respectively (Mao et al., 2005; Anders and Huber, 2012).

2.8 Statistical analysis

The differences among the treatments were analyzed with one-way ANOVA following the Tukey test.

3 Results

3.1 Effects of the uppermost monoterpenes on ROS content in *C. camphora*

With respect to 28°C, the O_2–· content in EuL significantly raised by 44.7% ($P< 0.05$) and 1.04 folds ($P< 0.05$) in the treatments with 38°C and Fos+38°C, respectively. Compared with Fos+38°C treatment, the O_2–· content significantly decreased by 34.8% ($P< 0.05$) and 49.3% ($P< 0.05$) in the treatments with Fos+38°C+E1 (1 μM eucalyptol) and Fos+38°C+E5 (5 μM eucalyptol), respectively (Figure 1A). Similarly, the O_2–· content in CmR, LnL and BeL also raised to the maximum level in the treatment with Fos+38°C, and remarkably reduced in the treatments with Fos+38°C+camphor, Fos+38°C+linalool and Fos+38°C+borneol, respectively. When the concentration of the 3 monoterpenes was at 5 μM, the O_2–· content also reduced to the level at 28°C (Figures 1B–D).

Similar to O_2–· content, the fumigation with the 4 uppermost monoterpenes also significantly ($P< 0.05$) declined the H_2O_2 content in the corresponding chemotypes, with the decrease gradually enhancing with raising the monoterpene concentration (Figures 1E–H).

10.3389/fpls.2022.1072931

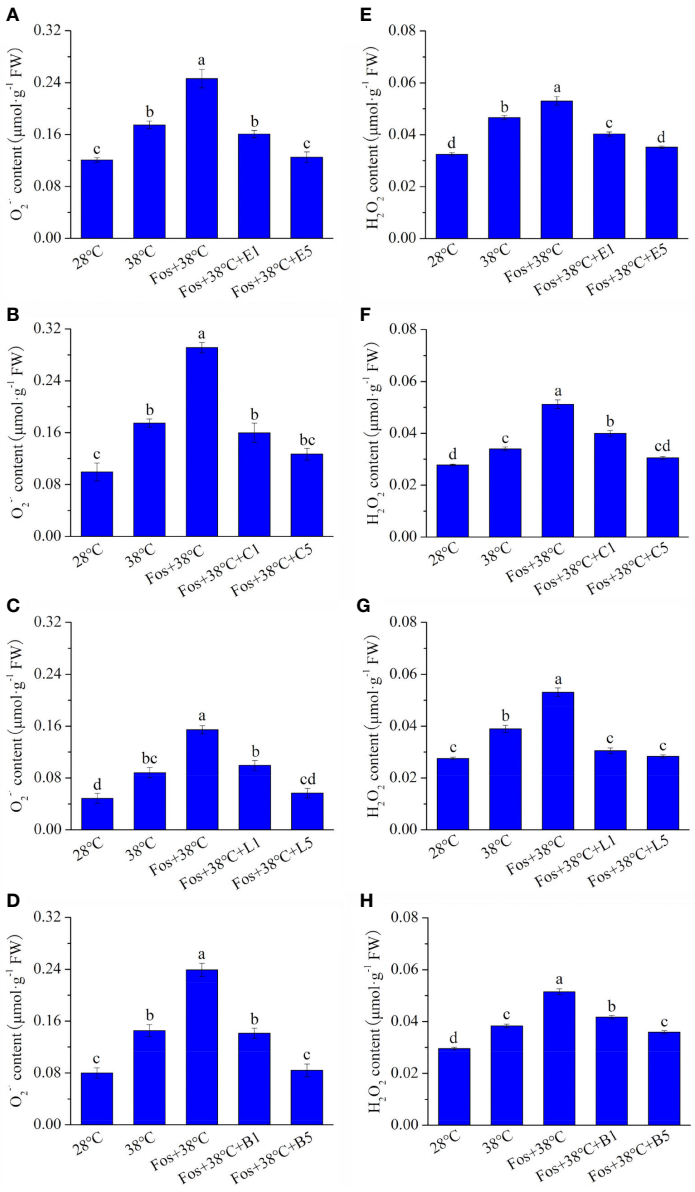

FIGURE 1
Effects of the uppermost monoterpenes on $O_2^{\cdot-}$ **(A–D)** and H_2O_2 **(E–H)** levels in *C. camphora*. **(A, E)** Eucalyptol chemotype (EuL); **(B, F)** Camphor chemotype (CmR); **(C, G)** Linalool chemotype (LnL); **(D, F)** Borneol chemotype (BeL). 28°C, 38°C, and Fos+38°C: *C. camphora* was treated with normal temperature, high temperature, and high temperature with fosmidomycin (Fos) pretreatment, respectively. Fos+38°C+E1 and Fos+38°C+E5: EuL blocked monoterpene synthesis with Fos was fumigated with 1 and 5 μM eucalyptol at 38°C, respectively. Fos+38°C+C1 and Fos+38°C+C5: CmR blocked monoterpene synthesis with Fos was fumigated with 1 and 5 μM camphor at 38°C, respectively. Fos+38°C+L1 and Fos+38°C+L5: LnL blocked monoterpene synthesis with Fos was fumigated with 1 and 5 μM linalool at 38°C, respectively. Fos+38°C+B1 and Fos+38°C+B5: BeL blocked monoterpene synthesis with Fos was fumigated with 1 and 5 μM borneol at 38°C, respectively. Different lowercase letters indicate the significant difference at $P< 0.05$. Means ± SE (n = 4).

3.2 Effects of the uppermost monoterpenes on membrane damage in *C. camphora*

Compared with 28°C, the TBARS content in the 4 chemotypes significantly increased in 38°C treatment, and further increased to the maximum level in the treatment with Fos+38°C. However, remarkable decreases were detected in Fos+38°C+monoterpene treatments compared with Fos+38°C treatment (Figure 2).

3.3 Effects of the uppermost monoterpenes on antioxidant enzyme activities in *C. camphora*

In the treatments with 38°C and Fos+38°C, the SOD activity in EuL significantly increased by 18.9% ($P< 0.05$) and 30.4% ($P< 0.05$), respectively, in contrast to that at 28°C. Compared with Fos+38°C treatment, the SOD activity significantly decreased by 10.8% ($P< 0.05$) and 16.4% ($P< 0.05$) in Fos+38°C+E1 and Fos +38°C+E5 treatments, respectively (Figure 3A). Similarly, the decline was also found in CmR treated with Fos+38°C +camphor, LnL treated with Fos+38°C+linalool, and BeL treated with Fos+38°C+borneol (Figures 3B–D).

The POD activity in EuL, CmR, LnL and BeL also raised to the maximum level in the treatment with Fos+38°C, and then reduced in the fumigation with eucalyptol, camphor, linalool and borneol, respectively (Figures 3E–H).

3.4 Effects of the uppermost monoterpenes on photosynthetic pigment levels in *C. camphora*

The Chl a content in EuL treated with 38°C and Fos+38°C showed remarkable reduction with respect to that at 28°C, and the lowest content was found in the treatment with Fos+38°C.

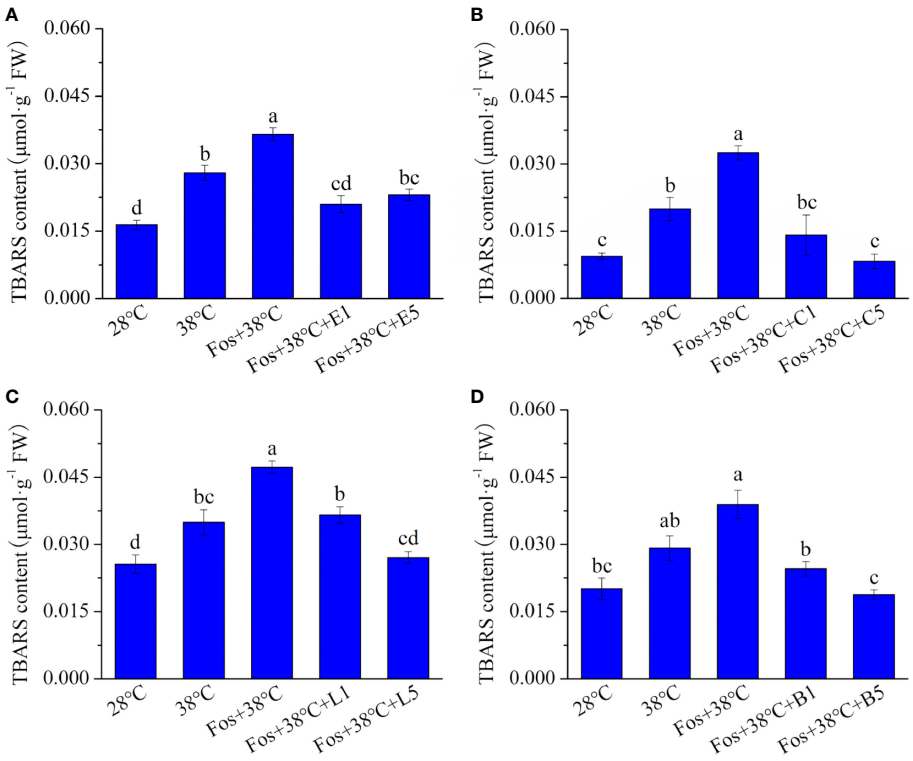

FIGURE 2
Effects of the uppermost monoterpenes on thiobarbituric acid reactive substance (TBARS) content in *C. camphora*. **(A)** Eucalyptol chemotype (EuL); **(B)** Camphor chemotype (CmR); **(C)** Linalool chemotype (LnL); **(D)** Borneol chemotype (BeL). 28°C, 38°C, and Fos+38°C: *C. camphora* was treated with normal temperature, high temperature, and high temperature with fosmidomycin (Fos) pretreatment, respectively. Fos+38°C +E1 and Fos+38°C+E5: EuL blocked monoterpene synthesis with Fos was fumigated with 1 and 5 μM eucalyptol at 38°C, respectively. Fos+38°C +C1 and Fos+38°C+C5: CmR blocked monoterpene synthesis with Fos was fumigated with 1 and 5 μM camphor at 38°C, respectively. Fos+38° C+L1 and Fos+38°C+L5: LnL blocked monoterpene synthesis with Fos was fumigated with 1 and 5 μM linalool at 38°C, respectively. Fos+38°C +B1 and Fos+38°C+B5: BeL blocked monoterpene synthesis with Fos was fumigated with 1 and 5 μM borneol at 38°C, respectively. Different lowercase letters indicate the significant difference at $P< 0.05$. Means ± SE (n = 4).

10.3389/fpls.2022.1072931

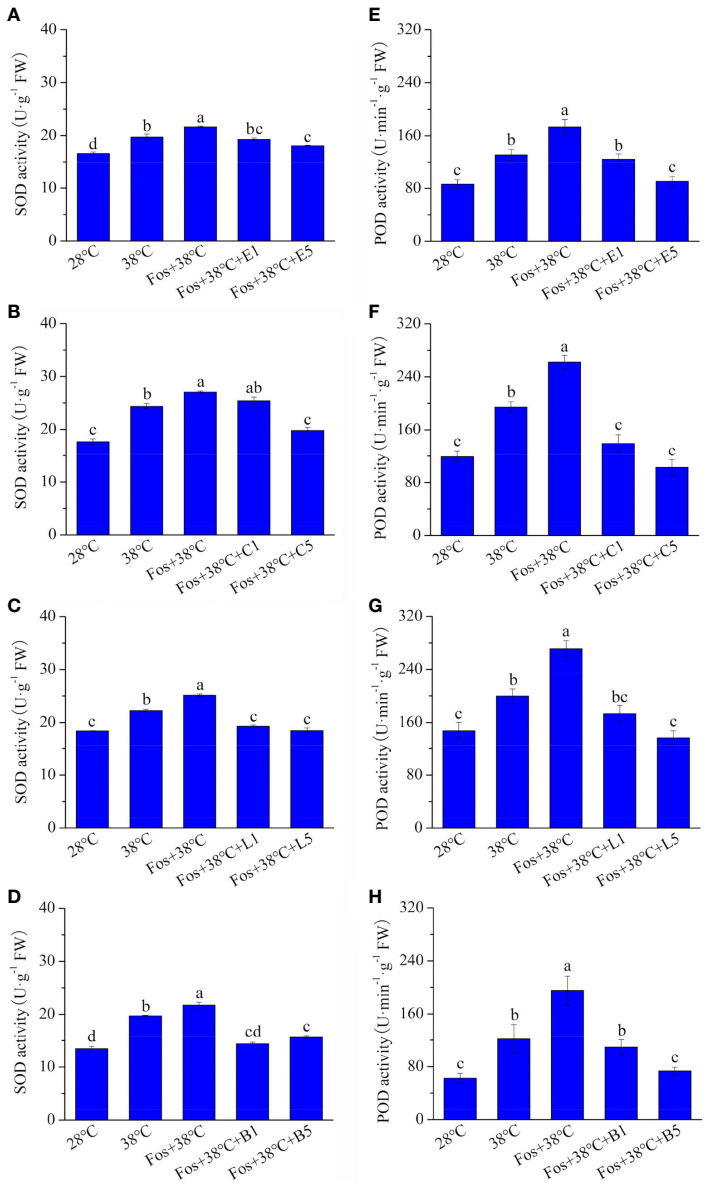

FIGURE 3
Effects of the uppermost monoterpenes on superoxide dismutase (SOD) **(A–D)** and peroxidase (POD) **(E–H)** activities in *C. camphora*. **(A, E)** Eucalyptol chemotype (EuL); **(B, F)** Camphor chemotype (CmR); **(C, G)** Linalool chemotype (LnL); **(D, F)** Borneol chemotype (BeL). 28°C, 38°C, and Fos+38°C: *C. camphora* was treated with normal temperature, high temperature, and high temperature with fosmidomycin (Fos) pretreatment, respectively. Fos+38°C+E1 and Fos+38°C+E5: EuL blocked monoterpene synthesis with Fos was fumigated with 1 and 5 μM eucalyptol at 38°C, respectively. Fos+38°C+C1 and Fos+38°C+C5: CmR blocked monoterpene synthesis with Fos was fumigated with 1 and 5 μM camphor at 38°C, respectively. Fos+38°C+L1 and Fos+38°C+L5: LnL blocked monoterpene synthesis with Fos was fumigated with 1 and 5 μM linalool at 38°C, respectively. Fos+38°C+B1 and Fos+38°C+B5: BeL blocked monoterpene synthesis with Fos was fumigated with 1 and 5 μM borneol at 38°C, respectively. Different lowercase letters indicate the significant difference at $P < 0.05$. Means ± SE (n = 4).

However, a significant ($P < 0.05$) increase was found in Fos +38°C+eucalyptol treatment in contrast to that in Fos+38°C treatment. When the eucalyptol concentration was at 5 μM, the Chl a content was even higher than that at 38°C. For the levels of Chl b and Car, they also showed the similar variations (Table 1).

In other 3 chemotypes, the photosynthetic pigment content also significantly ($P < 0.05$) declined in 38°C treatment with respect to that at 28°C, and declined to the lowest level in Fos+38°C treatment. In contrast to Fos+38°C treatment, the increase was detected in CmR, LnL and BeL treated with Fos+38°C+camphor, Fos+38°C +linalool and Fos+38°C+borneol, respectively (Table 1).

10.3389/fpls.2022.1072931

TABLE 1 Effects of the uppermost monoterpenes on photosynthetic pigment content in *C. camphora*.

		Chlorophyll a (μg·mm^{-2})	Chlorophyll b (μg·mm^{-2})	Carotenoids (μg·mm^{-2})
	28°C	1.01 ± 0.01a	0.37 ± 0.01a	0.28 ± 0.01a
	38°C	0.66 ± 0.02c	0.27 ± 0.01c	0.20 ± 0.02bc
EuL	Fos+38°C	0.49 ± 0.02d	0.23 ± 0.01d	0.13 ± 0.01d
	Fos+38°C+E1	0.68 ± 0.01c	0.26 ± 0.02cd	0.19 ± 0.01c
	Fos+38°C+E5	0.87 ± 0.01b	0.33 ± 0.01b	0.24 ± 0.01b
	28°C	0.92 ± 0.03a	0.38 ± 0.01a	0.27 ± 0.01a
	38°C	0.64 ± 0.01c	0.29 ± 0.01b	0.20 ± 0.01c
CmR	Fos+38°C	0.47 ± 0.01d	0.22 ± 0.01c	0.10 ± 0.01d
	Fos+38°C+C1	0.71 ± 0.01b	0.31 ± 0.01b	0.19 ± 0.01c
	Fos+38°C+C5	0.85 ± 0.01a	0.37 ± 0.03a	0.23 ± 0.01b
	28°C	0.80 ± 0.01a	0.30 ± 0.01a	0.23 ± 0.01a
	38°C	0.64 ± 0.01c	0.21 ± 0.03bc	0.17 ± 0.01b
LnL	Fos+38°C	0.56 ± 0.01d	0.16 ± 0.01c	0.12 ± 0.01c
	Fos+38°C+L1	0.71 ± 0.02b	0.24 ± 0.01b	0.16 ± 0.01b
	Fos+38°C+L5	0.79 ± 0.04ab	0.28 ± 0.03ab	0.22 ± 0.02ab
	28°C	0.71 ± 0.02a	0.21 ± 0.01a	0.21 ± 0.01a
	38°C	0.53 ± 0.01d	0.15 ± 0.02b	0.17 ± 0.01b
BeL	Fos+38°C	0.43 ± 0.01c	0.11 ± 0.01c	0.13 ± 0.01c
	Fos+38°C+B1	0.63 ± 0.02b	0.21 ± 0.01a	0.18 ± 0.01ab
	Fos+38°C+B5	0.67 ± 0.01ab	0.21 ± 0.01a	0.18 ± 0.01ab

EuL, Eucalyptol chemotype; CmR, Camphor chemotype; LnL, Linalool chemotype; BeL, Borneol chemotype. 28°C, 38°C, and Fos+38°C: *C. camphora* was treated with normal temperature, high temperature, and high temperature with fosmidomycin (Fos) pretreatment, respectively. Fos+38°C+E1 and Fos+38°C+E5: EuL pretreated with Fos was fumigated with 1 and 5 μM eucalyptol at 38°C, respectively; Fos+38°C+C1 and Fos+38°C+C5: CmR pretreated with Fos was fumigated with 1 and 5 μM camphor at 38°C, respectively; Fos+38°C+L1 and Fos+38°C+L5: LnL pretreated with Fos was fumigated with 1 and 5 μM linalool at 38°C, respectively; Fos+38°C+B1 and Fos+38°C+B5: BeL pretreated with Fos was fumigated with 1 and 5 μM borneol at 38°C, respectively. Different lowercase letters indicate the significant difference at $P< 0.05$. Means ± SE (n = 4).

3.5 Effects of the uppermost monoterpenes on photosynthetic abilities in *C. camphora*

In contrast to 28°C, the Chl fluorescence intensity in the 4 chemotypes from O to P remarkably decreased in 38°C treatment, and further decreased to the lowest level in the treatment with Fos +38°C. However, a remarkable increase was found in EuL, CmR, LnL and Bel in the treatments with Fos+38°C+eucalyptol, Fos+38° C+camphor, Fos+38°C+linalool and Fos+38°C+borneol, respectively, in contrast to Fos+38°C treatment (Figure 4).

Compared with 28°C, φP_O in EuL significantly reduced by 12.7% ($P< 0.05$) and 22.5% ($P< 0.05$) in 38°C and Fos+38°C treatments, respectively. In Fos+38°C+eucalyptol treatment, the φP_O significantly ($P< 0.05$) raised with respect to that in Fos+38° C treatment, and was remarkably ($P< 0.05$) higher than that at 38°C when eucalyptol concentration was at 5 μM. However, φD_O showed reverse variations, and Fos+38°C+eucalyptol treatment lowered its value (Table 2).

Similarly, the increase was also found in φP_O in CmR treated with Fos+38°C+camphor, LnL treated with Fos+38°C+linalool, and BeL treated with Fos+38°C+borneol, while the decrease in φD_O (Table 2).

3.6 Variation ratio of the physiological indexes with the 4 uppermost monoterpene fumigation

To compare the thermotolerance differences of the 4 uppermost monoterpenes, the variation ratio of these physiological indexes was calculated in Fos+38°C+monoterpene (5 μM) treatments compared with Fos+38°C treatment. For $O_2^{\cdot-}$ content, the high reduction ratio was detected in Fos+38°C+C5, Fos+38°C+L5 and Fos+38°C+B5 treatments, while the low in Fos +38°C+E5 treatment. For H_2O_2 content, the high reduction ratio was found in Fos+38°C+C5 and Fos+38°C+L5 treatments, while the low in Fos+38°C+E5 and Fos+38°C+B5 treatments. Although SOD activity and Chl b content exhibited the maximum variation ratio in Fos+38°C+B5 treatment, their variation ratio in Fos+38°C +C5 treatment was significantly ($P< 0.05$) higher than that in Fos +38°C+E5 treatment. In terms of other indexes (except Chl a content), they always showed strong variation in Fos+38°C+C5 treatment, but weak variation in Fos+38°C+E5 treatment. Fos+38° C+C5 treatment caused the maximum increase ratio in Chl a content, but without significant difference with Fos+38°C+E5 treatment (Table 3).

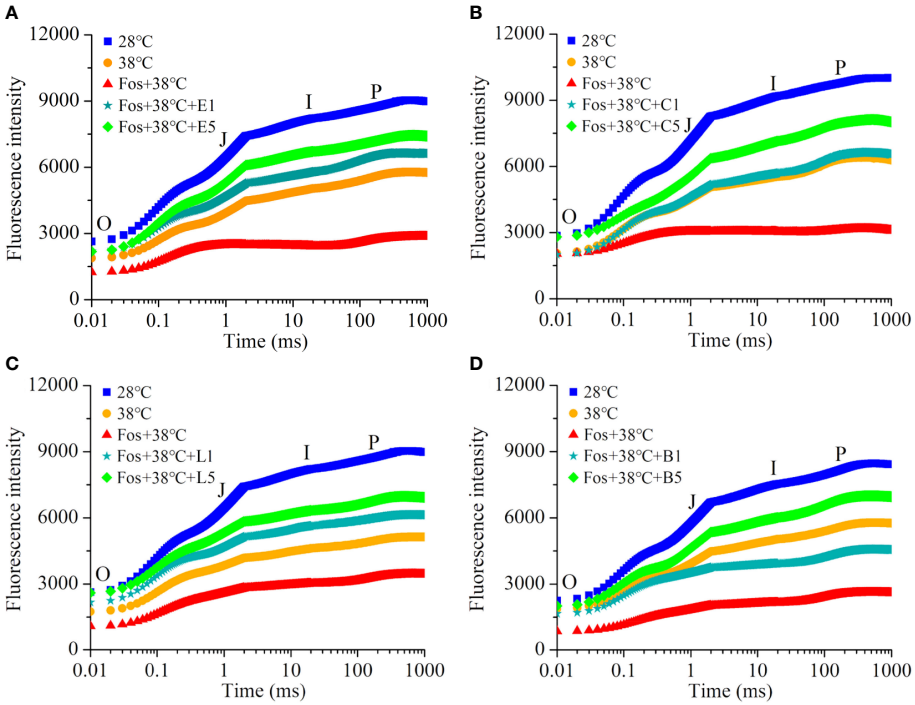

FIGURE 4
Effects of the uppermost monoterpenes on chlorophyll fluorescence kinetics in *C. camphora*. **(A)** Eucalyptol chemotype (EuL); **(B)** Camphor chemotype (CmR); **(C)** Linalool chemotype (LnL); **(D)** Borneol chemotype (BeL). 28°C, 38°C, and Fos+38°C: *C. camphora* was treated with normal temperature, high temperature, and high temperature with fosmidomycin (Fos) pretreatment, respectively. Fos+38°C+E1 and Fos+38°C +E5: EuL blocked monoterpene synthesis with Fos was fumigated with 1 and 5 μM eucalyptol at 38°C, respectively. Fos+38°C+C1 and Fos+38° C+C5: CmR blocked monoterpene synthesis with Fos was fumigated with 1 and 5 μM camphor at 38°C, respectively. Fos+38°C+L1 and Fos+38° C+L5: LnL blocked monoterpene synthesis with Fos was fumigated with 1 and 5 μM linalool at 38°C, respectively. Fos+38°C+B1 and Fos+38°C +B5: BeL blocked monoterpene synthesis with Fos was fumigated with 1 and 5 μM borneol at 38°C, respectively. Means (n = 4) are shown.

3.7 Effects of eucalyptol and camphor on gene expression in *C. camphora*

Compared with 28°C, EuL treated with 38°C changed expression of 12 genes related with antioxidation, including 2 genes encoding antioxidant enzymes (*SOD2* and *CAT*), 3 genes in ascorbate (AsA)-glutathione (GSH) cycle (*APX*, *gpx*, and *GSR*), 2 genes in AsA biosynthesis (*GGP* and *GME*), 3 genes in GSH metabolism (*OPLAH*, *GST*, and *frmA*), and 2 genes in tocopherol (vitamin E, VE) biosynthesis (*VTE3* and *E2.1.1.95*). This alteration further aggravated in the treatment with Fos+38°C. Interestingly, the expression levels of these genes in Fos+38°C+E5 treatment were similar with or trended to that at 28°C. The similar alterations were also found in expression of 7 genes in porphyrin and Chl biosynthesis (*chlI*, *chlD*, *EARS*, *UROD*, *HCAR*, *CPOX*, and *acsF*), 3 genes in carotenoid biosynthesis (*ZDS*, *VDE*, and *ZEP*), 1 gene encoding PSI antenna proteins (*LHCA2*), 2 genes encoding PSII antenna proteins (*LHCB2* and *LHCB5*), 3 genes in oxygen-evolving complex (*psbO*, *psbP*, and *psbQ*), 3 genes in PSII complex (*psbA*, *psbK*, and *psbW*), 4 genes in PSI complex (*psaA*, *psaE*, *psaK*, and *psaO*), 1 gene encoding homogentisate solanesyltransferase for plastoquinone (PQ) formation (*HST*), 2 genes associated with cytochrome b_6-f complex ($Cytb_6$-f) (*petA* and *petC*), 1 gene coding for plastocyanin (*petE*), 1 gene coding for ferredoxin-$NADP^+$ reductase (*petH*), 2 genes coding for ATP synthase (*ATPF1A* and *ATPF1B*), and 12 genes in carbon fixation (*MDH1*, *MDH2*, *E1.1.1.82*, *pckA*, *GAPDH*, *rbcS*, *ppdK*, *TPI*, *tktA*, *RPE*, *rpiA*, and *PRK*) (Figure 5). The detail functions and expression levels of these genes were provided in Supplementary Tables 2–4.

For antioxidation, CmR treated with 38°C up-regulated expression of 2 genes encoding antioxidant enzymes (*SOD1* and *CAT*), 1 gene in AsA-GSH cycle (*APX*), and 2 genes in GSH metabolism (*GST* and *frmA*), but down-regulated 1 gene in AsA biosynthesis (*GGP*), 2 genes in VE biosynthesis (*VTE3* and *E2.1.1.95*), 2 genes in phenylpropanoid biosynthesis (*4CL* and *CYP98A*), and 2 genes in flavonoid biosynthesis (*FLS* and *HCT*). For photosynthetic pigment biosynthesis, 38°C treatment down-regulated expression of 5 genes in porphyrin and Chl biosynthesis (*chlG*, *EARS*, *CPOX*, *chlH*, and *chlI*), and 5 genes in Car biosynthesis (*ispG*, *idi*, *GPS*, *crtB*, and *ZEP*). For the photosynthetic abilities, 38°C treatment down-regulated

TABLE 2 Effects of the uppermost monoterpenes on maximum quantum yield of primary photochemistry (φP_O) and non-photochemical deexcitation (φD_O) in *C. camphora*.

		φP_O	φD_O
EuL	28°C	0.71 ± 0.01a	0.29 ± 0.01d
	38°C	0.62 ± 0.01c	0.38 ± 0.01b
	Fos+38°C	0.55 ± 0.01d	0.45 ± 0.01a
	Fos+38°C+E1	0.64 ± 0.01c	0.36 ± 0.01b
	Fos+38°C+E5	0.67 ± 0.01b	0.33 ± 0.01c
CmR	28°C	0.73 ± 0.01a	0.27 ± 0.01d
	38°C	0.60 ± 0.01c	0.40 ± 0.01b
	Fos+38°C	0.43 ± 0.02d	0.57 ± 0.02a
	Fos+38°C+C1	0.62 ± 0.01c	0.38 ± 0.01b
	Fos+38°C+C5	0.66 ± 0.01b	0.34 ± 0.01c
LnL	28°C	0.71 ± 0.01a	0.29 ± 0.01e
	38°C	0.57 ± 0.01d	0.43 ± 0.01b
	Fos+38°C	0.51 ± 0.01e	0.49 ± 0.01a
	Fos+38°C+L1	0.63 ± 0.01c	0.37 ± 0.01c
	Fos+38°C+L5	0.65 ± 0.01b	0.35 ± 0.01d
BeL	28°C	0.69 ± 0.01a	0.31 ± 0.01e
	38°C	0.57 ± 0.01c	0.44 ± 0.01c
	Fos+38°C	0.41 ± 0.01e	0.59 ± 0.01a
	Fos+38°C+B1	0.51 ± 0.01d	0.49 ± 0.01b
	Fos+38°C+B5	0.65 ± 0.01b	0.35 ± 0.01d

EuL, Eucalyptol chemotype; CmR, Camphor chemotype; LnL, Linalool chemotype; BeL, Borneol chemotype. 28°C, 38°C, and Fos+38°C: *C. camphora* was treated with normal temperature, high temperature, and high temperature with fosmidomycin (Fos) pretreatment, respectively. Fos+38°C+E1 and Fos+38°C+E5: EuL pretreated with Fos was fumigated with 1 and 5 μM eucalyptol at 38°C, respectively; Fos+38°C+C1 and Fos+38°C+C5: CmR pretreated with Fos was fumigated with 1 and 5 μM camphor at 38°C, respectively; Fos+38°C+L1 and Fos+38°C+L5: LnL pretreated with Fos was fumigated with 1 and 5 μM linalool at 38°C, respectively; Fos+38°C+B1 and Fos+38°C+B5: BeL pretreated with Fos was fumigated with 1 and 5 μM borneol at 38°C, respectively. Different lowercase letters indicate the significant difference at $P< 0.05$. Means ± SE (n = 4).

expression of 2 genes encoding PSI antenna proteins (*LHCA1* and *LHCA2*), 2 genes encoding PSII antenna proteins (*LHCB1* and *LHCB2*), 2 genes in oxygen-evolving complex (*psbP* and *psbQ*), 3 genes in PSII complex (*psbK*, *psbS*, and *psbW*), 1 gene in PSI complex (*psaB*), 1 gene encoding ferredoxin-$NADP^+$ reductase (*petH*), 2 genes encoding ATP synthase (*ATPF1B* and *ATPF1G*), and 12 genes in carbon fixation (*ppc*, *MDH2*, *GOT2*, *maeB*, *pckA*, *GAPDH*, *rbcS*, *rbcL*, *TPI*, *tktA*, *rpiA*, and *PRK*). These alterations were further aggravated in the treatment with Fos+38°C, but their expression in the treatment with Fos +38°C+C5 trended to the levels at 28°C (Figure 6; Supplementary Tables 5–7).

TABLE 3 Variation ratio of the physiological indexes in the uppermost monoterpene fumigation (Fos+38°C+monoterpene) compared with non-fumigation (Fos+38°C).

	Fos+38°C+E5	Fos+38°C+C5	Fos+38°C+L5	Fos+38°C+B5
$O_2^{-\cdot}$ content (%)	-49.4 ± 5.1b	-56.4 ± 3.6ab	-63.3 ± 5.5a	-64.8 ± 4.7a
H_2O_2 content (%)	-25.0 ± 3.1b	-40.4 ± 2.1a	-46.6 ± 2.6a	-30.3 ± 1.2b
TBARS content (%)	-36.8 ± 5.5c	-74.6 ± 4.5a	-42.7 ± 3.6c	-51.7 ± 2.5b
SOD activity (%)	-16.6 ± 0.4c	-26.8 ± 1.9b	-26.5 ± 2.0b	-33.9 ± 1.4a
POD activity (%)	-47.6 ± 4.1bc	-51.6 ± 3.4ab	-45.6 ± 4.7c	-62.4 ± 3.0a
Chlorophyll a content (%)	77.6 ± 4.8a	80.6 ± 4.8a	40.4 ± 7.8c	56.0 ± 5.1b
Chlorophyll b content (%)	44.9 ± 3.1c	70.0 ± 8.3b	74.2 ± 5.7b	90.7 ± 6.7a
Carotenoids content (%)	84.9 ± 5.3b	128.0 ± 12.1a	86.0 ± 5.1b	41.4 ± 4.9c
φPo (%)	23.3 ± 1.6c	51.8 ± 5.0a	24.1 ± 3.4c	33.8 ± 2.8b
φD_O (%)	-28.0 ± 4.7bc	-39.4 ± 5.8a	-25.9 ± 2.2c	-31.8 ± 1.5ab

Fos+38°C: Treatment with high temperature at 38°C after pretreatment with fosmidomycin (Fos); Fos+38°C+E5: EuL pretreated with Fos was fumigated with 5 μM eucalyptol at 38°C; Fos +38°C+C5: CmR pretreated with Fos was fumigated with 5 μM camphor at 38°C; Fos+38°C+L5: LnL pretreated with Fos was fumigated with 5 μM linalool at 38°C; Fos+38°C+B5: BeL pretreated with Fos was fumigated with 5 μM borneol at 38°C. Positive value indicates the increase, while negative value indicates the decrease. Different lowercase letters indicate the significant difference at $P< 0.05$. Means ± SE (n = 4).

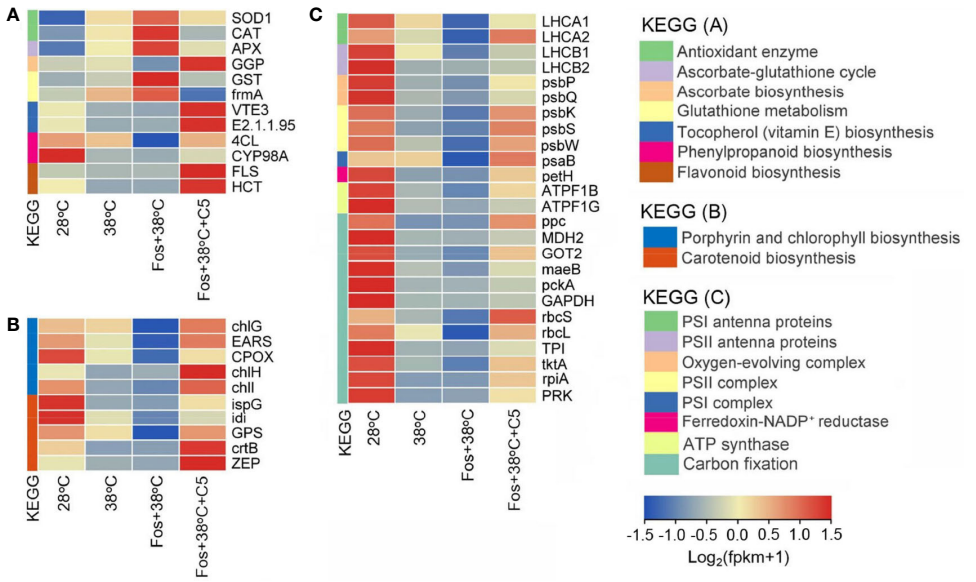

FIGURE 5
Effects of eucalyptol on gene expression in antioxidation **(A)**, photosynthetic pigment biosynthesis **(B)**, and photosynthetic abilities **(C)** in eucalyptol chemotype of *C. camphora* (EuL). 28°C, 38°C, and Fos+38°C: EuL was treated with normal temperature, high temperature, and high temperature with fosmidomycin (Fos) pretreatment, respectively. Fos+38°C+E5: EuL blocked monoterpene synthesis with Fos was fumigated with 5 μM eucalyptol at 38°C. KEGG: Kyoto encyclopedia of genes and genomes pathways. The heatmap was drawn using the FPKM (fragments per kilobase per million mapped reads) by using the software R packages pheatmap 1.0.12. Means (n = 3) are shown.

4 Discussion

Fos is an effective inhibitor for isoprene and monoterpene synthesis by blocking MEP pathway (Tian et al., 2021). In exposure to O_3, ROS accumulation was detected in *P. australis* leaves with blocking isoprene synthesis by Fos and in *Q. ilex* leaves with blocking monoterpene synthesis (Loreto and Velikova, 2001; Loreto et al., 2004). Meanwhile, *P. australis* that was blocked isoprene synthesis accumulated ROS under high temperature stress (Velikova and Loreto, 2005). Under high temperature, EuL seedlings and adult CmR plants remarkably increased ROS and TBARS content after their monoterpene synthesis was blocked (Zuo et al., 2017; Tian et al., 2020). In this study, the similar increase was also found in the 4 chemotypes of *C. camphora* in the treatment with Fos+38°C. Moreover, Fos+38°C+monoterpene (eucalyptol, camphor, linalool, and borneol) treatments significantly declined the ROS and TBARS content, demonstrating that the 4 uppermost monoterpenes served important functions in regulating ROS levels (Figures 1, 2). Although monoterpenes can quench ROS and free radicals *in vitro* (Wojtunik et al., 2014), their scavenging abilities against ROS *in vivo* are suspected for their internal low concentration and lacking a direct scavenging evidence.

ROS accumulation can cause oxidative stress, which is harmful to the cells. There are a large and integrated non-enzymatic and enzymatic antioxidants in plants to regulate ROS levels and reduce oxidative stress. For non-enzymatic antioxidants, Car, VE, AsA, GSH and flavonoids exhibit strong antioxidant abilities (Koopman et al., 2010; Ma et al., 2019; Shen et al., 2022). In the 4 chemotypes, Car content significantly decreased in 38°C treatment and further decreased in Fos+38°C treatment (Table 1), which should result from the down-regulation of the genes related with Car biosynthesis, such as *ZDS*, *VDE* and *ZEP* in EuL, as well as *ispG*, *idi*, *GPS*, *crtB* and *ZEP* in CmR. Compared with Fos+38°C treatment, Car content increased in Fos+38°C+monoterpene treatments for the up-regulation of the related genes. Meanwhile, the genes in VE, AsA, GSH and flavonoids biosynthesis and in GSH metabolic transformation were up-regulated and down-regulated, respectively, in Fos+38°C+monoterpene (eucalyptol and camphor) treatments compared with Fos+38°C treatment (Figures 5, 6; Supplementary Tables 2, 5), which were also beneficial to non-enzymatic antioxidant formation. These results were consistent with previous studies in CmR fumigated with terpinene and β-pinene (Tian et al., 2020), suggesting that monoterpenes may regulate expression of the genes associated with non-enzymatic antioxidant formation, and then adjust ROS levels.

Enzymatic antioxidants can scavenge ROS through enzymatic reaction, and the enhancement of their activities is induced by ROS accumulation. In the treatment with Fos associating with high temperature, Eul seedlings and adult CmR plants increased the activities of antioxidant enzymes in response to the ROS

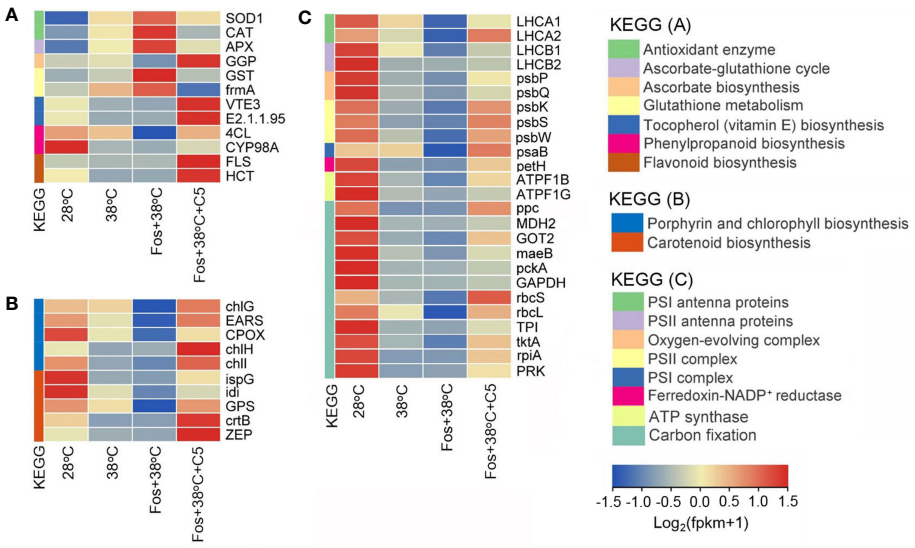

FIGURE 6
Effects of camphor on gene expression in antioxidation **(A)**, photosynthetic pigment biosynthesis **(B)**, and photosynthetic abilities **(C)** in camphor chemotype of *C. camphora* (CmR). 28°C, 38°C, and Fos+38°C: CmR was treated with normal temperature, high temperature, and high temperature with fosmidomycin (Fos) pretreatment, respectively. Fos+38°C+C5: CmR blocked monoterpene synthesis with Fos was fumigated with 5 μM camphor at 38°C. KEGG: Kyoto encyclopedia of genes and genomes pathways. The heatmap was drawn using the FPKM (fragments per kilobase per million mapped reads) by using the software R packages pheatmap 1.0.12. Means (n = 3) are shown.

accumulation (Zuo et al., 2017; Tian et al., 2020). In this study, the activities of SOD and POD also increased in the 4 chemotypes of *C. camphora* in the treatment with Fos+38°C. Moreover, Fos+38°C+monoterpene treatments declined their activities in contrast to Fos+38°C treatment (Figure 3). The corresponding alterations were also found in expression of the genes *SOD2* (encoding SOD) and *CAT* (encoding catalase) in EuL treated with Fos+38°C+E5 (Figure 5A, Supplementary Table 2), and the genes *SOD1* and *CAT* in CmR treated with Fos+38°C+C5 (Figure 6A, Supplementary Table 5). AsA-GSH cycle includes several enzymes to serve antioxidant function. *APX*, *gpx* and *GSR* encode AsA peroxidase, GSH peroxidase and GSH reductase, respectively (Caverzan et al., 2012; Passaia et al., 2014; Couto et al., 2016). High temperature and acid rain stresses increased their activities in *C. camphora* to quench ROS (Ma et al., 2019). In this study, the expression of the 3 genes in EuL and 1 gene *APX* in CmR increased in 38°C treatment, further increased in Fos+38°C treatment, and then decreased in Fos+38°C+E5 and Fos+38°C +C5 treatments, which may be caused by the variations of the ROS levels (Figures 5, 6; Supplementary Tables 2, 5). It can be speculated that monoterpenes reduce ROS levels by promoting non-enzymatic antioxidant formation, and ROS accumulation resulted from blocking monoterpene formation under high temperature stress raises antioxidant enzyme activities by inducing related gene expression.

In previous studies, Chl and Car content significantly reduced in adult CmR plants in Fos+38°C treatment, but increased in Fos +38°C+β-pinene and Fos+38°C+terpinene treatments, due to the alterations of related gene expression (Tian et al., 2020). Similarly, the down-regulation of the genes in Chl and Car biosynthesis in EuL and CmR may lead to the decrease of Chl and Car content, respectively, in the treatments with 38°C and Fos+38°C. In contrast to Fos+38°C treatment, Fos+38°C+E5 and Fos+38°C+C5 treatments increased the photosynthetic pigment content by raising expression of the related genes (Figures 5, 6; Supplementary Tables 3, 6).

In the 4 chemotypes, the Chl fluorescence intensity (O to P) decreased in 38°C treatment, and then reduced to the minimum level in the treatment with Fos+38°C (Figure 4), which were similar with previous findings in EuL seedlings and adult CmR plants (Zuo et al., 2017; Tian et al., 2020). The decline of O to J was interpreted as the decline of PQ pool (Strasser et al., 1995), as *HST* that coded for homogentisate solanesyltransferase in PQ biosynthesis was down-regulated in EuL (Figure 5C; Supplementary Table 4). For J to P, its decrease was caused by the blockage of electron transport at PSII donor side (Gao et al., 2016). The treatments with 38°C and Fos+38°C inhibited expression of the genes associated with PSII complex and PSII oxygen-evolving enhancer proteins in EuL and CmR, which may restrain PSII assembly and water photolysis and lead to the decline of electron supply at PSII donor side. Meanwhile, the down-regulation was also found in the genes associated with the assembly of $Cytb_6$-f, PSI and ATP synthase, as well as encoding plastocyanin and ferredoxin-$NADP^+$ reductase, which may block

electron transport, $NADP^+$ reduction and ATP formation, and lower assimilatory power (ATP and NADPH) generation. However, these cases reversed to better statuses in Fos+38°C+E5 and Fos+38°C+C5 treatments (Figures 5, 6; Supplementary Tables 4, 7).

Compared with 28°C, the fumigation with 1, 3 and 5 μM eucalyptol at 28°C not changed the φPo and φD_O in EuL, indicating that monoterpene fumigation no affect the photosynthetic abilities in *C. camphora* under normal temperature (Supplementary Figure 1). In contrast to 38°C, a decline was found in φPo in the 4 chemotypes of *C. camphora* treated with Fos+38°C (Table 2). This was similar with the reduction of ΔF/Fm′ in *Q. ilex* with blocking monoterpene synthesis under O_3 stress (Loreto et al., 2004). For φDo, Fos+38°C treatment aggravated its increase. These demonstrated that an aggravated suppression has happened in the quantum yield and electron transport in Fos+38°C treatment, with massive light energy absorbed by photosynthetic pigments consuming as heat (Zhao et al., 2016). The variations of the 2 Chl fluorescence transient parameters were consistent with that in EuL seedlings and adult CmR plants in Fos treatment associating with high temperature stress (Zuo et al., 2017; Tian et al., 2020). Compared with Fos+38°C treatment, Fos+38°C+monoterpene treatments increased φPo in the 4 chemotypes, but decreased φDo (Table 2), indicating that the uppermost monoterpene fumigation was beneficial to maintaining PSII efficiency. This was similar with *Q. ilex* maintaining higher ΔF/Fm′ in fumigation with sabinene, α-pinene and cis-β-ocimene (Loreto et al., 1998), and adult CmR plants maintaining higher PSII efficiency in fumigation with terpinene and β-pinene (Tian et al., 2020).

Under high temperature, blocking monoterpene synthesis reduced photosynthetic rate in *Q. ilex* (Loreto et al., 1998), *Q. suber* (Delfine et al., 2000) and EuL seedlings (Zuo et al., 2017) in indoor experiments. Compared with high temperature, blocking monoterpene synthesis under high temperature reduced the stomatal conductance in EuL seedlings, but raised the intercellular CO_2 concentration, indicating that the photosynthetic rate reduction with blocking monoterpene synthesis under high temperature is non-stoma limitation. Under high temperature weather, the reduction was also detected in the photosynthetic abilities in the 4 chemotypes of outdoor adult *C. camphora* with blocking monoterpene synthesis (Xu et al., 2022). This reduction should not only result from the decline of the photosynthetic pigment content, PSII efficiency and assimilatory power, but also result from the decline of CO_2 assimilation abilities, due to the down-regulation of related genes in EuL and CmR (Figures 5, 6; Supplementary Tables 4, 7). In contrast to Fos+38°C treatment, Fos+38°C+E5 and Fos+38°C+C5 treatments up-regulated expression of the genes associated with CO_2 assimilation, suggesting that the uppermost monoterpenes were beneficial to maintaining photosynthesis in *C. camphora* under high temperature.

In fumigation with monoterpenes (α-pinene, β-pinene, myrcene, and ocimene), *A. thaliana* up-regulated expression of the genes that were involved in defense (Godard et al., 2008) and innate immune responses (Riedlmeier et al., 2017; Wenig et al., 2019). Both endogenous (Zuo et al., 2019) and exogenous (Harvey and Sharkey, 2016) isoprene exhibited inducing effects on the gene expression in several biological pathways and stress responses. In previous study, terpinene and β-pinene served important functions in adult CmR tolerating high temperature by adjusting expression of the genes associated with ROS metabolism and photosynthetic abilities (Tian et al., 2020). In this study, the uppermost monoterpenes also exhibited similar roles in improving thermotolerance in *C. camphora*, indicating that they also serve signaling functions.

In previous studies, isoprene improved plant photosynthetic abilities by stabilizing thylakoid membranes (Pollastri et al., 2019), which has been hypothesized by intercalating into membranes against leakiness (Sharkey et al., 2008; Velikova et al., 2011). However, isoprene cannot dissolve into cellular membranes in great quantity, and is not involved in the formation of thylakoid membrane acyl lipids (Harvey et al., 2015). When CmR was treated with Fos+38°C+C5, a reduction was found in the cell membrane damage. The levels of membrane lipid molecules showed variation tendencies to the control at 28°C, and the expression of the genes related with these membrane lipid metabolism was also altered accordingly (submitted). This demonstrates that monoterpenes and isoprene might stabilize thylakoid membranes by regulating related gene expression, which is beneficial to maintaining plant photosynthetic abilities under high temperature.

In the previous study, the fumigation with β-pinene and terpinene at 10 μM (Fos+38°C+β-pinene and Fos+38°C+terpinene) recovered the ROS metabolism and photosynthetic pigment levels in CmR to the levels at 28°C (Tian et al., 2020), while the recovery effects were carried out in fumigation with the 4 uppermost monoterpenes at 5 μM, suggesting that the uppermost monoterpenes had stronger thermotolerance abilities. In contrast to Fos+38°C treatment, the fumigation with the 4 uppermost monoterpenes at 5 μM caused different variation ratio in the ROS metabolism, photosynthetic pigment levels and photosynthetic abilities in the corresponding chemotype. Among of them, camphor fumigation (Fos+38°C+C5) showed high variation ratio in most of indexes, while eucalyptol fumigation (Fos+38°C+E5) showed low variation ratio, indicating that camphor might have strong abilities in reducing ROS levels and maintaining photosynthesis under high temperature, and eucalyptol might have weak abilities (Table 3). These differences should be caused by the recovery effects of related gene expression, with high in Fos+38°C+C5 treatment but low in Fos+38°C+E5 treatment, which was similar with different monoterpene (α-pinene, β-pinene, myrcene, and

ocimene) fumigation inducing different defense responses in gene expression in *A. thaliana* (Godard et al., 2008; Riedlmeier et al., 2017; Wenig et al., 2019). This indicated that monoterpenes might have different signaling effects in improving *C. camphora* thermotolerance.

Data availability statement

The data presented in the study are deposited in the NCBI SRA database, accession number PRJNA909422.

Author contributions

ZZ and CX conceived the main idea of the study. CX, BW, and QL performed the experiments and analyzed the data. YM, TZ, YW, and YC took part in the experiments. ZZ wrote and modified the paper. All authors contributed to the article and approved the submitted version.

Funding

This research was supported by the National Natural Science Foundation of China (No. 31870585), the Basic Public Welfare Research Project of Zhejiang Province (No. LGN21C160003, LGN19C150006), and the Natural Science Foundation of Zhejiang Province (No. LY17C160004).

Conflict of interest

The authors declare that the research was conducted in the absence of any commercial or financial relationships that could be construed as a potential conflict of interest.

Publisher's note

All claims expressed in this article are solely those of the authors and do not necessarily represent those of their affiliated organizations, or those of the publisher, the editors and the reviewers. Any product that may be evaluated in this article, or claim that may be made by its manufacturer, is not guaranteed or endorsed by the publisher.

Supplementary material

The Supplementary Material for this article can be found online at: https://www.frontiersin.org/articles/10.3389/fpls.2022.1072931/full#supplementary-material

SUPPLEMENTARY FIGURE 1
Effects of eucalyptol on the maximum quantum yield of primary photochemistry (φPo) and non-photochemical deexcitation (φD_O) in eucalyptol chemotype of *C. camphora* under normal temperature. Compared with 28°C, the fumigation with 1, 3 and 5 μM eucalyptol (Eul) at 28°C not changed the φPo and φD_O, indicating that monoterpene fumigation no affect the photosynthetic abilities in *C. camphora* under normal temperature.

References

Anders, S., and Huber, W. (2012). *Differential expression of RNA-seq data at the gene level the DESeq package* (Heidelberg, Germany: European Molecular Biology Laboratory).

Behnke, K., Ehlting, B., Teuber, M., Bauerfeind, M., Louis, S., Hasch, R., et al. (2007). Transgenic, non-isoprene emitting poplars don't like it hot. *Plant J.* 51, 485–499. doi: 10.1111/j.1365-313X.2007.03157.x

Caverzan, A., Passaia, G., Rosa, S. B., Ribeiro, C. W., Lazzarotto, F., and Margis-Pinheiro, M. (2012). Plant responses to stresses: role of ascorbate peroxidase in the antioxidant protection. *Genet. Mol. Biol.* 35, 1011–1019. doi: 10.1590/S1415-47572012000600016

Couto, N., Wood, J., and Barber, J. (2016). The role of glutathione reductase and related enzymes on cellular redox homoeostasis network. *Free Radical Biol. Med.* 95, 27–42. doi: 10.1016/j.freeradbiomed.2016.02.028

Delfine, S., Csiky, O., Seufert, G., and Loreto, F. (2000). Fumigation with exogenous monoterpenes of a non-isoprenoid-emitting oak (*Quercus suber*): monoterpene acquisition, translocation, and effect on the photosynthetic properties at high temperatures. *New Phytol.* 146, 27–36. doi: 10.1046/j.1469-8137.2000.00612.x

Gao, P., Zuo, Z., Wu, X., Gao, Y., Gao, R., and Zhang, R. (2016). Effects of cycloheximide on photosynthetic abilities, reflectance spectra and fluorescence emission spectra in *Phyllostachys edulis*. *Trees – Struct. Funct.* 30, 719–732. doi: 10.1007/s00468-015-1315-z

Godard, K. A., White, R., and Bohlmann, J. (2008). Monoterpene-induced molecular responses in *Arabidopsis thaliana*. *Phytochemistry* 69, 1838–1849. doi: 10.1016/j.phytochem.2008.02.011

Grabherr, M. G., Haas, B. J., Yassour, M., Levin, J. Z., Thompson, D. A., Amit, I., et al. (2011). Full-length transcriptome assembly from RNA-seq data without a reference genome. *Nat. Biotechnol.* 29, 644–652. doi: 10.1038/nbt.1883

Guidolotti, G., Pallozzi, E., Gavrichkova, O., Scartazza, A., Mattioni, M., Loreto, F., et al. (2019). Emission of constitutive isoprene, induced monoterpenes, and other volatiles under high temperatures in *Eucalyptus camaldulensis*: a ^{13}C labelling study. *Plant Cell Environ.* 42, 1929–1938. doi: 10.1111/pce.13521

Harvey, C. M., Li, Z., Tjellstrm, H., Blanchard, G. J., and Sharkey, T. D. (2015). Concentration of isoprene in artificial and thylakoid membranes. *J. Bioenerg. Biomembr.* 47, 419–429. doi: 10.1007/s10863-015-9625-9

Harvey, C. M., and Sharkey, T. D. (2016). Exogenous isoprene modulates gene expression in unstressed *Arabidopsis thaliana* plants. *Plant Cell Environ.* 39, 1251–1263. doi: 10.1111/pce.12660

Holopainen, J. K. (2011). Can forest trees compensate for stress-generated growth losses by induced production of volatile compounds? *Tree Physiol.* 31, 1356–1377. doi: 10.1093/treephys/tpr111

Holopainen, J. K., and Blande, J. D. (2013). Where do herbivore-induced plant volatiles go? *Front. Plant Sci.* 4, 185. doi: 10.3389/fpls.2013.00185

Jardine, K. J., Jardine, A. B., Holm, J. A., Lombardozzi, D. L., Negron-Juarez, R. I., Martin, S. T., et al. (2017). Monoterpene 'thermometer' of tropical forest-atmosphere response to climate warming. *Plant Cell Environ.* 40, 441–452. doi: 10.1111/pce.12879

Koopman, W. J. H., Nijtmans, L. G. J., Dieteren, C. E. J., Roestenberg, P., Valsecchi, F., Smeitink, J. A. M., et al. (2010). Mammalian mitochondrial complex

I: biogenesis, regulation, and reactive oxygen species generation. *Antioxid. Redox Sign.* 12, 1431–1470. doi: 10.1089/ars.2009.2743

Lantz, A. T., Allman, J., Weraduwage, S. M., and Sharkey, T. D. (2019). Isoprene: new insights into the control of emission and mediation of stress tolerance by gene expression. *Plant Cell Environ.* 42, 2808–2826. doi: 10.1111/pce.13629

Lichtenthaler, H. K., and Welburn, A. (1983). Determination of total carotenoids and chlorophylls a and b of leaf extracts in different solvents. *Biochem. Soc T.* 11, 591–592. doi: 10.1042/bst0110591

Li, B., and Dewey, C. N. (2011). RSEM: accurate transcript quantification from RNA-seq data with or without a reference genome. *BMC Bioinf.* 12, 323. doi: 10.1186/1471-2105-12-323

Li, Y. R., Fu, C. S., Yang, W. J., Wang, X. L., Feng, D., Wang, X. N., et al. (2018). Investigation of constituents from *Cinnamomum camphora* (L.) j. presl and evaluation of their anti-inflammatory properties in lipopolysaccharide stimulated RAW 264.7 macrophages. *J. Ethnopharmacol.* 221, 37–47. doi: 10.1016/j.jep.2018.04.017

Llusia, J., Peñuelas, J., Guenther, A., and Rapparini, F. (2013). Seasonal variations in terpene emission factors of dominant species in four ecosystems in NE Spain. *Atmos. Environ.* 70, 149–158. doi: 10.1016/j.atmosenv.2013.01.005

Loivamäki, M., Gilmer, F., Fischbach, R. J., Sorgel, C., Bachl, A., Walter, A., et al. (2007). *Arabidopsis*, a model to study biological functions of isoprene emission? *Plant Physiol.* 14, 1066–1078. doi: 10.1104/pp.107.098509

Loreto, F., Forster, A., Durr, M., Csiky, O., and Seufert, G. (1998). On the monoterpene emission under heat stress and on the increased thermotolerance of leaves of *Quercus ilex* l. fumigated with selected monoterpenes. *Plant Cell Environ.* 21, 101–107. doi: 10.1046/j.1365-3040.1998.00268.x

Loreto, F., Pinelli, P., Manes, F., and Kollist, H. (2004). Impact of ozone on monoterpene emissions and evidence for an isoprene-like antioxidant action of monoterpenes emitted by *Quercus ilex* leaves. *Tree Physiol.* 24, 361–367. doi: 10.1093/treephys/24.4.361

Loreto, F., and Velikova, V. (2001). Isoprene produced by leaves protects the photosynthetic apparatus against ozone damage, quenches ozone products, and reduces lipid peroxidation of cellular membranes. *Plant Physiol.* 127, 1781–1787. doi: 10.1104/pp.010497

Luo, Q., Xu, C., Zheng, T., Ma, Y., Li, Y., and Zuo, Z. (2021). Leaf morphological and photosynthetic differences among four chemotypes of *Cinnamomum camphora* in different seasons. *Ind. Crop Prod.* 169, 113651. doi: 10.1016/j.indcrop.2021.113651

Mao, X., Cai, T., Olyarchuk, J. G., and Wei, L. (2005). Automated genome annotation and pathway identification using the KEGG orthology (KO) as a controlled vocabulary. *Bioinformatics* 21, 3787–3793. doi: 10.1093/bioinformatics/bti430

Mathur, S., Agrawal, D., and Jajoo, A. (2014). Photosynthesis: response to high temperature stress. *J. Photochem. Photobiol. B* 137, 116–126. doi: 10.1016/j.jphotobiol.2014.01.010

Ma, Y., Wang, B., Zhang, R., Gao, Y., Zhang, X., Li, Y., et al. (2019). Initial simulated acid rain impacts reactive oxygen species metabolism and photosynthetic abilities in *Cinnamonum camphora* undergoing high temperature. *Ind. Crop Prod.* 135, 352–361. doi: 10.1016/j.indcrop.2019.04.050

Mostafa, S., Wang, Y., Zeng, W., and Jin, B. (2022). Floral scents and fruit aromas: functions, compositions, biosynthesis, and regulation. *Front. Plant Sci.* 13, 860157. doi: 10.3389/fpls.2022.860157

Passaia, G., Caverzan, A., Fonini, L. S., Carvalho, F., Silveira, J., and Margis-Pinheiro, M. (2014). Chloroplastic and mitochondrial *GPX* genes play a critical role in rice development. *Biol. Plantarum.* 58, 375–378. doi: 10.1007/s10535-014-0394-9

Peñuelas, J., and Llusià, J. (2002). Linking photorespiration, monoterpenes and thermotolerance in *Quercus*. *New Phytol.* 155, 227–237. doi: 10.1046/j.1469-8137.2002.00457.x

Pollastri, S., Jorba, I., Hawkins, T. J., Llusià, J., Michelozzi, M., Navajas, D., et al. (2019). Leaves of isoprene-emitting tobacco plants maintain PSII stability at high temperatures. *New Physiol.* 223, 1307–1318. doi: 10.1111/nph.15847

Riedlmeier, M., Ghirardo, A., Wenig, M., Knappe, C., Koch, K., Georgii, E., et al. (2017). Monoterpenes support systemic acquired resistance within and between plants. *Plant Cell* 29, 1440–1459. doi: 10.1105/tpc.16.00898

Rodrigues, T. B., Baker, C. R., Walker, A. P., McDowell, N., Rogers, A., Higuchi, N., et al. (2020). Stimulation of isoprene emissions and electron transport rates as key mechanisms of thermal tolerance in the tropical species *Vismia guianensis*. *Global Change Biol.* 26, 5928–5941. doi: 10.1111/gcb.15213

Sasaki, K., Saito, T., Lamsa, M., Oksman-Caldentey, K. M., Suzuki, M., Ohyama, K., et al. (2007). Plants utilize isoprene emission as a thermotolerance mechanism. *Plant Cell Physiol.* 48, 1254–1262. doi: 10.1093/pcp/pcm104

Sharkey, T. D., Wiberley, A. E., and Donohue, A. R. (2008). Isoprene emission from plants: why and how. *Ann. Bot.* 101, 5–18. doi: 10.1093/aob/mcm240

Shen, N., Wang, T., Gan, Q., Liu, S., Wang, L., and Jin, B. (2022). Plant flavonoids: Classification, distribution, biosynthesis, and antioxidant activity. *Food Chem.* 383, 132531. doi: 10.1016/j.foodchem.2022.132531

Shi, X., Zhang, C., Liu, Q., Zhang, Z., Zheng, B., and Bao, M. (2016). *De novo* comparative transcriptome analysis provides new insights into sucrose induced somatic embryogenesis in camphor tree (*Cinnamomum camphora* l.). *BMC Genomics* 17, 26. doi: 10.1186/s12864-015-2357-8

Strasser, R. J., Srivastava, A., and Govindjee, (1995). Polyphasic chlorophyll a fluorescence transient in plants and cyanobacteria. *Photochem. Photobiol.* 61, 32–42. doi: 10.1111/j.1751-1097.1995.tb09240.x

Strasser, R. J., Srivastava, A., and Tsimilli-Michael, M. (2004). "Analysis of the chlorophyll a fluorescence transient," in *Advances in photosynthesis and respiration. vol. 19: Chlorophyll fluorescence: a signature of photosynthesis*. Eds. G. Papageorgiou and Govindjee, (the Netherlands: Kluwer Academic Publishers), 321–362.

Tian, Z., Luo, Q., Li, Y., and Zuo, Z. (2020). Terpinene and β-pinene acting as signaling molecules to improve *Cinnamomum camphora* thermotolerance. *Ind. Crop Prod.* 154, 112641. doi: 10.1016/j.indcrop.2020.112641

Tian, Z., Luo, Q., and Zuo, Z. (2021). Seasonal emission of monoterpenes from four chemotypes of *Cinnamomum camphora*. *Ind. Crop Prod.* 163, 113327. doi: 10.1016/j.indcrop.2021.113327

Velikova, V., and Loreto, F. (2005). On the relationship between isoprene emission and thermotolerance in *Phragmites australis* leaves exposed to high temperatures and during the recovery from a heat stress. *Plant Cell Environ.* 28, 318–327. doi: 10.1111/j.1365-3040.2004.01314.x

Velikova, V., Vrkonyi, Z., Szab, M., Maslenkova, L., Nogues, I., Kovcs, L., et al. (2011). Increased thermostability of thylakoid membranes in isoprene-emitting leaves probed with three biophysical techniques. *Plant Physiol.* 157, 905–916. doi: 10.1104/pp.111.182519

Vivaldo, G., Masi, E., Taiti, C., Caldarelli, G., and Mancuso, S. (2017). The network of plants volatile organic compounds. *Sci. Rep.* 7, 1–18. doi: 10.1038/s41598-017-10975-x

Wang, X., Cai, J., Liu, F., Dai, T., Cao, W., Wollenweber, B., et al. (2014). Multiple heat priming enhances thermo-tolerance to a later high temperature stress *via* improving subcellular antioxidant activities in wheat seedlings. *Plant Physiol. Biochem.* 74, 185–192. doi: 10.1016/j.plaphy.2013.11.014

Wenig, M., Ghirardo, A., Sales, J. H., Pabst, E. S., Breitenbach, H. H., Antritter, F., et al. (2019). Systemic acquired resistance networks amplify airborne defense cues. *Nat. Commun.* 10, 3813. doi: 10.1038/s41467-019-11798-2

Wojtunik, K. A., Ciesla, L. M., and Waksmundzka-Hajnos, M. (2014). Model studies on the antioxidant activity of common terpenoid constituents of essential oils by means of the 2,2-diphenyl-1-picrylhydrazyl method. *J. Agr. Food Chem.* 62, 9088–9094. doi: 10.1021/jf502857s

Xu, C., Ma, Y., Tian, Z., Luo, Q., Zheng, T., Wang, B., et al. (2022). Monoterpene emissions and their protection effects on adult *Cinnamomum camphora* against high temperature. *Trees – Struct. Funct.* 36, 711–721. doi: 10.1007/s00468-021-02242-4

Yakefu, Z., Huannixi, W., Ye, C., Zheng, T., Chen, S., Peng, X., et al. (2018). Inhibitory effects of extracts from *Cinnamomum camphora* fallen leaves on algae. *Water Sci. Technol.* 77, 2545–2554. doi: 10.2166/wst.2018.199

Zhao, J., Yang, L., Zhou, L., Bai, Y., Wang, B., Hou, P., et al. (2016). Inhibitory effects of eucalyptol and limonene on the photosynthetic abilities in *Chlorella vulgaris* (Chlorophyceae). *Phycologia* 55, 696–702. doi: 10.2216/16-38.1

Zheng, T., Zhou, M., Yang, L., Wang, Y., Wang, Y., Meng, Y., et al. (2020). Effects of high light and temperature on *Microcystis aeruginosa* cell growth and β-cyclocitral emission. *Ecotox. Environ. Safe.* 192, 110313. doi: 10.1016/j.ecoenv.2020.110313

Zuo, Z. (2019). Why algae release volatile organic compounds —–the emission and roles. *Front. Microbiol.* 10, 491. doi: 10.3389/fmicb.2019.00491

Zuo, Z., Wang, B., Ying, B., Zhou, L., and Zhang, R. (2017). Monoterpene emissions contribute to thermotolerance in *Cinnamomum camphora*. *Trees – Struct. Funct.* 31, 1759–1771. doi: 10.1007/s00468-017-1582-y

Zuo, Z., Weraduwage, S. M., Lantz, A. T., Sanchez, L. M., Weise, S. E., Wang, J., et al. (2019). Isoprene acts as a signaling molecule in gene networks important for stress responses and plant growth. *Plant Physiol.* 180, 124–152. doi: 10.1104/pp.18.01391

Zuo, Z., Yang, L., Chen, S., Ye, C., Han, Y., Wang, S., et al. (2018). Effects of nitrogen nutrients on the volatile organic compound emissions from *Microcystis aeruginosa*. *Ecotox. Environ. Safe.* 161, 214–220. doi: 10.1016/j.ecoenv.2018.05.095

frontiers | Frontiers in Plant Science

TYPE Original Research
PUBLISHED 06 January 2023
DOI 10.3389/fpls.2022.1081807

OPEN ACCESS

EDITED BY
Muhammad Mohsin Abrar,
Zhongkai University of Agriculture and Engineering, China

REVIEWED BY
Zhaowen Mo,
South China Agricultural University, China
Mahmood Ul Hassan,
China Agricultural University, China

*CORRESPONDENCE
Yongjin Zhou
zhouyongjin1111@163.com

†These authors have contributed equally to this work

SPECIALTY SECTION
This article was submitted to Plant Abiotic Stress, a section of the journal Frontiers in Plant Science

RECEIVED 27 October 2022
ACCEPTED 07 December 2022
PUBLISHED 06 January 2023

CITATION
Zhang M, Li Z, Feng K, Ji Y, Xu Y, Tu D, Teng B, Liu Q, Liu J, Zhou Y and Wu W (2023) Strategies for indica rice adapted to high-temperature stress in the middle and lower reaches of the Yangtze River.
Front. Plant Sci. 13:1081807.
doi: 10.3389/fpls.2022.1081807

Strategies for indica rice adapted to high-temperature stress in the middle and lower reaches of the Yangtze River

Man Zhang[1,2†], Zhong Li[1†], Kaixuan Feng[1,2], Yalan Ji[1], Youzun Xu[1], Debao Tu[1], Bin Teng[1], Qiumeng Liu[2], Jingwen Liu[2], Yongjin Zhou[1*] and Wenge Wu[1,2]

[1]Rice Research Institute, Anhui Academy of Agricultural Sciences, Hefei, Anhui, China, [2]School of Resources and Environment, Anhui Agricultural University, Hefei, Anhui, China

High temperatures caused by climate warming severely affect the grain yield and quality of rice. In this study, the rice cultivars Longliangyou Huazhan (LLYHZ) and Quanliangyou 2118 (QLY2118) were selected as the experimental materials for investigation of an optimal cultivation system under high-temperature treatment. In addition, the heat-resistant cultivar Huanghuazhan (HHZ) and heat-sensitive cultivar Huiliangyou 858 (HLY858) were chosen as the experimental materials to study the effects of exogenous plant growth regulators on heat stress responses under high-temperature treatment. The results showed that mechanical transplanting of carpet seedlings and delayed sowing effectively increased the leaf area index and reduced the canopy temperature of LLYHZ and QLY2118. Furthermore, carpet seedling mechanical transplantation and delayed sowing improved grain yield and quality. Spray application of five plant growth regulators revealed that brassinolide and salicylic acid had the strongest effects on significantly improving antioxidant enzyme activities in the panicle, which would reduce the damage caused by the accumulation of reactive oxygen species and enhance plant tolerance of high-temperature stress. In addition, brassinolide and salicylic acid enhanced the percentage of anther dehiscence and percentage seed set. In this study, a set of simplified eco-friendly cultivation techniques for single-season indica rice adaptation to high-temperature stress was established. These results will be of great importance in alleviating the effects of high-temperature stress on rice production.

KEYWORDS

rice, high temperature, carpet seedling mechanical transplantation, sowing date, growth regulator

1 Introduction

Global warming is primarily manifested as an increase in average temperature and the frequent incidence of extreme heat (Lobell and Gourdji, 2012). General circulation models estimate an average increase in global surface temperature of approximately 4°C (2.9°C to 5.5°C) (UI Hassan et al., 2021). The trend for climate change in China is essentially consistent with the general trend for global change, but distinct geographical characteristics are evident. The rate of warming in the northern region is significantly greater than that in the southern region, and that in the western region is greater than in the eastern region. The middle and lower reaches of the Yangtze River have frequently experienced extremely high temperatures over a prolonged period. High temperature and the impacts of extreme heat in this area occur mainly from mid-July to early August, with the highest frequency in late July. This coincides with the crucial period for the heading and flowering of mid-season rice in the middle and lower reaches of the Yangtze River. The increase in frequency and intensity of extremely high temperatures will greatly impact rice production (Stephen et al., 2022). Therefore, overcoming the effect of high temperatures on rice during the heading stage is an important focus of agricultural research (Bamagoos et al., 2021).

Heat injury caused by climate warming is a major contributor to the decreases in rice yield and quality (Liu et al., 2021). If the temperature during the vegetative growth period of rice exceeds 35°C, tiller production decreases, the rate of growth in plant height declines, the growth of aboveground and underground plant parts is reduced, and the overall rice development period is shortened. These changes affect the reproductive development of rice, reduce the rate of dry matter accumulation, affect the distribution of dry matter in various organs, and thus severely impact productivity and grain quality (Wassmann et al., 2009). High temperatures in the daytime or the nighttime can affect grain quality. Krishnan et al. (Krishnan et al., 2011) reported that short-term high temperature after flowering adversely affects rice quality and starch granules. In prolonged periods of high temperatures, the degree and frequency of chalkiness are increased, and short-term high-temperature stress reduces amylose accumulation in the grain.

Previous studies have confirmed that high temperature affects the growth of rice during various developmental periods (Yu et al., 2022), especially during the heading stage (Zhang et al., 2021). In response, various cultivation strategies have been adopted in rice production, including changing the planting method (Xing et al., 2017), adjusting the sowing date (Sadras et al., 2015), and spraying plants with chemical regulators (Cao and Hua, 2008). Appropriate rice-planting methods not only improve the soil structure and fertility but also promote grain production (Zhou et al., 2022). Altering the sowing date to adjust the growth period of rice can ensure that the crucial developmental stages coincide with an appropriate temperature and light environment, which is conducive to growth and yield formation (Patel et al., 2019). Spray application of plant growth regulators can increase photosynthetic capacity and promote the synthesis of endogenous hormones to reduce damage from high-temperature stress (Fahad et al., 2016a). With global warming, the frequency and extent of extreme weather are increasing, which has a significant impact on rice production. Farmers frequently choose rice cultivars with yield as their primary consideration and ignore the high-temperature resistance of cultivars; if the sowing date is inappropriate, heading and flowering may coincide with high temperatures. In the face of extremely high temperatures, there is currently a lack of preventative and control measures that can be implemented in rice production. Therefore, it is of considerable importance to establish environmentally friendly, simplified cultivation techniques for single-season indica rice to reduce the impact of high-temperature stress on rice production.

2 Materials and methods

2.1 Field test

2.1.1 Experimental design

The field experiment was conducted in 2019 at the Guohe Base Test Site in Lujiang County, Anhui Province, China. Temperature differences were achieved by employing two sowing dates to simulate high- and normal-temperature environments. The rice cultivars Longliangyou Huazhan (LLYHZ) and Quanliangyou 2118 (QLY2118), which are suitable for cultivation in the middle and lower reaches of the Yangtze River, were selected as the experimental materials. Two sowing dates (16 and 22 May) and two transplanting methods (manual transplanting and blanket seedling automated transplanting) were applied for a total of eight treatments. Transplanting was performed on 15 June. Three replicate plots, each 200 m^2 in area, were established for each treatment, comprising a total of 24 plots. To prevent the stacking of fertilizer between different plots, all ridges were covered with black plastic film, and the film was inserted on either side of the ridges to a depth of 20 cm. Nitrogen fertilizer (in the form of urea) was applied to each treatment at a rate of 225 kg N ha^{-1} and the ratio of base fertilizer to tiller fertilizer to panicle fertilizer was 5 : 2 : 3. Phosphate fertilizer (in the form of superphosphate) was applied at a rate of 75 kg P ha^{-1} as a base fertilizer. Potassium fertilizer (in the form of potassium chloride) was applied at a rate of 120 kg K ha^{-1} as a base fertilizer and ear fertilizer in two equal amounts. Base fertilizer, tillering fertilizer, and panicle fertilizer were applied 1 d before transplantation, at

early tillering (7 d after transplantation), and at the immature panicle differentiation stage, respectively. Water management during the experiment was conducted as follows: immediately after transplanting, irrigation to a depth of 3–5 cm was carried out, 80% sufficient to drain the field at the seedling stage to reduce ineffective tillering; and 7 d before maturity, the field was drained and sun-dried to facilitate harvesting. Strict control of diseases, pests, and weeds was applied throughout the growth period.

2.1.2 Determination of the leaf area index, meteorological data, and yield

At the heading stage, four holes were sampled in each plot based on the average number of tillers. Plants were divided into stems, leaves, and ears. The leaf area index was determined with an LI-3000 (LI-COR; America) leaf area meter.

The canopy temperature and relative humidity of each treatment was measured with a HOBO MX2301A (HOBO MX2301A ONSET HOBO; America) data logger. The air temperature and relative humidity at the heading stage were measured with a micro weather station.

At the maturity stage, an area of 5.0 m^2 with uniform growth was selected at the center of each plot to measure grain yield. The grain weight was determined after hygrometric adjustment; the grain water content was measured with a grain moisture meter (PM-8188-A kett; Japan), and then the yield with a water content of 13.5% was calculated. Four adjacent sides of the yield area were cut, with three points on each side. A total of 12 representative plants were placed in a net bag for seed testing. After drying in the shade, the total number of grains per sampling point was counted manually. The mean number of grains per panicle at the sampling point was calculated. All rice plants from one hole were placed in a grain separator to remove the husks and empty grains. Based on the number of filled grains obtained after separation, the percentage seed set of the total number of grains was calculated. Two sets of 1,000 grains were sampled from among the filled grains, and the 1,000-grain weight was measured.

2.2 Pot experiment

2.2.1 Experimental design

The pot experiment was reliant on the field experiment. At 15 d before heading in the field experiment, plants with comparable growth tillers were selected, and the plants and rhizosphere soil were dug up from the paddy field and transplanted into pots (height 30 cm and diameter 30 cm). At the heading stage, the plant was labeled and transferred to an artificial climate incubator for treatment for 7 d with a high temperature (37°C) or a normal temperature (32°C; the control).

2.2.2 Determination of grain quality and percentage seed set

The pot-grown plants from the same sampling points were cut and placed in a net bag, dried in a cool place, and then threshed manually. All plants from one sampling point were placed in a grain separator to remove the husks and empty grains. The number of filled grains was determined and the percentage seed set relative to the total number of filled grains was calculated.

The filled grains were dried after harvest and stored indoors for 3 months until the physical and chemical properties were stable. The gel consistency, relative crystallinity, and amylose content of the grains were determined using a PERTON IM9500 near-infrared grain analyzer.

2.3 Plant growth regulator control test

2.3.1 Experimental design

A screening test for plant growth regulators was conducted at the Hefei Branch of the National Rice Improvement Center, Anhui Academy of Agricultural Sciences, China, in 2020. The heat-resistant rice cultivar Huanghuazhan (HHZ) and the heat-sensitive cultivar Huiliangyou 858 (HLY858) were used in the pot experiment. The seeds were sown on 14 May and the seedlings were cultivated in the field. On 11 June, seedlings of uniform growth were selected and transferred to plastic buckets (height 30 cm and diameter 30 cm). At 1 d before transplantation, 1.0 g of pure nitrogen, 1.5 g of pure phosphorus, and 0.7 g of pure potassium were applied to each bucket and mixed well as a base fertilizer application. At 7 d after transplantation, 0.4 g of pure nitrogen was applied to each bucket as tillering fertilizer. At the immature panicle differentiation stage, 0.6 g of pure nitrogen and 0.7 g of pure potassium were applied to each bucket as panicle fertilizer. Other management measures were conducted in accordance with the requirements for high-yield rice cultivation. When the panicle head emerged from the flag leaf, tillers or main stems of consistent growth were selected for labeling, and the plants were placed in a greenhouse for treatment with high temperature (37°C) or a normal temperature (32°C; the control). Plant growth regulators [brassinolide (BR), 0.15 mg l^{-1} (Chen et al., 2019); salicylic acid (SA), 500 μmol l^{-1} (Yang et al., 2019); abscisic acid (ABA), 100 μmol l^{-1} (Rezaul et al., 2019); 6-benzylaminopurine (6-BA), 60 mg l^{-1} (Wu et al., 2016); and potassium dihydrogen phosphate (MP), 22.05 mmol l^{-1} (Yang et al., 2019)] were applied as a foliar spray on the first day before high-temperature treatment and the third day after treatment; water was applied as the control. After 5 d of high-temperature treatment, the plants were transferred to a greenhouse at ambient temperature for growth. Once there was no risk of high temperatures outdoors, the plants were moved outside to grow to maturity.

2.3.2 Determination of the percentage anther dehiscence and antioxidant enzyme activity

At noon on the third day of high-temperature treatment, anthers were observed under a stereomicroscope and the percentage dehiscence was calculated as follows: anther dehiscence (%) = (number of fully dehiscent anthers + number of partially dehiscent anthers)/total number of anthers examined × 100.

Fresh spikelets treated at high temperature for 3 d were ground in liquid nitrogen and suspended in 5 ml of precooled phosphate-buffered saline (PBS; 50 mM, pH 7.0). The homogenates were centrifuged at 22,000 × g for 10 min at 4°C, and the supernatant was analyzed for antioxidant enzymes superoxide dismutase (SOD), peroxidase (POD), and catalase (CAT). The activities of SOD, POD, and CAT were determined in accordance with the methods of Nahakpam (Nahakpam and Shah, 2011).

2.4 Statistical analysis

Three biological replicates were included for all measurements. The significance of differences among the treatments was statistically analyzed using one-way analysis of variance (ANOVA) followed by the least significant difference (LSD) multiple-range test ($p < 0.05$). The statistical packages OriginPro 8.0 (OriginLab, Northampton, MA, USA) and the Data Processing System (DPS) version 7.05 (Zhejiang University, Hangzhou, China) were used for the statistical analyses.

3 Results

3.1 Appropriate sowing date to alleviate high-temperature *stress*

High temperatures in the Jianghuai area of Anhui Province occur mainly from mid-July to mid-August, with the highest temperatures recorded from late July to early August. In 2019, high temperatures were recorded in late July and early August (in total 13 d) (Figure 1). In the present experiment, under the normal sowing date (NSD) (16 May), the heading and flowering period was prone to high-temperature stress. The heading and flowering period of LLYHZ and QLY2118 in the manual transplanting treatment experienced 3 d and 8 d of high temperatures, respectively, whereas in the carpet seedling mechanical transplanting treatment the two cultivars experienced only 1 d and 2 d of high temperatures, respectively. Under delayed sowing (22 May), the number of days of high-temperature stress in the heading and flowering period in the manual transplanting treatment (2 d and 3 d) was lower than that under the normal sowing date, but the plants were still exposed to high-temperature stress, whereas plants in the carpet seedling mechanical transplanting treatment under delayed sowing avoided exposure to high-temperature stress (Supplementary Table S1).

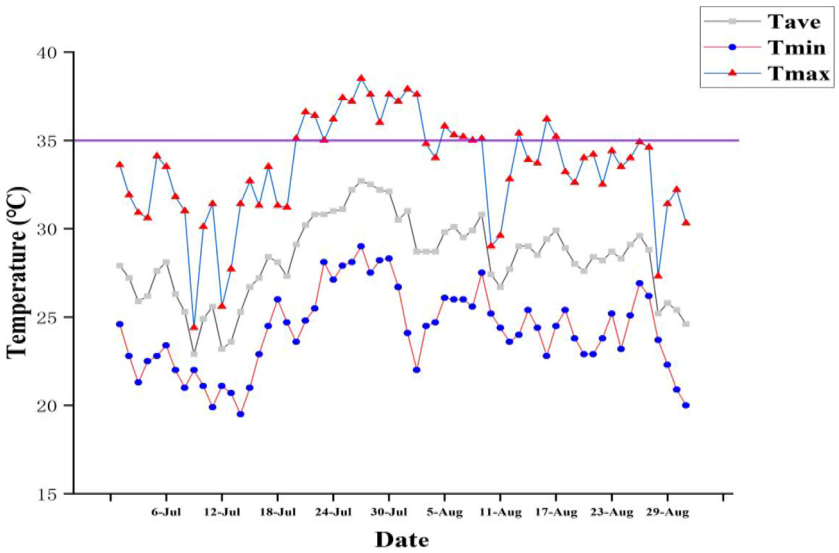

FIGURE 1
Daily maximum temperature, daily minimum temperature, and daily average temperature in Lujiang district from July to August in 2019. T_{ave}, daily average temperature; T_{min}, daily minimum temperature; T_{max}, daily maximum temperature. The horizontal line is the threshold (35°C) for high temperature.

3.2 Leaf area index and canopy temperature of rice plants at the heading stage

No significant difference in the leaf area index of LYYHZ was observed between the two sowing dates under the carpet seedling mechanical transplanting treatment [NSD: 11.46 m^2 m^{-2}; delayed sowing date (DSD): 11.28 m^2 m^{-2}] or under the manual transplanting treatment (NSD: 5.76 m^2 m^{-2}; DSD: 6.67 m^2 m^{-2}). The leaf area index of QLY2118 under mechanical transplanting with the normal sowing date (9.61 m^2 m^{-2}) was significantly lower than that with the delayed sowing date (11.56 m^2 m^{-2}). Under the manual transplanting treatment, the leaf area index of QLY2118 with the normal sowing date (7.91 m^2 m^{-2}) was significantly lower than that of the delayed sowing date (9.64 m^2 m^{-2}). Further analysis showed that, with the same sowing date, the leaf area indices of YLLHZ and QLY2118 in the carpet seedling mechanical transplanting treatment were significantly higher than those in the manual transplanting treatment (Figure 2).

The canopy temperature of plants at the heading stage under the two planting methods was lower than that of the air temperature, but the difference between the canopy temperature and air temperature under the different planting methods was significant. The canopy temperature of plants during the heading stage in the carpet seedling mechanical transplanting treatment was 0.31–0.63°C lower than the air temperature, whereas the canopy temperature during the heading stage in the manual transplanting treatment was 0.18–0.29°C lower than the air temperature (Table 1). These results show that the carpet seedling mechanical transplanting method led to a reduced canopy temperature by increasing the leaf area index.

3.3 Grain yield and yield components under the different treatments

A significant interaction was observed between sowing date and planting method on grain yield and percentage seed set. Under the carpet seedling mechanical transplanting treatment, no significant difference in effective panicle number, grain number per panicle, percentage seed set, or grain yield was observed among the sowing date treatments, but the 1,000-grain weight under the normal sowing date (LLYHZ, 187.6; QLY2118, 186) was significantly lower than that under the delayed sowing date (LLYHZ, 231.0; QLY2118, 210.0). Under the manual transplanting method, the grain yield of the normal sowing date treatment (LLYHZ, 11.6 t ha^{-1}; QLY2118, 10.6 t ha^{-1}) was significantly lower than that of the delayed sowing treatment (LLYHZ, 13.1 t ha^{-1}; QLY2118, 13.5 t ha^{-1}); the grain yields of LLYHZ and QLY2118 decreased by 11.5% and 21.5%, respectively (Table 2).

3.4 Effects of high temperature on percentage seed set and grain quality of pot-grown rice plants

High temperature had a significant effect on the percentage seed set under both planting methods (Figure 3). Under carpet seedling mechanical transplantation (70.7%) and manual transplanting (70.3%), the percentage seed set of LLYHZ under high-temperature treatment was 15.1% and 14.8% lower than that under normal temperature treatment (83.3% and 82.5%), respectively, and the percentage seed set of QLY2118

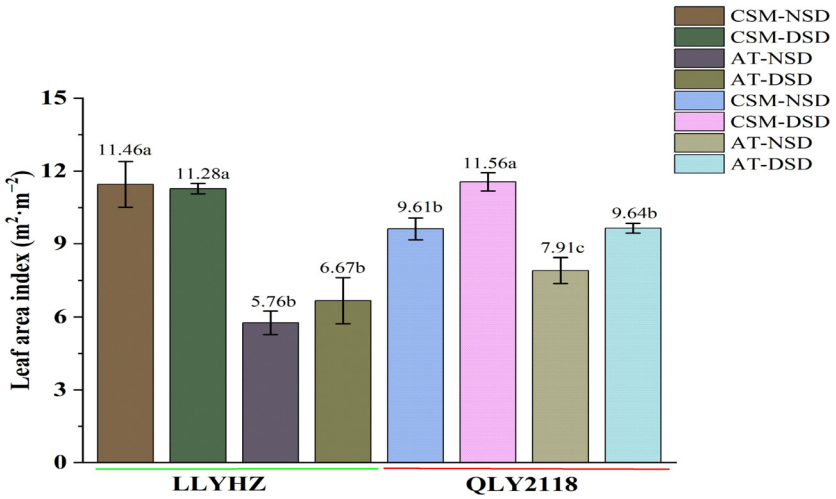

FIGURE 2
Leaf area index of two rice cultivars in the different treatments at the heading stage. Error bars indicate the SD of three biological replicates. Bars with different lowercase letters are significantly different (LSD test, $p < 0.05$). LLYHZ, Longliangyou Huazhan; QLY2118, Quanliangyou 2118; NSD, normal sowing date; DSD, delayed sowing date; CSM, carpet seedling mechanical transplantation; MT, manual transplanting; SD, standard deviation.

10.3389/fpls.2022.1081807

TABLE 1 Leaf area index, average maximum canopy temperature, and temperature difference between treatments at the heading stage of two rice cultivars.

Cultivar	SD	PM	MMTC (°C)	MMAC (°C)	TDV (°C)
LLYHZ	NSD	CSM	32.51 ± 1.97 a	33.14 ± 2.01 a	0.63
	DSD	CSM	29.71 ± 4.05 b	30.19 ± 4.03 b	0.48
	NSD	AT	33.15 ± 2.04 a	33.34 ± 2.02 a	0.19
	DSD	AT	33.41 ± 2.06a	33.59 ± 2.06 a	0.18
QLY2118	NSD	CSM	33.12 ± 2.16 a	33.43 ± 2.15 ab	0.31
	DSD	CSM	30.74 ± 3.74 b	31.53 ± 3.79 b	0.79
	NSD	AT	33.86 ± 2.22 a	34.01 ± 2.20 a	0.15
	DSD	AT	33.37 ± 1.59 a	33.66 ± 1.59 a	0.29

LLYHZ, Longliangyou Huazhan; QLY2118, Quanliangyou 2118; SD, sowing date; PM, planting method; MMTC, mean maximum canopy temperature; MMAC, mean maximum atmospheric temperature; TDV, temperature difference value; NSD, normal sowing date; DSD, delayed sowing date; CSM, carpet seedling mechanical transplantation; AT, manual transplanting; SD, standard deviation. Different lowercase letters within a column indicate a significant difference (LSD test, $p < 0.05$). Error values are the SD of three biological replicates.

under high-temperature treatment (67.6% and 68.6%) was 20.8% and 15.6% lower than that under normal temperature treatment (85.4% and 81.3%), respectively. Under exposure to high-temperature stress, grain quality decreased significantly. High temperature significantly decreased the amylose content, gel consistency, and relative crystallinity of the grain under both transplanting methods (Figures 4A–C).

3.5 Effects of plant growth regulators on anther dehiscence and percentage seed set

High-temperature treatment had a significant effect on the percentage seed set (Figures 5A, B). The percentage seed set of HHZ sprayed with BR, SA, ABA, 6-BA, MP, and CK was 19.6%, 22.1%, 26.1%, 29.3%, 32.2%, and 53.7%, respectively. The percentage seed set of HLY858 sprayed with BR, SA, ABA, 6-BA, MP, and CK was 42.6%, 43.5%, 45.7%, 51.6%, 53.4%, and 54.3%, respectively. The decrease in seed set under high-temperature treatment of the heat-sensitive cultivar HLY858 was greater than that of the heat-resistant cultivar HHZ. Under high-temperature treatment, compared with the water spray treatment, spray application of growth regulators increased the percentage seed set. Different growth regulators had different effects on alleviating high-temperature stress. The CK, BR, and SA treatments had the strongest effect on increasing the percentage seed set.

High-temperature treatment had a significant effect on anther dehiscence (Figure 5C, D). Compared with the normal temperature treatment, the average anther dehiscence

TABLE 2 Yield of two rice cultivars in the different treatments and their yield components.

Cultivar	SD	PM	NEP (no. m^{-2})	GNP	SSR (%)	TSW (g)	Yield (t ha^{-1})
LLYHZ	NSD	CSM	403.6 ± 17.6 a	187.6 ± 21.0 b	85.2 ± 1.2 a	21.8 ± 0.4 a	16.3 ± 1.0 a
	DSD	CSM	378.1 ± 19.2 a	196.7 ± 13.8 ab	84.3 ± 0.4 ab	22.9 ± 0.2 b	16.8 ± 0.7 a
	NSD	AT	295.9 ± 10.1 b	231.0 ± 34.2 a	80.6 ± 2.0 c	21.6 ± 0.1 bc	11.6 ± 0.4 c
	DSD	AT	311.1 ± 15.1 b	236.2 ± 12.1 a	82.3 ± 1.5 bc	21.3 ± 0.2 c	13.1 ± 0.2 b
QLY2118	NSD	CSM	381.1 ± 21.0 a	186.0 ± 11.4 b	86.0 ± 2.2 a	22.5 ± 0.3 a	14.0 ± 0.7 a
	DSD	CSM	405.8 ± 22.7 a	178.4 ± 5.7 b	87.1 ± 4.1 a	23.8 ± 0.3 b	14.0 ± 0.8 a
	NSD	AT	263.2 ± 22.4 b	210.0 ± 8.5 a	78.3 ± 1.6 b	22.7 ± 0.4 b	10.6 ± 0.4 a
	DSD	AT	289.8 ± 17.7 b	226.7 ± 11.0 a	85.6 ± 0.8 a	22.5 ± 0.3 b	13.5 ± 0.8 b

LLYHZ, Longliangyou Huazhan; QLY2118, Quanliangyou 2118; SD, sowing date; PM, planting method; NSD, normal sowing date; DSD, delayed sowing date; CSM, carpet seedling mechanical transplantation; AT, manual transplanting; NEP, number of effective panicles; GNP, grain number per panicle; SSR, percentage seed set; TSW, thousand-seed weight. Different lowercase letters within a column indicate a significant difference (LSD test, $p < 0.05$). Error values are the SD of three biological replicates.

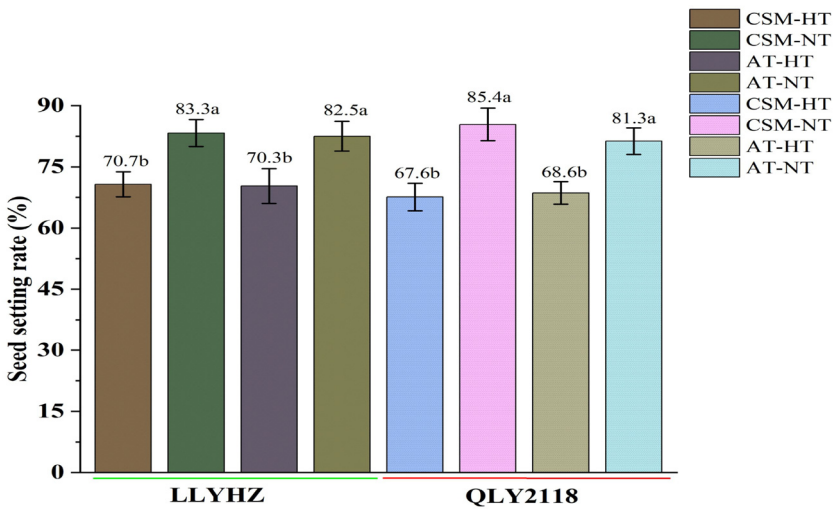

FIGURE 3
Effect of high temperature on seed set of two rice cultivars under different planting methods. Bars with different lowercase letters indicate a significant difference (LSD test, $p < 0.05$). Error bars indicate the SD of three biological replicates. LLYHZ, Longliangyou Huazhan; QLY2118, Quanliangyou 2118; CSM, carpet seedling mechanical transplantation; AT, manual transplanting; HT, high temperature; NT, normal temperature.

percentage of HHZ and HLY858 decreased by 34.5% and 54.2%, respectively, under high-temperature stress. Under the high-temperature treatment, compared with the control, spray application of growth regulators increased the anther dehiscence percentage. The growth regulators differed in their effect on alleviation of high-temperature stress, of which brassinolide and salicylic acid treatment had the greatest effect on increasing the anther dehiscence percentage.

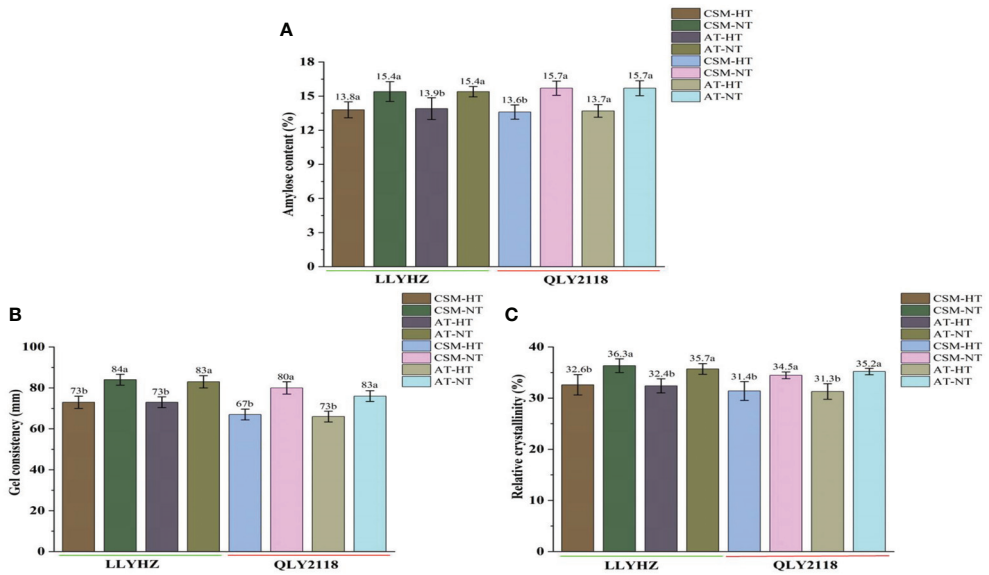

FIGURE 4
Effect of high temperature on grain quality of two rice cultivars. **(A)** Amylose content of the grains. **(B)** Gel consistency of the grains. **(C)** Relative crystallinity of the grains. Bars with different lowercase letters indicate a significant difference (LSD test, $p < 0.05$). Error bars indicate the SD of three biological replicates. LLYHZ, Longliangyou Huazhan; QLY2118, Quanliangyou 2118; CSM, carpet seedling mechanical transplantation; AT, manual transplanting; HT, high temperature; NT, normal temperature.

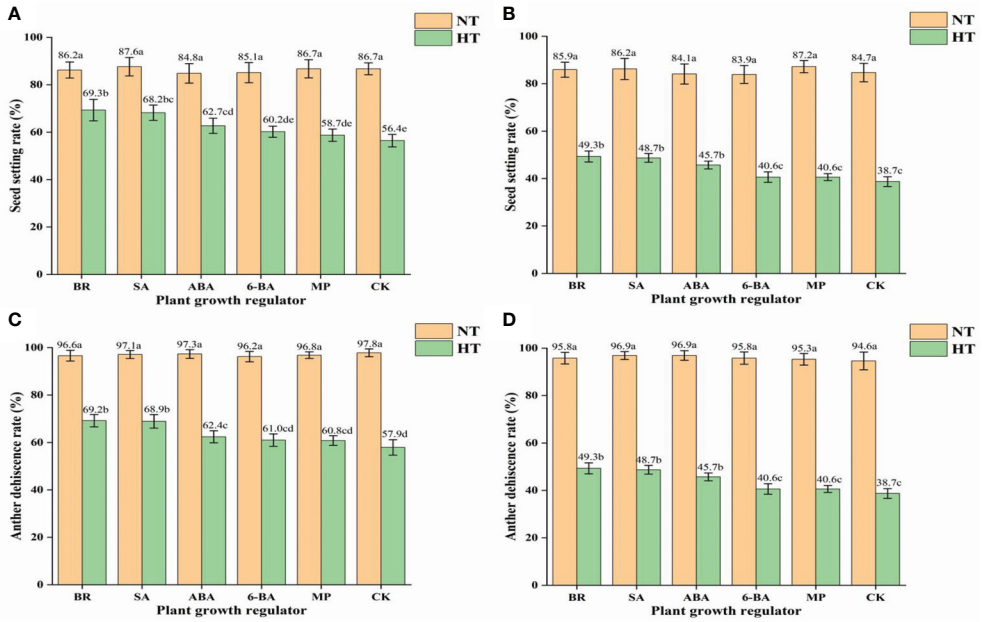

FIGURE 5
Effects of plant growth regulators on seed set and anther dehiscence of two rice cultivars under different temperature treatments. **(A)** Seed set of Huanghuazhan (HHZ). **(B)** Seed set of Huiliangyou 858 (HLY858). **(C)** Anther dehiscence of HHZ. **(D)** Anther dehiscence of HKY858. Bars with different lowercase letters indicate a significant difference (LSD test, $p < 0.05$). Error bars indicate the SD of three biological replicates. HT, high temperature; NT, normal temperature. BR, brassinolide; SA, salicylic acid; ABA, abscisic acid; 6-BA, benzylaminopurine; MP, potassium dihydrogen phosphate; CK, water.

3.6 Effects of plant growth regulators on *the* antioxidant enzyme activities of rice spikelets

High-temperature treatment had a significant effect on the antioxidant enzyme activity of rice spikelets (Figures 6A–C). Compared with the normal temperature, the SOD activity in spikelets of HHZ sprayed with BR, SA, and CK under high-temperature treatment decreased by 15.8%, 16.6%, and 23.5%, respectively, whereas that of HLY858 under high-temperature treatment decreased by 27.5%, 29.4%, and 44.3%, respectively. Compared with the normal temperature, the POD activity in spikelets of HHZ sprayed with BR, SA, and CK under high-temperature treatment decreased by 10.7%, 11.5%, and 18.2%, respectively, and that of HLY858 under high-temperature treatment decreased by 25.4%, 25.8%, and 41.5%, respectively. Compared with the normal temperature, the CAT activity in spikelets of HHZ sprayed with BR, SA, and CK under high-temperature treatment decreased by 19.6%, 17.5%, and 22.1%, and that of HLY858 under high-temperature treatment decreased by 23.5%, 24.6%, and 30.5%, respectively. The decrease in antioxidant enzyme activities of the heat-sensitive cultivar HLY858 was significantly greater than that of the heat-tolerant cultivar HHZ. Under high-temperature treatment, compared with the water treatment, spray application of growth regulators increased the activity of antioxidant enzymes in the two rice cultivars. The increase in activities of HLY858 was greater than that in HHZ.

4 Discussion

4.1 Effects of high temperature on *the* yield and quality of rice

The formation of crop yield is the process by which crops use environmental resources to complete their growth cycle to maturity and develop economically valuable products. Temperature is arguably the most easily monitored meteorological indicator among the many environmental factors that consistently affect yield. The components of rice yield include panicle number, grain number, percentage seed set, and 1,000-grain weight. The temperature requirements differ among the developmental stages of rice. Previous studies have shown that high-temperature stress in rice leads to pollen swelling and deformation (Wu et al., 2017) and 'sticky' pollen grains that adhere together in the anther, ultimately leading to a reduced frequency of pollen germination on the stigma (Rativa et al., 2020). In addition, high temperature at the heading stage affects the maturation and germination of pollen grains, reduces

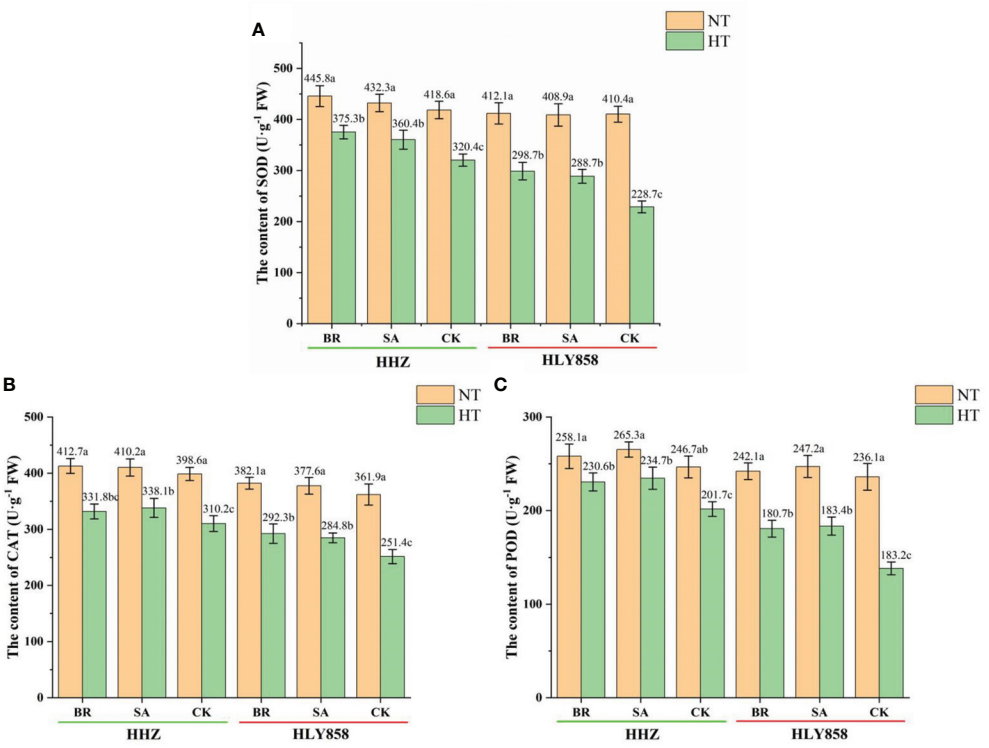

FIGURE 6
Effects of plant growth regulators on alleviating high temperature stress on antioxidant enzymes in the spikelet of two rice cultivars. **(A)** Superoxide dismutase (SOD); **(B)** catalase (CAT); **(C)** peroxidase (POD). Bars with different lowercase letters indicate a significant difference (LSD test, $p < 0.05$). Error bars indicate the SD of three biological replicates. HHZ, Huanghuazhan; HLY858, Huiliangyou 858; HT, high temperature; NT, normal temperature; BR, brassinolide; SA, salicylic acid; ABA, abscisic acid; 6-BA, 6-benzylaminopurine; MP, potassium dihydrogen phosphate; CK, water.

the percentage fertilization, and increases the number of empty grains, resulting in decreases in seed set and 1,000-grain weight (Satake et al., 1988). With regard to yield components in rice, the optimum temperature in the vegetative growth period is 28.4°C, and during the grain-filling period it is 21.7–26.7°C; the daily average maximum temperature should not exceed 35°C. If the temperature exceeds 27°C during the grain-filling period, it will cause a reduction in the percentage seed set and 1,000-grain weight and will affect the grain yield. This is consistent with the present results, which show that both natural high temperature and simulated high temperature reduced the percentage seed set. High temperature also affects the grain quality of rice. High temperature during the grain-filling stage leads to a reduction in the gel consistency and amylose content of the grain (Lin et al., 2010). Kobata et al. (Kobata et al., 2004) reported that high temperature leads to a lack of starch substrates in the endosperm and an increase in grain chalkiness, and the abnormal loss of endosperm moisture under high temperature also leads to the development of chalkiness (Ishimaru et al., 2009). Consistent with previous studies, the present results show that high temperature significantly reduced the amylose content, gel consistency, and relative crystallinity of rice grains, confirming that high temperature reduces the grain quality and yield of rice.

4.2 Reasonable sowing date to alleviate *high-temperature* damage *to* rice

One means of avoiding the risk of high-temperature stress is to adjust the sowing date to stagger the crucial stages of rice growth and the timing of high temperature to alleviate the effects of high temperature on rice. Selection of an appropriate sowing date is conducive to efficient development of the production potential in rice. In the present experiment, rice grown under a normal sowing date was more likely to suffer from high-temperature stress and significant decreases in the percentage seed set and grain yield than rice grown under a delayed sowing date. A delayed sowing date effectively avoided the effects of high temperature in the heading and flowering stages, which was beneficial to the growth of the plant. However, the delay in sowing date shortens the vegetative growth period, and the population growth is reduced, which negatively affects the

yield components and results in lower yield (Patel et al., 2019). An excessively early or overly late sowing date is not conducive to the coordinated development of rice plants (Kumar et al., 2012). In addition, the sowing date has a strong impact on grain quality. High temperature at the heading stage increases the amylose and protein contents and decreases the gel consistency of the grain (Krishnan et al., 2011). However, the decrease in amylose content under high temperature may reflect genotypic differences among cultivars (Sreenivasulu et al., 2015). The sowing date can alter the severity of damage of high temperature on rice, change the temperature and light resources during the grain-filling period, and indirectly or directly affect grain quality and yield. An early sowing date and short growth period are not conducive to most effectively utilizing the local temperature and light environment. Late-maturing cultivars with a relatively long growth period can be chosen to exploit local temperature and light resources. Late sowing of cultivars with a long growth period will affect the reliability of full heading and late grain filling, and the cultivar's yield potential will not be realized. Therefore, the selection of a cultivar with a slightly shorter growth period, rapid tillering, and favorable traits for early maturation will help to ensure grain filling and maturity and that a high yield is attained.

4.3 Alleviating heat injury *in* rice by different planting methods

Given differences in the utilization efficiency of resources, such as temperature and light, different planting methods will inevitably have a certain impact on the growth of rice. Differences were observed in the adaptability of rice to high temperatures in summer under different planting methods. For single-season indica rice cultivars with an initial sowing period of more than 94 d in the Jianghuai area of Anhui Province, the mechanical transplanting of carpet seedlings (sown on 16 May) effectively avoided high-temperature stress at the heading and flowering stages. In addition, carpet seedling mechanical transplantion can alleviate the damage from high temperature to a certain extent by increasing population growth and reducing the canopy temperature. The yield of rice under different planting methods was previously reported to be significantly positively correlated with the accumulation of total dry matter (San-Oh et al., 2008). The material output rate and conversion rate of rice leaves and stems are highest in hand-transplanted rice and lowest in direct-seeded rice.

The damage from high temperature differs among rice seedlings grown under different planting methods, which affects the entire development process. The duration of the seedling stage is used to avoid the risk of high-temperature exposure at a later developmental stage. In addition, the yield under different planting methods also differs. Thus, choosing the most appropriate planting method is crucial to maximize the potential benefits.

4.4 Chemical regulation alleviates high-temperature damage to rice

The application of exogenous plant growth regulators can reduce damage from high temperature. Mixed application of plant growth regulators under high temperature can increase the photosynthetic capacity of rice leaves and improve spikelet fertility and grain filling (Fahad et al., 2016b). Spray application of exogenous ABA may regulate stomatal closure in the leaves, induce the expression of responsive genes and the synthesis of endogenous ABA and heat shock proteins, and improve the high-temperature tolerance of plants (Rezaul et al., 2019). Spray application of brassinolide in the middle and late stages of pollen mother cell meiosis increases SOD activity and the contents of proline, soluble sugar, and ABA in florets at the heading stage, improves the high-temperature tolerance of plants at the heading stage, and reduces the decrease in percentage seed set under high-temperature stress at the heading stage (Chen et al., 2021; Raghunath et al., 2021). In addition, spray application of SA (Yang et al., 2022), auxin (Sharma et al., 2018), MP (Yang et al., 2019), and other substances can alleviate high-temperature stress to a certain extent. In the present study, spray application of five plant growth regulators effectively reduced damage from high temperatures on rice. The main responses were to improve SOD, POD, and CAT activities, percentage anther dehiscence, and percentage seed set. Among the growth regulators applied in this study, brassinolide and SA had the strongest beneficial effects.

4.5 Simplified green cultivation system for single-season indica rice adapted to high-temperature stress in the middle and lower reaches of the Yangtze River

Based on physiological and agronomic research on high-temperature resistance, it is very important to optimize the existing cultivation techniques and regulate the growth and development process of rice. These are useful in making rice plants adapt to the high-temperature stress caused by global warming. This study integrated high-temperature damage and control technology models for indica rice in the middle and lower reaches of the Yangtze River. The conclusions are as follows: (1) select the varieties with high quality, high yield, and high-temperature resistance; (2) determine a reasonable sowing date to avoid high temperature during the heading and flowering stages of rice; (3) mechanize rice transplanting to establish a healthy community structure and improve rice resistance to high temperature; and (4) compensate with

cultivation disaster reduction measures (i.e., application of plant growth regulators).

5 Conclusion

The present results show that carpet seedling mechanical transplantation and a delayed sowing date in combination effectively avoided high-temperature stress at the heading and flowering stages of rice. The carpet seedling transplanting method promoted population growth, thereby reducing the canopy temperature and alleviating the risk of high-temperature stress. However, high temperatures led to a decrease in the percentage seed set and reduced grain quality under both mechanical transplanting and manual transplanting. The plant growth regulators brassinolide and SA alleviated injury from high-temperature stress at the heading and flowering stages by increasing the activity of antioxidant enzymes in the panicles, thereby reducing the damage caused by accumulation of reactive oxygen species, enhancing the high-temperature tolerance of plants, and increasing the percentage of anther dehiscence and the percentage seed set.

Data availability statement

The original contributions presented in the study are included in the article/Supplementary Material. Further inquiries can be directed to the corresponding author.

Author contributions

MZ, ZL, and YZ: Conceptualization. MZ, ZL, KF, BT, QL, and YZ: investigation; MZ, YJ, YX, JL, DT, and WW: formal analysis. MZ, ZL, and YZ: writing. All authors have read and agreed to the published version of the manuscript.

Funding

This research was funded by National Natural Science Foundation of China (32101822), Anhui Provincial Natural Science Foundation (2108085QC109), Young Talents Program of Anhui Academy of Agricultural Sciences (QNYC-201904) Discipline leading talents Program of Anhui Academy of Agricultural Sciences (LJRC-202102), Anhui Provincial Special Project for Transformation and application of agricultural Scientific and Technological Achievements (2021ZH001), and the National Key Research and Development Program of China (2017YFD0300106).

Conflict of interest

The authors declare that the research was conducted in the absence of any commercial or financial relationships that could be construed as a potential conflict of interest.

Publisher's note

All claims expressed in this article are solely those of the authors and do not necessarily represent those of their affiliated organizations, or those of the publisher, the editors and the reviewers. Any product that may be evaluated in this article, or claim that may be made by its manufacturer, is not guaranteed or endorsed by the publisher.

Supplementary material

The Supplementary Material for this article can be found online at: https://www.frontiersin.org/articles/10.3389/fpls.2022.1081807/full#supplementary-material

References

Bamagoos, A., Alharby, H., and Fahad, S. (2021). Biochar coupling with phosphorus fertilization modifies antioxidant activity, osmolyte accumulation and reactive oxygen species synthesis in the leaves and xylem sap of rice cultivars under high-temperature stress. *Physiol. Mol. Biol. Plants* 27 (9), 2083–2100. doi: 10.1007/s12298-021-01062-7

Cao, Y., and Hua, Z. (2008). Protective roles of brassinolide on rice seedlings under high temperature stress. *Rice Sci.* 15 (1), 63–68. doi: 10.1016/S1672-6308(08)60021-9

Chen, Y., Chen, H., Xiang, J., Zhang, Y., Wang, Z., Zhu, D., et al. (2021). Rice spikelet formation inhibition caused by decreased sugar utilization under high temperature is associated with brassinolide decomposition. *Environ. Exp. Bot.* 190, 104585. doi: 10.1016/j.envexpbot.2021.104585

Chen, Y., Wang, Y., Zhu, D., Shi, Q., Chen, H., Xiang, J., et al. (2019). Mechanism of exogenous brassinolide in alleviating high temperature injury at panicle initiation stage in rice. *Chin. J. Rice Sci.* 33 (5), 457–466. doi: 10.16819/j.1001-7216.2019.9036

Fahad, S., Hussain, S., Saud, S., Hassan, S., Ihsan, Z., Shah, A. N., et al. (2016a). Exogenously applied plant growth regulators enhance the morpho-physiological growth and yield of rice under high temperature. *Front. Plant Sci.* 7, 1250. doi: 10.3389/fpls.2016.01250

Fahad, S., Hussain, S., Saud, S., Khan, F., Hassan, S., Nasim, W., et al. (2016b). Exogenously applied plant growth regulators affect heat-stressed rice pollens. *J. Agron. Crop Sci.* 202 (2), 139–150. doi: 10.1111/jac.12148

Ishimaru, T., Horigane, A. K., Ida, M., Iwasawa, N., San-oh, Y. A., Nakazono, M., et al. (2009). Formation of grain chalkiness and changes in water distribution in developing rice caryopses grown under high-temperature stress. *J. Cereal Sci.* 50 (2), 166–174. doi: 10.1016/j.jcs.2009.04.011

Kobata, T., Uemuki, N., Inamura, T., and Kagata, H. (2004). Shortage of assimilate supply to grain increases the proportion of milky white rice kernels under high temperatures. *Japanese J. Crop Sci.* 73 (3), 315–322. doi: 10.1626/jcs.73.315

Krishnan, P., Ramakrishnan, B., Reddy, K. R., and Reddy, V. (2011). High-temperature effects on rice growth, yield, and grain quality. *Adv. Agron.* 111, 187–206. doi: 10.1016/B978-0-12-387689-8.00004-7

Kumar, J., Singh, D., Singh, B., Singh, R., Panwar, S., and Gupta, A. K. (2012). Sowing time and weed management practices to enhance yield of direct-seeded rice. *Indian J. Weed Sci.* 44 (4), 207–209. doi: IJWS-2012-44-4-1

Lin, C., Li, C., Lin, S., Yang, F., Huang, J., Liu, Y., et al. (2010). Influence of high temperature during grain filling on the accumulation of storage proteins and grain quality in rice (Oryza sativa l.). *J. Agric. Food Chem.* 58 (19), 10545–10552. doi: 10.1021/jf101575j

Liu, W., Yin, T., Zhao, Y., Wang, X., Wang, K., Shen, Y., et al. (2021). Effects of high temperature on rice grain development and quality formation based on proteomics comparative analysis under field warming. *Front. Plant Sci.* 12, 746180. doi: 10.3389/fpls.2021.746180

Lobell, D., and Gourdji, S. (2012). The influence of climate change on global crop productivity. *Plant Physiol.* 160 (4), 1686–1697. doi: 10.1104/pp.112.208298

Nahakpam, S., and Shah, K. (2011). Expression of key antioxidant enzymes under combined effect of heat and cadmium toxicity in growing rice seeding. *Plant Growth Regul.* 63, 23–35. doi: 10.1007/s10725-010-9508-3

Patel, A., Patel, M., Patel, R., and Mote, B. (2019). Effect of different sowing date on phenology, growth and yield of rice–a review. *Plant Arch.* 19 (1), 12–16.

Raghunath, M., Beena, R., Mohan, V., Viji, V., Manju, R., and Stephen, R. (2021). High temperature stress mitigation in rice (Oryza sativa l.): Foliar application of plant growth regulators and nutrients. *J. Crop Weed* 17 (1), 34–47. doi: 10.22271/09746315.2021.v17.i1.1404

Rativa, A., de Araújo Junior, A., da Silva Friedrich, D., Gastmann, R., Lamb, T., dos Santos Silva, A., et al. (2020). Root responses of contrasting rice genotypes to low temperature stress. *J. Plant Physiol.* 255, 153307. doi: 10.1016/j.jplph.2020.153307

Rezaul, I., Feng, B., Chen, T., Fu, W., Zhang, C., Tao, L., et al. (2019). Abscisic acid prevents pollen abortion under high temperature stress by mediating sugar metabolism in rice spikelets. *Physiologia Plantarum* 165 (3), 644–663. doi: 10.1111/ppl.12759

Sadras, V., Vadez, V., Purushothaman, R., Lake, L., and Marrou, H. (2015). Unscrambling confounded effects of sowing date trials to screen for crop adaptation to high temperature. *Field Crops Res.* 177, 1–8. doi: 10.1016/j.fcr.2015.02.024

San-Oh, Y., Kondo, M., Ookawa, T., and Hirasawa, T. (2008). Ecophysiological analysis on effect of planting pattern on biomass production and grain yield in rice. *Japan Agric. Res. Quarterly: JARQ* 42 (2), 79–89. doi: 10.6090/jarq.42.79

Satake, T., Lee, S., Koike, S., and Kariya, K. (1988). Male Sterility caused by cooling treatment at the young microspore stage in rice plants: XXVIII. prevention of cool injury with the newly devised water management practices: Effects of the temperature and depth of water before the critical stage. *Japanese J. Crop Sci.* 57 (1), 234–241. doi: 10.1626/jcs.57.234

Sharma, L., Dalal, M., Verma, R., Kumar, S., Yadav, S., Pushkar, S., et al. (2018). Auxin protects spikelet fertility and grain yield under drought and heat stresses in rice. *Environ. Exp. Bot.* 150, 9–24. doi: 10.1016/j.envexpbot.2018.02.013

Sreenivasulu, N., Butardo, V., Misra, G., Cuevas, R., Anacleto, R., and Kavi Kishor, P. (2015). Designing climate-resilient rice with ideal grain quality suited for high-temperature stress. *J. Exp. Bot.* 66 (7), 1737–1748. doi: 10.1093/jxb/eru544

Stephen, K., Beena, R., Kiran, A., Shanija, S., and Saravanan, R. (2022). Changes in physiological traits and expression of key genes involved in sugar signaling pathway in rice under high temperature stress. *3 Biotech.* 12 (9), 183. doi: 10.1007/s13205-022-03242-y

UI Hassan, M., Rasool, T., Iqbal, C., Arshad, A., Abrar, M., Abrar, M., et al. (2021). Linking plants functioning to adaptive responses under heat stress conditions: a mechanistic review. *J. Plant Growth Regul.* 41, 2596–2613. doi: 10.1007/s00344-021-10493-1

Wassmann, R., Jagadish, S., Sumfleth, K., Pathak, H., Howell, G., Ismail, A., et al. (2009). Regional vulnerability of climate change impacts on Asian rice production and scope for adaptation. *Adv. Agron.* 102, 91–133. doi: 10.1016/S0065-2113(09)01003-7

Wu, C., Cui, K., Wang, W., Li, Q., Fahad, S., Hu, Q., et al. (2016). Heat-induced phytohormone changes are associated with disrupted early reproductive development and reduced yield in rice. *Sci. Rep.* 6 (1), 1–14. doi: 10.1038/srep34978

Wu, Q., Liu, X., Yin, D., Yuan, H., Xie, Q., Zhao, X., et al. (2017). Constitutive expression of OsDof4, encoding a C2-C2 zinc finger transcription factor, confesses its distinct flowering effects under long-and short-day photoperiods in rice (Oryza sativa l.). *BMC Plant Biol.* 17 (1), 1–13. doi: 10.1186/s12870-017-1109-0

Xing, Z., Pei, W., Ming, Z., Qian, H., Hu, Y., Guo, B., et al. (2017). Temperature and solar radiation utilization of rice for yield formation with different mechanized planting methods in the lower reaches of the Yangtze river, China. *J. Integr. Agric.* 16 (9), 1923–1935. doi: 10.1016/S2095-3119(16)61596-4

Yang, J., Cai, Z., Liu, D., Hu, L.-Y., Qu, W.-B., Zhang, C.-H., et al. (2019). Effects of spraying salicylic acid and potassium dihydrogen phosphate on physiological cha-racteristics and grain yield of single-season rice under high temperature condition. *J. Appl. Ecol.* 30 (12), :4202–:4210. doi: 10.13287/j.1001-9332.201912.029

Yang, J., Duan, L., He, H., Li, Y., Li, X., Liu, D., et al. (2022). Application of exogenous KH_2PO_4 and salicylic acid and optimization of the sowing date enhance rice yield under high-temperature conditions. *J. Plant Growth Regul.* 41 (4), 1532–1546. doi: 10.1007/s00344-021-10399-y

Yu, Y., Deng, L., Zhou, L., Chen, G., and Wang, Y. (2022). Exogenous melatonin activates antioxidant systems to increase the ability of rice seeds to germinate under high temperature conditions. *Plants* 11, (7). doi: 10.3390/plants11070886

Zhang, H., Xu, H., Jiang, Y., Zhang, H., Wang, S., Wang, F., et al. (2021). Genetic control and high temperature effects on starch biosynthesis and grain quality in rice. *Front. Plant Sci.* 12, 757997. doi: 10.3389/fpls.2021.757997

Zhou, Z., Jin, J., and Wang, L. (2022). Modeling the effects of elevation and precipitation on rice (Oryza sativa l.) production considering multiple planting methods and cultivars in central China. *Sci. Total Environ.* 813, 152679. doi: 10.1016/j.scitotenv.2021.152679

10.3389/fpls.2022.1081807

Glossary

LLYHZ	Longliangyou Huazhan
QLY2118	Quanliangyou 2118
HHZ	Huanghuazhan
HLY858	Huiliangyou 858
AT	Artificial transplanting
CSM	Carpet seedlings machine
SD	Sowing date
PP	Planting pattern
DSD	Delaying sowing date
NSD	Normal sowing date
TEP	The effective panicles
GNP	Grain number per panicle
SSR	Seed setting rate
TSW	Thousand seed weight
SOD	Superoxide dismutase
POD	Peroxidase
CAT	Catalase
BR	Brassinolide
SA	Salicylic acid
ABA	Abscisic acid
6-BA	6-benzylaminopurine
MP	Monopotassium phosphate
MMTC	Mean maximum canopy temperature
MMAC	Mean maximum atmospheric temperature
TDV	Temperature difference value

frontiers | Frontiers in Plant Science

TYPE Original Research
PUBLISHED 25 January 2023
DOI 10.3389/fpls.2023.1076331

OPEN ACCESS

EDITED BY
Biao Jin,
Yangzhou University, China

REVIEWED BY
Victor Gonzalez-Mendoza,
Consejo Nacional de Ciencia y Tecnología (CONACYT), Mexico
Marina Gavilanes-Ruiz,
National Autonomous University of Mexico, Mexico

*CORRESPONDENCE
Moddassir Ahmed
cmmanibge@yahoo.co.uk

SPECIALTY SECTION
This article was submitted to Plant Abiotic Stress, a section of the journal Frontiers in Plant Science

RECEIVED 21 October 2022
ACCEPTED 13 January 2023
PUBLISHED 25 January 2023

CITATION
Annum N, Ahmed M, Tester M, Mukhtar Z and Saeed NA (2023) Physiological responses induced by phospholipase C isoform 5 upon heat stress in *Arabidopsis thaliana*. *Front. Plant Sci.* 14:1076331. doi: 10.3389/fpls.2023.1076331

Physiological responses induced by phospholipase C isoform 5 upon heat stress in *Arabidopsis thaliana*

Nazish Annum[1], Moddassir Ahmed[1*], Mark Tester[2], Zahid Mukhtar[1] and Nasir Ahmad Saeed[1]

[1]Wheat Biotechnology Lab, Agricultural Biotechnology Division, National Institute for Biotechnology and Genetic Engineering Constituent College (NIBGE-C), Pakistan Institute of Engineering and Applied Sciences (PIEAS), Faisalabad, Pakistan, [2]Center for Desert Agriculture (CDA), King Abdullah University of Science and Technology (KAUST), Thuwal, Saudi Arabia

Plant's perception of heat stress involves several pathways and signaling molecules, such as phosphoinositide, which is derived from structural membrane lipids phosphatidylinositol. Phospholipase C (PLC) is a well-known signaling enzyme containing many isoforms in different organisms. In the present study, Phospholipase C Isoform 5 (*PLC5*) was investigated for its role in thermotolerance in *Arabidopsis thaliana*. Two over-expressing lines and one knock-down mutant of *PLC5* were first treated at a moderate temperature (37 °C) and left for recovery. Then again exposed to a high temperature (45 °C) to check the seedling viability and chlorophyll contents. Root behavior and changes in $^{32}P_i$ labeled phospholipids were investigated after their exposure to high temperatures. Over-expression of *PLC5* (*PLC5 OE*) exhibited quick and better phenotypic recovery with bigger and greener leaves followed by chlorophyll contents as compared to wild-type (*Col-0*) and *PLC5* knock-down mutant in which seedling recovery was compromised. *PLC5* knock-down mutant illustrated well-developed root architecture under controlled conditions but stunted secondary roots under heat stress as compared to over-expressing *PLC5* lines. Around 2.3-fold increase in phosphatidylinositol 4,5-bisphosphate level was observed in *PLC5 OE* lines upon heat stress compared to wild-type and *PLC5* knock-down mutant lines. A significant increase in phosphatidylglycerol was also observed in *PLC5 OE* lines as compared to *Col-0* and *PLC5* knock-down mutant lines. The results of the present study demonstrated that *PLC5* over-expression contributes to heat stress tolerance while maintaining its photosynthetic activity and is also observed to be associated with primary and secondary root growth in *Arabidopsis thaliana*.

KEYWORDS

PG, PIP_2, Thermotolerance, *Arabidopsis thaliana*, Root growth

Abbreviations: DAG, Diacylglycerol; DGK, Diacylglycerol Kinase; ER, Endoplasm Reticulum; HSR, Heat Shock Responsive; IP_3, Inositol 1,4,5 trisphosphate; IPP, Inositol polyphosphate; OE, Over-expression; PA, Phosphatidic acid; PG, Phosphatidylglycerol; PIP, Phosphatidylinositol monophosphate; PIP_2, Phosphatidylinositol 4,5-bisphosphate; PIPK, Phosphatidylinositol phosphate kinase; PI-PLC, Phosphoinositide specific phospholipase C; PLD, Phospholipase D; K_d, Knock-down; sHSP, small Heat Shock Protein.

1 Introduction

Temperature plays an important role in plant growth and productivity. Atmospheric temperature of earth is continually changing round the year and it is becoming quite distinct in the event of climate change. The frequency and magnitude of heat-wave events in the past decades point toward an alarming increase in the global mean temperature (3.7 ± 1.1°C) by the end of the 21st century (Zhu et al., 2022). So, it has become increasingly important to understand how plants respond to high temperatures. Usually, high temperature affects a variety of potential cellular targets, distressing plant growth and survival. In a normal atmosphere, plants experience day-to-day and periodic temperature changes that vary in range, frequency and magnitude. *Arabidopsis thaliana* as a model plant has differences in sensitivity and response to temperature extremities that help the plant adapt to changing local temperature patterns. Gene expression changes under rising temperature, leading to high-temperature tolerance. The genetic reprogramming and successive increase in thermotolerance are known as adaptive and/or acquired thermotolerance (Zhang et al., 2015). At the cellular level, high temperature leads to protein misfolding, perturbs membrane fluidity, transport and enzymatic reaction, cytoskeleton organization and metabolic balance by accumulating reactive oxygen species (ROS). Thus, as sessile eukaryotes, plants quickly sense temperature fluctuations in the environment and recruit timely adaptive tactics to preserve cell function and viability (Hayes et al., 2021).

Membrane plays an important role in vesicle transport and cell signaling, not only through host-specific proteins but also provides a substrate for the production of lipids (as a second messenger). Besides playing structural role as membrane components, lipids perform regulatory and signaling functions, thus activating cellular responses to environmental signals (Hou et al., 2016; Kosová et al., 2018). PIP_2 (Phosphatidylinositol 4,5-bisphosphate) and PA (Phosphatidic acid) lipids and their associated metabolic enzymes like PLC, PLD, DGK (Diacylglycerol Kinase) and PIP5K (Phosphatidylinositol 4 phosphate 5 kinase) have various regulatory and cellular functions in response to environmental stimuli. However, plants PLC signaling system are presumed to be different from animals in terms of lacking the primary targets for DAG and IP3, i.e. PKCs, TRP channels and IP3 receptors (Wheeler and Brownlee, 2008; Munnik, 2014). PIP_2 has been hardly detected in the plasma membrane of flowering plants which is supposed to be the substrate of PLC. PIP is also assumed to be a precursor of PLC as it is abundantly observed in the plasma membrane. Yet it is still debatable that, what is the typical precursor of PLC (Munnik et al., 1998; Munnik, 2014; Simon et al., 2014).

Acting very early in the response pathway, PLCs assumed to be physically close to the thermosensor. Phospholipases use PIP_2/PIP as a substrate to generate DAG and IP_s (Inositol phosphates) that could ultimately help in the activation of calcium (Ca^{+2}) channels, which in turn activates various sHSP (small heat shock proteins) and HSR (heat shock responsive) genes through various pathways. Furthermore, CaBP (calcium binding proteins), also known as "calcium sensor" recognize and decrypt the existing information in the calcium signatures. This information is then transported to initiate downstream phosphorylation cascade in order to regulate gene expression (Tuteja and Sopory, 2008; Niu and Xiang, 2018). Previously, (Hunt et al., 2004) reported the differential calcium sensitivities for AtPLC protein activities which may act as mechanistic attributes for generated calcium signatures. Beside PIP_2/PIP, PI is also a component of signaling system and take part in signal perception and transduction (Liu et al., 2019). Phosphatidylcholine (PC) and phosphatidyl ethanol (PE) ratio affects membrane stability (Yu et al., 2020). Phosphatidylglycerol (PG) was reported to be an important and major lipid component of chloroplast membrane (Demé et al., 2014). The level of PG was reported to be decreased under heat treatment to maintain chloroplast membrane stability and high photosynthetic activity (Zhu et al., 2022). Similarly, cardiolipin (CL) involved in various mitochondrial events, is also known as the signature phospholipid of mitochondria (Mileykovskaya and Dowhan, 2014).

Plant PLC signals in response to various abiotic stresses including cold, drought, and salt (Darwish et al., 2009; Arisz et al., 2013; Simon et al., 2014) to elicit various downstream mechanism to cope with these environmental stresses. Nine PLCs were reported to be found in *Arabidopsis thaliana*. Each PLC has unique role and tested against various stresses. Previously, *PLC2* has been reported to be involved in ER stress response pathway (Kanehara et al., 2015). Similarly, PLC involvement in thermotolerance had also been reported, where knockout mutant of *PLC3* and *PLC9* exhibited severely impaired basal and acquired thermotolerance, while their over-expression improved thermotolerance (Zheng et al., 2012; Gao et al., 2014; Ren et al., 2017). *PLC3* also reported to be involved in ABA (abscisic acid) signaling (Zhang et al., 2018a), likewise *PLC4* found to be a negative regulator of salt tolerance (Xia et al., 2017), while over-expression of *PLC5* improved drought tolerance (Zhang et al., 2018b). Although *AtPLC5* (multi stress tolerant gene) expression is reported to be induced by dehydration, salt and cold stresses (Hunt et al., 2004), it is yet to be tested against thermotolerance. The current study deals with evaluation of thermotolerance in *PLC5* mutant plants at seedling stage. The over expressed *PLC5* lines demonstrated improved plant vigor and enhanced recovery when subjected to acquired thermotolerance. In addition, *PLC5 OE* lines exhibited improved primary and lateral root growth (Supplementary data) as compared to knock down mutants and wild type plants when exposed to heat shock. This could be associated to less damage of chloroplast and thylakoid membranes and thus to less disruption in light capturing and photosynthetic activity as it has been described (Kato et al., 2020). In our case, this was supported by a decrease of chlorophyll amount in the wild type and Knocked-down mutant (which are sensitive to the heat treatments).

2 Materials and methods

2.1 Plant material

The seeds of *Arabidopsis thaliana* (*Col-0*) and its homozygous *AtPLC5* over-expressing and knockdown mutants *i.e.* OE_2, OE_3 and K_d were kindly provided by Dr. Teun Munnik, Research Cluster Green Life Sciences, Section Plant Cell Biology, Swammerdam Institute for Life Sciences, University of Amsterdam, Netherlands.

2.2 Seed sterilization

The seeds of *Arabidopsis thaliana* and its *AtPLC5* mutants were surface sterilized in a desiccator by using commercial bleach and 37% HCl for 3 h and then placed in a laminar air flow hood for an hour to allow complete evaporation of chlorine gas. This method is also called the "Dry method of seed sterilization" or "Chlorine gas seed sterilization" (Zhang et al., 2018b).

2.3 Seedling survival assay for acquired thermotolerance

Sterilized seeds were placed in round petri plates containing ½ strength MS medium (Murashige and Skoog, 1962) including Gamborg B_5Vitamins and 1% sucrose. Stratification was done at 4 °C in dark for 2 days. After stratification, petri plates containing seeds were placed at 22 °C (16/8 h light-dark period) in a growth chamber for 3 days to grow and then subjected to heat shock. Seedlings were first treated at 37 °C for 60 min, then placed at 22 °C for 120 min for recovery, and then again subjected to a new treatment at 45 °C for 0 min (Control) and 150 min (Heat shock). A water bath was used for heat shock treatment. After heat treatment, seeds were put at 22 °C (16/8 h light-dark period) to recover for 10-14 days. The seedling survival rate was calculated based on the visual color of tissue, as green seedlings were considered as alive and white seedlings as dead.

2.4 Determination of chlorophyll levels

The aerial part of the fresh seedling was collected in a 2 ml Eppendorf tube and ground partially with the help of a small pestle in order to facilitate the carotenoid extraction. Acetone (80%) was used for chlorophyll extraction and kept under dark conditions for 1.45 h in order to ensure maximum pigment diffusion. After centrifugation (12000xg for 2 min) the supernatant was collected and absorbance (A_x) was measured using a Spectrophotometer (U 5100 Spectrophotometer, Hitachi) at 663.2 nm and 646.8 nm wavelength by taking 80% acetone as a blank. Chlorophyll concentration was estimated by following (Lichtenthaler, 1987) protocol.

2.5 Root elongation assay

For root elongation assay Square Petri plates (12 x 12 cm) containing media described previously, were used. Seeds were put on Square Petri plates and stratified at 4 °C in a dark room for 2 days, then placed in a growth chamber vertically tilted at 70 degrees angle at 22 °C with 16/8 h light-dark period for 3 days before heat treatment. Sealed Square Petri plates were placed in a water bath for heat treatment at 44 °C for 0 min (Control) and for 36 min (Heat shock) in order to test the basal thermotolerance. Plates were scanned on daily basis before and after the heat treatment by using Epson Perfection V800 photo scanner, at 300 DPI for 12 days. *Smart Root* version 4.1 (Lobet et al., 2011) plugins of the *Fiji Image J* (RRID: SCR_003070, https://imagej.net/software/fiji/) software (Schindelin et al., 2012) was used to measure the root growth.

2.6 Radioactive phospholipid labeling, extraction and analysis

Five-day old seedlings of *Arabidopsis thaliana* (*Col-0*) and its *AtPLC5* mutants were metabolically labeled in 2 ml Eppendorf tubes by using 200 µl labeling buffer (MES-KOH 2.5 mM, pH 5.8, KCl 1 mM) containing carrier free $^{32}PO_4^{3-}$ (5-10 µCi) for overnight incubation. Three biological replicates were used per genotype for simple randomization. Three seedlings were used for each replicate. After overnight incubation for $^{32}P_i$ labeling, samples were subjected to heat shock at 40 °C for 30 min using heating block. Perchloric acid (5% v/v) was then added to stop the treatment and lipids were extracted and separated by following protocol of (Munnik and Zarza, 2013). Heat activated potassium oxalate impregnated thin layer chromatographic (TLC) plates were used to separate the lipids (Munnik et al., 1998). Extracted lipids were visualized on autoradiograph by overnight exposure of TLC plate to autoradiography film and quantified by using phosphoimaging (Typhon FLA 7000, GE Healthcare). Individual phospholipid level was determined as the percent fraction of total lipids.

2.7 Statistical analysis

Statistical analysis was performed using Microsoft Excel 2016 for Window 10 (RRID: SCR_016137, https://www.microsoft.com/en-gb/). Significance of data was determined using one way ANOVA with student's t test (***P <0.001).

3 Results

3.1 Seedling survival

Upon heat perception different downstream complex mechanisms are activated in plants, suggesting that various genes may be involved in thermotolerance. *Arabidopsis thaliana*, as a model system, is generally used for phenotypic characterization by different phenotypic assays (Silva-Correia et al., 2014). Among this seedling survival was one of the most regularly used method for evaluating heat tolerance in *Arabidopsis thaliana* (Yeh et al., 2012). Survival is usually scored based on the color of the tissue. Seedlings that remain green after being exposed to heat/high temperature stress and are actively growing and producing new leaves are considered viable. In contrast, yellowing or whitening of leaves demonstrate non-viable seedling because of their impaired photosynthetic activity (Zheng et al., 2012; Silva-Correia et al., 2014).

3.2 Acquired thermotolerance

In present study, acquired thermotolerance approach was used, in which seedling were acclimatized first by exposing to moderately elevated temperature, and then leaving them for recovery at optimum temperature before exposing to high temperature (Mueller et al., 2015). Schematic representation of the experimental conditions used

10.3389/fpls.2023.1076331

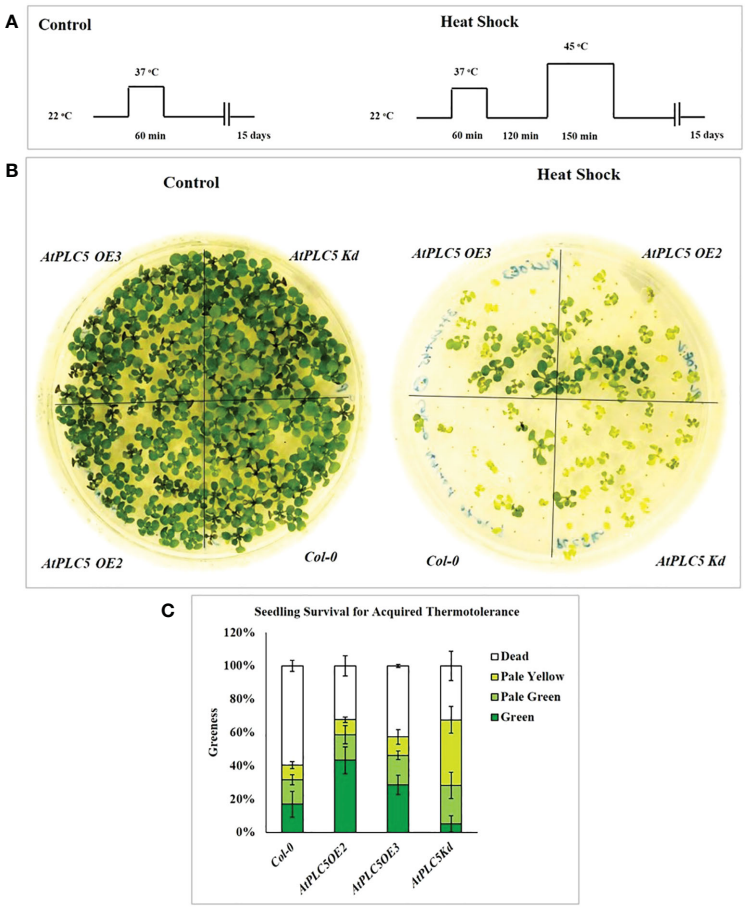

FIGURE 1
Seedling survival assay for acquired thermotolerance. **(A)** Schematic diagram of the heat shock conditions used to assess acquired thermotolerance phenotypes of *AtPLC5* mutants of *Arabidopsis thaliana*. Three days old seedlings were prior acclimatized by subjected to heat stress at 37 °C for 1 h, at 22 °C for 2 h (for recovery) and then exposed to 45 °C for 0 h (control) and 2.5 h (heat shock). Seedlings of mutants were daily monitored for 15 days after treatment. **(B)** Survival was observed and scored based on seedling leaves color. **(C)** Mean derived from 4 replicates, containing 34 seedlings for each genotype tested. Error bar represent standard deviation of the mean. Experiment was repeated 3 times independently. Data was represented in percentage.

in this experiment is shown in Figure 1A. Water bath was used as medium for heat stress since water is the better heat conductor. Three independent experiments were performed to assess the seedling viability of *Col-0* and *AtPLC5* OE_2, OE_3 and one knockdown (K_d) line of *Arabidopsis* after heat shock at condition referred above. The phenotype of the representative genotypes is presented in Figure 1B, while the viability as "greenness" is represented by Figure 1C.

The results revealed that all four genotypes survived (100% green seedlings) under control conditions when applied pre-treatment of 37 °C for 60 min and did not show any lethal effects on seedling viability. Subsequently, exposure to heat stress at 45 °C for 150 min was observed to significantly reduce seedling viability compared to control condition. This experiment demonstrated that *AtPLC5* mutants (OE_2, OE_3, K_d) exhibited a significant rate of survival upon exposure to heat shock for acquired thermotolerance as compared to wild-type *Col-0*. *AtPLC5* mutants OE_2, OE_3 and K_d indicated around 65-70% survival rate, while for wild-type it was approximated to 40% which means an improvement of around 25-30% in viability for OE_2 and K_d mutants of *AtPLC5* seedlings and around 20% for OE_3 seedlings. However, the seedlings of *AtPLC5* OE_2 and OE_3 mutants recovered at a better rate, having bigger and greener leaves than the K_d mutant which showed a relatively smaller and pale yellowish green phenotype.

It is assumed that *AtPLC5* over-expression might be involved in acquired thermotolerance as it speeds up the recovery period while knocking down this gene might compromise the rate of seedling recovery and duration of seedling revival.

3.3 Chlorophyll contents

Chlorophyll contents of seedlings have been considered an additional measure to verify the stay-green character of selected plant phenotype. The results obtained (Figure 2) illustrated the same trend which was observed in Figure 1B, with the *AtPLC5* OE_2 mutants, which indicated fast recovery and higher chlorophyll content (Figure 2A), seedling weight (ariel part) (Figure 2B) and superior plant morphology to other genotypes after heat stress treatment. However, at control conditions, all genotypes show approximately the same level of chlorophyll contents and their ariel part weight.

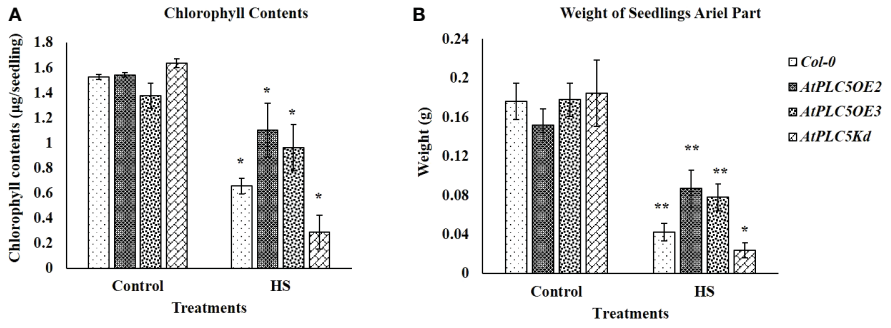

FIGURE 2
Fifteen days after acquired thermotolerance treatment **(A)** chlorophyll contents (µg/seedling) and **(B)** weight (g) of the aerial part of seedlings were determined. Mean derived from 4 replicates, containing 34 seedlings for each genotype tested. Error bar represent standard deviation of the mean. Students *t-test* (*P < 0.05, **P < 0.01) was used to test the significance.

3.4 Root length assay

Normally, round plates are used for seedling survival assays to be grown horizontally. However, it was almost impossible to explain the behavior of root growth upon heat stress. To tackle this situation, a new experimental setup was used by utilizing the square petri plates placed tilted at an angle of 70° to facilitate the visibility of root growth (Figure 3A). For this experiment, three-day old seedlings were treated with 0 min for control and 36 min at 44 °C (Heat Shock), in a water bath. After 12 days, it was observed that at the controlled conditions, *Col-0* and all *AtPLC5* mutants showed highly developed root architecture that was characterized by long main roots from which

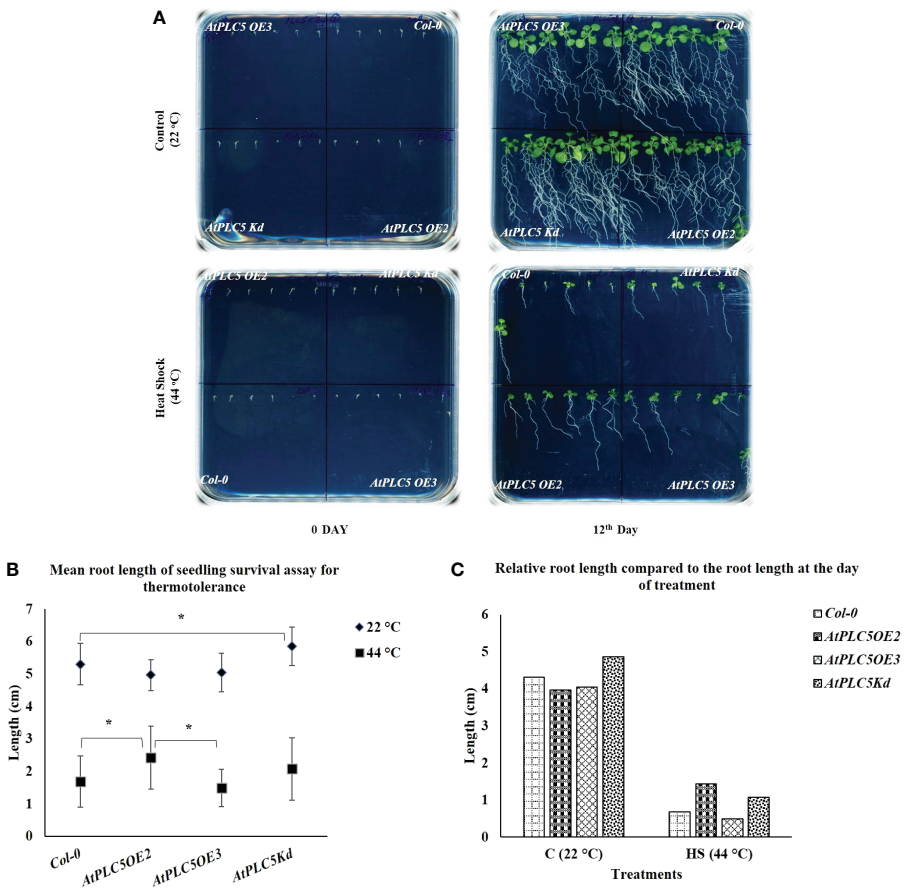

FIGURE 3
Root growth Assay. Square petri plate divided into 4 parts equally. Six seeds of *Col-0* and *AtPLC5 (OE2, OE3, Kd)* mutants placed on each part with an equal distance. Stratification was done for 2 days in cold dark room at 4 °C, then move to 22 °C (16 h L/8 h D) for growth. Three days old seedlings were treated with 0 min (Control) and 36 min at 44 °C (HS) in a water bath. **(A)** Plates were photographed after 12 days of treatment. **(B)** Mean was derived from 5 replicates, for each genotype tested containing 6 seedlings each. **(C)** Relative root length was also determined at the same time. Student's *t*-test (*P < 0.05) was used to test the level of significance.

several lateral roots emerged. After 12 days heat treated seedlings were compared, where all genotypes showed significant decrease in their root development (Figure 3C) and *Col-0* was hardly able to develop main and lateral roots as compared to *PLC5* OE_2, OE_3, K_d lines. Among *AtPLC5* over-expressing lines, OE_2 showed longer primary root length with few lateral roots (Supplementary Figure S1) as compared to OE_3 and K_d mutants (Figure 3A).

Smart root plugin was used to measure the main root length and results indicated that there were no significant differences between *Col-0* and all *AtPLC5* over-expressing lines under normal growth conditions. However, significant differences were observed in the average root length of *Col-0* and *AtPLC5* knockdown mutant at controlled conditions (grown at 22 °C) until 12 days (Figure 3B). Significant differences were observed in the mean root length of *Col-0* and *AtPLC5* OE_2 line after 12 days of heat shock (44 °C) exposure, non-significant differences were observed in root length between *Col-0*, OE_3 and K_d mutants of *AtPLC5* after 12^{th} day of heat treatment. There was a significant difference between OE_2 and OE_3 of *PLC5* lines in term of root length of *Arabidopsis thaliana* after 12 days of heat treatment.

3.5 Heat induced PPI and PA responses

$^{32}P_i$ labeling experiment was performed to investigate probable changes in PPI/PA levels as a consequence *PLC5* over-expression and in knockdown *Arabidopsis thaliana* lines when given heat shock (40 °C) for 30 min (Figure 4A). Heat treatment to *PLC5 OE* lines elicited a significant increase of ~2.3-fold in PIP_2 and ~1.4-fold in PA levels as compared to lines grown under control (22.5 °C) conditions (Figures 4B, C), validating a constitutively higher PLC activity *in vivo* setting. Moreover, it was witnessed that the absolute level of PIP_2 in *PLC OE* lines remained below wild-type under controlled conditions. Although a significant increase of ~1.6-fold in PA level was observed in *PLC5* K_d mutant upon heat treatment, the absolute level remained below *Wt* and *PLC5 OE* lines. Interestingly, a significant increase of ~1.85-fold was observed in structural lipid PG level (Figure 4D) in *PLC5* over-expressed lines as compared to *Wt* under controlled (22.5 °C) conditions. Although the level of PG was decreased slightly due to heat stress the absolute level remains higher than *Wt* and knockdown mutant. This presumably indicating their efficient photosynthetic machinery, as Kobayashi et al., 2015 also reported that the deficiency of PG yielded pale-yellow green phenotype. While the level of PIs remained same under control and heat stressed condition in both *Wt* and *PLC5* mutants.

4 Discussion

The extent and rate of global climate change increasingly poses a high-temperature threat to plant survival. Being the primary victim of external stimuli, plasma membrane (PM) guards the plant cells from environmental extremities through downstream signal transduction to generate suitable cellular responses. Membrane constitution and membrane protein operations are all regulated by lipid composition (Rawat et al., 2021). Regulation of phospholipases (PLCs) is not simple; it involves Ca^{+2} signaling, activation of G-proteins and modifications at post-translational stage (Munnik, 2014). PLCs have been investigated extensively for their regulatory role in various biotic and abiotic stress management (Gao et al., 2014). PI(4,5)P which is a

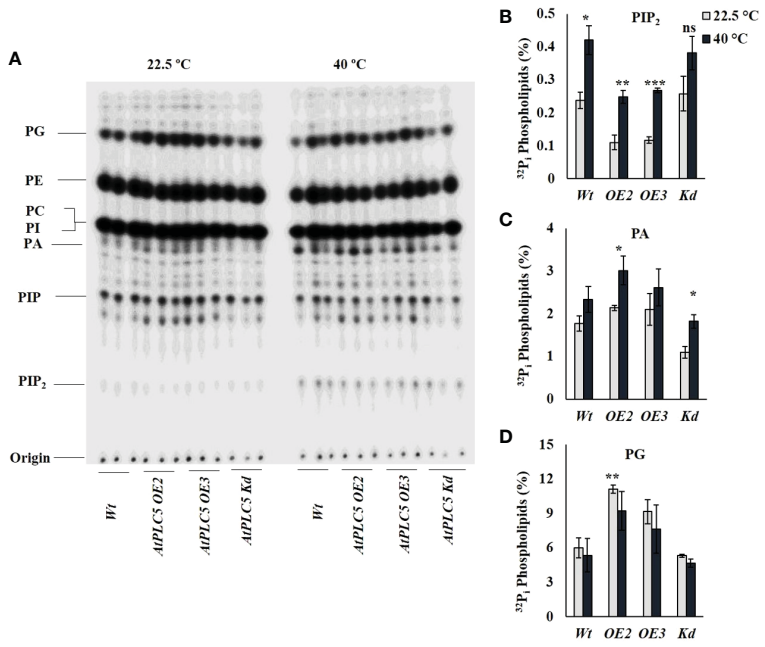

FIGURE 4
$^{32}P_i$ lipid profiling of *PLC5* mutants under heat stress. Five days old seedlings were radioactively labeled O/N and treated for 30 min at high temperature (40 °C) using heat block. Lipids were then extracted, analyzed and quantified by phosphoimaging. **(A)** Typical TLC profile of *PLC5* mutants containing lipid extract of 3 seedlings each. **(B)** PIP_2 **(C)** PA **(D)** PG lipids behavior of *Wt* and *PLC5* mutants under control and heat stressed condition. Data shown are the mean ± SE (n=3). Student's *t*-test (***P < 0.001) was used to test the level of significance.

presumable substrate of PLC could hardly be detected in flowering plants. However, the rapid elevation in PIP_2 and PA levels when exposed to heat stress suggest that these lipids are closely associated with thermosensing (Mishkind et al., 2009; Hayes et al., 2021). But still it is unclear how these lipid modifying enzymes are activated by elevated temperature. In this study *PLC5*, one of the nine isoforms of PLC family of *Arabidopsis thaliana*, was tested for thermotolerance to understand its role in heat signaling.

In the present study, phenotypic analysis showed that seedlings of *PLC5 OE* lines exhibited quick and better recovery from heat shock (Figure 1A) compared to wild-type and *PLC5* K_d seedlings. The phenotype of *PLC5 OE* lines was observed to have bigger and greener leaves as compared to knockdown mutant and wild-type that exhibited smaller leaves of pale-yellow green in color after heat shock, indicating slow or compromised recovery. Recently transgenic wheat containing *AtPLC5* transgene was also reported to retain their stay green character under heat stress (40°C) as compared to *Wt* wheat (Annum et al., 2022). Together these results suggested an involvement of *PLC5* gene in seedling survival under acquired thermotolerance.

Chlorophyll plays a significant role in light harvest, separation of charge and transport in photosynthesis (Kato et al., 2020). The loss of chlorophyll caused by high temperature is associated with heat sensitivity in plants (Shirdelmoghanloo et al., 2016; Zhou et al., 2017). In the present study although a significant decrease in chlorophyll level was observed in *Wt* and *PLC5* mutants when subjected to heat stress, *PLC5 OE* lines showed significantly higher chlorophyll contents as compared to *Wt* and *PLC5* knockdown mutant when exposed to heat stress, indicating higher photosynthetic activity and high temperature tolerance. Whereas, the severe and significant loss of chlorophyll in knockdown mutant of *PLC5* under high temperature showed impaired photosynthetic machinery and temperature sensitivity. Consequently, the chlorophyll contents of wild-type (*Col-0*) and *PLC5* over-expressed and knockdown mutant support the phenotypic observation with significant differences.

Previously, it was reported that abiotic stresses could hinder root development (Zhang et al., 2018b), and similar root growth retardation was observed in case of *PLC5 OE* lines. Under controlled condition (22 °C), *PLC5* K_d mutant showed significantly well-developed root architecture with primary and secondary root growth as compared to wild-type (Figure 3A), whereas *PLC5 OE* lines revealed reduction in well-developed root architecture which might be the result of decreased PIP_2 level as it was previously reported that induced *PIP5K3* over-expression in the *PLC5* background rescued the PIP_2 production and restored root hair phenotype (Van Leeuwen et al., 2007; Zhang et al., 2018b). Similarly, the root growth of *Col-0* and *PLC5* mutants after being subjected to heat shock (44 °C for 36 min) showed a clear reduction in root structure as compared to control (22 °C) condition, still *PLC5* over-expressing lines developed longer main root with fewer secondary roots as compared to K_d mutant that did not develop secondary roots, whereas *Col-0* was found to be hardly successful in developing main root.

Cell membrane, as a permeable barrier, is mainly composed of lipids and proteins. These lipids can be further divided structurally into 3 distinct groups *i.e.*, glycerolipids, sphingolipids and sterol. Among different glycerolipids, phospholipids include Phosphatidylinositol 4,5-bisphosphate (PIP_2), Phosphatidylinositol monophosphate (PIP), Phosphatidic acid (PA), Phosphatidylinositol (PI), Phosphatidylcholine (PC), Phosphatidylethanolamine (PE), Phosphatidylglycerol (PG), and Cardiolipin (CL) (Abdelrahman et al., 2020). The activation of phospholipid based signaling pathway had been reported to be involved in calcium based heat stress responses (Tuteja and Mahajan, 2007). Although PLC and the subsequent liberation of IP3 upon heat stress could provide mechanism for calcium release, still the signaling of PIP_2 and PLC is different in animals and plants (Mishkind et al., 2009).

Although PIP_2 is a genuine animal PLC substrate, it is present in relatively lower concentration in plants and is rarely detected in plasma membranes where most PLC activity is known to be perceived (Munnik, 2014). Whereas, PI4P is abundantly present in plasma membrane suggesting its role as a plant PLC substrate (Vermeer et al., 2017). Obviously, this might be changed under stress conditions where PIP_2 level is reported to be increased under osmotic stress, salinity stress, and heat stress (Darwish et al., 2009; Zhang et al., 2018b; Annum et al., 2022). In the current study, a clear reduction in PIP_2 level in *PLC5 OE* lines under normal condition was observed whereas, the level of PA was increased as compared to *Wt* and *PLC5* knockdown mutant which are also in agreement with (Zhang et al., 2018b). Subsequently, a significant increase in PIP_2 and PA level, when given heat shock (40 °C) has been observed in wild-type and *PLC5* mutants. However, PA level displayed a non-significant increase in *Wt* whereas, a significant increase in *PLC5* OE_2 which was assumed to an increase in PLC activity. Although a significant increase in PA level was also observed in *PLC5* K_d mutant, the total level was less than *Wt* and *PLC5 OE* lines, which might be due to PLD activity.

In plants, PG (phosphatidylglycerol) is mainly present in the thylakoid membrane of chloroplast and plays an important role in photosynthetic electron transport chain (Hagio et al., 2002; Kobayashi et al., 2017). Previous reports suggested the prerequisite activity of PG for chloroplast biogenesis, as its deficiency yielded a pale-yellow green phenotype and became unsuccessful in establishing thylakoid membrane networks inside leaf chloroplast (Haselier et al., 2010; Kobayashi et al., 2015). Interestingly, in the present study, over-expression of *PLC5* resulted in a significant increase in PG level (~1.85-fold) under controlled conditions as compared to *Wt* and knockdown mutant. Although a non-significant decrease was observed in PG level when exposed to heat stress the overall level remains higher, supporting the phenotypic greener color seedling leaves as compared to *PLC5* K_d mutant which exhibited pale yellow green phenotype that might be a result of compromised chloroplast biogenesis. Further research in this area is required to identify the exact role of PG against abiotic stresses. And how it contributes in plant phenotypes under abiotic stresses? And to decipher the exact role of PLCs and downstream targets of IPPs, PPIs and PA. Whether PIP_2 or PIP is an assumed substrate of PLC or PIPK? This work is in the process of extending the current understanding of plant signaling to thermal stress and provides a new perspective on the role of phosphoinositide as an important messenger in this process.

5 Conclusion

The seedling survival assay of *PLC5* over-expressing lines of *Arabidopsis thaliana* appeared to be more thermotolerant than *PLC5* knockdown mutant and *Col-0*, indicating the involvement of *PLC5* gene in high temperature tolerance. The chlorophyll analysis

and radioactive lipid profiling further support the results of this study, revealing that phosphatidylglycerol (PG) activity which is essential for chloroplast biogenesis and involved in photosynthetic electron transport chain, is increased by ~1.8-fold in *PLC5* over-expressed lines of *Arabidopsis thaliana*. Thus, we assume over-expression of *PLC5* increased thermotolerance and this is caused by the increased hydrolysis of PIP_2 and highly efficient photosynthetic machinery.

Data availability statement

The original contributions presented in the study are included in the article/Supplementary Material. Further inquiries can be directed to the corresponding author.

Author contributions

NA was responsible for Methodology, Investigation, Formal analysis, Writing – Original draft preparation, MA validated the data, review and edit the manuscript, MT and ZM critically reviewed the final manuscript and incorporated valuable intellectual input, NAS conceptualized, supervised and approved the final manuscript. All authors contributed to the article and approved the submitted version.

Funding

This work was supported by International Research Support Initiative Program (IRSIP) fellowship to NA, PhD scholar, funded by Higher Education Commission (HEC), Government of Pakistan (IRSIP Fellowship No. (PIN) IRSIP 39, BMS 43).

Acknowledgments

The authors like to thank Dr. Teun Munnik, Research Cluster Green Life Sciences, Section Plant Cell Biology, Swammerdam Institute for Life Sciences, University of Amsterdam, Netherlands for providing *AtPLC5* over-expressed/knockdown lines, excellent learning and experimental environment, technical guidance and support for this study.

Conflict of interest

The authors declare that the research was conducted in the absence of any commercial or financial relationships that could be construed as a potential conflict of interest.

Publisher's note

All claims expressed in this article are solely those of the authors and do not necessarily represent those of their affiliated organizations, or those of the publisher, the editors and the reviewers. Any product that may be evaluated in this article, or claim that may be made by its manufacturer, is not guaranteed or endorsed by the publisher.

Supplementary material

The Supplementary Material for this article can be found online at: https://www.frontiersin.org/articles/10.3389/fpls.2023.1076331/full#supplementary-material

References

Abdelrahman, M., Ishii, T., El-Sayed, M., and Tran, L. P. (2020). Heat sensing and lipid reprograming as a signaling switch for heat stress responses in wheat. *Plant Cell Physiol.* 61 (8), 1399–1407. doi: 10.1093/pcp/pcaa072

Annum, N., Ahmed, M., Imtiaz, K., Mansoor, S., Tester, M., and Saeed, N. A. (2022). (32)P(i) labeled transgenic wheat shows the accumulation of phosphatidylinositol 4,5-bisphosphate and phosphatidic acid under heat and osmotic stress. *Front. Plant Sci.* 13 (881188). doi: 10.3389/fpls.2022.881188

Arisz, S. A., van Wijk, R., Roels, W., Zhu, J. K., Haring, M. A., and Munnik, T. (2013). Rapid phosphatidic acid accumulation in response to low temperature stress in arabidopsis is generated through diacylglycerol kinase. *Front. Plant Sci.* 4 (1). doi: 10.3389/fpls.2013.00001

Darwish, E., Testerink, C., Khalil, M., El-Shihy, O., and Munnik, T. (2009). Phospholipid signaling responses in salt-stressed rice leaves. *Plant Cell Physiol.* 50 (5), 986–997. doi: 10.1093/pcp/pcp051

Demé, B., Cataye, C., Block, M. A., Maréchal, E., and Jouhet, J. (2014). Contribution of galactoglycerolipids to the 3-dimensional architecture of thylakoids. *FASEB J.* 28 (8), 3373–3383. doi: 10.1096/fj.13-247395

Gao, K., Liu, Y. L., Li, B., Zhou, R. G., Sun, D. Y., and Zheng, S. Z. (2014). Arabidopsis thaliana phosphoinositide-specific phospholipase c isoform 3 (AtPLC3) and AtPLC9 have an additive effect on thermotolerance. *Plant Cell Physiol.* 55 (11), 1873–1883. doi: 10.1093/pcp/pcu116

Hagio, M., Sakurai, I., Sato, S., Kato, T., Tabata, S., and Wada, H. (2002). Phosphatidylglycerol is essential for the development of thylakoid membranes in arabidopsis thaliana. *Plant Cell Physiol.* 43 (12), 1456–1464. doi: 10.1093/pcp/pcf185

Haselier, A., Akbari, H., Weth, A., Baumgartner, W., and Frentzen, M. (2010). Two closely related genes of arabidopsis encode plastidial cytidinediphosphate diacylglycerol synthases essential for photoautotrophic growth. *Plant Physiol.* 153 (3), 1372–1384. doi: 10.1104/pp.110.156422

Hayes, S., Schachtschabel, J., Mishkind, M., Munnik, T., and Arisz, S. A. (2021). Hot topic: Thermosensing in plants. *Plant Cell Environ.* 44 (7), 2018–2033. doi: 10.1111/pce.13979

Hou, Q., Ufer, G., and Bartels, D. (2016). Lipid signalling in plant responses to abiotic stress. *Plant Cell Environ.* 39 (5), 1029–1048. doi: 10.1111/pce.12666

Hunt, L., Otterhag, L., Lee, J. C., Lasheen, T., Hunt, J., Seki, M., et al. (2004). Gene-specific expression and calcium activation of arabidopsis thaliana phospholipase c isoforms. *New Phytol.* 162 (3), 643–654. doi: 10.1111/j.1469-8137.2004.01069.x

Kanehara, K., Yu, C. Y., Cho, Y., Cheong, W. F., Torta, F., Shui, G., et al. (2015). Arabidopsis AtPLC2 is a primary phosphoinositide-specific phospholipase c in phosphoinositide metabolism and the endoplasmic reticulum stress response. *PloS Genet.* 11 (9), e1005511. doi: 10.1371/journal.pgen.1005511

Kato, K., Shinoda, T., Nagao, R., Akimoto, S., Suzuki, T., Dohmae, N., et al. (2020). Structural basis for the adaptation and function of chlorophyll f in photosystem I. *Nat. Commun.* 11 (1), 238. doi: 10.1038/s41467-019-13898-5

Kobayashi, K., Endo, K., and Wada, H. (2017). Specific distribution of phosphatidylglycerol to photosystem complexes in the thylakoid membrane. *Front. Plant Sci.* 8. doi: 10.3389/fpls.2017.01991

Kobayashi, K., Fujii, S., Sato, M., Toyooka, K., and Wada, H. (2015). Specific role of phosphatidylglycerol and functional overlaps with other thylakoid lipids in arabidopsis chloroplast biogenesis. *Plant Cell Rep.* 34 (4), 631–642. doi: 10.1007/s00299-014-1719-z

Kosová, K., Vítámvás, P., Urban, M. O., Prášil, I. T., and Renaut, J. (2018). Plant abiotic stress proteomics: The major factors determining alterations in cellular proteome. *Front. Plant Sci.* 9 (122). doi: 10.3389/fpls.2018.00122

Lichtenthaler, H. K. (1987). CHLOROPHYLL AND CAROTENOIDS: PIGMENTS OF PHOTOSYNTHETIC BIOMEMBRANES. *Methods Enzymol.* 148, 350–382. doi: 10.1016/0076-6879(87)48036-1

Liu, S., Hu, Z.-M., Zhang, Q., Yang, X., Critchley, A. T., and Duan, D. (2019). PI signal transduction and ubiquitination respond to dehydration stress in the red seaweed gloiopeltis furcata under successive tidal cycles. *BMC Plant Biol.* 19 (1), 516. doi: 10.1186/s12870-019-2125-z

Lobet, G., Pagès, L., and Draye, X. (2011). A novel image-analysis toolbox enabling quantitative analysis of root system architecture. *Plant Physiol.* 157 (1), 29–39. doi: 10.1104/pp.111.179895

Mileykovskaya, E., and Dowhan, W. (2014). Cardiolipin-dependent formation of mitochondrial respiratory supercomplexes. *Chem. Phys. Lipids* 179, 42–48. doi: 10.1016/j.chemphyslip.2013.10.012

Mishkind, M., Vermeer, J. E., Darwish, E., and Munnik, T. (2009). Heat stress activates phospholipase d and triggers PIP accumulation at the plasma membrane and nucleus. *Plant J.* 60 (1), 10–21. doi: 10.1111/j.1365-313X.2009.03933.x

Mueller, S., Krause, D., Mueller, M., and Fekete, A. (2015). Accumulation of extra-chloroplastic triacylglycerols in arabidopsis seedlings during heat acclimation. *J. Exp. Bot.* 66 (15), 4517–4526. doi: 10.1093/jxb/erv226

Munnik, T. (2014). "PI-PLC: phosphoinositide-phospholipase c in plant signaling," in *Phospholipases in plant signaling* (Springer), 27–54.

Munnik, T., Irvine, R., and Musgrave, A. (1998). Phospholipid signalling in plants. *Biochim. Biophys. Acta (BBA)-Lipids Lipid Metab.* 1389 (3), 222–272. doi: 10.1016/S0005-2760(97)00158-6

Munnik, T., and Zarza, X. (2013). Analyzing plant signaling phospholipids through 32Pi-labeling and TLC. *Methods Mol. Biol.* 401–402_401. doi: 10.1007/978-1-62703-401-2_1

Murashige, T., and Skoog, F. (1962). A revised medium for rapid growth and bioassays with tobacco tissue cultures. *Physiol. Plant* 15, 473–497. doi: 10.1111/j.1399-3054.1962.tb08052.x

Niu, Y., and Xiang, Y. (2018). An overview of biomembrane functions in plant responses to high-temperature stress. *Front. Plant Sci.* 9 (915). doi: 10.3389/fpls.2018.00915

Rawat, N., Singla-Pareek, S. L., and Pareek, A. (2021). Membrane dynamics during individual and combined abiotic stresses in plants and tools to study the same. *Physiol. Plant.* 171 (4), 653–676. doi: 10.1111/ppl.13217

Ren, H., Gao, K., Liu, Y., Sun, D., and Zheng, S. (2017). The role of AtPLC3 and AtPLC9 in thermotolerance in arabidopsis. *Plant Signal Behav.* 12 (10), e1162368–e1162368. doi: 10.1080/15592324.2016.1162368

Schindelin, J., Arganda-Carreras, I., Frise, E., Kaynig, V., Longair, M., Pietzsch, T., et al. (2012). Fiji: an open-source platform for biological-image analysis. *Nat. Methods* 9 (7), 676–682. doi: 10.1038/nmeth.2019

Shirdelmoghanloo, H., Lohraseb, I., Rabie, H. S., Brien, C., Parent, B., and Collins, N. C. (2016). Heat susceptibility of grain filling in wheat (Triticum aestivum l.) linked with rapid chlorophyll loss during a 3-day heat treatment. *Acta Physiol. Plant.* 38 (8), 208. doi: 10.1007/s11738-016-2208-5

Silva-Correia, J., Freitas, S., Tavares, R., Lino-Neto, T., and Azevedo, H. (2014). Phenotypic analysis of the arabidopsis heat stress response during germination and early seedling development. *Plant Methods* 10, 7. doi: 10.1186/1746-4811-10-7

Simon, M. L., Platre, M. P., Assil, S., van Wijk, R., Chen, W. Y., Chory, J., et al. (2014). A multi-colour/multi-affinity marker set to visualize phosphoinositide dynamics in arabidopsis. *Plant J.* 77 (2), 322–337. doi: 10.1111/tpj.12358

Tuteja, N., and Mahajan, S. (2007). Calcium signaling network in plants. *Plant Signal Behav.* 2 (2), 79–85. doi: 10.4161/psb.2.2.4176

Tuteja, N., and Sopory, S. K. (2008). Chemical signaling under abiotic stress environment in plants. *Plant Signal Behav.* 3 (8), 525–536. doi: 10.4161/psb.3.8.6186

Van Leeuwen, W., Vermeer, J. E., Gadella, T. W.Jr., and Munnik, T. (2007). Visualization of phosphatidylinositol 4, 5-bisphosphate in the plasma membrane of suspension-cultured tobacco BY-2 cells and whole arabidopsis seedlings. *Plant J.* 52 (6), 1014–1026. doi: 10.1111/j.1365-313X.2007.03292.x

Vermeer, J. E. M., van Wijk, R., Goedhart, J., Geldner, N., Chory, J., Gadella, T. W. J.Jr., et al. (2017). *In vivo* imaging of diacylglycerol at the cytoplasmic leaflet of plant membranes. *Plant Cell Physiol.* 58 (7), 1196–1207. doi: 10.1093/pcp/pcx012

Wheeler, G. L., and Brownlee, C. (2008). Ca2+ signalling in plants and green algae–changing channels. *Trends Plant Sci.* 13 (9), 506–514. doi: 10.1016/j.tplants.2008.06.004

Xia, K., Wang, B., Zhang, J., Li, Y., Yang, H., and Ren, D. (2017). Arabidopsis phosphoinositide-specific phospholipase c 4 negatively regulates seedling salt tolerance. *Plant Cell Environ.* 40 (8), 1317–1331. doi: 10.1111/pce.12918

Yeh, C.-H., Kaplinsky, N., and Hu, C. (2012). Some like it hot, some like it warm: Phenotyping to explore thermotolerance diversity. *Plant Sci. an Int. J. Exp. Plant Biol.* 195, 10–23. doi: 10.1016/j.plantsci.2012.06.004

Yu, L., Fan, J., Zhou, C., and Xu, C. (2020). Chloroplast lipid biosynthesis is fine-tuned to thylakoid membrane remodeling during light acclimation. *Plant Physiol.* 185 (1), 94–107. doi: 10.1093/plphys/kiaa013

Zhang, N., Belsterling, B., Raszewski, J., and Tonsor, S. J. (2015). Natural populations of arabidopsis thaliana differ in seedling responses to high-temperature stress. *AoB Plants* 17 (7), 1–13. doi: 10.1093/aobpla/plv101

Zhang, Q., van Wijk, R., Shahbaz, M., Roels, W., Schooten, B. V., Vermeer, J. E. M., et al. (2018a). Arabidopsis phospholipase C3 is involved in lateral root initiation and ABA responses in seed germination and stomatal closure. *Plant Cell Physiol.* 59 (3), 469–486. doi: 10.1093/pcp/pcx194

Zhang, Q., van Wijk, R., Zarza, X., Shahbaz, M., van Hooren, M., Guardia, A., et al. (2018b). Knock-down of arabidopsis PLC5 reduces primary root growth and secondary root formation while overexpression improves drought tolerance and causes stunted root hair growth. *Plant Cell Physiol.* 59 (10), 2004–2019. doi: 10.1093/pcp/pcy120

Zheng, S. Z., Liu, Y. L., Li, B., Shang, Z. L., Zhou, R. G., and Sun, D. Y. (2012). Phosphoinositide-specific phospholipase C9 is involved in the thermotolerance of arabidopsis. *Plant J.* 69 (4), 689–700. doi: 10.1111/j.1365-313X.2011.04823.x

Zhou, R., Kjær, K. H., Rosenqvist, E., Yu, X., Wu, Z., and Ottosen, C.-O. (2017). Physiological response to heat stress during seedling and anthesis stage in tomato genotypes differing in heat tolerance. *J. Agron. Crop Sci.* 203 (1), 68–80. doi: 10.1111/jac.12166

Zhu, H., Wu, Y., and Zheng, Y. (2022). Effects of heat shock on photosynthesis-related characteristics and lipid profile of cycas multipinnata and c. panzhihuaensis. *BMC Plant Biol.* 22 (1), 442. doi: 10.1186/s12870-022-03825-0

frontiers | Frontiers in Plant Science

TYPE Original Research
PUBLISHED 30 January 2023
DOI 10.3389/fpls.2023.1083847

OPEN ACCESS

EDITED BY
Biao Jin,
Yangzhou University, China

REVIEWED BY
Jemaa Essemine,
Partner Institute for Computational Biology, China
Martina Spundova,
Palacký University, Olomouc, Czechia

*CORRESPONDENCE
Jin Xu
xjinhsh@njfu.edu.cn

†These authors have contributed equally to this work and share first authorship

SPECIALTY SECTION
This article was submitted to Plant Abiotic Stress, a section of the journal Frontiers in Plant Science

RECEIVED 29 October 2022
ACCEPTED 16 January 2023
PUBLISHED 30 January 2023

CITATION
Xue J, Zeng P, Cui J, Zhang Y, Yang J, Zhu L, Hu H and Xu J (2023) Physiological and gene expression changes of *Cryptomeria fortunei* Hooibrenk families under heat stress.
Front. Plant Sci. 14:1083847.
doi: 10.3389/fpls.2023.1083847

Physiological and gene expression changes of *Cryptomeria fortunei* Hooibrenk families under heat stress

Jinyu Xue[1†], Pingsheng Zeng[2†], Jiebing Cui[1], Yingting Zhang[1], Junjie Yang[1], Lijuan Zhu[1], Hailiang Hu[1] and Jin Xu[1*]

[1]Key Laboratory of Forest Genetics and Biotechnology of Ministry of Education, Co-innovation Center for Sustainable Forestry in Southern China, College of Forestry, Nanjing Forestry University, Nanjing, China, [2]Experimental Center of Subtropical Forestry, Chinese Academy of Forestry, Fenyi, China

Heat stress is one of the major abiotic stresses affecting plant growth and productivity. *Cryptomeria fortunei* (Chinese cedar) is an excellent timber and landscaping tree species in southern China thanks to its beautiful appearance, straight texture and ability to purify the air and improve the environment. In this study, we first screened 8 excellent *C. fortunei* families (#12, #21, #37, #38, #45, #46, #48, #54) in a second generation seed orchard. We then analyzed the electrolyte leakage (EL) and lethal temperature at 50% (LT_{50}) values under heat stress, to identify the families with the best heat resistance (#48) and the lowest heat resistance (#45) and determine the physiological and morphological response of different threshold-resistance of *C. fortune* to heat stress. The relative conductivity of the *C. fortunei* families showed an increasing trend with increasing temperature, following an "S" curve, and the half-lethal temperature ranges between 39°C and 43.2°C. The activities of SOD and POD fluctuated in the early stage of stress but decreased after 37°C. We observed the changes in the cell ultrastructure at 43°C, and the mesophyll cell structure of #48 was less damaged than that of #45. Eight heat resistance gene, including *CfAPX1*, *CfAPX2*, *CfHSP11*, *CfHSP21*, *CfHSP70*, *CfHSFA1a*, *CfHSFB2a* and *CfHSFB4*, were all up-regulated in #45 and #48, and there were significant differences between #45 and #48 under different heat stress treatments. We found a significant difference in heat tolerance between #45 and #48, such that #48 shows higher heat tolerance capability and could be exploited in breeding programs. We conclude that the strongly heat-resistant family had a more stable physiological state and a wider range of heat stress adaptations.

KEYWORDS

***Cryptomeria fortunei* Hooibrenk, heat stress, physiological analysis, plant cell ultrastructure, gene expression**

Abbreviations: *C. fortunei*, *Cryptomeria fortunei*; EL, electrolyte leakage; LT_{50}, lethal temperature at 50%; NBT, nitroblue tetrazolium; TEM, transmission electron microscope; SOD, superoxide dismutase; POD, peroxidase; CAT, catalase; APX, ascorbate peroxidase; HSPs, heat shock proteins; PCR, polymerase chain reaction; TFs, transcription factors; HSFs, heat stress transcription factors; OD, optical density.

1 Introduction

With the globe becoming warm, high temperature stress has become one of the major environmental stresses limiting plant growth, metabolism and productivity (Berry and Bjorkman, 1980; Hasanuzzaman et al., 2013). In recent years, the frequent occurrence of extremely high temperatures has posed a severe challenge to the ability of plants to withstand high temperatures (Borrell et al., 2020). In the published research on the effects of heat stress on plant physiology, there have been many studies on the relationship between heat tolerance and plant physiological indicators, but the types of plants studied have mainly included herbs and vegetables. In contrast, research on forest trees has been limited. Different plants have different heat-resistance mechanisms, and the same plant may also be affected by the synergistic effect of multiple heat-resistance mechanisms (Hasanuzzaman et al., 2010). Compared with agricultural crops, forest trees have more complex cultivation conditions, more resilience mechanisms and longer growth cycles (Bi and Zhuge, 2008). During their growth and development, trees are affected by various environmental factors, among which temperature, light and water are the most important abiotic factors influencing tree growth. When the damage caused by high-temperature stress exceeds a plant's own regulatory capacity, the plant exhibits heat-damage symptoms (Nahar et al., 2015).

Heat stress usually means that the temperature exceeds the threshold level for a period of time, which is enough to cause irreversible damage to plant growth and is a serious threat to global crop production (Vetter et al., 1958). The cell membrane is the critical barrier between cells and the external environment. Therefore, heat stress can initially cause changes in cell membrane permeability, leading to the denaturation of membrane proteins, separation of cell membrane lipids, and disruption of normal cell physiological activities (Hemantaranjan et al., 2014). Changes in cell membrane permeability will cause the cell membrane to lose its ability to select substances, the electrolytes in the cytoplasm to extravasate, and the conductivity of cell tissue fluids to increase (Jiang et al., 2016). Chlorophyll synthesis is sensitive to heat stress and is a good indicator of heat stress damage (Gosavi et al., 2014). Heat stress can cause various changes in chloroplasts, such as changes in thylakoid structure, the loss of granal stacking, and granal swelling (Ashraf and Hafeez, 2004; Rodríguez et al., 2005). In addition, heat stress-mediated changes in chloroplast ultrastructure can be used to indicate the heat tolerance of plant varieties at the cellular level (Zou et al., 2017).

The protective enzymes in plants mainly include catalase (CAT), peroxidase (POD), superoxide dismutase (SOD) and ascorbate peroxidase (APX) (Hong et al., 2021; Hu et al., 2021). For instance, there was a significant negative correlation between the activities of SOD and POD in different bottle gourd seedlings and the heat damage index of bottle gourds (Tian et al., 2020). SOD mainly scavenges superoxide anions in plants and converts them into H_2O_2 and O_2, thereby maintaining cellular homeostasis and protecting cells from oxidative damage (Talbi et al., 2015). One of the important physiological mechanisms of plants in response to heat stress is the accumulation of osmoregulatory factors. The main osmotic regulators in plant cells mainly include proline, soluble sugars, and soluble proteins (Kaplan et al., 2004).

The survival strategy of plants under heat stress conditions often involves altering gene expression during transcription/translation, resulting in the production of heat shock proteins (HSPs). During cell growth and development, HSPs participate in protein synthesis, folding, and target protein degradation, thereby maintaining the stability of the cell membrane system (Usman et al., 2015; Khan and Shahwar, 2020). In plant genomes, approximately 7% of the coding sequences are assigned to transcription factors (TFs). Compared with animals and yeast, many of them belong to large gene families, such as heat stress transcription factors (HSFs) (Fragkostefanakis et al., 2015). Mishra found that in tomato (*Solanum lycopersicum*), at each developmental stage, the plants with *HsfA1a* silencing were more sensitive to heat stress than the wild type (Mishra et al., 2002).

Cryptomeria fortunei Hooibrenk is an evergreen tree species of the Cupressaceae family. It is an excellent timber and garden tree species in southern China (Zhang et al., 2021). With increasing global warming, the living environment of *C. fortunei* is also worsening. Therefore, it is of great theoretical and practical significance to study the physiological mechanism and genes related to the heat tolerance of *C. fortunei* in response to heat stress for subsequent molecular genetics and breeding research. In this study, we preselected the most and least thermo sensitive families among the eight tested families. We then analyzed the changes in needle phenotype, antioxidant activity, and chlorophyll content and ultrastructure of the two families under heat stress. Finally, we used the transcriptome data of *C. fortunei* available in our laboratory to identify heat resistance-related genes and explore their expression levels in families of *C. fortunei* with different levels of heat resistance, which laid a foundation for molecular breeding of heat resistance in *C. fortunei*.

2 Materials and methods

2.1 Plant materials

Our collection of *C. fortunei* is mainly derived from the eastern part of China (Table 1). The seedlings of eight elite *C. fortunei* families that were the offspring of the second orchard of *C. fortunei* in Xiapu forest farm, Xiapu County, Fujian Province, were selected. The material was harvested in 2018, and the seedlings were raised in 2019. In May 2021, we moved these to our laboratory in Nanjing (118°50' E, 32°05' N) for this study. To carry out heat stress, we pretreated 2-year-old healthy *C. fortunei* plants in the growth chamber under a 12/12-h photoperiod (day/night) at 25 °C/20 °C and 60% humidity and conducted a 4-week preliminary experiment.

2.2 Heat stress treatment

The shoots with consistent growth across the families of *C. fortunei* were collected and subjected to heat stress treatment at 25° C, 29°C, 33°C, 37°C, 39°C, 41°C, and 43°C. Starting from 25°C, the first 3 temperatures were increased at 4°C/h, and the temperature was increased at 2°C/h after 37°C. When the target temperature was reached, the treatment was performed for 9 hours. Six needles from three positions were taken after 12 h of treatment. The plants of

TABLE 1 Materials and sources.

Families	Sources	Longitude (E)	Latitude (N)	Annual temperature range (oC)	Average Annual Precipitation (mm)
#12	Shuimen Forestry Farm, Xiapu County, Fujian Province	120°06'	27.00'	17-23	1640
#21	Shiyang Forest Farm, Wencheng County, Zhejiang Province	119°50'	27°50'	16-25	1725
#37	Lushan Forest Farm, Jiujiang County, Jiangxi Province	116°05'	29°45'	11-18	1745
#38, #45, #46, #48	Xiapu Forest Farm, Xiapu County, Fujian Province	119°57'	26°52'	17-23	1640
#54	Tianmushan Forest Farm, Lin'an County, Zhejiang Province	119°25'	30°20'	13-22	1386

families #45 and #48 were sampled after 0 h, 3 h, 6 h and 9 h of heat stress treatment (43°C). The plants of groups #45 and #48 were sampled after 0h, 3 h, 6 h and 9 hof heat stress treatment (43°C). These samples were wrapped in tin foil, placed in liquid nitrogen for rapid freezing, and then stored in an ultralow temperature refrigerator at -80°C. The experimental treatment was repeated three times, and three plants were treated each time.

2.3 Electrolyte leakage (EL) and lethal temperature at 50% (LT_{50})

EL was measured according to the method of Zhang with some modifications (Zhang et al., 2020). Here, 0.2 g of the treated sample needles was weighed; samples were placed in 10 ml of distilled water and shaken with a shaker at room temperature. After 4 hours of incubation, the conductivity was measured by a conductivity meter (DDS-307, Leici Instruments Co., Shanghai, China). The formula EL (%)=$(E_1-E_0)/(E_2-E_0)\times100$ was used, wherein the conductivity of distilled water was E_0 and that of the extract was E_1. The sample was heated in a boiling water bath for 15 min. After cooling to room temperature, the ultimate conductivity was measured as E_2.

In combination with the logistic equation, the relative conductivity was fitted with the logistic regression equation as $Y=K/(1+ae^{-bt})$, where Y is EL, t is temperature, K is the maximum EL, and a and b are unknown parameters. The equation was processed so that the second derivative was equal to zero, and the values of a and b and the correlation coefficient R were obtained. The inflection point temperature of the relative conductivity curve corresponding to the processing temperature is the half lethal temperature, that is, LT_{50}=lna/b (Janáček and Prášil, 1991; Huang et al., 2016).

2.4 Chlorophyll content

Needle samples (0.2 g) of #45 and #48 after heat stress treatment were weighed and placed in a mortar; calcium carbonate, quartz sand and 2-3 ml of 95% alcohol were added to grind the sample into a homogenate, and 7-8 ml of 95% alcohol was added until the tissue turned white. The supernatant was centrifuged at 500 rpm 3 times at room temperature for 10 minutes each time, and the OD_{665} (optical density at 665 nm) and OD_{649} (optical density at 649 nm) of the supernatant were measured with a spectrophotometer. The chlorophyll (a+b) content was measured according to the method described by Lichtenthaler and Wellburn (Lichtenthaler and Wellburn, 1983).

2.5 Determination of SOD and POD activity

The needles of #45 and #48 were collected as samples after heat stress treatment. We then weighed the needles (0.2 g), ground them in liquid nitrogen, and suspended them in 3.0 ml of a solution consisting of 50 mM phosphate buffer pH 7.8. The homogenate was centrifuged at 10000 rpm for 20 minutes at 4°C. The supernatant was taken to analyze SOD and POD activities. SOD activity analysis was based on the ability of SOD to inhibit the photochemical reduction of nitroblue tetrazolium (NBT) (Luo et al., 1999). The activity of SOD was expressed as the activity units of the enzyme that inhibited 50% of the NBT. SOD activity was expressed as U g^{-1} FW protein. POD activity was measured by using guaiacol as the substrate (Thomas et al., 1982). One unit of POD activity was defined as a change of 0.01 in 1 min at 470 nm. POD activity was expressed as U g^{-1} FW min^{-1}.

2.6 Ultrastructural observations

Needle samples # 45 and # 48 were collected and subjected to 37° C and 43°C for 24 hours, and samples at 25°C were collected as controls. After treatment, three mature needles were sampled. The needles were cut into a 3 mm segment size with a blade and placed in a 5 ml penicillin bottle; 2 ml of 3% glutaraldehyde solution was added, the air in the bottle was extracted with a syringe, which caused the needles to sink entirely to the bottom of the bottle. Samples were then stored in a 4°C refrigerator for 24 h. The specimens were rinsed with 0.1 mol L^{-1} phosphate buffer solution with a pH of 7.0 3 times for 30 minutes each time. The specimens were subsequently dehydratedin a series of graded alcohol solutions, namely, 15%, 30%, 50%, 70%, 80%,

90%, 95%, 100% solution, followed by acetone solution at room temperature. The samples were infiltrated and embedded with Poly Bed 812 epoxy resin, dried and stored for 8 hours. The samples were then sectioned using ultratome III ultramicrotome (LKB, Bromma, Stockholm, Sweden). The samples were subsequently stained in uranium dioxide acetate and lead citrate and then observed *via* the transmission electron microscope (TEM) (JEM-2100, JEOL Ltd., Tokyo, Japan). From the TEM images, ten chloroplasts were selected for observation. The shape of the chloroplast is approximated to be an ellipse, and the calculation formula of ellipse area is as follows: $S=\pi ab$, where S is the elliptical area (μm^2), a is the semimajor axis (μm), and b is the semiminor axis (μm).

2.7 Gene expression

The total RNA extracted from the needles of *C. fortunei* treated for 0, 3, 6, and 9 h under heat stress at 43°C was used as the template. A TaKaRa Mini BEST Plant RNA Extraction Kit was used to extract total RNA (Spin-column) (Takara, Beijing, China). The RNA concentration was measured by spectrophotometer (NanoDrop, 2000; Thermo Scientific, Waltham, Massachusetts, USA). Reverse transcription was performed with a HiScript III RT SuperMix for qPCR (+gDNA wiper) (Vazyme, Nanjing, China) reverse transcription kit according to the manufacturer's instructions. According to the existing *C. fortunei* transcriptome sequencing data in our laboratory, eight genes related to heat resistance were screened. Homologous sequences were identified by the NCBI online tool BLAST (https://blast.ncbi.nlm.nih.gov/Blast.cgi), and specific primers used were designed by Primer Premier 5.0. The CYP gene of *C. fortunei* was used as the internal reference gene. The reverse transcription cDNA template was diluted 10 times, and three replicates were evaluated. A ChamQ SYBR qPCR Master Mix (Low Rox Premixed) kit (Vazyme) was used for qRT-PCR analysis. All qPCRs were carried out on an Applied Biosystems 7500 real-time PCR system (ABI, Foster City, CA, USA). The expression levels were calculated using the $2^{-\Delta\Delta Ct}$ method (Zhang et al., 2021). Table 2 lists all primers used to quantify the reverse transcription polymerase chain reaction (PCR). Experimental consumables, including 96 well 0.2 ml semi-skirt PCR plates, were obtained from NEST Biotechnology Co. Ltd (Wuxi, China).

TABLE 2 qRT-PCR primer sequence.

Primer name	Primer sequence(5′-3′)
CfAPX1-F	TGTGAGCACCAGACAAAGCC
CfAPX1-R	AGCCTGAGCCACCAGAAGAG
CfAPX2-F	CTCAAAGCCAGAGCGTTCCT
CfAPX2-R	CCGTTTGCCTGATGCTACTC
CfHSP11-F	ATCACCGAGTAGAACGCTCG
CfHSP11-R	GTATGGCTTCGGCTCCTGTT
CfHSP21-F	GATTTGGTTGCTCTCCAGGC
CfHSP21-R	AAGGACACCAGGGCAATGTT
CfHSP70-F	AAGCGGATCACTTTCAGGCA
CfHSP70-R	CAGAGCTGTTTTGGATGCCG
CfHSFA1a-F	CGTCAGCTGTCTGGTCAAGT
CfHSFA1a-R	AACGGCCCTCCTGTAATTGG
CfHSFB2a-F	CCGTGGAAAACAAAGCATCT
CfHSFB2a-R	AAGATCGTTGCATTGCTGTG
CfHSFB4-F	GGAAGTCTGCGATCGATGTT
CfHSFB4-R	TGACACGACTCAACCGCTAC
CYP-F	TCTCGGGCAGCATTTCACGC
CYP-R	AGCCGAAACTGGCGCCAACA

2.8 Statistical analysis

GraphPad Prism 8 was used for statistical analysis and mapping. When $p \leq 0.05$, the Pearson rank correlation method was used to calculate the bivariate correlation between traits and corresponding gene expression levels. The data were analyzed by one-way ANOVA, and Duncan's test was conducted in accordance with $p \leq 0.05$. These analyses were conducted using SPSS 26.0.

3 Results

3.1 Individual *C. fortunei* families show varying degrees of heat resistance

We aimed to preselect the most and least heat resistant *C. fortunei* families from our set of 8 by analyzing the EL and LT_{50} values in response to heat stress. The EL values of all *C. fortunei* families increased gradually with increasing temperature, showing a consistent "S"-shaped curve response (Figure 1). We found that the lowest LT_{50} was for #45, which was 39.9°C, and the highest LT_{50} was for #48, which was 43.1°C (Table 3). Subsequently, we selected these two families for further physiological index tests and related experiments to study the widest possible range of heat-resistant responses within *C. fortunei*.

3.2 Heat stress causes needle damage in *C. fortunei* families

Heat stress often leads to changes in leaf color in plants. After heat stress treatment at 37°C, compared with the control (25°C), the needles of #45 and #48 showed no significant difference in needle shape or color (Figures 2A, B), yet at ≥ 39°C, they showed different degrees of etiolation. The degree of conifer browning damage increased significantly with increasing heat stress. After treatment at 39°C, the needles of #45 were browned and dried, and at 43°C, most of the needles had dried (Figures 2C, D) . Furthermore, heat stress also caused the top needles to wilt and droop, making them thicker and easier to detach. In addition, compared with the #45 family, phenotypic changes in the #48 family under high-temperature stress were not obvious, and the degree of needle browning and drying was

lower. This is consistent with the fact that the LT_{50} of the #48 family is higher than that of the #45 family (Table 3).

3.3 Chlorophyll contents of the *C. fortunei* families change under different heat stresses

Chlorophyll synthesis is sensitive to heat stress and is a good indicator of heat stress injury (Gosavi et al., 2014). Heat stress had an adverse effect on the chlorophyll content of seedlings of the *C. fortunei* families. We found that the chlorophyll a content of the #45 and #48 needles showed a decreasing trend with increasing temperature. Under the 25°C-39°C treatment, the change was relatively small, and the decrease was obvious after treatment at 39°C (Figure 3A). The chlorophyll a, b and chlorophyll (a+b) contents of #48 needles were less than those of #45 needles following heat stress treatment under 39°C but more than those of #45 needles at 39-43°C (Figures 3A–C). These results indicated that #48 changed slowly under heat stress and was more stable under heat stress than #45. However, the chlorophyll a/b ratio did not increase (Figure 3D).

3.4 The antioxidant system of the *C. fortunei* families changes under different heat stresses

Heat stress treatment significantly affected the activities of POD and SOD in #45 and #48. During heat stress, the SOD activities of #45 and #48 needles were the highest at 37°C; compared with 25°C, the increase was 182.61% and 158.22%, respectively (Figure 4). With increasing temperature stress, the POD activities of #45 and #48 showed a trend of first increasing and then decreasing, similar to the changes in SOD activities. The POD activity also showed a downward trend after 37°C, and #45 at 43°C decreased by 68.99% compared with that at 37°C. After treatment at 39°C, both the SOD and POD activities of #48 were higher than those of #45 (Figure 4).

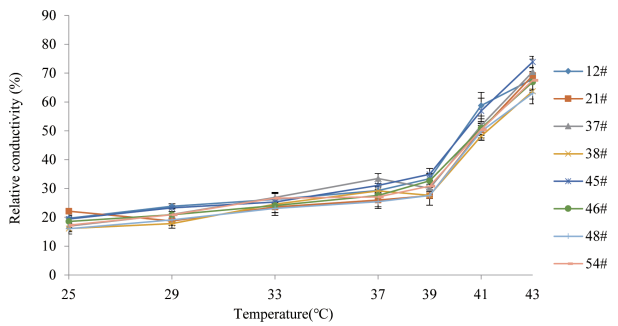

FIGURE 1
Variations of electrolyte leakage of eight *C. fortunei* families under heat stress.

3.5 Effect of heat stress on the ultrastructure of mesophyll cells of *C. fortunei*

Under heat stress, the ultrastructure of mesophyll cells of the #45 and #48 families changed obviously. Compared with the control (25° C) (Figures 5A–D), we found that the ultrastructure of #48 was not significantly different under heat stress at 37°C, but the number of osmiophilic granules in its chloroplasts was significantly increased, and no starch granules were observed (Figures 5G, H). In addition, we also found that #45 showed similar changes, but #45 had more obvious changes in chloroplast structure than #48, and it could be clearly seen that the thylakoid sheet structure in the chloroplast was distorted and loose (Figures 5E, F). Both #45 and #48 mesophyll cells exhibited severe plasmolysis at 43°C, and some organelles moved toward the center of the cell (Figures 5I, K). In the cells of #45, the tonoplast membrane was ruptured, the chloroplast structure was further expanded, deformed or even ruptured, and the internal osmiophilic granules increased. The thylakoid sheets were loose and disordered (Figure 5J). In contrast, the cells of #48 were less damaged. We observed a relatively intact plasma membrane, but a damaged nucleus and mitochondrial structure, in which chromatin within the nucleus aggregated into darker clumps, and the chloroplast structure was ruptured, but its thylakoid sheets remained tightly packed (Figure 5L). According to the above results, the ultrastructure of mesophyll cells in both families responded to heat stress, and the #45 family was more susceptible to heat stress damage than the #48 family.

3.6 Effect of heat stress on the chloroplast size of *C. fortunei*

The photosynthesis efficiency depends not only on the number of chloroplasts in cells but also on the surface area of chloroplasts (Bondada et al., 1994). The sectional area of #45 and #48 chloroplasts first increased and then decreased with increasing heat stress (Table 4). The changes in the chloroplast cross-sectional area of #45 at 37°C were significantly increased compared with the control (25°C), but the changes in #48 at 37°C were not significant. We found that the chloroplast cross-sectional area of #48 changed significantly when treated at 43°C, and the chloroplast cross-sectional area decreased significantly. We therefore conclude that the effect of heat stress on #45 was greater than that on #48, which showed weaker heat tolerance and more severe damage.

3.7 Expression of heat resistance genes in *C. fortunei* families under heat stress

To gain more insights into the response of *C. fortunei* to heat stress, we evaluated eight heat-resistance-related genes screened from the existing transcriptome data under 43°C culture conditions (Figure 6). We found that the transcript levels were significantly different in #45 and #48. The relative expression of *CfAPX1* under heat stress showed a trend of first increasing and then decreasing in both families, and its gene expression in #48 was higher than that in

TABLE 3 Regression equation of electrolyte leakage and temperature and lethal temperature of 50% of *C. fortunei.*

Families	Equation parameters		Fitting Degree (R^2)	Lethal temperature of 50% (°C)
	a	b		
#12	79.6	0.108	0.868	40.7
#21	68.9	0.099	0.791	42.6
#37	108.9	0.115	0.888	40.9
#38	100.5	0.108	0.893	42.8
#45	110.0	0.118	0.871	39.9
#46	85.2	0.106	0.877	41.9
#48	96.7	0.106	0.874	43.1
#54	89.8	0.107	0.874	41.9

#45 (Figure 6A). Under heat stress, the relative expression of *CfAPX2* showed a trend of first increasing and then decreasing in #45 and reached the highest level at 6 h, which was 6.0 times that of the control (0 h) (Figure 6B). The expression level of *CfHSFB2a* in #45 was higher than that in #48 at 0 h, 3 h and 6 h (Figure 6D). The relative expression of *CfHSP70* in #45 reached the highest level at 3 h and decreased significantly thereafter. We observed that between the two families, the relative expression levels of genes in #48 and #45 were not significantly different under the 0h and 3 h treatments, while gene expression in #48 was significantly higher than that in #45 under the 6 h and 9 h treatments (Figures 6F–H).

3.8 Correlation of various physiological indicators in *C. fortunei* families under heat stress

At 25°C, the EL of the #45 family was significantly positively correlated with five physiological parameters, and there was a positive correlation between these five physiological parameters (Table 5). At room temperature, the EL of #48 had no significant correlation with chlorophyll a; however, chlorophyll (a+b) content and SOD activity were negatively correlated. In addition, POD in #48 was significantly positively correlated with EL but negatively correlated with the other four physiological indicators.

Under 37 °C heat stress, the EL and POD of #45 and #48 were significantly positively correlated with each other and negatively correlated with the chlorophyll content (Table 5). In the #45 family, POD was negatively correlated with the other 4 physiological parameters. In addition, under 37 °C treatment, SOD in the #48 family was significantly negatively correlated with chlorophyll but extremely significantly positively correlated with POD and EL.

After heat stress at 43 °C, the POD activity in the #45 family was positively correlated with the five physiological indicators, while that in the #48 family was negatively correlated with the other four indicators except chlorophyll b, which was positively correlated and not significant. At the same time, after heat stress at 43 °C, the EL of the #48 family was negatively correlated with these five physiological parameters.

4 Discussion

The cell membrane constitutes the primary heat stress target in plants. The lipid molecules on the biofilm transform from a colloidal

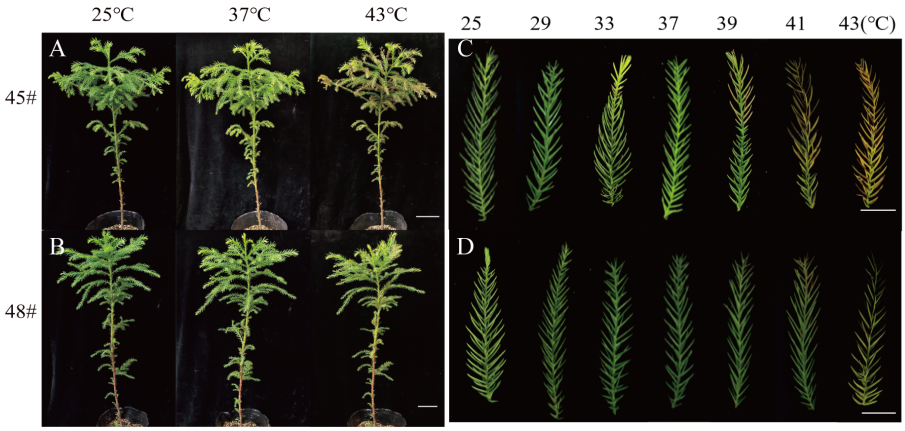

FIGURE 2
The phenotypes of the *C fortune* families changed significantly under heat stress. **(A)** #45 phenotype at 25°C, 37°C and 43°C; **(B)** #48 phenotype at 25 °C, 37 °C and 43 °C; **(C)** needle phenotype of #45; **(D)** needle phenotype of #48. **(A, B)** Bars=10 cm; **(C, D)** Bars=2 cm.

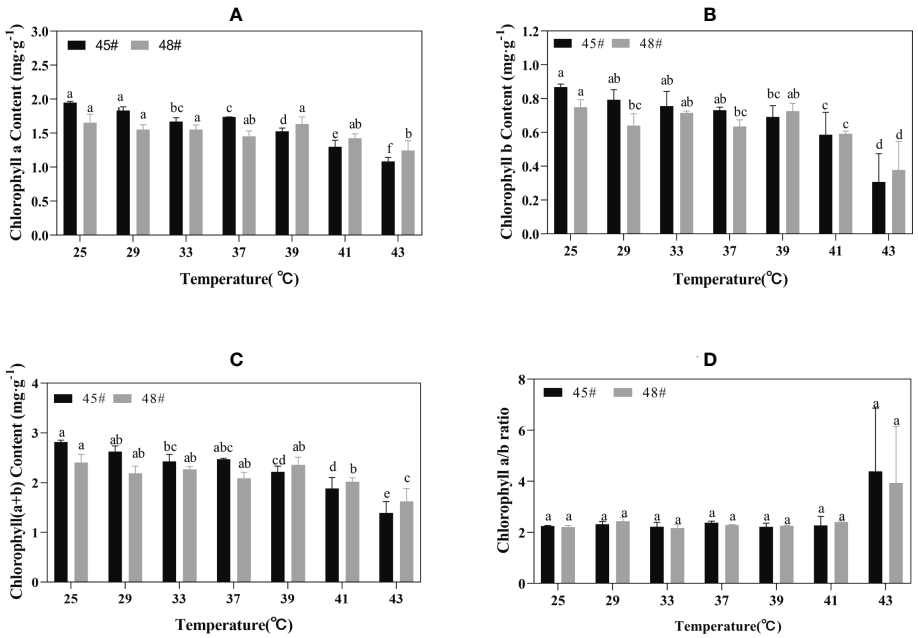

FIGURE 3
Chlorophyll changes in *C. fortune* families under heat stress. **(A)** Chlorophyll a content; **(B)** Chlorophyll b content; **(C)** Chlorophyll (a+b) content; **(D)** Chlorophyll a/b ratio. Each value in the graph is the mean ± standard error (n=3). The different patterns indicate different treatment temperatures, and the lowercase letters above each bar indicate significant differences ($p < 0.05$).

state to a liquid crystal state under thermal stress, which increases the permeability of the lipid membrane and allows the penetration of intracellular electrolytes, which leads to an increase in EL (Lastra et al., 1982). There is a positive correlation between the rate of lipid peroxidation and EL: with increasing heat stress, the relative permeability of the plasma membrane and EL also increases (Lukatkin, 2003). In the present study, the EL of each family of *C. fortunei* gradually increased with the intensification of heat stress and exhibited an overall "S"-shaped curve. At 25°C-37°C, the EL increased slowly and then increased sharply after 37°C. The EL of *C. fortunei* family #48 was at a lower level during the whole stress process, indicating that #48 had less electrolyte extravasation, less damage to the cell membrane, and stronger heat resistance.

We found that heat stress led to a decrease in photosynthetic pigment content and impaired chlorophyll biosynthesis in plastids (Marchand et al., 2005; Dutta et al., 2009). Chlorophyll content can reflect the degree of heat stress of plants to a certain extent, thus reflecting the heat tolerance of plants (Bhusal et al., 2018). Studies have shown that heat stress leads to increased decomposition of chlorophyll in plants. Part of the reason may be that high temperature inhibits chlorophyll biosynthesis, resulting in a lower synthesis rate than the decomposition rate. Another reason may be that the content of reactive oxygen species in plants increases under heat stress, thus causing oxidative damage, which then accelerates the degradation of chlorophyll (Sun et al., 2006). The chlorophyll a and chlorophyll b contents in #45 after heat stress (43°C) decreased by 44.4% and 64.6%, respectively, compared with those of the control, while the contents of chlorophyll a and chlorophyll b in #48 decreased by 24.8% and 49.6% respectively, indicating that chlorophyll b in *C. fortunei* was more sensitive to heat stress than chlorophyll a. With the intensification of heat stress, the chlorophyll a content in the cedar family showed a downward trend, and the chlorophyll b and chlorophyll (a+b) contents changed in the same way. However, chlorophyll contents of #45 and #48 increased at 37 °C and 39 °C respectively. Therefore,

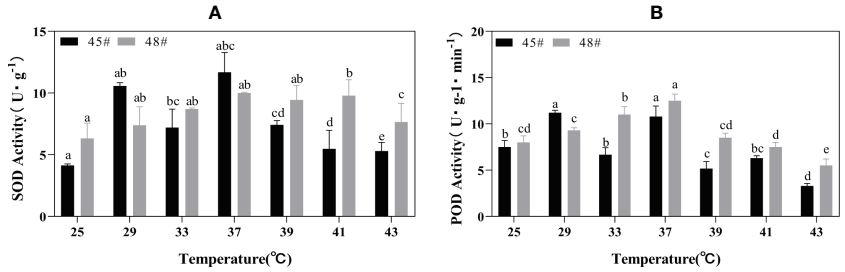

FIGURE 4
Changes in the POD and SOD contents of *C fortunei* families under heat stress. **(A)** SOD content; **(B)** POD content. Each value in the graph is the mean ± standard error (n=3). The different patterns indicate different treatment temperatures, and the lowercase letters above each bar indicate significant differences ($p < 0.05$).

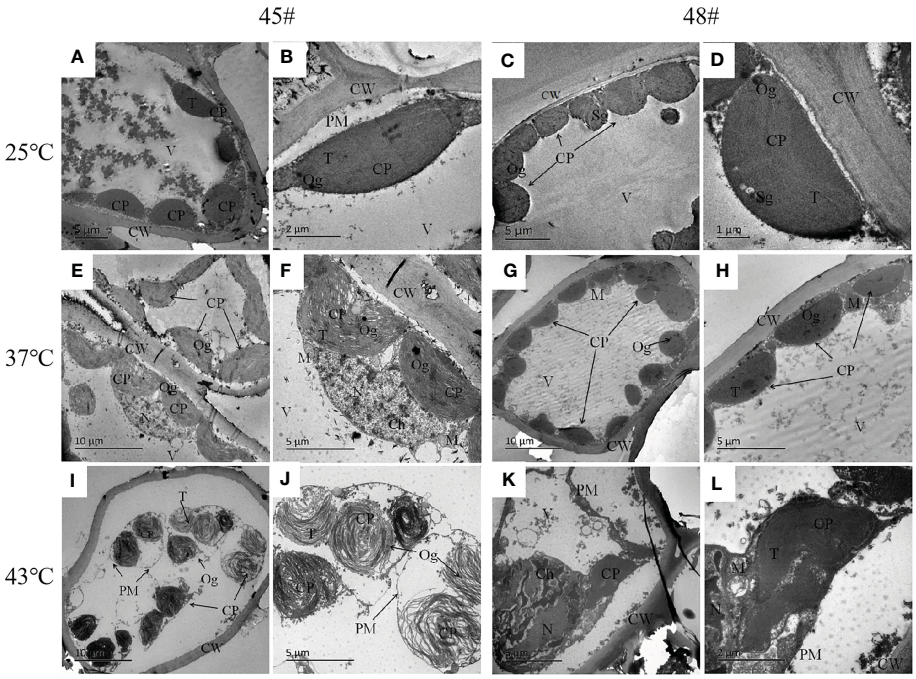

FIGURE 5
Changes in the ultrastructure of mesophyll cells in #45 and #48 under heat stress **(A, B)** #45 room-temperature treatment; **(C, D)** #48 room-temperature treatment; **(E, F)** #45 subjected to 37°C; **(G, H)** #48 subjected to 37°C; **(I, J)** #45 subjected to 43°C; **(K, L)** #48 subjected to 43°C. Cell wall, CW; Membrane, PM; Vacuole, V; Chloroplast: CP; Thylakoids, T; Starch granules, SG; Mitochondria, m; Nucleus, n; Chromatin, ch; Osmiophilic particles, Og.

we speculate that after adapting to high-temperature stress, *C. fortunei* scavenges reactive oxygen species to alleviate high-temperature damage through the initiation of various anti-high-temperature mechanisms, thus leading to the restoration of the chlorophyll content (Chang, 2013). The decrease in chlorophyll content at the beginning of stress may be due to the sudden high temperature affecting the normal physiological state of *C. fortunei* cells, and the accumulation of intracellular reactive oxygen species, which inhibits the biosynthesis of chlorophyll in cells and accelerates the decomposition of chlorophyll.

The enzyme reaction system formed during the long-term evolution of plants. To eliminate oxidative stress caused by heat stress and enhance plant protection, SOD and POD are key enzymes in the plant defense system (Larkindale and Vierling, 2008). These enzymes exist in various plant cells and can scavenge intracellular O^{2-}, balance oxygen free radicals, and maintain their metabolic stability (Vidya et al., 2018). In our study, the decrease in SOD activity in #45 at 33°C may be due to the sudden high temperature disrupting the normal physiological metabolism of cedar trees, whereas the subsequent increase in activity is due to a self-protective response to a stressful environment after thermos table exercise. The changes in POD activity in the two cedar families in this study were similar to those in SOD activity, showing a trend of first increasing and then decreasing. Chloroplasts are believed to be the most sensitive organelles (Lütz et al., 2012). Without heat stress, the SOD activity of #48 was higher than that of #45. After heat stress at 39°C, the SOD activity of #48 was significantly higher than that of #45, indicating that #48 could more effectively remove ROS. In addition, correlation analysis showed that under 43°C heat stress, the SOD activity and chlorophyll content of #48 were significantly positively correlated, while the chlorophyll content of #45 during this period was not significantly negatively correlated with SOD activity. Free radicals may cause damage to the chloroplast membrane in plants (Zhang et al., 2021). This result indicated that the increase in the active oxygen content in plants from the #45 family under heat stress caused more serious oxidative damage, which accelerated the degradation of chlorophyll. This further illustrated that #45 has a lower heat resistance than #48.

TABLE 4 Effects of heat stress on cross sections of chloroplasts in two families.

Temperature (°C)	#45			#48		
	Length of Long Axis (μm)	Length of Short Axis (μm)	Cross-Section Area of Chloroplast ($μm^2$)	Length of Long Axis (μm)	Length of Short Axis (μm)	Cross-Section Area of Chloroplast ($μm^2$)
25	6.46 ± 0.89b	3.75 ± 0.91b	18.63 ± 3.56b	5.67 ± 0.64b	3.71 ± 0.37b	16.51 ± 2.56ab
37	8.50 ± 0.71a	4.08 ± 0.45b	27.23 ± 3.35a	6.17 ± 0.84b	3.71 ± 0.55b	17.81 ± 2.86ab
43	5.96 ± 0.53b	5.08 ± 0.42a	23.90 ± 3.66a	6.34 ± 0.75b	2.79 ± 0.54c	14.09 ± 3.24c

a, b, and c indicate that the two families (#45 and #48) have significant differences in long axis, short axis, or chloroplast cross-sectional area under different heat stress ($p < 0.05$).

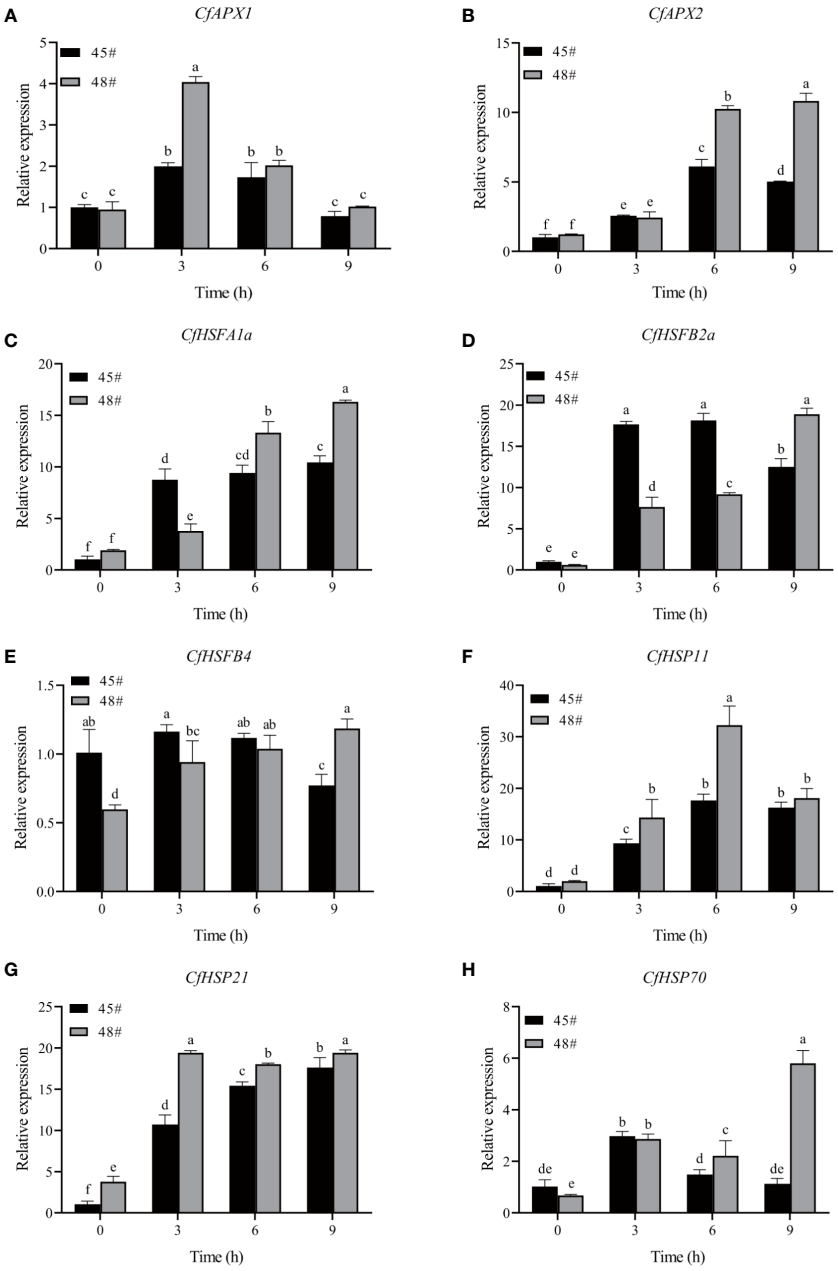

FIGURE 6
Effects of heat stress on gene expression in *C. fortunei* needles. The time course of heat in *C. fortune* shifted to 43°C. **(A)** *CfAPX1*; **(B)** *CfAPX2*; **(C)** *CfHSP11*; **(D)** *CfHSFB2a*; **(E)** *CfHSFB4*; **(F)** *CfHSP11*; **(G)** *CfHSP21*; **(H)** *CfHSP70*. Each value in the graph is the mean ± standard error (n=3).

We found that in the process of heat stress, the chloroplasts of plant leaves expanded and deformed, the thylakoid sheets were loose, the structure was disordered, the plastid globules increased, and the chloroplast envelope was ruptured and disintegrated. Among them, photosystem II on the thylakoid membrane was one of the most sensitive parts, and the damage from heat stress was irreversible (Sheng et al., 2006; Guo et al., 2018). In this study, with the intensification of heat stress, osmiophilic granules increased in the chloroplasts of both families, and the chloroplasts in the needles of the two families were damaged to different degrees under heat stress. Studies have shown that osmiophilic granules are the product of degradation of thylakoid membrane lipid aggregates, which reflects the increased degree of chloroplast damage under stress conditions (Zhou et al., 2018).

The expression of the APX gene was induced by high temperature, drought, low temperature, salt and other stresses. The product of this gene can efficiently remove H_2O_2 in plants, thereby maintaining cellular redox homeostasis and improving plant stress resistance (Krasensky and Jonak, 2012). Using wild-type and mutant Arabidopsis plants as materials, the results showed that *APX1*, *APX2* and *APX6* were significantly induced by heat stress, and *APX3* and *APX5* showed obvious inducible expression in response to heat stress (Li et al., 2019). The accumulation of HSPs is controlled by HSFs and plays a central role in the plant heat shock response and the acquisition of heat tolerance by plants or other organisms (Tian et al., 2021). For example, *AtHSFa* and *AtHSFb* in the Arabidopsis A1 subfamily can regulate the expression of related genes and the

TABLE 5 Correlation of various physiological indicators in *C. fortunei* families under heat stress.

		#45					#48				
		Chla	Chlb	Chl(a+b)	SOD	POD	Chla	Chlb	Chl(a+b)	SOD	POD
25°C	EL	0.710*	0.710*	0.991**	0.912**	0.965**	-0.771*	-0.296	-0.473	-0.042	0.949**
	Chla		1.000**	0.797*	0.358	0.500		0.836**	0.925**	0.668*	-0.933**
	Chlb			0.797*	0.358	0.500			0.982**	0.967**	-0.583
	ChI(a+b)				0.849**	0.921**				0.900**	-0.727
	SOD					0.988**					-0.356
37°C	EL	-0.771*	-0.296	-0.473	-0.042	0.949**	-0.958**	-0.974**	-0.964**	0.919**	0.997**
	Chla		0.836**	0.925**	0.668*	-0.933**		0.998**	1.000**	-0.993**	-0.935**
	Chlb			0.982**	0.967**	-0.583			0.999**	-0.985**	-0.955**
	ChI(a+b)				0.900**	-0.727*				-0.991**	-0.942**
	SOD					-0.356					0.888**
43°C	EL	-0.033	-0.207	-0.161	0.964**	0.902**	-0.025	-0.949**	-0.623	-0.216	-0.351
	Chla		0.985**	0.992**	-0.297	0.401		0.364	0.798**	0.982**	-0.927**
	Chlb			0.999**	-0.459	0.235			0.852**	0.535	0.012
	ChI(a+b)				-0.417	0.280				0.898**	-0.514
	SOD					0.756*					-0.839**

*Indicates $P < 0.05$; ** Indicates $P < 0.01$.

synthesis of HSP genes in the early stage of the plant response to heat stress, thus helping the plant resist to the damage caused by high temperature (Baniwal et al., 2004; Ikeda et al., 2011). In this study, during heat stress, the expression of each HSF gene in the #48 family was higher than that in the #45 family after 9 h of treatment. In general, the expression of heat resistance genes in the #48 family was higher under heat stress, which explained why the #48 family was more heat-tolerant than the #45 family at the molecular level, and the results were also consistent with previous research results.

5 Conclusions

We found that the LT_{50} values of #45 and #48 were the lowest at 39.9°C and the highest at 43.1°C, respectively, out of the eight *C. fortunei* families, which indicated that #45 had the weakest heat resistance and #48 had the strongest heat resistance. In addition, the chlorophyll content and the antioxidant system were closely related to heat tolerance. At the same time, we found that changes in mesophyll cell ultrastructure and chloroplast cross-sectional area were closely related heat stress parameters in *C. fortunei*. Heat stress also induced up-regulation of the *CfAPX1*, *CfAPX2*, *CfHSP11*, *CfHSP21*, *CfHSP70*, *CfHSFA1a*, *CfHSFB2a* and *CfHSFB4* genes, and each gene was significantly different under different heat stress treatments in families #45 and #48. This study lays a foundation for studying the molecular mechanisms of the response and tolerance of *C. fortunei* to heat stress.

Data availability statement

The data presented in the study are deposited in the NCBI repository, accession number PRJNA644276.

Author contributions

JYX: Methodology, Validation, Writing-original draft. PZ: Methodology, Validation. JX: Conceptualization, Writing-review & editing, Funding acquisition project administration. JC: Methodology, Validation, Data curation, Writing-original draft, Resources. YZ: Methodology, Validation, Data curation. JY: Data curation, Resources. LZ: Validation, Data curation. HH: Validation, Data curation. All authors contributed to the article and approved the submitted version.

Funding

This work was supported by Fujian Seed Industry Innovation and Industrialization Project of Fujian Province (ZYCX-LY-202101), and Priority Academic Program Development of Jiangsu Higher Education Institutions (PAPD).

Acknowledgments

We thank Nanjing Forestry University for providing the platform.

Conflict of interest

The authors declare that the research was conducted in the absence of any commercial or financial relationships that could be construed as a potential conflict of interest.

Publisher's note

References

Ashraf, M., and Hafeez, M. (2004). Thermotolerance of pearl millet and maize at early growth stages: Growth and nutrient relations. *Biol. Plantarum.* 48, 81–86. doi: 10.1023/B:BIOP.0000024279.44013.61

Baniwal, S. K., Bharti, K., Chan, K. Y., Fauth, M., Ganguli, A., Kotak, S., et al. (2004). Heat stress response in plants: a complex game with chaperones and more than twenty heat stress transcription factors. *J. Biosci.* 29, 471–487. doi: 10.1007/BF02712120

Berry, J., and Bjorkman, O. (1980). Photosynthetic response and adaptation to temperature in higher plants. *Annu. Rev. Plant Physiol.* 31, 491–543. doi: 10.1146/annurev.pp.31.060180.002423

Bhusal, N., Sharma, P., Sareen, S., and Sarial, A. K. (2018). Mapping QTLs for chlorophyll content and chlorophyll fluorescence in wheat under heat stress. *Biol. Plantarum.* 62, 721–731. doi: 10.1007/s10535-018-0811-6

Bi, Y., and Zhuge, Q. (2008). Progress in genetic engineering of forest trees under abiotic stresses. *World Forestry Res.* 21, 5. doi: 10.13348/j.cnki.sjlyyj.2008.05.006

Bondada, B. R., Oosterhuis, D. M., Wullschleger, S. D., Kim, K. S., and Harris, W. M. (1994). Anatomical considerations related to photosynthesis in cotton (*Gossypium hirsutum l.*) leaves, bracts, and the capsule wall. *J. Exp. Bot.* 45, 111–118. doi: 10.1093/jxb/45.1.111

Borrell, J. S., Dodsworth, S., Forest, F., Pérez-Escobar, O. A., Lee, M. A., Mattana, E., et al. (2020). The climatic challenge: which plants will people use in the next century? *Environ. Exp. Bot.* 170, 103872. doi: 10.1016/j.envexpbot.2019.103872

Chang, R. J. (2013). *Study on physiological and biochemical responses of two kinds of begonia semperflorens in leaf color under high temperature stress* (Zhejiang A&F University). [dissertation/master's thesis]. [Lin'an (ZJ)]. Available at: https://kns.cnki.net/kcms/detail/detail.aspx?dbcode=CMFD&dbname=CMFD201401&filename=1014101502.nh&uniplatform=NZKPT&v=ygfxUV4xHU9yXgtORfRkPPe6aqrNsyERsiEkctwmaNMaoI6WWRlyWTjN0bFQTJr

Dutta, S., Mohanty, S., and Tripathy, B. C. (2009). Role of temperature stress on chloroplast biogenesis and protein import in pea. *Plant Physiol.* 150, 1050–1061. doi: 10.1104/pp.109.137265

Fragkostefanakis, S., Röth, S., Schleiff, E., and Scharf, K. D. (2015). Prospects of engineering thermotolerance in crops throughmodulation of heat stress transcription factor and heatshock protein networks. *Plant Cell Environ.* 38, 1881–1895. doi: 10.1111/pce.12396

Gosavi, U., Jadhav, A. S., Kale, A. A., and Gadakh, S. R. (2014). Effect of heat stress on proline, chlorophyll content, heat shock proteins and antioxidant enzyme activity in sorghum (*Sorghum bicolor*) at seedlings stage. *Indian J. Biotechnol.* 13, 356–363.

Guo, Y., Zhang, Z., Fu, Q., Guang, X., Zheng, J., and Li., B. (2018). Effects of high temperature stress on leaf structures and physiological metabolism of *Potentilla fruticosa* l. *Northern Horticulture.* 23, 93–98. doi: 10.11937/bfyy.20173974

Hasanuzzaman, M., Hossain, M. A., and Fujita, M. (2010). Physiological and biochemical mechanisms of nitric oxide induced abiotic stress tolerance in plants. *Am. J. Plant Physiol.* 5, 295–324. doi: 10.3923/ajpp.2010.295.324

Hasanuzzaman, M., Nahar, K., Alam, M. M., Roychowdhury, R., and Fujita, M. (2013). Physiological, biochemical, and molecular mechanisms of heat stress tolerance in plants. *Int. J. Mol. Sci.* 14, 9643–9684. doi: 10.3390/ijms14059643

Hemantaranjan, A., Bhanu, A. N., Singh, M. N., Yadav, D. K., Patel, P. K., Singh, R., et al. (2014). Heat stress responses and thermotolerance. *Adv. Plants Agric. Res.* 1, 62–70. doi: 10.15406/apar.2014.01.00012

Hong, Z., Liu, S., Hong, C., and Lei, X. (2021). Resistance response of five afforestation tree species under drought stress. *J. Nanjing For. Univ. Nat. Sci. Ed.* 45, 111–119. doi: 10.12302/j.issn.1000-2006.202002019

Huang, H., Jian, Q., Jiang, Y., Duan, X., and Qu, H. (2016). Enhanced chilling tolerance of banana fruit treated with malic acid prior to low-temperature storage. *Postharvest Biol. Tec.* 111, 209–213. doi: 1016/j.postharvbio.2015.09.008

Hu, Q., Qian, R., Zhang, Y., Zhang, X., Ma., X., and Zheng, J. (2021). Physiological and gene expression changes of *Clematis crassifolia* and *Clematis cadmia* in response to heat stress. *Front. Plant Sci.* 12. doi: 10.3389/fpls.2021.624875

Ikeda, M., Mitsuda, N., and Ohme-Takagi, M. (2011). Arabidopsis *HsfB1* and *HsfB2b* act as repressors of the expression of heat-inducible hsfs but positively regulate the acquired thermotolerance. *Plant Physiol.* 157, 1243–1254. doi: 10.1104/pp.111.179036

Janáček, J., and Prášil, I. (1991). Quantification of plant frost injury by nonlinear fitting of an s-shaped function. *Cryo Letters.* 12, 47–52.

Jiang, Y., Qiu, Y., Hu, Y., and Yu, D. (2016). Heterologous expression of AtWRKY57 confers drought tolerance in *Oryza sativa*. front. *Plant Sci.* 7. doi: 10.3389/fpls.2016.00145

Kaplan, F., Kopka, J., Haskell, D. W., Zhao, W., Gatzke, N., Sung, D. Y., et al. (2004). Exploring the temperature-stress metabolome of arabidopsis. *Plant Physiol.* 136, 4159–4168. doi: 10.1104/pp.104.052142

Khan, Z., and Shahwar, D. (2020). "Role of heat shock proteins (HSPs) and heat stress tolerance in crop plants," in *Sustainable agriculture in the era of climate change*. Eds. R. Roychowdhury, S. Choudhury, M. Hasanuzzaman and S. Srivastava (Cham: Springer). doi: 10.1007/978-3-030-45669-6_9

Krasensky, J., and Jonak, C. (2012). Drought, salt, and temperature stress-inducedmetabolic rearrangements and regulatory networks. *J. Exp. Bot.* 63, 1593–1608. doi: 10.1093/jxb/err460

Larkindale, J., and Vierling, E. (2008). Core genome responses involved in acclimation to high temperature. *Plant Physiol.* 146, 748–761. doi: 10.1104/pp.107.112060

Lastra, O., Gómez, M., López-Gorgé, J., and del Río, L. A. (1982). Catalase activity and isozyme pattern of the metalloenzyme system, superoxide dismutase, as a function of leaf development during growth of *Pisum sativum l.* plants. *Physiologia Plantarum.* 5, 209–213. doi: 10.1111/j.1399-3054.1982.tb02289.x

Lichtenthaler, H. K., and Wellburn, A. R. (1983). Determinations of total carotenoids and chlorophylls *a* and *b* of leaf extracts in different solvents. *Biochem. Soc T.* 11, 591–592. doi: 10.1042/bst0110591

Li, Z., Li, J., Bing, J., and Zhang, C. (2019). The role analysis of APX gene family in the growth and developmental processes and in response to abiotic stresses in *Arabidopsis thaliana*. *Hereditas (Beijing).* 41 (6), 534–547. doi: 10.16288/j.yczz.19-026

Lukatkin, A. S. (2003). Contribution of oxidative stress to the development of cold-induced damage to leaves of chilling-sensitive plants: 3. *Injury Cell membranes by chilling temperatures. Russ. J. Plant Physiol.* 50, 243–246. doi: 10.1023/A:1022985500733

Luo, Y., Zhang, Y., Zhong, Y., and Kong, Z. (1999). Toxicological study of two novel pesticides on earthworm *Eisenia foetida*. *Chemosphere.* 39, 2347–2356. doi: 10.1016/S0045-6535(99)00142-3

Lütz, C., Bergweiler, P., Di, P. L., and Holzinger, A. (2012). "Cell organelle structure and function in alpine and polar plants are influenced by growth conditions and climate," in *Plants in alpine regions*. Ed. C. Lütz (Vienna: Springer). doi: 10.1007/978-3-7091-0136-0_5

Marchand, F. L., Mertens, S., Kockelbergh, F., Beyens, L., and Nijs, I. (2005). Performance of high arctic tundra plants improved during but deteriorated after exposure to a simulated extreme temperature event. *Global Change Biol.* 11, 2078–2089. doi: 10.1111/j.1365-2486.2005.01046.x

Mishra, S. K., Tripp, J., Winkelhaus, S., Tschiersch, B., Theres, K., Nover, L., et al. (2002). In the complex family of heat stress transcription factors, *HsfA1* has aunique role as master regulator of thermotolerance in tomato. *Genes Dev.* 16, 1555–1567. doi: 10.1101/gad.228802

Nahar, K., Hasanuzzaman, M., Ahamed, K. U., Hakeem, K. R., Ozturk, M., and Fujita, M. (2015). "Plant responses and tolerance to high temperature stress: Role of exogenous phytoprotectants," in *Crop production and global environmental issues*. Ed. K. Hakeem (Cham: Springer). doi: 10.1007/978-3-319-23162-4_17

Rodríguez, M. G., Canales, E., and Borrás-Hidalgo, O. (2005). Molecular aspects of abiotic stress in plants. *Biotecnol. Apl.* 22, 1–10.

Sheng, X., Li, J., Zhang, X., Wei, H., and Cui, L. (2006). Effects of heat acclimation pretreatment on changes of membrane lipid peroxidation, antioxidant metabolites, and ultrastructure of chloroplasts in two cool-season turfgrass species under heat stress. *Environ. Exp. Bot.* 56, 274–285. doi: 10.1016/j.envexpbot.2005.03.002

Sun, Y., Wei, J., and Fan, A. (2006). Effects of salicylic acid on chlorophyll fluorescence and xanthophyll cycle in cucumber leaves under high temperature and strong light. *Chin. J. Appl. Ecology.* 3, 399–402. doi: 10.13287/j.1001-9332.2006.0082

Talbi, S., Romero-Puertas, M. C., Hernández, A., Terrón, L., Ferchichi, A., and Sandalio, L. M. (2015). Drought tolerance in a saharian plant *Oudneya africana*: role of antioxidant defences. *Environ. Exp. Bot.* 111, 114–126. doi: 10.1016/j.envexpbot.2014.11.004

Thomas, R. L., Jen, J. J., and Morr, C. V. (1982). Changes in soluble and bound peroxidase-IAA oxidase during tomato fruit development. *J. Food Sci.* 47, 158–161. doi: 10.1111/j.1365-2621.1982.tb11048.x

Tian, S., Chen, C., and Zhang, Z. (2020). Physiological and biochemical response to heat stress and heat resistances evaluation of bottle gourds. *Acta Agriculturae Shanghai.* 36, 18–23. doi: 10.15955/j.issn1000-3924.2020.06.04

Tian, F., Hu, X., Yang, X., Yang, X., Chen, J., Lu, M., et al. (2021). Recent advances in the roles of HSFs and HSPs in heat stress response in woody plants. *Front. Plant Sci.* 12. doi: 10.3389/fpls.2021.704905

Usman, M. G., Rafii, M. Y., Ismail, M. R., Abdul Malek, M., and Abdul Latif, M. (2015). Expression of target gene *Hsp70* and membrane stability determine heat tolerance in chili pepper. *J. Am. Soc Hortic. Sci.* 140, 144–150. doi: 10.21273/JASHS.140.2.144

Vetter, J. L., Steinberg, M. P., and Nelson, A. I. (1958). Enzyme assay, quantitative determination of peroxidase in sweet corn. *J. Agric. Food Chem.* 6, 39–41. doi: 10.1021/jf60083a006

Vidya, M. K., Kumar, V. G., Sejian, V., Bagath, M., Krishnan, G., and Bhatta, R. (2018). Toll-like receptors: significance, ligands, signaling pathways, and functions in mammals. *Int. Rev. Immunol.* 37, 20–36. doi: 10.1080/08830185.2017.1380200

Zhang, M., Xu, G., Teng, Z., Liu, G., and Zhang, X. (2021). Effects of simulated acid rain on growth and photosynthetic physiological characteristics of *Populus simonii* × p. *nigra*. *J. Nanjing For. Univ. Nat. Sci. Ed.* 45, 57–64. doi: 10.12302/j.issn.1000-2006.202003068

Zhang, Y., Yang, J., Zhu, L., Xue, J., Hu, H., Cui, J., et al. (2021). Identification of microRNAs and their target genes related to needle discoloration of evergreen tree Chinese cedar (*Cryptomeria fortunei*) in cold winters. *Planta.* 254, 31. doi: 10.1007/s00425-021-03685-2

Zhang, Y., Zhu, L., Xue, J., Yang, J., Hu, H., Cui, J., et al. (2021). Selection and verification of appropriate reference genes for expression normalization in *Cryptomeria fortunei* under abiotic stress and hormone treatments. *Genes.* 12, 791. doi: 10.3390/genes12060791

Zhang, Y., Zhu, Q., Zhang, M., Guo, Z., Yang, J., Mo, J., et al. (2020). Individual *Cryptomeria fortunei* hooibrenk families show varying degrees of chilling stress resistance. *Forests.* 11, 189. doi: 10.3390/f11020189

Zhou, Y. W., Chen, J. H., Lu, L., Cheng, J., Yang, L., and Shi, J. (2018). Changes on leaf chloroplast ultrastructure and photosynthetic characteristics of *Liriodendron sino-americanum* somatic embryo regeneration seedlings under waterlogging stress. *Scientia Silvae Sinicae.* 54, 19–28. doi: 10.11707/j.1001-7488.20180303

Zou, M., Yuan, L., Zhu, S., Liu, S., Ge, J., and Wang, C. (2017). Effects of heat stress on photosynthetic characteristics and chloroplast ultrastructure of a heat-sensitive and heat-tolerant cultivar of wucai (*Brassica campestris* l.). *Acta Physiol. Plant* 39, 30. doi: 10.1007/s11738-016-2319-z

frontiers | Frontiers in Plant Science

TYPE Original Research
PUBLISHED 22 February 2023
DOI 10.3389/fpls.2023.1121852

OPEN ACCESS

EDITED BY
Biao Jin,
Yangzhou University, China

REVIEWED BY
Kunpeng Jia,
Henan University, China
Bo Li,
Lanzhou University, China

*CORRESPONDENCE
Yu Ling
lingyu820110@163.com
Dianfeng Zheng
zdffnj@263.net

SPECIALTY SECTION
This article was submitted to Plant Abiotic Stress, a section of the journal Frontiers in Plant Science

RECEIVED 12 December 2022
ACCEPTED 11 January 2023
PUBLISHED 22 February 2023

CITATION
Mo Y, Li G, Liu L, Zhang Y, Li J, Yang M, Chen S, Lin Q, Fu G, Zheng D and Ling Y (2023) *OsGRF4*^{AA} compromises heat tolerance of developing pollen grains in rice. *Front. Plant Sci.* 14:1121852. doi: 10.3389/fpls.2023.1121852

OsGRF4^{AA} compromises heat tolerance of developing pollen grains in rice

Yujian Mo[1,2], Guangyan Li[3], Li Liu[1], Yingjie Zhang[1], Junyi Li[1], Meizhen Yang[1], Shanlan Chen[1], Qiaoling Lin[1], Guanfu Fu[3], Dianfeng Zheng[1,2]* and Yu Ling[1,2]*

[1]College of Coastal Agricultural Sciences, Guangdong Ocean University, Zhanjiang, China, [2]South China Branch of National Saline-Alkali Tolerant Rice Technology Innovation Center, Zhanjiang, China, [3]State Key Laboratory of Rice Biology, China National Rice Research Institute, Hangzhou, China

Extreme high temperature at the meiosis stage causes a severe decrease in spikelet fertility and grain yield in rice. The rice variety grain size on chromosome 2 (GS2) contains sequence variations of *OsGRF4* (*Oryza sativa* growth-regulating factor 4; *OsGRF4*^{AA}), escaping the microRNA miR396-mediated degradation of this gene at the mRNA level. Accumulation of *OsGRF4* enhances nitrogen usage and metabolism, and increases grain size and grain yield. In this study, we found that pollen viability and seed-setting rate under heat stress (HS) decreased more seriously in GS2 than in its comparator, Zhonghua 11 (ZH11). Transcriptomic analysis revealed that, following HS, genes related to carbohydrate metabolic processes were expressed and regulated differentially in the anthers of GS2 and ZH11. Moreover, the expression of genes involved in chloroplast development and photosynthesis, lipid metabolism, and key transcription factors, including eight male sterile genes, were inhibited by HS to a greater extent in GS2 than in ZH11. Interestingly, pre-mRNAs of *OsGRF4*, and a group of essential genes involved in development and fertilization, were differentially spliced in the anthers of GS2 and ZH11. Taken together, our results suggest that variation in *OsGRF4* affects proper transcriptional and splicing regulation of genes under HS, and that this can be mediated by, and also feed back to, carbohydrate and nitrogen metabolism, resulting in a reduction in the heat tolerance of rice anthers.

KEYWORDS

***OsGRF4*, rice, heat tolerance, carbohydrate metabolism, gene transcription, pre-mRNA alternative splicing**

1 Introduction

Heat stress (HS) is an abiotic stress that causes severe loss in rice production (Tang et al., 2020; Qu et al., 2022; Shen et al., 2022). What is worse, the Intergovernmental Panel on Climate Change (IPCC) recently predicted that the mean temperature on Earth will continuously increase to 1.5–2°C above pre-industrial averages by 2050, even if net zero CO_2 emissions were to be achieved immediately (Shukla et al., 2022).

Developing pollen grains are more vulnerable to high temperatures than cells from other plant tissues. High temperatures cause production loss directly by decreasing pollen grain viability and seed formation in crops (Draeger and Moore, 2017; Peng et al., 2020; Bokshi et al., 2021; Naranjo et al., 2022). As a key modulator of HS response, heat stress transcription factor A2 (HSFA2) plays an essential role in the thermotolerance of meiocytes and microspores in plants (Frank et al., 2009; Akerfelt et al., 2010; Vihervaara et al., 2013; Fragkostefanakis et al., 2016). In tomato, male meiocytes and microspores are susceptible to HS owing to their inefficient regulatory response to increasing temperature. This sensitivity could be partially mitigated by enhanced expression of *HSFA2* and several other HS-responsive genes (Hedhly et al., 2016). Carbohydrate metabolites, energy status, and phytohormone abundance could also alter the thermotolerance of microspores and anthers of plants (Jambhekar and Amon, 2008; Hedhly et al., 2016; Smith and Zhao, 2016). In the grain sorghum (*Sorghum bicolor*), HS decreased cell wall invertase (CWI)-mediated sucrose hydrolysis in microspores and anthers, leading to altered carbohydrate metabolism and starch deficiency in pollen grains (Jain et al., 2010). A transient HS treatment at the tetrad stage of maize caused significant regulation of starch, lipid, and energy biosynthesis-related genes. Correspondingly, increased levels of sucrose and its monosaccharide components, and decreased levels of pyruvate, fatty acids, and saturated fatty acids, were found in plants grown under HS (Begcy et al., 2019). Similarly, differential expression changes in chlorophyll- and photosynthesis-related genes, together with a disturbance of carbohydrates, were found in heat-treated rice anthers (Liu et al., 2020). In rice, salicylic acid may increase the HS tolerance of pollen mother cells through hydrogen peroxide (H_2O_2)-mediated signaling pathways (Feng et al., 2018) and catalase (CAT)-mediated detoxification of reactive oxygen species (ROS) (Zhao et al., 2018; Gong et al., 2019). Furthermore, the exogenous application of abscisic acid prior to HS enhanced sucrose transport and accelerated sucrose metabolism to maintain the carbon balance and energy homeostasis, which consequently mitigated the heat damage to anthers (Rezaul et al., 2019).

Growth regulation factors (GRFs) are a group of plant-specific transcription factors. The N-terminal regions of the GRFs contain two highly conserved domains, the QLQ and WRC domains. The QLQ domain serves as a protein–protein interacting interface, and the WRC domain functions as the DNA-binding site of the protein (Kim and Tsukaya, 2015). Recently, many studies have demonstrated that expression levels of both *OsGRF4* and other GRF genes are post-transcriptionally regulated by the microRNA miR396 (Liu et al., 2014; Che et al., 2015; Duan et al., 2015; Li S. et al., 2016; Liebsch and Palatnik, 2020; Rossmann et al., 2020; Lu et al., 2021). Therefore, several rice varieties possessing, either naturally or artificially, a sequence variation on *OsGRF4* (*Oryza sativa* growth-regulating factor 4; $OsGRF4^{AA}$) that blocks the binding site of miR396 accumulate more *OsGRF4* transcripts and proteins (Hu et al., 2015). These rice varieties promote and integrate nitrogen assimilation, carbon fixation, and cellular growth, then increase grain size and weight by significantly up-regulating expression levels of *Adenine Methyltransferase 1.1 (AMT1.1)*, *glutamine synthetase 1.2 (GS1.2)*, *glutamine synthetase 2 (GS2)*, and *NADH-glutamate synthase 2 NADH–GOGAT2* (Li et al., 2018). Regulation of the expression of *OsGRF4* by miR396 has been shown to be essential for grain production in rice under nitrogen-deficient conditions (Zhang et al., 2020).

The GRF-mediated regulation of growth and stress response in plants usually requires the cooperation of other regulators. A transcription co-activator, GRF-interacting factor (GIF), modulates the growth of both vegetative and reproductive organs in rice (Duan et al., 2015; He et al., 2017), which can be mediated by gene transcriptional activation, which in turn is controlled by the GRF–GIF combination (Li S. et al., 2016). Similar cooperation between GRF and GIF has also been found in other plants (Li S. et al., 2016; Lee et al., 2018). Furthermore, OsGRF4-mediated up-regulation of brassinosteroid signaling genes and MYB61, a transcription factor relevant to cellulose accumulation, is also necessary for the promotion of grain development (Che et al., 2015; Gao et al., 2020).

As enhanced expression of *OsGRF4* in a gibberellic acid-independent manner has been shown to overcome the disadvantage of low nitrogen use efficiency (NUE) of green revolution varieties (Li et al., 2018), variations in *OsGRF4* are considered a target for rice breeding in order to increase production (Liebsch and Palatnik, 2020; Lu et al., 2021). However, whether and how the variation of *OsGRF4* affects stress tolerance in rice has not yet been studied. In this study, we compared the effects of HS on two rice genotypes, Zhonghua 11 (ZH11) and its $OsGRF4^{AA}$ near-isogenic line, grain size on chromosome 2 (GS2). Our experiment demonstrated that HS treatment at the meiotic stage caused a greater abundance of dead pollen grains and less seed setting in GS2 than in ZH11. Transcriptomic analysis demonstrated that a group of genes involved in abiotic stimuli and those relating to chloroplast and photosynthesis, including eight male sterile genes (MSGs), were, generally, inhibited more significantly by HS in anthers from GS2, which was consistent with the more serious heat damage to anthers and pollen grains in GS2. Furthermore, pre-mRNA alternative splicing (AS) analysis revealed differential AS regulation between the two genotypes in a considerable number of genes, including several genes that are important for meiosis development and the stress response, such as *CIRCADIAN CLOCK ASSOCIATED 1 (CCA1)*, *OsSPO11-5*, *HSFB2c*, and, interestingly, *OsGRF4* itself, suggesting that OsGRF4 affects the heat tolerance of rice anthers at both the transcription and pre-mRNA splicing levels.

2 Materials and methods

2.1 Plant materials, growth conditions, and treatments

The rice seeds of ZH11 and its $OsGRF4^{AA}$ near-isogenic line, GS2, were provided by Dr. Jiang Hu from the State Key Laboratory of Rice Biology, China National Rice Research Institute (Hu et al., 2015). The seeds were first grown in the China National Rice Research Institute (Hangzhou, China, 119°57′E, 30°03′N) under natural conditions until the pollen mother cell meiotic stage (Feng et al., 2018). Thereafter, the rice plants were divided into two groups and moved into separate transparent growth chambers with a relative humidity of around 70%–80% and natural sunlight conditions. Group 1 was subjected to a HS condition (i.e., 28°C from 16:01 to 8:59, and 38°C from 9:00 to 16:00), whereas the other group was grown under a normal

temperature condition (i.e., 23°C from 16:01 to 8:59 and 28°C from 9:00 to 16:00). The treatment time was 6 days. Anthers were sampled at 16:00 on the last day of the treatment. Sampled anthers were immediately submerged in liquid nitrogen for 1 min and stored at –80°C until RNA extraction and sequencing library preparation.

2.2 Pollen viability measurement

Pollen viability was determined using the method described by Feng et al. (2018). Briefly, mature pollen grains were removed from the anthers of the florets, and placed on a glass slide with a drop of potassium iodide/iodine (KI/I_2) solution. The slide was observed using a light microscope (DM4000B; Leica, Wetzlar, Germany). Eight replicates were investigated and photographed for the measurement of pollen viability.

2.3 Seed-setting rate measurement

Mature rice plants and panicles were photographed for phenotyping. Then the number of filled grains (FG) and abortive grains (AG) per panicle were measured. The seed-setting rate was calculated as FG/(FG + AG) × 100%.

2.4 RNA-sequencing and data analysis

RNA sequencing (RNA-Seq) and primary data analysis were performed at Shanghai Majorbio Bio-pharm Biotechnology Co., Ltd. (Shanghai, China). Total RNA was isolated from rice anthers using a plant RNA purification reagent (Invitrogen, California, USA). The quality and integrity of the RNA were measured by an Agilent Bioanalyzer 2100 system (Agilent Technologies, USA) and only high-quality RNA samples [$OD_{260/280}$ = 1.8–2.2, $OD_{260/230} \geq 2.0$, RNA integrity number (RIN) ≥ = 8.0, 28S : 18S ≥ 1.0, > 1 μg] were used to construct the sequencing library. RNA-Seq libraries were sequenced on an Illumina NovaSeq6000 platform to generate high-quality paired-end reads following the Illumina manufacturer's recommendations. Next, data processing for differentially expressed gene (DEG) analysis was carried out using Kallisto (Bray et al., 2016) and 3D RNA-Seq App (Guo et al., 2021), with default settings (adjusted p-value < 0.01 and absolute $\log_2$-fold change > 1) unless specifically indicated otherwise. Pre-mRNA splicing analysis was performed using rMATS (replicate multivariate analysis of transcript splicing) (Shen et al., 2014). RNA read coverages were visualized using the program Integrative Genomics Viewer (IGV) (http://www.igv.org) by Rice Annotation Project (RAP) International Rice Genome Sequencing Project (IRGSP) 1.0 genome (https://rapdb.dna.affrc.go.jp/) as the reference genome.

2.5 qRT-PCR and RT-PCR

Reverse transcription-PCR (RT-PCR) and reverse transcription-quantitative PCR (qRT-PCR) were slightly modified compared with the methods previously described in (Chen et al., 2022). DNA digestion of total RNA samples was performed after RNA extraction by using an RNase-Free DNase Set (Vazyme, Catalog No. R223-01). Total RNA was then reverse transcribed using a SuperScript First-Strand Synthesis System to generate the first-strand cDNA libraries. qPCR was performed using Power SYBR Green PCR Master Mix (Yeasen Biotech; Catalog No. 11201ES08) under the following conditions: 95°C for 5 min, then cycles of 95°C for 15 s and 60°C for 1 min. The validation was assessed with three biological replicates for each sample. An actin gene (*Os03g0718150*) was used as the internal control for normalization of qPCR. The fold change was evaluated using the standard $2^{(-\Delta\Delta CT)}$ method. Statistical analysis of gene expression in qRT-PCR was performed using Microsoft Excel 2013. In RT-PCR validation of AS events, primers flanking different exons were used. The PCR program was as follows: initial denaturation for 3 min at 95°C, followed by 40 cycles at 95°C for 30 s, 56°C for 30 s, and 72°C for 2 min. The final extension at 72°C lasted 5 min.

3 Results

3.1 Phenotypes of pollen grains and seed-setting of GS2 and ZH11 under different temperature conditions

Pollen grains from ZH11 and GS2 with and without HS treatment were observed and measured using a microscope after KI/I_2 staining (Figure 1). The viability of pollen grains from both genotypes grown under control conditions was high. No significant difference was found between ZH11 and GS2. Dead pollen grains accounted for only 5.4% and 3.8% of pollen grains in ZH11 and GS2, respectively. The viability of pollen grains was decreased significantly by HS treatment in both genotypes. However, more severe heat-induced damage of pollen grains was found in GS2 anthers. The percentage of dead pollen grains was 34.6% in ZH11 after HS treatment, whereas this proportion increased significantly, to 62.6%, in GS2.

Next, we calculated the seed-setting rates of both genotypes. The seed-setting rates of ZH11 and GS2 under control conditions were 82.3% and 83.3%, respectively. The seed-setting rate was decreased significantly by HS in both genotypes. In addition, the rate of decrease was greater in GS2 than in ZH11, as we found that fertilized grains accounted for 35.4% of all grains in ZH11 after HS treatment, whereas only 21.1% of grains were fertilized in GS2 after HS treatment.

3.2 Overview of RNA-Seq profiles of anthers from the two genotypes under normal and HS conditions

By running a RNA-Seq experiment with the collected anthers, we obtained 40–45 million raw reads from each of the 12 cDNA libraries, and at least 95.6% of raw reads from each library could be assembled to the reference sequence of the rice genome (Supplementary Table 1). In the 3D RNA-Seq analysis pipeline, low-count reads, that is, reads lower than one per million, and reads found only in one library, were removed from further analysis (Figures 2A, B). In principal component analysis, different samples separated from

10.3389/fpls.2023.1121852

each other, while all three replicates from the same sample grouped together, suggesting high similarity between replicates (Figure 2C). The large distances between the ZH11 control group and other samples indicate that their transcriptomic profiles are very different. In contrast, the ZH11 and GS2 HS groups were close to each other, suggesting less transcriptomic difference between these two samples. Correspondingly, the analysis of DEG numbers showed that the numbers of down-regulated and up-regulated DEGs were, respectively, 2,112 and 816 in the comparison of the ZH11 and GS2 control groups; 3,256 and 1,976 in the comparison of the ZH11 control group and the ZH11 HS group; 1,476 and 1,429 in the comparison of the GS2 control group and the GS2 HS group; and 451 and 507 in the comparison of the ZH11 and GS2 HS groups (Figure 2D). Furthermore, the Venn diagram demonstrated that there were considerable numbers of overlapping and specific DEGs in different comparisons (Figure 2E).

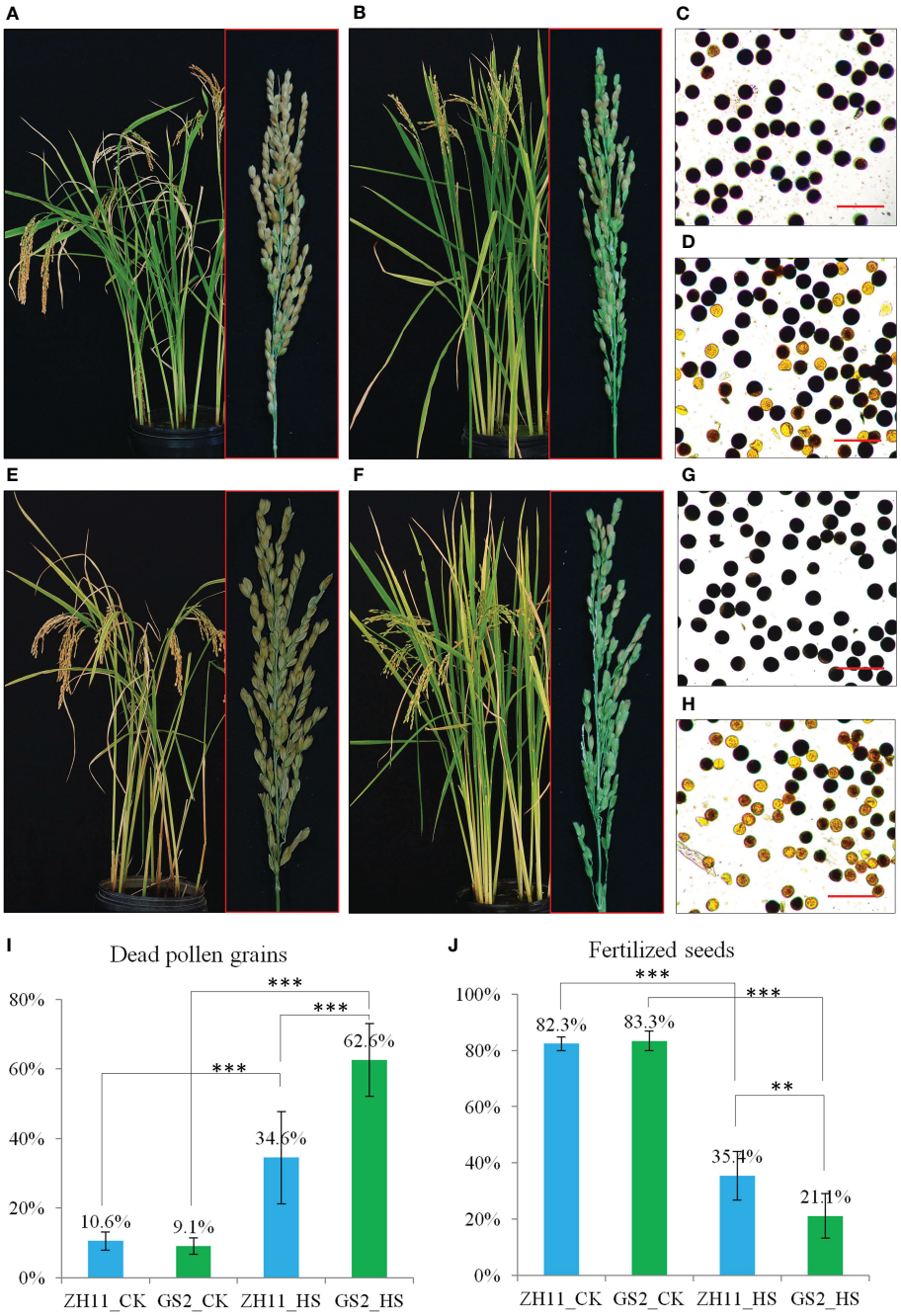

FIGURE 1
Phenotypes of Zhonghua 11 (ZH11) and grain size on chromosome 2 (GS2) under different temperature conditions at the pollen mother cell meiosis stage. **(A–D)** Photographs of whole plants, seed setting, and pollen grains in ZH11 with and without HS treatment. **(A, C)** Without heat stress (HS) treatment. **(B, D)** After HS treatment. **(E–H)** Photographs of whole plants, seed setting, and pollen grains in GS2 with and without HS treatment. **(E, G)** Without HS treatment. **(F, H)** After HS treatment. Scale bars in **(C, D, G, H)** represent 100 μm. **(I)** Ratios of dead pollen grains. **(J)** Ratios of fertilized seeds. Significance level for *t*-test: $^{**}p < 0.01$; $^{***}p < 0.001$.

3.3 Genes regulated by HS treatment in both ZH11 and GS2

Further analysis revealed a group of 961 genes that were up-regulated by HS in both ZH11 and GS2, and another group, of 820 genes, which were down-regulated in both varieties by HS (Supplementary Tables 2, 3). Gene ontology (GO) analysis revealed that HS up-regulated genes were enriched in the biological processes "response to heat", "protein folding", "response to hydrogen peroxide", "response to high light intensity", and so on (Figure 3A). On the other hand, HS-inhibited genes tend to be enriched in biological processes involved in cell differentiation and cell structure control, flower development, and gene transcription (Figure 3B). Inhibition of such genes explained why we observed a significant reduction in the viability of pollen grains from both genotypes.

Next, we employed two extra sets of RNA-Seq data,which have also been used to explore HS-induced transcriptomic changes in rice anthers (Zhang X. et al., 2012; Liu et al., 2020). Our analysis demonstrated that 103 and 84 genes from the commonly up-regulated DEGs in ZH11 and GS2, respectively, overlapped with one of the two RNA-Seq data sets employed, whereas another group of 55 DEGs overlapped with both data sets. In the case of HS-inhibited genes, 100, 138, and 32 genes from commonly down-regulated DEGs in ZH11 and GS2 were also found to be repressed in at least one of the employed data sets (Figure 3C). Further study showed that 40% of 55 commonly up-regulated genes in the three studies were enriched in the GO term of "response to heat". This group of genes comprised, among others, *HSFA2a*, *Heat Shock Protein 101 (HSP101)*, *Heat Stress-associated 32kd protein (HSA32)*, and a group of *sHSPs*. In addition, a gene encoding a splicing factor, *RNA-binding Protein 1 (RNP1)* (Os01g031660), was found to be commonly up-regulated by HS in anthers from different rice genotypes. In contrast, another group of 32 genes were commonly down-regulated by HS treatment. These commonly suppressed genes included genes involved in cell division and flower development, such as an aquaporin protein (Os01g0232000), two GDSL-like lipase/acylhydrolases (Os02g0816200 and Os06g0156600), a lipid transfer protein (LTPL65, Os01g0814100), a transcription factor (Os02g0791300), a hormone-responsive gene (Os11g0128300), a core histone H2A (Os05g0113900), and a chloroplast precursor (Os04g0678700) (Figure 3D). These results suggest that these 87 genes may play important roles in the HS response of anthers from different rice genotypes.

3.4 Genes that are differentially expressed in ZH11 and GS2 after HS treatment

As it has been found that the number of dead pollen grains in anthers after high-temperature treatment is greater in GS2 than in ZH11, we next

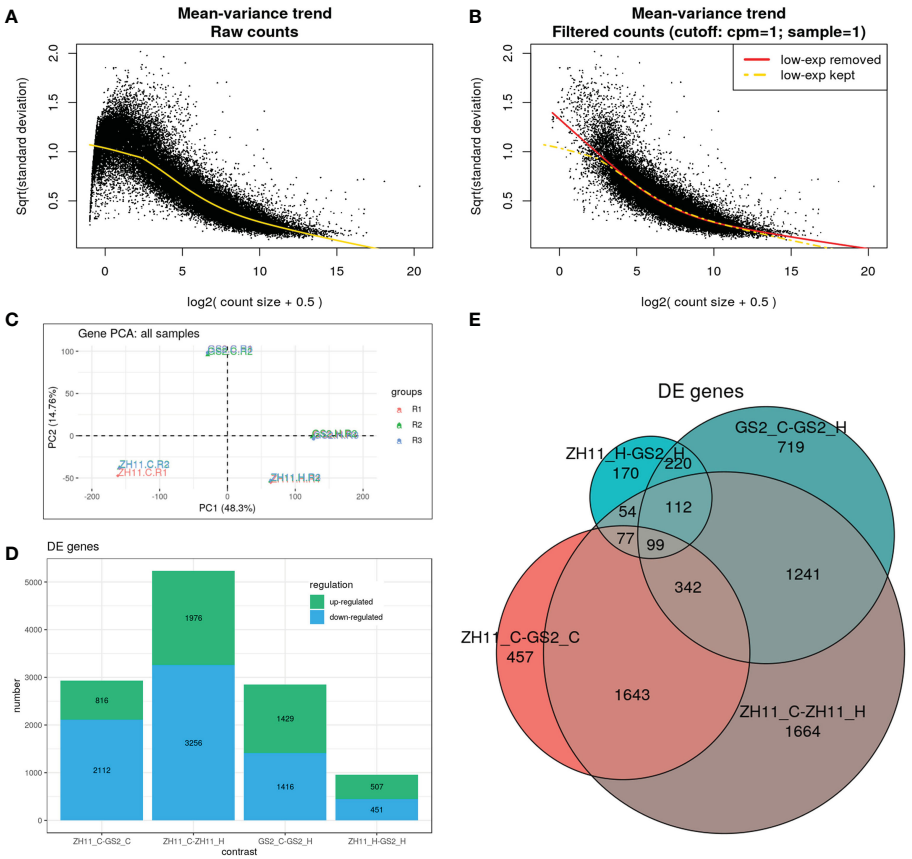

FIGURE 2
Gene expression patterns in Zhonghua 11 (ZH11) and grain size on chromosome 2 (GS2) under different temperature conditions. **(A)** Mean–variance trend of raw read counts (before filtering). **(B)** Mean–variance trend of filtered read counts (poorly expressed reads removed). **(C)** Principal component analysis (PCA) plots of 12 libraries. **(D)** Differentially expressed gene (DEG) numbers of four separate comparisons. The green box shows up-regulated genes and the blue box shows down-regulated genes. **(E)** Specific and overlapping DEG numbers across four different comparisons.

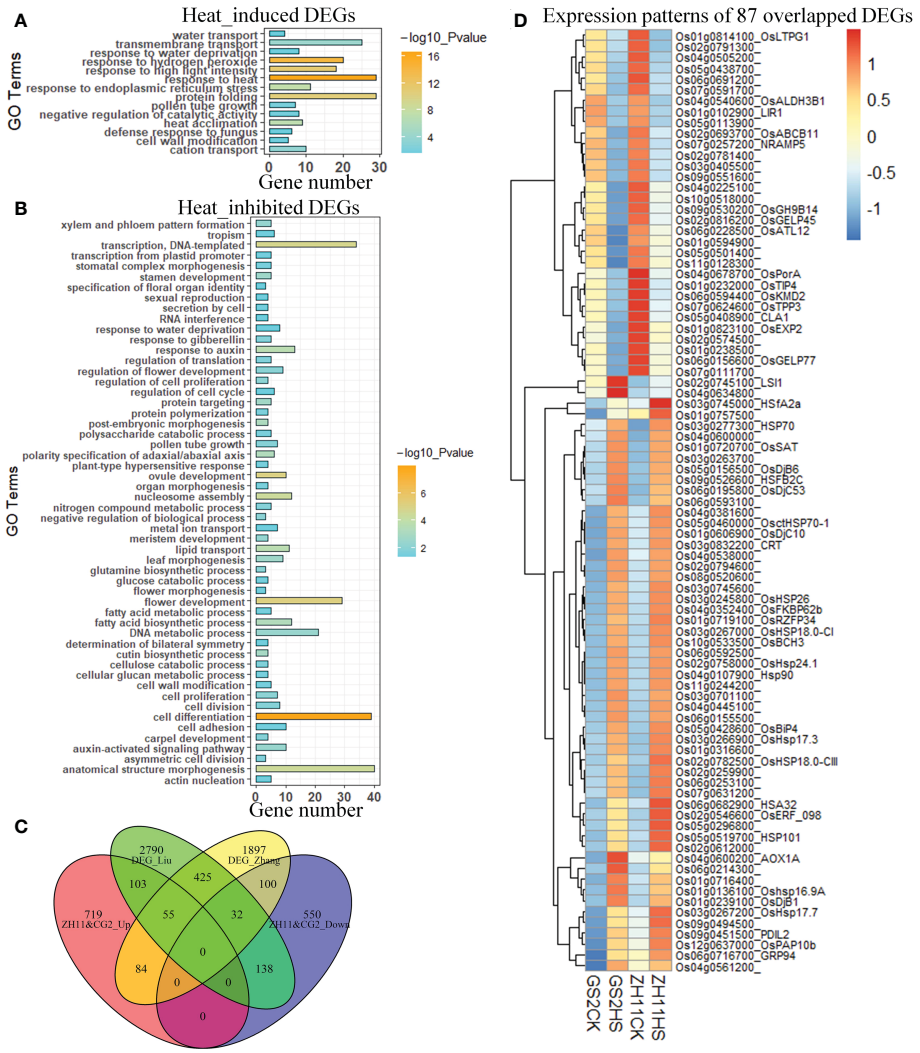

FIGURE 3
Heat-responsive differentially expressed genes (DEGs) in anthers from different genotypes. **(A)** Gene ontology analysis of genes up-regulated by heat stress (HS) in both Zhonghua 11 (ZH11) and grain size on chromosome 2 (GS2). **(B)** Gene ontology analysis of genes down-regulated by HS in both ZH11 and GS2. **(C)** Numbers of specific and overlapping DEGs in our experiment and in two other studies. **(D)** Expression of 87 genes (overlapping DEGs in three studies) in ZH11 and GS2 under normal and HS conditions.

aimed to uncover the transcriptomic difference between anthers from the two genotypes after HS. A heatmap comparing the patterns of expression of 958 DEGs in GS2 and ZH11 after HS treatment is shown in Figure 4A. The heatmap shows that the heat-mediated regulatory patterns of many genes were similar in the two genotypes. However, the same genes were expressed at different levels after HS treatment, resulting from either originally different levels under normal temperature conditions or different intensities of regulation between the two genotypes by HS treatment, or both. Interestingly, HS-mediated gene expression changes seemed to be more marked in GS2. After HS treatment, 80 HS-induced DEGs had higher levels of expression in GS2 than in ZH1, whereas 121 heat-suppressed DEGs were, in contrast, expressed at lower levels in GS2 than in ZH11 after HS treatment; one gene from this category was expressed at lower level in ZH11 than in GS2 after HS treatment (Figure 4B).

The change trends of genes detected from RNA-Seq data could be validated through qRT-PCR. Genes whose regulation under HS showed the same trend in ZH11 and GS2 included a B-box containing protein *BBX19*, *HSFA2a*, *MALE STERILITY 2 (MS2)*, and *ABA 8′-Hydroxylase (ABA8ox2)* (Figure 4C). Regulation of some other genes under HS showed opposing trends in ZH11 and GS2. For example, *Dehydration Responsive Element Binding Protein 1A (DREB1A)* and *Peroxidase 1* (*Pox1*, Os05g0499300) were induced in GS2, but inhibited in ZH11, after HS treatment.

3.5 Genes essential for the development of anthers and pollen grains are differentially affected in ZH11 and GS2

Under normal conditions, a group of genes with higher expression levels in ZH11 than GS2 was enriched in GO terms including “carbohydrate metabolic process”, “lipid metabolic process”, “lipid transport”, and “photosynthesis”. In contrast, genes expressed at higher levels in GS2 were highly enriched in biological processes involved in pollen tube germination and growth, pollination, cell growth,

10.3389/fpls.2023.1121852

transmembrane transport, and negative regulation of catalytic activity (Supplementary Figure 1). However, we did not find a significant difference in pollen viability under control conditions.

Further analysis revealed that DEGs with higher levels of expression in ZH11 after HS treatment are involved in tens of biological processes (Figure 5A). About 60 DEGs are thought to play roles in response to abiotic stress, and 40 genes are involved in the response to endogenous stimuli. Interestingly, a group of DEGs with significantly higher levels of expression in ZH11 than in GS2 after HS treatment play important roles in chloroplast development and photosynthesis. In contrast, further GO analysis demonstrated that DEGs with lower levels of expression in ZH11 than in GS2 after HS treatment were greatly enriched, and thus with relatively low numbers, in five biological processes (Figure 5B), implying that the biological processes these genes are involved in have not yet been identified.

In fact, a great number of DEGs involved in chloroplast and photosynthesis are also responsive to abiotic stress (Figures 5C, D). Only a few abiotic stress-responsive genes, such as *HSFA2a* and *OsBiP5*, were up-regulated by HS, whereas most of the remaining genes were down-regulated in both genotypes by HS treatment (Figure 5C). Similarly, many genes related to photosynthesis were also down-regulated in both genotypes. However, these photosynthesis genes were down-regulated to different levels in ZH11 and GS2 by the same HS treatment. All genes, except *CYP19-4*, were expressed at higher levels in ZH11 than in GS2 after HS treatment (Figure 5D). Given that the abundance of dead pollen grains was greater in GS2 than in ZH11 after HS, we supposed that sustaining the expression of these genes at relatively high levels might contribute to reduced heat-induced damage to rice anthers.

Next, we investigated a group of genes that have been identified as male sterile genes (MSGs) in rice, the mutation of which would cause total or partial male sterilization in rice [as reviewed by Abbas et al. (2021)]. Interestingly, 8 out of 77 MSGs were expressed at higher levels in ZH11 than in GS2 after HS treatment (Figure 5E). In contrast, no MSGs were expressed at significantly higher levels in GS2 than in ZH11 after the same HS treatment. The eight MSGs with higher levels of expression in ZH11 than in GS2 after HS were five genes involved in lipid metabolism [i.e., *OsC6* (Os11g0582500), *OsABCG26* (Os10g0494300), *OsDPW* (Os03g0167600), *OsSTRL2* (Os03g0263600), and *OsABCG3* (Os01g0836600], a bHLH transcription factor [*TIP2/TDR/bHLH142*

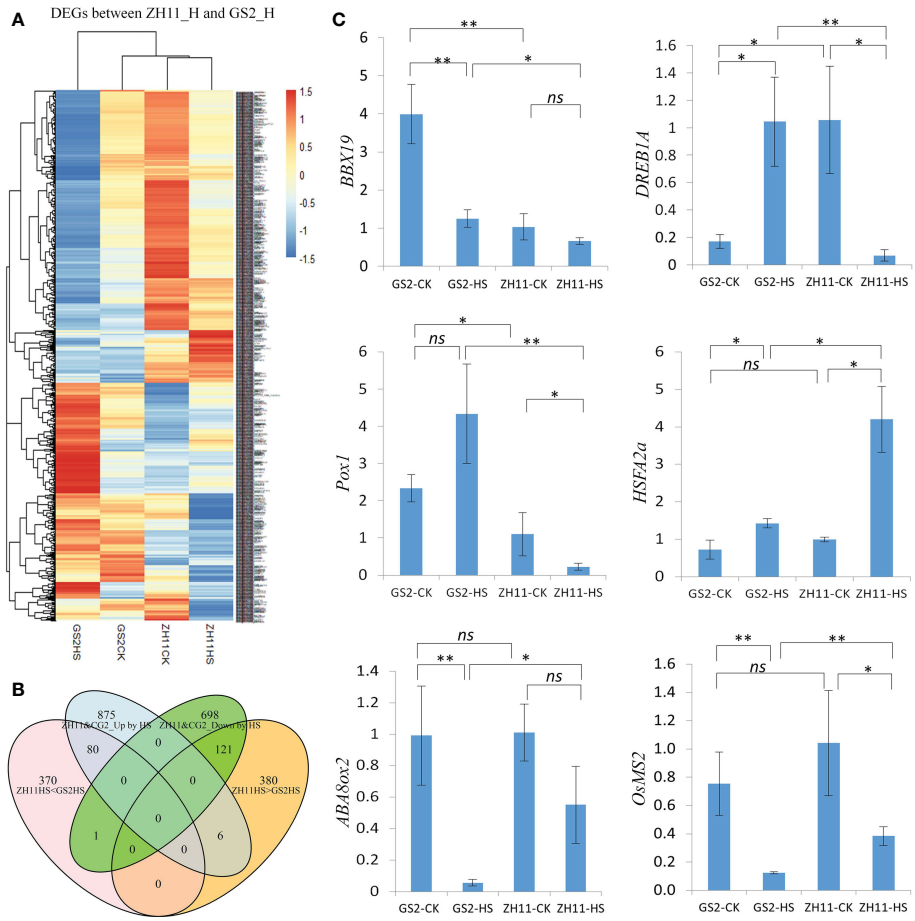

FIGURE 4
Expression patterns of differentially expressed genes (DEGs) between Zhonghua 11 (ZH11) and grain size on chromosome 2 (GS2) after heat stress (HS). **(A)** A heatmap showing expression patterns of DEGs in ZH11 and GS2 anthers after HS treatment. **(B)** Numbers of overlapping and specific DEGs between four comparisons in our study, namely ZH11HS < GS2HS (DEGs with lower expression levels in ZH11 than in GS2 after HS), ZH11&GS2_Up by HS (DEGs up-regulated by HS treatment in both ZH11 and GS2), ZH11&GS2_Down by HS (DEGs down-regulated by HS treatment in both ZH11 and GS2), and ZH11HS > GS2HS (DEGs with higher expression levels in ZH11 than in GS2 after HS). **(C)** Reverse transcription-quantitative PCR (qRT-PCR) validation of RNA sequencing (RNA Seq) data with some of these genes: *BBX19*, *DREB1A*, *Pox1*, *HSFA2a*, *ABA8ox2*, and *OsMS2*. Significance level for *t*-test: $*p < 0.05$; $**p < 0.01$. ns, non-significant.

(Os01g0293100)], an R2R3 MYB transcription factor *Carbon Starved Anther (CSA*, encoded by Os01g0274800), and a triterpene synthase [*OsC12/PTS1* (Os08g0223900)] (Figure 5F). *OsC6* was also one of the top 50 DEGs with much higher expression levels in ZH11 than in GS2 after HS treatment (Supplementary Figure 2).

3.6 Expression of the GRF gene family under different temperature conditions in GS2 and ZH11

As the difference between the two rice genotypes used here was thought to have resulted from a couple of nucleotide variations (1,187TC→AA) in a GRF, *OsGRF4*, we were curious to know the patterns of expression of this gene and of its family members in the anthers of the two genotypes. As shown in Figure 6A, among these 12 GRF genes, *OsGRF11* showed the highest level of expression in anthers, followed by *OsGRF8*, under either normal or high temperature. Almost all GRFs were suppressed by HS in both genotypes, except for *GRF10* and *GRF11*: the former was suppressed by HS in GS2 but induced in ZH11, whereas the latter was induced by HS in GS2 but suppressed in ZH11. The expression level of *OsGRF4* in anthers was lower than that of many other GRF genes. Furthermore, the transcripts of this gene seemed to accumulate less in ZH11 under HS conditions when tested by qPCR (Figure 6B).

When observing read coverages of *OsGRF4* using the IGV program, we found another sequence variation, in addition to the previously reported variation (1,187TC→AA). This novel variation is located at

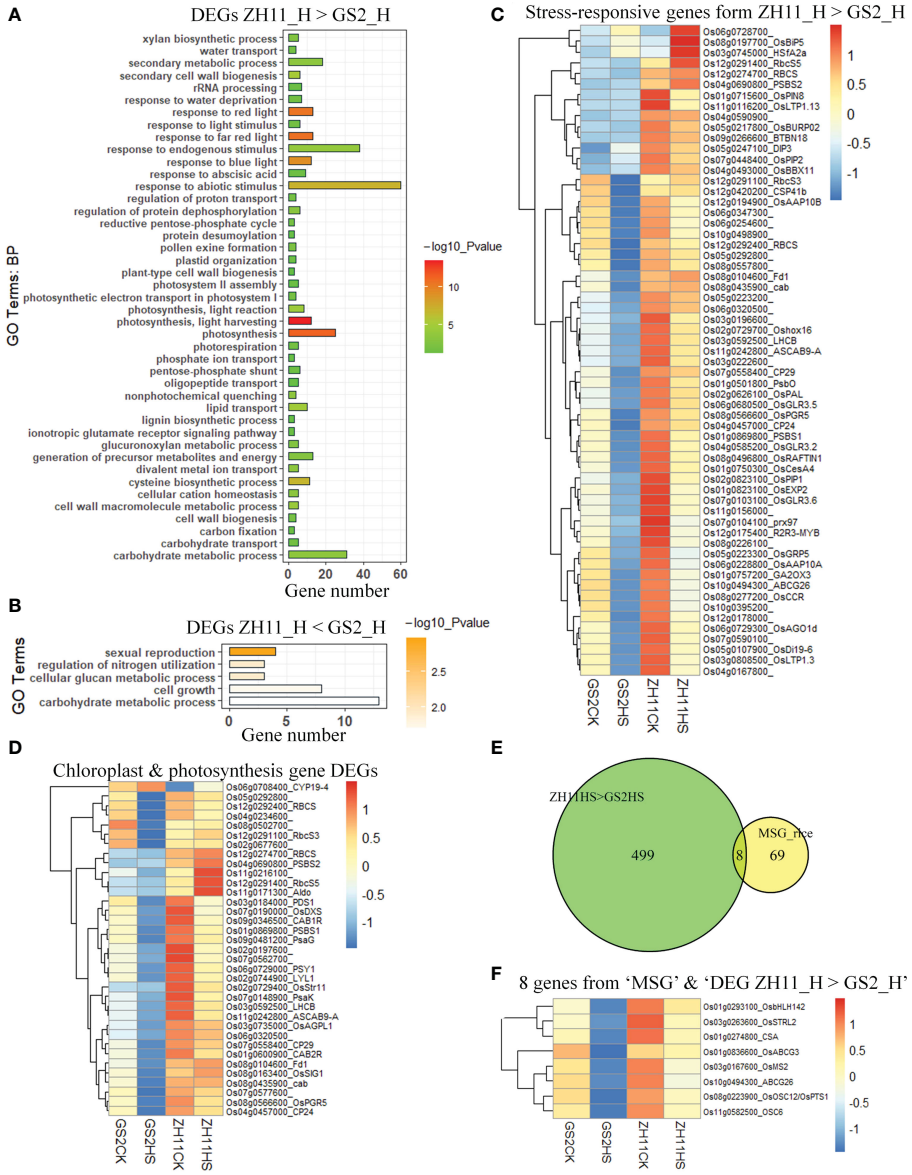

FIGURE 5
Differentially expressed genes (DEGs) essential for male fertility in anthers from Zhonghua 11 (ZH11) and grain size on chromosome 2 (GS2) after heat stress (HS) treatment. **(A)** Gene ontology (GO) analysis of DEGs with higher levels of expression in ZH11. **(B)** GO analysis of DEGs with lower levels of expression in ZH11. **(C)** Expression patterns of 60 stress-responsive DEGs with higher levels of expression levels ZH11. **(D)** Expression patterns of those DEGs involved in chloroplast development and photosynthesis. **(E)** The overlap of male sterile genes (MSGs) and those expressed at a higher level in ZH11 than in GS2. **(F)** Gene identifiers (IDs) and relative expression patterns of the eight MSGs in E.

3′-UTR of the last exon, where an 'A' was replaced by a 'T' in GS2 (as this variation was found in all GS2 genotype samples but not in any ZH11 genotypes, we suggest that it is not a random error caused by sequencing). More interestingly, we found that the pre-mRNA splicing patterns of *OsGRF4* were different in ZH11 and GS2 genotypes after HS, when read coverages of the target genes were visualized using the IGV program (Figure 6C). The last intron of this gene underwent intron retention (IR) in ZH11 after HS. This AS regulation was not found in any of the GS2 samples, either with or without HS treatment. In other words, the splicing patterns of the gene in the GS2 background remained the same as under the normal temperature condition. We further tested this AS event using RT-PCR. We found that an extra DNA fragment (252 bp) was amplified in ZH11 HS group samples (Figure 6D). This novel amplified fragment was predicted to be the intron-retained isoform owing to its size. Moreover, the AS of *OsGRF4* seemed to be carried out only in ZH11 anthers after HS treatment, as we could not detect the same AS event in leaves from either genotype under the same temperature conditions (Figure 6E). Bioinformatic analysis revealed that the resulting mRNA isoform of *OsGRF4* in ZH11 anthers induced a stop codon in the retained intron, which would induce RNA degradation if it triggered the nonsense-mediated degradation (NMD) system. Otherwise, the resulting mRNA isoform was predicted to be translated into a sequence-varied protein, with the last amino acid, D (Asp), at the C-terminal replaced by three contiguous T (Thr) residues (Figure 6F). Thus, the mechanism for the appearance of AS in *OsGRF4* is yet not clear, and determination of its biological significance for the heat tolerance of anthers and pollen grains in rice requires further observation.

3.7 Differential AS analysis between ZH11 and GS2 after HS treatment

Next, we employed a widely used pre-mRNA splicing analysis program, rMATS, to explore AS events in the RNA-Seq samples. As shown in Figure 7A, AS events were defined as a skip exon (SE), a retained intron (RI), mutually exclusive exons (MXE), an alternative 3′ splice site (A3'SS), and an alternative 5′ splice site (A5'SS) in our analysis. There were 2,838, 2,442, 1,673, and 1,205 significant differential AS (DAS) events in comparisons of ZH11 control group vs. ZH11 HS group, GS2 control group vs. GS2 HS group, ZH11 control group vs. GS2 control group, and ZH11 HS group vs. GS2 HS group, respectively. SE and A3′SS events accounted for more than two-thirds of the total AS events in each comparison, with IR and A5′SS events the next most frequent. Interestingly, only 23 genes were considered to be DEGs and also DAS genes across ZH11 and GS2 after HS, that is, less than 3% of these 1,960 disturbed genes were regulated together at transcriptional and splicing levels (Figure 7B). GO analysis revealed that DAS genes tend to be highly enriched in

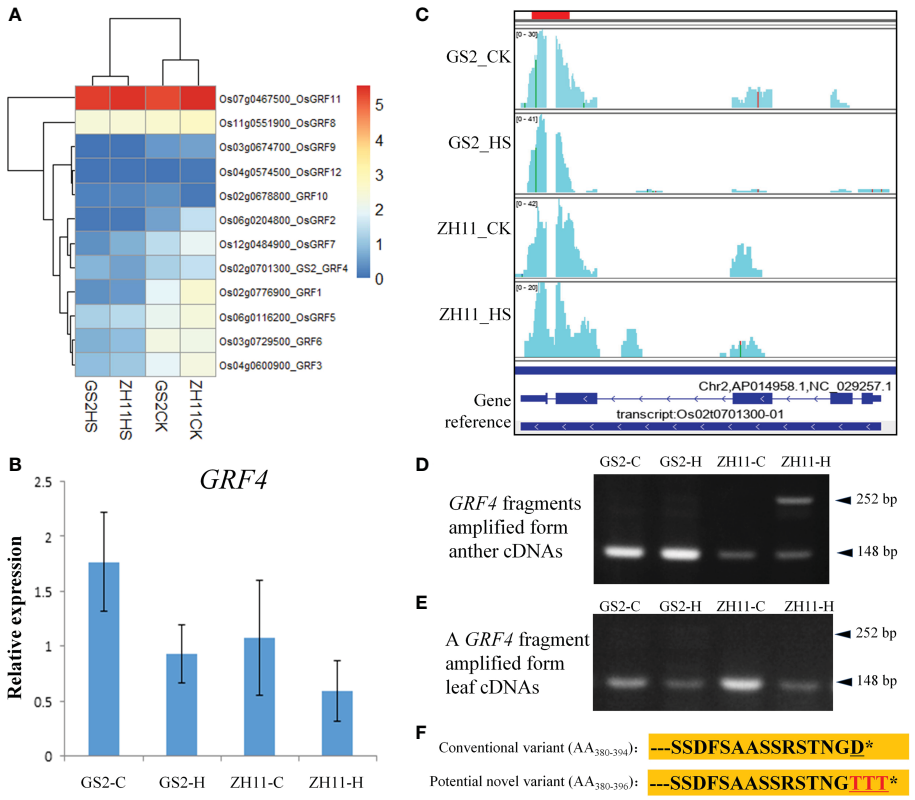

FIGURE 6
Expressions of growth regulation factors (GRFs) under different temperature conditions. **(A)** Expression patterns of GRFs in RNA sequencing (RNA-Seq) data. **(B)** Expression of *OsGRF4* (*Oryza sativa* growth-regulating factor 4) measured by reverse transcription-quantitative PCR (qRT-PCR). **(C)** Visualization of coverage of sequencing reads annotated to *OsGRF4* gene using the IGV program. **(D)** Reverse transcription-PCR (RT-PCR) validation of the intron retention (IR) event detected in *OsGRF4*. **(E)** RT-PCR amplification of *OsGRF4* by using leaf cDNA as a template. **(F)** Amino acid residues of the conventional OsGRF4 protein and that of the potential protein variant translated from the intron-retained mRNA isoform. Only amino acid residues from position 380 on are shown. * stands for the terminal point of the amino acid sequence.

nucleic acid-binding processes, such as DNA metabolism, RNA processing, gene transcription, etc. A group of genes involved in pollen grain development could also be differentially spliced. As we found that DAS genes were also enriched in GO terms, such as "starch biosynthetic process", "mitotic cell cycle", and "floral organ formation" (Figure 7C).

We randomly picked up several genes that was considered to be differently spliced in ZH11 and GS2 under heat stress conditions, and validated them through RT-PCR. It was demonstrated that encoding genes of important regulators, such as *CCA1*, *OsSPO11*, *HSFB2c*, and *OsDR11*, could amplify more than one target band (Figures 7D–J), suggesting that different mRNA isoforms could be generated after the pre-mRNA splicing process. Moreover, the intensities of amplified fragments of the same genes varied between ZH11 and GS2 after HS, suggesting different abundances of alternatively spliced mRNA isoforms in these two samples, which corresponds to snapshots from the IGV program (shown below each RT-PCR gel panel). Notably, not all AS events detected through RT-PCR and the IGV program were considered significant DAS events in the rMATS program. Reasons for this gap could be the relatively low read coverage of AS events in RNA-Seq data or the technical preference of the data analysis program (i.e., rMATS focusing on variations of junction counts between different exons, but not IR (Shen et al., 2014).

4 Discussion

A two-nucleotide substitution in the *OsGRF4* gene could enhance NUE and carbohydrate accumulation under normal conditions, ultimately resulting in enhanced grain size and yields (Che et al., 2015; Duan et al., 2015; Li et al., 2018). The meiotic stage is one of the developmental phases that is most sensitive to HS (Chen et al., 2016). Our experimental results demonstrate that heat-induced damage in anthers was more severe in the near-isogenic line GS2 (*OsGRF4* variation line) than in its wild-type background ZH11. This indicates a potential risk of more severe HS-induced productivity loss from this rice genotype if planted in areas that are frequently exposed to high temperatures and heatwaves during the meiotic stage.

The involvement of GRF family proteins in stress responses has been found before in plants. For example, it has been found that MYB61 is regulated by OsGRF4, and promotes nitrogen utilization and biomass production in rice (Gao et al., 2020). Thus, we did not find differential

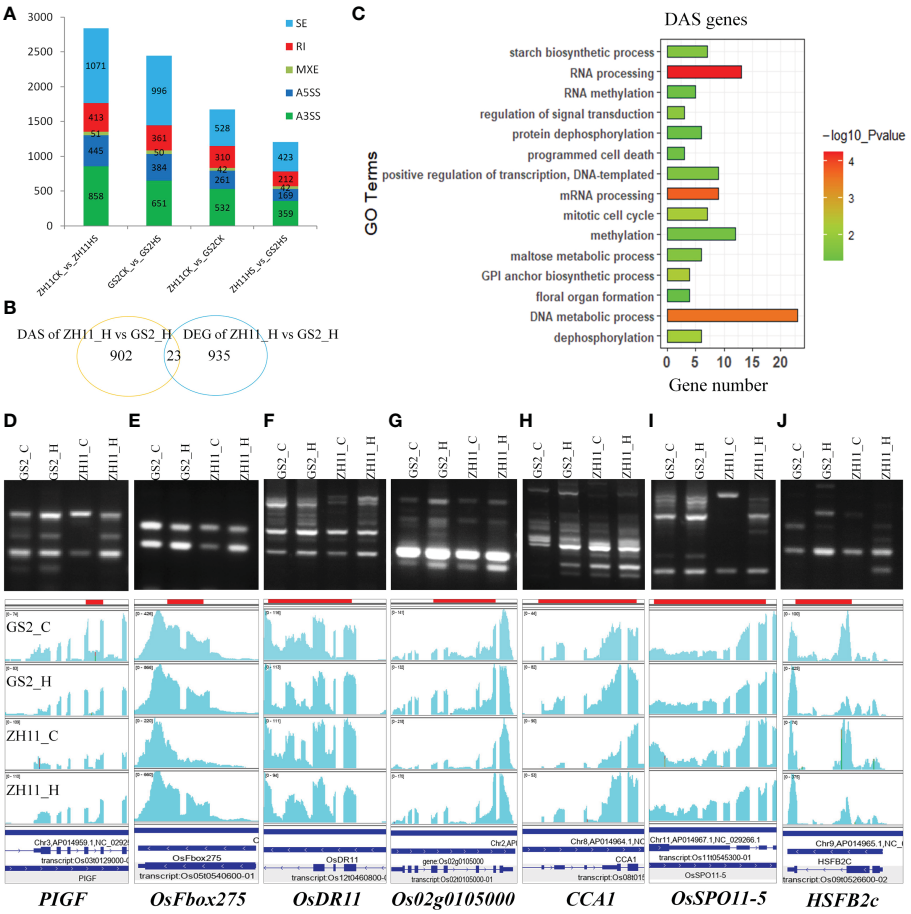

FIGURE 7
Detection of differential alternative splicing (DAS) genes in Zhonghua 11 (ZH11) and grain size on chromosome 2 (GS2). **(A)** Number of DAS events in four different comparisons. **(B)** Overlap of differentially expressed genes (DEGs) and DAS genes in the comparison of the ZH11 HS group and the GS2 HS group. **(C)** Gene ontology (GO) analysis of DAS genes in the comparison of the ZH11 HS group and the GS2 HS group. **(D–J)** Alternative splicing (AS) events on seven genes as determined through reverse transcription-PCR (RT-PCR) (upper) and the IGV program (bottom).

expression of MYB61 from our RNA-Seq data here, suggesting that there could be other downstream pathways involved in differentiated carbon and nitrogen metabolisms in rice. In *Arabidopsis*, a mutation of AtGRF7 enhances its drought and salt stress tolerance, because AtGRF7 suppresses the expression of stress-responsive genes and then decreases the stress resistance in wild-type plants (Kim et al., 2012). Transgenic seedlings of a hybrid poplar (i.e., *Populus alba* × *Populus glandulosa*) overexpressing a specific GRF15 mRNA lacking target sites of miR396a exhibited enhanced heat tolerance and photosynthetic efficiency (Zhao et al., 2021), suggesting that GRF15 plays an important role in responding to HS in poplar seedlings. However, it is still unclear whether or not, in this transgenic tree, the heat tolerance of the flowers as well of the vegetative tissues was enhanced.

GO analysis demonstrated that several biological processes, including "response to heat", "protein folding", "response to high light intensity", and "response to hydrogen peroxide", were highly enriched in both genotypes in response to high-temperature stress treatment. This result is similar to what had been found recently in wheat anthers (Browne et al., 2021). In this study, a great number of heat-responsive genes, including *HSFs* and *HSPs*, were up-regulated by HS in anthers from both genotypes. Heat induction of such genes was found in different organisms, and at different developmental stages of plants (McClellan et al., 2007; Gonzalez-Schain et al., 2016; Ling et al., 2018), suggesting that all of these genes play a role in facilitating heat tolerance in different plant tissues. In total, 87 genes are regulated in the anthers of both ZH11 and GS2, as well as in the rice genotypes "996", "SDWG005", and "9311" (Zhang X. et al., 2012; Liu et al., 2020). These common up-regulated DEGs include not only *HSFs* and *HSPs*, but also two pre-mRNA splicing factors, *SF2* (Os01g0316600) and *PRP4* (Os03g0701100), suggesting that they would function as regulators of pre-mRNA splicing under HS conditions.

Abiotic stress can alter the composition of core histone H2A and chromatin remodeling factors. It has been suggested that H2A.Z nucleosomes wrap DNA more tightly under low temperature while more loosely under high temperature, which influences the ability of RNA polymerase II to transcribe genes in response to temperature variation (Kumar and Wigge, 2010). Here, we found that the DEGs that were down-regulated in anthers from different rice genotypes included not only those involved in cell division and flower development, but also genes encoding core histones H2A and H3, SWI/SNF-related chromatin-binding proteins, HMG1/2 (Os09g0551600, and THION27 (Os01g0594900). Given that these genes may function in processes, such as preservation of membrane integrity and chromosome architecture, suppression of their expression was assumed to be a reason for the developmental deficiency of pollen grains after HS treatment.

Reduction and/or alteration in carbohydrate reserves causes developmental defects in pollen grains and male sterility under stress conditions (De Storme and Geelen, 2014). The transcriptomic analysis in our study revealed that, in addition to genes involved in abiotic and endogenous stimuli, genes involved in chloroplast development and photosynthesis and carbohydrate metabolism accounted for the majority of DEGs that after HS treatment were expressed at higher levels in the anthers of ZH11 than in those of GS2. Almost all of chloroplast- and photosynthesis-related genes were expressed at lower levels in GS2 than in ZH11 after HS treatment. More severe heat inhibition of photosynthesis-related genes is associated with a greater decrease in pollen grain viability in GS2 anthers. Although photosynthetic activity seems to be carried out mainly in the leaves of plants, several recent studies have confirmed that properly expressions of photosynthesis and chloroplast genes are essential for anther development in maize (Murphy et al., 2015; Zhu et al., 2020), petunias (Yue et al., 2018), wheat (Liu et al., 2018), and rice (Basnet et al., 2019). Nearly all (> 96%) photosynthesis-associated genes found in the maize leaf were expressed in most subepidermal and endothecial cells of the anthers, although no photosynthetic light reaction activity from the anthers was detected *in vitro* (Murphy et al., 2015). In wheat anthers, it was found that HS caused significant down-regulation of chloroplast-related genes together with the disturbance of starch and sucrose metabolism, and could ultimately result in severe decease of pollen fertility (Liu et al., 2018). By comparing gene expression profiles in anthers from wild-type rice and from *phyA* and *phyB* single and double mutants, it was found that carbohydrate metabolism and stress- and photosynthesis-related genes were significantly affected in the *phyA phyB* double mutant (Basnet et al., 2019), indicating a complex regulatory network underlying phytochrome-mediated anther and pollen development in rice. Another study of rice anthers demonstrated dynamic change in the expression of chlorophyll- and photosynthesis-related genes, which were up-regulated immediately after HS and then suppressed when the stress was prolonged (Liu et al., 2020).

More severe HS-induced male sterility in GS2 could be further attributed to more vulnerable lipid metabolic activity in anthers, as five of the eight MSGs that are differentially expressed in the anthers of GS2 and ZH11 are lipid metabolism genes, and all are consistently expressed at significantly lower levels in GS2 anthers than in ZH11 anthers. In support of this, premature programed cell death of tapetal cells was found from maize anthers with a mutation in *ZmGPAT6*, a male sterile gene that encodes a glycerol-3-phosphate acyltransferase. *ZmGPAT6*-mediated lipid biosynthesis maintains starch metabolism and photosynthetic activities of endothecium (En) chloroplasts, which are crucial for maize anther development (Zhu et al., 2020).

A more severe HS-induced abortion phenotype of GS2 is correlated with greater inhibition of the critical transcription factors necessary for pollen grain development and fertilization. *CSA* is a gene that encodes a MYB domain protein regulating sugar partitioning for rice pollen development (Zhang et al., 2010), and controls the development of the reverse photosensitive genic male sterile (rPGMS) trait (i.e., exhibiting male fertility under long-day conditions and male sterility under short-day conditions) in japonica rice (Zhang et al., 2013; Zhu et al., 2015). This gene was down-regulated to a significantly lower level in GS2 anthers under HS conditions. A comparative study in rice found that *OsHSFA2a* was induced significantly in anthers, and its induction intensity was positively correlated with the heat tolerance of anthers (Gonzalez-Schain et al., 2016). It has been reported that mutation in the *bHLH142* gene also causes complete male sterility (Ranjan et al., 2017; Abbas et al., 2021).

High temperatures target not only gene transcription, but also mRNA processing, in anthers and pollen grains. Global AS can be triggered by HS in different organisms (Ling et al., 2021) and in this study the number of AS events detected differed significantly between different genotypes and under different temperature conditions. Thus, the most frequent AS type detected here through rMATS was exon skipping (ES); this is inconsistent with previous reports, which suggest IR is the most prevalent AS type carried out in plants (Jiang et al., 2017; Ling et al., 2018). The divergence can likely be attributed to different preferences between AS analysis programs, as we know that rMATS was originally

designed for detecting AS events in mammal cells, where ES is the predominant type of AS (Shen et al., 2014). We detected a great numbers of IR events using the IGV program coupled with RT-PCR validation, but not in rMATS, suggesting that considerable numbers of novel IR events or those with relatively low intensity could be ignored by this program. Nevertheless, many IR events were detected in genes encoding stress regulators and also in those genes critical for gametophyte development, including *HSFB2c*, *CCA1*, *OsSPO11-5*, and *OsDR11*.

More interestingly, *OsGRF4* itself underwent IR specifically in anthers from ZH11 under the given HS conditions. There could be several reasons for this genotypic-specific AS event. The first reason could be the specific AS regulated by variation of *cis*-elements such as sequence changes in the *OsGRF4* gene between ZH11 and GS2 backgrounds. Second, differentiated expression of splicing factors could also affect the pre-mRNA splicing process. Third, different cellular states, such as different carbon and nitrogen supply, may also impact the pre-mRNA splicing patterns. In fact, some clues can be obtained from recent studies. A great number of genes encoding splicing factors, miRNAs, long non-coding RNAs (lncRNAs), and transcription factors were found to undergo AS in young panicles and florets of rice (Li et al., 2021). The same genes from different rice genotypes carried out differential AS regulations in response to salt stress stimulation (Jian et al., 2022). Interestingly, not only growth conditions but also nutrition status affect AS regulation of related genes in different plants (Zhang Y. M. et al., 2012; Li H. et al., 2016; Nishida et al., 2017; Wang et al., 2019). For example, nutrient stress caused differential AS regulation of the *NRR* gene in rice (Zhang Y. M. et al., 2012). Moreover, a recent study demonstrated that nitrogen starvation modulated differential AS and transcript usage of various metabolism-related genes in rice (Chaudhary and Kalkal, 2021), and AS of *OsGS1;1* affects NUE, grain development, and amylose content in rice (Liu et al., 2022).

In conclusion, under HS conditions, the rice variety GS2, containing $OsGRF4^{AA}$, caused the alteration of nutrition allocation and metabolism in reproductive tissues, which could be mediated by, and also feed back negatively to, transcriptional and splicing regulation of essential genes. The combined impact made GS2 anthers and the developing male gametophytes more sensitive to HS.

Data availability statement

The data sets presented in this study can be found in SRA repositories https://www.ncbi.nlm.nih.gov/bioproject/PRJNA915644. The names of the repository/repositories and accession number(s) can be found in the article/Supplementary Material.

Author contributions

YL and DZ had the idea, organized the whole program, and modified the manuscript. YM and GL ran most of the experiments, done the data analysis, and wrote the manuscript. LL, YZ, JL, MY, SC, and QL participated in some experiments and data analysis. GF provided suggestions for the experiments. All authors contributed to the article and approved the submitted version.

Funding

This study was funded by Guangdong Basic and Applied Basic Research Foundation, No. 2021A1515012391, Innovation & University Improvement Programs from Guangdong Ocean University, No. 230419099, and Open Project Program of State Key Laboratory of Rice Biology, No. 20210402.

Acknowledgments

We would like to thank Dr Jiang Hu from the China National Rice Research Institute for providing plant materials.

Conflict of interest

The authors declare that the research was conducted in the absence of any commercial or financial relationships that could be construed as a potential conflict of interest.

Publisher's note

Supplementary material

The Supplementary Material for this article can be found online at: https://www.frontiersin.org/articles/10.3389/fpls.2023.1121852/full#supplementary-material

SUPPLEMENTARY FIGURE 1
Biological process enrichment of differentially expressed genes (DEGs) between Zhonghua 11 (ZH11) and grain size on chromosome 2 (GS2) under normal conditions. **(A)** DEGs with higher expressional levels in ZH11. **(B)** DEGs with higher expression levels in GS2.

SUPPLEMENTARY FIGURE 2
Top 50 differentially expressed genes (DEGs) in comparisons of ZH11 HS group > GS2 HS group **(A)** and ZH11 HS group < GS2 HS group **(B)**.

References

Abbas, A., Yu, P., Sun, L., Yang, Z., Chen, D., Cheng, S., et al. (2021). Exploiting genic Male sterility in rice: From molecular dissection to breeding applications. *Front. Plant Sci.* 12, 629314. doi: 10.3389/fpls.2021.629314

Akerfelt, M., Vihervaara, A., Laiho, A., Conter, A., Christians, E. S., Sistonen, L., et al. (2010). Heat shock transcription factor 1 localizes to sex chromatin during meiotic repression. *J. Biol. Chem.* 285, 34469–34476. doi: 10.1074/jbc.M110.157552

Basnet, R., Hussain, N., and Shu, Q. (2019). *OsDGD2beta* is the sole digalactosyldiacylglycerol synthase gene highly expressed in anther, and its mutation confers Male sterility in rice. *Rice (N Y)* 12, 66. doi: 10.1186/s12284-019-0320-z

Begcy, K., Nosenko, T., Zhou, L. Z., Fragner, L., Weckwerth, W., and Dresselhaus, T. (2019). Male Sterility in maize after transient heat stress during the tetrad stage of pollen development. *Plant Physiol.* 181, 683–700. doi: 10.1104/pp.19.00707

Bokshi, A. I., Tan, D. K. Y., Thistlethwaite, R. J., Trethowan, R., and Kunz, K. (2021). Impact of elevated CO_2 and heat stress on wheat pollen viability and grain production. *Funct. Plant Biol.* 48, 503–514. doi: 10.1071/FP20187

Bray, N. L., Pimentel, H., Melsted, P., and Pachter, L. (2016). Near-optimal probabilistic RNA-seq quantification. *Nat. Biotechnol.* 34, 525–527. doi: 10.1038/nbt.3519

Browne, R. G., Li, S. F., Iacuone, S., Dolferus, R., and Parish, R. W. (2021). Differential responses of anthers of stress tolerant and sensitive wheat cultivars to high temperature stress. *Planta* 254, 4. doi: 10.1007/s00425-021-03656-7

Chaudhary, S., and Kalkal, M. (2021). Rice transcriptome analysis reveals nitrogen starvation modulates differential alternative splicing and transcript usage in various metabolism-related genes. *Life (Basel)* 11, 1–15. doi: 10.3390/life11040285

Chen, S., Mo, Y., Zhang, Y., Zhu, H., and Ling, Y. (2022). Insights into sweet potato SR proteins: from evolution to species-specific expression and alternative splicing. *Planta* 256, 72. doi: 10.1007/s00425-022-03965-5

Chen, Y., Muller, F., Rieu, I., and Winter, P. (2016). Epigenetic events in plant male germ cell heat stress responses. *Plant Reprod.* 29, 21–29. doi: 10.1007/s00497-015-0271-5

Che, R., Tong, H., Shi, B., Liu, Y., Fang, S., Liu, D., et al. (2015). Control of grain size and rice yield by GL2-mediated brassinosteroid responses. *Nat. Plants* 2, 15195. doi: 10.1038/nplants.2015.195

De Storme, N., and Geelen, D. (2014). The impact of environmental stress on male reproductive development in plants: Biological processes and molecular mechanisms. *Plant Cell Environ.* 37, 1–18. doi: 10.1111/pce.12142

Draeger, T., and Moore, G. (2017). Short periods of high temperature during meiosis prevent normal meiotic progression and reduce grain number in hexaploid wheat (*Triticum aestivum* l.). *Theor. Appl. Genet.* 130, 1785–1800. doi: 10.1007/s00122-017-2925-1

Duan, P., Ni, S., Wang, J., Zhang, B., Xu, R., Wang, Y., et al. (2015). Regulation of *OsGRF4* by OsmiR396 controls grain size and yield in rice. *Nat. Plants* 2, 15203. doi: 10.1038/nplants.2015.203

Feng, B., Zhang, C., Chen, T., Zhang, X., Tao, L., and Fu, G. (2018). Salicylic acid reverses pollen abortion of rice caused by heat stress. *BMC Plant Biol.* 18, 245. doi: 10.1186/s12870-018-1472-5

Fragkostefanakis, S., Mesihovic, A., Simm, S., Paupiere, M. J., Hu, Y., Paul, P., et al. (2016). HsfA2 controls the activity of developmentally and stress-regulated heat stress protection mechanisms in tomato Male reproductive tissues. *Plant Physiol.* 170, 2461–2477. doi: 10.1104/pp.15.01913

Frank, G., Pressman, E., Ophir, R., Althan, L., Shaked, R., Freedman, M., et al. (2009). Transcriptional profiling of maturing tomato (*Solanum lycopersicum* l.) microspores reveals the involvement of heat shock proteins, ROS scavengers, hormones, and sugars in the heat stress response. *J. Exp. Bot.* 60, 3891–3908. doi: 10.1093/jxb/erp234

Gao, Y., Xu, Z., Zhang, L., Li, S., Wang, S., Yang, H., et al. (2020). MYB61 is regulated by GRF4 and promotes nitrogen utilization and biomass production in rice. *Nat. Commun.* 11, 5219. doi: 10.1038/s41467-020-19019-x

Gong, P., Luo, Y., Huang, F., Chen, Y., Zhao, C., Wu, X., et al. (2019). Disruption of a Upf1-like helicase-encoding gene *OsPLS2* triggers light-dependent premature leaf senescence in rice. *Plant Mol. Biol.* 100, 133–149. doi: 10.1007/s11103-019-00848-4

Gonzalez-Schain, N., Dreni, L., Lawas, L. M., Galbiati, M., Colombo, L., Heuer, S., et al. (2016). Genome-wide transcriptome analysis during anthesis reveals new insights into the molecular basis of heat stress responses in tolerant and sensitive rice varieties. *Plant Cell Physiol.* 57, 57–68. doi: 10.1093/pcp/pcv174

Guo, W., Tzioutziou, N. A., Stephen, G., Milne, I., Calixto, C. P., Waugh, R., et al. (2021). 3D RNA-seq: A powerful and flexible tool for rapid and accurate differential expression and alternative splicing analysis of RNA-seq data for biologists. *RNA Biol.* 18, 1574–1587. doi: 10.1080/15476286.2020.1858253

Hedhly, A., Vogler, H., Schmid, M. W., Pazmino, D., Gagliardini, V., Santelia, D., et al. (2016). Starch turnover and metabolism during flower and early embryo development. *Plant Physiol.* 172, 2388–2402. doi: 10.1104/pp.16.00916

He, Z., Zeng, J., Ren, Y., Chen, D., Li, W., Gao, F., et al. (2017). *OsGIF1* positively regulates the sizes of stems, leaves, and grains in rice. *Front. Plant Sci.* 8, 1730. doi: 10.3389/fpls.2017.01730

Hu, J., Wang, Y., Fang, Y., Zeng, L., Xu, J., Yu, H., et al. (2015). A rare allele of *GS2* enhances grain size and grain yield in rice. *Mol. Plant* 8, 1455–1465. doi: 10.1016/j.molp.2015.07.002

Jain, M., Chourey, P. S., Boote, K. J., and Allen, L. H.Jr. (2010). Short-term high temperature growth conditions during vegetative-to-reproductive phase transition irreversibly compromise cell wall invertase-mediated sucrose catalysis and microspore meiosis in grain sorghum (*Sorghum bicolor*). *J. Plant Physiol.* 167, 578–582. doi: 10.1016/j.jplph.2009.11.007

Jambhekar, A., and Amon, A. (2008). Control of meiosis by respiration. *Curr. Biol.* 18, 969–975. doi: 10.1016/j.cub.2008.05.047

Jiang, J., Liu, X., Liu, C., Liu, G., Li, S., and Wang, L. (2017). Integrating omics and alternative splicing reveals insights into grape response to high temperature. *Plant Physiol.* 173, 1502–1518. doi: 10.1104/pp.16.01305

Jian, G., Mo, Y., Hu, Y., Huang, Y., Ren, L., Zhang, Y., et al. (2022). Variety-specific transcriptional and alternative splicing regulations modulate salt tolerance in rice from early stage of stress. *Rice (N Y)* 15, 56. doi: 10.1186/s12284-022-00599-9

Kim, J. S., Mizoi, J., Kidokoro, S., Maruyama, K., Nakajima, J., Nakashima, K., et al. (2012). Arabidopsis growth-regulating factor7 functions as a transcriptional repressor of abscisic acid- and osmotic stress-responsive genes, including *DREB2A*. *Plant Cell* 24, 3393–3405. doi: 10.1105/tpc.112.100933

Kim, J. H., and Tsukaya, H. (2015). Regulation of plant growth and development by the GROWTH-REGULATING FACTOR and GRF-INTERACTING FACTOR duo. *J. Exp. Bot.* 66, 6093–6107. doi: 10.1093/jxb/erv349

Kumar, S. V., and Wigge, P. A. (2010). H2A.Z-containing nucleosomes mediate the thermosensory response in arabidopsis. *Cell* 140, 136–147. doi: 10.1016/j.cell.2009.11.006

Lee, S. J., Lee, B. H., Jung, J. H., Park, S. K., Song, J. T., and Kim, J. H. (2018). Growth-regulating factor and grf-interacting factor specify meristematic cells of gynoecia and anthers. *Plant Physiol.* 176, 717–729. doi: 10.1104/pp.17.00960

Liebsch, D., and Palatnik, J. F. (2020). MicroRNA miR396, GRF transcription factors and GIF co-regulators: A conserved plant growth regulatory module with potential for breeding and biotechnology. *Curr. Opin. Plant Biol.* 53, 31–42. doi: 10.1016/j.pbi.2019.09.008

Li, S., Gao, F., Xie, K., Zeng, X., Cao, Y., Zeng, J., et al. (2016). The OsmiR396c-OsGRF4-OsGIF1 regulatory module determines grain size and yield in rice. *Plant Biotechnol. J.* 14, 2134–2146. doi: 10.1111/pbi.12569

Li, H., Liang, Z., Ding, G., Shi, L., Xu, F., and Cai, H. (2016). A natural Light/Dark cycle regulation of carbon-nitrogen metabolism and gene expression in rice shoots. *Front. Plant Sci.* 7, 1318. doi: 10.3389/fpls.2016.01318

Li, H., Li, A., Shen, W., Ye, N., Wang, G., and Zhang, J. (2021). Global survey of alternative splicing in rice by direct RNA sequencing during reproductive development: Landscape and genetic regulation. *Rice (N Y)* 14, 75. doi: 10.1186/s12284-021-00516-6

Ling, Y., Mahfouz, M. M., and Zhou, S. (2021). Pre-mRNA alternative splicing as a modulator for heat stress response in plants. *Trends Plant Sci.* 26, 1153–1170. doi: 10.1016/j.tplants.2021.07.008

Ling, Y., Serrano, N., Gao, G., Atia, M., Mokhtar, M., Woo, Y. H., et al. (2018). Thermopriming triggers splicing memory in arabidopsis. *J. Exp. Bot.* 69, 2659–2675. doi: 10.1093/jxb/ery062

Li, S., Tian, Y., Wu, K., Ye, Y., Yu, J., Zhang, J., et al. (2018). Modulating plant growth-metabolism coordination for sustainable agriculture. *Nature* 560, 595–600. doi: 10.1038/s41586-018-0415-5

Liu, H., Guo, S., Xu, Y., Li, C., Zhang, Z., Zhang, D., et al. (2014). OsmiR396d-regulated OsGRFs function in floral organogenesis in rice through binding to their targets *OsJMJ706* and *OsCR4*. *Plant Physiol.* 165, 160–174. doi: 10.1104/pp.114.235564

Liu, X., Tian, Y., Chi, W., Zhang, H., Yu, J., Chen, G., et al. (2022). Alternative splicing of *OsGS1;1* affects nitrogen-use efficiency, grain development, and amylose content in rice. *Plant J.* 110, 1751–1762. doi: 10.1111/tpj.15768

Liu, G., Zha, Z., Cai, H., Qin, D., Jia, H., Liu, C., et al. (2020). Dynamic transcriptome analysis of anther response to heat stress during anthesis in thermotolerant rice (*Oryza sativa* l.). *Int. J. Mol. Sci.* 21, 1–17. doi: 10.3390/ijms21031155

Liu, H., Zhang, G., Wang, J., Li, J., Song, Y., Qiao, L., et al. (2018). Chemical hybridizing agent SQ-1-induced male sterility in *Triticum aestivum* l.: A comparative analysis of the anther proteome. *BMC Plant Biol.* 18, 7. doi: 10.1186/s12870-017-1225-x

Lu, Y., Zeng, J., and Liu, Q. (2021). The rice miR396-GRF-GIF-SWI/SNF module: A player in GA signaling. *Front. Plant Sci.* 12, 786641. doi: 10.3389/fpls.2021.786641

McClellan, A. J., Xia, Y., Deutschbauer, A. M., Davis, R. W., Gerstein, M., and Frydman, J. (2007). Diverse cellular functions of the Hsp90 molecular chaperone uncovered using systems approaches. *Cell* 131, 121–135. doi: 10.1016/j.cell.2007.07.036

Murphy, K. M., Egger, R. L., and Walbot, V. (2015). Chloroplasts in anther endothecium of *Zea mays* (Poaceae). *Am. J. Bot.* 102, 1931–1937. doi: 10.3732/ajb.1500384

Naranjo, T., Cunado, N., and Santos, J. L. (2022). Assessing the heat tolerance of meiosis in Spanish landraces of tetraploid wheat *Triticum turgidum*. *Plants (Basel)* 11, 1–11. doi: 10.3390/plants11131661

Nishida, S., Kakei, Y., Shimada, Y., and Fujiwara, T. (2017). Genome-wide analysis of specific alterations in transcript structure and accumulation caused by nutrient deficiencies in *Arabidopsis thaliana*. *Plant J.* 91, 741–753. doi: 10.1111/tpj.13606

Peng, Y., Zhang, X., Liu, Y., and Chen, X. (2020). Exploring heat-response mechanisms of MicroRNAs based on microarray data of rice post-meiosis panicle. *Int. J. Genomics* 2020, 7582612. doi: 10.1155/2020/7582612

Qu, X., Zou, J., Wang, J., Yang, K., Wang, X., and Le, J. (2022). A rice R2R3-type MYB transcription factor OsFLP positively regulates drought stress response *via* OsNAC. *Int. J. Mol. Sci.* 23, 1–16. doi: 10.3390/ijms23115873

Ranjan, R., Khurana, R., Malik, N., Badoni, S., Parida, S. K., Kapoor, S., et al. (2017). bHLH142 regulates various metabolic pathway-related genes to affect pollen development and anther dehiscence in rice. *Sci. Rep.* 7, 43397. doi: 10.1038/srep43397

Rezaul, I. M., Baohua, F., Tingting, C., Weimeng, F., Caixia, Z., Longxing, T., et al. (2019). Abscisic acid prevents pollen abortion under high-temperature stress by mediating sugar metabolism in rice spikelets. *Physiol. Plant* 165, 644–663. doi: 10.1111/ppl.12759

Rossmann, S., Richter, R., Sun, H., Schneeberger, K., Topfer, R., Zyprian, E., et al. (2020). Mutations in the miR396 binding site of the growth-regulating factor gene *VvGRF4* modulate inflorescence architecture in grapevine. *Plant J.* 101, 1234–1248. doi: 10.1111/tpj.14588

Shen, S., Park, J. W., Lu, Z. X., Lin, L., Henry, M. D., Wu, Y. N., et al. (2014). rMATS: robust and flexible detection of differential alternative splicing from replicate RNA-seq data. *Proc. Natl. Acad. Sci. U.S.A.* 111, E5593–E5601. doi: 10.1073/pnas.1419161111

Shen, Q., Xie, Y., Qiu, X., and Yu, J. (2022). The era of cultivating smart rice with high light efficiency and heat tolerance has come of age. *Front. Plant Sci.* 13, 1021203. doi: 10.3389/fpls.2022.1021203

Shukla, P. R., Skea, J., Slade, R., Al Khourdajie, A., van Diemen, R., McCollum, D., et al. (2022). "IPCC 2022: Climate change 2022: Mitigation of climate change," in *Contribution of working group III to the sixth assessment report of the intergovernmental panel on climate change*. Cambridge University Press, Cambridge, UK and New York, NY, USA. doi: 10.1017/9781009157926

Smith, A. R., and Zhao, D. (2016). Sterility caused by floral organ degeneration and abiotic stresses in arabidopsis and cereal grains. *Front. Plant Sci.* 7, 1503. doi: 10.3389/fpls.2016.01503

Tang, Y., Gao, C. C., Gao, Y., Yang, Y., Shi, B., Yu, J. L., et al. (2020). OsNSUN2-mediated 5-methylcytosine mRNA modification enhances rice adaptation to high temperature. *Dev. Cell* 53, 272–286.e277. doi: 10.1016/j.devcel.2020.03.009

Vihervaara, A., Sergelius, C., Vasara, J., Blom, M. A., Elsing, A. N., Roos-Mattjus, P., et al. (2013). Transcriptional response to stress in the dynamic chromatin environment of cycling and mitotic cells. *Proc. Natl. Acad. Sci. U.S.A.* 110, E3388–E3397. doi: 10.1073/pnas.1305275110

Wang, Z., Zhang, H., and Gong, W. (2019). Genome-wide identification and comparative analysis of alternative splicing across four legume species. *Planta* 249, 1133–1142. doi: 10.1007/s00425-018-03073-3

Yue, Y., Tian, S., Wang, Y., Ma, H., Liu, S., Wang, Y., et al. (2018). Transcriptomic and GC-MS metabolomic analyses reveal the sink strength changes during petunia anther development. *Int. J. Mol. Sci.* 19, 1–15. doi: 10.3390/ijms19040955

Zhang, H., Liang, W., Yang, X., Luo, X., Jiang, N., Ma, H., et al. (2010). Carbon starved anther encodes a MYB domain protein that regulates sugar partitioning required for rice pollen development. *Plant Cell* 22, 672–689. doi: 10.1105/tpc.109.073668

Zhang, X., Li, J., Liu, A., Zou, J., Zhou, X., Xiang, J., et al. (2012). Expression profile in rice panicle: Insights into heat response mechanism at reproductive stage. *PloS One* 7, e49652. doi: 10.1371/journal.pone.0049652

Zhang, H., Xu, C., He, Y., Zong, J., Yang, X., Si, H., et al. (2013). Mutation in *CSA* creates a new photoperiod-sensitive genic male sterile line applicable for hybrid rice seed production. *Proc. Natl. Acad. Sci. U.S.A.* 110, 76–81. doi: 10.1073/pnas.1213041110

Zhang, Y. M., Yan, Y. S., Wang, L. N., Yang, K., Xiao, N., Liu, Y. F., et al. (2012). A novel rice gene, NRR responds to macronutrient deficiency and regulates root growth. *Mol. Plant* 5, 63–72. doi: 10.1093/mp/ssr066

Zhang, J., Zhou, Z., Bai, J., Tao, X., Wang, L., Zhang, H., et al. (2020). Disruption of MIR396e and MIR396f improves rice yield under nitrogen-deficient conditions. *Natl. Sci. Rev.* 7, 102–112. doi: 10.1093/nsr/nwz142

Zhao, Y., Xie, J., Wang, S., Xu, W., Chen, S., Song, X., et al. (2021). Synonymous mutation in growth regulating factor 15 of miR396a target sites enhances photosynthetic efficiency and heat tolerance in poplar. *J. Exp. Bot.* 72, 4502–4519. doi: 10.1093/jxb/erab120

Zhao, Q., Zhou, L., Liu, J., Cao, Z., Du, X., Huang, F., et al. (2018). Involvement of CAT in the detoxification of HT-induced ROS burst in rice anther and its relation to pollen fertility. *Plant Cell Rep.* 37, 741–757. doi: 10.1007/s00299-018-2264-y

Zhu, X., Liang, W., Cui, X., Chen, M., Yin, C., Luo, Z., et al. (2015). Brassinosteroids promote development of rice pollen grains and seeds by triggering expression of carbon starved anther, a MYB domain protein. *Plant J.* 82, 570–581. doi: 10.1111/tpj.12820

Zhu, T., Li, Z., An, X., Long, Y., Xue, X., Xie, K., et al. (2020). Normal structure and function of endothecium chloroplasts maintained by ZmMs33-mediated lipid biosynthesis in tapetal cells are critical for anther development in maize. *Mol. Plant* 13, 1624–1643. doi: 10.1016/j.molp.2020.09.013

frontiers | Frontiers in Plant Science

TYPE Original Research
PUBLISHED 01 March 2023
DOI 10.3389/fpls.2023.1090774

OPEN ACCESS

EDITED BY
Biao Jin,
Yangzhou University, China

REVIEWED BY
Geetha Govind,
University of Agricultural Sciences, Bangalore, India
Sombir Rao,
Cornell University, United States

*CORRESPONDENCE
Syariful Mubarok
syariful.mubarok@unpad.ac.id

SPECIALTY SECTION
This article was submitted to Plant Abiotic Stress, a section of the journal Frontiers in Plant Science

RECEIVED 06 November 2022
ACCEPTED 15 February 2023
PUBLISHED 01 March 2023

CITATION
Mubarok S, Jadid N, Widiastuti A, Derajat Matra D, Budiarto R, Lestari FW, Nuraini A, Suminar E, Pradana Nur Rahmat B and Ezura H (2023) Parthenocarpic tomato mutants, *iaa9-3* and *iaa9-5*, show plant adaptability and fruiting ability under heat-stress conditions. *Front. Plant Sci.* 14:1090774. doi: 10.3389/fpls.2023.1090774

Parthenocarpic tomato mutants, *iaa9-3* and *iaa9-5*, show plant adaptability and fruiting ability under heat-stress conditions

Syariful Mubarok[1*], Nurul Jadid[2], Ani Widiastuti[3], Deden Derajat Matra[4], Rahmat Budiarto[1], Fitrianti Widya Lestari[5], Anne Nuraini[1], Erni Suminar[1], Bayu Pradana Nur Rahmat[6] and Hiroshi Ezura[7,8]

[1]Department of Agronomy, Faculty of Agriculture, Universitas Padjadjaran, Sumedang, Indonesia, [2]Department of Biology, Institut Teknologi Sepuluh Nopember, Surabaya, Indonesia, [3]Department of Plant Protection, Faculty of Agriculture, Universitas Gadjah Mada, Yogyakarta, Indonesia, [4]Department of Agronomy and Horticulture, Faculty of Agriculture, IPB University, Bogor, Indonesia, [5]Plantation Seed Supervision and Certification Center, Bandung, Indonesia, [6]Master Graduate Program of Agronomy, Faculty of Agriculture, Universitas Padjadjaran, Sumedang, Indonesia, [7]Faculty of Life and Environmental Sciences, University of Tsukuba, Tsukuba, Japan, [8]Tsukuba Plant Innovation Research Center, University of Tsukuba, Tsukuba, Japan

Fruit set is one of the main problems that arise in tomato plants under heat-stress conditions, which disrupt pollen development, resulting in decreased pollen fertility. Parthenocarpic tomatoes can be used to increase plant productivity during failure of the fertilisation process under heat-stress conditions. The aim of this study were to identify the plant adaptability and fruiting capability of ?*iaa9-3* and *iaa9-5* tomato mutants under heat-stress conditions. The *iaa9-3* and *iaa9-5* and wild-type Micro-Tom (WT-MT) plants were cultivated under two temperature conditions: normal and heat-stress conditions during plant growth. The results showed that under the heat-stress condition, *iaa9-3* and *iaa9-5* showed delayed flowering time, increased number of flowers, and increased fruit set and produced normal-sized fruit. However, WT-MT cannot produce fruits under heat stress. The mutants can grow under heat-stress conditions, as indicated by the lower electrolyte leakage and H_2O_2 concentration and higher antioxidant activities compared with WT-MT under heat-stress conditions. These results suggest that *iaa9-3* and *iaa9-5* can be valuable genetic resources for the development of tomatoes in high-temperature environmental conditions.

KEYWORDS

tomato, parthenocarpic, auxin, heat stress, mutant

1 Introduction

Tomato (*Solanum lycopersicum*) is an essential Solanaceae horticultural commodity in the world (Anas et al., 2022). Tomatoes are generally used as a source of nutrients and antioxidants, such as vitamins A, C and B, calcium, potassium, magnesium, sodium, iron, phenolic antioxidants, flavonoids, lycopene and ascorbic acid (Oboulbiga et al., 2017; Mubarok et al., 2019a; Mubarok et al., 2023). Tomato production is affected by several factors, such as genetics, nutrition and cultivation methods and environmental factors, including temperature.

Temperature is a very important environmental factor for the growth and development of tomato plants. Heat stress is an external factor that often becomes an obstacle to tomato cultivation. In general, heat stress occurs when temperatures are 10 °C–15 °C higher than optimum cultivation temperatures; for tomato growth, the optimum temperature is 26 °C and heat stress starts to occur when air temperature exceeds 32 °C (Sato et al., 2000; Pham et al., 2020). Heat stress is one of the principal abiotic stresses in tropical countries that limit plant growth and development, affecting production. Failure in pollen development and increased pollen sterility are the main problems in tomato production under heat stress, resulting in a low fruit set (Ezura et al., 2019). The Intergovernmental Panel on Climatic Change reported that in 2014, each country's average world temperature increased by 0.3° C due to global warming and is predicted to increase by 3°C from the usual temperature in 2100. Increased temperature due to global warming has become a severe problem in the agricultural sector. Thus, new tomato cultivars suitable for high-temperature conditions must be developed.

Environmental temperatures above 35 °C in tomato cultivation damage plant growth and development, including seed germination, vegetative and reproductive growth, fruit setting and photosynthetic activity (Ariizumi et al., 2013; Rahmat et al., 2023). The severity of heat stress depends on the duration and time of heat-stress exposure. Ariizumi et al. (2013) reported that ambient temperature 4 degrees above optimal temperature will increase tomato flower abortion. Flower abortion occurred due to the failure of pollination and fertilisation, and flower abortion reduces fruit set initiation. Generation of parthenocarpic tomatoes can be an alternative option to resolving the problem in fruit set initiation under heat-stress conditions, which causes reduced fruit formation due to pollen sterility.

Auxin (AUX) triggers fruit set in tomatoes by activating cell division in the pericarp (i.e. phase II); therefore, induction of parthenocarpic fruits can be artificially attained by the application of exogenous AUX in tomato flowers or flower buds (Ariizumi et al., 2013). By mutation methods, two parthenocarpic tomatoes, namely, *iaa9-3* and *iaa9-5*, have been generated from the Micro-Tom (MT) library. Compared with the wild type, *iaa9-3* and *iaa9-5* produced higher rates of parthenocarpic fruit production, with values reaching up to 70.0% ± 4.7% and 63.3% ± 5.4%, respectively, from an emasculated flower. Meanwhile, in the wild-type MT (WT-MT), almost none of the emasculated WT-MT flowers exhibited fruit formation (Saito et al., 2011).

iaa9-3 and *iaa9-5* have a mutation in *IAA9*, which is a member of the AUX/indole-3-acetic acid (IAA) gene family and acts as a transcriptional repressor of the signalling pathway of the plant hormone AUX (Guilfoyle and Hagen, 2007). Different locations of mutations occur in *iaa9-3* and *iaa9-5*. In *iaa9-3*, a single-DNA substitution causing a T to A substitution was found at the 237th nucleotide, whereas in *iaa9-5*, a 32 bp deletion was located at the 133rd nucleotide position. These mutations by DNA substitution or deletion in these mutants result in the modification of the functional activity of *IAA9*, which triggers fruit development prior to pollination or parthenocarpy (Saito et al., 2011).

Parthenocarpic mutants, such as *iaa9-3* and *iaa9-5*, can produce fruits under heat-stress conditions and help maintain stable tomato production in the future. Those two mutants also can growth under drought stress (Suminar et al., 2022). However, the ability of such mutants for plant growth and development, especially in the fruit set under heat-stress conditions, should be carefully evaluated. In this study, we evaluated the fruit set ability of two mutants under tropical heat-stress conditions.

2 Materials and methods

2.1 Plant materials and cultivation condition

The *iaa9-3* (TOMPJE2811) and *iaa9-5* (TOMJPG0114-1) mutants were isolated and characterised from a mutant population based on MT cultivars (Saito et al., 2011). These mutants and WT-MT as control were cultivated in the greenhouse of the experimental field of the Laboratory of Horticulture, Faculty of Agriculture, Universitas Padjadjaran, with four biological replications; each replication consisted of six individual plants for vegetative analysis. The *iaa9-3* and *iaa9-5* mutants and WT-MT seeds were sown in plug trays, in accordance with the methods described by Rahmat et al. (2023). After the seedling produced 4–5 leaves, they were transplanted into a 12 cm-diameter pot that was filled with a mixture of soil and commercial coir coco peat (1:1/v:v) and cultivated in two greenhouse conditions, i.e. heat-stress (40 °C/45 °C) and control (30 °C/35 ° C) conditions. The heat stress condition was treated for the whole lifespan of the plant, starting from transplanting until the fruit harvest. During the cultivation periods, the plants were fertigated with a commercial nutrient solution with an electrical conductivity (EC) level of 2.0–2.5 dS m^{-1}.

2.2 Agronomic-related yield evaluation of iaa9-3 and iaa9-5 mutants

The agronomic features related to plant growth and yield were evaluated. For plant growth, plant canopy diameter that measured as the method described by Iizuka et al. (2017) and the number of shoots were evaluated at 8 weeks after sowing. For plant yield, several characteristics were evaluated; these characteristics included

flowering time that was the number of days from sowing until 1st flowering from each plant (Mubarok et al., 2019c), the number flowers per plant, the number of fruits per plant, the rate of fruit set, fruit weight, length and diameter and the number of seeds. The fruit weight per plant was calculated by dividing the total fruit weight by the total fruit number. The total number of flowers and fruits and the rate of fruit set were counted similarly to those in the study by Pham et al. (2020) at 115 days after sowing. Meanwhile, the rate of fruit set was calculated by dividing the total number of fruits by the total number of flowers. The fruit weight, length and diameter and the number of seeds per fruit were obtained from five individual fruits of each plant.

2.3 Pollen viability analysis

Pollen viability testing was carried out using 2,3,5-triphenyl tetrazolium chloride (TTC) in accordance with the method used by Ezura et al. (2019). TTC staining is an indicator of cellular survival based on the mitochondrial reduction reaction, where the viable pollen will turn red, and the non-viable pollen will be colourless. Pollens were obtained from five individual flowers, soaked in 1% TTC +50% sucrose and shaken for dispersal in the solution. Afterwards, the TTC solution containing the pollens was left in a dark room at 38°C for 3 h for pollen colouration. Then, 2 µg supernatant was collected and placed in the cell counter. The pollens were then observed under a microscope. The criterion for viable pollens was the absorption of red colour from the TTC solution per 1 mm^2 cell counter.

2.4 H_2O_2 concentration analysis

H_2O_2 concentration was measured following the method used by the Association of Official Analytical Chemists (AOAC) with modifications (Association of Official Analytical Chemists, 1990). A total of 5 g leaf sample was mixed with 5 mL Aqua Bidest using mortar and pestle in an ice bath. Then, 5 mL ground leaf sample mixture was combined with 25 mL sulfuric acid. The mixture was titrated with 0.1 N potassium permanganate. Each 1 mL of potassium permanganate used in titration corresponded to 1.07 mg H_2O_2. Titration was stopped when the sample mixture changed colour. H_2O_2 was calculated using the following formula:

$$H_2O_2 = \frac{V \times 0.1\ (KMnO_4) \times\ 1.701}{W \times 0.01\ (H_2SO_4)} \times 100\,\%$$

V = Titrate used in titration (mL)

W = Weight of the leaf sample (g)

The H_2O_2 values were then converted from percentage to µmol/g of fresh weight (FW).

2.5 Antioxidant activity analysis

Antioxidant activity was analysed following the method used by Sami and Rahimah (2016). A total of 3 g leaf sample was macerated using methanol (99.8%) for 24 h. After 24 h, the mixture was filtrated using filter paper, and the filtrate was thickened utilising a rotary evaporator. The leaf extract solution (1000 ppm) was created by combining 50 mg thickened leaf extract with 50 mL methanol (99.8%). Next, 0.5 mL 0.4 mM 2,2- diphenyl-2-picrylhydrazyl (DPPH) solution was added to a test tube containing 500 µL leaf extract solution (1000 ppm). The test tubes containing the mixture were then incubated in the dark for 30 min at room temperature. After incubation, each sample absorbance was observed using a spectrophotometer (Orion™ AquaMate 8000, Thermo Fisher Scientific, UK) at 516 nm (Mubarok et al., 2019b). A blank solution containing methanol and DPPH only was also prepared. Sample antioxidant activity was measured using the following equation:

$$Antioxidant\ \ activity\ \ (\%) = \frac{Blank\ \ absorbance - Sample\ \ absorbance}{Blank\ \ absorbance} \times 100\,\%$$

2.6 Statistical data analysis

The normalities of data distributions were tested using the Kolmogorov–Smirnov test. For statistical data analysis, data were subjected to a two-factor analysis of variance followed by Duncan's multiple range test at $p < 0.05$ for comparisons among the investigated data. The data are represented as the mean values ± standard error (SE) of four replicates. All statistical analyses were performed using SPSS 20.0 statistical software.

3 Results

3.1 iaa9-3 and iaa9-5 exhibited a reduction in vegetative plant growth compared with WT-MT

The response of plant vegetative growth can be observed from the plant appearance, which was characterised by the plant canopy diameter and the number of shoots. Based on statistical data analysis, the plant canopy diameter of WT-MT, *iaa9-3* and *iaa9-5* mutants were significantly different in either normal temperature or heat-stress conditions (Figures 1A–C, respectively). High-temperature/heat-stress condition greatly influenced the size of the plant canopy diameter. Under heat-stress conditions, the plant canopy diameter decreased significantly in all plant genotypes compared with plants under normal conditions. The highest reduction in the plant canopy diameter was observed in WT-MT, and it decreased by approximately 41.3% compared with that under normal condition. The plant canopy diameters of *iaa9-3* and *iaa9-5* decreased by 40.6% and 36.7%, respectively (Figures 1A, C).

At both temperatures tested, the plant canopy diameter of WT-MT was larger than those of *iaa9-3* and *iaa9-5*. As shown in Figure 1A, the plant canopy diameter of WT-MT under normal conditions showed

10.3389/fpls.2023.1090774

the highest diameter, but it was not significantly different from that of *iaa9-3*. Meanwhile, *iaa9-5* had significantly lower values compared with WT-MT and *iaa9-3* (Figure 1A). The large plant canopy diameter of WT-MT can also be monitored under heat-stress condition, where the plant canopy diameters of *iaa9-3* and *iaa9-5* were significantly lower than that of WT-MT (Figure 1A).

Many lateral shoots caused the large plant canopy diameter of WT-MT. Statistical data analysis showed a significant difference in the number of lateral shoots between WT-MT and *iaa9-3* and *iaa9-5* under normal and heat-stress conditions. The heat-stress condition significantly inhibited the growth of new lateral shoots in all investigated plant genotypes, which resulted in a low number of lateral shoots under heat-stress conditions. However, no further reduction in lateral shoots was observed in *iaa9-3* under heat stress (Figure 2B). The decrease in the number of lateral shoots under heat-stress condition was 23.50%, 17.35% and 38.36% lower compared with those under normal conditions for WT-MT, *iaa9-3* and *iaa9-5*, respectively. Under normal and heat-stress conditions, the mutation in the *IAA9* gene significantly reduced the number of lateral shoots in *iaa9-3* and *iaa9-5*. In *iaa9-3*, the number of lateral shoots was 5.75 and 4.25 fewer compared with that in WT-MT under normal and heat-stress conditions, respectively. *Iaa9-5* showed 5.25 and 4.45 fewer lateral shoots compared with WT-MT under normal and heat-stress conditions, respectively (Figures 2A–C).

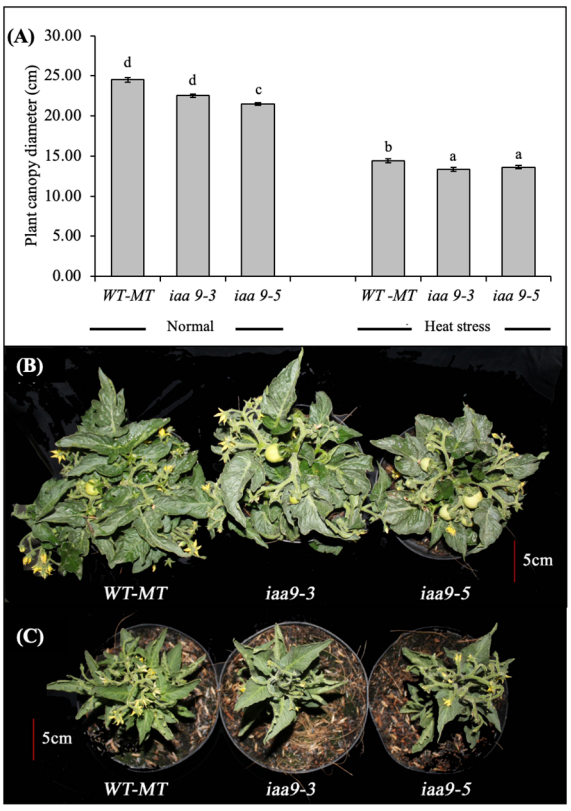

FIGURE 1
(A) The average value of the plant canopy diameter of WT-MT, *iaa9-3*, and *iaa9-5* under two temperature conditions. The plant canopy of WT-MT, *iaa9-3* and *iaa9-5* under **(B)** normal temperature and **(C)** heat stress condition. The average value ± standard error (SE) (n = 4) followed by the same lowercase letters is not significantly different based on Duncan's Multiple Range Test at 5%.

3.2 Mutant genotypes iaa9-3 and iaa9-5 experienced delayed flowering under the heat-stress condition

Flowering is strongly influenced by internal and external factors. The time of flowering is one of the several indicators of a plant entering the generative phase. The results showed that the flowering time of the three observed tomato genotypes, namely, *iaa9-3*, *iaa9-5* and WT-MT, differed depending on environmental conditions. Under the normal-temperature condition, the mutation in *iaa9-3* and *iaa9-5* significantly accelerated flowering time by 3 and 6.7 days earlier than WT-MT, respectively (Figure 3). This result was different from that observed under heat-stress condition. Accelerated flowering time was observed in WT-MT, but *iaa9-3* and *iaa9-5* experienced a delay in flowering time. The mutants behaved as WT under normal condition when subjected to heat stress.

3.3 The number of flowers increased under heat stress condition

The flower is an important generative organ for fruit formation. Statistical analysis showed a significant difference in the number of flowers among the tested genotypes under normal and heat-stress conditions. WT-MT had 94.5 and 122.5 more flowers in normal and heat-stress conditions, respectively. Meanwhile, *iaa9-3* and *iaa9-5* had 68.7 and 74.1 flowers under normal conditions and 91.6 and 84.8 flowers under heat-stress conditions, respectively. Raising the ambient temperature to 45°C during the growth period significantly increased the number of flowers on all tested plants. The number of flowers of WT-MT, *iaa9-3* and *iaa9-5* increased by 29.63%, 33.33% and 14.43%, respectively; under heat stress compared with those under normal condition (Figure 3).

3.4 Pollen viability decreased under heat-stress conditions

In the microscopic analysis of pollen viability, three groups, namely, viable, semi-viable and non-viable pollens were determined based on pollen viability level. Based on statistical data analysis, under normal conditions, the percentage of viable, semi-viable and non-viable pollens in the three genotypes of investigated plants did not show any significant difference. Among the three levels of the proportion of pollens, the group of viable pollens had the highest percentage compared with the semi-viable and non-viable pollen groups.

This study proved that the decrease in pollen viability occurred under heat-stress conditions. Raising the temperature up to 45°C significantly reduced the level of pollen viability in all investigated genotypes. The decrease in the percentage of viable pollen under

10.3389/fpls.2023.1090774

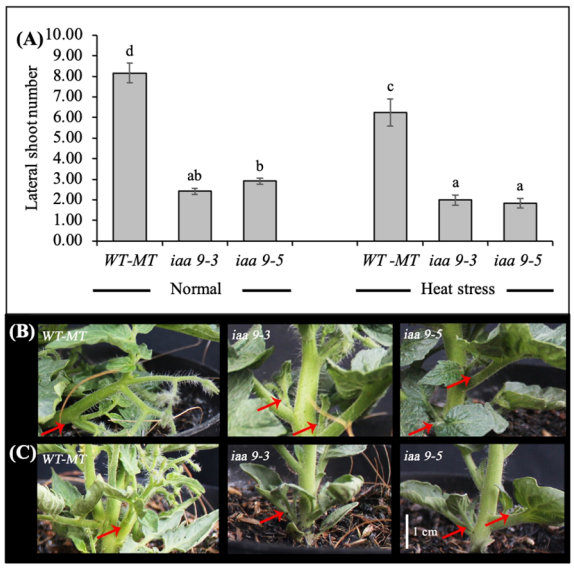

FIGURE 2
(A) The average value of lateral shoot number of WT-MT, *iaa9-3* and *iaa9-5* under two temperature conditions. The lateral shoot number of WT-MT, *iaa9-3* and *iaa9-5* under **(B)** normal temperature and **(C)** heat stress condition. The average value ± standard error (SE) (n = 4) followed by the same lowercase letters is not significantly different based on Duncan's Multiple Range Test at 5%.

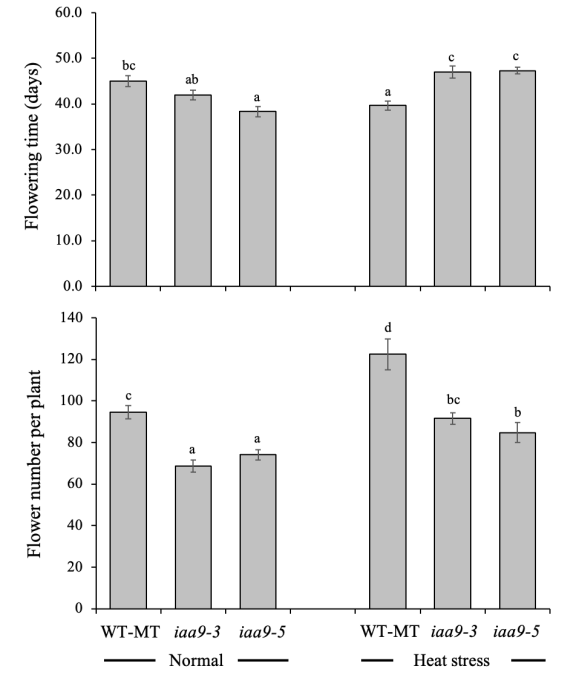

FIGURE 3
Flowering time and flower number per plant of WT-MT, *iaa9-3* and *iaa9-5* under two temperature conditions, i.e., normal temperature and heat stress condition. The average value ± standard error (SE) (n = 4) followed by the same lowercase letters is not significantly different based on Duncan's Multiple Range Test at 5%.

heat-stress conditions occurred in WT-MT, where the percentage of viable pollen decreased by almost 87.15% compared with that under normal condition. Mutations in the *IAA9* gene can prevent pollen damage under heat-stress condition, as indicated by the percentages of viable pollen in *iaa9-3* and *iaa9-5*, which reached 32.62% and 33.42%, respectively. The percentages decreased by 49.73% and 47.51%, respectively, compared with those under normal condition. The decrease in the number of viable pollens under heat-stress condition was caused by the increase in pollen sterility, which resulted in a very high number of non-viable pollens in WT-MT (67.57%) due to high temperature, and the decreases in *iaa9-3* and *iaa9-5* reached 32.97% and 32.56%, respectively (Figure 4B).

3.5 iaa9-3 and iaa9-5 can produce fruit under heat stress

The fruit set is the percentage ratio of the number of fruits and the number of flowers in the same individual plant. Statistical analysis showed that the fruit set in *iaa9-3* and *iaa9-5* was significantly higher than that in WT-MT under normal and heat-stress conditions (Figures 5A, B, respectively). Plant capacity to produce fruit also differed between normal and heat-stress conditions, irrespective of genotypes. Under normal conditions, the fruit sets of *iaa9-3* and *iaa9-5* were 81.24% and 64.89% or 21.57% and 5.22% higher than that of WT-MT, respectively. The percentage of fruit set from all tested plants decreased dramatically under the heat-stress condition at 45°C (Figure 5C). Under the heat-stress condition, WT-MT was unable to produce fruits, whereas *iaa9-3* and *iaa9-5* did. Thus, mutations in the *IAA9* gene can increase the percentage of fruit set in *iaa9-3* and *iaa9-5* compared with WT-MT under heat-stress conditions. Although both mutants can produce fruit sets under heat-stress conditions, the fruit set was lower compared with that in normal conditions. The fruit sets of *iaa9-3* and *iaa9-5* under heat-stress conditions were 34.98% and 32.84% or 46.26% and 32.05% lower than those under normal conditions, respectively (Figure 5C).

3.6 iaa9-3 and iaa9-5 can produce normal fruit size under heat stress

The number of fruits per plant, individual fruit weight and fruit diameter can be used as yield and yield quality variables of tomato fruit. Under the normal-temperature condition, all tested genotypes produced fruits. WT-MT plant produced the highest fruit number and significantly differed from the *iaa9-3* and *iaa9-5*. Under normal conditions, the number of fruits for WT-MT, *iaa9-3* and *iaa9-5* were 53.3, 47.8 and 46.8 fruits per plant, respectively. The heat condition affected the fruit yield of all investigated genotypes, with the lowest value detected in WT-MT. WT-MT had a small fruit size with no seed inside. However, *iaa9-3* and *iaa9-5* can still produce fruits under heat-stress condition, with the value being reduced compared with that under normal condition. Under heat condition,

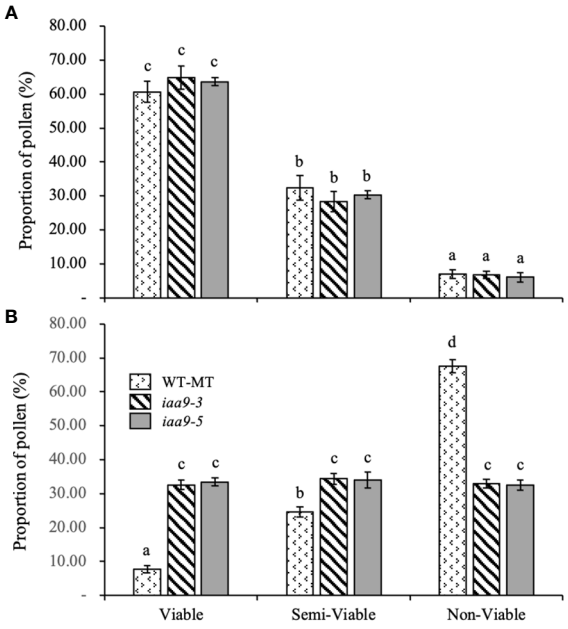

FIGURE 4
The proportion of pollen of WT-MT, *iaa9-3* and *iaa9-5* under two temperature conditions, i.e., **(A)** normal temperature and **(B)** heat stress condition. The average value ± standard error (SE) (n = 4) followed by the same lowercase letters is not significantly different based on Duncan's Multiple Range Test at 5%.

the reduction of fruit number varied compared to that in normal condition, i.e. 97.75%, 42.34% and 48.68% for WT-MT, *iaa9-3* and *iaa9-5*, respectively (Figure 6A).

Fruit size can be indicated by individual fruit weight, length and diameter. Under normal condition, *iaa9-3* and *iaa9-5* had a smaller fruit size, indicated by shorter fruit length and diameter and smaller fruit weight, compared with WT-MT. However, the fruit length of *iaa9-3* was comparable to that of WT-MT. Under the heat-stress condition, *iaa9-3* and *iaa9-5* resulted in a longer fruit length and higher fruit diameter compared with WT-MT (Figures 6B–D). Although *iaa9-3* and *iaa9-5* had a few fruit numbers under heat-stress condition, both mutants had a larger fruit size compared with that under normal condition. From the data obtained, Figure 6 indicate a positive relationship between fruit number and fruit size, where more fruits were produced (Figure 6A), which resulted in smaller fruit sizes and weights (Figures 6B–D). Statistical data analysis showed that the individual fruit weights of *iaa9-3* and *iaa9-5* were significantly smaller than those of WT-MT under normal condition. However, both mutants had significantly higher fruit weight than WT-MT under heat-stress condition (Figure 6B).

In all investigated plants, the number of seeds was highly affected by genetic factors and environmental conditions. Mutation in the *IAA9* gene had a significant effect on the number of seeds. Under normal conditions, *iaa9-3* and *iaa9-5* had lower numbers of seeds compared with WT-MT, with reductions of up to 55.82% and 37.73%, respectively (Figure 6E). Heat stress significantly reduced the number of seeds in all investigated plants. Under the heat-stress condition, although *iaa9-3* and *iaa9-5* resulted in a larger fruit size compared with that under normal conditions, both mutants and WT-MT cannot produce seeds because of the heat-stress condition (Figure 6E).

3.7 Mutation in the *IAA9 gene* significantly reduced H_2O_2 content but showed increased antioxidant activity

H_2O_2 content was analysed to predict the accumulation of reactive oxygen species (ROS) within their leaves as an effect of *IAA9* mutation under two different environmental conditions. Statistical data analysis showed that H_2O_2 content differed under various plant genotypes and environmental conditions. Under normal conditions, the H_2O_2 content was lower than that under heat-stress conditions in all plant genotypes. Mutation in the *IAA9* gene significantly reduced H_2O_2 content in *iaa9-3* and *iaa9-5* compared with WT-MT, with values of 0.44 and 1.90 μmol/g FW, respectively, which is lower than that of WT-MT

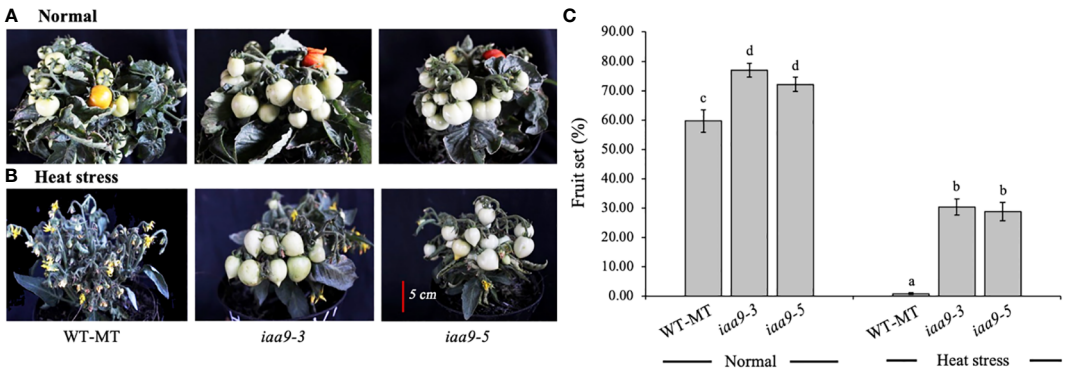

FIGURE 5
Fruit set of WT-MT, *iaa9-3* and *iaa9-5* under two temperature conditions, i.e., **(A)** normal temperature and **(B)** heat stress condition. **(C)** The average value of fruit set under normal temperature and heat stress conditions. The average value ± standard error (SE) (n = 4) followed by the same lowercase letters is not significantly different based on Duncan's Multiple Range Test at 5%.

10.3389/fpls.2023.1090774

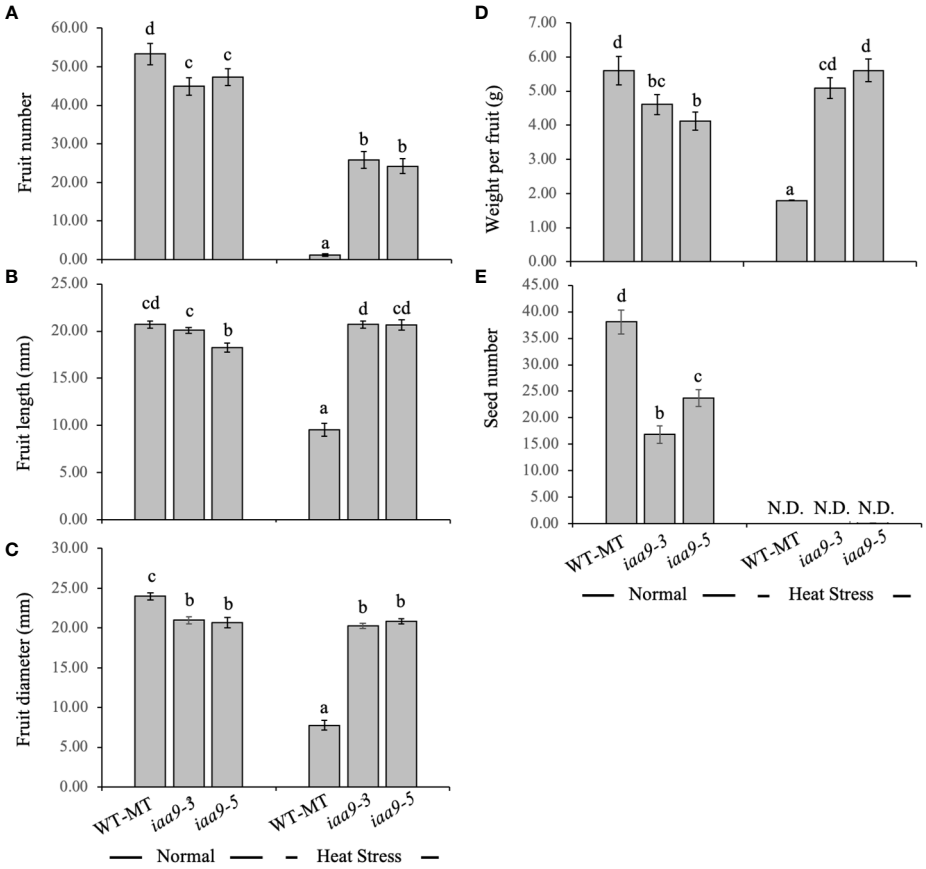

FIGURE 6
(A) Fruit number, **(B)** fruit length, **(C)** fruit diameter, **(D)** individual fruit weight, and **(E)** seed number of WT-MT, *iaa9-3* and *iaa9-5* under two temperature conditions, i.e., normal temperature and heat stress condition. The average value ± standard error (SE) (n = 4) followed by the same lowercase letters is not significantly different based on Duncan's Multiple Range Test at 5%.

(Figure 7A). Environmental conditions significantly affected the content of H_2O_2 in plants. The rise in temperature resulted in the increased H_2O_2 content in all investigated plants, but *iaa9-3* and *iaa9-5* showed a lower H_2O_2 content compared with WT-MT. WT-MT had a significantly higher H_2O_2 content than *iaa9-3* and *iaa9-5*, but it was comparable between *iaa9-3* and *iaa9-5*. The increase in H_2O_2 content under heat-stress conditions varied among genotypes, with values of 1.22, 0.56 and 1.82 µmol/g FW for WT-MT, *iaa9-3* and *iaa9-5*, respectively. These values were higher than those under normal conditions (Figure 7A).

Antioxidant activity values directly influence ROS accumulation in plants. Antioxidant activity varied among genotypes under normal

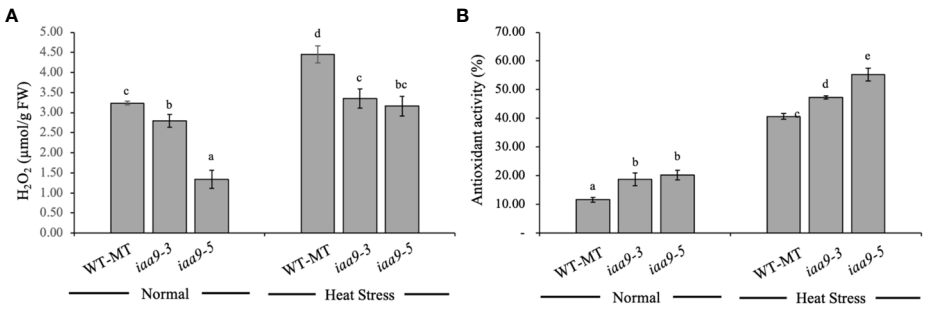

FIGURE 7
(A) H_2O_2 and **(B)** Antioxidant activity of WT-MT, *iaa9-3*, and *iaa9-5* leaves under two temperature conditions, normal temperature, and heat stress conditions. The average value ± standard error (SE) (n = 4) followed by the same lowercase letters is not significantly different based on Duncan's Multiple Range Test at 5%.

or heat-stress conditions. The statistical data analysis of antioxidant activity revealed a significant difference in antioxidant activity among genotypes under normal or heat-stress conditions (Figure 7). Under normal conditions, *iaa9-5* showed the highest leaf antioxidant activity, followed by *iaa9-3* whose value was significantly higher than that of WT-MT. A significant increase in antioxidant activity was detected when the plant was exposed to high temperatures or heat stress. Under heat-stress conditions, similar findings with normal conditions were observed. *iaa9-3* had the highest antioxidant activity, followed by *iaa9-3* and WT-MT, with increased antioxidant activities of 248.90%, 152.22% and 171.92% compared to the under normal conditions for WT-MT, *iaa9-3* and *iaa9-5*, respectively (Figure 7C).

4 Discussion

Tomato productivity is greatly affected by heat stress. Heat stress-induced male gametophyte abortion leads to fruit set reduction (Alsamir et al., 2021). The reduction of fruit set showed a consequence in reducing plant yield, which is a major problem in tomato production. The use of parthenocarpic tomatoes is an interesting approach to improving tomato production in heat-exposed locations, especially in the tropics. *iaa9-3* and *iaa9-5* resulted in a parthenocarpic tomato without any fertilisation process. Therefore, these tomatoes can be developed with a high-temperature characteristic for growing in the tropics. However, these mutants should be further evaluated to gain more information regarding their growth and development performances under heat-stress condition.

The diameter of the plant canopy is one of the plant growth variables that can show the response of plants to environmental conditions. Heat stress greatly affects plant growth, which can be characterised by a decline in vegetative growth, resulting in small plant size, such as the small canopy diameter observed compared with that under normal condition (Figure 1). Mutations in *iaa9-3* and *iaa9-5* resulted in smaller plant canopy diameters compared with that of WT-MT under normal or heat-stress conditions. The small number of lateral shoots produced caused the small diameter in the mutants. By contrast, the WT-MT compound leaf shape formed a longer leaf stalk and wider plant shape, resulting in a wider plant diameter (Figure 1). According to Valladares et al. (2007), the shape of a plant canopy is determined by the shape of leaves, lateral shoots and branching patterns. A high number of branching results in a wide plant canopy development.

The loss function of *IAA9* caused changes in the growth pattern of the shoot, which inhibited the growth of the lateral shoot. Inhibition of lateral shoot growth decreased the number of lateral shoots of *iaa9-3* and *iaa9-5* (Figure 2). Tezuka et al. (2011) stated that a high AUX level can inhibit lateral shoot regeneration in tomato plants. Wang et al. (2005) reported a contradictive study that the *AS-IAA9* plant showed decreased apical dominance. Heat stress also reduces plant growth by lowering plant stomatal conductance (Camejo et al., 2005). A low stomatal conductance reduces CO_2 fixation while increasing leaf temperature, resulting in reduced photosynthesis and more oxidative damage in leaf tissue (Hemantaranjan, 2014).

The *iaa9-3* and *iaa9-5* experienced lateral shoot growth reduction, which led to a decline in the number of flowers compared with that in WT-MT under normal and heat-stress conditions (Figures 2 and 3). Under normal conditions, the flowering times of *iaa9-3* and *iaa9-5* were shorter than that of WT-MT. Possibly, mutations in *iaa9-3* and *iaa9-5* sped up flowering. According to Cheng and Zhao (2007) AUX plays an important role in the initiation of flower primordia. The shoot apical meristem turns into a flowering meristem that can initiate the floral meristem, in which AUX plays a role in regulating the proliferation of flower meristematic cells (Merelo et al., 2022). The role of AUX in primordial formation was evidenced by the increase in AUX concentration at the primordial tip of the flower (Vanneste and Friml, 2009). Accelerated flowering in WT-MT under heat stress was caused by the shortened plant life cycle (Solankey et al., 2015), but mutation in the *IAA9* gene can slow down the flowering process.

The highest number of lateral shoots was identified in WT-MT, resulting in a higher number of flowers on WT-MT either in normal or heat-stress conditions. Apical meristem can transform either into vegetative organs, such as leaves or reproductive organs, such as flowers (Ohta, 2018). Lateral shoots at certain points on determinate tomatoes can form bunches as a growth site of flowers and fruit (Park et al., 2016). AUX is directly involved in the formation of axillary buds. With the mutation of the *IAA9* gene, the number of lateral shoots in *iaa9-3* and *iaa9-5* mutants and the number of flowers produced decreased. Heat stress treatment up to 45°C caused a significant increase in the number of flowers on all tested genotypes than those under normal conditions, with a higher number of flowers observed on WT-MT than on *iaa9-3* and *iaa9-5* (Figure 3). The increased number of flowers under heat stress was in accordance with the statement of Park et al. (2016), who stated that high temperatures can induce flower growth as a plant adaptation to maintain its generation.

Pollen viability is a crucial factor in determining the success of fruit formation. The results of this study showed that mutations in *iaa9-3* and *iaa9-5* can increase the number of viable and semi-viable pollens and reduce the number of non-viable pollens under normal temperature or heat stress. According to Aloni et al. (2006) endogenous AUX plays an important role in the growth of the pollen tube that will penetrate the ovule, as evidenced by the increased concentration of IAA in the pistil after pollination. Sakata et al. (2010) stated that the application of AUX can increase the anther length, prevent pollen abortion and improve the viability of mature pollens. AUX can block transcriptional changes, which result in normal pollen production and prevent pollen sterility under heat stress (Higashitani, 2013). According to Pan et al. (2019) IAA can increase the fresh weight of stamens and pistils in tomato flowers when exposed to heat stress. At temperatures of 40°C–45°C, WT-MT had the lowest number of viable and semi-viable pollen and the highest number of non-viable pollens compared with both mutants. Thus, WT-MT had the

highest potential for male sterility, which can affect fruit formation (Figure 4).

Tomato reproduction is extremely sensitive to heat stress. High temperatures can cause abortion of the male gametophyte, which leads to a reduction in fruit set. The increased fruit set in *iaa9-3* and *iaa9-5* under normal and heat-stress conditions was caused by the mutation in the *IAA9* gene. AUX synthesis can increase fruit set in tomato plants by preventing flowering and fruit fall (Batlang, 2008; Pramanik and P. Mohapatra, 2017). Mutations in the *IAA9* gene caused a reduction in the accumulation of mRNA, which triggered tomato fruit development before pollination, resulting in parthenocarpic fruit formation (Wang et al., 2005). AUX accumulation in the ovary vasculature and the micropylar pole of the ovule embryo sac for six days before anthesis was distributed to the ovule for two days before anthesis and finally localised to the interior and surface of the ovarian wall during anthesis (Pattison and Catalá, 2012). Under the heat-stress condition, WT-MT showed no ability to produce fruit (Figure 5) although it produced a large number of flowers (Figure 4). Solankey et al. (2015) stated that the rise in temperature affected the development of gametes and embryos and inhibited the ability of pollinated flowers to develop into seeds. Saito et al. (2011) stated that *iaa9-3* and *iaa9-5* are parthenocarpic tomato mutants with the ability to form fruit without fertilisation. Therefore, these tomatoes are very good candidates for tomato development in areas with the high-temperature condition that generally limits tomato productivity.

Both *iaa9-3* and *iaa9-5* can produce fruit without fertilisation due to a mutation in the *IAA9* gene under normal or heat-stress conditions. Heat stress caused a decrease in plant growth and development, which affected the yield, especially the number of fruits. Kumar et al. (2022) stated that exposure of plants to extreme temperatures limits their ability to produce fruit due to disruption of the pollination process. At normal temperatures, the number of fruits in both mutants was less than that in WT-MT. This finding was caused by the small number of flowers that formed in the mutants compared with WT-MT, which resulted in the formation of fewer fruits. Under the heat-stress condition, WT-MT did not produce fruits due to the failure of the fertilisation process as the effect of lowered pollen viability (Figure 4). Extremely high temperatures during the reproductive stage affect pollen viability, fertilisation and grain or fruit formation (Hatfield and Prueger, 2015). Non-viable pollens cannot pollinate flowers, causing failure in the fruit set (Sato et al., 2000). Meanwhile, *iaa9-3* and *iaa9-5* can produce fruits under heat stress. This result was due to the nature of the two tomatoes, which were parthenocarpic tomatoes, to form fruit without fertilisation (Ariizumi et al., 2013). The results showed that *iaa9-5* had the lowest fruit weight at normal temperatures. *IAA9* gene mutation in *iaa9-5* affected fruit weight due to genetic changes. Mutation locations in different alleles resulted in varied responses between *iaa9-3* and *iaa9-5*, such as fruit size and weight. Fruit weight was affected by the number of fruits on the plant. Under normal conditions, *iaa9-5* had a higher fruit number compared with that in heat-stress condition, but it had a lower fruit size (Figure 6). Burge et al. (1987) stated that fruit weight decreased with the increase in fruit number per vine in kiwifruit. A similar finding was reported by Puspitasari et al. (2014) who revealed that the more fruits produced, the less the individual fruit size.

IAA9 gene mutations in *iaa9-3* and *iaa9-5* caused a decrease in the number of seeds under normal conditions. This study was in line with the research of Liu et al. (2018) on *SlARF5-6* parthenocarpic transgenic tomato, which showed a high AUX response, resulting in a lower number of seeds compared with the WT. According to Takisawa et al. (2019) low seed production was attributed to two reasons, i.e. (1) formation of pseudo-embryo from the innermost layer of the embryo sac and (2) inhibition of pollen tube elongation. A few seeds that were found in both mutants at 40° C–45°C indicated that only a few viable pollens in both mutants can fertilise.

Heat stress increases ROS, such as H_2O_2, accumulation within plant tissues (Suzuki and Mittler, 2006). This continuous accumulation of ROS within plant tissues damages the cell plasma membrane (Dhanda and Munjal, 2009). In this study, *iaa9-3* and *iaa9-5* showed a lower H_2O_2 accumulation compared with WT-MT and higher antioxidant activities (Figures 7A, B). Antioxidants scavenge ROS and break it down into less radical compounds that are less harmful to plant cells (Moons, 2005). The higher antioxidant activity observed in *iaa9-3* and *iaa9-5* leaves was likely caused by the heightened AUX response in both *IAA9* mutants. Increased AUX concentration has been linked to increased antioxidant synthesis (Moons, 2005; Duan et al., 2010), DELLA protein stability (Paponov et al., 2008), and ethylene synthesis (Tognetti et al., 2012). AUX enhances antioxidant enzyme synthesis by activating the redox genes responsible for catalase, superoxide dismutase, guaiacol peroxidase, ascorbate peroxidase and glutathione-*S*-transferase synthesis (Tognetti et al., 2012; Sergiev et al., 2018).

In conclusion, the results showed that *iaa9-3* and *iaa9-5* exhibited a reduction in vegetative plant growth, delayed flowering time, increased number of flowers, ability to produce fruit and adaptability to heat-stress conditions. Thus, *iaa9-3* and *iaa9-5* can potentially contribute to breeding programs to generate new heat-tolerant commercial tomato cultivars.

Data availability statement

The raw data supporting the conclusions of this article will be made available by the authors, without undue reservation.

Author contributions

All authors listed have made a substantial, direct, and intellectual contribution to the work and approved it for publication.

Funding

We thank Universitas Padjadjaran, Indonesia, for supporting this work through a grant on the scheme of Indonesian Research Collaboration year 2022 with grant number 2203/UN6.3.1/PT.00/2022, and the APC was funded by Universitas Padjadjaran.

Acknowledgments

We also thank the National BioResearch Project (NBRP), MEXT, Japan, for providing the seeds of *S. lycopersicum* cv. Micro-Tom, *iaa9-3* and *iaa9-5*. We also thank all of the members of our laboratory for helpful discussions throughout the work.

Conflict of interest

The authors declare that the research was conducted in the absence of any commercial or financial relationships that could be construed as a potential conflict of interest.

Publisher's note

All claims expressed in this article are solely those of the authors and do not necessarily represent those of their affiliated organizations, or those of the publisher, the editors and the reviewers. Any product that may be evaluated in this article, or claim that may be made by its manufacturer, is not guaranteed or endorsed by the publisher.

References

Aloni, R., Aloni, E., Langhans, M., and Ullrich, C. I. (2006). Role of auxin in regulating arabidopsis flower development. *Planta* 223, 315–328. doi: 10.1007/s00425-005-0088-9

Alsamir, M., Mahmood, T., Trethowan, R., and Ahmad, N. (2021). An overview of heat stress in tomato (Solanum lycopersicum l.). *Saudi. J. Biol. Sci.* 28, 1654–1663. doi: 10.1016/j.sjbs.2020.11.088

Anas, A., Wiguna, G., Damayanti, F., Mubarok, S., Setyorini, D., and Ezura, H. (2022). Effect of ethylene *Sletr1-2* receptor allele on flowering, fruit phenotype, yield, and shelf-life of four F1 generations of tropical tomatoes (*Solanum lycopersicum* l.). *Horticulturae* 8, 1098. doi: 10.3390/horticulturae8121098

Ariizumi, T., Shinozaki, Y., and Ezura, H. (2013). Genes that influence yield in tomato. *Breed. Sci.* 63, 3–13. doi: 10.1270/jsbbs.63.3

Association of Official Analytical Chemists (1990). *Ofdicial methods of analysis*. (Gaithersburg, MD, USA: AOAC International).

Batlang, U. (2008). Benzyladenine plus gibberellins (GA4+7) increase fruit size and yield in greenhouse-grown hot pepper (Capsicum annuum l.). *J. Biol. Sci.* 8, 659–662. doi: 10.3923/jbs.2008.659.662

Burge, G. K., Spence, C. B., and Marshall, R. R. (1987). Kiwifruit: Effects of thinning on fruit size, vegetative growth, and return bloom. *New Z. J. Exp. Agric.* 15, 317–324. doi: 10.1080/03015521.1987.10425577

Camejo, D., Rodríguez, P., Angeles Morales, M., Miguel Dell'Amico, J., Torrecillas, A., and Alarcón, J. J. (2005). High temperature effects on photosynthetic activity of two tomato cultivars with different heat susceptibility. *J. Plant Physiol.* 162, 281–289. doi: 10.1016/j.jplph.2004.07.014

Cheng, Y., and Zhao, Y. (2007). A role for auxin in flower development. *J. Integr. Plant Biol.* 49, 99–104. doi: 10.1111/j.1744-7909.2006.00412.x

Dhanda, S., and Munjal, R. (2009). Cell membrane stability: Combining ability and gene effects under heat stress conditions. *Cereal Res. Commun.* 37, 409–417. doi: 10.1556/CRC.37.2009.3.10

Duan, Q., Kita, D., Li, C., Cheung, A. Y., and Wu, H.-M. (2010). FERONIA receptor-like kinase regulates RHO GTPase signaling of root hair development. *Proc. Natl. Acad. Sci.* 107, 17821–17826. doi: 10.1073/pnas.1005366107

Ezura, H., Hoshikawa, K., Fukumoto, S., Ooshima, S., and Mina, A. (2019). Heat-tolerant tomato mutant and method for producing the same.

Guilfoyle, T. J., and Hagen, G. (2007). Auxin response factors. *Curr. Opin. Plant Biol.* 10, 453–460. doi: 10.1016/j.pbi.2007.08.014

Hatfield, J. L., and Prueger, J. H. (2015). Temperature extremes: Effect on plant growth and development. *Weather. Clim. Extrem.* 10, 4–10. doi: 10.1016/j.wace.2015.08.001

Hemantaranjan, A. (2014). Heat stress responses and thermotolerance. *Adv. Plants Agric. Res.* 1, 1–10. doi: 10.15406/apar.2014.01.00012

Higashitani, A. (2013). High temperature injury and auxin biosynthesis in microsporogenesis. *Front. Plant Sci.* 4. doi: 10.3389/fpls.2013.00047

Iizuka, K., Yonehara, T., Itoh, M., and Kosugi, Y. (2017). Estimating tree height and diameter at breast height (DBH) from digital surface models and orthophotos obtained with an unmanned aerial system for a Japanese cypress (Chamaecyparis obtusa) forest. *Remote Sens. (Basel).* 10, 13. doi: 10.3390/rs10010013

Kumar, S., Thakur, M., Mitra, R., Basu, S., and Anand, A. (2022). Sugar metabolism during pre- and post-fertilization events in plants under high temperature stress. *Plant Cell Rep.* 41, 655–673. doi: 10.1007/s00299-021-02795-1

Liu, S., Zhang, Y., Feng, Q., Qin, L., Pan, C., Lamin-Samu, A. T., et al. (2018). Tomato AUXIN RESPONSE FACTOR 5 regulates fruit set and development *via* the mediation of auxin and gibberellin signaling. *Sci. Rep.* 8, 2971. doi: 10.1038/s41598-018-21315-y

Merelo, P., González-Cuadra, I., and Ferrándiz, C. (2022). A cellular analysis of meristem activity at the end of flowering points to cytokinin as a major regulator of proliferative arrest in arabidopsis. *Curr. Biol.* 32, 749–762.e3. doi: 10.1016/j.cub.2021.11.069

Moons, A. (2005). *Regulatory and functional interactions of plant growth regulators and plant glutathione s-transferases (GSTs)*. Vitamins & hormones 155–202. doi: 10.1016/S0083-6729(05)72005-7

Mubarok, S., Ezura, H., Qonit, M. A. H., Prayudha, E., Suwali, N., and Kurnia, D. (2019b). Alteration of nutritional and antioxidant level of ethylene receptor tomato mutants, Sletr1-1 and Sletr1-2. *Sci. Hortic.* 256, 108546. doi: 10.1016/j.scienta.2019.108546

Mubarok, S., Ezura, H., Rostini, N., Suminar, E., and Wiguna, G. (2019a). Impacts of Sletr1-1 and Sletr1-2 mutations on the hybrid seed quality of tomatoes. *J. Integr. Agric.* 18 (5), 1170–1176. doi: 10.1016/S2095-3119(19)62614-6

Mubarok, S., Hoshikawa, K., Okabe, Y., Yano, R., Tri, M. D., Ariizumi, T., et al. (2019c). Evidence of the functional role of the ethylene receptor genes *SlETR4* and *SlETR5* in ethylene signal transduction in tomato. *Mol. Genet. Genomics* 294, 301–313. doi: 10.1007/s00438-018-1505-7

Mubarok, S., Qonit, M. A. H., Rahmat, B. P. N., Budiarto, R., Suminar, E., and Nuraini, A. (2023). An overview of ethylene insensitive tomato mutants: Advantages and disadvantages for postharvest fruit shelf-life and future perspective. *Front. Plant Sci.* 14. doi: 10.3389/fpls.2023.1079052

Oboulbiga, E. B., Parkouda, C., Sawadogo-Lingani, H., Compaoré, E. W. R., Sakira, A. K., and Traoré, A. S. (2017). Nutritional composition, physical characteristics and sanitary quality of the tomato variety Mongol F1 from Burkina Faso. *Food Nutr. Sci.* 08, 444–455. doi: 10.4236/fns.2017.84030

Ohta, K. (2018). "Branch formation and yield by flower bud or shoot removal in tomato," in *Physical methods for stimulation of plant and mushroom development (InTech)*. doi: 10.5772/intechopen.71519

Pan, C., Yang, D., Zhao, X., Jiao, C., Yan, Y., Lamin-Samu, A. T., et al. (2019). Tomato stigma exsertion induced by high temperature is associated with the jasmonate signalling pathway. *Plant Cell Environ.* 42, 1205–1221. doi: 10.1111/pce.13444

Paponov, I. A., Paponov, M., Teale, W., Menges, M., Chakrabortee, S., Murray, J. A. H., et al. (2008). Comprehensive transcriptome analysis of auxin responses in arabidopsis. *Mol. Plant* 1, 321–337. doi: 10.1093/mp/ssm021

Park, H. J., Kim, W.-Y., Pardo, J. M., and Yun, D.-J. (2016). *Molecular interactions between flowering time and abiotic stress pathways*. 371–412. doi: 10.1016/bs.ircmb.2016.07.001

Pattison, R. J., and Catalá, C. (2012). Evaluating auxin distribution in tomato (Solanum lycopersicum) through an analysis of the PIN and AUX/LAX gene families. *Plant J.* 70, 585–598. doi: 10.1111/j.1365-313X.2011.04895.x

Pham, D., Hoshikawa, K., Fujita, S., Fukumoto, S., Hirai, T., Shinozaki, Y., et al. (2020). A tomato heat-tolerant mutant shows improved pollen fertility and fruit-setting under long-term ambient high temperature. *Environ. Exp. Bot.* 178, 104150. doi: 10.1016/j.envexpbot.2020.104150

Pramanik, K., and P. Mohapatra, ,. P. (2017). Role of auxin on growth, yield and quality of tomato - a review. *Int. J. Curr. Microbiol. Appl. Sci.* 6, 1624–1636. doi: 10.20546/ijcmas.2017.611.195

Puspitasari, Y. D., Aini, N., and Koesriharti, K. (2014). *Respon dua varietas tomat (Lycopersicon esculentum mill.) terhadap aplikasi zat pengatur tumbuh naphthalene acetic acid (Naa)*. Doctoral dissertation, Brawijaya University. Indonesia.

Rahmat, B. P. N., Octavianis, G., Budiarto, R., Jadid, N., Widiastuti, A., Matra, D. D., et al. (2023). SlIAA9 mutation maintains photosynthetic capabilities under heat-stress conditions. *Plants* 12, 378. doi: 10.3390/plants12020378

Saito, T., Ariizumi, T., Okabe, Y., Asamizu, E., Hiwasa-Tanase, K., Fukuda, N., et al. (2011). TOMATOMA: A novel tomato mutant database distributing micro-tom mutant collections. *Plant Cell Physiol.* 52, 283–296. doi: 10.1093/pcp/pcr004

Sakata, T., Oshino, T., Miura, S., Tomabechi, M., Tsunaga, Y., Higashitani, N., et al. (2010). Auxins reverse plant male sterility caused by high temperatures. *Proc. Natl. Acad. Sci.* 107, 8569–8574. doi: 10.1073/pnas.1000869107

Sami, F. J., and Rahimah, S. (2016). Uji aktivitas antioksidan ekstrak metanol bunga brokoli (*Brassica oleracea l. var. italica*) dengan metode DPPH (2,2 diphenyl-1-picrylhydrazyl) dan metode abts (2,2 azinobis (3-etilbenzotiazolin)-6-asam sulfonat). *Jurnal. Fitofarmaka. Indonesia.* 2, 107–110. doi: 10.33096/jffi.v2i2.179

Sato, S., Peet, M. M., and Thomas, J. F. (2000). Physiological factors limit fruit set of tomato (Lycopersicon esculentum mill.) under chronic, mild heat stress. *Plant Cell Environ.* 23, 719–726. doi: 10.1046/j.1365-3040.2000.00589.x

Sergiev, I., Todorova, D., Shopova, E., Jankauskienė, J., Jankovska-Bortkevič, E., and Jurkonienė, S. (2018). Effects of auxin analogues and heat stress on garden pea. *Zemdirbyste-Agriculture* 105, 243–248. doi: 10.13080/z-a.2018.105.031

Solankey, S. S., Singh, R. K., Baranwal, D. K., and Singh, D. K. (2015). Genetic expression of tomato for heat and drought stress tolerance: An overview. *Int. J. Vegetable. Sci.* 21, 496–515. doi: 10.1080/19315260.2014.902414

Suminar, E., Budiarto, R., Nuraini, A., Mubarok, S., and Ezura, H. (2022). Morpho-physiological responses of iaa9 tomato mutants to different levels of PEG simulated drought stress. *Biodivers. J. Biol. Diversity* 23 (6), 3115–3126. doi: 10.13057/biodiv/d230639

Suzuki, N., and Mittler, R. (2006). Reactive oxygen species and temperature stresses: A delicate balance between signaling and destruction. *Physiol. Plant* 126, 45–51. doi: 10.1111/j.0031-9317.2005.00582.x

Takisawa, R., Koeda, S., and Nakazaki, T. (2019). Effects of the <i<pat-2</i< gene and auxin biosynthesis inhibitor on seed production in parthenocarpic tomatoes (<i<Solanum lycopersicum</i< l.). *Hort. J.* 88, 481–487. doi: 10.2503/hortj.UTD-085

Tezuka, T., Harada, M., Johkan, M., Yamasaki, S., Tanaka, H., and Oda, M. (2011). Effects of auxin and cytokinin on *In vivo* adventitious shoot regeneration from decapitated tomato plants. *HortScience* 46, 1661–1665. doi: 10.21273/HORTSCI.46.12.1661

Tognetti, V. B., Mühlenbock, P., and van Breusegem, F. (2012). Stress homeostasis - the redox and auxin perspective. *Plant Cell Environ.* 35, 321–333. doi: 10.1111/j.1365-3040.2011.02324.x

Valladares, F., Gianoli, E., and Gómez, J. M. (2007). Ecological limits to plant phenotypic plasticity. *New Phytol.* 176, 749–763. doi: 10.1111/j.1469-8137.2007.02275.x

Vanneste, S., and Friml, J. (2009). Auxin: A trigger for change in plant development. *Cell* 136, 1005–1016. doi: 10.1016/j.cell.2009.03.001

Wang, H., Jones, B., Li, Z., Frasse, P., Delalande, C., Regad, F., et al. (2005). The tomato *Aux/IAA* transcription factor *IAA9* is involved in fruit development and leaf morphogenesis. *Plant Cell* 17, 2676–2692. doi: 10.1105/tpc.105.033415

frontiers | Frontiers in Plant Science

TYPE Original Research
PUBLISHED 14 April 2023
DOI 10.3389/fpls.2023.1125324

OPEN ACCESS

EDITED BY
Nianjun Teng,
Nanjing Agricultural University, China

REVIEWED BY
Dilek Ünal,
Bilecik Şeyh Edebali University, Türkiye
Tse-Min Lee,
National Sun Yat-sen University, Taiwan

*CORRESPONDENCE
Jianjun Cui
cuijianjun29@163.com
Enyi Xie
xieenyi@163.com

SPECIALTY SECTION
This article was submitted to Plant Abiotic Stress, a section of the journal Frontiers in Plant Science

RECEIVED 16 December 2022
ACCEPTED 28 March 2023
PUBLISHED 14 April 2023

CITATION
Huang Y, Cui J, Wang S, Chen X, Liao J, Guo Y, Xin R, Huang B and Xie E (2023) Transcriptome analysis reveals the molecular mechanisms of adaptation to high temperatures in *Gracilaria bailinae*. *Front. Plant Sci.* 14:1125324. doi: 10.3389/fpls.2023.1125324

Transcriptome analysis reveals the molecular mechanisms of adaptation to high temperatures in *Gracilaria bailinae*

Yongjian Huang, Jianjun Cui*, Sipan Wang, Xinyi Chen, Jiawei Liao, Youyou Guo, Rong Xin, Bowen Huang and Enyi Xie*

Fishery College, Guangdong Ocean University, Zhanjiang, China

Global warming causes great thermal stress to macroalgae and those species that can adapt to it are thought to be better able to cope with warmer oceans. *Gracilaria bailinae*, a macroalgae with high economic and ecological values, can survive through the hot summer in the South China Sea, but the molecular mechanisms underlying its adaptation to high temperatures are unclear. To address this issue, the present study analyzed the growth and transcriptome of *G. bailinae* after a 7-day exposure to 15°C (LT: low temperature), 25°C (MT: middle temperature), and 35°C (HT: high temperature). Growth analysis showed that the HT group had the highest relative growth rate (RGR = 2.1%) with the maximum photochemical quantum yield of PSII (F_v/F_m = 0.62) remaining within the normal range. Transcriptome analysis showed more differentially expressed genes (DEGs) in the comparison between MT and HT groups than in that between MT and LT, and most of these DEGs tended to be downregulated at higher temperatures. The KEGG pathway enrichment analysis showed that the DEGs were mainly enriched in the carbohydrate, energy, and lipid metabolisms. In addition, the genes involved in NADPH and ATP synthesis, which are associated with photosynthesis, the Calvin cycle, pyruvate metabolism, and the citrate cycle, were downregulated. Downregulation was also observed in genes that encode enzymes involved in fatty acid desaturation and alpha-linolenic acid metabolism. In summary, *G. bailinae* regulated the synthesis of NADPH and ATP, which are involved in the above-mentioned processes, to reduce unnecessary energy consumption, and limited the synthesis of enzymes in the metabolism of unsaturated fatty acids and alpha-linolenic acid to adapt to high environmental temperatures. The results of this study improve our understanding of the molecular mechanisms underlying the adaptation of *G. bailinae* to high temperatures.

KEYWORDS

heat-tolerance mechanism, gene regulation, *Gracilaria bailinae*, macroalgae, temperature, transcriptome

1 Introduction

Since the industrial revolution, increasing anthropogenic CO_2 and other greenhouse gas emissions have resulted in an energy imbalance on Earth; specifically, in a positive radiative imbalance at the highest atmospheric layers (Hansen et al., 2011; Von Schuckmann et al., 2016; Association, 2022). As a result, energy began to accumulate as heat in the Earth system, which is what ultimately drives global warming (Hansen et al., 2011; Von Schuckmann et al., 2016; Association, 2022). The global average temperature in 2021 was approximately 1.11 ± 0.13°C warmer than the pre-industrial average recorded between 1850 and 1900, and the 2015–2021 period has been the hottest on record (Association, 2022). Our oceans have absorbed over 90% of the energy accumulated in the Earth system through human-induced greenhouse gas emissions, causing a rise in ocean heat content, which in 2021 was the highest on record (Association, 2022). The Special Report published by the Intergovernmental Panel on Climate Change in 2019 also noted that the oceans have warmed unabated since 2005 (Bindoff et al., 2019). In addition, the frequency of marine heatwaves (MHWs) has increased during the past century, with potential consequences for marine organisms and the communities that depend on them (Smale et al., 2019). Between 1982 and 2020, the duration and frequency of MHWs in the South China Sea increased significantly (Yao and Wang, 2021). The continued warming of the oceans is having an enormous impact on macroalgae. One of the most crucial aspects affecting their dispersion is temperature, since it has an influence on their physiology, growth, and adaptation (Graba-Landry et al., 2018; Ji and Gao, 2021). Ocean warming hinders the growth of some tropical brown algae and subtropical macroalgae, forces tropical species to exist at their maximum temperature limit, and can even cause the entire macroalgal community to retreat (Wernberg et al., 2011; Koch et al., 2013; Bender et al., 2014; Graba-Landry et al., 2018; Ji and Gao, 2021). Increasing sea surface temperatures have already led to the loss of important habitat-forming kelp and macroalgae (Graba-Landry et al., 2018). If global warming persists, the distribution of certain seaweeds will change even more, and some might go extinct (Wernberg et al., 2011; Yao and Somero, 2014). It is thought that macroalgal species that can adapt to heat stress would do better in the increasingly warmer oceans (Ji and Gao, 2021).

The ability of plants to sense temperature stimuli, generate and transmit signals, and activate the proper morpho-anatomical, physiological, and molecular responses plays a vital role in their survival in hot environments (Hasanuzzaman et al., 2013; Zhang et al., 2020). Algae generally employ a variety of coping and repair mechanisms, including the regulation of photosynthesis to balance energy output and consumption, the modification of membrane fluidity by altering the degree of fatty acid saturation, the accumulation of compatible solutes to keep cell osmolality constant, and the activation of the enzymatic antioxidant system to remove excessive reactive oxygen species (Barati et al., 2019). RNA sequencing (RNA-seq) is a comprehensive technique for analyzing gene function and revealing the molecular mechanisms behind certain biological processes (Lim et al., 2016). This technique has steadily been employed in the study of macroalgae's molecular biology in recent years (Wang et al., 2015; Wenlei et al., 2018; Qin et al., 2021). For example, RNA-seq has been crucial in 1) tracking the expression of essential genes and critical metabolic processes in the growth and development of *Gracilariopsis lemaneiformis* (Wang et al., 2015; Qin et al., 2021), 2) investigating the molecular processes of *G. lemaneiformis'* reaction to low temperature environments (Qin et al., 2021), and 3) understanding *Pyropia haitanensis'* thermal adaptation to high temperatures (Wenlei et al., 2018).

Gracilaria bailinae is a red alga generally used for agar extraction, animal farming, and aquaculture water treatments (Elle et al., 2017; Xu et al., 2021). Specifically, this species has the potential to limit the spread of pathogenic *Vibrio*, reduce unionized ammonia, and promote the steady growth of advantageous phytoplankton (*Nannochloropsis* and *Chlorella*) (Elle et al., 2017). Additionally, due to its high agar yield of 29.8% dw (Skriptsova and Nabivailo, 2009), *G. bailinae* is greatly sought after for uses in the processed food, cosmetic, and pharmaceutical industries, and also in the fields of microbiology and molecular biology (Endoma et al., 2020). Preliminary studies found that *G. bailinae* can grow at a temperature range between 15 and 35°C and shows several traits associated with high-temperature tolerance (unpublished). Within the context of global warming, this species has a great potential for future applications as it can be farmed on a large scale all year round in tropical areas, continuously providing the raw materials for ecological restoration programs, sewage purification, agar and feed manufacturing, etc. However, the molecular mechanisms behind *G. bailinae's* reaction to high temperatures remain unknown. The present study specifically aims to reveal the mechanism of gene network regulation at the transcriptional level in *G. bailinae* subjected to extreme temperatures using the RNA-seq technique and combining the growth and physiological performances. The results obtained will not only provide a theoretical basis for understanding the molecular mechanisms of adaptation to high temperature in *G. bailinae*, but also guidance to breed temperature-tolerant seaweed species.

2 Materials and methods

2.1 Macroalgal samples and temperature treatments

Wild *G. bailinae* specimens were collected from Wushi (N 20° 33′, E 109°51′), Guangdong Province, China, in July 2021.The samples were brought back to the lab in a portable fridge at 4°C. Fresh algae were randomly selected and cleaned thoroughly using sterilized seawater. They were then temporarily cultivated in a tank filled with sterile seawater that had been enhanced with f/2 media at 25°C under a 12 L:12 D photoperiod and light intensity of 100 $\mu mol \cdot m^{-2} \cdot s^{-1}$. Three beakers containing 1 L of fresh sterile seawater enriched with f/2 medium were prepared and 3 g of healthy algae was added to each of them. The beakers were then transferred to incubators set at 15°C (LT: low temperature), 25°C (MT: middle

temperature), and 35°C (HT: high temperature) for 7 days. Three biological replicates were prepared per treatment and the medium was changed every 2 days. After 7 days of culture, the algae were used for growth and F_v/F_m measurements, as well as transcriptomic analysis.

2.2 Growth and F_v/F_m measurements

After the treatment, the fresh weight of *G. bailinae* was measured and the relative growth rate (RGR) was determined using the formula supplied by Yong (Yong et al., 2013):

$$RGR(\%\cdot d^{-1}) = \frac{ln\, M_7 - ln\, M_0}{7} \times 100\,\%$$

where M_0 represents the starting weight of the algae and M_7 represents their weight after the 7-day treatment.

The maximum photochemical quantum yield of PSII (F_v/F_m) was measured based on Li et al. (Li et al., 2016) after 7 days of treatment at different temperatures using a Hansatech FMS-2 modulated fluorometer (Hansatech Instruments, Norfolk, UK). The formula used was $F_v = F_m - F_0$; the minimum (F_0) and maximum (F_m) fluorescence were obtained by exposing algae that had adapted to darkness for 30 minutes to actinic light and saturated light provided by the fluorometer (Li et al., 2016).

2.3 Total RNA extraction, cDNA library construction, and transcriptome sequencing

Total RNA was isolated from *G. bailinae* using the Trizol reagent kit (Invitrogen, Carlsbad, CA, USA) in accordance with the manufacturer's instructions after 7 days of LT, MT, and HT treatments. An Agilent 2100 Bioanalyzer (Agilent Technologies, Palo Alto, CA, USA) was used to analyze the quality of total RNA and the results were validated *via* RNase-free agarose gel electrophoresis. Following total RNA extraction, Oligo (dT) beads were used to enrich *G. bailinae's* mRNA. Using random primers, the enriched mRNA was reverse transcribed into cDNA after being broken into small fragments by applying fragmentation buffer. Subsequently, DNA polymerase I, RNase H, dNTP, and buffer were used to create second-strand cDNA. Following purification with Qia Quick PCR extraction kit (Qiagen, Venlo, Netherlands), the cDNA fragments were ligated to the Illumina sequencing adapter after end repair and poly(A) addition. The ligation products were size selected *via* agarose gel electrophoresis, amplified *via* PCR, and then sequenced using Illumina NovaSeq 6000 (Gene Denovo Biotechnology Co., Guangzhou, China).

2.4 Analysis of the relationship between samples

Principal component analysis (PCA) was carried out using R (http://www.r-project.org/) on all nine transcriptome datasets to investigate variations in expression patterns between samples. The three duplicates of each temperature treatment were subjected to Pearson correlation analysis in order to evaluate the reproducibility of the transcriptome data.

2.5 Filtering of clean reads, *de novo* assembly, and annotation

The raw reads were trimmed by removing those containing adapters, more than 10% of unknown nucleotides, and more than 50% of low quality (Q-value ≤ 20) bases using fastp (version 0.18.0) (Chen et al., 2018). The transcriptome's *de novo* assembly was carried out using the short-read assembling program Trinity (Grabherr et al., 2011). BLASTx (http://www.ncbi.nlm.nih.gov/BLAST/) with an E-value threshold of 10^5 was used to compare transcripts to the NCBI non-redundant protein (Nr) database (http://www.ncbi.nlm.nih.gov), the Swiss-Prot protein database (http://www.expasy.ch/sprot), the Kyoto Encyclopedia of Genes and Genomes (KEGG) database (http://www.genome.jp/kegg), and the COG/KOG database (http://www.ncbi.nlm.nih.gov/COG), and annotate the unigenes. Protein function annotations were then obtained based on the best alignment results.

2.6 Analysis of differentially expressed genes

The differential expression analysis of RNAs between different groups and between samples was performed using DESeq2 (Love et al., 2014) and edgeR (Robinson et al., 2010) software, respectively. The genes with a parameter of false discovery rate (FDR) below 0.05 and absolute fold change ≥ 3 were considered DEGs.

2.7 Verification *via* real-time quantitative PCR

Nine genes associated with temperature changes were randomly selected from the transcriptome results to validate the transcriptome using the 18sRNA (Liu et al., 2021a) gene as a reference gene. The following reaction steps were adopted: 95°C for 300 s, followed by 45 cycles at 95°C for 10 s, 60°C for 15 s, 72°C for 15 s, and reading the fluorescence signal, followed by 1 cycle at 95°C for 10 s, 65°C for 60 s, and 95°C for 1 s. Each reaction was conducted in triplicate. Primer Premier 5.0 (Premier, Toronto, ON, Canada) was used to design each primer. The $2^{-\Delta\Delta Ct}$ (RQ) method was used to determine the relative transcript level (Qin et al., 2021). Primer sequences and qRT-PCR validation results are included in Supplementary Table S1.

2.8 Statistical analyses

The RGR and F_v/F_m data were expressed as means ± SD (n ≥ 3). The statistical significance of different treatments was assessed using

one-way ANOVA and Duncan's test in SPSS 25 (IBM Corp., Armonk, NY, USA) with a significance level of $P< 0.05$.

3 Results

3.1 Growth and F_v/F_m changes in *G. bailinae* under different temperatures

G. bailinae maintained a positive growth during the period of culture under the three different temperatures. The HT treatment (35°C) resulted in a maximum growth rate of 2.1%, which was significantly higher than the values obtained at 15°C and 25°C ($P< 0.01$); in particular, it was 15 times higher than that obtained at 15°C (0.14%) (Figure 1A). The F_v/F_m values at 25°C and 35°C were 0.65 and 0.62, respectively, which were significantly higher than the value at 15°C (0.36) ($P< 0.01$) (Figure 1B).

3.2 Data quality summary

The raw data obtained from the nine samples sequenced were subjected to quality control to obtain clean data (Supplementary Table S2). Out of a total of 494,707,094 reads 492,443,386 were retained after removing adapters and low-quality sequences. In each sample, the yield of clean reads was above 99%, the GC content was between 50.94% and 51.56%, and the Q20(%) value was above 98%. The clustering of the assembled transcripts of *G. bailinae* yielded a total of 20,049 single genes (> 200 base pairs) with an N50 count of 4,140 and a length of 1,072 base pairs. The size of single genes ranged from 201 to 8,602 base pairs, with an average length of 769 base pairs and a total length of 15,419,753 base pairs (Supplementary Table S3).

3.3 Evaluation of the reproducibility of data

The three duplicate samples in each treatment had Pearson correlation coefficients (r) of less than 0.96 (r > 0.80 indicates a strong correlation) (Supplementary Figure S1A). PCA showed that the expression patterns of *G. bailinae* differed under the three temperatures (Supplementary Figure S1B). Furthermore, qRT-PCR and mRNA-Seq analyses showed that nine randomly selected genes had a similar expression tendency (Supplementary Table S1).

3.4 Gene function annotation

At present, the whole-genome sequencing of *G. bailinae* has not been completed, therefore, only 20,049 gene transcript sequences were compared to the NCBI non-redundant protein databases Nr, Swiss-Prot, KEGG, and COG/KOG (evalue< 0.00001) using BLASTx. The proteins with the highest sequence similarity to the given unigene and its functional annotation information were obtained. In total, 20,049 genes were assembled from the transcriptome data in this study and 13,095 (65.31%) of them were compared to the four major databases. Of these 20,049 genes, 12,828 (63.98%), 5,246 (26.17%), 5,027 (25.07%), and 9,714 (48.45%) genes matched the Nr, KEGG, KOG, and GO databases, respectively.

In the Nr database, the main match obtained was *Gracilariopsis chorda* (84.82%), which belongs to the same genus as *G. bailinae*, in line with the taxonomic status distinction (Supplementary Figure S2). Cellular processes, environmental information processing, genetic information processing, metabolism, and organic systems were the five primary functional categories of the genes that matched the KEGG database. Each category was subdivided into secondary groups of functions. In particular, the largest number of unigenes were involved in "global and overview maps" (1,445), followed by "translation" (750) and "folding, sorting, and degradation" (409) (Supplementary Figure S3). The genes that matched the KOG database were divided into 25 groups: the largest was "translation, ribosomal structure and biogenesis" (781), followed by "general function prediction only" (701), and the smallest was "cell motility" (5) (Supplementary Figure S4). A total of 5,824 (29.05%) genes were matched to Swiss-Prot database. The number of genes matched in all databases was 4611 (23.00%) (Supplementary Figure S5).

Based on the Nr annotation information, Blast2GO was used to obtain the GO function annotations (Ashburner et al., 2000;

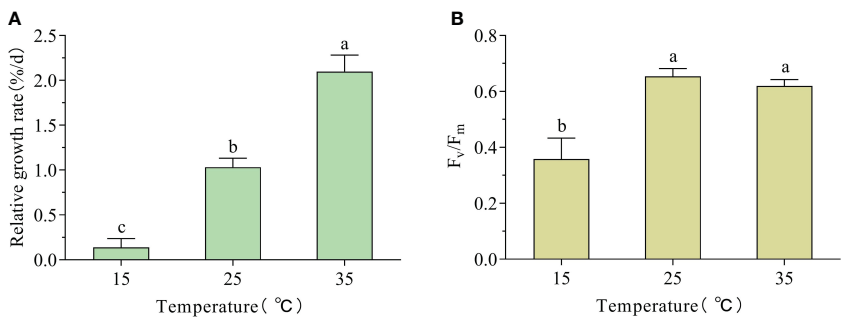

FIGURE 1
Relative growth rate (RGR) and F_v/F_m changes in *G. bailinae* exposed to different temperatures. **(A)** RGR. **(B)** Maximum photochemical quantum yield of PSII (F_v/F_m). Different small letters above the columns indicate a significant difference between different temperature treatments (P< 0.05).

Conesa et al., 2005). Three ontologies in GO were used to categorize the genes' molecular functions (MF), cellular components (CC), and biological processes (BP). The 9,714 unigenes annotated into the GO database by GO annotation were classified into 50 subclasses, accounting for 48.45% of all unigenes, and the same unigenes could be annotated to different subclasses. The top three subclasses of the GO ontologies were: cellular process, metabolic process, and localization with 6,637, 5,845, and 1,497, genes, respectively, for BP; cellular anatomical entity, protein-containing complex, and virion component, with 4,253, 1,958 and 110 genes, respectively, for CC; and catalytic activity, binding, and transporter activity, with 5,066, 4,771, and 802 genes, respectively, for MF (Supplementary Figure S6).

3.5 Analysis of DEGs

3.5.1 Overview of DEGs under stress

Two comparison groups, MT *vs* LT and MT *vs* HT, were established to investigate the variations in gene expression under different temperature treatments using log2(FC) ≥ 1.5 and FDR ≤ 0.05 as screening conditions. A total of 1,868 genes differentially expressed under different temperatures were identified: 1137 DEGs (389 upregulated and 748 downregulated) and 864 DEGs (466 up-regulated and 398 down-regulated) were identified in MT *vs* HT and MT *vs* LT, respectively (Figures 2A, B); 133 DEGs were co-regulated under LT and HT treatments (Figure 2D). In addition, to explore the gene expression patterns of *G. bailinae* under varying temperatures, a trend analysis of DEGs was performed for MT *vs* LT, and MT *vs* HT. All DEGs were clustered into eight trend profiles, and 1183 DEGs were significantly enriched in four of them, i.e., 3, 1, 0, and 7 ($P< 0.05$), which is shown in colored blocks in Figure 2C. Three of the four significantly enriched trends, i.e., about 80% of the significantly enriched DEGs in the trend analysis, showed a decrease with increasing temperature, while only one trend showed an increase with temperature.

3.5.2 GO classification and KEGG pathway analysis of DEGs in MT *vs* LT and MT *vs* HT

GO and KEGG analyses were conducted to examine the functions of DEGs. The GO classification results showed that DEGs were involved in three groups of functions, i.e., biological processes, molecular functions, and cellular components, and most genes were specifically classified as being involved in cellular processes (LT: 275, HT: 388), metabolic processes (LT: 241, HT: 344), and catalytic activity (LT: 200, HT: 311) both in MT *vs* LT and MT *vs* HT (Supplementary Figure S7). KEGG enrichment analysis indicated that DEGs were mainly enriched in four KEGG B classes: carbohydrate metabolism, energy metabolism, global and overview maps, and lipid metabolism (Supplementary Figure S8 and Table 1).

3.5.3 Effect of different temperatures on specific metabolic pathways

Based on the DEG analysis in KEGG, the following nine pathways related to the energy, carbohydrate, and lipid metabolisms were selected to investigate the specific effects of high and low temperatures on *G. bailinae*: photosynthesis (ko00195), photosynthesis-antenna proteins (ko00196), carbon fixation in photosynthetic organisms (ko00710), glycolysis/gluconeogenesis (ko00010), pentose phosphate pathway (PPP)

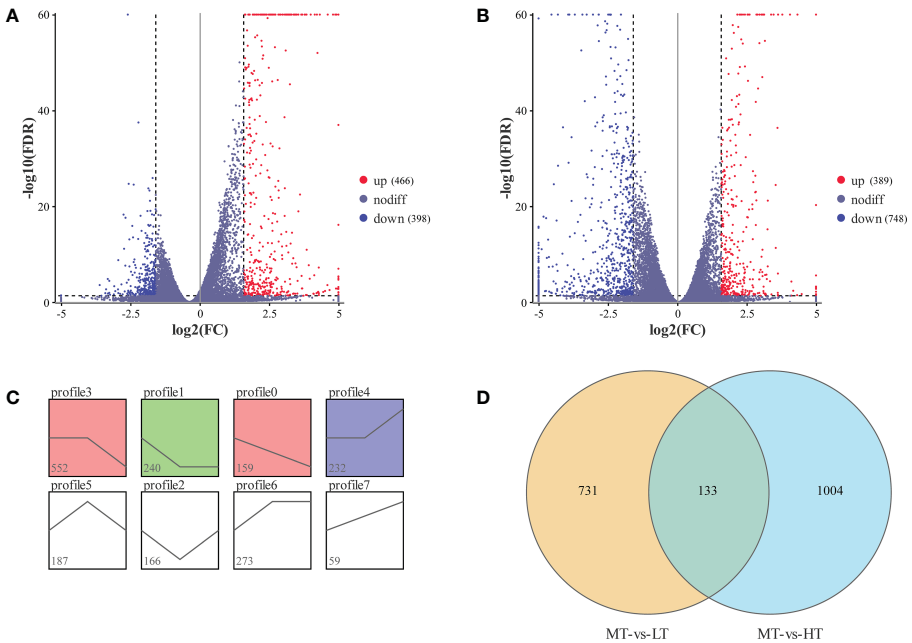

FIGURE 2
Overview of DEGs in *G. bailinae* exposed to different temperatures. **(A)** Volcano plots of the DEGs in MT *vs* LT. **(B)** Volcano plots of the DEGs in MT *vs* HT. **(C)** Trend analysis of DEGs in MT *vs* LT and MT *vs* HT. Significant enrichment trends are shown by colored blocks ($P< 0.05$). The bottom-left number represents the number of genes. **(D)** Venn diagram depicting the number of DEGs obtained in the MT *vs* LT and MT *vs* HT comparisons.

TABLE 1 Significantly enriched KEGG pathways in MT *vs* HT and MT *vs* LT.

Pathway ID	Pathway	KEGG_B_class	No. of DEGs	Pvalue
MT *vs* LT				
ko01200	Carbon metabolism	Global and overview maps	20	7.28E-04
ko00196	Photosynthesis - antenna proteins	Energy metabolism	7	1.07E-03
ko00520	Amino sugar and nucleotide sugar metabolism	Carbohydrate metabolism	7	1.25E-03
ko01040	Biosynthesis of unsaturated fatty acids	Lipid metabolism	4	3.50E-03
ko01100	Metabolic pathways	Global and overview maps	74	3.71E-03
ko00785	Lipoic acid metabolism	Metabolism of cofactors and vitamins	2	9.72E-03
ko01110	Biosynthesis of secondary metabolites	Global and overview maps	40	1.32E-02
ko02010	ABC transporters	Membrane transport	4	2.37E-02
ko00051	Fructose and mannose metabolism	Carbohydrate metabolism	5	2.83E-02
ko00592	alpha-Linolenic acid metabolism	Lipid metabolism	2	3.13E-02
ko00260	Glycine, serine and threonine metabolism	Amino acid metabolism	6	3.39E-02
ko00710	Carbon fixation in photosynthetic organisms	Energy metabolism	7	3.43E-02
ko00630	Glyoxylate and dicarboxylate metabolism	Carbohydrate metabolism	7	3.89E-02
ko00562	Inositol phosphate metabolism	Carbohydrate metabolism	4	4.58E-02
MT *vs* HT				
ko01100	Metabolic pathways	Global and overview maps	124	3.93E-06
ko00195	Photosynthesis	Energy metabolism	17	1.22E-05
ko03010	Ribosome	Translation	43	4.28E-04
ko00450	Selenocompound metabolism	Metabolism of other amino acids	7	8.26E-04
ko00710	Carbon fixation in photosynthetic organisms	Energy metabolism	13	9.64E-04
ko04712	Circadian rhythm - plant	Environmental adaptation	3	1.75E-02
ko00051	Fructose and mannose metabolism	Carbohydrate metabolism	7	1.79E-02
ko01200	Carbon metabolism	Global and overview maps	23	1.89E-02
ko00030	Pentose phosphate pathway	Carbohydrate metabolism	8	2.06E-02
ko00010	Glycolysis/Gluconeogenesis	Carbohydrate metabolism	13	2.28E-02
ko00190	Oxidative phosphorylation	Energy metabolism	17	2.77E-02
ko00196	Photosynthesis - antenna proteins	Energy metabolism	6	4.39E-02

(ko00030), pyruvate metabolism (ko00620), citrate cycle (TCA cycle) (ko00020), biosynthesis of unsaturated fatty acids (ko01040), and alpha-linolenic acid metabolism (ko00592).

3.5.3.1 Pathways related to photosynthesis

Comparative transcriptome analysis identified 17 DEGs involved in photosynthesis, which participated in the formation of PS II (psaA, psaB, psaD, psaH), PS I (psbB, psbC, psbD, psbO, psbV), the cytochrome b6/f complex (petB), F-type ATPase (atpA, atpG), and photosynthetic electron transport (petH, petJ) (Figure 3). All these DEGs were significantly downregulated in MT *vs* HT, while only one significantly downregulated gene (petB) was enriched in MT *vs* LT. In addition, the analysis identified 10 DEGs associated with photosynthetic antenna proteins and involved in the synthesis of allophycocyanin beta subunit (apcB), phycocyanobilin lyase subunit alpha (cpcE), and light-harvesting complex I chlorophyll a/b binding proteins 1, 2, and 4 (LHCA1, LHCB2, and LHCB4). Most of these DEGs were upregulated in LT and HT treatments, and only three related to LHCB2, apcB, and cpcE were significantly downregulated in MT *vs* HT.

3.5.3.2 Pathways related to carbohydrate and energy metabolism

Transcriptome analysis showed that DEGs were significantly enriched in the pathways related to carbohydrate and energy metabolisms and played a role in the response to temperature changes in *G. bailinae*. The NADPH and ATP produced by photosynthesis can be used for carbon dioxide fixation

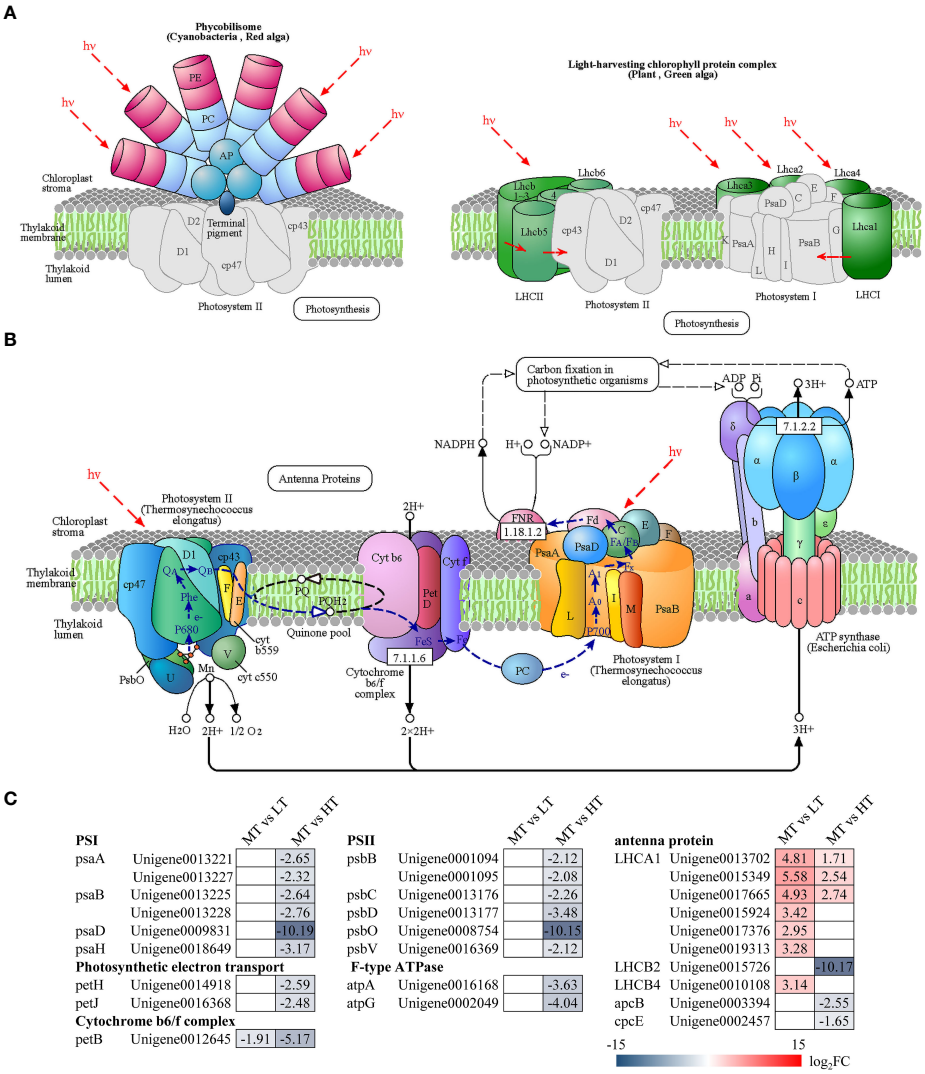

FIGURE 3
Pathways of photosynthesis and photosynthetic antenna proteins: **(A)** photosynthetic antenna protein pathway (ko00196), **(B)** photosynthesis pathway (ko00195), **(C)** DEGs involved in photosynthesis and photosynthetic antenna proteins. The number in each cell is the log2 fold change (log2FC). Red and blue gradients indicate the upregulation and downregulation of unigenes, respectively, while the white color represents log2FC< 1.5 or FDR > 0.05. The diagrams of photosynthesis and photosynthetic antenna proteins were obtained from the KEGG website.

(Figure 3B). A total of 11 DEGs were significantly enriched in the pathway of carbon fixation in photosynthetic organisms (Calvin cycle), encoding ALDO, E3.1.3.37, rbcS, FBP, FBA, rpe, TPI, and GAPA. Most of the genes involved in this pathway were significantly downregulated under the HT treatment, while the opposite was observed under the LT treatment (Figure 4). In addition, it is worth noting that the gene encoding rbcS was significantly downregulated under both treatments, which may be associated with different temperature response mechanisms.

The intermediate products synthesized by the Calvin cycle, i.e., propyl phosphates (glyceraldehyde phosphate and dihydroxyacetone phosphate), can be further used in the glycolysis/glycogenesis pathway to synthesize sucrose and starch, enter the TCA cycle to produce energy, or flow to PPP to produce NADPH. In MT *vs* HT, 15 DEGs were significantly enriched in the above pathways, encoding ALDO, FBA, TPI, FBP, GPI, ENO, IDH3, ACLY, rpe, PDHB, and DLAT. Most of the DEGs were downregulated under the HT treatment, and only one DEG encoding GPI was upregulated (Figure 4). In MT *vs* LT, a total of 10 DEGs were significantly enriched in the glycolysis/gluconeogenesis, PPP, TCA cycle, and pyruvate metabolism pathways, encoding ALDO, TPI, GPI, ENO, MDH1, SDHB, DLST, FH, rpe, and tal. Specifically, the DEGs encoding ENO, DLST, and FH were significantly downregulated, while the remaining seven DEGs were significantly upregulated.

3.5.3.3 Analysis of pathways related to lipid metabolism

Transcriptome analysis revealed that temperature induced the differential expression of genes related to lipid metabolism, especially those involved in the biosynthesis of unsaturated fatty acids and alpha-linolenic acid metabolism. Four DEGs encoding desaturation-

10.3389/fpls.2023.1125324

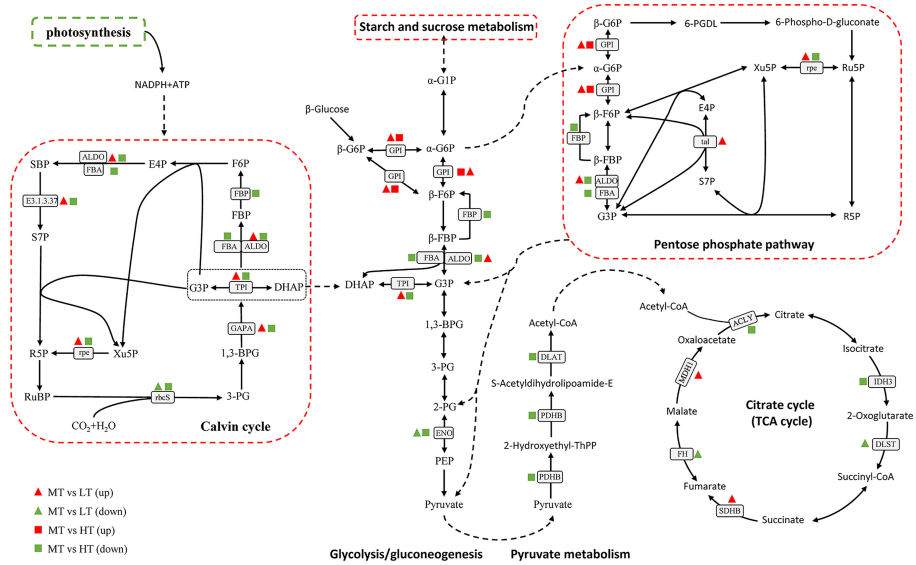

Reactants or products are abbreviated as follows:

1,3-BPG: 1,3-Bisphospho-D-glycerate
2-PG: D-Glycerate 2-phosphate
3-PG: D-Glycerate 3-phosphate
6-PGDL: D-Glucono-1, 5-lactone 6-phosphate
DHAP: Dihydroxyacetone phosphate
E4P: D-Erythrose 4-phosphate
F6P: D-Fructose 6-phosphate
FBP: D-Fructose 1,6-bisphosphate
G1P: D-Glucose 1-phosphate
G3P: D-Glyceraldehyde 3-phosphate
G6P: alpha-D-Glucose 6-phosphate
PEP: Phosphoenolpyruvate
R5P: D-Ribose 5-phosphate
Ru5P: D-Ribulose 5-phosphate
RuBP: D-Ribulose 1,5-bisphosphate
S7P: D-Sedoheptulose 7-phosphate
SBP: D-Sedoheptulose 1,7-bisphosphate
Xu5P: D-Xylulose 5-phosphate

Each enzyme is abbreviated as follows:

ACLY: ATP citrate (pro-S)-lyase [EC:2.3.3.8]
ALDO: fructose-bisphosphate aldolase, class I [EC:4.1.2.13]
BP: fructose-1,6-bisphosphatase I [EC:3.1.3.11]
DLST: 2-oxoglutarate dehydrogenase E2 component (dihydrolipoamide succinyltransferase) [EC:2.3.1.61]
E3.1.3.37: sedoheptulose-bisphosphatase [EC:3.1.3.37]
ENO: enolase [EC:4.2.1.11]
FBA: fructose-bisphosphate aldolase, class II [EC:4.1.2.13]
FDLAT: pyruvate dehydrogenase E2 component (dihydrolipoamide acetyltransferase) [EC:2.3.1.12]
FH: fumarate hydratase, class II [EC:4.2.1.2]
GAPA: glyceraldehyde-3-phosphate dehydrogenase (NADP+) (phosphorylating) [EC:1.2.1.13]
GPI: glucose-6-phosphate isomerase [EC:5.3.1.9]
IDH3: isocitrate dehydrogenase (NAD+) [EC:1.1.1.41]
MDH1: malate dehydrogenase [EC:1.1.1.37]
PDHB: pyruvate dehydrogenase E1 component beta subunit [EC:1.2.4.1]
rbcS: ribulose-bisphosphate carboxylase small chain [EC:4.1.1.39]
rpe: ribulose-phosphate 3-epimerase [EC:5.1.3.1]
SDHB: succinate dehydrogenase (ubiquinone) iron-sulfur subunit [EC:1.3.5.1]
tal: transaldolase [EC:2.2.1.2]
TPI: triosephosphate isomerase (TIM) [EC:5.3.1.1]

FIGURE 4
Pathways of carbon fixation in photosynthetic organisms, glycolysis/gluconeogenesis, pyruvate metabolism, pentose phosphate, and citrate cycle (TCA cycle). Detailed descriptions of the DEGs are included in Supplementary Table S4.

related enzymes (SCD) and chain extension-related enzymes (KAR) in the biosynthesis of unsaturated fatty acids were significantly differentially expressed in different comparison groups. Both SCD and KAR were upregulated under the LT treatment, while only SCD was downregulated under the HT treatment (Figure 5).

Figure 6 shows the effect of temperature on the metabolism of alpha-linolenic acid in *G. bailinae*. Phosphatidylcholine in the plastid membrane is oxidized by lipase to form alpha-linolenic acid, which then undergoes a series of oxidations to form oxo-phytodienoic acid (OPDA) in the plastid. Then, OPDA enters the peroxisomes through the ABC transporter and forms (+)-7-iso-jasmonic acid after reduction and 3-step β-oxidation. In the present study, three DEGs encoding acyl-CoA oxidase (ACX) and 12-oxophytodienoic acid reductase (SCD) were significantly activated after the LT and HT treatments. Under HT, only SCD was significantly downregulated, while under LT both ACX and SCD were significantly upregulated.

4 Discussion

As ocean warming continues to increase, there are inevitable consequences for the survival of macroalgae; however, species that can adapt to heat stress are better prepared to cope with the warmer conditions (Ji and Gao, 2021; Association, 2022). The present study found that the optimum growth state of *G. bailinae* was at 35°C. Based on this observation, transcriptomic analysis was first conducted to reveal the mechanism behind the adaptability of this macroalgae to high temperatures. The results of RNA-seq analysis showed that the process is associated with the regulation of the energy, carbohydrate, and lipid metabolism.

4.1 Growth and F_v/F_m response to temperature changes

Macroalgae are expected to be especially sensitive to ocean warming since the rates of their biochemical and physiological processes are substantially regulated by ambient temperature (as observed in ectotherms) (Davison, 1991; Brown et al., 2004; Graba-Landry et al., 2018). Typically, within a species' thermal tolerance range, the rates of physiological processes and other parameters (e.g., growth) increase with temperature until they reach a thermal optimum and rapidly decline thereafter (Brown et al., 2004; Graba-Landry et al., 2018). Different algae show different adaptations to temperature variation, and growth rate is an important indicator that visually reflects their growth status (Yang et al., 2021; Gao et al.,

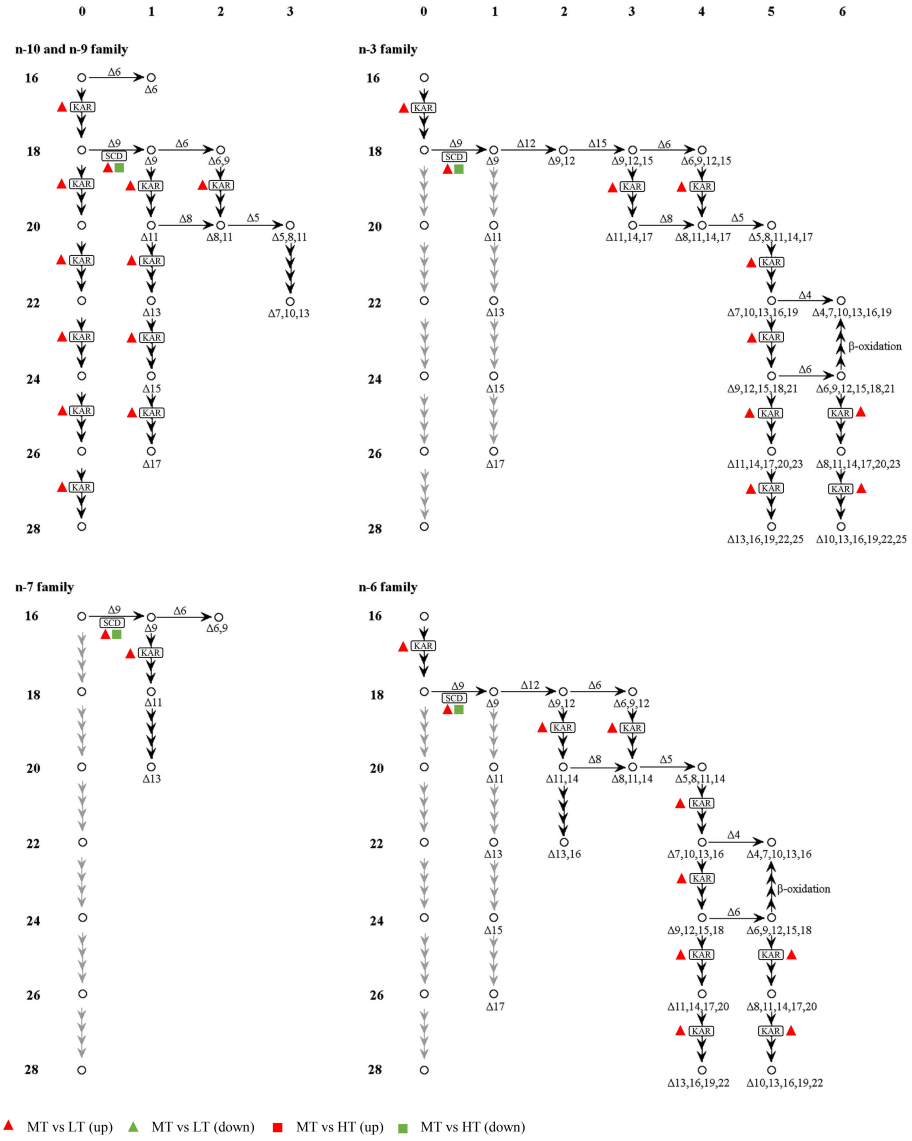

FIGURE 5
Pathways of biosynthesis of unsaturated fatty acids. The left side and top of the figure show the number of carbon atoms (16~28), and number of double bonds (1~6), respectively. The detailed descriptions of the DEGs are included in Supplementary Table S4.

2022): the highest growth rate is recorded at the optimum growth temperature. For example, the highest growth rate of *G. lemaneiformis* (Liu et al., 2017), *Ulva prolifera* (Cui et al., 2015), and *Caulerpa sertularioides* (Zhong et al., 2021) was observed at 23°C, 20°C, and 26°C, respectively. In the present study, the RGR of *G. bailinae* reached its maximum at 35°C and growth was significantly inhibited under the lower temperatures tested. F_v/F_m is the maximum photochemical quantum yield of PSII, which reflects the potential maximum photosynthetic capacity of macroalgae and can also indirectly reflect their growth state and living environment (Goltsev et al., 2016; Cui et al., 2019; Zhong et al., 2021). Studies have indicated that F_v/F_m is a heat-sensitive indicator, which makes it an important tool for the evaluation of plants' heat tolerance (Yamada et al., 1996; Wahid et al., 2007; Wu et al., 2019). For example, in *G. lemaneiformis*, this parameter was shown to decrease under unsuitable temperatures (Liu et al., 2017). A notable drop in F_v/F_m was also observed in *Saccharina japonica* under high temperature stress, which was caused by the deactivation of PSII (Shindo et al., 2022). In the present study, the analysis of F_v/F_m in *G. bailinae* indicated that 25°C and 35°C were suitable temperatures, but the parameter decreased significantly at 15°C. Obviously, the changes in RGR and F_v/F_m under different temperatures indicate that *G. bailinae* has a remarkable capacity to adapt to high temperatures.

4.2 Effect of temperature on photosynthesis

It has long been acknowledged that plant photosynthesis is one of the most temperature-sensitive processes (Li et al., 2019). This process depends on electron transport into the photosynthetic system and it gives algae the energy they need to grow and develop

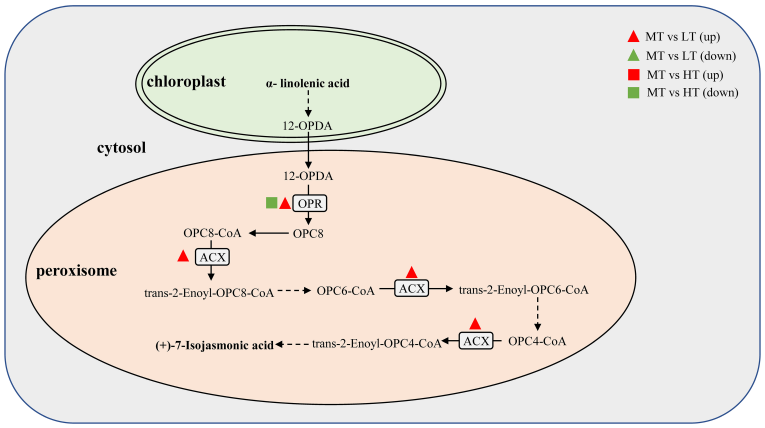

FIGURE 6
Pathways of the alpha-linolenic acid metabolism. The solid and dashed arrows indicate one-step and multi-step processes, respectively. The detailed descriptions of the DEGs are included in Supplementary Table S4.

(Qin et al., 2021). In the cells of red algae, light energy absorbed by the phycobillisome and the light-harvesting chlorophyll protein complex (LHC) drives the flow of electrons from H_2O to $NADP^+$, which promotes the reduction of $NADP^+$ to NADPH (Croce and Van Amerongen, 2014). At the same time, ATP synthase uses the electrochemical gradient generated simultaneously across the thylakoid membrane for ATP synthesis (Croce and Van Amerongen, 2014). NADPH and ATP represent the basis for all subsequent chemical reactions (Croce and Van Amerongen, 2014). Algae can regulate the above processes by controlling gene expression to resist or adapt to environmental changes, that is, regulating the synthesis of NADPH and ATP. Wang et al. (2018) reported that the protein-related genes of the photosynthetic antenna in wild-type *P. haitanensis* were significantly downregulated under high temperature stress, impeding the absorption of sufficient light to activate photosynthesis, and therefore resulting in insufficient energy to resist heat stress (Wang et al., 2018). Another study on *Amphiroa fragilissima* revealed that the expression levels of several DEGs involved in photosynthesis were suppressed under high temperature stress compared to those in the control group (Yang et al., 2021). However, in the present study, the photosynthetic activity of *G. bailinae* remained normal despite the downregulation of photosynthesis-related genes, which was not in line with the results of the above-mentioned studies. The downregulation of genes in most heat-sensitive algae under temperature stress may lead to fatal results, but *G. bailinae* has a high temperature adaptability, and 35°C is its suitable growth temperature. A study on the high-temperature tolerant *P. haitanensis* showed that this species can reduce unnecessary energy consumption by decreasing the rate of photosynthesis and energy metabolism (Wenlei et al., 2018). A proteomic analysis similarly indicated that the *P. haitanensis* strain Z-61 resists high temperature stress by downregulating photosynthesis (Xu et al., 2014). Similarly, *G. bailinae* regulates NADPH and ATP synthesis by downregulating photosynthesis-related genes to decrease the electron transfer rate and H^+ production in the photosynthetic system, thereby potentially reducing unnecessary energy consumption and ultimately adapting to high temperature environments. In addition, as observed for the compensatory reaction of gene expression (Dal Bosco et al., 2004), the high expression of LHCA1-related genes in photosynthetic antenna proteins may compensate for the decreased light capture efficiency caused by the downregulation of genes related to LHCB2, apcB, and cpcE, so as to meet the light energy demand of *G. bailinae* and achieve a higher growth rate.

4.3 Effect of temperature on carbohydrate and energy metabolisms

In plants, a metabolic regulatory network is frequently engaged in the response to abiotic stimuli (Wenlei et al., 2018). Previous studies have shown that *P. haitanensis* under stress can reduce unnecessary energy consumption to prevent cell damage (Xu et al., 2014; Xu et al., 2016). However, when stress levels become excessive, the corresponding energy shortage in algae would result in an enhancement of the inherent pathways of carbohydrate metabolism and the induction of alternative pathways, such as glycolysis, to provide energy and the related carbon skeletons for key metabolic processes (Obata and Fernie, 2012; Wenlei et al., 2018). Wang et al. (Wang et al., 2018) corroborated this claim by studying the heat-tolerant *P. haitanensis*, whose genes showed a tendency to be upregulated under high temperature stress to maintain the energy and associated carbon skeleton for key metabolic processes. In the present study, a joint analysis was performed for the following five pathways related to the carbohydrate and energy metabolisms: Calvin cycle, glycolysis/gluconeogenesis, PPP, pyruvate metabolism, and TCA cycle. In our study, we found that only the DEG encoding GPI was significantly upregulated under HT treatment, while other DEGs enriched in these pathways were downregulated (Figure 4). The accumulation of sugar phosphates associated with glycolysis and the oxidative pentose phosphate pathway (OPPP) indicated that glycolytic carbon flow may be rerouted into the OPPP to produce NADPH for antioxidative action (Obata and Fernie, 2012; Wenlei

et al., 2018). GPI catalyzes the interconversion between F6P and G6P. Further oxidation of G6P in the PPP can produce a large amount of NADPH, which may be one of the remedies for the decrease in NADPH synthesis during photosynthesis. The Calvin cycle, which comprises 13 chemical steps and 11 enzymes that catalyze them, is the main mechanism for carbon fixation in C3 plants (Tamoi et al., 2005). The cycle converts atmospheric CO_2 into carbon skeletons that are utilized to produce starch and sucrose using the byproducts of the light reactions of photosynthesis (i.e., ATP and NADPH) (Raines, 2003). Gene downregulation during the Calvin cycle is generally thought to lead to a reduced synthesis of related enzyme proteins, especially the key protein Rubisco. However, in this study, the expression of genes related to the Rubisco small subunit rbcS was downregulated under HT treatment, but the biomass of *G. bailinae* was relatively high. Related research shows that Rubisco activase induced the activation of Rubisco, but the synthesis of this protein (transcription and translation) and enzyme had different sensitivities to long-term heat stress (Almeselmani et al., 2012). Therefore, due to the adaptability of *G. bailinae* to high temperatures, Rubisco activase may activate Rubisco more obviously under high temperature conditions, thereby improving the carbon sequestration efficiency of the protein and reducing its absolute content during the Calvin cycle. However, further studies are needed to confirm this. The TCA cycle promotes the oxidation of respiratory substrates for ATP generation, and therefore plays a crucial role in plant resistance to abiotic challenges (Sweetlove et al., 2010; Obata and Fernie, 2012; Wenlei et al., 2018). It is worth noting that the genes encoding ACLY and IDH3 were significantly downregulated in the TCA cycle. IDH3 catalyzes the conversion of isocitrate to alpha-ketoglutarate to produce NADH. The downregulation of IDH3 indicated that *G. bailinae* adapts to high temperatures by reducing unnecessary energy consumption. In addition, the downregulation of other genes in the Calvin cycle, glycolysis/gluconeogenesis, and pyruvate metabolism pathways also indicated that *G. bailinae* slows the rate of energy or carbohydrate metabolisms to adapt to high temperatures. On the contrary, under low temperature stress, due to energy shortage, this macroalgae needs to produce more energy by overexpressing genes associated with the synthesis of energy molecules, such as MDH1 and SDHB, to maintain the key life activities of cells.

4.4 Effect of temperature on lipid metabolism

In response to temperature stress, plants typically control the percentage of polyunsaturated fatty acids to alter membrane fluidity (Sun et al., 2015). Two aspects are involved in the production of unsaturated fatty acids: fatty acid peptide chain extension and desaturation (Qin et al., 2021). Fatty acids, which are the major components of membrane phospholipids, induce desaturation to promote cell membrane fluidity and stability, hence minimizing cellular damage (Qin et al., 2021). Transcriptome analysis of *G. lemaneiformis* revealed that the expression levels of genes associated with fatty acid extension and desaturation under normal temperatures were significantly lower than those under low temperature stress (Qin et al., 2021). Wang et al. (2018) also pointed out that genes related to unsaturated fatty acid synthesis in *P. haitanensis* were more significantly downregulated under normal temperatures than under high temperature stress. In this study, the genes associated with desaturation (SCD) were significantly downregulated under the HT treatment, while those associated with both fatty acid chain extension (KAR) and desaturation (SCD) were significantly upregulated under the LT treatment. This indicates that *G. bailinae* may regulate the membrane's lipid fluidity to adapt to high temperatures by gradually downregulating the genes related to the biosynthesis of unsaturated fatty acids.

Alpha-linolenic acid (a C18 polyunsaturated acid) is a biosynthetic substrate for jasmonic acid (JA) and its diverse derivatives, which are lipid-derived signaling molecules involved in the regulation of numerous plant processes, including growth, reproductive development, photosynthesis, and responses to abiotic and biotic stresses (Bhatla, 2018). In plants, alpha-linolenic acid is perhaps the most prevalent and chemically diverse source of polyunsaturated fatty acids (Gerwick et al., 1991; Leung et al., 2022). JA can further form methyl jasmonate, which is considered to be crucial for algae's ability to withstand heat (Qin et al., 2021). Exogenous methyl jasmonate has been found to reduce the negative effects of high temperature stress on a number of pathways in *G. lemaneiformis* (Wang et al., 2017). A transcriptome analysis of this species under low temperature stress also revealed that the activation of crucial genes associated with methyl jasmonate production was dramatically elevated (Qin et al., 2021). Su et al. (Su et al., 2019) reported that heat stress induced the upregulation of genes involved in the metabolism of alpha-linolenic acid in wheat. In the present study, it was revealed that the genes encoding OPR (the enzyme 12-oxophytodienoic acid reductase that catalyzes the conversion of 12-OPDA to OPC8) were significantly downregulated under the HT treatment. In contrast, those encoding OPR and ACX (acyl-CoA oxidase, which plays a crucial role in the three rounds of β-oxidation for the synthesis of JA acid from alpha-linolenic acid (Liu et al., 2021b)) were significantly upregulated in the LT treatment (Figure 6). These results suggest that *G. bailinae* can adapt to high temperatures by gradually limiting JA synthesis.

5 Conclusions

In summary, this study proved that the appropriate growth temperature for *G. bailinae* is 25–35°C, and the optimum is 35°C. It also revealed that this species modifies nine metabolic pathways related to the energy, carbohydrate, and lipid metabolisms to adapt to high temperatures. *G. bailinae* regulates the synthesis of NADPH and ATP by downregulating genes related to pathways of the energy and carbohydrate metabolisms to reduce unnecessary energy consumption. In addition, it controls the synthesis of unsaturated fatty acids and JA by downregulating the genes related to lipid metabolism to regulate the fluidity of membrane lipids and the content of lipid-derived signaling molecules, respectively. These

results provide us with a better understanding of the molecular mechanisms underlying the adaptation of *G. bailinae* to high temperatures, which may assist in the development of technologies and breeding strategies to improve the heat tolerance of *Gracilaria* spp.

Data availability statement

The datasets presented in this study can be found in online repositories. The names of the repository/repositories and accession number(s) can be found below: BioProject, PRJNA925653.

Author contributions

YH, JC and EX conceived and designed this study. YH conducted the experiments, analyzed the results, and wrote the original manuscript. EX is responsible for obtaining research funding. JC revised and improved the original manuscript. SW and XC conducted a preliminary analysis of the data. JL, YG, RX and BH assisted the completion of the experiment. All authors discussed the results at various stages. All authors contributed to the article and approved the submitted version.

Funding

This research was supported by Natural Science Research Project of Guangdong Ocean University (R19049) and Chinese National Key Research and Development Program (2020YFD0901101)

Acknowledgments

We would like to express our deepest gratitude to all of those who helped us in this paper.

Conflict of interest

The authors declare that the research was conducted in the absence of any commercial or financial relationships that could be construed as a potential conflict of interest.

Publisher's note

Supplementary material

The Supplementary Material for this article can be found online at: https://www.frontiersin.org/articles/10.3389/fpls.2023.1125324/full#supplementary-material

References

Almeselmani, M., Deshmukh, P., and Chinnusamy, V. (2012). Effects of prolonged high temperature stress on respiration, photosynthesis and gene expression in wheat (*Triticum aestivum* l.) varieties differing in their thermotolerance. *Plant Stress* 6, 25–32.

Ashburner, M., Ball, C. A., Blake, J. A., Botstein, D., Butler, H., Cherry, J. M., et al. (2000). Gene ontology: tool for the unification of biology. *Nat. Genet.* 25, 25–29. doi: 10.1038/75556

Association, W. M. (2022) *). state of the global climate 2021*. Available at: https://policycommons.net/artifacts/2434625/1290_statement_2021_en/3456217/.

Barati, B., Gan, S.-Y., Lim, P.-E., Beardall, J., and Phang, S.-M. (2019). Green algal molecular responses to temperature stress. *Acta Physiol. Plant* 41, 1–19. doi: 10.1007/s11738-019-2813-1

Bender, D., Diaz-Pulido, G., and Dove, S. (2014). The impact of CO_2 emission scenarios and nutrient enrichment on a common coral reef macroalga is modified by temporal effects. *J. Phycol.* 50, 203–215. doi: 10.1111/jpy.12153

Bhatla, S. C. (2018). "Jasmonic acid," in *Plant physiology, development and metabolism*. Eds. S. C. Bhatla and M. A. Lal (Singapore: Springer), 671–679. doi: 10.1007/978-981-13-2023-1_21

Bindoff, N. L., Cheung, W. W. L., Kairo, J. G., Arístegui, J., Guinder, V. A., Hallberg, R., et al. (2019). "2019: Changing ocean, marine ecosystems, and dependent communities," in *IPCC special report on the ocean and cryosphere in a changing climate*. Eds. H.-O. Pörtner, D. C. R., V. Masson-Delmotte, P. Zhai, M. Tignor, E. Poloczanska, K. Mintenbeck, A. Alegría, A. O. XXXM. Nicolai, J. Petzold and B. Rama (UK and New York: Cambridge), 447–587. doi: 10.1017/9781009157964.007

Brown, J. H., Gillooly, J. F., Allen, A. P., Savage, V. M., and West, G. B. (2004). Toward a metabolic theory of ecology. *Ecology* 85, 1771–1789. doi: 10.1890/03-9000

Chen, S., Zhou, Y., Chen, Y., and Gu, J. (2018). Fastp: an ultra-fast all-in-one FASTQ preprocessor. *Bioinformatics* 34, i884–i890. doi: 10.1093/bioinformatics/bty560

Conesa, A., Götz, S., García-Gómez, J. M., Terol, J., Talón, M., and Robles, M. (2005). Blast2GO: a universal tool for annotation, visualization and analysis in functional genomics research. *Bioinformatics* 21, 3674–3676. doi: 10.1093/bioinformatics/bti610

Croce, R., and Van Amerongen, H. (2014). Natural strategies for photosynthetic light harvesting. *Nat. Chem. Biol.* 10, 492–501. doi: 10.1038/nchembio.1555

Cui, J., Zhang, J., Huo, Y., Zhou, L., Wu, Q., Chen, L., et al. (2015). Adaptability of free-floating green tide algae in the yellow Sea to variable temperature and light intensity. *Mar. pollut. Bull.* 101, 660–666. doi: 10.1016/j.marpolbul.2015.10.033

Cui, J., Zhang, J., Monotilla, A. P., Huo, Y., Shi, J., Zhao, X., et al. (2019). Assessment of blooming *Ulva* macroalgae production potential in the yellow Sea, China. *Phycologia* 58, 535–541. doi: 10.1080/00318884.2018.1551016

Dal Bosco, C., Lezhneva, L., Biehl, A., Leister, D., Strotmann, H., Wanner, G., et al. (2004). Inactivation of the chloroplast ATP synthase γ subunit results in high non-photochemical fluorescence quenching and altered nuclear gene expression in arabidopsis thaliana. *J. Biol. Chem.* 279, 1060–1069. doi: 10.1074/jbc.M308435200

Davison, I. R. (1991). Environmental effects on algal photosynthesis: temperature. *J. Phycol.* 27, 2–8. doi: 10.1111/j.0022-3646.1991.00002.x

Elle, B. J., Corre, V.Jr., Felarca, K. G., and Pedroso, F. (2017). Potential of *Gracilariopsis bailiniae* and *Oreochromis mossambicus* in improving water quality in intensive *Litopenaeus vannamei* tank culture. *AACL Bioflux* 10, 1309–1318.

Endoma, L. F., Nuñal, S. N., Traifalgar, R. F. M., and Luhan, M. R. J. (2020). Photo-bleached agar extracts from *Gracilariopsis heteroclada*. *Bot. Mar.* 63, 559–569. doi: 10.1515/bot-2020-0028

Gao, X., Liu, W., Zhong, Y., Xing, H., Zhang, J., Chang, J., et al. (2022). Effect of different temperatures on the growth and photosynthetic physiology of *Zostera marina* l. *Chin. J. Appl. Environ. Biol.* 28, 175–181. doi: 10.19675/j.cnki.1006-687x.2020.10008

Gerwick, W. H., Moghaddam, M., and Hamberg, M. (1991). Oxylipin metabolism in the red alga *Gracilariopsis lemaneiformis*: mechanism of formation of vicinal dihydroxy fatty acids. *Arch. Biochem. Biophys.* 290, 436–444. doi: 10.1016/0003-9861(91)90563-X

Goltsev, V., Kalaji, H., Paunov, M., Bąba, W., Horaczek, T., Mojski, J., et al. (2016). Variable chlorophyll fluorescence and its use for assessing physiological condition of plant photosynthetic apparatus. *Russ. J. Plant Physiol.* 63, 869–893. doi: 10.1134/S1021443716050058

Graba-Landry, A., Hoey, A. S., Matley, J. K., Sheppard-Brennand, H., Poore, A. G., Byrne, M., et al. (2018). Ocean warming has greater and more consistent negative effects than ocean acidification on the growth and health of subtropical macroalgae. *Mar. Ecol. Prog. Ser.* 595, 55–69. doi: 10.3354/meps12552

Grabherr, M. G., Haas, B. J., Yassour, M., Levin, J. Z., Thompson, D. A., Amit, I., et al. (2011). Full-length transcriptome assembly from RNA-seq data without a reference genome. *Nat. Biotechnol.* 29, 644–652. doi: 10.1038/nbt.1883

Hansen, J., Sato, M., Kharecha, P., and Von Schuckmann, K. (2011). Earth's energy imbalance and implications. *Atmos. Chem. Phys.* 11, 13421–13449. doi: 10.5194/acp-11-13421-2011

Hasanuzzaman, M., Nahar, K., Alam, M. M., Roychowdhury, R., and Fujita, M. (2013). Physiological, biochemical, and molecular mechanisms of heat stress tolerance in plants. *Int. J. Mol. Sci.* 14, 9643–9684. doi: 10.3390/ijms14059643

Ji, Y., and Gao, K. (2021). Effects of climate change factors on marine macroalgae: a review. *Adv. Mar. Biol.* 88, 91–136. doi: 10.1016/bs.amb.2020.11.001

Koch, M., Bowes, G., Ross, C., and Zhang, X. H. (2013). Climate change and ocean acidification effects on seagrasses and marine macroalgae. *Global Change Biol.* 19, 103–132. doi: 10.1111/j.1365-2486.2012.02791.x

Leung, K. S., Oger, C., Guy, A., Bultel-Poncé, V., Vigor, C., Durand, T., et al. (2022). Alpha-linolenic acid, phytoprostanes and phytofurans in plant, algae and food. *Adv. Bot. Res.* 101, 437–468. doi: 10.1016/bs.abr.2021.09.005

Li, C., Nong, Q., Solanki, M. K., Liang, Q., Xie, J., Liu, X., et al. (2016). Differential expression profiles and pathways of genes in *sugarcane* leaf at elongation stage in response to drought stress. *Sci. Rep.* 6, 1–11. doi: 10.1038/srep25698

Li, Q., Zhang, L., Pang, T., and Liu, J. (2019). Comparative transcriptome profiling of *Kappaphycus alvarezii* (Rhodophyta, gigartinales) in response to two extreme temperature treatments: an RNA-seq-based resource for photosynthesis research. *Eur. J. Phycol.* 54, 162–174. doi: 10.1080/09670262.2018.1536283

Lim, E.-L., Siow, R.-S., Abdul Rahim, R., and Ho, C.-L. (2016). Global transcriptome analysis of *Gracilaria changii* (Rhodophyta) in response to agarolytic enzyme and bacterium. *Mar. Biotechnol.* 18, 189–200. doi: 10.1007/s10126-015-9680-6

Liu, S., Zhang, J., Hu, C., Chen, X., Sun, X., and Xu, N. (2021a). Physiological and transcriptome analysis of exogenous l-arginine in alleviation of high temperature stress in *Gracilariopsis lemaneiformis*. *Front. Mar. Sci.* 8, 784586. doi: 10.3389/fmars.2021.784586

Liu, S., Zhang, J., Hu, C., Sun, X., and Xu, N. (2021b). Physiological and transcriptome analysis of γ-aminobutyric acid (GABA) in improving *Gracilariopsis lemaneiformis* stress tolerance at high temperatures. *Algal Res.* 60, 102532. doi: 10.1016/j.algal.2021.102532

Liu, C., Zou, D., Yang, Y., Chen, B., and Jiang, H. (2017). Temperature responses of pigment contents, chlorophyll fluorescence characteristics, and antioxidant defenses in *Gracilariopsis lemaneiformis* (Gracilariales, rhodophyta) under different CO_2 levels. *J. Appl. Phycol.* 29, 983–991. doi: 10.1007/s10811-016-0971-8

Love, M. I., Huber, W., and Anders, S. (2014). Moderated estimation of fold change and dispersion for RNA-seq data with DESeq2. *Genome Biol.* 15, 1–21. doi: 10.1186/s13059-014-0550-8

Obata, T., and Fernie, A. R. (2012). The use of metabolomics to dissect plant responses to abiotic stresses. *Cell. Mol. Life Sci.* 69, 3225–3243. doi: 10.1007/s00018-012-1091-5

Qin, F., Zang, X., Shui, G., and Wang, Z. (2021). Transcriptome analysis of *Gracilariopsis lemaneiformis* at low temperature. *J. Appl. Phycol.* 33, 4035–4050. doi: 10.1007/s10811-021-02514-z

Raines, C. A. (2003). The Calvin cycle revisited. *Photosynth. Res.* 75, 1–10. doi: 10.1023/A:1022421515027

Robinson, M. D., McCarthy, D. J., and Smyth, G. K. (2010). edgeR: a bioconductor package for differential expression analysis of digital gene expression data. *bioinformatics* 26, 139–140. doi: 10.1093/bioinformatics/btp616

Shindo, A., Borlongan, I. A., Nishihara, G. N., and Terada, R. (2022). Interactive effects of temperature and irradiance including spectral light quality on the photosynthesis of a brown alga *Saccharina japonica* (Laminariales) from Hokkaido, Japan. *Algal Res.* 66, 102777. doi: 10.1016/j.algal.2022.102777

Skriptsova, A. V., and Nabivailo, Y. V. (2009). Comparison of three gracilarioids: growth rate, agar content and quality. *J. Appl. Phycol.* 21, 443–450. doi: 10.1007/s10811-008-9389-2

Smale, D. A., Wernberg, T., Oliver, E. C., Thomsen, M., Harvey, B. P., Straub, S. C., et al. (2019). Marine heatwaves threaten global biodiversity and the provision of ecosystem services. *Nat. Clim. Change* 9, 306–312. doi: 10.1038/s41558-019-0412-1

Su, P., Jiang, C., Qin, H., Hu, R., Feng, J., Chang, J., et al. (2019). Identification of potential genes responsible for thermotolerance in wheat under high temperature stress. *Genes* 10, 174. doi: 10.3390/genes10020174

Sun, P., Mao, Y., Li, G., Cao, M., Kong, F., Wang, L., et al. (2015). Comparative transcriptome profiling of *Pyropia yezoensis* (Ueda) MS hwang & HG choi in response to temperature stresses. *BMC Genom.* 16, 1–16. doi: 10.1186/s12864-015-1586-1

Sweetlove, L. J., Beard, K. F., Nunes-Nesi, A., Fernie, A. R., and Ratcliffe, R. G. (2010). Not just a circle: flux modes in the plant TCA cycle. *Trends Plant Sci.* 15, 462–470. doi: 10.1016/j.tplants.2010.05.006

Tamoi, M., Nagaoka, M., Yabuta, Y., and Shigeoka, S. (2005). Carbon metabolism in the Calvin cycle. *Plant Biotechnol.* 22, 355–360. doi: 10.5511/plantbiotechnology.22.355

Von Schuckmann, K., Palmer, M., Trenberth, K. E., Cazenave, A., Chambers, D., Champollion, N., et al. (2016). An imperative to monitor earth's energy imbalance. *Nat. Clim. Change* 6, 138–144. doi: 10.1038/nclimate2876

Wahid, A., Gelani, S., Ashraf, M., and Foolad, M. R. (2007). Heat tolerance in plants: an overview. *Environ. Exp. Bot.* 61, 199–223. doi: 10.1016/j.envexpbot.2007.05.011

Wang, W., Li, H., Lin, X., Yang, S., Wang, Z., and Fang, B. (2015). Transcriptome analysis identifies genes involved in adventitious branches formation of *Gracilaria lichenoides in vitro*. *Sci. Rep.* 5, 1–16. doi: 10.1038/srep17099

Wang, W., Lin, Y., Teng, F., Ji, D., Xu, Y., Chen, C., et al. (2018). Comparative transcriptome analysis between heat-tolerant and sensitive *Pyropia haitanensis* strains in response to high temperature stress. *Algal Res.* 29, 104–112. doi: 10.1016/j.algal.2017.11.026

Wang, F., Wang, C., Zou, T., Xu, N., and Sun, X. (2017). Comparative transcriptional profiling of *Gracilariopsis lemaneiformis* in response to salicylic acid-and methyl jasmonate-mediated heat resistance. *PloS One* 12, e0176531. doi: 10.1371/journal.pone.0176531

Wenlei, W., Fei, T., Yinghui, L., Dehua, J., Yan, X., Changsheng, C., et al. (2018). Transcriptomic study to understand thermal adaptation in a high temperature-tolerant strain of *Pyropia haitanensis*. *PloS One* 13, e0195842. doi: 10.1371/journal.pone.0195842

Wernberg, T., Russell, B. D., Thomsen, M. S., Gurgel, C. F. D., Bradshaw, C. J., Poloczanska, E. S., et al. (2011). Seaweed communities in retreat from ocean warming. *Curr. Biol.* 21, 1828–1832. doi: 10.1016/j.cub.2011.09.028

Wu, J., Lian, W., Liu, Z., Zeng, X., Jiang, J., and Wei, Y. (2019). High temperature response of chlorophyll fluorescence parameters and heat tolerance evaluation in different grape cultivars. *J. Northwest A F University(Natural Sci. Edition)* 47, 80–88. doi: 10.13207/j.cnki.jnwafu.2019.06.011

Xu, Y., Chen, C., Ji, D., Hang, N., and Xie, C. (2014). Proteomic profile analysis of *Pyropia haitanensis* in response to high-temperature stress. *J. Appl. Phycol.* 26, 607–618. doi: 10.1007/s10811-013-0066-8

Xu, C., Xu, R., Huang, B., Chen, H., Chen, B., and Xie, E. (2021). Indoor polyculture of *Gracilaria bailinae* and *Litopenaeus vannamei* with zero water exchange. *J. Guangdong Ocean Univ.* 41, 131–137. doi: 10.3969/j.issn.1673-9159.2021.03.017

Xu, K., Xu, Y., Ji, D., Xie, J., Chen, C., and Xie, C. (2016). Proteomic analysis of the economic seaweed *Pyropia haitanensis* in response to desiccation. *Algal Res.* 19, 198–206. doi: 10.1016/j.algal.2016.08.010

Yamada, M., Hidaka, T., and Fukamachi, H. (1996). Heat tolerance in leaves of tropical fruit crops as measured by chlorophyll fluorescence. *Sci. Hortic.* 67, 39–48. doi: 10.1016/S0304-4238(96)00931-4

Yang, F., Wei, Z., and Long, L. (2021). Transcriptomic and physiological responses of the tropical reef calcified macroalga *Amphiroa fragilissima* to elevated temperature. *J. Phycol.* 57, 1254–1265. doi: 10.1111/jpy.13158

Yao, C., and Somero, G. N. (2014). The impact of ocean warming on marine organisms. *Chin. Sci. Bull.* 59, 468–479. doi: 10.1007/s11434-014-0113-0

Yao, Y., and Wang, C. (2021). Variations in summer marine heatwaves in the south China Sea. *JGR: Oceans* 126, e2021JC017792. doi: 10.1029/2021JC017792

Yong, Y. S., Yong, W. T. L., and Anton, A. (2013). Analysis of formulae for determination of seaweed growth rate. *J. Appl. Phycol.* 25, 1831–1834. doi: 10.1007/s10811-013-0022-7

Zhang, X., Wu, C., Hu, C., Li, Y., Sun, X., and Xu, N. (2020). Lipid remodeling associated with chitooligosaccharides-induced heat tolerance of marine macroalgae *Gracilariopsis lemaneiformis*. *Algal Res.* 52, 102113. doi: 10.1016/j.algal.2020.102113

Zhong, Y., Yang, Y., Gao, X., Xing, H., Liu, W., Duan, Y., et al. (2021). Effects of salinity, temperature and light intensity on growth and photosynthetic activity of *Caulerpa sertularioides*. *J. Trop. Subtropical Bot.* 29, 626–633. doi: 10.11926/jtsb.4378

frontiers | Frontiers in Plant Science

TYPE Original Research
PUBLISHED 14 April 2023
DOI 10.3389/fpls.2023.1155504

OPEN ACCESS

EDITED BY
Biao Jin,
Yangzhou University, China

REVIEWED BY
Chongde Sun,
Zhejiang University, China
Da-Gang Hu,
Shandong Agricultural University, China

*CORRESPONDENCE
Haiying Ren
jbxie@bjfu.edu.cn
Jianbo Xie
jbxie@bjfu.edu.cn

SPECIALTY SECTION
This article was submitted to Plant Abiotic Stress, a section of the journal Frontiers in Plant Science

RECEIVED 31 January 2023
ACCEPTED 20 March 2023
PUBLISHED 14 April 2023

CITATION
Xu W, Ren H, Qi X, Zhang S, Yu Z and Xie J (2023) Conserved hierarchical gene regulatory networks for drought and cold stress response in *Myrica rubra*. *Front. Plant Sci.* 14:1155504. doi: 10.3389/fpls.2023.1155504

Conserved hierarchical gene regulatory networks for drought and cold stress response in *Myrica rubra*

Weijie Xu[1,2], Haiying Ren[1,3,4]*, Xingjiang Qi[1,3,4], Shuwen Zhang[1,3], Zheping Yu[1,3] and Jianbo Xie[2,5]*

[1]State Key Laboratory for Managing Biotic and Chemical Treats to the Quality and Safety of Agro-Products, Institute of Horticulture, Institute of Agro-product Safety and Nutrition, Zhejiang Academy of Agricultural Sciences, Hangzhou, China, [2]State Key Laboratory of Tree Genetics and Breeding, College of Biological Sciences and Technology, Beijing Forestry University, Beijing, China, [3]State Key Laboratory for Managing Biotic and Chemical Treats to the Quality and Safety of Agro-products, Hangzhou, China, [4]Xianghu Lab., Hangzhou, China, [5]The Tree and Ornamental Plant Breeding and Biotechnology Laboratory of National Forestry and Grassland Administration, Beijing Forestry University, Beijing, China

Stress response in plant is regulated by a large number of genes co-operating in diverse networks that serve multiple adaptive process. To understand how gene regulatory networks (GRNs) modulating abiotic stress responses, we compare the GRNs underlying drought and cold stresses using samples collected at 4 or 6 h intervals within 48 h in Chinese bayberry (*Myrica rubra*). We detected 7,583 and 8,840 differentially expressed genes (DEGs) under drought and cold stress respectively, which might be responsive to environmental stresses. Drought- and cold-responsive GRNs, which have been built according to the timing of transcription under both abiotic stresses, have a conserved trans-regulator and a common regulatory network. In both GRNs, basic helix-loop-helix family transcription factor (bHLH) serve as central nodes. *MrbHLHp10* transcripts exhibited continuous increase in the two abiotic stresses and acts upstream regulator of *ASCORBATE PEROXIDASE* (*APX*) gene. To examine the potential biological functions of *MrbHLH10*, we generated a transgenic *Arabidopsis* plant that constitutively overexpresses the *MrbHLH10* gene. Compared to wild-type (WT) plants, overexpressing transgenic *Arabidopsis* plants maintained higher APX activity and biomass accumulation under drought and cold stress. Consistently, RNAi plants had elevated susceptibility to both stresses. Taken together, these results suggested that *MrbHLH10* mitigates abiotic stresses through the modulation of ROS scavenging.

KEYWORDS

Chinese bayberry, ROS scavenging, abiotic stress tolerance, bHLH transcription factor, gene regulatory networks

Introduction

A disturbance in the environment triggers rapid and global reprogramming of cells, which requires the spatial and temporal coordination of multiple TFs (Zhang et al., 2019; Zhou et al., 2021). Transcriptional regulation occurs on a multitude of time scales, from minutes to days, making temporally dynamic patterns possible (Wang et al., 2021). The

regulation of phytohormone signaling pathways, light-signaling pathways, circadian clock regulation, and reactive oxygen species homeostasis at the transcriptional, epigenetic, and post-translational levels have been identified during environmental stress including heat, drought and cold stress (Ohama et al., 2017; Li et al., 2018; Ding et al., 2020).

In the presence of excess ROS, for example due to environmental stress, the cells are subjected to oxidative conditions that are detrimental to them (Wang et al., 2008; Kuge et al., 2010). H_2O_2, as ROS, is an important indicator of the generation of ROS (Bhattacharjee, 2012; De la Garma et al., 2015; He et al., 2018). Thus, the maintenance of steady state ROS by scavenging routes is necessary in order to prevent oxidative damage due to adverse environmental stress (Mittler et al., 2004; Miller et al., 2010; Jiang and Jie, 2002). The AsA-GSH cycle and Superoxide Dismutase (SOD) are both essential for scavenging ROS (Shi et al., 2013; Hernández et al., 2015). Superoxide dismutase (SOD) is the primary defense mechanism against ROS in plants, and it converts superoxide to oxygen (O_2) and H_2O_2 at the molecular level (Huang et al., 2016; He et al., 2018; Wang et al., 2021). In the AsA-GSH cycle, APX uses AsA to reduce H_2O_2 to H_2O (Hernández et al., 2015; Xing et al., 2018). In previous studies, APX is present in many organelles as well as in the cytosol. It has a unique ability to adapt to stress in various environments. (He et al., 2018; Xing et al., 2018). For example, it has been shown that overexpression of *APX2* gene increases tolerance to exogenous hydrogen peroxide and assists in ROS detoxification under both stress and normal conditions in *A. thaliana* (Mittler et al., 2006; Rossel et al., 2007).

bHLH superfamily, a TF family with a large number of members, is prevalent throughout eukaryotes (Pires and Dolan, 2010; Sánchez-Pérez et al., 2019; Guo et al., 2021). In general, bHLH is composed of about 60 amino acids and has two functional areas: a base area with 13 to 17 predominantly base amino acids for DNA binding, and an HLH area capable of forming a homodimer or heterodimer with one or more partners. (Tian et al., 2019; Guo et al., 2021). bHLH TFs are important regulators in controlling responses to environmental stresses, development processes (Sun et al., 2020), and the biosynthesis of secondary metabolites (Groszmann et al., 2010; Zhao et al., 2020) by targeting dehydration and cold responsive genes (Guo et al., 2021). In *Arabidopsis*, AtAIB (ABA-inducible bHLH-type transcription factor), which enhance drought tolerance, control stomatal closure by modulating stomatal movement associated with H_2O_2 signalling (Cui et al., 2015; Li et al., 2017). In wheat, CBF (ICE1, bHLH116), a MYC-type bHLH TFs, was upregulated by cold stress and the knock-down *bHLH116* seedling displayed reduced cold stress tolerance accompanied with increased ROS levels and reduced antioxidant enzyme activities (Guo et al., 2021). Extensive studies uncovered several downstream genes of *bHLH*. For example, bHLH122, can directly bind to the promoters of *CYP707A3* gene, repressing its expression and increasing the APX content. AtbHLH68, AtbHLH112 and AtbHLH122, have been reported to control abiotic stress responses by regulating the APX and ABA signaling pathway genes in *A. thaliana*. These results indicate that *bHLH* genes play important roles in plant abiotic stress tolerance through crossing with phytohormone ABA and ROS scavenging pathway. However, the functional importance of *bHLH* gene in controlling plant response to multiple abiotic stresses remains to be investigated and the downstream genes extending the bHLH pathway remain unclear.

The Chinese bayberry (*Myrica rubra* Sieb. and Zucc.), which is widespread in tropical and subtropics, is one of the most important sub-tropical fruit crops. It is also a good candidate for studying fruit quality (Ren et al., 2019; Ren et al., 2021). *M. rubra species* are sensitive to drought and cold stress, which will directly decrease the yield and quality of *M. rubra* (Larcheveque et al., 2011; Windt et al., 2011). Moreover, the whole genome of *M. rubra* will be helpful to study the function genome and improve its genetics. (Ren et al., 2019). In this study, we performed a time-course transcriptome investigation in response to drought and cold stress, in an effort to identify the potential multifunctional TFs involved abiotic stress in *M. rubra*.

Materials and methods

Plant materials

The 1-year-old *M. rubra* seedlings were grown in a greenhouse at Lanxi, Zhejiang Province, China (29.22 N, 119.45 E) (15.0 h light, 22–25°C, 75% humidity). We watered the seedlings once a day to maintain the optimum level of moisture in the field. In order to carry out the cold-treatment, the plants in the treatment group were transferred to the growing room (Sanyo) where they grew under the same conditions as those of the control (He et al., 2018). Three biological replicates were used for each group of seedlings, with each group exposed to 4°C for 0, 30 min, 1, 3, 6, 9, 12, 24, 36, or 48 h in growth chambers (Sanyo). Treatment groups were moved to Sanyo growth chambers with the same growth conditions as those in the control group when performing drought treatments. The seedlings were also divided into ten groups with three biological replicates each, and seedlings from each group were treated with 8% polyethylene glycol (PEG) for either 0, 30 min, 1, 3, 6, 9, 12, 24, 36 or 48 h in growth chambers (Sanyo) at 23°C. Each of the three to five fully expanded leaves of the seedling were measured.

Antioxidant enzyme and H_2O_2 assay

The pigment content and enzyme activity of *M. rubra* leaves were determined immediately after freezing in liquid nitrogen at the same time. In few words, 0.1 g of the leaf sample was frozen in liquid nitrogen, homogenized in cold 0.01M phosphate buffer (1.5 mL, pH 7.2),and centrifuged at 14,000 grams for 10 minutes at 4°C for 10 minutes, and then Plant superoxide dismutase (SOD) Assay Kit (Nanjing Jiancheng Bioengineering Institute, Jiangsu Province, China) was used to measure the activity of SOD. First, 1.5 mL reaction buffer (6.5×10^{-6} M riboflavin, 0.013 M met, 6.3×10^{-6} M NBT, 1×10^{-4} M Ethylene Diamine Tetraacetic Acid (EDTA), 0.05 M phosphate buffer, pH=7.8) was added to the supernatant followed by incubation at 25°C for 30 min, and absorbance at 560 nm was measured with a spectrophotometer. The activity of

malondialdehyde (MDA) was measured in accordance with the manufacturer's specification using Catalase Assay Kit (Nanjing Jiancheng Bioengineering Institute). Using a plastic pestle and an ice-cold 0.01 M phosphate buffer (pH 7.2) with 1.13 mg dithiothreitol, the leaf specimens were crushed in a micro-centrifuge. A centrifuge was used for 10 minutes at 4°C, weighing 14,000 g. We assayed the supernatant for MDA activity by measuring the linear rate of decrease in absorbance at 240 nm with a spectrophotometer. For APX and peroxidase (POD) activity, 0.1 g samples of leaves were homogenized in 1.5 mL ice-cold 0.01 M phosphate buffer (pH 7.2) for 30 min and centrifuged at 14,000 g for 10 min at 4°C. A Plant APX and POD Assay Kit (Nanjing Jiancheng Bioengineering Institute) were used to measure APX and POD activity in the supernatant. The supernatant was added to a mixture of 0.5 mL 0.1 M phosphate buffer, 0.5 mL 0.1 M guaiacol buffer and incubated at 30°C for 8 min. The absorbance of the sample at 470 nm was measured with an optical spectrophotometer.

RNA-sequencing and data analysis

In the case of drought and cold-stress, the 3rd to 5th leaves of M. rubra were picked up, then frozen in liquid nitrogen, and kept at -80 degrees Celsius until application. According to the manufacturer's guidelines, RNeasy Kit (Qiagen) was used to extract the total RNA. NanoDrop ND-2000 (A260/A280 1.9-2.1) and Agilent 2100 bioanalyzer (28S/18S 1.8-2.0) were used for the determination of RNA quality. A strand-specific RNA-seq library was constructed on an Illumina HiSeq 4000 platform according to the manufacturer's instructions and index codes. The Beijing Novogene Technologies performed the construction of the libraries and the paired-end sequencing. Following quality control and removal of adapter-and poly(N)-containing reads, clean reads acquired after mapping on the reference genome of *M. rubra* (http://www.bayberrybase.cn/) were analyzed (http://www.bayberrybase.cn/) as previously described (Ren et al., 2019) with TopHat (v. 2.0.0) with default parameters (Trapnell et al., 2009). Transcript levels were normalized based on FPKM with Cufflinks (v. 2.1.1) with default options (Trapnell et al., 2012). It was considered significant that genes with P-value<0.05 (adjusted for the false discovery rate, Q-value< 0.05) and >2-fold change were differentially expressed.

Functional enrichment analysis and visualization

A GO analysis was performed on DEGs and a GO annotation was obtained from *M. rubra* (http://www.bayberrybase.cn/) (Ren et al., 2019). The result of the GO enrichment analysis along with the P-value modified using the Benjamini and Hochberg (1995) FDR method were input into OmicShare platform (https://www.omicshare.com/tools), and created a visual tree map of the outcome of the GO analysis. Significant enrichment of GO terms with corrected P value < 0.05 and Q value < 0.05 was observed.

Measurement of tissue specificity

The tissue specificity score was calculated as previously described (Liao and Zhang, 2006). The tissue specificity score was generated as follows in order to further quantify the tissue specificity of gene expression: n represents the sum of tissues, aij is the mean expression of the gene i in tissue j, and the tissue specificity of the gene i is defined as:

$$Ti = \frac{1}{n\text{-}1}\sum_{j=1}^{n}\left(1 - \frac{aij}{(aij)\max j}\right)$$

Construction of a multi-layered hierarchical gene regulatory network using the BWERF algorithm

Using PlantPAN v.2.0, it was determined that cis-regulatory elements were found in the 2 kb promoter region of the candidate genes (Chow et al., 2016; Xu et al., 2022). It was predicted that these motifs are TF target sites based on 80% confidence values. Then, a backward elimination random forest (BWERF) algorithm is employed to construct ML-hGRNs, which uses the genes and TFs encoding transport, photosynthesis and oxidoreductases (Deng et al., 2017; Xu et al., 2022).

Phylogenetic and bioinformatics analyses

ExPASy (http://web.expasy.org/computepi/) was used for the analysis of the isoelectric point (pI) and the molecular weight of the bHLH protein (Kumar et al., 2018). In order to analyze genetic variation and phylogenetic relationships, a plurality of sequence alignment of bHLH protein sequences was performed in MEGA 7 (Kumar et al., 2018). To deal with the gaps and lack of data, we chose a partial deletion with an 80% coverage limit. Therefore, Jones-Taylor-Thornton (JTT) + (G) + (F) was chosen as the optimum amino acid replacement model. The Maximum Likelihood (ML) method in MEGA 7 was utilized to construct a phylogenetic tree of protein sequences with 1000 bootstrapping replicas (Kumar et al., 2022). For all positions, 90 per cent of the site coverage was removed; in other words, no more than 10 per cent of the alignment space, no data, and no clear basis were permitted. A phylogenetic tree was visualized using Figtree software (http://tree.bio.ed.ac.uk/software/figtree/).

Plasmid construction and *A. thaliana* genetic transformation

Generic transformation, cloning and expression analysis were carried out on *A. thaliana* seedlings at long time (16 hours/8 hours darkness) to produce overexpression and RNAi lines (Quan et al., 2021; Zhang et al., 2022). With the help of gene-specific primers, we

cloned the full-length coding region of *MrbHLH10* gene from a *M. rubra* clone template cDNA. During the process of cloning the full-length gene, the coding region of *MrbHLH10* gene was cloned into pDONR222 vector. Subsequently, LR reactions were employed to re-sequence the encoding area and target vector pGWB405 in accordance with Nakagawa et al. (2007), verified by sequencing. Two kinds of vector were introduced to *Agrobacterium* GV3101 *via Agrobacterium*-mediated transformation together with gene silencing inhibitor P19, and then transformed into *Nicotiana benthamiana* based on previous study (Zhang et al., 2022). The *Agrobacterium*-mediated floral dipping approach was used to create transgenic *A. thaliana* seedlings (Wang et al., 2022). Transgenic plants were confirmed by PCR analysis using vector- and gene-specific primers in Table S1.

Measurement of the physiological characteristics of transgenic plants

On a plate containing 1% sucrose and ½×MS medium (0.1 mM $MgSO_4$, 0.1 mM $CaCl_2$, 0.6 mM NaCl, and 0.3 mM $ZnSO_4$), seeds of WT and transgenic *A. thaliana* were grown. The germination count was calculated up to the 5 days (d) after stratification (nearly emerged radicle). Based on the prior research, we obtained the germination rate (GR) by the number of seeds on each side of WT *A. thaliana* and transgenic plants (Quan et al., 2020; Zhang et al., 2022). Leaf physiological traits were measured in mature leaves of WT and transgenic *A. thaliana* seedlings at 20 days after germination (DAG). Seedling length of *A. thaliana* was calculated by ImageJ software (https://imagej.en.softonic.com/) (Banugopan et al., 2012).

Statistical analyses

The statistical significance of treatment differences was assessed with either one way or twoway analysis of variance, with SPSS 17.0 (IBM, Chicago, IL, USA) and Excel 2013 (Microsoft Corp., Redmond, WA) on the basis of prior research (Xu et al., 2022). For the calculation of *P* values, the Students't test (* $P < 0.05$, * * $P < 0.01$) was adopted. After normalization, all samples had a normal distribution with respect to variance homogeneity (Xu et al., 2022).

Results

Physiological and transcriptomic changes response to drought and cold stress

In order to determine the effects of drought and cold stress on physiological activity, we first examined the activity of SOD, POD, MDA, APX, CAT and H_2O_2 under drought and cold stress. As expected, the activity of SOD, POD, MDA, APX, CAT and H_2O_2 showed an overall increase during the drought and cold treatment (Figures 1A–H). For example, under drought stress, the activities of SOD, MDA, APX and CAT and H_2O_2 increased significantly from 6 to 36 h (Figures 1B–D); the activities of SOD, MDA and APX peaked at 36 h, 36 h and 12 h, respectively (Figures 1B, C). By contrast, the activities of SOD and APX peaked at 12 h after cold treatment (Figures 1B, D). Interestingly, the activities of APX and MDA were positively correlated with each other ($P>0.05$, $R>0.6$) under the two stresses. Totally, the anti-oxidant enzyme activities were strongly induced under drought and cold stress.

To identify the stress-responsive genes under both stresses, we sequenced the total RNAs of the leaf tissues across all the time points. A total of 7,583 and 8,840 differentially expressed genes (DEGs) were obtained under drought stress and cold stress, respectively (Fold Change>2 and FDR < 0.01) (Figure 2A; Table S1). To gain insight into the transcriptome dynamics under the two stresses, we performed principal component analysis (PCA; Figures 2B, C). As a result, the transcriptome data can be generally divided into four and two clusters under drought and cold stress, respectively (Figures 2B, C). Consistent with this, a previous study reported that abiotic stress response in higher plants occurs in different phases (Wu et al., 2021). Notably, the cold-

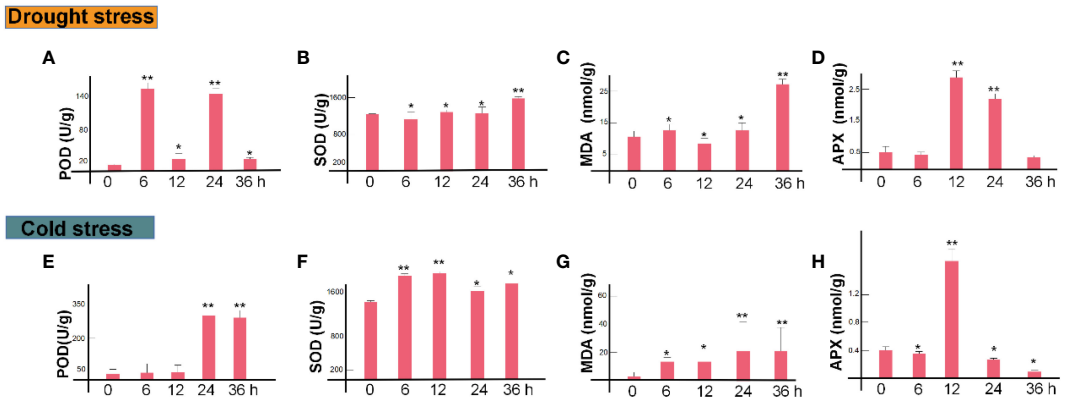

FIGURE 1
Temporal dynamics of *M. rubra* physiological characteristics during drought and cold treatment. Peroxidase (POD) activity **(A)**, superoxide dismutase (SOD) activity **(B)**, MDA **(C)** and APX content **(D)**, in *M. rubra* under drought stress. Peroxidase (POD) activity **(E)**, superoxide dismutase (SOD) activity **(F)**, MDA content **(G)** and APX content **(H)**, in *M. rubra* under cold stress. (*$P < 0.05$, **$P < 0.01$, Student's t-test).

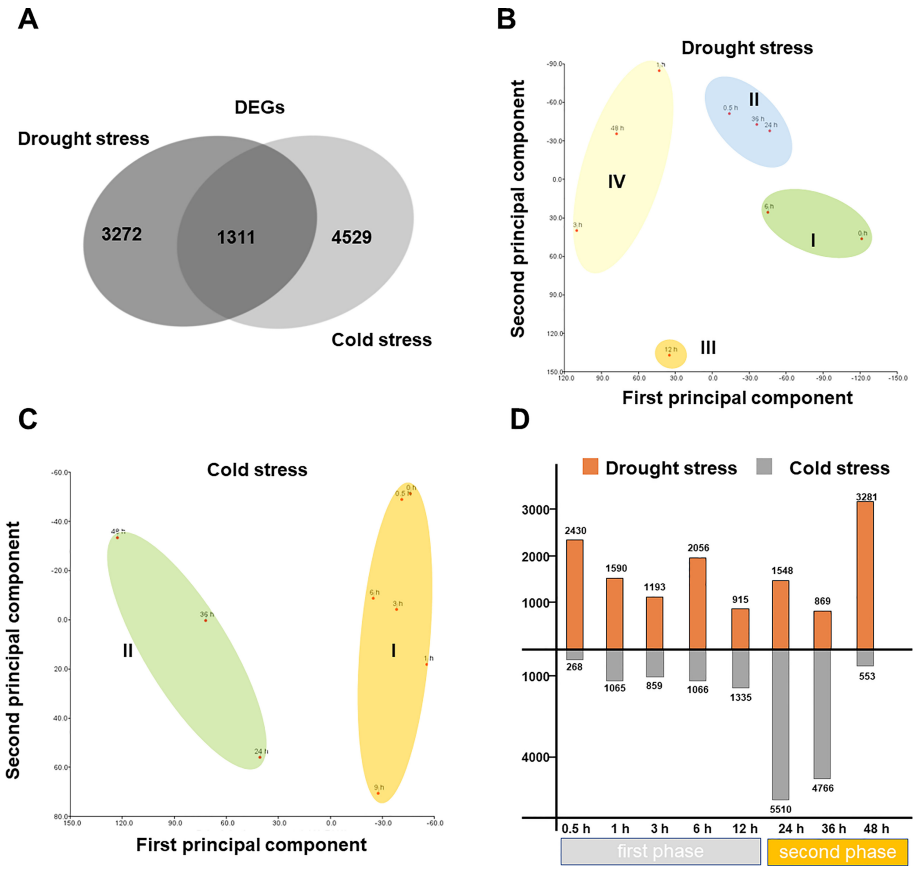

FIGURE 2
Temporal dynamics of *M. rubra* transcriptome during drought and cold treatment. **(A)** Venn diagrams of DEGs overlapping between drought stress and cold stress. DEG indicates differentially expressed gene. **(B)** PCA of the transcriptomes of the 8 time point samples under drought stress and **(C)** cold stress. **(D)** Number of drought-responsive (upper bars) and cold-responsive (lower bars) genes at each time point compared to the control group (0 h).

responsive transcription profile was clearly divided into two phases, and the majority of cold-responsive DEGs were induced in the second phase timepoint from 24 to 48 h (Figure 2D). By contrast, there were only <1500 DEGs in the first phase (0 to 24 h. The fewer DEGs within the early response might be reminiscent of *M. rubra* species that lived in freezing environment (under 4°C) with consistent cold pressure (Ren et al., 2019).

The GO analysis of the drought and cold-response genes showed that there were 251 and 227 significant enrichment terms (P<0.001). The upregulated DEGs under drought stress were enriched for terms including "response to hormone-mediated signaling pathway," "oxidoreductase activity," "photosynthesis," "transcription factor activity," "abscisic acid biosynthetic process," and "ABA signal transduction pathway" (Table S3). By contrast, upregulated cold-responsive DEGs were enriched for terms of photosynthesis, response to "oxidoreductase activity," "photosynthesis," "external biotic stimulus," "transcription factor activity," "transcription regulation," "calcium-binding," "DNA binding," and "serine/threonine kinase activity" (Table S3). These indicates that the patterns of the functional shifts were consistent with the physiological changes under the two stresses.

Conserved and divergent dynamic transcription profile between the two abiotic stresses

To examine the shared and unique transcriptomic network under drought and cold stresses, DEGs were clustered into 20 dynamic groups by using K-means clustering algorithm (Wu et al, 2021). The ten largest dynamic groups in response to drought and cold stress contained most of the stress-responsive DEGs—83.4% (3,142 drought-responsive genes) and 88.7% (4,108 cold-responsive genes) respectively (Figure 3A). The genes in the D2, D3, C3, C9, and C10 groups were continuously down- or up-regulated under both stresses (Figure 3A). On the other hand, the D1 and C2 groups were observed to have transient changes in gene expression at earlier timepoints, presumably in response to early stress. Thus, the groups with similar expression dynamics probably kept similar biological processes regardless of the stress they were exposed to. Under the two types of stress, the D4 and C4 groups with transient gene expression peaks at 36 hours showed a higher level of photosynthetic gene accumulation (Figures 3A, B). Likewise, the D3 and C7 groups that showed an increasing tendency to continue

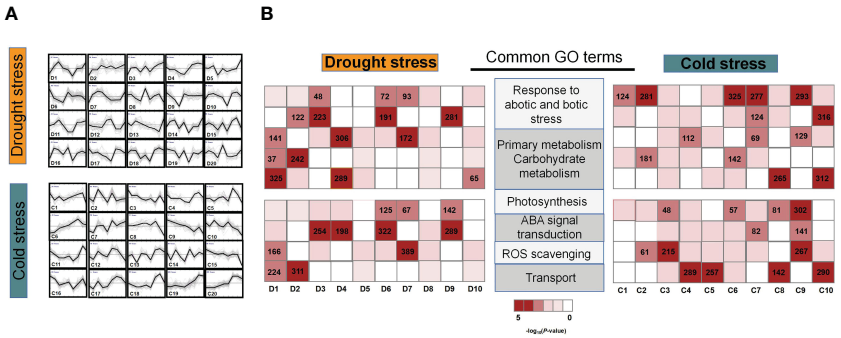

FIGURE 3
Temporal dynamics of *M. rubra* transcriptome during drought and cold treatment. **(A)** Expression dynamics of the 20 largest gene clusters over time under drought (D1–D20) and cold stress (C1–C20). **(B)** GO terms enriched in DEGs, with red indicating more significant enrichment (–log10(*P*-value)). The heatmaps show enriched GO terms detected in temporally dynamic groups of both drought and cold stress from 1 to 48 h.

showed oxidoreductase activity, as well as the genes associated with abiotic stress reaction (Figures 3A, B). These GO terms are consistent with the early and late physiological changes, which were observed in plant cells under drought and cold stress (Muns et al., 2007; Guo et al., 2021). This similarity in biological functions indicates that abiotic stress-response genes have maintained conserved expression dynamics.

Our objective was to gain insight into the regulatory mechanism underpinning drought and cold stress by using hierarchical clustering (Figures S1, S2). Under drought and cold stress response, the hierarchical clustering network consist of differentially expressed genes with 6 cluster (DI-VI) and 4 cluster (CI-IV) (Figures S1, S2), respectively. Cluster enrichment analyses revealed that, despite the presence of multiple metabolic pathways, some patterns could be discerned in a single cluster. For example, in drought stress response, genes involved in "membrane," "abiotic stress stimulus," "oxidoreductase activity," "response to abiotic stress," "response to stress," "ADP metabolic process," and "oxidation-reduction process," were mainly enriched in cluster D-III, which exhibited an increasing trend from 12 to 36 h, indicating that membrane biosynthesis, ADP metabolic process and oxidoreductase activity pathways are enhanced in response to drought stress (Figure S1). In cold stress response, genes involved in "oxidoreductase activity," "abiotic stress stimulus," "antioxidant activity," "photosynthesis," and "plant-pathogen interactions" were enriched in cluster C-IV and exhibited an increasing trend from 0 to 12 h, suggesting active ROS scavenging. DEGs involved in "response to abiotic stimulus" and "organic substance biosynthetic process," and "response to cold," were enriched in cluster C-II and showed continuously decreasing trends to 48 h (Figure S2). As a result of drought and cold stress, *M. rubra* exhibits early and late physiological changes that are consistent with these two GO terms.

Transcriptional regulatory networks involved in drought and cold stress

Expression dynamics are conserved, indicating that some regulators are common to both early and late responses in two abiotic stresses (Wu et al., 2021). Gene expression profiles under abiotic stress were sample-specific for TFs, which dominated the network rather than other genes (Yin et al., 2019; Wu et al., 2021). In our current research, a total of 1,923 and 1,731 stress-responsive TFs were identified under drought and cold stress, respectively, 26.6% (548) of which are stress-conserved TFs (Figure 4A). TFs had more sample-specific expression profiles under different abiotic stresses (Wu et al., 2021), and the number of stress-responsive TFs increased significantly across the samples in our study (Figure 4B). Specially, TF families of bHLH, MYB, ethylene responsive factor (ERF), MYB, WRKY, and NAM, ATAF, and CUC (NAC) showed one of the highest enrichments under drought and cold stress (Figure 4B). The bHLHs proteins, for instance, form a large family of plant-specific TFs that play an important role in plant defense and biotic and abiotic stresses (Yoda et al., 2002; Journot-Catalino et al., 2006; Zheng et al., 2006; Liu et al., 2007). Interestingly, the transcription of *MrbHLH18*, *MrbHLH31*, *MrbHLH10* and *MrbHLH75* increased significantly under both drought and cold stress, which are grouped in cluster D3 and C7 related to response to abiotic stimulus and oxidoreductase activity in both abiotic stresses.

To further examine the potential regulatory relationships, we constructed gene regulatory network (GRN) that interlinks TFs with their potential target genes (PTGs) based on the expression data and examined the presence of *MrbHLH10* potential TF binding site (TFBS) to verify the GRN (Figure 4C). As a result,

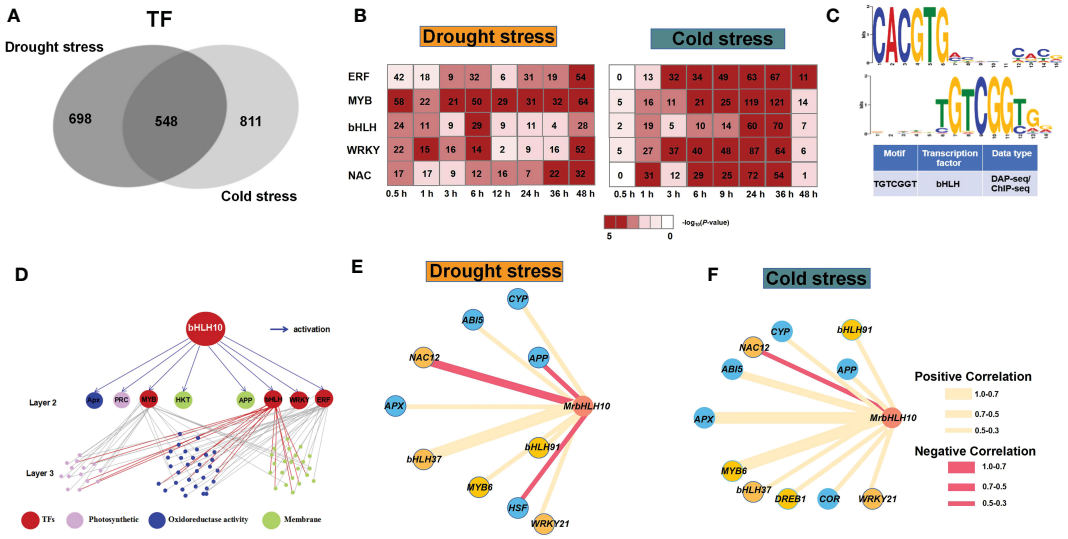

FIGURE 4
Gene regulatory networks of drought and cold-responsive transcriptional modulators. **(A)** Venn diagrams of TFs overlapping between drought stress and cold stress. **(B)** Enrichment (−log10 (P-value)) of TF families in timepoint (0–48 h) under drought stress (left) and cold stress (right). The number represents the number of differentially expressed TF genes. The heatmap presents TF families enriched in at least one of 20 groups. **(C)** Bioinformatic analysis of bHLH Binding Site (TFBS) Motifs based on PlantTFDB database (http://planttfdb.gao-lab.org/). **(D)** Gene regulatory network of photosynthesis, oxidoreductase activity and membrane regulation under drought stress and cold stress. **(E)** Coexpression network of genes that are differentially expressed under drought stress and cold stress **(F)** treatment in *M. rubra* at different timepoints.

totally 227 TF-PTG pairs were identified, and we observed that MYBs, WRKYs, bHLHs and ERFs which targeted large numbers of genes (twenty or more target genes from each TF as indicated by solid or arrows line, Figure 4D). Notably, *MrbHLH10* regulated 39 downstream ROS signaling pathway genes, and clear functional associations were observed in both stresses—*MrbHLH10* were connected to *APX* (GENE_006840) gene (Figures 4E, F; $R > 0.6$; $P < 0.05$), while multiple previously stress-responsive gene, such as *WRKY21* (Zhang et al., 2017) and *MYB6* (Li et al., 2020) were also associated with *MrbHLH10* (Figures 4E), indicating a role as the master regulators under the cold and drought stress.

Molecular characterization of MrbHLH10

The bHLH superfamily, one of the largest TF families, is widespread in eukaryotes (Pires & Dolan, 2010). Among the amino acid sequences of the MrbHLH proteins, there is a high

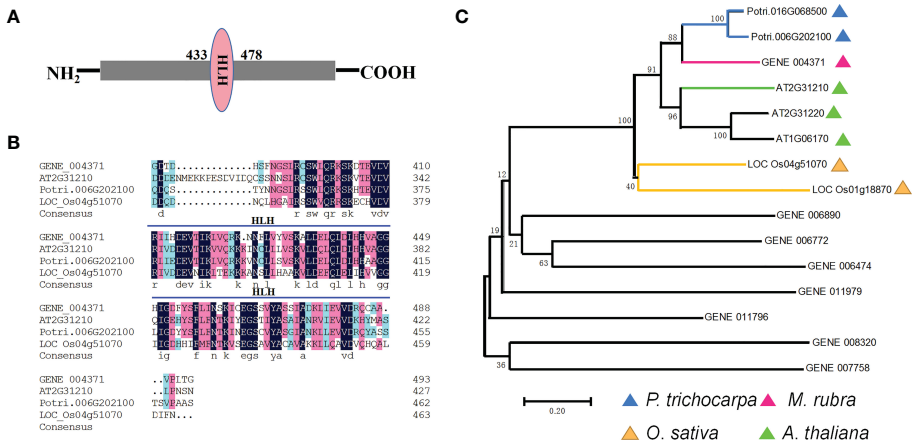

FIGURE 5
Bioinformatics analysis of *bHLH* gene **(A)** Domain architecture analysis of MrbHLH protein. **(B)** Multiple amino acid sequence alignment of bHLH10 from *M. rubra*, *O. sativa*, *P. trichocarpa* and *A. thaliana*. **(C)** Phylogenetic analysis of bHLH homologs from *M. rubra*, *O. sativa*, *P. trichocarpa* and *A. thaliana*. Scale bars, 0.2.

conservation domain comprising 60 amino acids with two distinct functional areas (Figure 5A). The base region, which is located at the N-terminal end of the domain, participates in DNA binding, is composed of 15 amino acids with many base residues (Tian et al., 2019). The MrbHLH10 coding sequencing (CDS) is 1,483 bp long, encoding 493 amino acids and having a molecular mass of ~54 kD and an isoelectric point of 5.42 (Table S6). The multiple amino acid sequence alignment and a phylogenetic tree indicated that the bHLH protein sequences from multiple species consist of the same conserved domains (Guo et al., 2021) (Figures 5B, C). Therefore, MrbHLH10 and ATbHLH10 might have the same biological function, which has been demonstrated to respond to various abiotic stresses (Guo et al., 2021).

In order to probe into the potential biology function of *MrbHLH10* gene in *M. rubra*, we made a deep analysis on the expression mode of bHLH. Notably, a total of 241 *MrbHLH* members are detected in *M. rubra*, which show four major expression patterns (Figure S3). MrbHLH10 showed different expression patterns in 12 of the selected organs or tissues (Figure S3), for instance, the expression profiles of *bHLH10* gene in the branch, xylem and mature leaf show similar trends, and expression patterns in the young leaf, phloem and petiole grouped in one cluster (Figure S3), indicating that *bHLH10* gene regulate plant growth and stress response in *M. rubra*.

MrbHLH10 promotes APX and ROS scavenging in response to environmental stresses

To investigate the potential function of bHLH10 in the response to enviromental stresses, we generated transgenic *A. thaliana* seedling overexpressing (OE) and RNAi bHLH10 *via Agrobacterium tumefaciens*-mediated transformation (Figure 6A) (Zhang et al., 2022). Compared to the WT and RNAi line, the OE line had a significantly longer root length and heavier fresh weight increased by 22.9% and 62.8% respectively under normal condition ($P<0.05$; Figure S3), indicating that *MrbHLH10* gene is implicated in plant growth (Figures 6A–C).

Compared with WT and RNAi lines, the primary root length of OE was obviously increased ($P<0.05$; Figure 6D). After 7 days of treatment at 4 °C, the WT and RNAi lines showed a significant increase in the primary root length of OE line compared with WT and RNAi ($P<0.05$; Figure 6G), indicating that *bHLH10* can

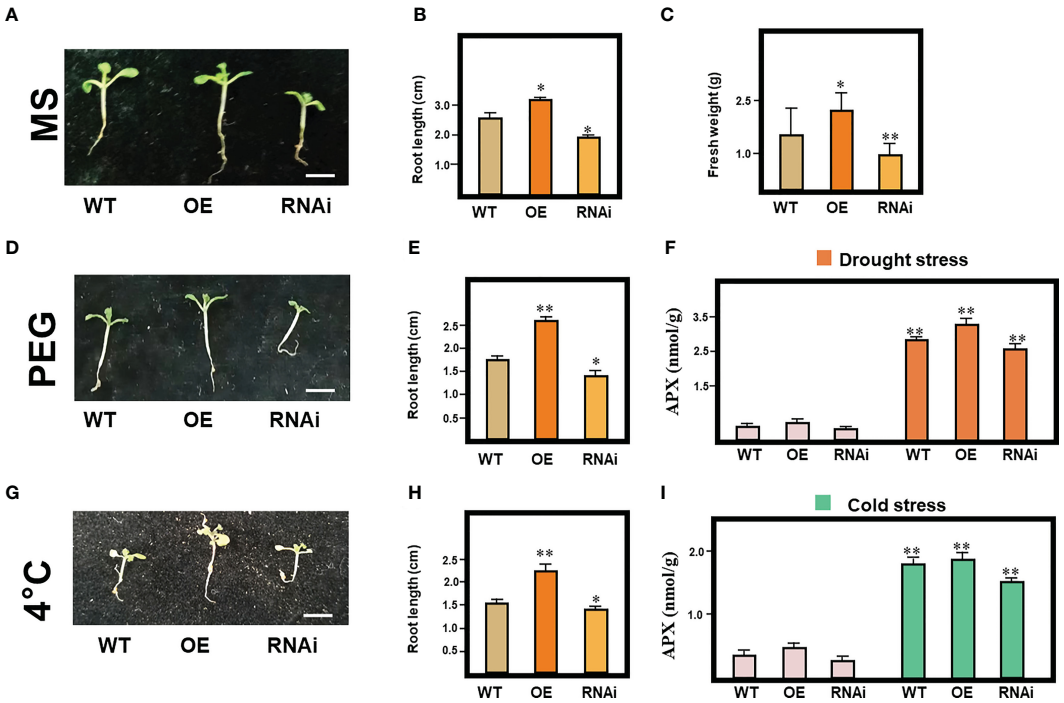

FIGURE 6
MrbHLH10 expression in response to drought and cold stress. **(A)** Time course of *MrbHLH10* expression in *A. thaliana* exposed to drought and cold stress on standard ½ MS medium. **(B)** Root length and **(C)** fresh weight of wild-type (WT), *MrbHLH10*-OE and *MrbHLH10*-RNAi lines grown on standard ½ MS medium for 1 weeks. **(D)** Time course of *MrbHLH10* expression in *A. thaliana* exposed to drought stress on standard ½ MS medium with 8% PEG for 1 weeks. **(E)** Root length of wild-type (WT), *MrbHLH10*-OE and *MrbHLH10*-RNAi lines grown on standard ½ MS medium with 8% PEG for 1 weeks. **(F)** APX content in leaves of wild-type (WT), *MrbHLH10*-OE and *MrbHLH10*-RNAi lines grown on standard ½ MS medium with 8% PEG for 1 weeks. **(G)** Time course of *MrbHLH10* expression in *A. thaliana* exposed to drought stress on standard ½ MS medium with 4 °C for 1 weeks. **(H)** Root length of wild-type (WT), *MrbHLH10*-OE and *MrbHLH10*-RNAi lines grown on standard ½ MS medium, with 4 °C for 1 weeks. **(I)** APX content of wild-type (WT), *MrbHLH10*-OE and *MrbHLH10*-RNAi lines grown on standard ½ MS medium, with 4 °C for 1 weeks. Data are presented as means ± SD (n = 3). (*$P < 0.05$, **$P < 0.01$, Student's t-test).

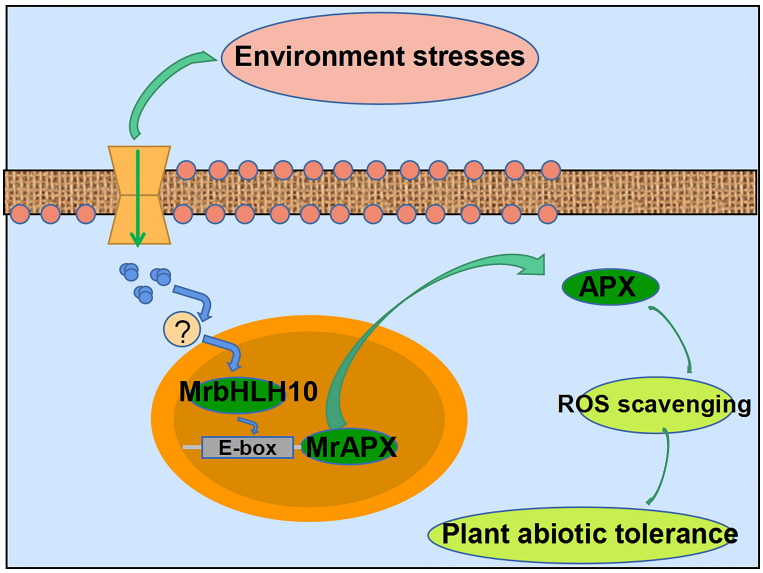

FIGURE 7
A potential working model for bHLH10 response to abiotic stresses in *M. rubra*. Under drought and cold stress, activating the environmental stresses signaling pathway and stimulating downstream stress signal transduction in plant cells, the upregulated bHLH10 acts upstream of APX and directly regulates its expression by binding to the E-box motif of its promoter. The activated APX then promotes cytosolic ascorbate peroxidase accumulation to scavenge ROS content under environmental stresses.

positively increase the growth of plants under drought and cold stress. Ascorbate peroxidase (APX) maintain cellular ROS homeostasis and is major ROS scavengers (Xing et al., 2018; Wang et al., 2021). APX activity were measured in OE, RNAi and WT line. Total APX activity was strongly induced, and OE line showed distinctly APX activity higher than WT plants and RNAi line respectively under drought and cold stress ($P<0.05$; Figures 6F, I). Thus, bHLH10 could be used as an indirect way to improve drought and cold-tolerance by keeping ROS in a stable state.

Discussion

Presence of conserved gene regulatory network in response to environmental stresses

The improvement of the plant's ability to withstand many kinds of stress is one of the fundamental objectives of breeding. It is of great importance to enhance the comprehensive resistance of plants by means of core functional genes in molecular breeding. (Hu et al., 2017; Xu et al., 2023). In this study, we constructed a high-temporal-resolution dynamic transcriptome landscape of drought and cold stress responses using nine time points. The dynamic transcriptome profiles were clealy grouped into four and two stages within the drought and cold stress response respectively, indicating the early-responsive and late-responsive phase (Hickman, 2017; Wu et al., 2021). We found there were 7,453 and 9,614 genes mainly expressed at the stages of early- and late-responsive phase respectively. Biological processes in the K-Means groups with similar expression dynamics were probably maintained across the two types of abiotic stresses. It is also possible that there are common regulators of early and late responses in both stressors due to the conserved expression dynamics. Specifically, we have identified 2,311 stress-conserved genes, among them 548 TFs, which will undoubtedly become the goal of functional genomics in the future. Because of this vast array of genes, we will be able to carry out further functional research, which will significantly improve our knowledge of the genetic mechanisms that govern the response to environmental stresses.

The TFs of bHLH, MYB, NAC, WRKY and ERF are known to regulate stress-responsive genes (He et al., 2018; Wu et al., 2021). Some TFBSs, which were enriched in the promoter, were related to the up-regulation of TF genes. The *bHLH* TF gene and some bHLH binding sites were significantly enriched (Guo et al., 2019; Yu et al., 2021). Therefore, transcriptomic regulation during salt stress in *M. rubra* is mediated by dynamic regulation of bHLHs and other TFs. In *A. thaliana*, these TFs are also associated with a cold stress response (Xu et al., 2014; Guo et al., 2021; Yu et al., 2021). In addition, *bHLH* genes function in leaf formation and growth as well as heat and drought stress responses (Khadiza et al., 2017; Zhao et al., 2021), indicating that in the two main dicotyledons and probably in other plants, bHLH orthologues are thought to confer a stress-tolerance mechanism.

bHLH is implicated in environmental stresses tolerance and plant growth

To adapt to abiotic stress conditions including extreme temperatures (heat and freezing), plants regulate a series of genes, so as to form a GRN in previous study (Guo et al., 2021; Jia et al.,

2022). In the absence of a central trans-regulator gene, a GRN could be deleted completely or network connectivity could be reorganized (Wu et al., 2021; Xu et al., 2022). However, there is still little investigation on the construction of GRNs in response to abiotic stresses combination (Reményi et al., 2004; Song et al., 2016; Vihervaara et al., 2018).

Systemic signaling in plants during abiotic stress combination (Zandalinas et al., 2020). In the bHLH10-mediated GRN, direct target genes including MYB6, WRKY41, TCP4, CYP1, STZ and APX1 were identified. In *O. sativa*, overexpression of *OsbHLH148* gene increases the plant's drought tolerance by regulating the JA pathway and the expression of OsJAZ protein (jasmonate ZIM domain) (Seo et al., 2011). With the expression of *MfbHLH38* gene from resurrection plants (*Myrothamnus flabellifolius*), transgenic *Arabidopsis* has improved water retention and drought tolerance, as well as the increase of their oxidative stress tolerance and osmotic regulatory ability, which is associated with the ABA response and elevated ABA content. In our study, multiple target genes of bHLH10, such as APX1 and WRKY41 were known to function in ROS scavenging and ABA signal processes (Reményi et al., 2004; Song et al., 2016; Vihervaara et al., 2018). In addition, recent studies showed that AtSTZ, a downstream transcription repressor, enhances abiotic stress tolerance after growth delay in *Arabidopsis* (Park et al., 2015; Sakamoto, 2004), may be regulated by MAP kinases in *Arabidopsis* (Nguyen et al., 2016). CYP1 mediate the last steps of auxin biosynthesis, as well as root growth inhibition in response to stress (Rodríguez et al., 2010).

The bHLH TFs are also involved in the course of development and growth, including the germination of seeds and the development of root, epidermis, xylem, carpels, anthers, fruits and stomata (Groszmann et al., 2010; Guo et al., 2021). In our study, root length significantly increased 131%, 114% and 78% in the *MrbHLH10*-OE line compared to the WT under drought, cold and normal condition respectively. Currently, there is evidence that bHLHs directly regulate cytokinin synthesis genes or cytokinin degradation genes such as CKXs (Hezhong et al., 2008; Hozain et al., 2012). bHLH10 may directly regulate *MrCKX* by GRN analysis, enhancing root development and cell division in root of OE plants, in agreement with prior reports (Hezhong et al., 2008). In contrast to other stress-tolerant genes like MYB6, DREB2C, WRKY45, and AtSAP5 (Lim et al., 2007; Hozain et al., 2012), overexpression of *bHLH10* gene enhances plant growth and environmental stresses tolerance.

MrAPX1 may be a key downstream gene involved in ROS scavenging

Excess ROS, for example, caused by environmental stresses, such as heat, salt, cold, and drought stress, results in oxidative conditions that are detrimental to plant cells (Wang et al., 2008; He et al., 2018). In response to environmental stresses, plants accumulate cryoprotectant molecules such as soluble sugars, sugar alcohols, and low-molecular-weight nitrogenous compounds (proline and glycinebetaine; Zhuo et al., 2017; He et al., 2018; Xing et al., 2018), and activated antioxidant defence systems which include MDA, CAT, SOD, POD and APX (He et al., 2018; Wang et al., 2021; Xie et al., 2018; Zhuo et al., 2017). These antioxidative enzymes can suppress ROS accumulation in plant cells due to environmental stress (Wang et al., 2021; Wu et al., 2018). The cycle of AsA-GSH and SOD is of great significance to the scavenging of ROS (He et al., 2018; Shi et al., 2014). SOD acts as a first defence mechanism for ROS, it catalyzes the conversion of oxygen ions (O_2^-) into oxygen (O_2) and hydrogen peroxide (H_2O_2) (Huang et al., 2016; He et al., 2018), in the AsA-GSH cycle, AsA reduces H_2O_2 to water (H_2O) (Xing et al., 2018). Our findings indicate that bHLH10 may activate stress-responsive gene including APX1 to modulate ROS accumulation under environmental stresses by GRN analysis. Further physiological analyses support this hypothesis, activities of APX increased in transgenic plants under normal, cold and drought stress conditions in our study. In previous study, APX subtypes are present in a variety of organelles as well as in the cytosol, whose adjustment modes differ under environmenta stress conditions (He et al., 2018; Xing et al., 2018). Recent studies shown that *APX1* is induced by heat, cold, drought and H_2O_2 stresses, and *APX* genes confer tolerance to various abiotic stresses when overexpressed in transgenic plants (Wang et al., 2016; He et al., 2018; Wang et al., 2020). Absence of cytosolic APX1 in Wassilewskija background results in a breakdown of the H_2O_2-scavenging system in *Arabidopsis* chloroplasts, causing an increase in H_2O_2 and protein oxidation (Davletova et al., 2005). A knockout of APX1 also significantly inhibits *Arabidopsis* growth and development, leading to increase sensitivity to oxidative stress, stunted growth and delayed flowering (Davletova et al., 2005; Miller et al., 2007; He et al., 2018). In *Populus*, activated PeAPX1 promotes cytosolic APX that scavenges ROS under cold and heat stress, and transgenic *Populus* overexpressing *PtAPX1* showed increased cold tolerance and led to lower MDA and H_2O_2 levels in leaf and roots, resulting in higher plant height and root biomass under cold stress, phenocopying the *MrbHLH10* OE plants in our study (He et al., 2018; Zhou et al., 2020; Guo et al., 2021).

In this study, we present a systematic review of ROS scavenging regulation first, as well as the complex GRNs that accompany it, and such networks have an essential role to play in understanding plant responses to environmental stresses. Together, the results show that MrbHLH10, a versatile TF, can increase environmental stresses by regulating the expression of MrAPX1, a direct downstream gene, which in turn keeps ROS stable (Figure 7). These results indicate that over-expression of bHLH10 can enhance the antioxidative function of transgenic plants, which might be helpful to prevent hyperosmolar and excess ROS due to environmental stresses.

Data availability statement

Raw data for RNA-seq are available at the BIGD Genome Sequence Archive (https://bigd.big.ac.cn) under accession number CRA006695

Ethics statement

This study was completed within the laws of the People's Republic of China. No specific permits were required for our field research. The study species is not included in the 'List of Protected Plants in China.

Author contributions

HR and JX designed the conception and experiment; WX, HR, XQ, SZ and ZY performed the experiments; WX wrote the manuscript; JX and HR helped to analyze and assess the data; XQ and SZ provided the valuable suggestions on the manuscript; JX helped to revise the manuscript; HR and JX obtained the funding and were responsible for this manuscript; all authors read and approved the manuscript.

Funding

This study was supported by Breeding for Agricultural New Varieties in Zhejiang Province (2021C02066-2) and Key R&D Projects in Zhejiang Province (2019C02038, 2020C02001, and 2021C02009), State Key Laboratory for Managing Biotic and Chemical Threats to the Quality and Safety of Agro-products (2021DG700024-KF202306), the Key Laboratory of Horticultural Plant Genetic and Improvement of Jiangxi Province, the open project of the Key Laboratory of Horticultural Plant Genetic and Improvement of Jiangxi Province (2021KFJJ001), National Key R&D Program of China (No.2022YFD2201600; 2022YFD2200602), the Project of the National Natural Science Foundation of China (NOs., 32022057 and 31972954), Forestry and Grassland Science and Technology Innovation Youth Top Talent Project of China (No. 2020132607).

Acknowledgments

We thank Ms. Liju Yan, Mr. Qi Zhang, and Ms. Xiuzhu Guo for collecting samples.

Conflict of interest

The authors declare that the research was conducted in the absence of any commercial or financial relationships that could be construed as a potential conflict of interest.

Publisher's note

Supplementary material

The Supplementary Material for this article can be found online at: https://www.frontiersin.org/articles/10.3389/fpls.2023.1155504/full#supplementary-material

References

Benjamini, Y., and Hochberg, Y. (1995). Controlling the false discovery rate: a practical and powerful approach to multiple testing. *J. R. Stat. society: Ser. B (Methodological)* 57 (1), 289–300.

Bhattacharjee, S. (2012). The language of reactive oxygen species signaling in plants. *J. Bot.* 2012, 1–22. doi: 10.1155/2012/985298

Chow, C. N., Zheng, H. Q., Wu, N. Y., Chien, C. H., Huang, H. D., Lee, T. Y., et al. (2016). PlantPAN 2.0: an update of plant promoter analysis navigator for reconstructing transcriptional regulatory networks in plants. *Nucleic Acids Res.* 44, D1154–D1160. doi: 10.1093/nar/gkv1035

Cui, L. G., Shan, J. X., Shi, M., Gao, J. P., and Lin, H. X. (2015). DCA1 acts as a transcriptional co-activator of DST and contributes to drought and salt tolerance in rice. *PloS Genet.* 11, e1005617. doi: 10.1371/journal.pgen.1005617

Davletova, S., Rizhsky, L., Liang, H., Shengqiang, Z., Oliver, D. J., Coutu, J., et al. (2005). Cytosolic ascorbate peroxidase 1 is a central component of the reactive oxygen gene network of arabidopsis. *Plant Cell* 17 (1), 268–281.

De la Garma, J. G., Fernandez-Garcia, N., Bardisi, E., Pallol, B., Rubio-Asensio, J. S., Bru, R., et al. (2015). New insights into plant salt acclimation: the roles of vesicle trafficking and reactive oxygen species signalling in mitochondria and the endomembrane system. *New Phytol.* 205, 216–239. doi: 10.1111/nph.12997

Deng, W., Zhang, K., Busov, V., and Wei, H. (2017). Recursive random forest algorithm for constructing multilayered hierarchical gene regulatory networks that govern biological pathways. *PloS One* 12, e0171532. doi: 10.1371/journal.pone.0171532

Ding, Y., Shi, Y., and Yang, S. (2020). Molecular regulation of plant responses to environmental temperatures. *Mol. Plant* 13, 544–564. doi: 10.1016/j.molp.2020.02.004

Groszmann, M., Bylstra, Y., Lampugnani, E. R., and Smyth, D. R. (2010). Regulation of tissue-specific expression of SPATULA, a bHLH gene involved in carpel development, seedling germination, and lateral organ growth in *Arabidopsis*. *J. Exp. Bot.* 61, 1495–1508. doi: 10.1093/jxb/erq015

Guo, J., Sun, B., He, H., Zhang, Y., and Wang, B. (2021). Current understanding of bhlh transcription factors in plant abiotic stress tolerance. *Int. J. Mol. Sci.* 22 (9), 4921. doi: 10.3390/ijms22094921

Guo, J., Dong, X., Han, G., and Wang, B. (2019). Salt-enhanced reproductive development of suaeda salsa l. coincided with ion transportergene upregulation in flflowers and increased pollen k+ content. *Front. Plant Sci.* 10, 333.

He, F., Wang, H. L., Li, H. G., Su, Y., Li, S., Yang, Y., et al. (2018). PeCHYR1, a ubiquitin eligase from *Populus euphratica*, enhances drought tolerance *via* ABA-induced stomatal closure by ROS production in *Populus*. *Plant Biotechnol. J.* 16, 1514–1528. doi: 10.1111/pbi.12893

Hernández, L. E., Sobrino-Plata, J., Montero-Palmero, M. B., Carrasco-Gil, S., Flores-Cáceres, M. L., Ortega-Villasante, C., et al. (2015). Contribution of glutathione to the control of cellular redox homeostasis under toxic metal and metalloid stress. *J. Exp. Bot.* 66, 2901–2911. doi: 10.1093/jxb/erv063

Hickman, R. (2017). Architecture and dynamics of the jasmonic acid gene regulatory network. *Plant Cell* 29, 2086–2105. doi: 10.1105/tpc.16.00958

Huang, S. B., Van Aken, O., Schwarzlander, M., Belt, K., and Millar, A. H. (2016). The roles of mitochondrial reactive oxygen species in cellular signaling and stress response in plants. *Plant Physiol.* 171, 1551–1559. doi: 10.1104/pp.16.00166

Hezhong, J. (2008). Study on technique of extracting volatile oils of notopterygium incisum ting ex HT Chang by SFE-CO~ 2. *J. Of Anhui Agric. Sci.* 36 (5), 1740.

Hozain, M. D., Abdelmageed, H., Lee, J., Kang, M., Fokar, M., Allen, R. D., et al. (2012). Expression of AtSAP5 in cotton up-regulates putative stress-responsive genes and improves the tolerance to rapidly developing water deficit and moderate heat stress. *J. Plant Physiol.* 169 (13), 1261–1270.

Hu, Y., Jiang, Y., Han, X., et al. (2017). Jasmonate regulates leaf senescence and tolerance to cold stress: crosstalk with other phytohormones. *J. Exp. Bot.* 68, 1361–1369.

Jiang Jiye, L. (2002). The algorithm on Knowledge Reduction in incomplete information system. *Int. J. Uncertainty Fuzziness Knowledge-Based Syst.* 24 (1), 95–103.

Jia, Y. Q., Niu, Y. N., Zhao, H. M., and Wang, Z. B. (2022). Hierarchical transcription factor and regulatory network for drought response in betula platyphylla. *Hortic. Res.* 9, 40. doi: 10.1093/hr/uhac040

Journot-Catalino, N., Somssich, I. E., Roby, D., and Kroj, T. (2006). The transcription factors WRKY11 and WRKY17 act as negative regulators of basal resistance in arabidopsis thaliana. *Plant Cell* 18 (11), 3289–3302.

Khadija, A., Lahlou, Y., Chemlali, S., Kissa, J., Gharibi, A., and Baite, M. (2017). Cone beam computed tomography study of intra-sinus calcifications. *Glob J. Med. Res.* 17 (1), 4–13.

Kesavaraju, B., and Dickson, S. (2012). New technique to count mosquito adults: using imagej software to estimate number of mosquito adults in a trap. *J. Am. Mosq. CONTR* 28 (4), 330–333. doi: 10.2987/12-6254R.1

Kuge, Y., Takai, N., Ogawa, Y., Temma, T., Zhao, Y., Nishigori, K., et al. (2010). Imaging with radiolabelled anti-membrane type 1 matrix metalloproteinase (mt1-mmp) antibody: potentials for characterizing atherosclerotic plaques. *Eur. J. Nucl. Med. Mol. Imaging* 37 (11), 2093–2104.

Kumar, S., Thambiraja, T. S., Karuppanan, K., and Subramaniam, G. (2022). Omicron and delta variant of SARS-CoV-2: a comparative computational study of spike protein. *J. Med. Virol.* 94 (4), 1641–1649.

Kumar, S., Stecher, G., Li, M., Knyaz, C., and Tamura, K. (2018). Mega x: molecular evolutionary genetics analysis across computing platforms. *Mol. Biol. Evol.* 6, 6. doi: 10.1093/molbev/msy096

Larchevêque Maurel, M., Desrochers, A., and Larocque, G. R. (2011). How does drought tolerance compare between two improved hybrids of balsam poplar and an unimproved native species?. *Tree Physiology*, 31(3), 240–249.

Li, B., Gao, K., Ren, H., and Tang, W. (2018). Molecular mechanisms governing plant responses to high temperatures. *J. Integr. Plant Biol.* 60, 757–779. doi: 10.1111/jipb.12701

Li, H., Yang, Z., Zeng, Q., Wang, S., Luo, Y., Huang, Y., et al. (2020). Abnormal expression of bHLH3 disrupts a flflavonoid homeostasis network, causing differences in pigment composition among mulberry fruits. *Hortic. Res.* 7, 83.

Li, J. J., Li, Y., Yin, Z. G., Jiang, J. H., Zhang, M. H., Guo, X., et al. (2017). OsASR5 enhances drought tolerance through a stomatal closure pathway associated with ABA and H2O2 signalling in rice. *Plant Biotechnol. J.* 15, 183–196. doi: 10.1111/pbi.12601

Liao, B. Y., and Zhang, J. (2006). Evolutionary conservation of expression profiles between human and mouse orthologous genes. *Mol. Biol. Evol.* 23, 530–540. doi: 10.1093/molbev/msj054

Lim, P. O., Kim, H. J., and Gil Nam, H. (2007). Leaf senescence. *Annu. Rev. Plant Biol.* 58, 115–136.

Liu, X. Q., Bai, X. Q., Wang, X. J., and Chu, C. C. (2007). OsWRKY71, a rice transcription factor, is involved in rice defense response. *J. Plant Physiol.* 164 (8), 969–979.

Miller, G. E., Chen, E., and Zhou, E. S. (2007). If it goes up, must it come down? chronic stress and the hypothalamic-pituitary-adrenocortical axis in humans. *psychol. Bull.* 133 (1), 25.

Miller, G., Suzuki, N., Ciftci-Yilmaz, S., and Mittler, R. (2010). Reactive oxygen species homeostasis and signalling during drought and salinity stresses. *Plant Cell Environ.* 33, 453–467. doi: 10.1111/j.1365-3040.2009.02041.x

Mittler, R. (2006). Abiotic stress, the field environment and stress combination. *Trends Plant Sci.* 11 (1), 15–19.

Mittler, R., Vanderauwera, S., Gollery, M., and Breusegem, F. V. (2004). Reactive oxygen gene network of plants. *Trends Plant Sci.* 9, 490–498. doi: 10.1016/j.tplants.2004.08.009

Mun, S., Decker, E. A., and McClements, D. J. (2007). Influence of emulsifier type on *in vitro* digestibility of lipid droplets by pancreatic lipase[J]. *Food Res. Int.* 40 (6), 770–781.

Nakagawa, T., Kurose, T., Hino, T., Tanaka, K., Kawamukai, M., Niwa, Y., et al. (2007). Development of series of gateway binary vectors, pGWBs, for realizing efficient construction of fusion genes for plant transformation. *J. bioscience bioengineering* 104 (1), 34–41.

Nguyen, P. K., Rhee, J. W., and Wu, J. C. (2016). Adult stem cell therapy and heart failurTo 2016: a systematic review. *JAMA Cardiol.* 1 (7), 831–841.

Ohama, N., Sato, H., Shinozaki, K., and Yamaguchi-Shinozaki, K. (2017). Transcriptional regulatory network of plant heat stress response. *Trends Plant Sci.* 22, 53–65. doi: 10.1016/j.tplants.2016.08.015

Park, S., Lee, C. M., Doherty, C. J., Gilmour, S. J., Kim, Y., and Thomashow, M. F. (2015). Regulation of the *Arabidopsis* CBF regulon by a complex low-temperature regulatory network. *Plant J.* 82, 193–207. doi: 10.1111/tpj.12796

Pires, N., and Dolan, L. (2010). Origin and diversification of basic-helix-loop-helix proteins in plants. *Mol. Biol. Evol.* 27, 862–874. doi: 10.1093/molbev/msp288

Quan, M., Liu, X., Xiao, L., Chen, P., Song, F., Lu, W., et al. (2021). Transcriptome analysis and association mapping reveal the genetic regulatory network response to cadmium stress in populus tomentosa[J]. *J. Exp. Bot.* 72 (2), 576–591.

Quan, M., Liu, X., Xiao, L., Chen, P., Song, F., Lu, W., et al. (2020). Transcriptome analysis and association mapping reveal the genetic regulatory network response to cadmium stress in populus tomentosa[J]. *J. Exp. Bot* 72 (2), 576-591. doi: 10.1093/jxb/eraa434

Reményi, A., Schöler, H. R., and Wilmanns, M. (2004). Combinatorial control of gene expression. *Nat. Struct. Mol. Biol.* 11, 812–815. doi: 10.1038/nsmb820

Ren, H. Y., He, Y. H., Qi, X. J., Zheng, X. L., Zhang, S. W., Yu, Z. P., et al. (2021). The bayberry database: a multiomic database for myrica rubra, an important fruit tree with medicinal value. *BMC Plant Biol.* 21, 452. doi: 10.1186/s12870-021-03232-x

Ren, H., Yu, H., Zhang, S., Liang, S., and Qi, X. (2019). Genome sequencing provides insights into the evolution and antioxidant activity of chinese bayberry. *BMC Genomics* 20 (1), 458. doi: 10.1186/s12864-019-5818-7

Rodríguez, P., Luna, A., Candela, I., Mujal, R., Teodorescu, R., and Blaabjerg, F. (2010). Multiresonant frequency-locked loop for grid synchronization of power converters under distorted grid conditions. *IEEE Trans. Ind. Electron.* 58 (1), 127–138.

Rossel, J. B., Wilson, P. B., Hussain, D., Woo, N. S., Gordon, M. J., Mewett, O. P., et al. (2007). Systemic and intracellular responses to photooxidative stress in arabidopsis. *Plant Cell* 19 (12), 4091–4110.

Sakamoto, Y., Suzuki, T., Kobayashi, M., Gao, Y., Fukai, Y., Inoue, Y., et al. (2004). Perfluoropentacene: high-performance p– n junctions and complementary circuits with pentacene. *J. Am. Chem. Soc.* 126 (26), 8138–8140.

Sánchez-Pérez, R., Pavan, S., Mazzeo, R., and Moldovan, C. (2019). Mutation of a bHLH transcription factor allowed almond domestication. *Science* 364, 1095–1098. doi: 10.1126/science.aav8197

Seo, J. H., Gutacker, A., Sun, Y., Wu, H., Huang, F., Cao, Y., et al. (2011). Improved high-efficiency organic solar cells *via* incorporation of a conjugated polyelectrolyte interlayer. *J. Am. Chem. Soc.* 133 (22), 8416–8419.

Shi, H., Ye, T., Chen, F., Cheng, Z., Wang, Y., Yang, P., et al. (2013). Manipulation of arginase expression modulates abiotic stress tolerance in arabidopsis: effect on arginine metabolism and ROS accumulation. *J. Exp. Bot.* 64, 1367–1379.

Shi, H., Ye, T., Zhu, J. K., and Chan, Z. (2014). Constitutive production of nitric oxide leads to enhanced drought stress resistance and extensivetranscriptional reprogramming in arabidopsis. *J. Exp. Bot.* 65, 4119–4131.

Song, L., Huang, S. S. C., Wise, A., Castanon, R., Nery, J. R., Chen, H., et al. (2016). A transcription factor hierarchy defines an environmental stress response network. *Science* 354, 1550. doi: 10.1126/science.aag1550

Sun, W., Jin, X., Ma, Z., Chen, H., and Liu, M. (2020). Basic helix–loop–helix (bHLH) gene family in tartary buckwheat (*Fagopyrum tataricum*): Genome-wide identification, phylogeny, evolutionary expansion and expression analyses. *Int. J. Biol. Macromol.* 155, 1478–1490. doi: 10.1016/j.ijbiomac.2019.11.126

Tian, Q., Chen, J., Wang, D., Wang, H.-L., Liu, C., Wang, S., et al. (2016). Overexpression of a populus euphratica CBF4 gene in poplar confers tolerance to multiple stresses. *Plant Cell Tissue Organ Culture* 128, 391– 407.

Trapnell, C., Pachter, L., and Salzberg, S. L. (2009). TopHat: discovering splice junctions with RNA-seq. *Bioinformatics* 25 (9), 1105–1111.

Trapnell, C., Roberts, A., Goff, L., Pertea, G., Kim, D., Kelley, D. R., et al. (2012). Differential gene and transcript expression analysis of RNA-seq experiments with TopHat and cufflinks. *Nat. Protoc.* 7 (3), 562–578.

Vihervaara, A., Duarte, F. M., and Lis, J. T. (2018). Molecular mechanisms driving transcriptional stress responses. *Nat. Rev. Genet.* 19, 385–397. doi: 10.1038/s41576-018-0001-6

Wang, C., Liu, S., Dong, Y., Zhao, Y., Geng, A., Xia, X., et al. (2016). PdEPF1 regulates water-use efficiency and drought tolerance by modulating stomatal density in poplar. *Plant Biotechnol. J.* 14, 849–860. doi: 10.1111/pbi.12434

Wang, L. Q., Wen, S. S., Wang, R., and Wang, C. (2021). Pagwox11/12a activates pagcyp736a12 gene that facilitates salt tolerance in poplar. *Plant Biotechnol. J.* 33, 128–139. doi: 10.1111/pbi.13653

Wang, Y. Y., Cao, Y. B., and Liang, X. Y. (2022). A dirigent family protein confers variation of casparian strip thickness and salt tolerance in maize. *Nat. Commun.*, 13.

Wang, R. G., Chen, S. L., Zhou, X. Y., Shen, X., Deng, L., Zhu, H. J., et al. (2008). Ionic homeostasis and reactive oxygen species control in leaves and xylem sap of two poplars subjected to NaCl stress. *Tree Physiol.* 28, 947–957.

Wang, M., Gong, J., and Bhullar, ,. N. K. (2020). Iron defificiency triggered transcriptome changes in bread wheat. *Comput. Struct. Biotechnol. J.* 18, 2709–2722.

Windt, C. W., Soltner, H., Van Dusschoten, D., and Blümler, P. (2011). A portable halbach magnet that can be opened and closed without force: The NMR-CUFF. *J. Magnetic Resonance* 208 (1), 27–33.

Wu, B. M., Li, L., Qiu, T. H., Zhang, X., and Cui, S. X. (2018). Cytosolic APX2 is a pleiotropic protein involved in H2O2 homeostasis, chloroplast protection, plant architecture and fertility maintenance. *Plant Cell Rep.* 37, 833– 848.

Wu, W., Li, J., Wang, Q., Lv, K., Du, K., Zhang, W., et al. (2021). Growth-regulating factor 5 (GRF5)-mediated gene regulatory network promotes leaf growth and expansion in poplar. *New Phytol.* 230 (2), 612–628.

Xing, C., Liu, Y., Zhao, L., Zhang, S., and Huang, X. (2018). A novel MYB transcription factor regulates ascorbic acid synthesis and affects cold tolerance. *Plant Cell Environ.* 42, 830–841. doi: 10.1111/pce.13387

Xu, W. J., Wang, Y., Xie, J. B., and Tan, S. X. (2022). Growth-regulating factor 15-mediated gene regulatory network enhances salt tolerance in poplar[J]. *Plant Physiol.* 1-18, kiac600. doi: 10.1093/plphys/kiac600

Xie, Y. P., Chen, P. X., Yan, Y., Bao, C. N., Li, X. W., Wang, L. P., et al. (2018). An atypical R2R3 MYB transcription factor increases cold hardiness by CBF-dependent and CBF-independent pathways in apple. *New Phytol.* 218, 201– 218.

Xu, W., Wang, Y., Xie, J., Tan, S. X., Wang, H., Zhao, Y., et al. (2023). Growth-regulating factor 15-mediated gene regulatory network enhances salt tolerance in poplar. *Plant Physiol.* 00, 1–18.

Xu, W., Zhang, N., Jiao, Y., Li, R., Xiao, D., and Wang, Z. (2014). The grapevine basic helix-loop-helix (bHLH) transcription factor positively modulates CBF-pathway and confers tolerance to cold-stress in arabidopsis. *Mol. Biol. Rep.* 41, 5329–5342. doi: 10.1007/s11033-014-3404-2

Yin, H., Li, M., Li, D., Khan, S. A, Hepworth, S. R, Wang, S. M, et al. (2019). Transcriptome analysis reveals regulatory framework for salt and osmotic tolerance in a succulent xerophyte. *BMC Plant Biol.* 19, 1–15. doi: 10.1186/s12870-019-1686-1

Yoda, H., Ogawa, M., Yamaguchi, Y., Koizumi, N., Kusano, T., and Sano, H. (2002). Identification of early-responsive genes associated with the hypersensitive response to tobacco mosaic virus and characterization of a WRKY-type transcription factor in tobacco plants. *Mol. Genet. Genomics* 267, 154–161.

Yu, C., Yan, M., Dong, H., Luo, J., Ke, Y., Guo, A., et al. (2021). Maize bHLH55 functions positively in salt tolerance through modulation of AsA biosynthesis by directly regulating GDP-mannose pathway genes. *Plant Sci.* 302, 110676. doi: 10.1016/j.plantsci.2020.110676

Zandalinas, S. I., Fichman, Y., Devireddy, A. R., Sengupta,, and Mittler, R. (2020). Systemic signaling during abiotic stress combination in plants. *PNAS.* 117 (24), 202005077. doi: 10.1073/pnas.2005077117

Zhang, C., Wang, D., Yang, C., Kong, N., Shi, Z., Zhao, P., et al. (2017). Genome-wide identification of the potato WRKY transcription factor family[J]. *PloS One* 12 (7), e0181573.

Zhang, X., Zhang, P., Wang, G., Bao, Z., and Ma, F. (2022). Chrysanthemum lavandulifolium homolog clmad1 modulates the floral transition during temperature shift. *Environ. Exp. Bot.* 194, 104720. doi: 10.1016/j.envexpbot.2021.104720

Zhao, Y., Xie, J., Wang, S., Zu, W., Chen, S., Song, X., et al. (2021). Synonymous mutation in growth regulating factor 15 of miR396a target sites enhances photosynthetic efficiency and heat tolerance in poplar[J]. *J. Exp. Bot.* 72 (12), 4502–4519.

Zhang, M., Liang, X., Wang, L., Cao, Y., Song, W., Shi, J., et al. (2019). A HAK family na+ transporter confers natural variation of salt tolerance in maize. *Nat. Plants* 5 (12), 1297–1308.

Zhao, R., Song, X., Yang, N., Chen, L., Xiang, L., Liu, X. Q., et al. (2020). Expression of the subgroup IIIf bHLH transcription factor CpbHLH1 from chimonanthus praecox (L.) in transgenic model plants inhibits anthocyanin accumulation. *Plant Cell Rep.* 39, 891–907. doi: 10.1007/s00299-020-02537-9

Zheng, Z. Y., Abu Qamar, S., Chen, Z. X., and Mengiste, T. (2006). Arabidopsis WRKY33 transcription factor is required for resistance to necrotrophic fungal pathogens. *Plant J.* 48 (4), 592–605.

Zhou, J., Li, Z., Xiao, G., Zhai, M., Pan, X., Huang, R., et al. (2020). CYP71D8L is a key regulator involved in growth and stress responses.

Zhou, P., Enders, T. A., Myers, Z. A., Erika, M., Crisp, P. A., and Noshay, J. M. (2021). Prediction of conserved and variable heat and cold stress response in maize using cis-regulatory information. *Plant Cell.* 1, 1. doi: 10.1093/plcell/koab267

Zhuo, C., Liang, L., Zhao, Y., Guo, Z., and Lu, S. (2017). A cold responsive ethylene responsive factor from medicago falcata confers cold tolerance by up-regulation of polyamine turnover, antioxidant protection, and proline accumulation. *Plant Cell Environ.* 41, 2021–2032. doi: 10.1111/pce.13114

frontiers | Frontiers in Plant Science

TYPE Original Research
PUBLISHED 09 May 2023
DOI 10.3389/fpls.2023.1136037

OPEN ACCESS

EDITED BY
Biao Jin,
Yangzhou University, China

REVIEWED BY
Georg Leitinger,
University of Innsbruck, Austria
Raquel Lobo-do-Vale,
University of Lisbon, Portugal

*CORRESPONDENCE
Yafei Li
l.yafei@outlook.com;
yafei.li@usys.ethz.ch

RECEIVED 02 January 2023
ACCEPTED 04 April 2023
PUBLISHED 09 May 2023

CITATION
Li Y, Eugster W, Riedl A, Lehmann MM, Aemisegger F and Buchmann N (2023) Dew benefits on alpine grasslands are cancelled out by combined heatwave and drought stress. *Front. Plant Sci.* 14:1136037. doi: 10.3389/fpls.2023.1136037

Dew benefits on alpine grasslands are cancelled out by combined heatwave and drought stress

Yafei Li[1]*, Werner Eugster[1], Andreas Riedl[1], Marco M. Lehmann[2], Franziska Aemisegger[3] and Nina Buchmann[1]

[1]Institute of Agricultural Sciences, ETH Zurich, Zurich, Switzerland, [2]Forest Dynamics, Swiss Federal Institute for Forest, Snow and Landscape Research (WSL), Birmensdorf, Switzerland, [3]Institute for Atmospheric and Climate Science, ETH Zurich, Zurich, Switzerland

Increasing frequencies of heatwaves combined with simultaneous drought stress in Europe threaten the ecosystem water and carbon budgets of alpine grasslands. Dew as an additional water source can promote ecosystem carbon assimilation. It is known that grassland ecosystems keep high evapotranspiration as long as soil water is available. However, it is rarely being investigated whether dew can mitigate the impact of such extreme climatic events on grassland ecosystem carbon and water exchange. Here we use stable isotopes in meteoric waters and leaf sugars, eddy covariance fluxes for H_2O vapor and CO_2, in combination with meteorological and plant physiological measurements, to investigate the combined effect of dew and heat-drought stress on plant water status and net ecosystem production (NEP) in an alpine grassland (2000 m elevation) during the June 2019 European heatwave. Before the heatwave, enhanced NEP in the early morning hours can be attributed to leaf wetting by dew. However, dew benefits on NEP were cancelled out by the heatwave, due to the minor contribution of dew in leaf water. Heat-induced reduction in NEP was intensified by the combined effect of drought stress. The recovery of NEP after the peak of the heatwave could be linked to the refilling of plant tissues during nighttime. Among-genera differences of plant water status affected by dew and heat-drought stress can be attributed to differences in their foliar dew water uptake, and their reliance on soil moisture or the impact of the atmospheric evaporative demand. Our results indicate that dew influence on alpine grassland ecosystems varies according to the environmental stress and plant physiology.

KEYWORDS

heatwave, dew, alpine grassland, drought, stable isotope, net ecosystem production

1 Introduction

A record-breaking heatwave struck Europe in June 2019 (Mitchell et al., 2019; WMO, 2019), one in a series of severe heatwaves and droughts since summer 2003 (Ciais et al., 2005), 2010 (Barriopedro et al., 2011), 2016 (Zschenderlein et al., 2018), and 2018 (Gharun et al., 2020). Drought often is associated with a concurrent heatwave that affects terrestrial ecosystems (Overpeck, 2013), creating a so-called compound extreme event or period (Zscheischler and Fischer, 2020; Zscheischler et al., 2020). Compared to forests, grasslands are less vulnerable to drought stress, because of their relatively stable water use efficiency (i.e., the ratio of gross primary productivity per unit ecosystem evapotranspiration; Wolf et al., 2013) during a drought period. However intense and prolonged droughts and heatwaves do negatively affect grasslands (e.g., Gharun et al., 2020). A heatwave increases evapotranspiration of grasslands, thereby relieving the vegetation from heat stress, but at the expense of available water supply, which becomes scarcer the longer the heatwave persists (Teuling et al., 2010). Cremonese et al. (2017) reported that the combined drought and heat stress caused a reduction of canopy greenness in a mountain grassland. Also, De Boeck et al. (2016) reported that a heatwave combined with drought stress caused a reduction in above-ground biomass of alpine grassland plants. Li et al. (2020) found that gross primary production (GPP) in a semi-arid grassland was reduced more by drought than by a heatwave. However, Gharun et al. (2020) showed very different responses to the 2018 summer drought (as compared to the previous two years) among temperate grasslands at different elevations, with annual GPP decreasing at lower elevations but increasing at the alpine elevation due to abundant soil water after snowmelt. Thus, our understanding of the response of grasslands to a compound extreme drought and heatwave is controversial, particularly for alpine grasslands.

Dew was widely observed across arid (Uclés et al., 2013), temperate (Jacobs et al., 2006) and tropical (Clus et al., 2008) ecosystems, and can contribute up to 0.7–0.8 mm of water per day (Beysens, 2018). Dew amounts were quantified by lysimeters (Riedl et al., 2022), eddy-covariance (Jacobs et al., 2006), and isotopic (Kim and Lee, 2011) approaches. Nocturnal dew formation and its evaporation in the early morning hours is expected to alleviate drought and heat stress imposed by a compound extreme event due to the following reasons: (1) Dew formation is driven by radiative cooling of plant canopies with stronger long-wave outgoing radiation than that of atmospheric air on clear and calm nights (Oke, 1970), hence relieving canopy heat stress. (2) High humidity conditions under dew formation and dew water films covering foliage reduce plant transpiration (Gerlein-Safdi et al., 2018). (3) Foliar uptake of dew droplets or atmospheric water vapor alleviates plant water stress (Boucher et al., 1995; Dawson and Goldsmith, 2018). (4) Leaf gas exchange during the morning hours — when dew evaporates — might be highly relevant to alleviate plant stress, since transpiration and photosynthesis during most of the day are strongly impaired during a compound heat-drought event (Gharun et al., 2020). Oliveira et al. (2021) pointed out that evaporation of dew induced CO_2 loss of a maritime pine forest during the rain-free period after wildfire. On the contrary, Simonin et al. (2009) reported that carbon gain was improved by fog which alleviated leaf water deficit, and addressed that the effect of dew/fog on net ecosystem exchange can vary by the duration of canopy wetting and the wettability of the leaf surface. However, it remains to be shown whether dew alleviates negative effects of a combined heat-drought on plant water status and ecosystem carbon exchange of grasslands, and which of the above mechanisms might dominate such a response.

Leaf water isotope signatures ($\delta^{18}O$ and $\delta^{2}H$) are useful to assess this question because they are natural tracers that can be used to assess plant physiological responses to environmental conditions (Bachmann et al., 2015; Prechsl et al., 2015). Evapotranspiration causes ^{18}O enrichment in leaf water compared to the source water (Dongmann et al., 1974; Farquhar and Lloyd, 1993). The magnitude of leaf water ^{18}O enrichment is strongly affected by the isotope signal of water vapor (Cernusak et al., 2002) and dew/fog (Kim and Lee, 2011; Goldsmith et al., 2017; Gerlein-Safdi et al., 2018), but also affected by foliar transpiration rates (Gessler et al., 2013). Typically, the leaf water ^{18}O signal is transferred onto leaf sugars *via* photosynthetic processes during daytime (Brandes et al., 2006; Gessler et al., 2013), and *via* the non-photosynthetic oxygen isotope exchange between leaf water and carbonyl groups of sugars (Wang et al., 2021). Leaf sugars are typically more enriched in ^{18}O compared to the leaf water due to the isotopic fractionation occurring during carbonyl hydration (Yakir and Deniro, 1990). Chamber experiments also suggested the transfer of the isotope signal of dew/fog on leaf water isotope signal during light and dark conditions (Kim and Lee, 2011; Gerlein-Safdi et al., 2018; Lehmann et al., 2020), and on leaf sugars during daytime conditions (Lehmann et al., 2020). However, it is not clear how large the photosynthetic and non-photosynthetic isotope imprints of leaf water on sugars are during nighttime as well as under low light and temperature conditions in the field.

Therefore, the main goals of this study focus on these three aims:

1) Quantify the combined effects of heat-drought stress and dew on net ecosystem production (NEP) by comparing the NEP before and during the heatwave, and analyzing leaf water-sugar isotope exchange in a chamber tracer experiment.
2) Quantify the combined effect of heat-drought stress and dew on plant water status by physiological and water isotope measurements.
3) Identify controls of atmospheric and soil conditions on plant water *via* analyzing the correlations of environmental variables with plant physiological and isotopic indicators.

We addressed these three aims using field data collected at an alpine grassland before and during the June 2019 heatwave, when a combined daytime heat-drought stress for the vegetation occurred during the day and dew formed during the night. H_2O vapor and net ecosystem CO_2 exchange were measured with the eddy-

covariance (EC) technique to assess the effects of these environmental conditions on the vegetation at the ecosystem scale. Physiological and water isotope measurements were employed to analyze the response of vegetation to these environmental conditions at plant scales.

2 Materials and methods

2.1 Study site

The Alp Weissenstein research site (CH-AWS, at 2000 m.a.s.l.) is part of a managed (grazed) alpine grassland ranging from 1900 to 2500 m.a.s.l. The vegetation composition was classified as *Deschampsio cespitosae–Poetum alpinae* community with red fescue (*Festuca rubra*), Alpine cat's tail (*Phleum rhaeticum*), white clover (*Trifolium repens*) and dandelion (*Taraxacum officinale*) as dominant species (Keller, 2006), complemented by alpine meadow-grass (*Poa alpina*) and lady's mantle (*Alchemilla vulgaris*). The soil types are slightly humous to humous sandy loam (Hiller et al., 2008), hence the permanent wilting point is estimated at around 0.1 m^3 m^{-3}. The mean annual air temperature and precipitation were 1.9 °C (2015–2020; measured all year round at the site between 2015 and 2020; before 2015, data were only collected between May and October at the site) and 1213 mm (2013–2020; measured all year round between 2013 and 2020; before 2012, only the liquid precipitation was measured at the site), respectively. During the main growing season (May to September), monthly mean air temperatures were between 5.0 °C and 10.8 °C (2006–2018) with July as the hottest month (Figure 1A), while average monthly precipitation ranged from 87 to 128 mm (Figure 1B). During the growing season in 2019, the monthly temperature ranged from 0.8 °C to 11.7 °C with June as the hottest month (Figure 1A), whilst the monthly precipitation ranged from 61 mm to 173 mm (Figure 1B).

2.2 Eddy covariance and meteorological measurements

EC measurements for H_2O vapor and net ecosystem CO_2 exchange have been carried out during the growing season since 2006 (tower coordinates: 46°34'59.5" N, 9°47'25.5" E at 1978 m.a.s.l.). In mid-November 2014, the site was equipped with mains power for year-round operation. The EC instruments at CH-AWS in 2019 consisted of a three-dimensional sonic anemometer (model HS-50, Gill Instruments, Solent, UK) and an enclosed-path infrared gas analyzer (IRGA; Li-7200, Li-Cor, Lincoln, NB, USA), installed at 1.4 m agl (above ground level). EC measurements were recorded at 20 Hz and processed to 30 min averages using the EddyPro software Version 7.0.6 (LI-COR, 2019) following established community guidelines (Aubinet et al., 2012) for H_2O (F_{H_2O} in mmol m^{-2} s^{-1}) and CO_2 fluxes (F_{CO_2} in µmol m^{-2} s^{-1}; net ecosystem exchange NEE). The micro-meteorological sign convention was used, with negative values denoting a downward flux, while positive values stand for upward fluxes. See details of footprint analysis of eddy-covariance measurements in Zeeman et al. (2010). Vapor pressure deficit (VPD) was quantified for 30-min intervals from ancillary air temperature and relative humidity measurements at 1.4 m agl (HygroClip HC2, Rotronic, Bassersdorf, Switzerland). Photosynthetic photon flux density (PPFD in µmol m^{-2} s^{-1}) was measured at 1.3 m agl every 10 s (PARlite, Kipp & Zonen B.V., Delft, The Netherlands) and then averaged to 30-min

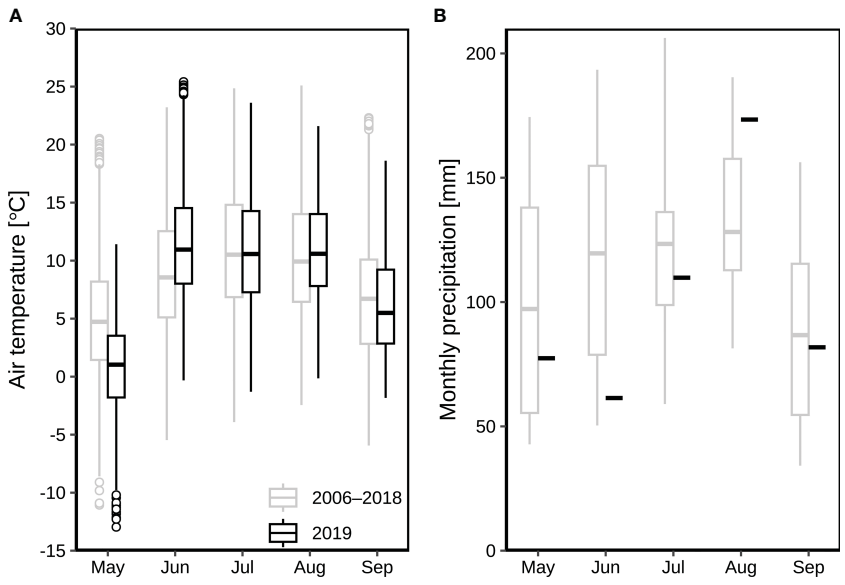

FIGURE 1
Air temperature and precipitation at the alpine grassland site CH-AWS in 2019 as compared to the period 2006–2018 (all data collected at the site): **(A)** average monthly air temperatures from May to September; **(B)** monthly precipitation from May to September. The boxplots show the medians, 25, and 75 quantile values (the inter-quartile range, IQR), with whiskers showing the data range up to 1.5 times the IQR. Values outside that range are shown with symbols.

intervals. Volumetric soil water content (SWC) was measured by two sensors (EC-5, Decagon Devices, Inc., Pullman, WA, USA) at 5 cm depth. NEP was calculated with the opposite sign of NEE (NEP = –NEE).

Diurnal NEP (g C m^{-2}) was calculated from the CO_2 flux (F_{CO_2}):

$$\mathrm{NEP} = \sum(a \cdot t \cdot F_{\mathrm{CO}_2} \cdot M_{\mathrm{C}}) \quad (1)$$

where M_c is the molar mas of carbon (12 g C mol^{-1}), t is measurement intervals (1800 s) of F_{CO_2}, and a is a unit conversion factor (10^{-6} mol µmol^{-1}).

For a long-term data series of air temperature at standard 2 m agl, an additional meteorological measurement setup was operating since 2006, installed at about 1180 m distance to the east and at approximately 40 m higher elevation compared to the flux tower (Michna et al., 2013). This additional setup provided air temperature (T_a) at 2 m agl (shaded, sheltered HydroClip S3, Rotronic AG, Basserdorf, Switzerland), and precipitation from an unheated pluviometer (LC, Texas Electronics, Dallas, USA). In November 2012, a precipitation gauge (1518H3, LAMBRECHT meteo GmbH, Göttingen, Germany) with a heatable orifice was installed between these two measurement stations (Michna et al., 2013) and provided annual total precipitation, including snowfall. Leaf wetness data were averaged from the measurements of two leaf wetness sensors (BNS, G. Lufft Mess-und Regeltechnik GmbH, Fellbach, Germany) installed since 2005 at 0.1 m agl close to the grassland canopy, using blotting paper inside a clip holder. The leaf wetness data was recorded by the voltage signal resulting from a fixed current applied from the center to the rim of the blotting paper. When the paper got wet by dew, fog, or rain, the blotting paper became conductive, and an increase in voltage signal was observed. We note that the leaf wetness sensors overestimated the leaf wetting duration (Figure S2), because the blotting paper dries out slower than the vegetation. By comparing the BNS sensor with a more accurate leaf wetness sensor (PHYTOS 31, Meter Group AG, Munich, Germany) at a later time of our observation campaigns (5–6 July 2020), the termination of leaf wetting was defined as the point when leaf wetness by BNS steeply and linearly decreased (Figure S2).

All variables were aggregated to 30 min averages or sums. The time series was recorded in CET (UTC+1 hour).

The evapotranspiration rate (ET in mm h^{-1}) was calculated from the H_2O flux (F_{H_2O}) as (Stull, 1988):

$$\mathrm{ET} = b \cdot F_{\mathrm{H_2O}} \cdot M_{\mathrm{H_2O}} \quad (2)$$

where M_{H_2O} is the molar mass of H_2O (18 g mol^{-1}), and b is a unit conversion factor [= (10^{-3} mol $mmol^{-1}$) · (10^{-6} m^3 g^{-1}) · (3600 s h^{-1}) · (10^3 mm m^{-1}) = 0.0036 mol m^2 s mm $mmol^{-1}$ g^{-1} h^{-1}].

2.3 June 2019 heatwave and drought

According to our measurements at the CH-AWS site during 2006 to 2018, the hottest three months were typically June, July, and August, with average air temperatures (at standard 2 m agl) of 8.9, 10.8 and 10.3 °C (Figure 1A), respectively. As compared to the long-term averages, the respective three months in 2019 were hotter with 11.7, 10.9, 10.8 °C (Figure 1A). The precipitation in June 2019 was 61 mm, which was only 51% of the long-term average of 120 mm in June during 2006–2018 (Figure 1B).

The 2019 heatwave occurred in Switzerland from 25 June to 1 July in 2019 (MeteoSwiss, 2019). No rain was recorded at the site from 23 June to 30 June 2019, but 0.2 mm rain was collected at 16:00 CET on 1 July 2019. Therefore, in this study, we only considered the 8-day rain-free period between 23 and 30 June 2019, with 23–24 June before the heatwave, and 25–30 June during the heatwave. Sunrise was around 04:30, and sunset was around 20:20 during the heatwave.

2.4 Experimental setup during measurement campaigns

To assess the combined effect of a well-developed natural drought during the heatwave in June 2019, we conducted two intensive measurement campaigns as intensive observation periods (IOP) at the end of the heatwave. These campaigns were carried out during two consecutive dew nights on 28–29 (IOP1 from 12:00 to 12:00 the next day) and on 29–30 (IOP2) June 2019.

2.4.1 Destructive sampling for isotope composition of water samples

To measure the isotope composition ($\delta^{18}O$ and $\delta^{2}H$) of leaf water, xylem water of root crowns, soil water, and dew droplets on leaf surfaces, destructive sampling was carried out during the IOP within 1 h before sunset (19:30 of IOP1 and IOP2), during the night (00:00 and 03:00 of IOP1 and IOP2), and after sunrise (06:00 of IOP1). Bulk leaf samples were taken in triplicates from randomly selected plants of four genera within an area of 70×20 m^2, i.e., *Alchemilla* with palmately-lobed and hairy leaves, as well as toothed leaf edges; *Poa* with long and narrow grass leaves; *Taraxacum* with a rosette of long and wide jagged leaves; and *Trifolium* with obovate leaves (Figure S1). The average vegetation height was around 20 cm during our field campaigns. Root crown xylem samples were taken in triplicates after removing the attached soil and debris from randomly selected plants for each genus. Dew droplets were absorbed with cotton balls in six replicates from randomly selected plants. Soil cores were taken with a soil auger in triplicates and were then cut into slabs to separate four soil depths of 0–5 cm, 5–10 cm, 10–15 cm, and 15–20 cm. Leaf samples were taken at 19:30, 00:00, 03:00 and 06:00 during IOP1, as well as at 19:30, 00:00 and 03:00 during IOP2. Root crown samples were taken at 19:30, 00:00 and 03:00 during IOP1 and IOP2. Dew droplets were taken at 03:00 during IOP1 (no dew droplets were observed at 00:00), as well as at 00:00 and 03:00 during IOP2. The 0–5 cm soil samples were taken at 19:30, 00:00 and 03:00 during IOP1 and IOP2, while soil samples of 5–10 cm, 10–15 cm and 15–20 cm depth were taken at 19:30 and 03:00 during IOP1 and IOP2.

All samples were immediately transferred into glass tubes (Labco Exetainer® 12 ml Vial, Labco Ltd., Lampeter, UK), sealed

with caps and parafilm, and stored in a portable freezing box filled with dry ice blocks. Samples were then taken back to the laboratory and stored at −19 °C. Dew water from cotton balls, and water from all plant and soil samples were extracted using a cryogenic vacuum extraction system (Prechsl et al., 2015). Using the high-temperature carbon reduction method (Werner and Brand, 2001; Gehre et al., 2004), the isotope composition of the respective water samples was determined by an isotope ratio mass spectrometer (IRMS, DeltaplusXP, Finnigan MAT, Bremen, Germany) coupling with a high-temperature conversion elemental analyzer (TC/EA, Finnigan MAT, Bremen, Germany) *via* a ConFlo III reference unit (Finnigan MAT, Bremen, Germany). The precision of $\delta^{18}O$ and $\delta^{2}H$ measurements for all the samples was ±0.3‰ and ±0.7‰, respectively. All isotope values of this study are expressed in the delta notation $\delta=(R_{sample}/R_{standard}-1)$ in per mil (‰), where $R_{standard}$ and R_{sample} are the molar ratios of either $^{2}H/^{1}H$ or $^{18}O/^{16}O$ of the standard (Vienna Standard Mean Ocean Water, V-SMOW) and the sample (IAEA, 2009; Coplen, 2011).

2.4.2 Isotope composition of atmospheric water vapor

The atmospheric water vapor at around 1 m agl was collected during IOP2 from 20:30 to 23:30, and from 00:00 to 03:00. Atmospheric air was pulled through a U-shaped glass tube that was placed in a Dewar filled with a cold slurry of ethanol and dry ice. After 3 h, the trapped water vapor frozen to the inner walls of the U-shaped glass tube was thawed, and the liquid water was filtered (Syringe filter, PTFE-Hydrophobic, 0.45µm) and transferred into glass vials. The samples were measured with the TC/EA-IRMS for their isotope composition ($\delta^{18}O_{vapor}$ and $\delta^{2}H_{vapor}$) as described above. To compare the isotope composition of atmospheric water vapor with the liquid water pools (i.e., dew droplets, leaf water, xylem water of root crowns, and soil water), the isotope composition of the liquid ($\delta^{18}O_{eq}$ and $\delta^{2}H_{eq}$) in equilibrium with this vapor was calculated under the corresponding air temperature measured at 1.4 m agl following Horita and Wesolowski (1994).

2.4.3 Leaf water potential

To investigate the mechanism of dew influence on ecosystem water and carbon exchanges, leaf water status was measured at the end of the heatwave during our intensive observation campaigns (IOP1 and IOP2). The comparison of LWP before and after 29 June heatwave as well as two dew nights (the 28–29 and 29–30 nights) allows to compare the influence of heatwave and dew on leaf water status.

Leaf water potential (LWP) of the four genera *Alchemilla*, *Poa*, *Taraxacum*, and *Trifolium* was measured in triplicates with a Scholander pressure chamber (Model 1505D, PMS Instruments Co., Albany, OR, USA) using a grass compression gland for *Poa* and *Taraxacum*, and a round compression gland for *Alchemilla* and *Trifolium*. The LWP was measured within 1 h before sunset (19:30; before-sunset) and 2 h before sunrise (03:00; predawn) during IOP1 and IOP2.

2.4.4 Complementary *in-situ* chamber tracer experiment

Complementary to the sampling campaigns under natural conditions, an *in-situ* chamber tracer experiment was carried out during IOP1 (28–29 June) to investigate whether dew signal was used for carbon assimilation by determining the $\delta^{18}O$ and $\delta^{2}H$ values of leaf water and sugars. Within around 1 h before sunset, a 50 × 50 cm^2 grassland plot was marked for the chamber tracer experiment. We used liquid water depleted in ^{18}O and ^{2}H as tracer ($\delta^{18}O$ = −364.7 ± 1.9‰ and $\delta^{2}H$ = −775.0 ± 0.3‰) and homogenously sprayed it onto the plot at around 19:30. After spraying, the vegetation was immediately covered with a custom-made canopy chamber (50 × 50 × 50 cm^3) wrapped with 0.1 mm thick polyethylene film, with a 76% transmissivity for thermal (longwave) infrared radiation (Horiguchi et al., 1982). With this tracer addition, we simulated dew, which was much more depleted in ^{18}O and ^{2}H than natural dew droplets. We note that we did not isolate the soil during the tracer amending on the grassland plot, hence the tracer could drip into the soil, and the amended tracer on vegetation can also drip to the soil, both of which can occur during natural dew formation processes. The canopy chamber did not fully isolate the grassland from the surrounding; thus, gas emission could still occur from the bottom rim of the chamber. But the chamber sufficiently suppressed the water vapor exchange between the within-chamber air and the open atmosphere. About 2 h before (03:00; predawn) and after sunrise (06:00), bulk leaf samples were taken in triplicates from randomly selected plants per genus in the plot. In addition, bulk leaf samples taken before sunset (19:30) acted as control for this experiment. Leaf water was extracted for isotope analyses ($\delta^{18}O_{lw}$ and $\delta^{2}H_{lw}$) as described in Section 2.3.1.

Leaf dry matter after cryogenic water extraction was milled to fine powder for $\delta^{18}O_{ls}$ and $\delta^{13}C_{ls}$ analysis of leaf sugars. Bulk sugars were extracted from 60 mg of this leaf powder with 1.5 mL deionized water at 85 °C for 30 min (Lehmann et al., 2020). The neutral sugar fraction (defined here as "sugars") was then further purified from ionic and phenolic substances by ion-exchange cartridges (OnGuard II A, H and P, Dionex; Thermo-Fisher Scientific, Bremen, Germany) following the protocol by Rinne et al. (2012). For the analysis of $\delta^{18}O_{ls}$, the purified bulk leaf sugars were filled into silver capsules, frozen and freeze-dried. The measurement precision (standard deviation) of the quality control standard (cellulose with 27.6‰ for $\delta^{18}O$) was ≤ 0.3‰ for $\delta^{18}O_{ls}$ (Lehmann et al., 2018), and 0.1‰ for $\delta^{13}C_{ls}$ (Bögelein et al., 2019). $\delta^{13}C$ is the carbon isotope ratio in δ-notation in per mill (‰), relative to the international Vienna-Pee Dee Belemnite (V-PDB) standard, and were normalized by IAEA-CH7 (polyethylene, −32.2‰) and IAEA-CH3 (cellulose, −24.7‰) (Bögelein et al., 2019). Higher $\delta^{13}C_{ls}$ indicated lower water use efficiency (WUE) of plants.

In the chamber tracer experiment, the contribution of the tracer (f_{tracer}) to leaf water at 03:00 ($\delta^{18}O_{lw\_03:00}$) was simulated using a linear two-pool mixing model. One source of the leaf water was assumed to be the $\delta^{18}O_{root}$ at 03:00 of IOP1 ($\delta^{18}O_{root,\ 03:00}$) under natural conditions and the second source was the mean tracer $\delta^{18}O$ ($\delta^{18}O_{tracer,\ mean}$) taken up by the leaves during the night. We calculated $\delta^{18}O_{tracer,\ mean}$ as the mean of the original tracer $\delta^{18}O$

($\delta^{18}O_{tracer,\ 19:30}$ = −364.7 ± 1.9‰) and the $\delta^{18}O$ of the tracer which remained on the leaf surfaces by 03:00 ($\delta^{18}O_{tracer,\ 03:00}$ measured by absorbing the remaining tracer in form of simulated dew from the leaf surfaces at 03:00). f_{tracer} was calculated as:

$$f_{tracer} = \frac{\delta^{18}O_{lw,\ 03:00} - \delta^{18}O_{root,\ 03:00}}{\delta^{18}O_{tracer,\ mean} - \delta^{18}O_{root,\ 03:00}} \quad (3)$$

Due to the chamber acting as a heat-trap, the within-chamber temperature should be slightly higher than the open-air temperature. This temperature difference might affect the leaf-air water vapor exchange, but was assumed to have minor effect on foliar water uptake of liquid-phase dew and water-sugar isotope exchange.

2.5 Statistics

Tukey's honest significance test was used to assess differences among averages over sampling times and genera by the R-function agricolae::HSD.test (Steel, 1997) and one-way ANOVA. Reported statistical significance represents $p < 0.05$ with capital letters indicating temporal differences, and lower-case letters denoting genera or soil-depth differences. The isotopic and LWP results were reported in mean and standard errors of mean (SEM). We note that differences of isotope composition are always reported in absolute terms in per mil (‰). Correlation coefficients of regressions of NEP with T_a, PPFD, and RH were analyzed before and during the heatwave, with "***", "**", "*" and "ns" indicating $p < 0.001$, $p < 0.01$, $p < 0.05$, and $p \geq 0.05$, respectively. During IOP1 and IOP2 at the end of the heatwave, considering the individual variability of plants, median values of leaf water isotope ($\delta^{18}O_{lw}$) and LWP by species at each sampling time were used for analyzing their correlations with environmental conditions (RH, SWC, and $\delta^{18}O_{soil}$), with "***", "**", "*" and "ns" indicating $p < 0.001$, $p < 0.01$, $p < 0.05$, and $p \geq 0.05$, respectively. All analyses were carried out with R version 4.1.2 (R Core Team, 2021).

3 Results

3.1 Diel environmental variability before and during the heatwave

The diurnal and nocturnal air temperature averaged 14.5 °C and 7.3 °C before the heatwave during 23-24 June, but was 20.1 °C and 11.2 °C on average during the heatwave from 25 to 30 June (Figure 2A). The highest temperature of 25.4 °C was observed on 26 June 2019 (15:30; Figure 2A), indicating the peak of the heatwave, followed by 27 June 2019, the second hottest day. H_2O fluxes varied from −0.3 to 13.7 mmol m^{-2} s^{-1} (Figure 2B), corresponding to 3.0–4.7 mm of diurnal ET before the heatwave, and 4.9–5.7 mm during the heatwave (Figure 3A). SWC decreased from 0.32 to 0.15 m^3 m^{-3} during this rain-free period from 23 to 30 June (Figure 2C). NEP varied from −22 to 21 µmol m^{-2} s^{-1} (Figure 2D). The daytime NEP was 4.2–6.3 g C m^{-2} before the heatwave, but ranged from 5.4 to −2.9 g C m^{-2} during the heatwave (Figure 3B). Negative NEP (−2.9 g C m^{-2}) occurred on 27 June, the day after the hottest day (26 June). Highest VPD was 2.06 kPa and 2.65 kPa before and during the heatwave (Figure 2E), respectively. The leaf wetness levels indicated that dew occurred during each night of the rain-free period, being fully evaporated from vegetation surfaces after 07:30 of day (Figure 2F). With dew occurrence during each night of the rain-free period (23–30 June), the corresponding nocturnal VPD was as low as 0.14–1.41 kPa (Figure 2E).

3.2 Effects of heat-drought and dew on net ecosystem production

Before the heatwave, NEP almost linearly increased with PPFD (Figure 4), with higher diurnal NEP (6.3 g C m^{-2}) on 23 June than that on 24 June (4.2 g C m^{-2}; Figure 3B). The suppression of heat-drought stress on NEP was substantial on the hottest day (26 June with 2.0 g C m^{-2}) during the heatwave (Figure 3B), with 63% of reduction in NEP compared to the previous day (25 June with 5.4 g C m^{-2} of NEP). Negative diurnal NEP (−2.9 g C m^{-2}) occurred on the second hottest day (27 June; Figure 3B), with longer period (09:00–15:00) of net carbon emission (negative NEP) under PPFD > 1300 µmol m^{-2} s^{-1} and T_a > 22.5 °C (Figure 4E), as compared to the hottest day during 14:00–16:30 under PPFD > 1800 µmol m^{-2} s^{-1} and T_a > 25.3 °C (Figure 4D). Daily NEP recovered to the levels of 4.7–5.0 g C m^{-2} on 28–30 June after the hottest two days on 26–27 June (Figure 3B).

During the early morning hours before 07:30 with leaf wetting by dew, NEP increased by T_a before and during the heatwave (Figure 5A; $p < 0.01$ and $p < 0.001$ before and during the heatwave, respectively), but the turning T_a from negative (net carbon emission) to positive (net carbon sequestration) NEP was higher during the heatwave period (13.7 °C for 25-30 June) than that before the heatwave (8.2 °C for 23-24 June). With vegetation wetting by dew in the early morning hours, NEP exponentially increased with PPFD ($p < 0.01$ and $p < 0.001$ before and during the heatwave, respectively), but NEP was lower during the heatwave than that before the heatwave under same levels of PPFD (Figure 5B). In the early morning hours with vegetation wetting, NEP slightly increased by leaf wetness levels before the heatwave (Figure 5C; $p \geq 0.05$), but significantly decreased by leaf wetness levels at the beginning of the heatwave on 25–26 June (Figure 5D; $p < 0.01$).

3.3 Effects of heat-drought and dew on leaf water status and leaf isotopes

3.3.1 Leaf water status

Comparing predawn (03:00) periods of IOP1 and IOP2 (Figure 6), *Poa* LWP significantly decreased from −0.9 to −1.5 MPa ($p < 0.05$), *Trifolium* LWP slightly decreased from −0.4 to −0.7 MPa ($p \geq 0.05$), *Taraxacum* LWP was at similar levels (−0.6 to −0.6 MPa; $p \geq 0.05$), whilst *Alchemilla* LWP slightly increased from −0.7 to −0.3 MPa ($p \geq 0.05$). Comparing before-sunset (19:30) periods of IOP1 and IOP2 (Figure 6), *Poa* LWP

10.3389/fpls.2023.1136037

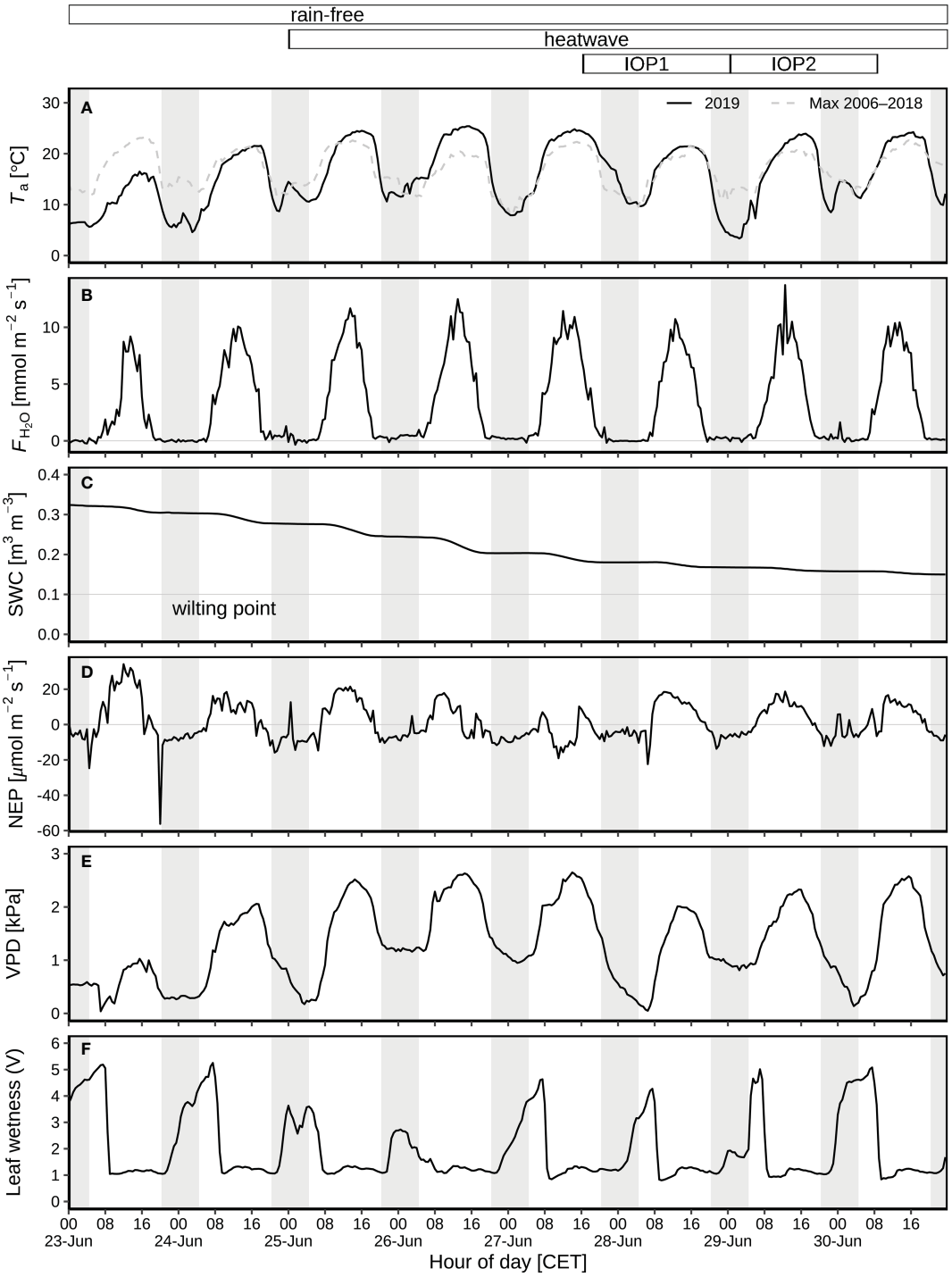

FIGURE 2
Environmental variables during the rain-free period (23–30 June) at CH-AWS site before the heatwave on 23–24 June, and during the June 2019 heatwave on 25–30 June: **(A)** air temperature (T_a) at 2 m agl as compared to the long-term maximum 2006–2018. **(B)** Eddy-covariance H_2O flux. **(C)** Volumetric soil water content (SWC) at 5 cm depth. **(D)** Net ecosystem production (NEP); positive numbers indicate CO_2 emission, and negative numbers represent CO_2 uptake. **(E)** Vapor pressure deficit (VPD). **(F)** Leaf wetness recorded by the voltage signal resulting from a fixed current applied from the center to the rim of the blotting paper; substantial increase in leaf wetness during nighttime and early morning indicate leaf wetting by dew during the rain-free period; dew occurred on each night of the period. Field campaigns were carried out during two intensive observation periods (IOP) on 28–29 (IOP1) and 29–30 (IOP2) June 2019. Hours of day are given in CET. The grey shaded areas represent nocturnal periods.

significantly decreased from −0.9 to −1.8 MPa ($p < 0.05$), *Taraxacum* LWP (−1.1 to −1.1 MPa) was at similar levels, whilst *Trifolium* LWP slightly increased from −1.3 to −1.0 MPa ($p \geq 0.05$) and *Alchemilla* LWP increased from −1.6 to −0.6 MPa ($p \geq 0.05$). The LWP of all four genera slightly increased during both IOP nights ($p \geq 0.05$; Figure 6), i.e., from before-sunset (19:30) to predawn periods (03:00). Among the four genera, *Alchemilla* had the lowest LWP before sunset of IOP1 ($p \geq 0.05$), but had slightly

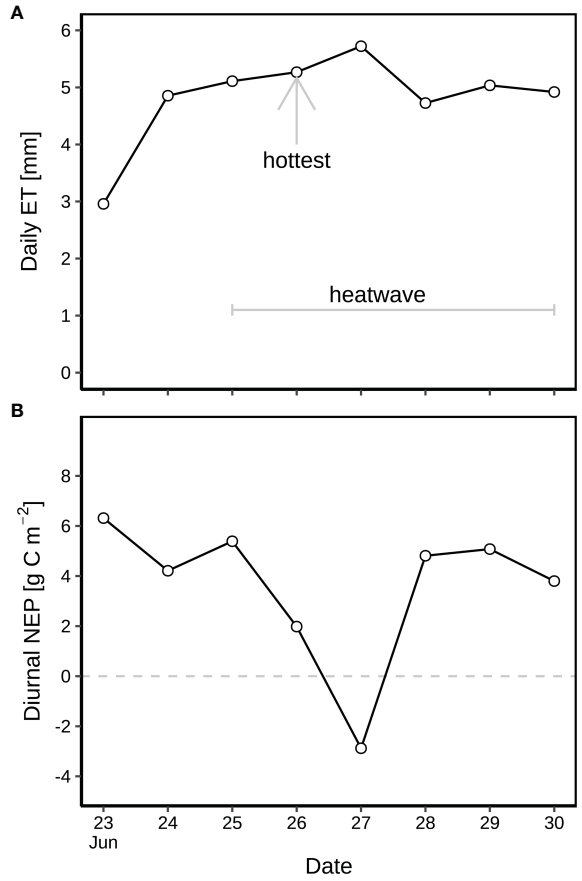

FIGURE 3
(A) Diurnal evapotranspiration (ET) and **(B)** net ecosystem production (NEP) during the rain-free period (23–30 June) at CH-AWS site before the heatwave on 23–24 June, and during the June 2019 heatwave on 25–30 June. Dew occurred on each night of the period. 26 June was hottest during the heatwave.

higher LWP than the other three genera before sunset of IOP2 ($p \geq 0.05$). On the contrary, *Poa* had slightly lower LWP than the other three genera at the predawn period of IOP1 ($p \geq 0.05$), but had much lower LWP than the other three genera at predawn of IOP2 ($p < 0.05$). Therefore, *Poa* LWP significantly decreased ($p < 0.05$) at the end of the heatwave, whilst *Alchemilla* LWP significantly increased ($p < 0.05$), *Taraxacum* and *Trifolium* slightly increased ($p \geq 0.05$) although heat-drought stress.

3.3.2 Isotope composition of different water pools at natural isotope abundances

The $\delta^{18}O_{soil}$ (–9.5 ± 1.6‰; Figure 7A) varied with depth ($p < 0.05$), with higher $\delta^{18}O_{soil}$ (–8.1 ± 1.4‰) in top soil layer (0–5 cm depth) and lower $\delta^{18}O_{soil}$ (–10.2 ± 1.2‰) in subsoil layers (5–20 cm depth). $\delta^{18}O_{root}$ was within the range of $\delta^{18}O_{soil}$ (Figures 7A, B), indicating soil water as the main source of plant water. $\delta^{18}O_{root}$ of *Alchemilla* and *Trifolium* was between the topsoil and the subsoil $\delta^{18}O_{soil}$, whilst $\delta^{18}O_{root}$ of *Poa* and *Taraxacum* was close to subsoil $\delta^{18}O_{soil}$. $\delta^{18}O_{root}$ varied with plant genera ($p < 0.05$; Figure 7B), with higher $\delta^{18}O_{root}$ for *Alchemilla* and *Trifolium* (–9.0 ± 1.0‰), but lower $\delta^{18}O_{root}$ for *Poa* and *Taraxacum* (–10.6 ± 1.0‰). The comparison of $\delta^{18}O_{soil}$ and $\delta^{18}O_{root}$ (Figure 7B) indicated that *Alchemilla* and *Trifolium* used shallower soil water as compared to *Poa* and *Taraxacum*.

Across all four genera, leaf water $\delta^{18}O_{lw}$ (–2.6 ± 4.8‰; Figure 7C) was on average higher than $\delta^{18}O_{root}$ (–9.8 ± 1.3‰; Figure 7B), indicating evaporative processes of leaf water as compared to xylem water. *Poa* had the highest $\delta^{18}O_{lw}$ among the four genera ($p < 0.05$; Figure 7C), indicating strongest water stress of *Poa* derived from their stronger evaporation or stress-induced partial stomatal closure. *Taraxacum* tended to have the lowest $\delta^{18}O_{lw}$, but not significantly different from *Alchemilla* and *Trifolium* ($p \geq 0.05$). $\delta^{18}O_{dew}$ changed over time, with –7.5 ± 0.4‰ at 03:00 of IOP1, increasing to –6.7 ± 1.0‰ at 00:00 and –5.7 ± 0.5‰ at 03:00 during IOP2 ($p \geq 0.05$; Figure 7B). $\delta^{18}O_{eq}$ of the liquid water in equilibrium with atmospheric water vapor was –5.0‰ to –4.7‰ during 20:30 to 03:00 of IOP2. Compared to the local meteoric water line (LMWL; $\delta^{2}H = 7.83\ \delta^{18}O + 12.97$; following Prechsl et al., 2014), $\delta^{2}H_{eq}$–$\delta^{18}O_{eq}$ was above the LMWL. In contrast, all $\delta^{2}H$–$\delta^{18}O$ pairs for dew droplets, plants and soil water fell below the LMWL, indicating evaporation of these water pools compared to local precipitation, particularly of leaf water (Figure 7D).

3.3.3 Effect of isotopically labelled dew on leaf water and sugar isotopes

Adding isotopically ^{18}O-depleted water as a tracer in the chamber tracer experiment on IOP1 night induced a substantial ^{18}O-depletion in leaf water ($\delta^{18}O_{lw}$; $p < 0.05$), but not so in leaf sugars ($\delta^{18}O_{ls}$; $p \geq 0.05$; Figure 8A). Before applying the tracer at 19:30 (before sunset), $\delta^{18}O$ of leaf sugar ($\delta^{18}O_{ls}$) for the four genera (29.9 ± 2.9‰; Figure 8A) was 30.1‰ higher than their respective $\delta^{18}O_{lw}$ (–0.2 ± 3.4‰). During the following 7.5 h overnight (until 03:00), $\delta^{18}O_{lw}$ of the four genera decreased by a further 26.6 ± 10.4‰ as compared to before-sunset levels. In contrast, $\delta^{18}O_{ls}$ (29.2 ± 4.5‰) of the four genera did not change after tracer amendment, and consequently $\delta^{18}O_{ls}$ of the four genera was 55.7‰ higher than the respective $\delta^{18}O_{lw}$ (Figure 8A). Wet foliage due to tracer application persisted for 10.5 h, thus after sunrise (06:00), $\delta^{18}O_{lw}$ of the four genera increased to –14.6 ± 4.7‰ in respect to predawn $\delta^{18}O_{lw}$, whereas the corresponding $\delta^{18}O_{ls}$ (26.3 ± 1.3‰) remained almost constant over the night until sunrise, indicating minor effect of amended tracer on soil moisture. As a result, $\delta^{18}O_{ls}$ of the four genera after sunrise was 40.9‰ higher than the corresponding $\delta^{18}O_{lw}$ (Figure 8A).

The changes in $\delta^{18}O_{lw}$ varied by genus before and during the chamber tracer experiment. Before sunset and tracer amendment, *Poa* $\delta^{18}O_{lw}$ (4.7 ± 1.3‰) was 6.6‰ higher than $\delta^{18}O_{lw}$ of the other three genera (–1.9 ± 1.8‰; Figure 8A), indicating more severe water stress of *Poa*. However, the difference for predawn (03:00) $\delta^{18}O_{lw}$ of *Poa* (–15.4 ± 2.8‰; Figure 8A) increased to 15.3‰ compared to the corresponding $\delta^{18}O_{lw}$ of the other three genera (–30.7 ± 8.9‰; Figure 8), which might be due to the stronger evaporation and less foliar water uptake of *Poa*, or stress-induced partial stomatal closure. Overall, the ranking of the genera stayed relatively stable, with *Poa* typically showing the highest $\delta^{18}O_{lw}$.

10.3389/fpls.2023.1136037

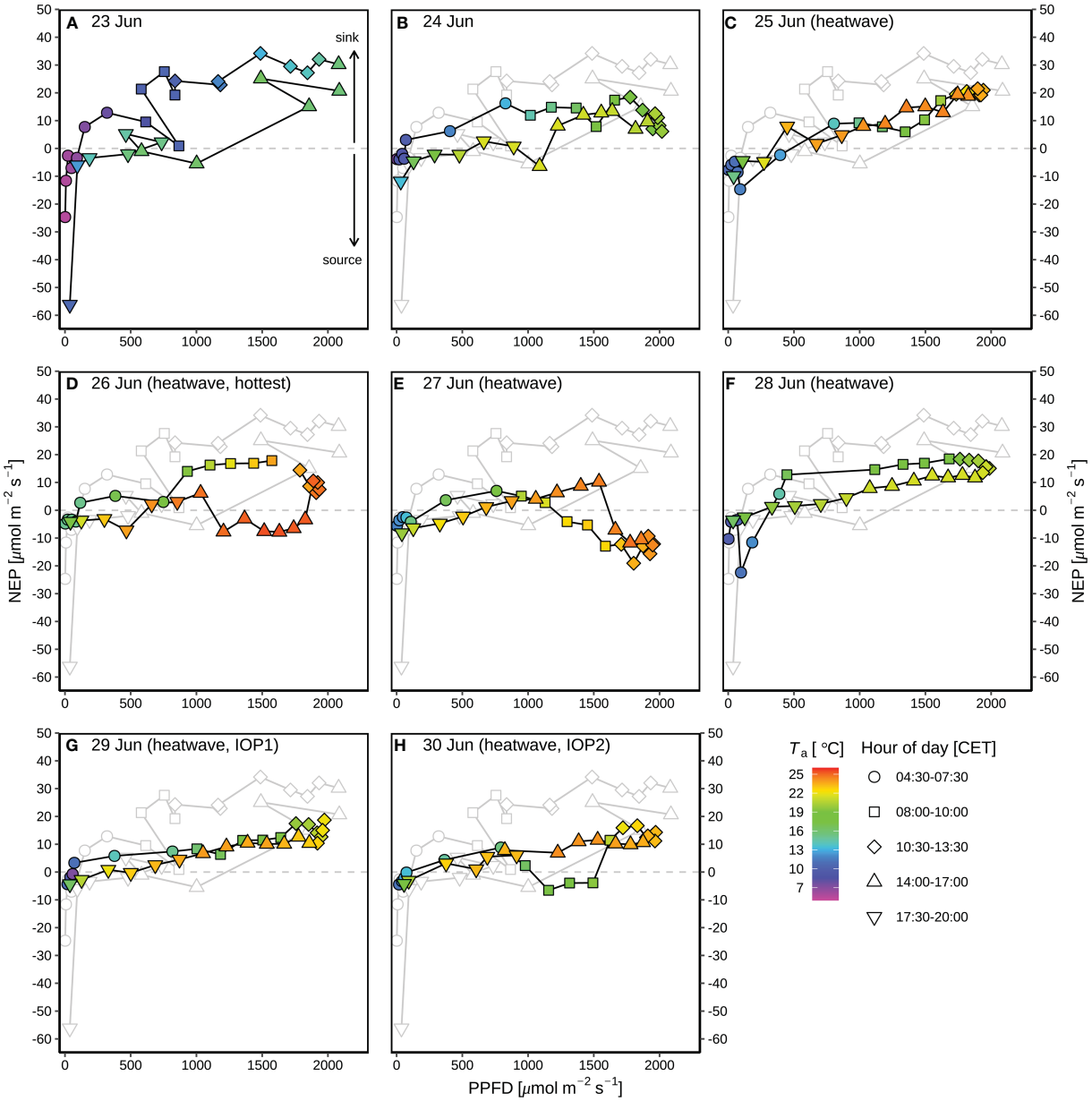

FIGURE 4
Response curves of diurnal net ecosystem production (NEP) to photosynthetic photon flux density (PPFD) during the rain-free period (23–30 June) at CH-AWS site before the heatwave on 23–24 June **(A, B)**, and during the June 2019 heatwave on 25–30 June **(C–H)**. Different hours of day (CET) are shown in different shapes; the colors of the symbols indicate the corresponding air temperature (T_a). Dew occurred during each night of the period. For comparison, the grey plots in panels **(B–H)** show the NEP-PPFD response curve on 23 June 2019 before the heatwave.

During the experiment, $\delta^{18}O$ of the added tracer increased from −364.7‰ at 19:30 to −19.5 ± 1.8‰ at 03:00 (Figure 8C). The contribution (f_{tracer}) of the added tracer ($\delta^{18}O_{tracer\_mean}$ of −192.1‰) to plant leaf water was 3–14%, highest for *Alchemilla* and lowest for *Poa* (Figure 8D). f_{tracer} was positively correlated with the corresponding predawn LWP, except for *Alchemilla* with large variability in their predawn LWP (Figure 8E).

$\delta^{13}C_{ls}$ was rather constant over the IOP1 night. Higher $\delta^{13}C_{ls}$ of *Alchemilla* and *Poa* indicated their lower WUE, as compared to *Taraxacum* and *Trifolium* (Figure 8B). $\delta^{13}C_{ls}$ of *Poa*, *Taraxacum* and *Trifolium* was negatively correlated with f_{tracer} (Figure 8F), whilst *Alchemilla* with highest f_{tracer} showed highest $\delta^{13}C_{ls}$ and thus lowest WUE.

3.4 Controls of atmospheric and soil conditions on plant water

LWP of *Taraxacum* and *Trifolium* were positively correlated with RH (Figure 9A), indicating the controls of atmospheric humidity on their LWP. LWP of *Poa* was positively correlated with SWC (Figure 9B), indicating the controls of soil moisture on

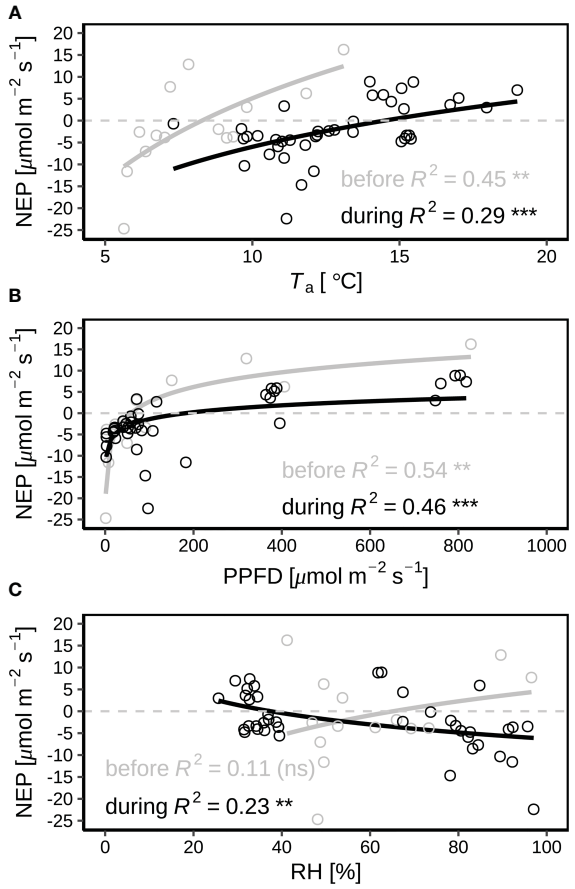

FIGURE 5
Correlations of net ecosystem production (NEP) with **(A)** air temperature (T_a at 2 m agl), **(B)** photosynthetic photon flux density (PPFD), and **(C)** relative humidity (RH) in the early morning hours (from sunrise to 07:30) with wet leaves by dew before (23–24 June in grey) and during the June 2019 heatwave (25–30 June in black). Dew occurred during each night of the period. 26 June was hottest during the heatwave. The values of p for the correlation coefficients are indicated by "***", "**", "*" and "ns" for $p < 0.001$, $p < 0.05$, $p < 0.01$, and $p \geq 0.05$.

their LWP. This corresponded to the significant decline of *Poa* LWP at the end of the heatwave (Figure 6), under the conditions of low SWC (0.15 m^3 m^{-3}; Figure 2C) close to wilting point. LWP and $\delta^{18}O_{lw}$ of *Alchemilla*, *Taraxacum* and *Trifolium* were negatively correlated (Figure 9C), indicating the controls of leaf water content on their $\delta^{18}O_{lw}$. Stronger drought-stress of *Poa* might induce partial stomatal closure, and thus result in their more enriched leaf water isotopes (higher $\delta^{18}O_{lw}$) not relevant to LWP. The slightly improved *Alchemilla* LWP at the end of the heatwave might be derived from the accumulated benefits by dew, which contributed more to *Alchemilla* leaf water (14%; Figure 8D) compared to the other three genera (≤ 12%). $\delta^{18}O_{lw}$ of *Alchemilla*, and *Taraxacum* was negatively correlated with RH (Figure 9D), indicating the control of atmospheric conditions on their $\delta^{18}O_{lw}$. $\delta^{18}O_{lw}$ did not show significant correlation with SWC and $\delta^{18}O_{soil}$ (Figures 9E, F), indicating the minor control of soil water on leaf water isotopes.

4 Discussion

4.1 Dew benefits cancelled out by heat-drought stress

The benefits of dew on NEP were observed in the early morning hours of 23–24 June before the heatwave (Figure 10). From sunrise to 06:30 on 23 and 24 June, PPFD was at similar levels (Figure 10C), hence higher NEP on 24 June (Figure 10A) might be induced by higher temperature (Figure 10D) as compared to 23 June. But from 06:30 to 07:30, although higher PPFD and temperature on 24 June, NEP was at the similar levels as that on 23 June (Figure 10C), probably induced by higher potential of dew formation as indicated in higher RH on 23 June (Figure 10B).

However, with the occurrence of heatwave, dew benefits on NEP were cancelled out, as shown in the reduced NEP with increasing RH (Figure 5C). The chamber tracer experiment at the end of the heatwave showed that dew isotope signal was not transferred to leaf sugar (Figure 8A), indicating that dew water did not participate in carbon assimilation during the heatwave. The possible reason could be derived from the minor contribution (3–14%) of dew water to plant leaf water (Figure 8D), corresponding to previous research that foliar water uptake can only increase leaf water content by 2–11% (Limm et al., 2009). Due to the heat-drought stress, partial stomatal closure and vapor pressure gradient (Li et al., 2023) from leaf to atmosphere (saturated leaf internal environment vs unsaturated atmospheric conditions) might limit the uptake of dew water *via* leaf, thus most of the dew water during the heatwave could evaporate after sunrise instead of being used for carbon assimilation. Oliveira et al. (2021) showed that dew evaporation processes induced CO_2 loss of a maritime pine forest during the rain-free period after wildfire, but Simonin et al. (2009) reported that the reduction in leaf water deficit by fog water can result in improved carbon gain. Therefore, the effect of dew on ecosystem exchange varied by environmental conditions, e.g., environmental stress (Oliveira et al., 2021), the duration of canopy wetting (Simonin et al., 2009), the wettability of the leaf surface (Brewer and Smith, 1994; Hanba et al., 2004), and the foliar water uptake capacity of plants (Simonin et al., 2009).

Our tracer chamber experiment was carried out in a single chamber, and with only once sampling after sunrise, thus it was not possible to investigate the effect of dew on carbon assimilation after dew totally evaporating from surfaces. Future research on hourly resolution and longer period of after-sunrise isotope measurements is recommended to answer this question.

4.2 Ecosystem water and carbon exchange

Despite heat-drought stress, alpine grassland kept high ET during the heatwave (Figure 3A), as long as soil moisture was available (Figure 2C) to meet its evaporative demand (Teuling et al., 2010; Wolf et al., 2013).

De Boeck et al. (2016) showed that a combined heatwave and drought stress induced a reduction in above-ground biomass of

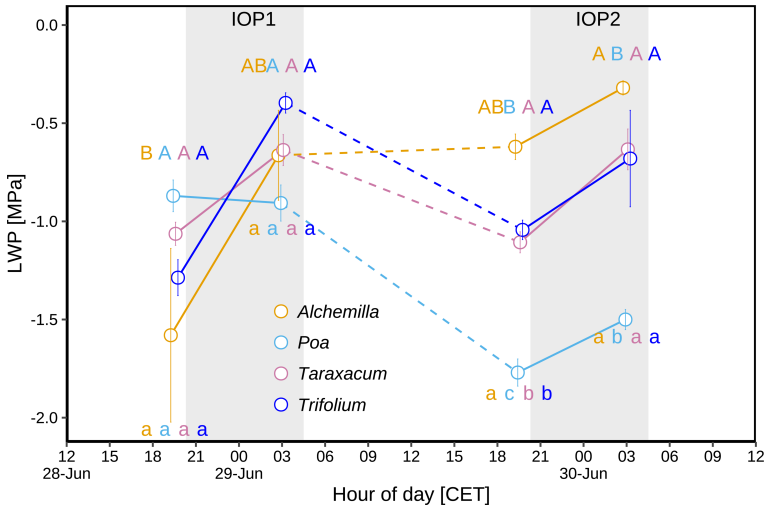

FIGURE 6
Leaf water potential (LWP) during two intensive observation periods (IOP1 and IOP2) with nocturnal dew occurrence at the end of the June 2019 heatwave: LWP of different plant genera (*Alchemilla*, *Poa*, *Taraxacum*, and *Trifolium*) were measured before sunset (at 19:30 within around 1 h before sunset) and before sunrise (03:00 within around 2 h before sunrise) of two dew events. Different letters indicate statistically significant differences ($p < 0.05$), with capital letters indicating temporal comparison, and lower cases indicating among-genera comparison. The grey shaded areas represent nocturnal periods.

alpine grassland plants. In this study, the reduction of NEP by the heat-drought stress was most pronounced during the two hottest days (26 and 27 June; Figures 4D, E) of the heatwave period, Compared to 26 June (25.4 °C; Figure 4B), 27 June showed a longer period of net carbon emission (Figure 4E) despite lower maximum T_a (24.8 °C; Figure 5E) and SWC (Figure 2C). This might be explained by an intensifying effect of drought stress, corresponding to previous research by De Boeck et al. (2016), and the influence of severe heat stress on nighttime refilling. Nevertheless, heat stress was a bit relieved after the heatwave peak, when temperatures only reached 21.5 °C, and NEP recovered immediately. The rapid re-growth ability of alpine plants after heat-drought stress (Brilli et al., 2011) might explain the recovery of NEP during 28–30 June (Figure 3B) after the hottest two days. This also corresponded to the fact that LWP of plants (except *Poa*) did not significantly decreased at the end of the heatwave (Figure 6). The refilling of plant tissues during the night is a well-known phenomenon (Schulze et al., 2019), helping to relieve water losses during heat-drought stress, and might contribute to the recovery of diurnal NEP on 28–30 June after the peak of the heatwave to the levels slightly lower than the beginning of the heatwave on 23–25 June. The redistribution of soil water by deeper plant roots to the shallower soil depths might provide sufficient soil moisture sources for plant tissue refilling (Burgess and Bleby, 2006) after the peak of the heatwave. This may also explain why the predawn LWP of *Alchemilla*, *Taraxacum*, and *Trifolium* did not decline at the end of the heatwave. Yet, the nighttime refilling mechanism of plant tissues might not always lead to a full recovery of NEP at daily scales, particularly in the case of extreme heat-drought stress. As a result, the most severe decline of NEP was observed during the peak of the heatwave on 26–27 June. The most severe heat stress on 26 June might cause the suppression of tissue refilling during the following night, and thus more pronounced NEP reduction was observed on the next day (27 June) instead of on the hottest day (26 June). The decline of *Poa* LWP (Figure 6) might be due to their more severe drought stress (as indicated in their higher $\delta^{18}O_{lw}$ as compared to the other three genera; Figures 7A, 8A) and dependence on soil moisture (Figure 9B). The decline of Poa LWP had minor effect on NEP, probably due to their small plant size and stress-induced partial stomatal closure. We could not quantify the individual contribution of different genera on ecosystem water and carbon fluxes, and effect of eddy-covariance footprint; thus, we suggest that future research can combine ecosystem-scale eddy-covariance fluxes, footprint models and plant-scale chamber fluxes, complemented by plant community compositions to quantify the effect of different genera on ecosystem exchange.

Dew amount was found to be underestimated by eddy-covariance H_2O fluxes because dew occurs on clear and calm nights with stably stratified nocturnal boundary layer (Jacobs et al., 2006; Li et al., 2021). High accuracy weighing lysimeters can be an option to quantify dew amount into ecosystems (Riedl et al., 2022; Ucles et al., 2013). CO_2 fluxes can be measured by eddy-variance (Eugster and Siegrist, 2000) and laser (Maier et al., 2022) approaches. For alpine ecosystems, a challenge is the topographic variability that induces large uncertainties of CO_2 fluxes (Hammerle et al., 2007). Due to the low quality of CO_2 fluxes during nighttime by eddy-covariance measurements, we could not assess the dew effect in darkness. Furthermore, the benefits of dew on ecosystems can continue after dew drying out on vegetation surfaces, which could be traced by high-resolution measurements of H_2O and CO_2 isotopes, but was not possible in this study based on 3–13 h intervals of destructive isotope sampling. Therefore, additional methods, e.g., synchronized and continuous laser measurements of H_2O and CO_2 fluxes (Li et al., 2021; Maier et al., 2022) and their isotopic fluxes (Siegwolf et al., 2021) at both plant and ecosystem scales need to be

10.3389/fpls.2023.1136037

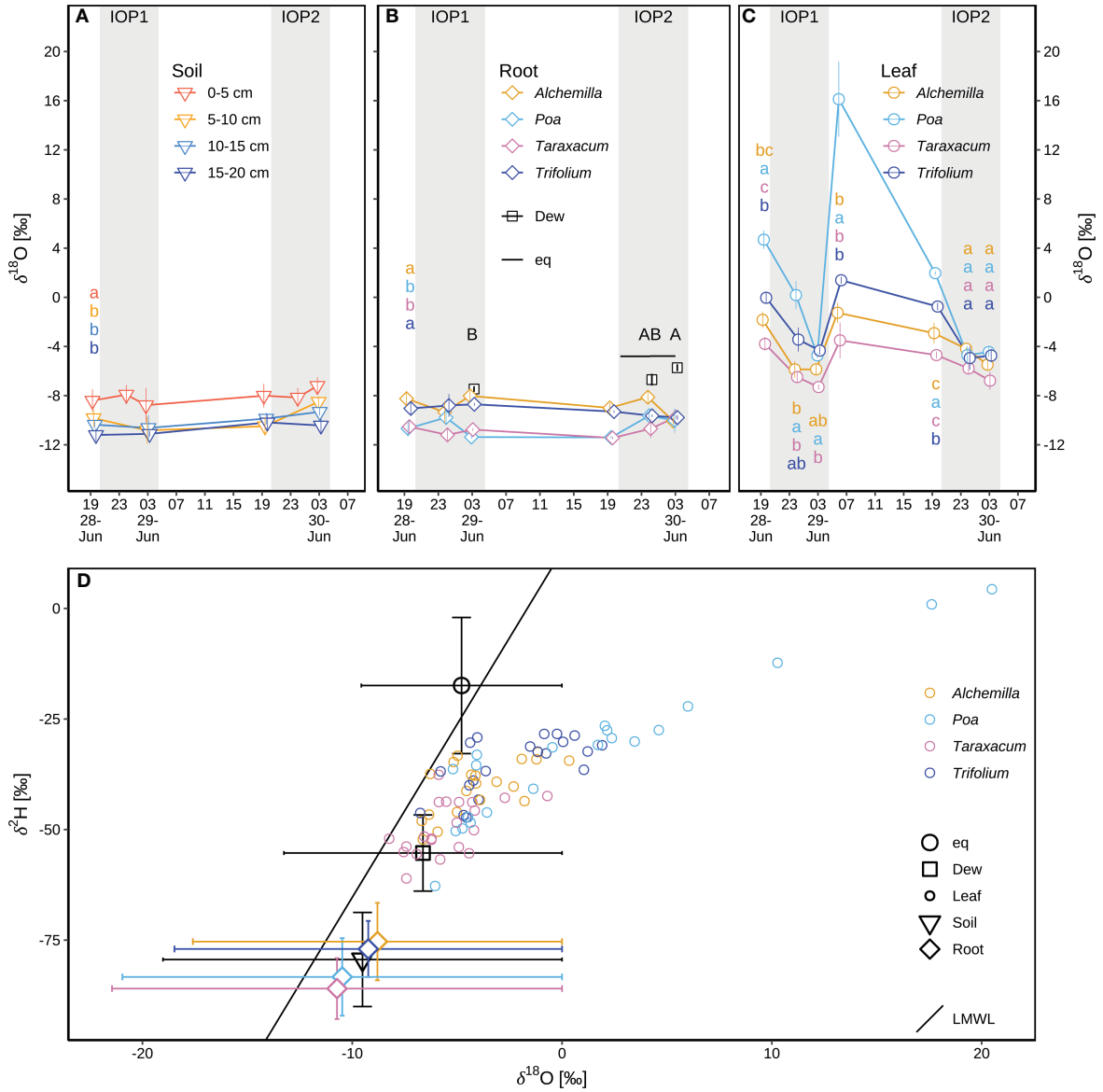

FIGURE 7
Isotope composition of different water pools during two consecutive intensive observation periods (IOP1 and IOP2) with nocturnal dew formation at the end of the June 2019 heatwave: **(A)** soil water $\delta^{18}O_{soil}$ at different depths (0–5, 5–10, 10–15, and 15–20 cm); different lower-case letters indicate statistical significance of among-soil-depth difference ($p < 0.05$) of $\delta^{18}O_{soil}$ over IOPs. **(B)** Dew droplets $\delta^{18}O_{dew}$ on plant surfaces; the liquid $\delta^{18}O_{eq}$ in equilibrium with atmospheric water vapor; xylem water of root crown $\delta^{18}O_{root}$ for four genera (*Alchemilla*, *Poa*, *Taraxacum*, *Trifolium*); different lower-case letters indicate statistical significance of among-genera difference ($p < 0.05$) of $\delta^{18}O_{root}$ over IOPs; different capital letters in black indicate statistical significance of among-sampling-time difference ($p < 0.05$) of $\delta^{18}O_{dew}$. **(C)** Leaf water $\delta^{18}O_{lw}$ for four genera; different lower-case letters indicate statistical significance of among-genera difference ($p < 0.05$) for $\delta^{18}O_{lw}$ at each sampling time. Mean and standard errors of mean (SEM) are shown in panels **(A–C)**. **(D)** $\delta^{2}H$–$\delta^{18}O$ pairs compared to the local meteoric water line (LMWL: $\delta^{2}H = 7.83\delta^{18}O + 12.97$) following Prechsl et al. (2014); $\delta^{2}H$–$\delta^{18}O$ of equilibrium liquid, dew samples, and soil samples was mean and SEM over IOPs; $\delta^{2}H$–$\delta^{18}O$ of xylem water of root crown was mean and SEM by species over IOPs; raw data of leaf water $\delta^{2}H$–$\delta^{18}O$ were shown for four genera at each sampling time. The grey shaded areas in panels **(A-C)** represent nocturnal periods.

explored to assess the long-term benefits of dew at plant (e.g., among species difference) and ecosystem scales.

4.3 Genus variability

Plant water stress can be induced by low soil moisture or high atmospheric water demand (Liu et al., 2020). In this study, leaf water status of *Poa* was dependent on soil moisture (Figure 9B), whilst LWP of *Alchemilla*, *Taraxacum*, and *Trifolium* were mainly controlled by atmospheric humidity conditions (Figure 9C). Among the four genera, *Poa* was most substantially affected by heat-drought stress as indicated in their lower LWP (Figure 6), higher $\delta^{18}O_{lw}$ and $\delta^{13}C_{ls}$ (Figures 7A, 8A, B). This could be induced by the reliance of *Poa* on soil moisture (Figure 9B), and lower foliar water uptake of *Poa* (Figure 8D). More severe drought stress of *Poa* induced their lower WUE (higher $\delta^{13}C_{ls}$; Figure 8F) as compared to *Taraxacum*, and *Trifolium*. Palmately-lobed and hairy leaves of

10.3389/fpls.2023.1136037

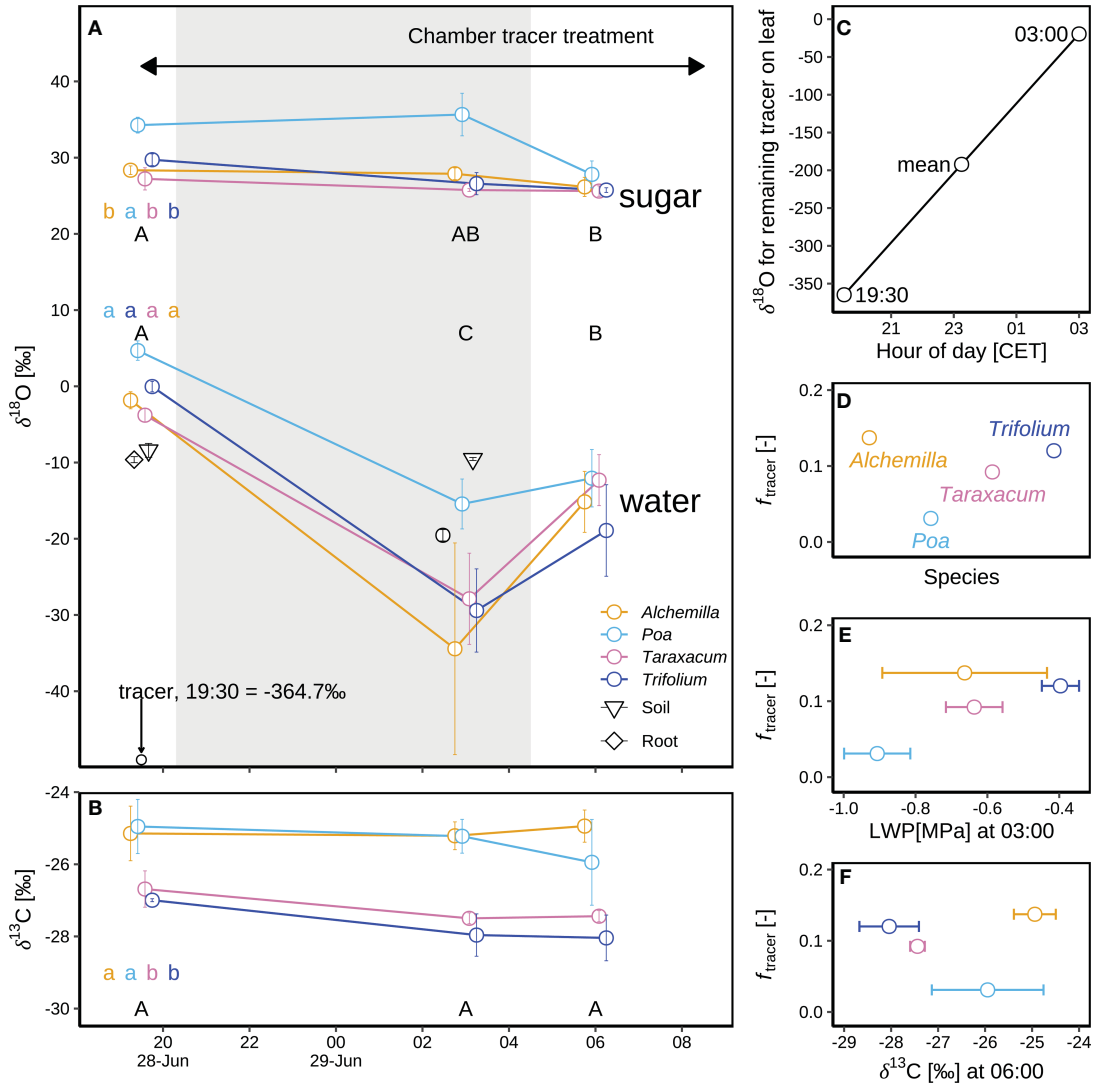

FIGURE 8
Oxygen isotope composition of leaf sugars ($\delta^{18}O_{ls}$ and $\delta^{13}C_{ls}$) and leaf water ($\delta^{18}O_{lw}$) in a chamber tracer experiment during an intensive observation period (IOP1) for four plant genera (*Alchemilla*, *Poa*, *Taraxacum*, and *Trifolium*) at the end of the June 2019 heatwave: **(A)** Mean and standard errors of mean (SEM) for the isotope composition of bulk leaf sugar ($\delta^{18}O_{ls}$) and leaf water ($\delta^{18}O_{lw}$) with the corresponding xylem water of root crown, soil water (at 5 cm soil depth) and tracer on leaf surface. The grey shaded area corresponds to the nocturnal period. Leaf samples taken before sunset in IOP1 (19:30 CET) acted as a control for natural isotope abundances. **(B)** Mean and SEM for the carbon isotope composition of bulk leaf sugar ($\delta^{13}C_{ls}$) for four genera. **(C)** Changes in $\delta^{18}O$ of tracer remaining on the leaves, from 19:30 ($\delta^{18}O_{tracer\_19:30}$) when the tracer was sprayed on the leaves until 03:00 ($\delta^{18}O_{tracer\_03:00}$) before sunrise; the mean tracer $\delta^{18}O$ ($\delta^{18}O_{tracer\_mean}$) was calculated as arithmetic mean. **(D)** Contributions of $\delta^{18}O_{tracer}$ in leaf water (f_{tracer}) at 03:00 on 29 June 2019 are based on a two-pool mixing model. **(E)** Correlation of f_{tracer} with leaf water potential (LWP) for four genera. **(F)** Correlation of f_{tracer} with $\delta^{13}C_{ls}$. Different letters in panels a–b indicate statistically significant difference ($p < 0.05$) of leaf water and sugar with capital letters representing temporal differences and lower-cases representing among-genera differences over IOP1.

Alchemilla might prolong the dew water retention on their leaves, and thus induced stronger foliar water uptake (Figure 8D) and slightly increased LWP (Figure 6) compared to the other three genera.

Both *Alchemilla* and *Trifolium* depended on shallower soil water depth (Figure 7B), but they probably benefited from dew water to maintain their plant water status (Figure 6) in response to heat and drought stress. In the case of *Trifolium*, the hairy trichomes on the edges of the leaves probably promoted foliar water uptake (Figure 8D). Many high-elevation plants have hairy structures to help reduce water loss, reflect excess radiation, and protect plants from pathogens (Zeng et al., 2013; Hamaoka et al., 2017). The control experiment at the same site by Prechsl et al. (2015) found that C_3-grasses did not shift to deeper soil water under drought treatment, indicating that high-elevation plants could benefit from leaf structures regulating their energy and water balances. On the contrary, with deeper soil water sources, the plant water status of *Poa* strongly declined (Figure 6) in response to heat-drought stress. The maintenance of *Taraxacum* LWP (Figure 6) in response to heat-drought stress might be beneficial from their waxy leaf surfaces (Figure S1) and deeper soil water uptake (Figure 7B). These results indicated that both soil moisture and atmospheric conditions can affect the ecosystem carbon and water exchange

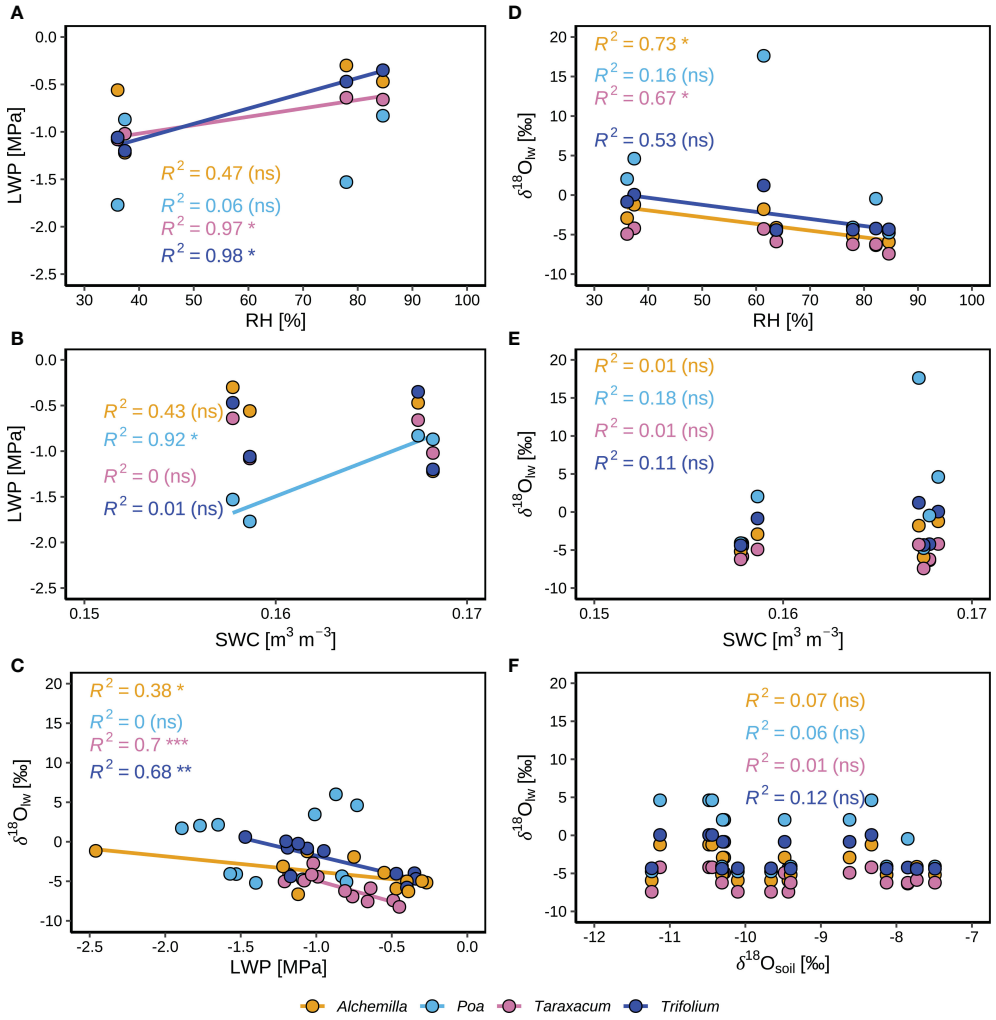

FIGURE 9
Correlations between different environmental and plant variables for four plant genera (*Alchemilla*, *Poa*, *Taraxacum*, and *Trifolium*) during two consecutive intensive observation periods (IOP1 and IOP2) with nocturnal dew formation at the end of the June 2019 heatwave: **(A)** Median leaf water potential (LWP) and corresponding relative humidity (RH, at 2 m agl). **(B)** Median LWP and corresponding volumetric soil water content (SWC) at 5 cm depth. **(C)** Leaf water isotopes ($\delta^{18}O_{lw}$) and LWP. **(D)** Meidian $\delta^{18}O_{lw}$ and corresponding RH. **(E)** Median $\delta^{18}O_{lw}$ and corresponding SWC. **(F)** Median $\delta^{18}O_{lw}$ and median soil water isotopes ($\delta^{18}O_{soil}$).

under heat-drought stressed conditions through their varied influence on different plant genera. Due to the similar $\delta^{18}O$ values for dew and soil water (Figure 7B), we could not split the contributions of dew (foliar water uptake) and nighttime plant tissue refilling (root water uptake; Schulze et al., 2019) on plant water status using the natural-conditioned data, because both root water uptake and foliar water uptake could occur during nighttime, and dew water can also drip off to the soil (Dawson, 1998) and disturb the isotopic signal of root water uptake fluxes. But our chamber-tracer experiment indicated that the contribution of dew on leaf water can vary from 3% to 14% (Figure 8D). We did not isolate the soil from the vegetation when amending tracer on the grassland plots, hence the tracer could have been directly applied on the soil, and the tracer sprayed on leaf surfaces could also have dripped into the soil. But according to the slight depletion of $\delta^{18}O_{lw}$ in our chamber-tracer experiment, the drip-off effect of dew was probably minor compared to direct foliar uptake of dew and atmospheric water vapor. Based on the facts of similar isotopic signal of dew and soil moisture in natural conditions, previous research used excised leaves and isotopically depleted/enriched water to distinguish the two (root and foliar) water sources (Kim and Lee, 2011; Goldsmith et al., 2017). However, these controlled experiments were performed with self-made chambers acting as a heat trap preventing radiative cooling, which is the most important driver of dew formation in natural conditions (Curtis, 1936; Li et al., 2023), and may thus not reflect natural conditions. Future research should therefore apply approaches that allow to estimate the dew influence on plant water under varying soil moisture conditions in the field (Li et al., 2021).

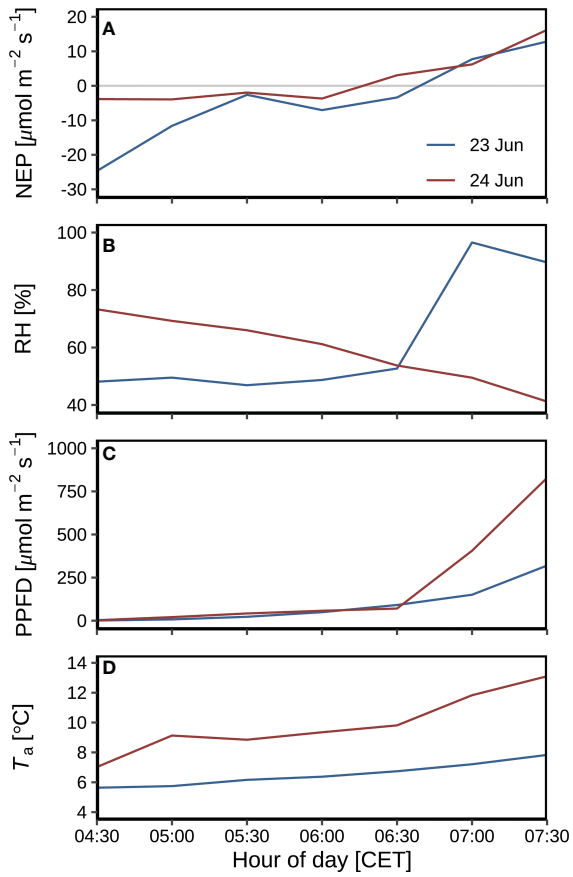

FIGURE 10
Environmental variables during leaf wetting by dew in the early mornings of 23-24 June before the heatwave: **(A)** Net ecosystem production (NEP). **(B)** Leaf wetness. **(C)** Photosynthetic photon flux density (PPFD). **(D)** air temperature (T_a) at 2 m agl.

5 Conclusions

The combination of stable isotope analyses in meteoric waters and leaf sugars, meteorological and plant physiological measurements, complemented by eddy-covariance fluxes for H_2O vapor and CO_2 provided novel insights into the effects of combined heat-drought stress on the water and carbon exchange of an alpine grassland.

(1) Before the heatwave, NEP increased with RH levels, but the dew benefits were cancelled out during the heatwave. NEP decreased with RH levels at the beginning of the heatwave, and showed no significant correlation with leaf wetness at the later stages of the heatwave.

(2) The isotope signal of amended dew in the chamber tracer experiment was not transferred to leaf sugar, indicating that dew water did not participate in the carbon assimilation. The minor effect of dew on NEP might be derived from low contribution (3-14%) of dew in leaf water, and the partial stomatal closure induced by heat-drought stress.

(3) NEP reduction was most severe on the hottest two days, with the shift from net ecosystem uptake to net ecosystem emission on the second hottest day just after the peak of the heatwave, indicating that the heat effect was intensified by drought stress.

(4) The recovery of NEP after the peak of the heatwave indicated the regrowth ability of alpine plants. Plants benefited from the minor effect of heat-drought stress on their water status, which could be recovered *via* the refilling of plant tissues during nighttime.

(5) The among-genera difference of leaf water status and isotopes in response to heat-drought stress and dew occurrence indicated the varied controls of soil moisture and atmospheric evaporative demand on plant water status, with soil-dependent genera suffering from more severe drought stress compared to the atmospheric-reliant genera.

Our results thus reveal that dew influence on ecosystem water and carbon exchange varied by the levels and stages of environmental stress and plant physiology.

Data availability statement

The datasets presented in this study can be found in the ETH Zurich research collection at https://doi.org/10.3929/ethz-b-000537314.

Author contributions

YL, WE, AR, and ML designed the experiment. YL conducted the field and laboratory work. YL and ML performed the purification of plant sugars. YL wrote and revised the manuscript, with contributions and feedback from NB, WE, ML, FA and AR. All authors contributed to the article and approved the submitted version. WE passed away on 23 May 2022 before the final submission of this study.

Funding

This study was funded by the Swiss National Science Foundation (grant no. 175733). We also acknowledge funding from the EU project SUPER-G (Developing SUstainable PERmanent Grassland systems and polices; project 774124) and open access funding by ETH Zurich. ML was funded by the Swiss National Science Foundation (grant no. 179978).

Acknowledgments

We thank Dr. Lukas Hörtnagl (Grassland Sciences group at ETH Zurich) and Dr. Shiva Ghiasi (Agroscope, the Swiss Center of Excellence for Agricultural Research) for flux data processing. We thank Annika Ackermann and Dr. Roland A. Werner (Grassland Sciences group at ETH Zurich) as well as Manuela Oettli and Dr.

Matthias Saurer (Stable Isotope Research Center at WSL Birmensdorf) for their assistance with isotope analyses. We further thank Oliver Rehmann at WSL for laboratory assistance, Tobia Lezuo at ETH Zurich for field work, as well as the AgroVet-Strickhof staff (Eschikon, Switzerland) and the technician team of the Grassland Sciences group for their field site support.

Conflict of interest

The authors declare that the research was conducted in the absence of any commercial or financial relationships that could be construed as a potential conflict of interest.

Publisher's note

Supplementary material

The Supplementary Material for this article can be found online at: https://www.frontiersin.org/articles/10.3389/fpls.2023.1136037/full#supplementary-material

References

Aubinet, M., Vesala, T., and Papale, D. (2012). *Eddy covariance: a practical guide to measurement and data analysis* (Dordrecht: Springer). doi: 10.1007/978-94-007-2351-1

Bachmann, D., Gockele, A., Ravenek, J. M., Roscher, C., Strecker, T., Weigelt, A., et al. (2015). No evidence of complementary water use along a plant species richness gradient in temperate experimental grasslands. *PloS One* 10 (1), e0116367. doi: 10.1371/journal.pone.0116367

Barriopedro, D., Fischer, E. M., Luterbacher, J., Trigo, R. M., and García-Herrera, R. (2011). The hot summer of 2010: redrawing the temperature record map of Europe. *Science* 332 (6026), 220–224. doi: 10.1126/science.1201224

Beysens, D. (2018). *Dew water* (Denmark: River Publishers).

Bögelein, R., Lehmann, M. M., and Thomas, F. M. (2019). Differences in carbon isotope leaf-to-phloem fractionation and mixing patterns along a vertical gradient in mature European beech and Douglas fir. *New Phytol.* 222 (4), 1803–1815. doi: 10.1111/nph.15735

Boucher, J. F., Munson, A. D., and Bernier, P. Y. (1995). Foliar absorption of dew influences shoot water potential and root-growth in pinus-strobus seedlings. *Tree Physiol.* 15 (12), 819–823. doi: 10.1093/treephys/15.12.819

Brandes, E., Kodama, N., Whittaker, K., Weston, C., Rennenberg, H., Keitel, C., et al. (2006). Short-term variation in the isotopic composition of organic matter allocated from the leaves to the stem of pinus sylvestris: effects of photosynthetic and postphotosynthetic carbon isotope fractionation. *Global Change Biol.* 12 (10), 1922–1939. doi: 10.1111/j.1365-2486.2006.01205.x

Brewer, C. A., and Smith, W. K. (1994). Influence of simulated dewfall on photosynthesis and yield in soybean isolines (Glycine max [L.] merr. cv williams) with different trichome densities. *Int. J. Plant Sci.* 155 (4), 460–466. doi: 10.1086/297183

Brilli, F., Hörtnagl, L., Hammerle, A., Haslwanter, A., Hansel, A., Loreto, F., et al. (2011). Leaf and ecosystem response to soil water availability in mountain grasslands. *Agric. For. Meteorology* 151 (12), 1731–1740. doi: 10.1016/j.agrformet.2011.07.007

Burgess, S. S. O., and Bleby, T. M. (2006). Redistribution of soil water by lateral roots mediated by stem tissues. *J. Exp. Bot.* 57 (12), 3283–3291. doi: 10.1093/jxb/erl085

Cernusak, L. A., Pate, J. S., and Farquhar, G. D. (2002). Diurnal variation in the stable isotope composition of water and dry matter in fruiting lupinus angustifolius under field conditions. *Plant Cell Environ.* 25 (7), 893–907. doi: 10.1046/j.1365-3040.2002.00875.x

Ciais, P., Reichstein, M., Viovy, N., Granier, A., Ogee, J., Allard, V., et al. (2005). Europe-Wide reduction in primary productivity caused by the heat and drought in 2003. *Nature* 437 (7058), 529–533. doi: 10.1038/nature03972

Clus, O., Ortega, P., Muselli, M., Milimouk, I., and Beysens, D. (2008). Study of dew water collection in humid tropical islands. *J. Hydrol* 361 (1-2), 159–171. doi: 10.1016/j.jhydrol.2008.07.038

Coplen, T. B. (2011). Guidelines and recommended terms for expression of stable-isotope-ratio and gas-ratio measurement results. *Rapid Commun. Mass Spectrometry* 25 (17), 2538–2560. doi: 10.1002/rcm.5129

Cremonese, E., Filippa, G., Galvagno, M., Siniscalco, C., Oddi, L., di Cella, U. M., et al. (2017). Heat wave hinders green wave: the impact of climate extreme on the phenology of a mountain grassland. *Agric. For. Meteorology* 247, 320–330. doi: 10.1016/j.agrformet.2017.08.016

Curtis, O. F. (1936). Leaf temperatures and the cooling of leaves by radiation. *Plant Physiol.* 11 (2), 343–364. doi: 10.1104/pp.11.2.343

Dawson, T. E. (1998). Fog in the California redwood forest: ecosystem inputs and use by plants. *Oecologia* 117 (4), 476–485. doi: 10.1007/s004420050683

Dawson, T. E., and Goldsmith, G. R. (2018). The value of wet leaves. *New Phytol.* 219 (4), 1156–1169. doi: 10.1111/nph.15307

De Boeck, H. J., Bassin, S., Verlinden, M., Zeiter, M., and Hiltbrunner, E. (2016). Simulated heat waves affected alpine grassland only in combination with drought. *New Phytol.* 209 (2), 531–541. doi: 10.1111/nph.13601

Dongmann, G., Nurnberg, H. W., Forstel, H., and Wagener, K. (1974). On the enrichment of $H_2{}^{18}O$ in the leaves of transpiring plants. *Radiat. Environ. Biophysics* 11 (1), 41–52. doi: 10.1007/BF01323099

Eugster, W., and Siegrist, F. (2000). The influence of nocturnal CO2 advection on CO2 flux measurements. *Basic Appl. Ecol.* 1 (2), 177–188. doi: 10.1078/1439-1791-00028

Farquhar, G. D., and Lloyd, J. (1993). "Carbon and oxygen isotope effects in the exchange of carbon dioxide between terrestrial plants and the atmosphere," in *Stable isotopes and plant carbon-water relations*. Eds. J. R. Ehleringer, A. E. Hall and G. D. Farquhar (San Diego: Academic Press), 47–70. doi: 10.1016/B978-0-08-091801-3.50011-8

Gehre, M., Geilmann, H., Richter, J., Werner, R. A., and Brand, W. A. (2004). Continuous flow $^2H/^1H$ and $^{18}O/^{16}O$ analysis of water samples with dual inlet precision. *Rapid Commun. mass spectrometry* 18 (22), 2650–2660. doi: 10.1002/rcm.1672

Gerlein-Safdi, C., Gauthier, P. P. G., and Caylor, K. K. (2018). Dew-induced transpiration suppression impacts the water and isotope balances of colocasia leaves. *Oecologia* 187 (4), 1041–1051. doi: 10.1007/s00442-018-4199-y

Gessler, A., Brandes, E., Keitel, C., Boda, S., Kayler, Z. E., Granier, A., et al. (2013). The oxygen isotope enrichment of leaf-exported assimilates–does it always reflect lamina leaf water enrichment? *New Phytol.* 200 (1), 144–157. doi: 10.1111/nph.12359

Gharun, M., Hortnagl, L., Paul-Limoges, E., Ghiasi, S., Feigenwinter, I., Burri, S., et al. (2020). Physiological response of Swiss ecosystems to 2018 drought across plant types and elevation. *Philos. T R Soc. B* 375 (1810), 20190521. doi: 10.1098/rstb.2019.0521

Goldsmith, G. R., Lehmann, M. M., Cernusak, L. A., Arend, M., and Siegwolf, R. T. W. (2017). Inferring foliar water uptake using stable isotopes of water. *Oecologia* 184 (4), 763–766. doi: 10.1007/s00442-017-3917-1

Hamaoka, N., Yasui, H., Yamagata, Y., Inoue, Y., Furuya, N., Araki, T., et al. (2017). A hairy-leaf gene, BLANKET LEAF, of wild oryza nivara increases photosynthetic water use efficiency in rice. *Rice* 10 (1), 20. doi: 10.1186/s12284-017-0158-1

Hammerle, A., Haslwanter, A., Schmitt, M., Bahn, M., Tappeiner, U., Cernusca, A., et al. (2007). Eddy covariance measurements of carbon dioxide, latent and sensible energy fluxes above a meadow on a mountain slope. *Bound-Lay Meteorol* 122 (2), 397–416. doi: 10.1007/s10546-006-9109-x

Hanba, Y. T., Moriya, A., and Kimura, K. (2004). Effect of leaf surface wetness and wettability on photosynthesis in bean and pea. *Plant Cell Environ.* 27 (4), 413–421. doi: 10.1046/j.1365-3040.2004.01154.x

Hiller, R., Zeeman, M. J., and Eugster, W. (2008). Eddy-covariance flux measurements in the complex terrain of an alpine valley in Switzerland. *Bound-Lay Meteorol* 127 (3), 449–467. doi: 10.1007/s10546-008-9267-0

Horiguchi, I., Sugaya, H., and Tani, H. (1982). The measurement of longwave radiation properties upon plastic films used in greenhouses. *J. Agric. Meteorology* 38 (1), 9–14. doi: 10.2480/agrmet.38.9

Horita, J., and Wesolowski, D. J. (1994). Liquid-vapor fractionation of oxygen and hydrogen isotopes of water from the freezing to the critical temperature. *Geochimica Cosmochimica Acta* 58 (16), 3425–3437. doi: 10.1016/0016-7037(94)90096-5

IAEA (2009). Reference sheet for VSMOW2 and SLAP2 international measurement standards. *Int. Atomic Energy Agency (IAEA) Vienna Austria* pp, 8. Available at: https://nucleus.iaea.org/sites/ReferenceMaterials/Shared%20Documents/ReferenceMaterials/StableIsotopes/VSMOW2/VSMOW2_SLAP2.pdf.

Jacobs, A. F. G., Heusinkveld, B. G., Kruit, R. J. W., and Berkowicz, S. M. (2006). Contribution of dew to the water budget of a grassland area in the Netherlands. *Water Resour Res.* 42 (3), W03415. doi: 10.1029/2005WR004055

Keller, P. (2006). *Vegetationskundliche Untersuchungen und Ertrag der Grünlandflächen im Gebiet der ETH-Forschungsstation Alp Weissenstein GR* (Zurich, Switzerland: University of Zurich), 119 pp.

Kim, K., and Lee, X. (2011). Transition of stable isotope ratios of leaf water under simulated dew formation. *Plant Cell Environ.* 34 (10), 1790–1801. doi: 10.1111/j.1365-3040.2011.02375.x

Lehmann, M. M., Goldsmith, G. R., Mirande-Ney, C., Weigt, R. B., Schonbeck, L., Kahmen, A., et al. (2020). The ^{18}O-signal transfer from water vapour to leaf water and assimilates varies among plant species and growth forms. *Plant Cell Environ.* 43 (2), 510–523. doi: 10.1111/pce.13682

Lehmann, M. M., Goldsmith, G. R., Schmid, L., Gessler, A., Saurer, M., and Siegwolf, R. T. W. (2018). The effect of ^{18}O-labelled water vapour on the oxygen isotope ratio of water and assimilates in plants at high humidity. *New Phytol.* 217 (1), 105–116. doi: 10.1111/nph.14788

Li, Y., Aemisegger, F., Riedl, A., Buchmann, N., and Eugster, W. (2021). The role of dew and radiation fog inputs in the local water cycling of a temperate grassland during dry spells in central Europe. *Hydrol. Earth Syst. Sci.* 25 (5), 2617–2648. doi: 10.5194/hess-25-2617-2021

Li, Y., Riedl, A., Eugster, W., Buchmann, N., Cernusak, L. A., Lehmann, M. M., et al. (2023). The role of radiative cooling and leaf wetting in air–leaf water exchange during dew and radiation fog events in a temperate grassland. *Agric. For. Meteorology* 328, 109256. doi: 10.1016/j.agrformet.2022.109256

Li, L. F., Zheng, Z. Z., Biederman, J. A., Qian, R. Y., Ran, Q. W., Zhang, B., et al. (2020). Drought and heat wave impacts on grassland carbon cycling across hierarchical levels. *Plant Cell Environ.* doi: 10.1111/pce.13767

LI-COR (2019). *Eddy covariance processing software (Version 7.0.6)* (Bad Homburg, Germany: LI–COR. LI–COR, Inc). Available at: https://www.licor.com/env/products/eddy_covariance/software.html.

Limm, E. B., Simonin, K. A., Bothman, A. G., and Dawson, T. E. (2009). Foliar water uptake: a common water acquisition strategy for plants of the redwood forest. *Oecologia* 161 (3), 449–459. doi: 10.1007/s00442-009-1400-3

Liu, L., Gudmundsson, L., Hauser, M., Qin, D., Li, S., and Seneviratne, S. I. (2020). Soil moisture dominates dryness stress on ecosystem production globally. *Nat. Commun.* 11 (1), 4892. doi: 10.1038/s41467-020-18631-1

Maier, R., Hörtnagl, L., and Buchmann, N. (2022). Greenhouse gas fluxes (CO_2, N_2O and CH_4) of pea and maize during two cropping seasons: drivers, budgets, and emission factors for nitrous oxide. *Sci. Total Environ.* 849, 157541. doi: 10.1016/j.scitotenv.2022.157541

MeteoSwiss. (2019). "Climate bulletin summer 2019." In.: *Federal Office for Meteorology and Climatology MeteoSwiss*. Available at: https://www.meteoswiss.admin.ch/home/search.subpage.html/en/data/publications/2019/9/klimabulletin-sommer-2019.html?pageIndex=1&query=Climate%20bulletin%20summer%202019&tab=search_tab.

Michna, P., Eugster, W., Hiller, R. V., Zeeman, M. J., and Wanner, H. (2013). Topoclimatological case-study of alpine pastures near the albula pass in the eastern Swiss Alps. *Geogr. Helv.* 68 (4), 249–263. doi: 10.5194/gh-68-249-2013

Mitchell, D., Kornhuber, K., Huntingford, C., and Uhe, P. (2019). The day the 2003 European heatwave record was broken. *Lancet Planetary Health* 3 (7), e290–e292. doi: 10.1016/S2542-5196(19)30106-8

Oliveira, B. R. F., Schaller, C., Keizer, J. J., and Foken, T. (2021). Estimating immediate post-fire carbon fluxes using the eddy-covariance technique. *Biogeosciences* 18 (1), 285–302. doi: 10.5194/bg-18-285-2021

Overpeck, J. T. (2013). Climate science: the challenge of hot drought. *Nature* 503 (7476), 350–351. doi: 10.1038/503350a

Prechsl, U. E., Burri, S., Gilgen, A. K., Kahmen, A., and Buchmann, N. (2015). No shift to a deeper water uptake depth in response to summer drought of two lowland and sub-alpine C_3-grasslands in Switzerland. *Oecologia* 177 (1), 97–111. doi: 10.1007/s00442-014-3092-6

Prechsl, U. E., Gilgen, A. K., Kahmen, A., and Buchmann, N. (2014). Reliability and quality of water isotope data collected with a lowbudget rain collector. *Rapid Commun. Mass Spectrometry* 28 (8), 879–885. doi: 10.1002/rcm.6852

R Core Team (2021). *R: a language and environment for statistical computing* (Vienna, Austria: R Foundation for Statistical Computing).

Riedl, A., Li, Y., Eugster, J., Buchmann, N., and Eugster, W. (2022). High-accuracy weighing micro-lysimeter system for long-term measurements of non-rainfall water inputs to grasslands. *Hydrology and Earth System Sciences* 26(1), 91–116. doi: 10.5194/hess-26-91-2022

Rinne, K. T., Saurer, M., Streit, K., and Siegwolf, R. T. W. (2012). Evaluation of a liquid chromatography method for compound-specific δ^{13}C analysis of plant carbohydrates in alkaline media. *Rapid Commun. Mass Spectrometry* 26 (18), 2173–2185. doi: 10.1002/rcm.6334

Schulze, E., Beck, E., Buchmann, N., Clemens, S., Müller-Hohenstein, M., and Scherer-Lorenzen, M. (2019). Plant ecology (Heidelberg, Germany: Springer Berlin, Heidelberg). doi: 10.1007/978-3-662-56233-8

Siegwolf, R., Lehmann, M., Goldsmith, G., Churakova, O., Mirande-Ney, C., Gruspante, G., et al. (2021). The dual c and O isotope–gas exchange model: a concept review for understanding plant responses to the environment and its application in tree rings. *Authorea Preprints*. doi: 10.22541/au.163844646.68129291/v1

Simonin, K. A., Santiago, L. S., and Dawson, T. E. (2009). Fog interception by sequoia sempervirens (D. don) crowns decouples physiology from soil water deficit. *Plant Cell Environ.* 32 (7), 882–892. doi: 10.1111/j.1365-3040.2009.01967.x

Steel, R. G. (1997). *Pinciples and procedures of statistics a biometrical approach* (Auckland: McGraw-Hill Kogakusha, Ltd.), 633 pp.

Stull, R. B. (1988). "Stable boundary layer," in *An introduction to boundary layer meteorology*. Ed. R. B. Stull (Dordrecht: Springer, Dordrecht), 499–543. doi: 10.1007/978-94-009-3027-8_12

Teuling, A. J., Seneviratne, S. I., Stöckli, R., Reichstein, M., Moors, E., Ciais, P., et al. (2010). Contrasting response of European forest and grassland energy exchange to heatwaves. *Nat. Geosci.* 3 (10), 722–727. doi: 10.1038/ngeo950

Uclés, O., Villagarcía, L., Cantón, Y., and Domingo, F. (2013). Microlysimeter station for long term non-rainfall water input and evaporation studies. *Agri. For. Meteorology* 182, 13–20. doi: 10.1016/j.agrformet.2013.07.017

Wang, A., Siegwolf, R. T. W., Joseph, J., Thomas, F. M., Werner, W., Gessler, A., et al. (2021). Effects of soil moisture, needle age and leaf morphology on carbon and oxygen uptake, incorporation and allocation: a dual labeling approach with $^{13}CO_2$ and $H_2{}^{18}O$ in foliage of a coniferous forest. *Tree Physiol.* 41 (1), 50–62. doi: 10.1093/treephys/tpaa114

Werner, R. A., and Brand, W. A. (2001). Referencing strategies and techniques in stable isotope ratio analysis. *Rapid Commun. Mass Spectrometry* 15 (7), 501–519. doi: 10.1002/rcm.258

WMO (2019). *European Heatwave sets new temperature records* (Geneva, Switzerland: World Meteorological Organization).

Wolf, S., Eugster, W., Ammann, C., Häni, M., Zielis, S., Hiller, R., et al. (2013). Contrasting response of grassland versus forest carbon and water fluxes to spring drought in Switzerland. *Environ. Res. Lett.* 8 (3), 35007. doi: 10.1088/1748-9326/8/3/035007

Yakir, D., and Deniro, M. J. (1990). Oxygen and hydrogen isotope fractionation during cellulose metabolism in *Lemna-Gibba* l. *Plant Physiol.* 93 (1), 325–332. doi: 10.1104/pp.93.1.325

Zeeman, M. J., Hiller, R., Gilgen, A. K., Michna, P., Plüss, P., Buchmann, N., et al. (2010). Management and climate impacts on net CO_2 fluxes and carbon budgets of three grasslands along an elevational gradient in Switzerland. *Agric. For. Meteorology* 150 (4), 519–530. doi: 10.1016/j.agrformet.2010.01.011

Zeng, Y., Zhu, Y., Lian, L., Xie, H., Zhang, J., and Xie, H. (2013). Genetic analysis and fine mapping of the pubescence gene GL6 in rice (Oryza sativa l.). *Chin. Sci. Bull.* 58 (24), 2992–2999. doi: 10.1007/s11434-013-5737-y

Zscheischler, J., and Fischer, E. M. (2020). The record-breaking compound hot and dry 2018 growing season in Germany. *Weather Clim Extreme* 29, 100270. doi: 10.1016/j.wace.2020.100270

Zscheischler, J., Martius, O., Westra, S., Bevacqua, E., Raymond, C., Horton, R. M., et al. (2020). A typology of compound weather and climate events. *Nat. Rev. Earth Env.* 1 (7), 333–347. doi: 10.1038/s43017-020-0060-z

Zschenderlein, P., Fragkoulidis, G., Fink, A. H., and Wirth, V. (2018). Large-Scale rossby wave and synoptic-scale dynamic analyses of the unusually late 2016 heatwave over Europe. *Weather* 73 (9), 275–283. doi: 10.1002/wea.3278

frontiers | Frontiers in Plant Science

TYPE Original Research
PUBLISHED 08 June 2023
DOI 10.3389/fpls.2023.1172078

OPEN ACCESS

EDITED BY
Biao Jin,
Yangzhou University, China

REVIEWED BY
Francisco M. Del Amor,
Instituto Murciano de Investigación y Desarrollo Agrario y Alimentario (IMIDA), Spain
Hongbo Zhao,
Zhejiang Agriculture and Forestry University, China

*CORRESPONDENCE
Zaiqiang Yang
yzq@nuist.edu.cn

RECEIVED 23 February 2023
ACCEPTED 18 May 2023
PUBLISHED 08 June 2023

CITATION
Luo J, Yang Z, Zhang F and Li C (2023) Effect of nitrogen application on enhancing high-temperature stress tolerance of tomato plants during the flowering and fruiting stage.
Front. Plant Sci. 14:1172078.
doi: 10.3389/fpls.2023.1172078

Effect of nitrogen application on enhancing high-temperature stress tolerance of tomato plants during the flowering and fruiting stage

Jing Luo, Zaiqiang Yang*, Fengyin Zhang and Chunying Li

Jiangsu Key Laboratory of Agricultural Meteorology, School of Applied Meteorology, Nanjing University of Information Science and Technology, Nanjing, China

This study was conducted to investigate the effects of nitrogen application on growth, photosynthetic performance, nitrogen metabolism activities, and fruit quality of tomato plants under high-temperature (HT) stress. Three levels of daily minimum/daily maximum temperature were adopted during the flowering and fruiting stage, namely control (CK; 18°C/28°C), sub-high temperature (SHT; 25°C/35°C), and high-temperature (HT; 30°C/40°C) stress. The levels of nitrogen (urea, 46% N) were set as 0 (N_1), 125 (N_2), 187.5 (N_3), 250 (N_4), and 312.5 (N_5) kg hm^2, respectively, and the duration lasted for 5 days (short-term). HT stress inhibited the growth, yield, and fruit quality of tomato plants. Interestingly, short-term SHT stress improved growth and yield via higher photosynthetic efficiency and nitrogen metabolism whereas fruit quality was reduced. Appropriate nitrogen application can enhance the high-temperature stress tolerance of tomato plants. The maximum net photosynthetic rate (P_{Nmax}), stomatal conductance (g_s), stomatal limit value (L_S), water-use efficiency (WUE), nitrate reductase (NR), glutamine synthetase (GS), soluble protein, and free amino acids were the highest in N_3, N_3, and N_2, respectively, for CK, SHT, and HT stress, whereas carbon dioxide concentration (C_i), was the lowest. In addition, maximum SPAD value, plant morphology, yield, Vitamin C, soluble sugar, lycopene, and soluble solids occurred at N_3-N_4, N_3-N_4, and N_2-N_3, respectively, for CK, SHT, and HT stress. Based on the principal component analysis and comprehensive evaluation, we found that the optimum nitrogen application for tomato growth, yield, and fruit quality was 230.23 kg hm^2 (N_3-N_4), 230.02 kg hm^2 (N_3-N_4), and 115.32 kg hm^2 (N_2), respectively, at CK, SHT, and HT stress. Results revealed that the high yield and good fruit quality of tomato plants at high temperatures can be maintained by higher photosynthesis, nitrogen efficiency, and nutrients with moderate nitrogen.

KEYWORDS

high-temperature stress, nitrogen, tomato, abiotic stress tolerance, principal component analysis, comprehensive evaluation

1 Introduction

Tomato (*Solanum lycopersicum* L.) is one of the most widely grown, consumed, and produced crops in the greenhouse worldwide (Liu and Wang, 2020). It has attracted attention due to its rich Vitamin C and other nutrients, especially lycopene, which is related to its effects as a natural antioxidant (Alenazi et al., 2020; Imran et al., 2020).

Global warming has continued to raise concerns in recent years (Marlon et al., 2021; Hoffmann et al., 2022). The effect of global warming may cause irreversible damage to the growth and development of plants (Mathur et al., 2014; Ezquer et al., 2020). Tomato is a temperature-loving crop and is sensitive to temperature throughout fertility (Birje et al., 2020; Hao et al., 2020). The optimum growth temperature of tomatoes is between 18°C and 32°C (Berry and Bjorkman, 1980; Van Ploeg and Heuvelink, 2005). Prolonged exposure to temperature exceeding this range will restrict the growth and production of tomatoes more frequently and seriously (Bertin et al., 2000; Nicola et al., 2009). Therefore, global warming will negatively affect the growth and productivity of tomato plants, especially in the summer seasons.

High temperature (HT) has adverse effects on photosynthesis, such as significantly reducing the maximum net photosynthetic rate (P_{Nmax}), apparent quantum efficiency (AQE), and light-compensation point (LCP), and significantly increasing the light-saturation point (LSP) (Djanaguiraman et al., 2020; Li et al., 2023). Previous studies demonstrated that gas exchange and photosynthesis had marked reduction under HT stress due to the inhibition of chloroplast and photosystem II (PSII) activity (Salvucci and Crafts-Brandner, 2004; Allakhverdiev et al., 2008). HT stress also reduces nitrogen metabolism via lower photosynthesis, resulting in the loss of nutrients (Prasad et al., 2008; Hammer et al., 2018). In addition, HT stress also influences morphological symptoms in tomato plants after the decline of photosynthesis and metabolism appear. It is well known that HT stress can reduce cell division and restrict cell elongation, thereby delaying plant growth (Ashraf and Harris, 2004; Camejo et al., 2005). Since plants cannot maintain some fundamental processes, HT stress may severely affect plant growth, yield, and fruit quality (Wahid et al., 2007; Bita and Gerats, 2013).

Although high temperatures have many adverse effects on plants, nitrogen application can enhance high-temperature stress tolerance (James et al., 2018). First, nitrogen can increase the photosynthesis and the scavenging capacity of reactive oxygen species, which in turn improves leaves to resist high-temperature adversity (Liu et al., 2019). Second, the smooth and efficient functioning of the nitrogen metabolic system in the leaves is ensured with increased nitrogen application, improving the nitrogen metabolism, and reducing the damage caused by HT stress (Iqbal et al., 2020; Ru et al., 2022). Specifically, excessive nitrogen application at high-temperature stress will exacerbate the damage to plants, which is characterized by lower yield (Peng et al., 2017).

Plants will continue to be challenged by HT stress in the future. Temperature and nitrogen both play important roles in plant growth (Sun et al., 2012; Alvar-Beltrán et al., 2019). However, to our knowledge, little is known about the effects of nitrogen application on tomato growth, development, and fruit quality under HT stress. In our study, we hypothesize that appropriate nitrogen would effectively increase the photosynthetic progress, and nitrogen metabolism and further affect the yield and fruit quality of tomato plants. Our objectives were (1) to compare the growth, photosynthetic performance, nitrogen metabolism activities, and fruit quality of tomatoes under different temperatures, (2) to investigate the effects of nitrogen application on the growth, yield, and fruit quality of tomatoes under high-temperature stress, (3) to determine the optimum nitrogen level to be applied under different high-temperature conditions, hoping to provide scientific contribution for high yield and good fruit quality of tomatoes in the greenhouse.

2 Materials and methods

2.1 Plant material and experimental treatments

The experiments were conducted in a Venlo-type greenhouse of the Nanjing University of Information Science and Technology (NUIST) from March 2022 to August 2022. Tomato seedlings (*Solanum lycopersicum* L., "Caesar") were planted into pots of 30 cm (height) × 30 cm (upper diameter) × 25 cm (lower diameter) filled with peat soil: perlite: vermiculite = 2:1:1 (v/v/v). The soil was a medium loam with pH=7.4, 12.93 g kg^{-1}organic carbon (C), 22.29 g kg^{-1} organic matter content, 69.36 mg kg^{-1} effective phosphorus (P), 13.80 mg L^{-1} available potassium (K), and 0.13% total nitrogen (N). To ensure proper soil nutrient content, base fertilizers were applied in phosphorus (calcium superphosphate, 12%P_2O_5, 200 kg hm^2) and potassium (potassium sulfate, 52%K_2O, 300 kg hm^2). Five levels of nitrogen (urea, 46%N) were set as 0 (0N, N_1), 125 (0.5N, N_2), 187.5 (0.75N, N_3), 250 (1.0N, N_4), and 312.5 (1.25N, N_5) kg hm^2 (250 kg hm^2 as the percentage of standard nutrient requirements (Yang et al., 2017; Wang et al., 2020)). The ratio of nitrogen was 30%:30%:20%:20% at the seedling, flowering and fruiting, green ripening, and color change stages, respectively.

Uniform-sized tomato seedlings with one young fruit were chosen to conduct high-temperature and nitrogen experiments during the flowering and fruiting stage. Three levels of daily minimum/daily maximum temperature were adopted, namely control (CK; 18°C/28°C), sub-high temperature (SHT; 25°C/35°C), and high-temperature (HT; 30°C/40°C) stress, and the duration lasted for 5 days. All seedlings were divided into 15 groups with each group containing 9 pots (Table 1). Plants uptaking nitrogen after 5 days were moved into artificial climate chambers (BDW 40, Conviron, Canada). During the treatment, the relative humidity was set at 50-80%, and the light was 6:00-18:00 (daytime) with photosynthetic active radiation between 0 to 1000 μmol m^{-2} s^{-1}.

After the treatments, all plants were removed to the Velno-type greenhouse for the recovery period. Measurements were taken with 3 random pots at the end of treatments and conducted on the third to fifth functional leaves. Additionally, to measure the fruit quality, three tomato fruits of relatively uniform size and without mechanical damage were chosen at maturity for each treatment. Water is supplied twice a day during the treatment and at least every two days (in most cases once or twice a day) during the seedling and recovery stages. All plants were irrigated to 80% field capacity (monitoring by soil moisture content tester) to avoid water deficiency.

TABLE 1 Treatment combination of nitrogen level and temperature level for tomato in the greenhouse.

Nitrogen treatment (kg hm^{-2})	Temperature treatment (daily maximum/daily minimum)		
	CK (28°C/18°C)	SHT (35°C/25°C)	HT (40°C/30°C)
N_1:0N (0kg hm^{-2})	CKN_1	$SHTN_1$	HTN_1
N_2:0.5N (125kg hm^{-2})	CKN_2	$SHTN_2$	HTN_2
N_3:0.75N (187.5kg hm^{-2})	CKN_3	$SHTN_3$	HTN_3
N_4:1.0N (250kg hm^{-2})	CKN_4	$SHTN_4$	HTN_4
N_5:1.25N (312.5kg hm^{-2})	CKN_5	$SHTN_5$	HTN_5

CK, SHT and HT are the control, sub-high temperature and high temperature treatment, respectively.

2.2 The methods of measurement

2.2.1 Gas exchange parameters and SPAD value

Gas exchange parameters, including the stomatal conductance (g_s) and intercellular carbon dioxide concentration (C_i), were measured by an LI-6400XT photosynthesis system (LI-COR Inc., Lincoln, NE, USA) from 9:00-11:00. The leaf chamber temperature was set to 25°C, the relative humidity was set to 65%, and the CO_2 concentration was kept at 390 μmol mol^{-1}. Photosynthetically active radiation (PAR) was set to 1800, 1600, 1400, 1200, 1000, 800, 600, 400, 200, 150, 100, 50, and 0 μmol m^{-2} s^{-1}, respectively. The stomatal limit (L_s) value was determined by equation (1).

$$L_s = 1 - \frac{C_i}{C_a} \quad (1)$$

Where C_a indicates the atmospheric CO_2 concentration.

And

$$\text{water-use efficiency (WUE)} = \frac{\text{net photosynthetic rate } (P_n)}{\text{transpiration rate } (T_r)} \quad (2)$$

The P_{Nmax} was obtained by the photosynthesis-light response curves based on the photosynthetic electron transport of photosystem II in C_3 and C_4 species (Ye, 2012; Ye et al., 2013).

SPAD value was measured by Chlorophyll Meter Model (SPAD-502, Konica Minolta, Japan).

2.2.2 Nitrogen metabolism and nutrients

The third to fifth function leaves were picked from the top of tomato plants, frozen rapidly with liquid nitrogen for 15 min, and then store at -20°C for measurement. Nitrate reductase (NR, EC 1.6.6.1) was determined according to the method of Miflin and Habash (2002). NR can be expressed in terms of the amount of nitroso-nitrogen produced, which has a maximum absorption peak at 540nm. Glutamine synthetase (GS, EC 2.7.7.42) activity was measured using the method of Du et al. (2008). One unit of GS activity was determined by the absorbance values at 540 nm using the spectrophotometer (UV-1800, Shimadzu, Japan). The NR and GS activities were calculated per germ of fresh weight (FW).

Soluble protein was determined by the coomassie brilliant blue method (Sedmak and Grossberg, 1977), which was measured by the absorbance of the solution at 595 nm, and the protein content was found by the standard curve. The content of free amino acids was determined by the ninhydrin chromogenic method according to Friedman (2004), which was colorimetric at 570 nm.

2.2.3 Morphological characters

Plant height, stem diameter, main root length, and leaf area were measured by tape ruler, electronic vernier caliper, rule, and leaf area meter (LI-3100C, Li-Cor, Inc., USA), respectively. Plant height growth, stem diameter height growth, and leaf area index (LAI) were calculated as:

$$\text{Plant height growth} = \text{Plant height}_{5d} - \text{Plant height}_{0d} \quad (3)$$

$$\text{Stem diameter growth} = \text{Stem diameter}_{5d} - \text{Stem diameter}_{0d} \quad (4)$$

$$\text{LAI} = \frac{\text{leaf area per plant} \times \text{total number of plants per unit of land area}}{\text{unit area of land}} \quad (5)$$

Where 0d and 5d are the value measured at 0d and 5d, respectively.

2.2.4 Fruit quality

Extrinsic quality (single fruit weight, fruit length, maximum and minimum fruit diameter, etc.) and intrinsic quality (Vitamin C, anthocyanin, organic acid content, and soluble sugar content, etc.) are two aspects of fruit quality (Ashalley, 2014). Fruit hardness, single fruit weight, and maximum and minimum fruit diameter were measured by fruit hardness meter (GY-4, Aipli, China), electronic balance (ES-220D, China), and electronic Vernier caliper, respectively. Fruit shape index and yield were calculated as:

$$\text{Fruit shape index} = \frac{\text{fruit longitudinal diameter}}{\text{fruit horizontal diameter}} \quad (6)$$

$$\text{Yield} = \text{plants per hectare} \times \text{normal fruits per plant} \times \text{single weight fruit} \quad (7)$$

The content of Vitamin C (VC), titratable acid, and soluble sugar was determined by the 2,6-dichloroindophenol titrimetric (JAOAC, 1984), micro alkaline titration (Wei, 2020), and the anthrone method (Wei, 2020), respectively. Lycopene was determined according to Zhao et al. (2022). Nitrate (NO_3^-) was determined according to Wang et al. (2017). Soluble solids were measured by a hand-held refractometer (ATC, Aipli, China).

2.3 Statistical analysis

2.3.1 Variance analysis

All data were the mean ± standard deviation (SD) of 3 biological replications. SPSS 24.0 (SPSS, Chicago, IL, USA) for one-way analysis of variance (ANOVA), interaction analysis, Duncan's multiple comparisons (at P=0.05), correlation analysis, and principal component analysis.

2.3.2 Principal component analysis

The indicators of tomato photosynthesis, nitrogen metabolism, nutrients, growth, and fruit quality were evaluated by correlation analysis and principal component analysis. The comprehensive index (CI) is constructed by the indicators with high contribution rates and most of the information in principal component analysis (Li et al., 2019). The standardized values, weights, and comprehensive index are calculated as follows.

This study uses the opposite difference approach (8) to normalize the indicators so that their ranges were between [0,1].

$$X_i' = \begin{cases} \frac{X_i - X_{mini}}{X_{maxi} - X_{mini}} & \textbf{Positive indicators} \\ \frac{X_{maxi} - X_i}{X_{maxi} - X_{mini}} & \textbf{Negative indicators} \end{cases} \quad (8)$$

Where X_i' is the standardized value of the i^{th} indicator, (i=1, 2, 3, …, 23); X_{mini} is the minimum value of the i^{th} indicator; X_{maxi} is the maximum value of the i^{th} indicator.

The weight of the indicators in Principal Component A_k can be calculated as:

$$W_{ki} = \frac{C_{ki}}{\sqrt{E_k}} \quad (9)$$

Where W_{ki} is the weight of the i^{th} indicator in A_k, (k=1, 2, …., p); C_{ki} is the loadings of the i^{th} indicator in A_k; E_k is the eigenvalues of A_k.

The results of the comprehensive index in Principal Component A_k are obtained as:

$$CI_k = \sum_{i=1}^{n} W_{ki} \times X_i' \quad (10)$$

Where CI_k is the comprehensive index of A_k.

The results of comprehensive evaluation in Principal Component analysis are obtained as:

$$W_k = P_k / \sum_{k=1}^{n} P_k \quad (11)$$

$$CI = \sum_{k=1}^{n} W_k \times CI_k \quad (12)$$

Where P_k is the contribution rate of Principal Component A_k; W_k is the weight of Principal Component A_k.

3 Results

3.1 Effects of nitrogen application on gas exchange parameters and SPAD value under high-temperature stress

High-temperature (HT) stress had negative impacts on the gas exchange parameters of tomato leaves, which was characterized by the decrease in P_{Nmax}, g_s, L_S, and WUE but the increase in C_i (Table 2).

TABLE 2 Effects of nitrogen application on gas exchange parameters of tomato leaves under high-temperature stress.

Treatment	P_{Nmax} (μmol $m^{-2}s^{-1}$)	g_s (mol m^{-2} s^{-1})	C_i (μmol mol^{-1})	L_s	WUE (μmol $mmol^{-1}$)
CKN_1	6.34 ± 0.07 k	0.04 ± 0.01 i	363.82 ± 1.82 a	0.09 ± 0.01 d	1.11 ± 0.13 hi
CKN_2	8.62 ± 0.13 h	0.08 ± 0.01 i	358.63 ± 1.19 b	0.10 ± 0.01 d	1.42 ± 0.05 gh
CKN_3	14.54 ± 0.08 d	0.33 ± 0.05 ef	329.78 ± 2.48 d	0.18 ± 0.03 bc	2.56 ± 0.17 d
CKN_4	17.82 ± 0.26 b	0.49 ± 0.04 bc	307.01 ± 2.79 g	0.23 ± 0.03 a	3.94 ± 0.11 b
CKN_5	7.89 ± 0.14 i	0.06 ± 0.01 i	360.83 ± 2.42 ab	0.10 ± 0.03 d	1.49 ± 0.12 g
$SHTN_1$	10.30 ± 0.12 g	0.22 ± 0.05 h	335.29 ± 1.86 c	0.16 ± 0.01 c	1.83 ± 0.14 f
$SHTN_2$	14.65 ± 0.39 d	0.37 ± 0.04 de	325.71 ± 1.59 e	0.19 ± 0.01 abc	2.68 ± 0.18 d
$SHTN_3$	20.59 ± 0.27 a	0.60 ± 0.05 a	307.37 ± 1.14 g	0.23 ± 0.01 a	4.49 ± 0.24 a
$SHTN_4$	18.00 ± 0.09 b	0.50 ± 0.02 b	309.26 ± 1.81 g	0.23 ± 0.02 a	3.90 ± 0.03 b
$SHTN_5$	16.03 ± 0.17 c	0.43 ± 0.02 cd	317.60 ± 1.45 f	0.21 ± 0.02 ab	3.23 ± 0.09 c
HTN_1	6.11 ± 0.12 k	0.04 ± 0.01 i	363.08 ± 3.22 a	0.09 ± 0.01 d	1.15 ± 0.15 hi
HTN_2	14.69 ± 0.20 d	0.38 ± 0.05 de	323.68 ± 2.53 e	0.19 ± 0.02 abc	2.64 ± 0.11 d
HTN_3	12.74 ± 0.05 e	0.30 ± 0.01 fg	330.49 ± 0.98 d	0.17 ± 0.01 bc	2.26 ± 0.12 e
HTN_4	10.85 ± 0.12 f	0.24 ± 0.01 gh	332.86 ± 1.28 cd	0.17 ± 0.02 bc	1.92 ± 0.07 f
HTN_5	7.03 ± 0.11 j	0.05 ± 0.01 i	361.66 ± 1.57 ab	0.10 ± 0.01 d	1.20 ± 0.09 hi
Temperature (T)	**	**	**	**	**
Nitrogen (N)	**	**	**	**	**
T x N	**	**	**	**	**

Different lowercase letters indicate significant differences among treatments at the P< 0.05 level by Duncan's test. CK, SHT and HT are the control, sub-high temperature and high temperature treatment, respectively. Values are mean ± SD (n = 3). ** indicates significance at P ≤ 0.01.

Compared to the CK and HT, the P_{Nmax}, g_s, L_S, and WUE in the SHT group increased significantly, but the C_i was reduced significantly (P<0.05). The P_{Nmax}, g_s, L_S, C_i, and WUE were significantly influenced by appropriate nitrogen applications under different temperature treatments. Maximum P_{Nmax}, g_s, L_S and WUE occurred at CKN_3, $SHTN_3$, and HTN_2, respectively, whereas the C_i was the lowest. P_{Nmax}, g_s, and WUE in HTN_2 were lower than those of the CKN_3. However, those parameters significantly increased by 15.54%, 22.45%, and 13.96%, respectively, under $SHTN_3$. L_S showed no significant difference among CKN_3, $SHTN_3$, and HTN_2. Furthermore, C_i under HTN_2 was 5.43% higher than that of CKN_3, but no significant differences between CKN_3 and $SHTN_3$ (P>0.05).

The SPAD value was also influenced by HT stress (Figure 1). Meanwhile, appropriate nitrogen application significantly mitigated the effects of HT stress on SPAD value, with a marked improvement in CKN_3, $SHTN_4$, and HTN_2. SPAD value under CKN_3 was 13.70% higher than that of HTN_2, while no significant difference with $SHTN_3$.

3.2 Response of nitrogen application on nitrogen metabolism and nutrients to high-temperature stress

The responses of nitrogen application on nitrogen metabolism and nutrients to HT stress were shown in Figure 2. The NR, GS, soluble protein, and free amino acids in CK were significantly greater than in HT but were lower than in SHT, without nitrogen application. Appropriate nitrogen application significantly increased the contents of NR, GS, soluble protein, and free amino acids in the leaves of tomato plants. The NR, GS, soluble protein and free amino acids were highest in CKN_3, $SHTN_3$, and HTN_2, respectively. Compared to CKN_3, the activity of NR and GS was greater than HTN_2, whereas was significantly reduced by 21.26% and 17.14%, respectively, under $SHTN_3$. Similar to NR and GS, free amino acids decreased significantly by 11.91% in HTN_2 but improved significantly by 2.19% in $SHTN_3$. Soluble protein under CKN_3 was 14.90% lower than that of $SHTN_3$. However, for soluble protein, there was no significant difference between CKN_3 and HTN_2 treatments.

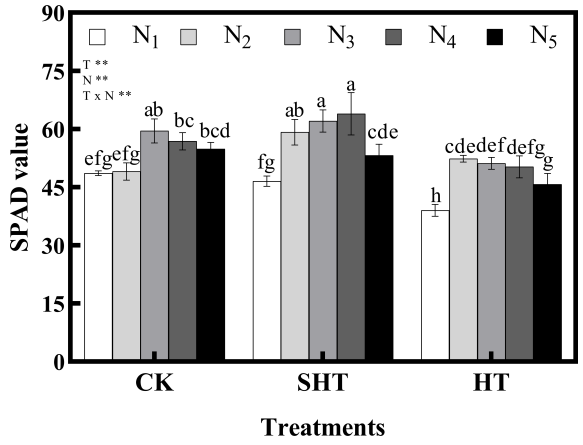

FIGURE 1
Effects of nitrogen application on SPAD value of tomato leaves under high-temperature stress. Different lowercase letters indicate significant differences among treatments at the P< 0.05 level by Duncan's test. CK, SHT and HT are the control, sub-high temperature and high temperature treatment, respectively. T, temperature; N, nitrogen. Values are mean ± SD (n = 3). ** indicates significance at $P \leq 0.01$.

3.3 Effects of nitrogen application on morphological characters under high-temperature stress

HT stress was reflected in the morphological characters (Table 3). Without nitrogen application, compared to CK, the plant height growth, stem diameter growth, main root length, and LAI were inhibited under HT, whereas were improved under SHT. Nitrogen application significantly affected the morphological characters of tomato plants under high-temperature stress. The plant height growth in CK increased with the increase of N_1-N_3, while they decreased with a further increase of N_4-N_5. Maximum plant height growth occurred at CKN_3, $SHTN_4$, and HTN_3, respectively. Similarly, stem diameter growth was the highest in CKN_3, $SHTN_3$, and HTN_3. The stem diameter growth in the CKN_3 was greater than that of the HTN_3, while significantly decreasing by 57.89% under the $SHTN_3$. The main root length and LAI also had appropriate nitrogen application under different temperature treatments. Compared to CK, the maximum main root length and LAI were significantly reduced by 6.76% and 20.29%, respectively, under HT conditions. In contrast, these two indicators under SHT were significantly increased by 3.72% and 50.72%, respectively, compared to the CK group.

3.4 Response of nitrogen application on fruit quality to high-temperature stress

The effects of nitrogen application on fruit shape index, fruit hardness, and yield of tomatoes under HT stress were shown in Table 4. The fruit shape index showed no significant difference among treatments of N_2-N_3 except N_4-N_5. However, fruit hardness was no significant difference among different temperature treatments. The yield in CK was significantly greater than in HT but was no significant difference in SHT, without nitrogen application. Appropriate nitrogen application could enhance high-temperature stress tolerance. The yield was the highest in N_4 under CK and SHT treatment, while the highest occurred at N_2 under HT treatment. Compared to HTN_2, the yield was significantly increased by 104.54% and 110.04%, respectively, for CKN_4 and $SHTN_4$ treatments.

HT stress inhibited the intrinsic quality of tomato fruit, while nitrogen application could significantly reduce the negative effects of HT stress (Figure 3). The VC, soluble sugar, lycopene, and soluble solids in CK and SHT increased with the increase of N_1-N_4, while they decreased with a further increase of N_5. However, these four indicators in HT increased with the increase of N_1-N_3, while they decreased with a further increase of N_4-N_5. Maximum VC occurred at N_4, N_4, and N_3, respectively, for CK, SHT, and HT

10.3389/fpls.2023.1172078

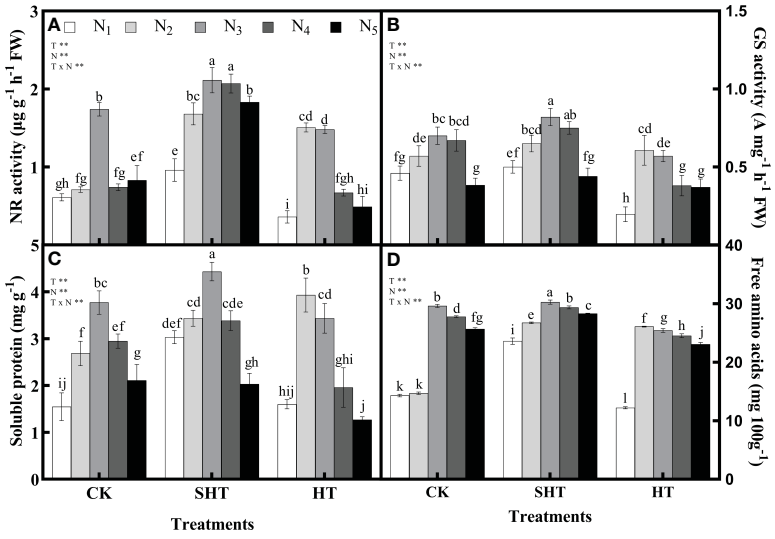

FIGURE 2
Effects of nitrogen application on the nitrate reductase (NR) activity **(A)**, glutamine synthetase (GS) activity **(B)**, soluble protein **(C)**, and free amino acids **(D)** in tomato leaves under high-temperature stress. Different lowercase letters indicate significant differences among treatments at the $P< 0.05$ level by Duncan's test. CK, SHT and HT are the control, sub-high temperature and high temperature treatment, respectively. T, temperature; N, nitrogen. Values are mean ± SD (n = 3). ** indicates significance at $P \leq 0.01$.

TABLE 3 Effects of nitrogen application on morphological characters of tomato leaves under high-temperature stress.

Treatment	Plant height growth (cm)	Stem diameter growth (mm)	Main root length (cm)	LAI
CKN_1	3.04 ± 0.07 hi	-0.27 ± 0.13 e	5.67 ± 0.10 g	0.89 ± 0.06 g
CKN_2	3.29 ± 0.02 h	0.34 ± 0.08 bcd	5.98 ± 0.05 f	1.04 ± 0.06 f
CKN_3	4.45 ± 0.18 e	0.57 ± 0.02 b	8.78 ± 0.05 b	1.22 ± 0.06 e
CKN_4	3.71 ± 0.08 g	0.50 ± 0.07 bc	8.88 ± 0.14 b	1.38 ± 0.06 d
CKN_5	4.15 ± 0.34 f	-0.16 ± 0.27 e	5.09 ± 0.09 hi	1.14 ± 0.06 ef
$SHTN_1$	5.33 ± 0.12 d	-0.08 ± 0.20 e	6.26 ± 0.05 e	1.45 ± 0.04 d
$SHTN_2$	5.91 ± 0.06 c	0.25 ± 0.08 d	6.45 ± 0.02 e	1.72 ± 0.02 c
$SHTN_3$	6.30 ± 0.10 b	0.90 ± 0.03 a	5.20 ± 0.15 hi	1.92 ± 0.04 b
$SHTN_4$	7.49 ± 0.14 a	0.54 ± 0.02 bc	9.21 ± 0.26 a	2.08 ± 0.07 a
$SHTN_5$	6.22 ± 0.02 b	0.31 ± 0.10 bcd	5.36 ± 0.04 h	1.62 ± 0.06 c
HTN_1	2.55 ± 0.09 j	-0.50 ± 0.04 f	5.08 ± 0.10 hi	0.75 ± 0.05 h
HTN_2	2.84 ± 0.17 ij	0.31 ± 0.02 cd	8.28 ± 0.28 c	0.84 ± 0.03 gh
HTN_3	3.00 ± 0.11 i	0.34 ± 0.05 bcd	6.73 ± 0.05 d	1.10 ± 0.07 f
HTN_4	2.76 ± 0.10 ij	-1.07 ± 0.09 h	6.18 ± 0.11 ef	0.81 ± 0.06 gh
HTN_5	2.27 ± 0.14 k	-0.80 ± 0.09 g	4.97 ± 0.10 i	0.73 ± 0.04 h
Temperature (T)	**	**	**	**
Nitrogen (N)	**	**	**	**
T x N	**	**	**	**

Different lowercase letters indicate significant differences among treatments at the P< 0.05 level by Duncan's test. CK, SHT and HT are the control, sub-high temperature and high temperature treatment, respectively. Values are mean ± SD (n = 3). LAI, leaf area index. ** indicates significance at P ≤ 0.01.

conditions. Compared to CKN_4, the VC was significantly decreased by 17.68% and 20.47%, respectively, for $SHTN_4$ and HTN_3 treatments. Similarly, the contents of soluble sugar, lycopene, and soluble solids in the SHT and HT groups were lower than those of the CK group. On the contrary, the titratable acid and NO_3^- were lowest in N_3/N_4, N_3/N_4, and N_2/N_3, respectively, for CK, SHT, and HT conditions. However, minimum titratable acid and NO_3^- were no significant differences among treatments.

TABLE 4 Effects of nitrogen application on external quality of tomato fruit under high-temperature stress.

Treatment	Fruit shape index	Fruit hardness (kg cm^{-2})	Yield (t hm^{-2})
CKN_1	0.96 ± 0.07 abc	2.16 ± 0.20 abcd	4.54 ± 0.89 ef
CKN_2	0.93 ± 0.04 abcde	2.12 ± 0.38 abcd	9.47 ± 2.13 c
CKN_3	0.89 ± 0.03 bcdef	1.45 ± 0.05 cd	15.38 ± 2.67 b
CKN_4	0.92 ± 0.01 abcde	1.51 ± 0.08 cd	18.94 ± 4.32 ab
CKN_5	0.94 ± 0.02 abcd	1.33 ± 0.24 d	7.45 ± 1.31 cde
$SHTN_1$	0.97 ± 0.01 ab	2.53 ± 0.12 ab	5.01 ± 0.22 def
$SHTN_2$	0.83 ± 0.02 def	3.03 ± 0.22 a	9.35 ± 0.93 c
$SHTN_3$	0.84 ± 0.07 cdef	2.67 ± 0.31 ab	15.76 ± 2.55ab
$SHTN_4$	0.91 ± 0.05 abcde	1.82 ± 0.22 bcd	19.45 ± 1.36 a
$SHTN_5$	0.96 ± 0.03 abc	2.55 ± 0.63 ab	4.21 ± 1.05 efg
HTN_1	1.03 ± 0.06 a	2.68 ± 0.07 ab	0.66 ± 0.02 g
HTN_2	0.86 ± 0.10 bcdef	2.60 ± 0.32 ab	9.26 ± 1.06 c
HTN_3	0.83 ± 0.04 cdef	2.51 ± 0.72 ab	8.68 ± 0.29 cd
HTN_4	0.80 ± 0.07 ef	2.42 ± 0.03 abc	7.73 ± 0.36 cde
HTN_5	0.76 ± 0.10 f	2.85 ± 1.11 a	2.27 ± 0.97 fg
Temperature (T)	*	**	**
Nitrogen (N)	**	n.s.	**
T x N	*	n.s.	**

Different lowercase letters indicate significant differences among treatments at the P< 0.05 level by Duncan's test. CK, SHT and HT are the control, sub-high temperature and high temperature treatment, respectively. Values are mean ± SD (n = 3). n.s., *, ** indicate non-significance and significance at P ≤ 0.05 and 0.01, respectively.

3.5 Comprehensive evaluation of tomato yield, fruit quality, and related traits under different treatments

3.5.1 Correlation analysis between different traits

Figure 4 showed that there were different degrees of positive and negative correlations between the trait indicators of the different treatments. The absolute values of the correlation coefficients for most indicators ranged from 0.60 to 0.98. Gas exchange parameters and SPAD value were highly significantly correlated (P<0.01), with the absolute values of the correlation coefficients ranging from 0.60 to 0.98. It can be assumed that the gas exchange parameters and SPAD value provide 60% to 98% of the common information. Similarly, indicators of nitrogen metabolism and nutrients had a highly significant positive correlation, providing 61% to 81% of the common information. The majority of morphological characters showed highly significant positive correlations, with correlation coefficients ranging from 0.45 to 0.59. Furthermore, the correlation coefficients for yield, VC, soluble sugar, soluble solids, and lycopene among the fruit quality varied from 0.47 to 0.77, giving 47% to 77% of the common information.

The 23 indicators measured contained a great deal of information and were highly correlated with each other. However, they were not suitable for determining indicators of nitrogen regulation under HT stress. Therefore, a principal component analysis was introduced to reduce the number of indicators to a few aggregated indicators for further analysis, without losing too much information.

3.5.2 Principal component and fitting analysis

The principal component analysis of the 23 indicators showed that the cumulative variance contribution of the first four components had reached 86.255%, satisfying the principle of eigenvalues greater than 1 and cumulative contribution greater than 85% (Table 5). Table 5 showed that the first principal component could characterize 58.676% of the information, with P_{Nmax}, WUE, g_s, C_i, L_s, SPAD value, GS, soluble sugar, yield, stem diameter growth, NR, free amino acids, soluble protein, LAI, and lycopene having larger absolute values of the eigenvectors. P_{Nmax} is the strongest indicator of photosynthesis and has the largest eigenvector, containing information common with g_s, WUE, C_i, L_s, and SPAD value. Thus, P_{Nmax} was selected. GS can represent NR, free amino acids, and soluble protein as an indicator of the strength of nitrogen metabolism and be therefore selected. Similarly, yield, stem diameter growth, soluble sugar, and lycopene were selected. The larger absolute values of eigenvectors in the second principal components were fruit shape index, NO_3^- and titratable acid. However, the third and fourth principal components were fruit hardness and soluble solids, plant height growth and main root length, respectively.

Although the four principal components above combined most of the indicator information, the characteristic information overlapped to some extent, and the number of input parameters was large. Therefore, further screening was needed. P_{Nmax}, yield,

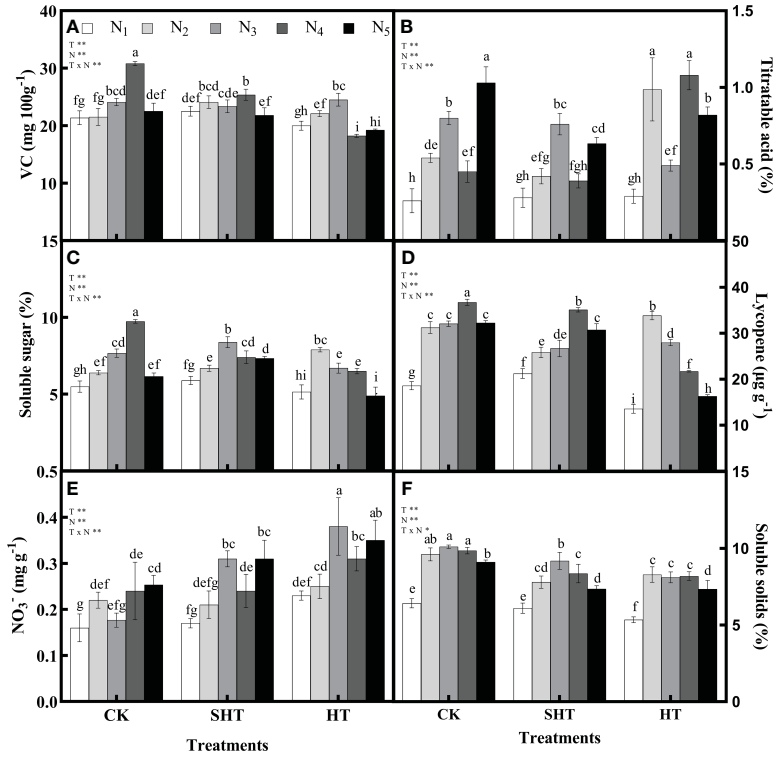

FIGURE 3
Effects of nitrogen application on the Vitamin C (VC; A), titratable acid (B), soluble sugar (C), lycopene (D), nitrate (NO_3^-; E), and soluble solids (F) of tomato fruit under high-temperature stress. Different lowercase letters indicate significant differences among treatments at the $P < 0.05$ level by Duncan's test. CK, SHT and HT are the control, sub-high temperature and high temperature treatment, respectively. T, temperature. N, nitrogen. Values are mean ± SD (n = 3). ** indicates significance at $P \leq 0.01$.

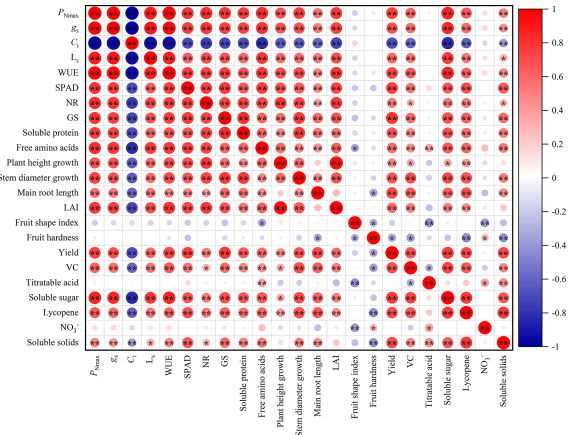

FIGURE 4
Correlation analysis among leaves and fruit indexes of tomato (n = 45). P_{Nmax}, the maximum net photosynthetic rate. g_s, stomatal conductance. C_i, carbon dioxide concentration. L_S, stomatal limit value. WUE, water-use efficiency. NR, nitrate reductase. GS, glutamine synthetase. LAI, leaf area index. VC, Vitamin C; NO_3^-, nitrate. * and ** indicate the statistical significance exceeding 95% and 99%, respectively.

soluble sugar, GS, stem diameter growth, and lycopene were selected to construct the CI, considering the correlation, the contribution of principal component analysis and eigenvectors, the biological significance of the indicators and the ease of determination.

Soluble sugar, GS, yield, P_{Nmax}, stem diameter growth, and lycopene were again subjected to principal component analysis and the eigenvectors obtained were 0.419, 0.417, 0.416, 0.413, 0.400, and 0.384, respectively (Table 6). The standardized indicators and eigenvectors were used to CI under different treatments.

$$CI = 0.419X'_{\text{soluble sugar}} + 0.417X'_{GS} + 0.416X'_{\text{yield}} + 0.413X'_{P_{Nmax}} + 0.400X'_{\text{stem diameter growth}} + 0.384X'_{\text{lycopene}} \quad (13)$$

The CI was highest at moderate nitrogen application under different temperatures, decreasing at low and high nitrogen applications (Figure 5). The response fits the regression models:

$$CI_{CK} = -4.659e^{-7}N^3 + 0.0001850N^2 - 0.01110N + 0.5670 \quad R^2 = 0.9788 \quad (14)$$

$$CI_{SHT} = -3.264e^{-7}N^3 + 0.0001253N^2 - 0.005834N + 0.8253 \quad R^2 = 0.9854 \quad (15)$$

$$CI_{HT} = 2.444e^{-7}N^3 - 0.0001671N^2 + 0.02879N + 0.1386 \quad R^2 = 0.9991 \quad (16)$$

Based on the regression equations, the highest CI of CK, SHT, and HT were obtained at the nitrogen of 230.23 kg hm^2 (N_3-N_4), 230.02 kg hm^2 (N_3-N_4), and 115.32 kg hm^2 (N_2), respectively.

TABLE 5 Contribution rate of principle components and eigenvectors of each index.

Principle component factor		PC1	PC2	PC3	PC4
Eigenvalue		13.495	2.761	2.494	1.088
Variance contribution rate (%)		58.676	12.003	10.846	4.731
Cumulative variance contribution (%)		58.676	70.678	81.524	86.255
Eigenvector	P_{Nmax}	0.262	-0.094	-0.090	-0.101
	WUE	0.255	-0.063	-0.104	-0.102
	g_s	0.255	-0.111	-0.126	-0.150
	C_i	-0.250	0.100	0.110	0.222
	L_s	0.249	-0.109	-0.111	-0.190
	SPAD value	0.247	-0.015	0.055	0.298
	GS	0.245	0.038	0.007	0.019
	Soluble sugar	0.241	0.036	0.137	-0.253
	Yield	0.241	0.114	0.172	-0.039
	Stem diameter growth	0.225	0.165	-0.066	0.051
	NR	0.225	-0.117	-0.188	0.250
	Free amino acids	0.224	-0.221	0.049	0.142
	Soluble protein	0.223	-0.019	-0.019	-0.031
	LAI	0.214	0.060	-0.300	0.279
	Lycopene	0.214	0.119	0.257	0.099
	VC	0.200	0.262	0.067	-0.286
	Plant height growth	0.188	0.066	-0.331	0.421
	Main root length	0.179	0.192	0.195	-0.312
	NO_3^-	-0.011	0.484	-0.046	0.152
	Fruit shape index	0.055	-0.476	0.175	-0.051
	Soluble solids	0.175	-0.013	0.430	0.160
	Fruit hardness	0.073	0.343	0.403	0.238
	Titratable acid	-0.018	0.374	-0.399	-0.281

P_{Nmax}, the maximum net photosynthetic rate; g_s, stomatal conductance; C_i, carbon dioxide concentration; L_S, stomatal limit value; WUE, water-use efficiency; NR, nitrate reductase; GS, glutamine synthetase; LAI, leaf area index; VC, Vitamin C; NO_3^-, nitrate.

4 Discussion

High temperature is one of the main disasters affecting the growth, yield, and fruit quality of plants (Mathur et al., 2014). The effect of high-temperature stress on plants receives more attention as the frequency and intensity of high-temperature stress increase globally (IPCC, 2021). Nitrogen plays an important role in plant growth, development, and yield. Appropriate nitrogen application can significantly improve high-temperature stress tolerance (James et al., 2018). In this study, we explored how nitrogen affects tomato plants under high-temperature stress.

First, short-term high-temperature stress affects the photosynthetic process of tomato leaves. Photosynthesis is one of the most fundamental metabolic activities in plants (Yin et al., 2006). The P_{Nmax} was inhibited under high-temperature (HT) stress, accompanied by different declines of g_s, L_s, and WUE (Table 2). However, C_i increased, which indicated that the decrease was due to non-stomatal limitation and mainly resulted from photosystem damage, and inhibition of ribulose bisphosphate (Rubisco) (Farquhar and Sharkey, 1982; Liu et al., 2013). In addition, HT also significantly decreased the SPAD value of tomato leaves (Figure 2), which reflected that the chloroplast development and photosynthetic performance were inhibited (Lu et al., 2019). Interestingly, short-term sub-high temperature (SHT) stress had positive impacts on the photosynthetic process, which was characterized by higher P_{Nmax}, g_s, L_s, WUE, SPAD value, and lower C_i, compared to CK. The SHT may improve chloroplast and cytoplasmic

TABLE 6 Contribution of principal components and eigenvectors of each index after the secondary screening.

Principle component factor		PC1
Eigenvalue		4.850
Variance contribution rate (%)		80.829
Cumulative variance contribution (%)		80.829
Eigenvector	Soluble sugar	0.419
	GS	0.417
	Yield	0.416
	P_{Nmax}	0.413
	Stem diameter growth	0.400
	Lycopene	0.384

GS, glutamine synthetase; P_{Nmax}, the maximum net photosynthetic rate.

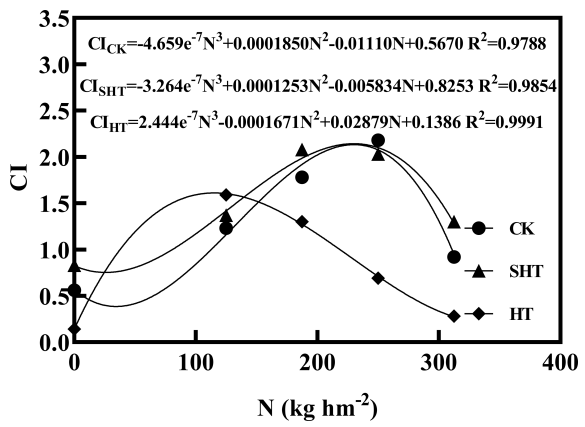

FIGURE 5
Comprehensive value (CI) of tomatoes as affected by nitrogen application under high-temperature stress. CK, SHT and HT are the control, sub-high temperature and high temperature treatment, respectively. N, nitrogen. R^2, coefficient of determination.

structure. Consequently, the Rubisco carboxylation activities and ribulose diphosphate (RuBP) carboxylation regeneration ability increased, thereby maintaining higher photosynthetic efficiency (Dias and Brüggemann, 2010; Han et al., 2019; Li et al., 2020). Nitrogen has positive impacts on photosynthetic reactions (Hamner, 1936; Liu et al., 2013; Ru et al., 2022). Appropriate nitrogen application not only can alleviate the damage of Chl-containing structure and function by high-temperature stress but also maintain the photosynthetic capacity of chloroplasts under high-temperature stress. In our study, maximum P_{Nmax}, g_s, L_s, WUE, and SPAD value occurred at N_2 under HT treatments. Similarly, these photosynthetic parameters were the highest in N_3, for CK and SHT stress. High-temperature stress was the main cause of the decrease in photosynthetic rate when nitrogen was overused, which was similar to the result of Han et al. (2019).

Second, nitrogen metabolism is tightly associated with nitrogen uptake and photosynthesis and is also closely related to the ultimate life state of the plants, such as growth and development under stress conditions (Xu and Zhou, 2006; Liu et al., 2013; Shu et al., 2016). In this study, short-term HT stress significantly hampered nitrogen metabolism, which further influenced the content of nutrients (Figure 2). Previous studies suggested that the decrease in nitrogen metabolism was due to the increase of NH_4^+ accumulation in plants, which hindered ammonia assimilation and ATP synthesis required for nitrate (Crawford and Glass, 1998; Yuan et al., 2017). However, under short-term SHT stress, the content of soluble protein and free amino acids increased in tomato leaves, accompanied by different improvements in the activity of NR and GS. These results showed that short-term SHT stress could stimulate enzyme activity in plants. Appropriate nitrogen can effectively enhance the high-temperature tolerance of tomato plants. The findings had also been confirmed on wheat (Ru et al., 2022), cotton (Iqbal et al., 2020), etc. In this study, NR, GS, soluble protein, and free amino acids were the highest in N_3-N_4, N_3-N_4, and N_2-N_3, respectively, for CK, SHT, and HT stress.

Third, plant morphology is also significantly affected by high-temperature stress (Źróbek-Sokolnik, 2012; Fahad et al., 2016). The plant height growth, stem diameter growth, main root length, and LAI were remarkably declined in tomatoes (Table 3), which were recognized as sensitive to HT stress. In contrast, short-term SHT stress improved plant morphology. An early study indicated that the maintenance of normal transfer and distribution of photosynthetic products in tomatoes ensured plant growth and development (Xu et al., 2020). Plant morphology changed with nitrogen levels (Boussadia et al., 2010; Bhuvaneswari et al., 2014; Razaq et al., 2017). For example, the results of LAI were consistent with those of previous studies, which found that moderate nitrogen with increased LAI (Meier and Leuschner, 2008). In addition, appropriate nitrogen can effectively alleviate the symptoms brought by high-temperature stress. The high LAI of appropriate nitrogen under high-temperature stress was caused by the increase

of the photosynthetic rate during growth and the increase of facilitating nutrient uptake.

Therefore, tomato plants are affected by many factors. The fruit quality is also sensitive to changes in the environment (Gajc-Wolska et al., 2008; Alenazi et al., 2020). In our study, under HT stress, the yield and intrinsic fruit quality were both significantly decreased (Table 4; Figure 3). This result was also consistent with Hernández et al. (2022). Although the intrinsic quality was also obviously reduced after SHT stress, which was characterized by lower VC, soluble sugar, lycopene, and soluble solids, SHT stress had an improvement in yield. These results indicated that short-term SHT stress maintained higher photosynthetic efficiency and nitrogen metabolism to uptake nutrients, thereby maintaining the high growth and yield of tomatoes. However, high yield is not always conducive to good fruit quality (Sansavini and Corelli-Grappadelli, 1996). Appropriate nitrogen can effectively enhance the heat stress tolerance of plants (Iqbal et al., 2020). On one hand, moderate nitrogen can increase the absorbance of light energy by increasing the leaf area, thus increasing the rate of photosynthesis (Fois et al., 2009; Gautam et al., 2021). On the other hand, it can enhance the activities of nitrogen metabolism via higher photosynthesis, causing enough nutrients, which in turn increases the yield and fruit quality (Nava et al., 2007; Ru et al., 2022). Consequently, the highest yield and fruit quality occurred at N_3-N_4, N_3-N_4, and N_2-N_3, respectively, for CK, SHT, and HT stress.

Temperature and nitrogen interaction affects fruit development and quality through the regulation of various plant physiological processes. For example, temperature and nitrogen interaction might regulate the balance between vegetative and reproductive growth in plants. Additionally, the interaction between nitrogen and temperature might influence the activity of enzymes involved in the biosynthesis of plant hormones such as auxins and cytokinins, which play a critical role in fruit development and quality (Ding et al., 2013). The production and signaling of reactive oxygen species (ROS) in plants have been shown to influence fruit development and quality (Tian et al., 2013). Therefore, temperature and nitrogen interaction might influence fruit development and quality via ROS production and signaling. In summary, the mechanism of nitrogen and temperature interaction in co-regulating fruit development and quality involves the regulation of several physiological processes such as plant metabolic rate, gene expression, and hormone signaling, which collectively influence fruit growth, development, and quality.

Principal component analysis is a very useful method for evaluating objects that are influenced by many factors (Wold et al., 1987). Previous studies had demonstrated that using this method to make comprehensive evaluations was feasible (Shi et al., 2021; Xu et al., 2021). According to our results, P_{Nmax}, yield, soluble sugar, GS, stem diameter growth, and lycopene were selected to construct the CI (Table 6). P_{Nmax} plays a vital role in photosynthesis (Xu et al., 2013). Meanwhile, GS is tightly associated with some fundamental processes, including nitrogen uptake and photosynthesis (Thum et al., 2003). Soluble sugar is considered an important factor in the fruit quality and anti-adversity of plants, and it is mainly accumulated by photosynthesis (Wahid et al., 2007). Additionally, lycopene also can reflect the intrinsic fruit quality due to the pigment principally responsible for the characteristic deep-red color of ripe tomato fruits, and it also acts as a natural antioxidant (Shi and Maguer, 2000). Therefore, these six indicators could be used to construct the CI to respond to the effects of nitrogen application under high-temperature stress. Based on the CI, the tomato growth, yield, and fruit quality were the highest in 230.23 kg hm^2 (N_3-N_4), 230.02 kg hm^2 (N_3-N_4), and 115.32 kg hm^2 (N_2), respectively, at CK, SHT, and HT stress, which can provide scientific contributions for higher yield and better fruit quality of tomato plants in the greenhouse.

5 Conclusions

In this study, the growth, yield, and fruit quality of tomato plants were inhibited by short-term high-temperature (HT) stress. However, sub-high temperature (SHT) stress improved growth and yield whereas fruit quality was reduced. Appropriate nitrogen application could enhance the HT stress tolerance of tomato plants. The P_{Nmax}, g_s, L_S, WUE, NR, GS, soluble protein, and free amino acids were the highest in CKN_3, $SHTN_3$, and HTN_2, respectively, whereas C_i, was the lowest. Maximum SPAD value, plant height growth, stem diameter growth, main root length, LAI, yield, VC, soluble sugar, lycopene, and soluble solids occurred at N_3-N_4, N_3-N_4, and N_2-N_3, respectively, for CK, SHT, and HT. The appropriate nitrogen maintained higher photosynthetic efficiency, nitrogen efficiency, and protein synthesis, thereby maintaining the high yield and quality of tomato plants. This study suggested that the optimum nitrogen application for tomato growth, yield, and fruit quality was 230.23 kg hm^2 (N_3-N_4), 230.02 kg hm^2 (N_3-N_4), and 115.32 kg hm^2 (N_2), respectively, at CK, SHT, and HT stress.

Data availability statement

The original contributions presented in the study are included in the article/Supplementary Material. Further inquiries can be directed to the corresponding author.

Author contributions

JL: Methodology, Data curation, Software, Formal analysis, Writing-original draft. ZY: Conceptualization, Methodology, Validation, Supervision, Writing-original draft. FZ: Methodology, Supervision, Writing-review and editing. CL: Supervision, Writing-review and editing. All authors contributed to the article and approved the submitted version.

Funding

This work was supported by the National Natural Science Foundation of China (41975142).

Conflict of interest

The authors declare that the research was conducted in the absence of any commercial or financial relationships that could be construed as a potential conflict of interest.

Publisher's note

All claims expressed in this article are solely those of the authors and do not necessarily represent those of their affiliated organizations, or those of the publisher, the editors and the reviewers. Any product that may be evaluated in this article, or claim that may be made by its manufacturer, is not guaranteed or endorsed by the publisher.

Supplementary material

The Supplementary Material for this article can be found online at: https://www.frontiersin.org/articles/10.3389/fpls.2023.1172078/full#supplementary-material

References

Alenazi, M. M., Shafiq, M., Alsadon, A. A., Alhelal, I. M., Alhamdan, A. M., Solieman, T. H., et al. (2020). Improved functional and nutritional properties of tomato fruit during cold storage. *Saudi J. Biol. Sci.* 27 (6), 1467–1474. doi: 10.1016/j.sjbs.2020.03.026

Allakhverdiev, S. I., Kreslavski, V. D., Klimov, V. V., Los, D. A., Carpentier, R., and Mohanty, P. (2008). Heat stress: an overview of molecular responses in photosynthesis. *Photosynth. Res.* 98, 541–550. doi: 10.1007/s11120-008-9331-0

Alvar-Beltrán, J., Dao, A., Dalla Marta, A., Saturnin, C., Casini, P., Sanou, J., et al. (2019). Effect of drought, nitrogen fertilization, temperature and photoperiodicity on quinoa plant growth and development in the sahel. *Agronomy* 9 (10), 607. doi: 10.3390/agronomy9100607

Ashalley, R. N. (2014). *Effectiveness and efficacy of different waxing materials on the quality of cucumber fruits stored under different storage conditions* [master's thesis]. (Legon: University of Ghana).

Ashraf, M., and Harris, P. (2004). Potential biochemical indicators of salinity tolerance in plants. *Plant Sci.* 166 (1), 3–16. doi: 10.1016/j.plantsci.2003.10.024

Berry, J., and Bjorkman, O. (1980). Photosynthetic response and adaptation to temperature in higher plants. *Annu. Rev. Plant Physiol.* 31 (1), 491–543. doi: 10.1146/annurev.pp.31.060180.002423

Bertin, N., Guichard, S., Leonardi, C., Longuenesse, J., Langlois, D., and Navez, B. (2000). Seasonal evolution of the quality of fresh glasshouse tomatoes under Mediterranean conditions, as affected by air vapour pressure deficit and plant fruit load. *Ann. Bot.* 85 (6), 741–750. doi: 10.1006/anbo.2000.1123

Bhuvaneswari, G., Sivaranjani, R., Reetha, S., and Ramakrishan, K. (2014). Application of nitrogen fertilizer on plant density, growth, yield and fruit of bell peppers (*Capsicum annuum* l.). *Int. Lett. Nat. Sci.* 8 (2), 81–90. doi: 10.56431/p-t5jc5t

Birje, P., Kshirsagar, D., and Shinde, S. (2020). Performance study of fl hybrids of tomato (*Solonum lycopersicum* l.). *J. Pharmacogn. Phytochem.* 9 (5S), 01–03. doi: 10.22271/phyto.2020.v9.i5Sa.12298

Bita, C. E., and Gerats, T. (2013). Plant tolerance to high temperature in a changing environment: scientific fundamentals and production of heat stress-tolerant crops. *Front. Plant Sci.* 4. doi: 10.3389/fpls.2013.00273

Boussadia, O., Steppe, K., Zgallai, H., El Hadj, S. B., Braham, M., Lemeur, R., et al. (2010). Effects of nitrogen deficiency on leaf photosynthesis, carbohydrate status and biomass production in two olive cultivars 'Meski'and 'Koroneiki'. *Sci. Hortic.* 123 (3), 336–342. doi: 10.1016/j.scienta.2009.09.023

Camejo, D., Rodríguez, P., Morales, M. A., Dell'Amico, J. M., Torrecillas, A., and Alarcón, J. J. (2005). High temperature effects on photosynthetic activity of two tomato cultivars with different heat susceptibility. *J. Plant Physiol.* 162 (3), 281–289. doi: 10.1016/j.jplph.2004.07.014

Crawford, N. M., and Glass, A. D. (1998). Molecular and physiological aspects of nitrate uptake in plants. *Trends Plant Sci.* 3 (10), 389–395. doi: 10.1016/S1360-1385(98)01311-9

Dias, M., and Brüggemann, W. (2010). Limitations of photosynthesis in phaseolus vulgaris under drought stress: gas exchange, chlorophyll fluorescence and Calvin cycle enzymes. *Photosynthetica* 48, 96–102. doi: 10.1007/s11099-010-0013-8

Ding, J. G., Chen, B. W., Xia, X. J., Mao, W. H., Shi, K., Zhou, Y. H., et al. (2013). Cytokinin-induced parthenocarpic fruit development in tomato is partly dependent on enhanced gibberellin and auxin biosynthesis. *PloS One* 8 (7), e70080. doi: 10.1371/journal.pone.0070080

Djanaguiraman, M., Narayanan, S., Erdayani, E., and Prasad, P. V. (2020). Effects of high temperature stress during anthesis and grain filling periods on photosynthesis, lipids and grain yield in wheat. *BMC Plant Biol.* 20, 1–12. doi: 10.1186/s12870-020-02479-0

Du, X. H., Zhou, X. J., and Peng, F. R. (2008). Determination and analysis of ammonium assimilation enzyme activities in different organs of tea plants. *Non-wood For. Res.* 26 (2), 23–28. doi: 10.3969/j.issn.1003-8981.2008.02.005

Ezquer, I., Salameh, I., Colombo, L., and Kalaitzis, P. (2020). Plant cell walls tackling climate change: biotechnological strategies to improve crop adaptations and photosynthesis in response to global warming. *Plants* 9 (2), 212. doi: 10.3390/plants9020212

Fahad, S., Hussain, S., Saud, S., Hassan, S., Ihsan, Z., Shah, A. N., et al. (2016). Exogenously applied plant growth regulators enhance the morpho-physiological growth and yield of rice under high temperature. *Front. Plant Sci.* 7. doi: 10.3389/fpls.2016.01250

Farquhar, G. D., and Sharkey, T. D. (1982). Stomatal conductance and photosynthesis. *Annu. Rev. Plant Physiol.* 33 (1), 317–345. doi: 10.1146/annurev.pp.33.060182.001533

Fois, S., Motzo, R., and Giunta, F. (2009). The effect of nitrogenous fertiliser application on leaf traits in durum wheat in relation to grain yield and development. *Field Crops Res.* 110 (1), 69–75. doi: 10.1016/j.fcr.2008.07.004

Friedman, M. (2004). Applications of the ninhydrin reaction for analysis of amino acids, peptides, and proteins to agricultural and biomedical sciences. *J. Agric. Food. Chem.* 52 (3), 385–406. doi: 10.1021/jf030490p

Gajc-Wolska, J., Bujalski, D., and Chrzanowska, A. (2008). Effect of a substrate on yielding and quality of greenhouse cucumber fruits. *J. Elementol.* 13 (2), 205–210.

Gautam, H., Sehar, Z., Rehman, M. T., Hussain, A., AlAjmi, M. F., and Khan, N. A. (2021). Nitric oxide enhances photosynthetic nitrogen and sulfur-use efficiency and activity of ascorbate-glutathione cycle to reduce high temperature stress-induced oxidative stress in rice (*Oryza sativa* l.) plants. *Biomolecules* 11 (2), 305. doi: 10.3390/biom11020305

Hammer, K. J., Borum, J., Hasler-Sheetal, H., Shields, E. C., Sand-Jensen, K., and Moore, K. A. (2018). High temperatures cause reduced growth, plant death and metabolic changes in eelgrass zostera marina. *Mar. Ecol. Prog. Ser.* 604, 121–132. doi: 10.3354/meps12740

Hamner, K. C. (1936). Effects of nitrogen supply on rates of photosynthesis and respiration in plants. *Bot. Gaz.* 97 (4), 744–764. doi: 10.1086/334601

Han, W., Yang, Z. Q., Huang, L. D., Sun, C. X., Yu, X. J., and Zhao, M. F. (2019). Fuzzy comprehensive evaluation of the effects of relative air humidity on the morpho-physiological traits of pakchoi (*Brassica chinensis* l.) under high temperature. *Sci. Hortic.* 246, 971–978. doi: 10.1016/j.scienta.2018.11.079

Hao, P. F., Qiu, C. W., Ding, G. H., Vincze, E., Zhang, G. P., Zhang, Y. S., et al. (2020). Agriculture organic wastes fermentation CO2 enrichment in greenhouse and the fermentation residues improve growth, yield and fruit quality in tomato. *J. Clean. Prod.* 275, 123885. doi: 10.1016/j.jclepro.2020.123885

Hernández, V., Hellín, P., Botella, M.Á., Vicente, E., Fenoll, J., and Flores, P. (2022). Oligosaccharins alleviate heat stress in greenhouse-grown tomatoes during the spring-summer season in a semi-arid climate. *Agronomy* 12 (4), 802. doi: 10.3390/agronomy12040802

Hoffmann, R., Muttarak, R., Peisker, J., and Stanig, P. (2022). Climate change experiences raise environmental concerns and promote green voting. *Nat. Clim. Change* 12 (2), 148–155. doi: 10.21203/rs.3.rs-738080/v1

Imran, M., Ghorat, F., Ul-Haq, I., Ur-Rehman, H., Aslam, F., Heydari, M., et al. (2020). Lycopene as a natural antioxidant used to prevent human health disorders. *Antioxidants* 9 (8), 706. doi: 10.3390/antiox9080706

IPCC. (2021). Summary for Policymakers. In: Climate Change 2021: The Physical Science Basis. *Contribution of Working Group I to the Sixth Assessment Report of the Intergovernmental Panel on Climate Change*. Eds. V. Masson-Delmotte, P. Zhai, A. Pirani, S. L. Connors, C. Péan, S. Berger, et al. (Cambridge, United Kingdom and New

York, NY, USA: Cambridge University Press), pp. 3–32. doi: 10.1017/9781009157896.001

Iqbal, A., Dong, Q., Wang, X., Gui, H., Zhang, H., Zhang, X., et al. (2020). High nitrogen enhance drought tolerance in cotton through antioxidant enzymatic activities, nitrogen metabolism and osmotic adjustment. *Plants* 9 (2), 178. doi: 10.3390/plants9020178

James, D., Borphukan, B., Fartyal, D., Ram, B., Singh, J., Manna, M., et al. (2018). Concurrent overexpression of OsGS1; 1 and OsGS2 genes in transgenic rice (*Oryza sativa* l.): impact on tolerance to abiotic stresses. *Front. Plant Sci.* 9. doi: 10.3389/fpls.2018.00786

JAOAC (1984). *Official methods of analysis. Vitamin c (ascorbic acid) in vitamin preparation and juices: 2, 6-dicholoindophenol titrimetric method* (Washington, DC: Association of Official Analytical Chemists).

Li, Z. J., Ji, W., Hong, E., Fan, Z., Lin, B. Y., Xia, X. Z., et al. (2023). Study on heat resistance of peony using photosynthetic indexes and rapid fluorescence kinetics. *Horticulturae* 9 (1), 100. doi: 10.3390/horticulturae9010100

Li, X., Li, M. H., Deng, W. W., Ahammed, G. J., Wei, J. P., Yan, P., et al. (2020). Exogenous melatonin improves tea quality under moderate high temperatures by increasing epigallocatechin-3-gallate and theanine biosynthesis in *Camellia sinensis* l. *J. Plant Physiol.* 253, 153273. doi: 10.1016/j.jplph.2020.153273

Li, Y. G., Yang, W. X., Shen, X. J., Yuan, G. H., and Wang, J. W. (2019). Water environment management and performance evaluation in central China: a research based on comprehensive evaluation system. *Water* 11 (12), 2472. doi: 10.3390/w11122472

Liu, Z. X., Bie, Z. L., Huang, Y., Zhen, A., Niu, M. L., and Lei, B. (2013). Rootstocks improve cucumber photosynthesis through nitrogen metabolism regulation under salt stress. *Acta Physio. Plant* 35, 2259–2267. doi: 10.1007/s11738-013-1262-5

Liu, K., Deng, J., Lu, J., Wang, X. Y., Lu, B. L., Tian, X. H., et al. (2019). High nitrogen levels alleviate yield loss of super hybrid rice caused by high temperatures during the flowering stage. *Front. Plant Sci.* 10. doi: 10.3389/fpls.2019.00357

Liu, J., and Wang, X. W. (2020). Tomato diseases and pests detection based on improved yolo V3 convolutional neural network. *Front. Plant Sci.* 11. doi: 10.3389/fpls.2020.00898

Lu, T., Yu, H. J., Li, Q., Chai, L., and Jiang, W. J. (2019). Improving plant growth and alleviating photosynthetic inhibition and oxidative stress from low-light stress with exogenous GR24 in tomato (*Solanum lycopersicum* l.) seedlings. *Front. Plant Sci.* 10. doi: 10.3389/fpls.2019.00490

Marlon, J. R., Wang, X., Mildenberger, M., Bergquist, P., Swain, S., Hayhoe, K., et al. (2021). Hot dry days increase perceived experience with global warming. *Global Environ. Change* 68, 102247. doi: 10.1016/j.gloenvcha.2021.102247

Mathur, S., Agrawal, D., and Jajoo, A. (2014). Photosynthesis: response to high temperature stress. *J. Photochem. Photobiol. B* 137, 116–126. doi: 10.1016/j.jphotobiol.2014.01.010

Meier, I. C., and Leuschner, C. (2008). Leaf size and leaf area index in fagus sylvatica forests: competing effects of precipitation, temperature, and nitrogen availability. *Ecosystems* 11, 655–669. doi: 10.1007/s10021-008-9135-2

Miflin, B. J., and Habash, D. Z. (2002). The role of glutamine synthetase and glutamate dehydrogenase in nitrogen assimilation and possibilities for improvement in the nitrogen utilization of crops. *J. Exp. Bot.* 53 (370), 979–987. doi: 10.1093/jexbot/53.370.979

Nava, G., Dechen, A. R., and Nachtigall, G. R. (2007). Nitrogen and potassium fertilization affect apple fruit quality in southern Brazil. *Commun. Soil Sci. Plant Anal.* 39 (1-2), 96–107. doi: 10.1080/00103620701759038

Nicola, S., Tibaldi, G., Fontana, E., Crops, A.-V., and Plants, A. (2009). Tomato production systems and their application to the tropics. *Acta Hortic.* 821 (821), 27–34. doi: 10.17660/ActaHortic.2009.821.1

Peng, Y., Yuanquan, C., Adamou, D., Zhiqiang, T., and Peng, S. (2017). Effect of nitrogen regimes on narrowing the magnitude of maize yield penalty caused by high temperature stress in north China plain. *Plant Soil Environ.* 63 (3), 131–138. doi: 10.17221/6/2017-PSE

Prasad, P., Staggenborg, S., and Ristic, Z. (2008). Impacts of drought and/or heat stress on physiological, developmental, growth, and yield processes of crop plants. *Response Crops to limited water: Understanding modeling Water Stress effects Plant Growth processes* 1, 301–355. doi: 10.2134/advagricsystmodel1.c11

Razaq, M., Zhang, P., and Shen, H.-l. (2017). Influence of nitrogen and phosphorous on the growth and root morphology of acer mono. *PloS One* 12 (2), e0171321. doi: 10.1371/journal.pone.0171321

Ru, C., Hu, X. T., Chen, D. Y., Song, T. Y., Wang, W., Lv, M. W., et al. (2022). Nitrogen modulates the effects of short-term heat, drought and combined stresses after anthesis on photosynthesis, nitrogen metabolism, yield, and water and nitrogen use efficiency of wheat. *Water* 14 (9), 1407. doi: 10.3390/w14091407

Salvucci, M. E., and Crafts-Brandner, S. J. (2004). Relationship between the heat tolerance of photosynthesis and the thermal stability of rubisco activase in plants from contrasting thermal environments. *Plant Physiol.* 134 (4), 1460–1470. doi: 10.1104/pp.103.038323

Sansavini, S., and Corelli-Grappadelli, L. (1996). "Yield and light efficiency for high quality fruit in apple and peach high density planting," in VI International Symposium on Integrated Canopy, Rootstock, Environmental Physiology in Orchard Systems. Eds. B. H. Barritt and F. Kappel (Leuven, Belgium: International Society for Horticultural Science (ISHS)), 451, 559–568.

Sedmak, J. J., and Grossberg, S. E. (1977). A rapid, sensitive, and versatile assay for protein using coomassie brilliant blue G250. *Anal. Biochem.* 79 (1-2), 544–552. doi: 10.1016/0003-2697(77)90428-6

Shi, J., and Maguer, M. L. (2000). Lycopene in tomatoes: chemical and physical properties affected by food processing. *Crit. Rev. Food Sci. Nutr.* 40 (1), 1–42. doi: 10.1080/07388550091144212

Shi, S. J., Wang, E. T., Li, C. X., Zhou, H., Cai, M. L., Cao, C. G., et al. (2021). Comprehensive evaluation of 17 qualities of 84 types of rice based on principal component analysis. *Foods* 10 (11), 2883. doi: 10.3390/foods10112883

Shu, S., Tang, Y. Y., Yuan, Y. H., Sun, J., Zhong, M., and Guo, S. R. (2016). The role of 24-epibrassinolide in the regulation of photosynthetic characteristics and nitrogen metabolism of tomato seedlings under a combined low temperature and weak light stress. *Plant Physiol. Biochem.* 107, 344–353. doi: 10.1016/j.plaphy.2016.06.021

Sun, P., Mantri, N., Lou, H. Q., Hu, Y., Sun, D., Zhu, Y. Q., et al. (2012). Effects of elevated CO_2 and temperature on yield and fruit quality of strawberry (*Fragaria× ananassa* duch.) at two levels of nitrogen application. *PloS One* 7 (7), e41000. doi: 10.1371/journal.pone.0041000

Thum, K. E., Shasha, D. E., Lejay, L. V., and Coruzzi, G. M. (2003). Light-and carbon-signaling pathways. modeling circuits of interactions. *Plant Physiol.* 132 (2), 440–452. doi: 10.1104/pp.103.022780

Tian, S. P., Qin, G. Z., and Li, B. Q. (2013). Reactive oxygen species involved in regulating fruit senescence and fungal pathogenicity. *Plant Mol. Biol.* 82, 593–602. doi: 10.1007/s11103-013-0035-2

Van Ploeg, D., and Heuvelink, E. (2005). Influence of sub-optimal temperature on tomato growth and yield: a review. *J. Hortic. Sci. Biotech.* 80 (6), 652–659. doi: 10.1080/14620316.2005.11511994

Wahid, A., Gelani, S., Ashraf, M., and Foolad, M. R. (2007). Heat tolerance in plants: an overview. *Environ. Exp. Bot.* 61 (3), 199–223. doi: 10.1016/j.envexpbot.2007.05.011

Wang, Z. H., Chen, X. J., Lyu, D. S., Li, W. H., Wang, T. Y., and Wei, C. L. (2020). Effects of water and fertilizer coupling on the yield and quality of processing tomato under aerated drip irrigation. *Trans. Chin. Soc Agric. Eng.* 36 (18), 66–75. doi: 10.11975/j.issn.1002-6819.2020.19.008

Wang, F., Li, G. A., Wang, L. L., Zhou, J. B., Lou, Y. D., and Yao, H. Y. (2017). Examining the effects of reduced nitrogen fertilization on the yield and fruit quality of greenhouse cultivated cucumber. *Chin. J. Appl. Ecol.* 28 (11), 3627–3633. doi: 10.13287/j.1001-9332.201711.041

Wei, T. T. (2020). *Effects of elevated air humidity at high temperature on organic acid metabolism and intrinsic quality of facility tomato fruits* [master's thesis]. (Nanjing, China: Nanjing University of Information Science and Technology).

Wold, S., Esbensen, K., and Geladi, P. (1987). Principal component analysis. *Chemometr. Intell. Lab.* 2 (1-3), 37–52. doi: 10.1016/0169-7439(87)80084-9

Xu, S. G., Cui, Y. X., Yang, C. X., Wei, S. J., Dong, W. P., Huang, L. H., et al. (2021). The fuzzy comprehensive evaluation (FCE) and the principal component analysis (PCA) model simulation and its applications in water quality assessment of nansi lake basin, China. *Environ. Eng. Res.* 26 (2), 200022. doi: 10.4491/eer.2020.022

Xu, W. Z., Deng, X. P., and Xu, B. C. (2013). Effects of water stress and fertilization on leaf gas exchange and photosynthetic light-response curves of bothriochloa ischaemum l. *Photosynthetica* 51, 603–612. doi: 10.1007/s11099-013-0061-y

Xu, C., Yang, Z. Q., Yang, S. Q., Wang, L., and Wang, M. T. (2020). High humidity alleviates photosynthetic inhibition and oxidative damage of tomato seedlings under heat stress. *Photosynthetica* 58 (1), 146–155. doi: 10.32615/ps.2019.168

Xu, Z. Z., and Zhou, G. S. (2006). Combined effects of water stress and high temperature on photosynthesis, nitrogen metabolism and lipid peroxidation of a perennial grass leymus chinensis. *Planta* 224, 1080–1090. doi: 10.1007/s00425-006-0281-5

Yang, Y. Z., Meng, C. R., Zhang, X. J., Bai, R. X., and Wei, C. Z. (2017). Effect of nitrogen and potassium fertilizer on yield and quality of processing tomato under drip irrigation with plastic film mulching. *Soil Fert. Sci. China* 1), 61–67. doi: 10.11838/sfsc.20170111

Ye, Z. P. (2012). Nonlinear optical absorption of photosynthetic pigment molecules in leaves. *Photosynth. Res.* 112 (1), 31–37. doi: 10.1007/s11120-012-9730-0

Ye, Z. P., Suggett, D. J., Robakowski, P., and Kang, H. J. (2013). A mechanistic model for the photosynthesis–light response based on the photosynthetic electron transport of photosystem II in C_3 and C_4 species. *New Phytol.* 199 (1), 110–120. doi: 10.1111/nph.12242

Yin, C. Y., Berninger, F., and Li, C. Y. (2006). Photosynthetic responses of populus przewalski subjected to drought stress. *Photosynthetica* 44 (1), 62–68. doi: 10.1007/s11099-005-0159-y

Yuan, L. Y., Tang, L., Zhu, S. D., Hou, J. F., Chen, G. H., Liu, F., et al. (2017). Influence of heat stress on leaf morphology and nitrogen–carbohydrate metabolisms in two wucai (*Brassica campestris* l.) genotypes. *Acta Soc Bot. Pol.* 86 (2), 3554. doi: 10.5586/asbp.3554

Zhao, R. L., Chen, X. Y., Xie, X. X., Lin, W., and Lin, F. (2022). Effects of the compound substrate of *Sparassiscris pa* fungi residues on the yield and quality of greenhouse tomatoes. *Fujian Agric. Sci. Technol.* 53 (8), 28–32. doi: 10.13651/j.cnki.fjnykj.2022.08.005

Źróbek-Sokolnik, A. (2012). ""Temperature stress and responses of plants,"," in *Environmental adaptations and stress tolerance of plants in the era of climate change*. Eds. P. Ahmad and M. N. V. Prasad (New York, NY: Springer New York), 113–134.

Frontiers in
Plant Science

Cultivates the science of plant biology and its applications

The most cited plant science journal, which advances our understanding of plant biology for sustainable food security, functional ecosystems and human health.

Discover the latest Research Topics

See more →

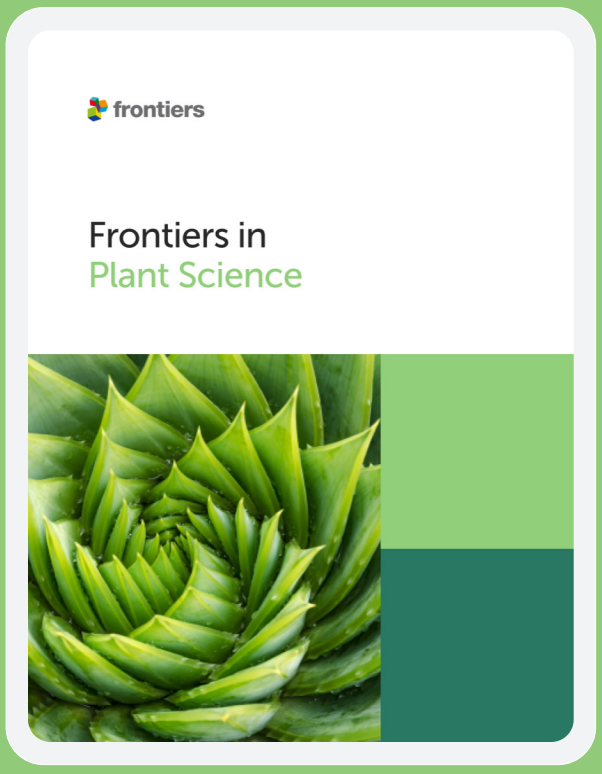

Frontiers

Avenue du Tribunal-Fédéral 34
1005 Lausanne, Switzerland
frontiersin.org

Contact us

+41 (0)21 510 17 00
frontiersin.org/about/contact